DISSERTATION ZUR ERLANGUNG DES DOKTORGRADES

DER FAKULTÄT FÜR CHEMIE UND PHARMAZIE

DER LUDWIG-MAXIMILIANS-UNIVERSITÄT MÜNCHEN

The Dual Use of Energetic Coordination Compounds – Stabilization of Sensitive Materials and Performance Enhancement through Complexation

MAXIMILIAN HANS HORST WURZENBERGER

AUS

MÜNCHEN, DEUTSCHLAND

2020

Erklärung

Diese Dissertation wurde im Sinne von § 7 der Promotionsordnung vom 28. November 2011 von Herrn Professor Dr. Thomas M. Klapötke betreut.

Eidesstattliche Versicherung

Diese Dissertation wurde eigenständig und ohne unerlaubte Hilfsmittel erarbeitet.

München, den 27. Oktober 2020

_____

MAXIMILIAN HANS HORST WURZENBERGER

Dissertation eingereicht am:	28.10.2020
1. Gutachter:	Prof. Dr. Thomas M. Klapötke
2. Gutachter:	Prof. Dr. Konstantin Karaghiosoff
Mündliche Prüfung am:	17.12.2020

Danksagung

Mein größter Dank gilt meinem Doktorvater Herrn Prof. Dr. Thomas M. Klapötke für die Möglichkeit in seinem Arbeitskreis zu promovieren und seine finanziellen Zuwendungen die letzten Jahre. Ihre tolerante Betreuung ermöglichte eine ungeheure Forschungsfreiheit und bei Problemen waren Sie jederzeit hilfsbereit und eine große Unterstützung. Der von Ihnen stets großzügig gewährte Freiraum für das Besuchen zahlreicher verschiedener Konferenzen erlaubte es mir, meinen wissenschaftlichen Horizont zu erweitern und interessante Kontakte zu knüpfen.

Bei Herrn Prof. Dr. Konstantin Karaghiosoff möchte ich mich nicht nur für die Anfertigung des Zweitgutachtens bedanken, sondern auch für deine freundschaftliche und lockere Art, die wesentlich zur Erheiterung des Arbeitsalltags beitrug. Man konnte immer auf deine enorm große Hilfe bezüglich NMR oder Einkristallmessungen vertrauen und (fast noch besser) mit dir das ein oder andere Bier in der Kaffeeküche trinken und Geschichten aus alten Unitagen lauschen. Ich hoffe es macht dir auch weiterhin so viel Spaß, dein Wissen mit so viel Elan und Freude an zukünftige Chemikergenerationen weiterzugeben, denn es ist definitiv eine große Bereicherung für diese Universität.

Des Weiteren bedanke ich mich bei Prof. Dr. Hans-Christian Böttcher, Prof. Dr. Robert Schmucker, Prof. i. R. Dr. Ingo-Peter Lorenz und Prof. em. Dr. Wolfgang Beck für ihre Bereitschaft Teil des Prüfungskomitees zu sein.

Ein enorm großer Dank gebührt Herrn Dr. Jörg Stierstorfer, der maßgeblich für die hervorragende Betreuung und das Gelingen dieser Doktorarbeit verantwortlich ist. Du hattest immer gute Ideen und Lösungsvorschläge bei auftretenden Problemen. Du hast mir viel über das Anfertigen von Publikationen und Vorträgen sowie das erfolgreiche Lösen von Kristallstrukturen beigebracht. Trotzdem hattest du immer die Geduld, bei problematischen Strukturen zu helfen und kritisches Feedback zu geben, was besonders die Qualität der Veröffentlichungen enorm gesteigert hat. Des Weiteren möchte ich mich für deine Korrektur dieser Arbeit und deinen guten Input für mehr farbige Bilder (ich weiß nicht wie viele Jahre ich noch brauche, um dich da auf Anhieb zufrieden zu stellen) bedanken. Auch wenn man nicht immer einer Meinung ist, war das Verhältnis zu dir bedeutend mehr als rein arbeitstechnisch und diese Freundschaft hätte ich die letzten Jahre nicht missen wollen!

Ein ähnlich großer Dank gilt Frau Irene Scheckenbach, ohne die dieser Arbeitskreis bei Weitem nicht so rund laufen würde wie er es tut. Sie sind eine stets gut gelaunte und freundliche Person und waren immer eine bemerkenswert große Hilfe bei allen bürokratischen und organisatorischen Angelegenheiten.

Ein weiterer sehr wichtiger Bestandteil dieser Doktorarbeit, der für einen meist harmonischen und angenehmen Arbeitsalltag sorgte, sind viele der ehemaligen und derzeitigen Mitglieder dieses grandiosen Arbeitskreises. Dadurch wurde nicht nur die tägliche Arbeit kurzweiliger, sondern auch diverse gemeinsame Freizeitaktivitäten, wie Saalfeste, Fußballturniere, Skiausflüge, Bier- und Weintastings, Paintballmatches, Beer Pong Abende, Pokerturniere, Wochenendausflüge nach Prag und gemeinsame Besuche von Wiesn und Starkbierfest sorgten für eine ausgeglichene und extrem unterhaltsame Work-Life Balance während meiner Zeit hier. Ich bin dankbar, dass ich die in den letzten Jahren eingetretene Gruppendynamik miterleben durfte und viele der hier kennengelernten Leute als Freunde bezeichnen würde. Besonders hervorheben möchte ich dabei Alicia Dufter, Elena Reinhardt, Maximilian Benz, Tobias Lenz, Alexander Harter, Michael Gruhne, Marcus Lommel, Moritz Kofen, Simon Endraß, Maurus Völkl, Daniel Shem Tov, Dr. Teresa Küblböck, Dr. Cornelia Unger und Dr. Ivan Gospodinov. Mein Dank gilt nicht nur für die angenehme gemeinsame Zeit mit all den Leuten, sondern auch für ihre wissenschaftliche Hilfe, wie Toxizitätsmessungen von Dr. Cornelia Unger, theoretische Rechnungen von Dr. Teresa Küblböck, Feuchtigkeitsbestimmungen von Tobias Lenz und die Hilfe bei Reparaturen von Maurus Völkl, die einen wichtigen Beitrag zu dieser Arbeit leisteten. Weiterhin möchte ich Dr. Ivan Gospodinov für das Korrekturlesen dieser Arbeit danken, sowie für seine Entertainmenteinlagen während der gemeinsamen Arbeitszeit, wobei es nicht unerwähnt bleiben darf, dass seit seiner Abwesenheit eine ruhigere Arbeitsatmosphäre eingetreten ist.

Nicht vergessen werden dürfen natürlich die Mitglieder Dr. Marco Reichel und Christin Kirst der „Subgroup“ Karaghiosoff, mit denen man immer eine gute Zeit verbringen konnte. Vor allem sei die gemeinsame Teilnahme am 15. Koordinationschemie-Treffen in München mit ihren lustigen Unterhaltungen erwähnt.

Besonders möchte ich mich bei meinen Bacheloranden und F-Praktikanten, Andreas Bartonek, Andreas Hess, Benjamin Bissinger, Jasmin Lechner, Marcus Lommel, Marina Schönherr, Michael Gruhne, Olga Zhuzhgova, Philipp Spieß, Sebastian Hagenreiner, Simon Endraß, Valentin Bockmair und Vanessa Braun bedanken, die mir eine große Hilfe bei der praktischen Arbeit dieser Dissertation waren. Insbesondere Vanessa, Jasmin, Benjamin, Michael, Marcus und Simon zeichneten sich nicht nur durch ihre bemerkenswerten Arbeitsleistungen aus, sondern waren auch außerhalb des Labors eine wertvolle Bereicherung und beteiligten sich aktiv beim Verfassen von Publikationen.

Des Weiteren gilt mein Dank Michael Gruhne, Vanessa Braun und Moritz Kofen, die alle herausragende und motivierte Chemiker sind, dass ich ihre Masterarbeiten betreuen durfte. Bei meinem Laborkollegen Moritz Kofen möchte ich mich außerdem für eine gute Zusammenarbeit bedanken, die stets ruhig und entspannt verlief, wenn er nicht gerade wieder aus Versehen etwas in die Luft jagte. Auch konnte man

für kurze Ablenkungen vom chemischen Alltagstrott mit ihm jederzeit über alle möglichen Themen interessante und unterhaltsame Gespräche führen.

Zwei ausgesprochen erstaunlichen Menschen, Michael Gruhne und Marcus Lommel, bin ich ganz besonders dankbar. Seit nun annähernd drei Jahren darf ich euren erfolgreichen Werdegang von kleinen schüchternen Bacheloranden zu Promotionsstudenten, die es Faust dick hinter den Ohren haben, bei uns im Arbeitskreis miterleben. Dabei bewundere ich stets eure riesige Motivation, Wissbegierde, Intelligenz und wie schnell ihr neue Sachen erlernt. Ihr wart mir die letzten Jahre eine beispiellos große Hilfe indem ihr beim Schreiben der Publikationen, Korrekturlesen, Erstellen von Graphiken und Sensitivitätsbestimmungen mitgewirkt habt. Ohne euch wäre dieses Arbeitspensum bei Weitem nicht möglich gewesen und ihr seid maßgeblich mit für die Qualität dieser Arbeit verantwortlich. Aber ihr seid nicht nur für mich, sondern auch für viele Andere hier im Arbeitskreis jederzeit zur Stelle, sei es mit Kristallmessungen, jeglicher Art von PC-Problemen oder bei der Bedienung der Kamera. Ohne euch und eure Lausbubenstreiche wäre dieser Arbeitskreis ein bedeutend tristerer Ort. Ihr habt definitiv beide eine große Zukunft vor euch.

Ein weiterer Dank gilt der EMTO GmbH, allen voran meinen beiden Chefs Prof. Dr. Thomas M. Klapötke und Dr. Jörg Stierstorfer, die mir eine Anstellung bei ihnen und somit ein Arbeiten außerhalb des akademischen Forschens erlaubten. Durch diverse Industrieprojekte war es möglich, einen interessanten Einblick über den Unitellerrand hinaus zu erlangen und Abläufe bei der Entwicklung in großen Firmen kennenzulernen.

Unserem CTA Stefan Huber möchte ich für seine Hilfe bei technischen Problemen, die zuverlässige Organisation von Chemikalien sowie sonstigem Labormaterialien und die netten Pläuschchen, die stets zur Erheiterung beitrugen, bedanken.

Prof. Dr. Jürgen Evers und Dr. Peter Meyer bin ich dankbar für die Messung von Pulverdiffraktogrammen und Einkristallen sowie die Hilfe bei besonderen Problemstrukturen.

Des Weiteren gilt mein Dank meinem ehemaligem Betreuer Dr. Norbert Szimhardt, der mich damals zuerst als F-Praktikant und später als Masterand betreute. Du warst es, der mir die Welt der energetischen Komplexverbindungen nähergebracht hat und mir die wichtigsten Grundlagen auf diesem Gebiet beibrachte. Ohne dich stünde ich heute nicht da, wo ich jetzt stehe.

Bei Niko Langhammer, Kurt Brandl, Lisa Eichacker und Sara Eichacker bedanke ich mich herzlichst für das Korrekturlesen von Teilen dieser Arbeit

Zu guter Letzt möchte ich mich bei meiner Familie, meinen Eltern Barbara und Michael sowie meiner Schwester Julia und meinen Freunden bedanken, ohne die all das hier nicht möglich gewesen wäre. Ihr wart all die Jahre immer für mich da, habt an mich geglaubt uns seid zu einem großen Teil für diesen Erfolg verantwortlich. Danke dafür!

Table of Contents

1. Introduction

1.1. Coordination Compounds and their Use as Energetic Materials

Coordination chemistry covers the vast majority of the Periodic Table of the Elements and combines various branches of chemistry. While the basic main group chemistry of stable substances, especially organic chemistry, is comparatively limited concerning binding behavior, the metal coordination chemistry possesses coordination numbers ranging from one to twelve and more.[1] Examples for extraordinary binding situations can be found in the monomeric compound 2,6-Trip$_2$C$_6$H$_3$Tl (Trip = 2,4,6-triisopropylphenyl) with single bounden thallium and ceric ammonium nitrate $(NH_4)_2[Ce(NO_3)_6]$ with six bidentate nitrato ligands.[2,3] In combination with the possible alternating oxidation state of the central metal as well as the variation of ligands and anions, coordination chemistry opens the door to an almost infinite amount of substances with unique properties. On the other hand, this same immense variety poses a demanding challenge for scientists, requiring enormous patience and effort.

In its present form, the concept of coordination chemistry was first postulated in the 1890s by ALFRED WERNER, a pioneer of modern inorganic chemistry. Later, it successfully replaced JØRGENSEN's flawed concept.[4] Both were investigating various transition metal ammine complexes and developed rules for interpreting their structures. While JØRGENSEN's idea was based on BLOMSTRAND's "chain theory" and relied on nitrogen chains similar to the carbon chains from organic chemistry, WERNER formulated higher linkages to the central metal divorced from its valency, which led to the first postulation of an octahedral coordination sphere. He also demonstrated the chirality of inorganic compounds, including the carbon-free so-called hexol (Figure 1), whose name is derived from the old and nowadays obsolete term "dodecaammine-hexol-tetracobalt salt".[5,6] Apart from very few exceptions (*e.g.*, radical ligands), the coordination bond is formed by donating an electron pair from the ligand to an empty orbital of the central metal, which contrasts with covalent bonds where both binding partners contribute equally. Therefore, the formation of complexes can be regarded as a Lewis acid-base reaction whereby the ligands are Lewis bases (electron pair donors) and the central metals Lewis acids (electron pair acceptors), leading to the development of a σ-bond between them.[1,7] Furthermore, ligands in oxo (O^{2-}), carbene (CR_2^{2-}), or nitrido (N^{3-}) complexes can create double or triple bonds to the central atom when acting as π-donor molecules. In the case of empty π*-orbitals, it is also possible that π-backbonding occurs, whereby electrons from the metal d orbitals are donated toward the ligand. Typical examples for π-backdonations are carbonyl (CO) or cyanido (CN^-) coordination compounds.[8] Even though their structural constitution and many of

their properties could not be explained, complexes have been known since the beginning of modern chemistry and have been playing an essential role in both research and industry.

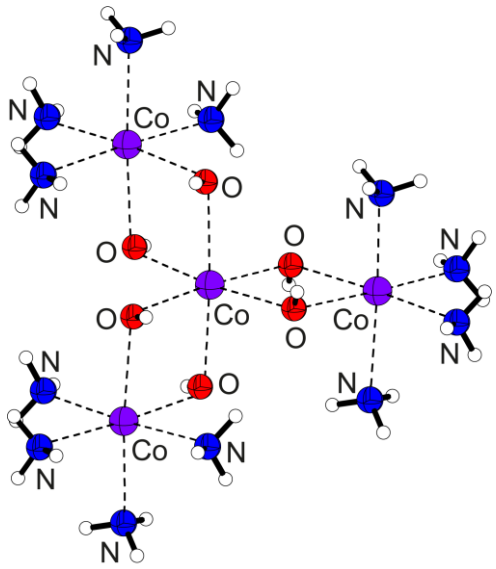

Figure 1. Illustration of the enantiomeric cation of hexol $[Co\{Co(NH_3)_4(OH)_2\}_3]^{6+}$ with octahedrally coordinated Co^{3+} central metals.[9]

For example, Prussian blue ($Fe_4[Fe(CN)_6]_3$), a primary modern synthetic pigment, and Zeise's salt, ($K[PtCl_3(C_2H_4)] \bullet H_2O$), the first organometallic complex in history, were synthesized in the early 18th and 19th centuries, respectively (Figure 2).[7,10]

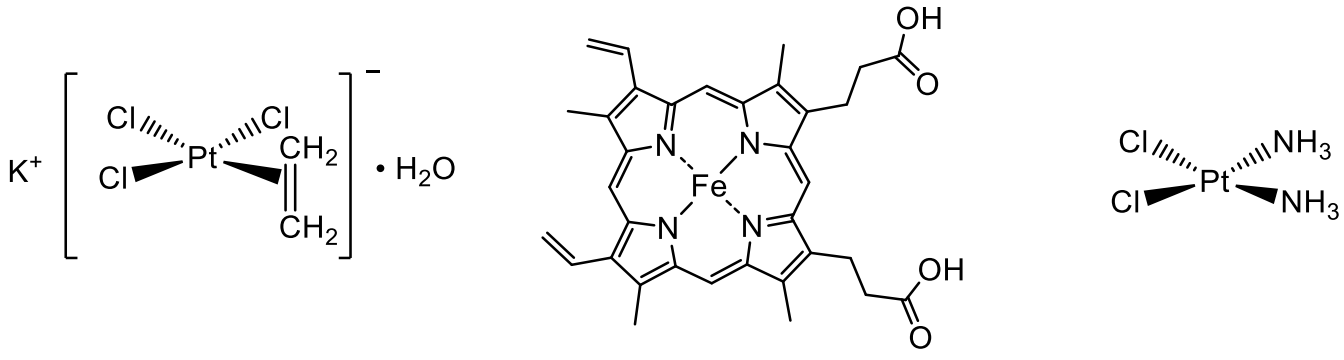

Figure 2. Overview and structure of some well-known coordination compounds.

Both substances' molecular structures were finally solved at the end of the 20th century using single-crystal X-ray diffraction experiments.[11,12] The coordination compounds investigated by WERNER were based on relatively few ligands such as simple primary amines, hydroxide, or pyridine and were mainly present as complex monomers. The polynuclear compounds he detected, like hexol, were correctly explained by the simple conjunction of several monomers.[5,13] Things he had not in mind at all were the formation of higher coordination polymers and the possible presence of metal-metal bonds in polynuclear

compounds. It took until the middle of the 20th century to recognize and further investigate metal-metal bonding in coordination chemistry. This discovery opened the field to a whole new class of compounds with unique properties and is still a research area of growing interest. Especially the effect of a variety of catalysts can be explained by the presence of metal-metal bonds within the complexes.[14] Besides their crucial role in catalysis, coordination compounds occur in numerous scientific fields and play an essential part in daily life. Their vital capacity becomes apparent when metal-containing biomolecules such as hemoglobin or chlorophyll are considered. The most commonly occurring transition metals in enzymes are iron, zinc, and manganese, but more exotic ones like molybdenum, vanadium, cobalt, or chromium can also be found.[1] The bioactivity of complexes furthermore enables their application as drugs for medical treatments as so-called metallodrugs. The most famous one is cisplatin, which is used as a chemotherapeutic medication. In addition to the use of platinum substances for cancer treatment, there exists a large number of coordination compounds with such diverse applications as in antimicrobial silver drugs, technetium- and gadolinium-based diagnostics, as well as gold and vanadium complexes for the therapy of rheumatoid arthritis or as insulin mimetics.[15] Apart from those already mentioned, complexation also plays an essential role in many other industrial applications, *e.g.*, fluorescent substances for fluoroimmunoassays, new materials for optical light-emitting diodes (OLEDs) as well as in the mining and extraction of various metals.[1]

A relatively small subsection of complex chemistry is taken up by so-called energetic coordination compounds (ECC). The history of ECC is almost as old as modern chemistry itself, and JUSTUS VON LIEBIG already investigated the first simple substances of this class, such as potassium difulminatoargentate(I) ($K[Ag(CNO)_2]$).[16] Several other fulminate complexes sharing the energetic character and lack of recognition of coordination compounds, such as $Na[Ag(CNO)_2]$ and $Na_4[Fe(CNO)_6]$, were subsequently investigated.[17] Following WERNER's concept, AMIEL investigated several basic primary ammine complexes of copper(II) chlorate, bromate as well as perchlorate in the early 1930s and described their explosive behavior.[18,19] Soon the principle explosive nature of metal ammine complexes or similar nitrogen-donor molecules with oxidizing anions was recognized. Fundamental studies revealed the energetic character of 3d metal coordination compounds based on nitrate, nitrite, iodate, chlorite, chlorate, or perchlorate as the anion.[20] Nevertheless, it took until the mid-1990s before SINDITSKII and SERUSHKIN first formulated the concept of energetic coordination compounds on the basis of complexes consisting of nitrogen-rich and highly endothermic ligands together with oxidizing anions.[21] Two prominent and well investigated ECC are pentaammine(5-cyano-2*H*-tetrazolato-N^2) cobalt(III) perchlorate (CP) and tetraammine-*cis*-bis(5-nitro-2*H*-tetrazolato-N^2) cobalt(III) perchlorate (BNCP) (Figure 3). Both were developed as potential replacements for toxic and

very sensitive lead-containing explosives. CP was first synthesized in the late 1960s and had already been tested for applications when its production was forbidden due to the use of toxic starting materials.[22] In the 1980s, an appropriate replacement for CP was found in BNCP. With the discovery of the laser initiation capability of BNCP, many new ECC, such as 5-hydrazino-1*H*-tetrazolemercury(II) perchlorate (HTMP), were synthesized and investigated concerning their behavior when irradiated with a laser diode.[23–25] However, many of them suffer from the toxicity of the applied central metals (*e.g.*, cobalt and mercury are highly carcinogenic), leading to high demand for new and more eco-friendly materials.

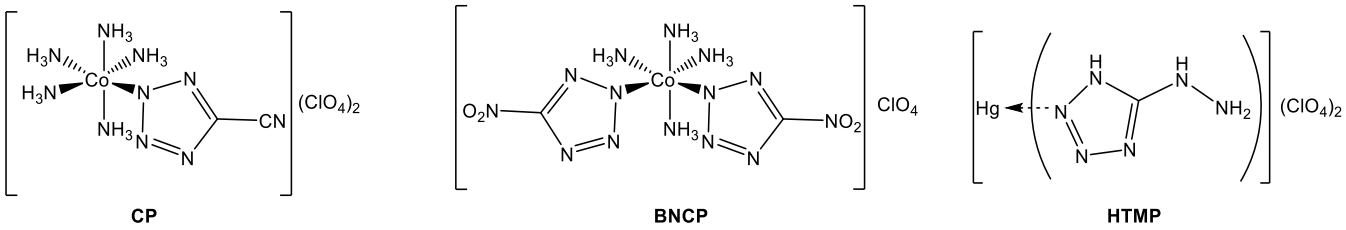

Figure 3. Depiction of prominent laser ignitable energetic coordination compounds.

1.2. Classification of Explosives

Explosives have a long tradition in human history and a decisive influence on historical development. With the rising number and types of different energetic materials, various classifications exist, *e.g.*, according to detonation velocity, application, or chemical composition.[26–29] From a chemical perspective, the most straightforward distinction is an explosive presence either as a pure single chemical substance or a mixture of several different components. In general, explosives derive their energy from a chemical reaction producing a large gas volume within a short time, which manifests itself as an explosion.[29] A feasible and easy classification of energetic materials is according to their three different main applications in pyrotechnics, propellants, and explosives, all of which can be further subdivided (Figure 4).

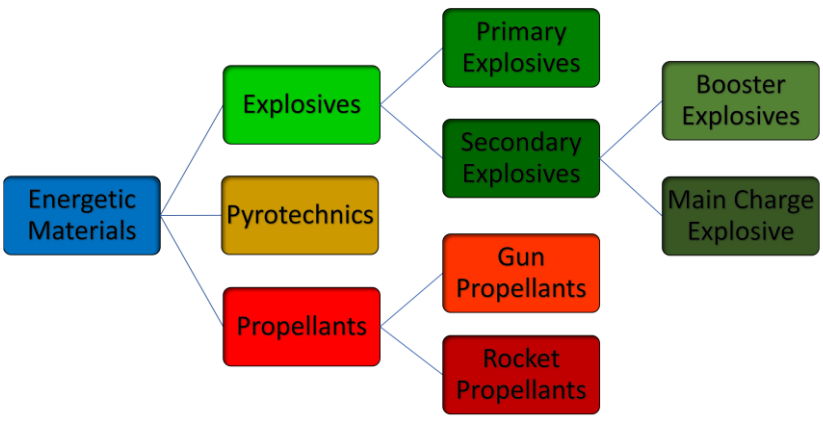

Figure 4. Primary classification of energetic materials according to their utilization.

Depending on their specific application, the classes of energetic materials must meet different criteria and show varying characteristics that allow an easy distinction between them. The most important properties of these materials are their sensitivity toward impact (*IS*), friction (*FS*), and electrostatic discharge (*ESD*), as well as performance parameters such as the detonation velocity.

Primary Explosives: Substances, which can be easily detonated via a simple initiating impulse (SII) and are used to generate a shock wave transferring the detonation to a less sensitive explosive, are designated as primary explosives. For the ability to produce a shock wave, primary explosives must possess a rapid deflagration-to-detonation transition (DDT) (deflagration: expanding velocity of reaction front < sonic velocity in combusting medium; detonation: expanding velocity of reaction front > sonic velocity in combusting medium) and small external non-explosive stimuli such as an electric spark, flame, heat, impact, or friction are used as SII. The most crucial distinction between primary and secondary explosives is the fast transition from the SII to the detonation of the former. Therefore, primary explosives typically show very high sensitivities toward impact (≤ 4 J), friction (≤ 10 N), and electrostatic discharge (≤ 20 mJ). Furthermore, classical primary explosives such as LS and LA usually possess a relatively low detonation velocity around 5000 m s^{-1}. In addition to their use as detonating agents, primary explosives can also be applied as sensitizers in priming mixtures, thus ensuring a reliable ignition. Detonations of such pyrotechnic compositions are highly undesirable, and they are usually used to generate heat, flame, or sound.[28] The first substance ever to be used as a primary explosive was mercury fulminate (MF) (Figure 5). It is known since the 17th century, and igniters based on MF were already patented in 1807. Due to mercury's high toxicity, it was replaced at the beginning of the 19th century by lead azide (LA) and lead styphnate (LS).[30]

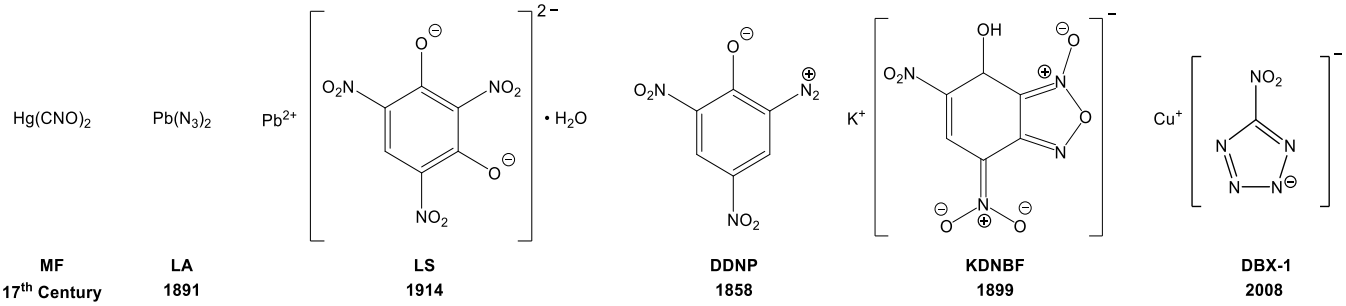

Figure 5. Most common materials of different generations of primary explosives and the year of their first preparation.

Both materials are still the most commonly used primary explosives today. However, because of the environmentally harmful and health-damaging effects of lead, more and more new ecologically compatible primary explosives have been investigated in recent years and have slowly started replacing them. The most prominent representatives nowadays of lead-free primary explosives are compounds such

as diazodinitrophenol (DDNP), potassium 4,6-dinitrobenzofuroxan (KDNBF), and copper(I) 5-nitrotetrazole (DBX-1). They consist of salts with less toxic metals or are present as completely organic compounds.[28]

Secondary Explosives: Compounds described as secondary or high explosives are characterized by a missing detonation capability solely using SII and therefore need to be initiated using a primary explosive. In general, high explosives are distinguished by higher performances and lower sensitivities toward external stimuli (*IS*: ≥ 4 J; *FS*: ≥ 50 N; *ESD*: ≥ 100 mJ) compared to primary explosives. Several parameters define the capability of energetic materials, most importantly, the heat of explosion (*Q* in kJ kg^{-1}), detonation velocity (*D* in m s^{-1}), and detonation pressure (*P* in kbar). While nowadays, commonly used secondary explosives are relatively few in numbers, their properties can be perfectly adapted when applying them in mixtures or formulation, *e.g.*, plastic explosives. Compared to the high-performance explosives hexogen (RDX) as well as octogen (HMX), trinitrotoluene (TNT) and hexanitrostilbene (HNS) show relatively low-performance parameters but are still commonly used compounds. The melting point of 80 °C of TNT and its manageable sensitivities allow utilizing it to prepare melt-cast formulations. In contrast, HNS, with a melting-point of 320 °C, is applied in high-temperature devices. Due to their brisance and the resulting relatively high price, RDX and HMX are almost exclusively used for military applications. Cheaper substances with a different major focus concerning the performance parameters are employed for civil purposes. Commercial explosives are mainly used for mining, road engineering, and demolition work. In contrast to the characteristics mentioned above, these tasks require a high release of gas volume per kg explosive to demolish bedrock or buildings. Favorable formulations that meet these requirements are so-called blasting gelatin, gelled explosives, and emulsion explosives. They are all different mixtures consisting of either nitrocellulose and nitroglycerin or ammonium nitrate and fuel oils (ANFO) with different additives such as aluminum, sawdust, or methylamine.[26] Apart from the subdivision of high explosives for military and civil applications, a more significant distinction is made between the so-called booster and main charge explosives.[31] The difference of booster explosives lies in their ease of detonation, and thus they are often interposed between primary explosive and main charge to augment and transmit the shock wave. The most commonly used booster explosive is pentaerythritol tetranitrate (PETN), also known as nitropenta (Figure 6). An essential feature of high explosives is their balanced oxygen content ensuring a full conversion of the material into oxidized products, ideally all gaseous. Therefore, many energetic materials contain nitro or nitrate ester groups for increasing the oxygen content. Both substituents have a high impact on living organisms and cause ecological problems. In recent years, the toxicity of commonly used secondary explosives has strongly shifted research toward new high explosives that show comparable or

even better energetic performances while possessing a decreased toxic effect on the environment. One of the most popular replacement candidates is TKX-50 (dihydroxylammonium 5,5'-bistetrazole-1,1'-diolate), which is entirely free of nitro as well as nitrate ester substituents and shows superior detonation parameters.[32]

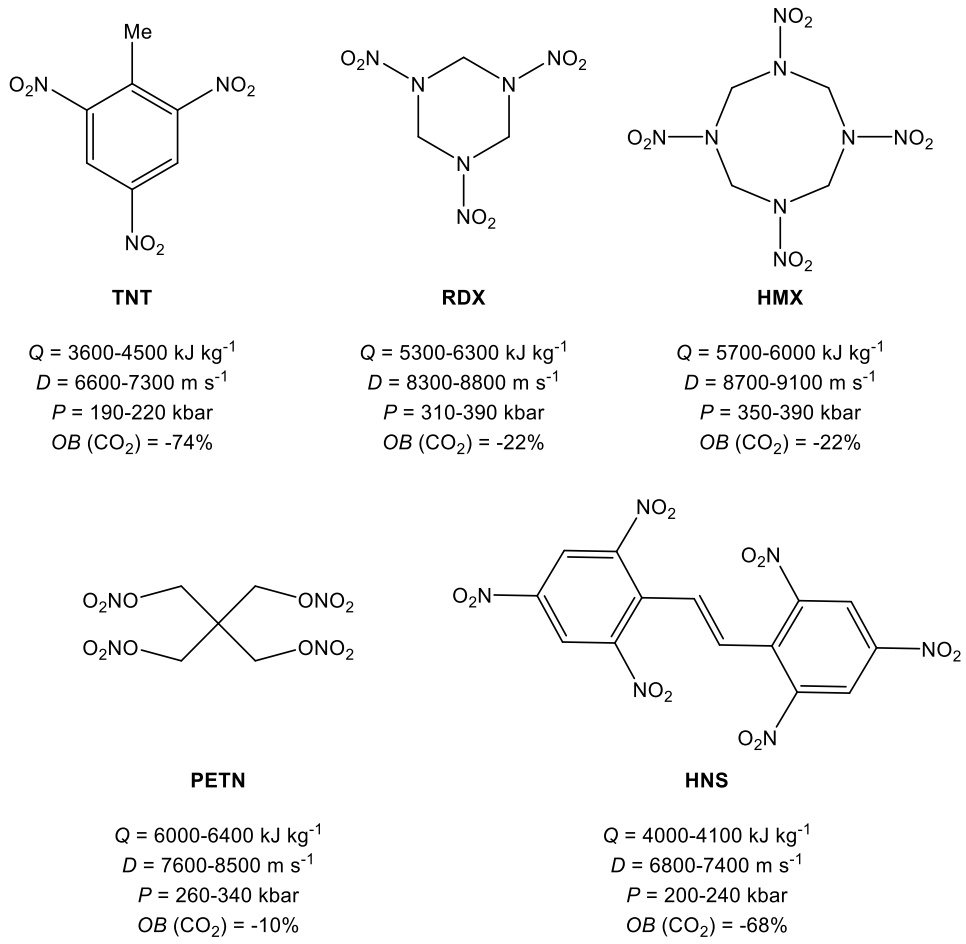

Figure 6. Most commonly used high explosives and their performance parameters.[33]

Pyrotechnics and Propellants: In contrast to explosives, pyrotechnics and propellants can be distinguished by much slower reaction time, and a DDT in both subsets is usually undesirable. While propellants are used to form a large volume of gases to perform mechanical work, pyrotechnics have a wide range of different applications, such as the generation of heat, light, sound, or other effects. Both can be further subdivided according to their applications or compositions, but common to all subsections is the assembly consisting of a fuel and an oxidizer. The only exceptions are monopropellants (rocket propellant) and base propellants (gun propellant). An example of the latter is nitrocellulose (NC). It can be regarded as an independent redox system in which the carbon backbone represents the fuel, and the nitro groups are the oxidizing agents. On the other hand, monopropellants consist of chemicals that decompose exothermically, which is usually triggered by contact with a catalyst. Typical examples of substances used in monopropellant systems are hydrazine, hydrogen peroxide, or propylene glycol

dinitrate (PGDN), also known as “Otto fuel”, which is often utilized to drive torpedoes or other weapon systems (Figure 7). Other major rocket engines use either solid propellants based on mixtures such as ammonium perchlorate (AP) and aluminum, or liquid bipropellants. Examples are nitrogen tetraoxide (NTO) and monomethylhydrazine (MMH), which react hypergolically on contact. The most crucial parameter of propellants is their specific impulse describing the effective exhaust velocity.[34]

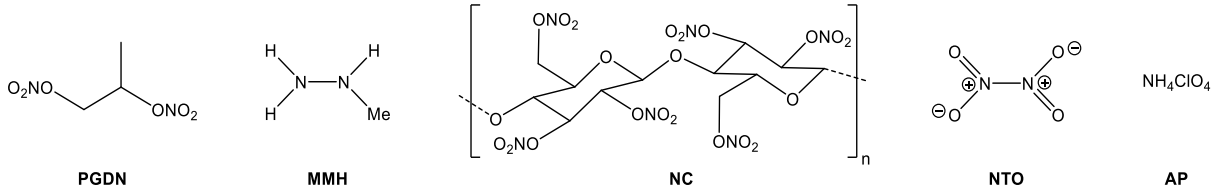

Figure 7. Major propellant representatives.

Other than the redox system, many different additives can be found in pyrotechnics depending on the intended application. Common admixtures are, *e.g.*, flame colorants for flares and fireworks, smoke agents, burn rate modifiers, or the aforementioned primary explosives to increase sensitivity. With respect to the initiation of energetic materials, pyrotechnic composition or so-called priming mixtures play an important role. One of the most famous ones is the 1928 invented SINOXID priming mixture, which is still in use today. It is mainly designed to initiate propellant powders in ammunition and consists of LS, tetrazene, barium nitrate, lead dioxide, antimony trisulfide, and calcium disilicide.[34,35]

The segmentation of energetic materials into different categories is a useful tool for ensuring safe handling of the substances. Nevertheless, it is an idealistic concept and many exceptions can be found of explosives whose properties lie in between two different subunits. The best examples are nickel(II) hydrazine nitrate (NHN), potassium 1,1’-dinitramino-5,5’-bistetrazolate (K_2DNABT), and hexanitrohexaazaisowurtzitane (CL-20) (Figure 8). The energetic coordination compound NHN was successfully investigated as a replacement for lead-based primary explosives in detonators.[36,37] However, its sensitivities lie outside the range of typical primary explosives, suggesting a classification somewhere between a booster and a primary explosive. Nevertheless, the most crucial characteristic, the fast transition from SII to detonation, allows its classification as a primary explosive. NHN exhibits lower initiation reliability compared to lead azide, and both nickel and hydrazine are highly carcinogenic, thus inhibiting its broader suitability in applications.[28] In the case of K_2DNABT, it is the other way round. It was investigated as a green, heavy metal-free primary explosive and is highly sensitive toward outer stimuli. Unlike NHN, it has a very fast DDT and shows an immediate detonation upon contact with flame. This property, together with its low solubility, makes it a perfect lead azide replacement. However, it combines the high sensitivities of primary explosives with a detonation velocity of 8330 m s^{-1}, which is in the range of high-performance explosive RDX, preventing safe handling of this compound and its use in any application until today.[38]

A similar problem exists with CL-20, one of the most powerful new high explosives with a detonation velocity above 9500 m s^{-1}. The sensitivities (4 J, 48 N) of this cage compound, together with the complicated and costly synthesis, thwart its establishment for any implementations.[26]

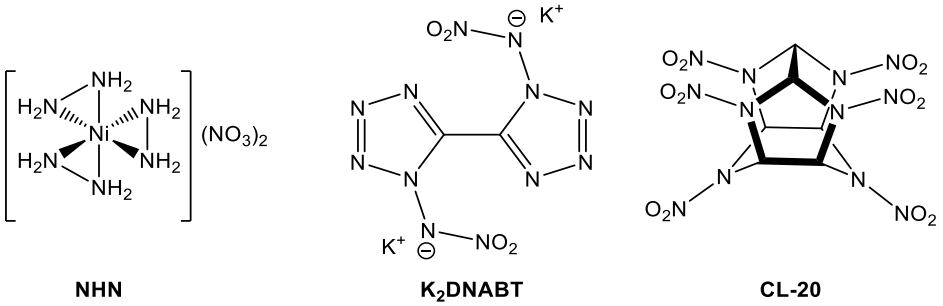

Figure 7. Non-classical representatives of explosives.

The applicability of ECC is described in the literature throughout almost all the different subdivisions. Like the aforementioned NHN, many complexes can be used as lead-free primary explosives. Furthermore, copper(II) complexes based on nitrogen-rich ligands 1-methyl-5*H*-tetrazole and 1,5-diaminotetrazole were investigated as green colorants in pyrotechnics as well as burn rate catalysts in new propellant systems.[39,40] Moreover, attempts were made to replace LS, which is often used to sensitize priming mixtures, using copper(II) azide stabilized with ditetrazolylethane ligands. Unfortunately, the results revealed a too strong performance of the lead-free primer caps.[41]

1.3. Initiation of Explosives

The military and civil applications take advantage of the fact that various outer stimuli can initiate energetic materials. There are two significant initiation modes, whereby devices for producing shockwaves are called detonators, initiation systems which only need to produce a flame or spark are called igniters.[26] The simplest devices for the ignition of energetic materials are non-electrical initiators, which work either by generating a flame or by a mechanical stimulus, like friction, stab, or percussion. Common examples of non-electrical systems are fuse type blasting caps, in which a primary explosive detonates, or a percussion primer, which contains the aforementioned priming mixture for the ignition of propellants. The most widespread devices, such as electric match type detonators (Figure 8), are electrical initiators. In these, a wire is in contact with the ignition charge, and when an electrical current is applied, the wire heats up until the energetic material reaches its ignition temperature. Depending on the application, the ignition charge is either a pyrotechnic mixture or a primary explosive. A pyrotechnic composition is first initiated in the electric match type, triggering a cascade effect transferring the reaction to a primary explosive and further to a secondary one. A particular class of electrical initiators are so-called exploding-bridgewire detonators (EBWs) with wires typically consisting of gold, platinum, or

respective alloys. Hereby the energetic material is not simply initiated by heating the bridgewire. Instead, a powerful electric current is sent through the thin wire, vaporizing it and leading to its explosion. Thus, the shockwave is directly transferred to the explosive. The benefits of EWBs is their exact and consistent function times (≤ 0.1 µs). They also allow the omission of the primary explosive and the direct transmission of the shockwave to PETN, significantly increasing safety compared to other initiation devices.[42]

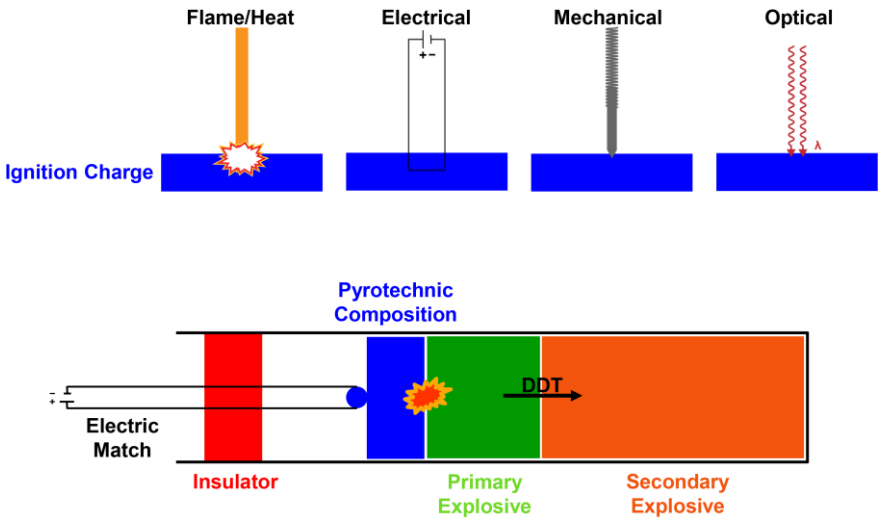

Figure 8. Top: schematic overview of different initiation mechanisms; bottom: illustration of electric match type detonator, the most common typ.

All of the initiating systems suffer from several drawbacks. Most critical is the use of very sensitive primary explosives, which predispose the systems to unintended explosion through outer stimuli if handled incorrectly. Furthermore, electrical initiators are susceptible to electromagnetic interference and electrostatic discharge. Safe EWBs, on the other hand, can easily be damaged through stray currents and require huge power sources.[26] Due to the disadvantages of conventional devices, there is a strong demand for new and safer initiation systems, which is represented by the already briefly mentioned laser initiation of energetic materials. First laser initiation experiments with LA and PETN were already performed in 1966, and the detonation of both by irradiation was successfully demonstrated.[43] Furthermore, laser ignition systems are also under current investigation for new combustion engines and propellant systems.[44,45] The significant advantages of using laser diodes for the initiation of energetic materials are the very short function time, the application of less sensitive substances, and the high isolation of the energetic materials, preventing accidental initiation. The mechanism for laser initiation of explosives is still not fully understood, but is most likely based on a photothermal effect. Most of the results in literature can be explained by the absorption of laser light by the energetic material and its subsequent conversion into heat. At first, so-called hot spots are formed, followed by a self-sustained decomposition of the material.[26] In recent years it has been found that ECC are particularly well suited for the use as laser

ignitable explosives. Therefore, many complexes based on various nitrogen-rich ligands systems, such as tetrazoles,[46] tetrazines,[47] or triazoles,[48] have been investigated for their behavior when irradiated with laser beams.

1.4. Sensitivity Determination of Energetic Materials

As already mentioned in the previous chapter, the sensitivity of energetic substances plays an essential role in initiation systems. More critical are the sensitivities to ensuring safe handling and transportation of the materials, and therefore a precise and accurate examination of these values is essential. The significant parameters of explosives are their sensitivities toward impact, friction, electrostatic discharge, and heat.[26] Two main reasons complicate the determination and comparison of sensitivities. First of all, the sensitivity of a substance is highly dependent on several factors, such as atmospheric humidity, type of initiation, and crystal size as well as shape. Secondly, the development of test procedures and equipment has so far proceeded mainly on a national basis leading to an extensive worldwide heterogeneity of machines and evaluation of results.[28] This inconsistency causes a broad range of values for identical compounds and makes their exact estimation and thus handling more difficult. Therefore, it is not easy to compare different substances and measured values. For example, within the NATO states, tetryl's impact sensitivity is stated between 3–18 J.[31] In the UN "Recommendations on the Transport of Dangerous Goods" alone, three different friction and six different impact testing methods are accepted. Most of the devices for determining the impact sensitivity are based on drop hammer machines. They use a defined weight of mass, which is allowed to fall onto the test substance. The affected impact energy can be adjusted according to the height. One of the most common devices, which is also recommended by the UN for testing, is the BAM (Bundesanstalt für Materialforschung und -prüfung) drop hammer. It should be used according to the 1 out of 6 evaluation method, representing an approximate ignition probability of 16.6% ($E_{16.6}$).[49] It represents the minimal initiation energy but does not give the no-fire limit for the absolute safe handling of a substance.[28] Another standard analysis method is the 50% initiation probability (E_{50}), which is generally obtained by applying the Bruceton or so-called up-and-down method. The most significant disadvantage of the E_{50} value is its missing information about reliability (100% ignition rate) and safety (0% ignition rate). Hence, it only can be used for rough comparisons of different materials. Furthermore, the Bruceton method is very time-consuming, while at the same time, it is very error-prone, leading to a lack of validity. To overcome these problems, the also laborious but beneficial Probit analysis can be applied for sensitivity determination. It provides the complete sensitivity curve of an energetic material, allowing the definition of a compound's reliability, safety, and the E_{50} value.[50]

Another sensitivity determination, especially common in the United States, employs the so-called ball drop impact tester. Instead of a simple weight, a free-falling ball is utilized to test a compound's sensitivity value. This test is applied particularly to primary explosives. Again, the E_{50} investigation is the most common choice of testing method, which restricts thorough characterization and limits comparability with other substances.[31]

1.5. Motivation and Objectives

Although energetic materials have been intensively investigated in recent years and many new compounds were synthesized, lead azide (LA), lead styphnate (LS), and RDX are still most commonly used in applications. However, these all suffer from their toxicity and have a massive impact on the environment. The goal of replacing lead styphnate and lead azide has received increasing attention in recent years as both were added to the REACH "candidate list of substances of very high concern for authorization," and therefore, restrictions on both are very likely within the next years.[51] To overcome the use of toxic lead-based primary explosives and to allow the implementation of energetic materials as laser ignitable explosives, new materials have to fulfill several criteria. The prime requirement is a fast DDT after the ignition using a SII and successfully transferring the detonation to a booster or main charge explosive. Therefore, they must show a certain degree of sensitivity against external stimuli to ensure their reliability. Furthermore, the compounds have to possess thermal stability of at least 150 °C, have to be long-term stable, and during the manufacturing and degradation process, the absence of toxic materials has to be ensured.[31,49] Together with subsidiary facts, such as price, compatibility, and solubility issues, it becomes clear why only a few new explosives have been considered as potential replacements within the last decades. The aforementioned concept of energetic coordination compounds is beneficial for designing novel explosives, and several fundamental studies in recent years set the stage for future applications.[23–25,47,52] ECC are composed of three different building blocks: ligand, transition metal, and anion (Figure 9). Especially suitable for the syntheses of energetic materials is the use of nitrogen-rich azoles as ligands, such as non-acidic triazoles and tetrazoles. They possess a strongly endothermic character and act mainly as fuel with the accompanying driving force to decompose into molecular nitrogen. The second building block is represented by the transition metal, which acts as a catalyst and matrix to build up the system. Familiar representatives are silver and metals from the second half of the 3d series (Mn–Zn). Last but not least, the anion functions as a fine-tuning agent for the energetic framework. It is either an oxidizing (*e.g.*, (per)chlorate, nitrate, bromate, polynitrophenolates) or endothermic (*e.g.*, azide, fulminate, dicyanamide) element for further increasing the energy of the resulting substance. By varying the building blocks, the resulting complexes' properties can be easily

adapted to specific requirements. Therefore, a straightforward optimization of the desired characteristic, like laser ignition, thermal stability, solubility, and sensitivity, can be achieved.

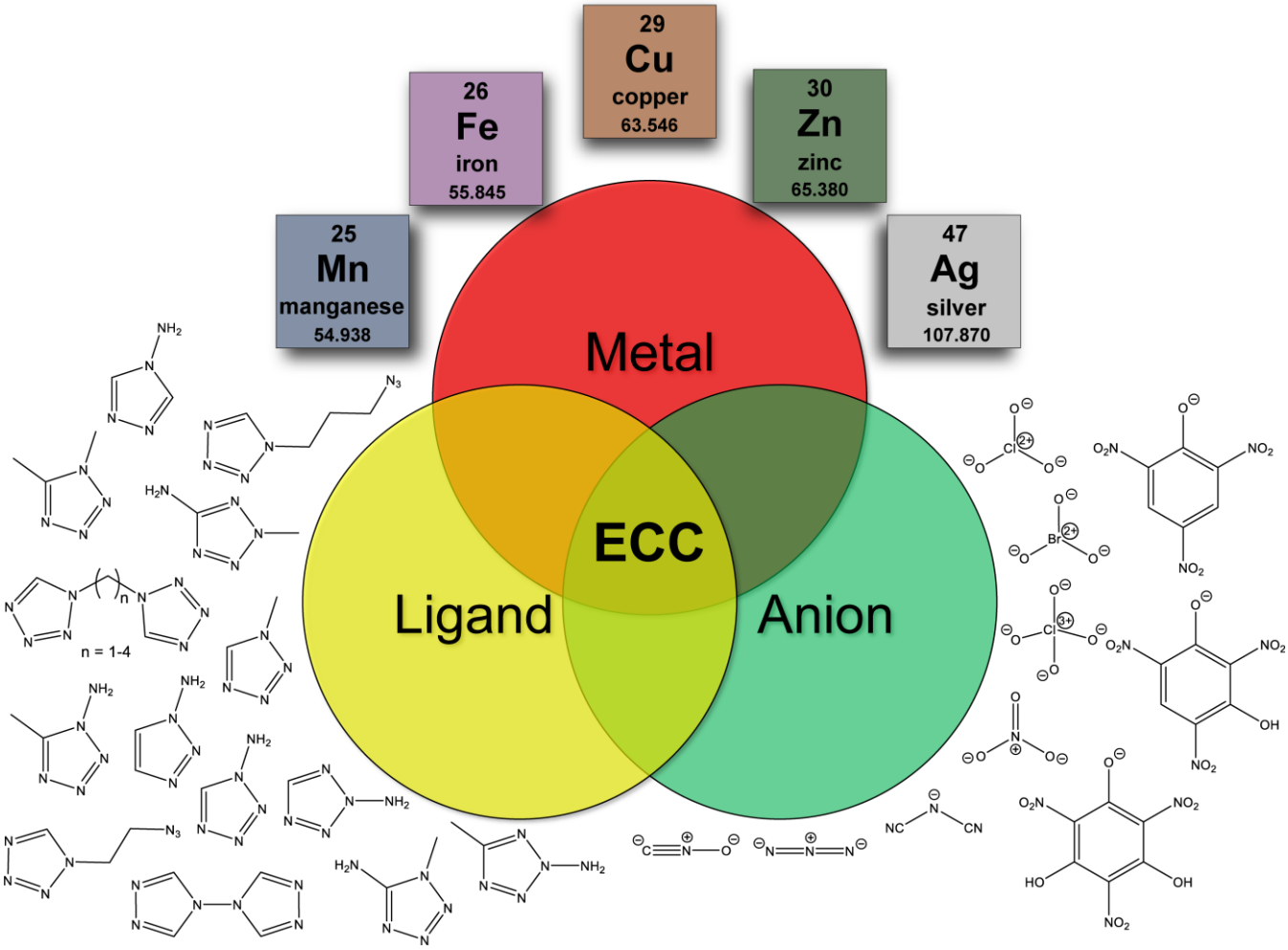

Figure 9. The concept of energetic coordination compounds and all components utilized in this thesis.

Consequently, this thesis mainly focuses on the exploration of new and less environmentally harmful energetic materials. Special attention was paid to pure single explosives, especially primary explosives, but also mixtures consisting of more than one substance were investigated concerning their possible implementation in energetic devices. The dual use of the concept of energetic coordination compounds allows the creation of explosives by implementing ligands in both non-energetic salts as well as very sensitive materials. Therefore, they either can be used to enhance the performance or stabilize highly sensitive substances like copper(II) azide and silver fulminate, in order to reveal new explosives with manageable properties. Besides the main interest in their application, complexes were developed to further deepen the understanding of the fundamental concept of energetic coordination compounds. Many different anions and ligands were applied to study their influence on sensitivities as well as thermal stability and to identify trends in energetic performance in detail. The newly synthesized ECC in this thesis were thoroughly characterized and tested for their behavior when exposed to a laser beam to classify

them and further investigate the laser ignition mechanism. In addition to the preparation and investigation of new explosives, well-known primary explosives were synthesized, and their sensitivities determined using different test setups as well as evaluation methods. In order to ensure an exact classification, a novel type of impact tester similar to the US ball drop impact tester was introduced, and the obtained values compared with those from using standard BAM techniques. The knowledge gained now allows a comparison of the various test apparatuses.

1.6. References

[1] G. A. Lawrance, *Introduction to Coordination Chemistry*, 1st ed., John Wiley & Sons, Ltd., Chinchester, **2010**.

[2] M. Niemeyer, P. P. Power, *Angew. Chem. Int. Ed.* **1998**, *37*, 1277–1279.

[3] T. A. Beineke, J. Delgaudio, *Inorg. Chem.* **1968**, *7*, 715–721.

[4] A. Werner, *Z. anorg. Chem.* **1893**, *3*, 267–330.

[5] H. Werner, *Angew. Chem. Int. Ed.* **2013**, *52*, 6146–6153.

[6] A. Werner, *Ber. Dtsch. Chem. Ges.* **1914**, *47*, 3087–3094.

[7] D. Astruc, *Organometallic Chemistry and Catalysis*, 1st ed., Springer, Berlin, **2007**.

[8] A. F. Holleman, E. Wiberg, N. Wiberg, *Anorganische Chemie*, 103rd ed., De Gruyter, Berlin, Boston **2007**.

[9] I. Bernal, J. Cetrullo, S. Berhane, *J. Coord. Chem.* **2000**, *52*, 185–205.

[10] J. Bartoll, *9th International Conference on NDT of Art*, Jerusalem, Israel, May 25–30, **2008**, 1–9.

[11] F. Herren, P. Fischer, A. Ludi, W. Haelg, *Inorg. Chem.* **1980**, *19*, 956–959.

[12] J. A. J. Jarvis, B. T. Kilbourn, P. G. Owston, *Acta Crystallogr. Sect. B* **1971**, *27*, 366–372.

[13] K.-H. Ernst, F. R. W. P. Wild, O. Blacque, H. Berke, *Angew. Chem. Int. Ed.* **2011**, *11*, 10780–10787.

[14] F. A. Cotton, C. A. Murillo, R. A. Walton, *Multiple Bonds Between Metal Atoms*, 3rd ed., Springer, New York, **2005**.

[15] K. D. Mjos, C. Orvig, *Chem. Rev.* **2014**, *114*, 4540–4563.

[16] J. v. Liebig, *Ann. Phys. Chem.* **1823**, *75*, 393–420.

[17] W. Beck, *Eur. J. Inorg. Chem.* **2003**, *2003*, 4275–4288.

[18] J. Amiel, *Compt. rend.* **1934**, *199*, 51−53.

[19] J. Amiel, *Compt. rend.* **1935**, *200*, 672−674.

[20] W. R. Tomlinson, K. G. Ottoson, L. F. Audrieth, *J. Am. Chem. Soc.* **1949**, *71*, 375–376.

[21] V. P. Sinditskii, V. V. Serushkin, *Def. Sci. J.* **1996**, *46*, 371–383.

[22] M. B. Talawar, A. P. Agrawal, S. N. Asthana, *J. Hazard. Mater.* **2005**, *120*, 25–35.

[23] J. W. Fronabarger, W. B. Sanborn, T. Massis, *22nd International Pyrotechnics Seminar*, Fort Collins, USA, July 15–19, **1996**, 645–652.

[24] M. A. Ilyushin, I. V. Tselinsky, I. A. Ugryumov, A. Y. Zhilin, A. S. Kozlov, *6th New Trends in Research of Energetic Materials Seminar*, Pardubice, Czech Republic, April 22–24, **2003**, 146–152.

[25] A. Y. Zhilin, M. A. Ilyushin, I. V. Tselinskii, A. S. Kozlov, I. S. Lisker, *Russ. J. Appl. Chem.* **2003**, *76*, 572–576.

[26] T. M. Klapötke, *Chemistry of High-Energy Materials*, 5th ed., De Gruyter, Berlin, **2019**.

[27] J. P. Agrawal, *High Energy Materials: Propellants, Explosives and Pyrotechnics*, 1st ed., Wiley, Weinheim, **2010**.

[28] R. Matyáš, J. Pachman, *Primary Explosives*, 1st ed., Springer, Berlin, **2013**.

[29] F. Zapata, C. García-Ruiz, *Crit. Rev. Anal. Chem.* **2020**, 1−18.

[30] U. Brede, R. Hagel, K. H. Redecker, W. Weuter, *Propellants Explos. Pyrotech.* **1996**, *21*, 113–117.

[31] NATO Allied Ordnance Publication 7, 2nd ed., June **2003**.

[32] N. Fischer, D. Fischer, T. M. Klapötke, D. G. Piercey, J. Stierstorfer, *J. Mater. Chem.* **2012**, *22*, 20418–20422.

[33] T. M. Klapötke, *Energetic Materials Encyclopedia*, 1st ed., De Gruyter, Berlin, Boston, **2018**.

[34] E.-C. Koch, Sprengstoffe, Treibmittel, Pyrotechnika, 2nd ed., De Gruyter, Berlin, Boston, **2019**.

[35] J. Köhler, R. Meyer, A. Homburg, *Explosivstoffe*, 10th ed., Wiley-VCH, Weinheim, **2008**.

[36] M. B. Talawar, A. P. Agrawal, J. S. Chhabra, C. K. Ghatak, S. N. Asthana, K. U. B. Rao, *J. Sci. Ind. Res.* **2004**, *63*, 677–681.

[37] B. Hariharanath, K. S. Chandrabhanu, A. G. Rajendran, M. Ravindran, C. B. Kartha, *Defence Sci. J.* **2006**, *56*, 383–389.

[38] D. Fischer, T. M. Klapötke, J. Stierstorfer, *Angew. Chem. Int. Ed.* **2014**, *53*, 8172–8175.

[39] J. J. Sabatini, J. M. Raab, R. K. Hann, R. Damavarapu, T. M. Klapötke, *Chem. – Asian J.* **2012**, *7*, 1657–1663.

[40] Z. Li, T. Zhang, J. Zhang, L. Wang, Y. Zhong, Beijing Institute Tech, CN Patent 201910821846, China **2019**.

[41] M. M. Puszynski, N. Mehta, G. Cheng, K. D. Oyler, D. Fischer, T. M. Klapötke, J. Stierstorfer, *J. J. Inorg. Chem.* **2016**, *1*, 003.

[42] P. W. Cooper, *Explosives Engineering*, 1st ed., Wiley-VCH, Weinheim, **1996**.

[43] A. A. Brish, I. A. Galeev, B. N. Zaitsev, E. A. Sbitnev, L. V. Tatarintsev, *Fiz. Goreniya Vzryva* **1966**, *3*, 132–133.

[44] C. Manfletti, *J. Propul. Power* **2014**, *30*, 952–961.

[45] M. Weinrotter, H. Kopecek, E. Wintner, *Laser Phys.* **2005**, *15*, 947–953.

[46] J. Evers, I. Gospodinov, M. Joas, T. M. Klapötke, J. Stierstorfer, *Inorg. Chem.* **2014**, *53*, 11749–11756.

[47] T. W. Myers, J. A. Bjorgaard, K. E. Brown, D. E. Chavez, S. K. Hanson, R. J. Scharff, S. Tretiak, J. M. Veauthier, *J. Am. Chem. Soc.* **2016**, *138*, 4685–4692.

[48] M. A. Ilyushin, I. V. Tselinskiy, A. V. Smirnov, I. V. Shigalei, *Cent. Eur. J. Energ. Mater.* **2012**, *9*, 3–16.

[49] UN Recommendations on the Transport of Dangerous Goods, 5th ed., **2009**.

[50] J. Šelešovský, J. Pachman, *Cent. Eur. J. Energ. Mater.* **2010**, *7*, 269–277.

[51] https://echa.europa.eu/de/candidate-list-table, (accessed September 2020).

[52] Q. Zhang, J. M. Shreeve, *Angew. Chem. Int. Ed.* **2014**, *53*, 2540–2542.

2. OZM Ball Drop Impact Tester (BIT-132) vs. BAM Standard Method – a Comparative Investigation

Michael S. Gruhne, Marcus Lommel, Maximilian H. H. Wurzenberger, Norbert Szimhardt, Thomas M. Klapötke, and Jörg Stierstorfer

Published in *Propellants, Explosives, Pyrotechnics* **2020**, *45*, 147–153.

DOI: 10.1002/prep.201900286

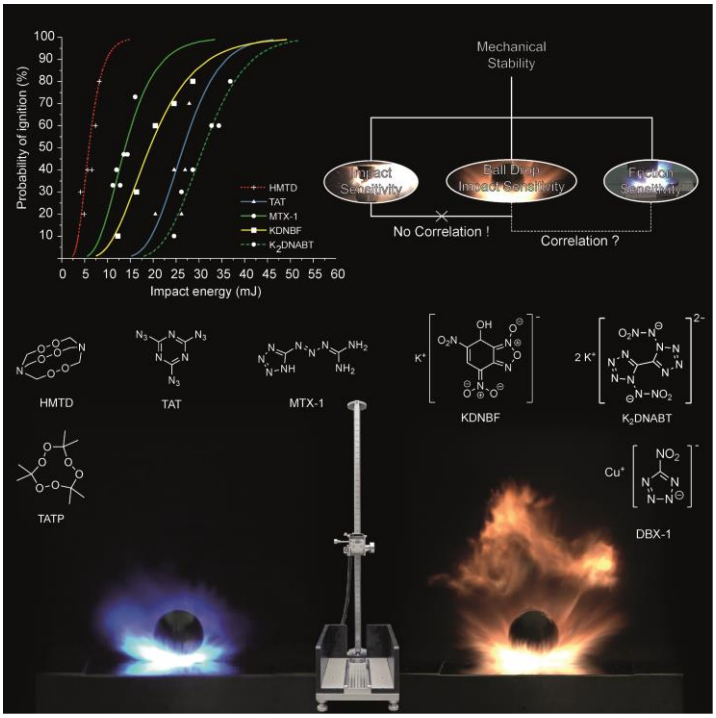

Abstract: Safety, performance, cost efficient synthesis and toxicity are the most important aspects of modern explosives. Sensitivity measurements are performed in accordance with different protocols all around the world. Sometimes the BAM drop hammer does not accurately reflect the sensitivity of an energetic material, in particular the sensitivity of primary explosives. Therefore, we present here preliminary results obtained using the novel ball drop tester (BIT-132), manufactured by OZM research, following MIL-STD-1751 A (method 1016). The ball drop impact sensitivity tester is a device in which a free-falling steel ball is dropped onto an unconfined sample, and is expected to produce more realistic results than the currently commonly used BAM method. The results obtained using the probit analysis were compared to those from the BAM drop hammer and friction tester. The following sensitive explosives were investigated: HMTD, TATP, TAT, Tetrazene, MTX-1, KDNBF, KDNP, K_2DNABT, Lead Styphnate Monohydrate, DBX-1, Nickel(II) Hydrazine Nitrate, Silver Acetylide, AgN_3, $Pb(N_3)_2$ RD-1333, AgCNO, and $Hg(CNO)_2$.

2.1. Introduction

In the field of applicable energetic materials chemistry, the safe handling of explosives is as important as a tailored performance or an economic synthesis. Nowadays, theoretical calculations based on quantum chemical models or structural relationships are possible and allow an estimation of the sensitivity of an energetic material toward mechanical or electrostatic stimuli.[1] Nevertheless, the experimental determination of sensitivities cannot be replaced by calculations, since many reliable calculations focus on a limited set of CHNO-based compounds and are based on empirical data. Unfortunately, sensitivity measurements are performed and evaluated using different methods all over the world, making comparisons of the sensitivity values difficult. The method for impact sensitivity testing which is recommended by the UN is the BAM (Bundesanstalt für Materialforschung und -prüfung) drop hammer, and has therefore become the most frequently used standard measuring method.[2] Besides its major advantages, some particular aspects must be taken into account when using the BAM drop hammer. The substance is placed between two steel cylinders enclosed by a steel guide, and a weight is dropped onto the steel cylinders from variable heights which may lead to an ignition. This ignition scenario facilitates the interpretation of the testing outcome, but it doesn't correspond to realistic conditions as the setup could cause hot spots during impact, leading to ignition.[3] An ignition could also be induced by adiabatic compression of the air trapped between the two cylinders.[4]

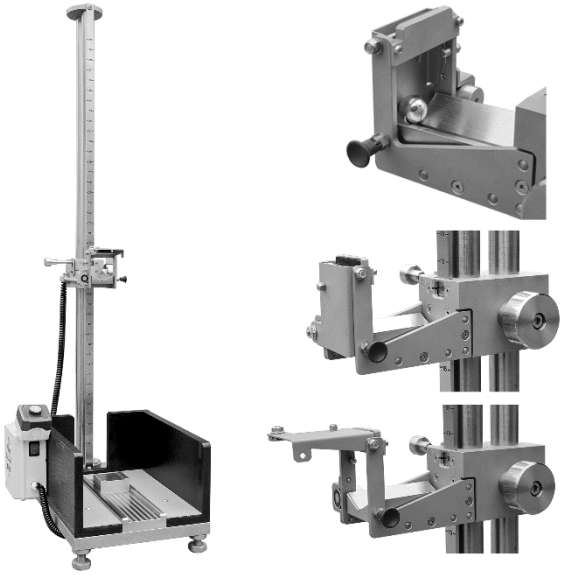

Figure 1. OZM BIT-132 (left side) and its release mechanism (right side).

An alternative method which can be used is the ball drop impact tester (BIT) in accordance with MIL-STD-1751 A, method 1016.[5] Similar ball drop impact testing devices are mostly used in the US. In this method, a free-falling steel ball is dropped onto an unconfined layer of substance. This testing scenario takes more realistic circumstances into account, *e.g.*, the slight spin of the ball when hitting the sample.[6]

This enables an alternative, more realistic result, to be obtained which allows a simpler and more reliable ignition mechanism and therefore safer handling of energetic materials. The lack of uniformity of results, especially regarding ball drop impact sensitivities, (*e.g.*, energy, force, height, etc.) and different evaluation procedures (E_{50}, nofire-level, 1-out-of-10, etc.) are problems that urgently needed to be addressed. Consequently, an intensive study applying the BIT method to the most common sensitive energetic materials under uniform testing conditions was long overdue.[7–9] In order to obtain the largest possible data set, the probit method is used as the evaluation method of choice.[10]

In this work, a variety of different sensitive energetic materials were chosen in order to compare the ball drop impact sensitivities. The selected primary explosives included a range of typical, commercially used ones such as tetrazene (**4a**, **4b**), KDNBF (**6**), lead styphnate monohydrate (LS, **9a**, **9b**), nickel(II) hydrazine nitrate (NHN, **11**), AgN_3 (SA, **13a**, **13b**), $Pb(N_3)_2$ RD-1333 (LA, **14**), AgCNO (SF, **15**)), and mercury fulminate (MF, **16**). In addition, several homemade explosives such as HMTD (**1**), TATP (**2**) and silver acetylide (**12**) were chosen, as well as a series of potential green primary explosives (TAT (**3**), MTX-1 (**5**), KDNP (**7**), K_2DNABT (**8**), and DBX-1 (**10**)).

2.2. Experimental Section

CAUTION! *All of the compounds which were investigated are potentially explosive energetic materials, which show increased sensitivities toward various stimuli (e.g., elevated temperatures, impact, friction, or electrostatic discharge). Therefore, proper safety precautions (safety glasses, face shield, earthed equipment and shoes, leather jacket, Kevlar gloves, Kevlar sleeves and ear plugs) must be worn while synthesizing and handling these compounds. Each compound that was tested was synthesized on a 1.5–3 g batch size, depending on the sensitivity of the compound and its bulk density. This should guarantee that all measurements could be carried out from the same batch. The crystal shapes and sizes were established using light microscopy, and the results - together with the particle size distributions - are shown in Figures S16–17 and Table S17.*

2.2.1. Synthesis of the Explosives

Common primary explosives were synthesized according to standard literature procedures. The organic peroxides **1** and **2** were prepared by the reaction of hexamine (**1**) or acetone (**2**) with hydrogen peroxide under acid catalysis.[11,12] Compound **3** was precipitated from a mixture of acetone and water by the reaction of cyanuric chloride and sodium azide.[13] Tetrazene (**4b**) was synthesized by dissolving aminoguanidine bicarbonate in acetic acid and further reaction with sodium nitrite.[14] Compound **5** was

obtained by treating tetrazene with sodium nitrite.[15] Compound **6** was obtained using a two-step synthesis, in which picryl chloride was reacted with sodium azide and potassium carbonate.[16] The reaction of 3-bromo-2,4,6-trinitroanisole with potassium azide and diethyl carbonate resulted in compound **7**.[17]

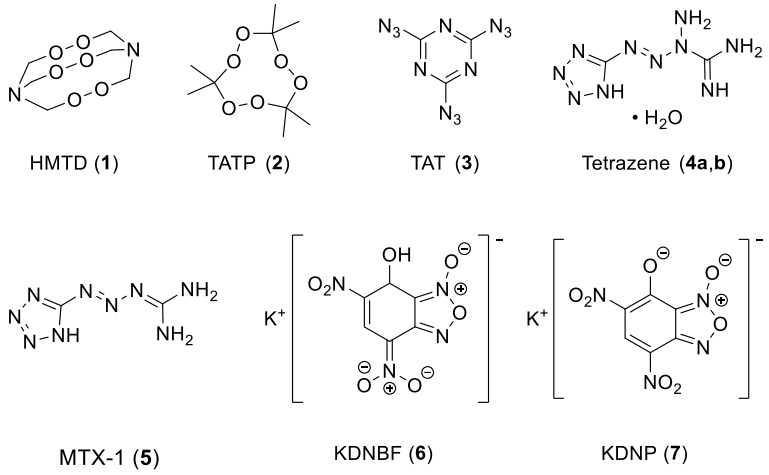

Chart 1. Prepared primary explosives **1**–**7**.

Compounds **4a**, **9a**, **13a**, and **14** were provided by DynITEC GmbH Germany, whereas **4b**, **9b**, and **13b** were synthesized in the lab according to literature procedures.

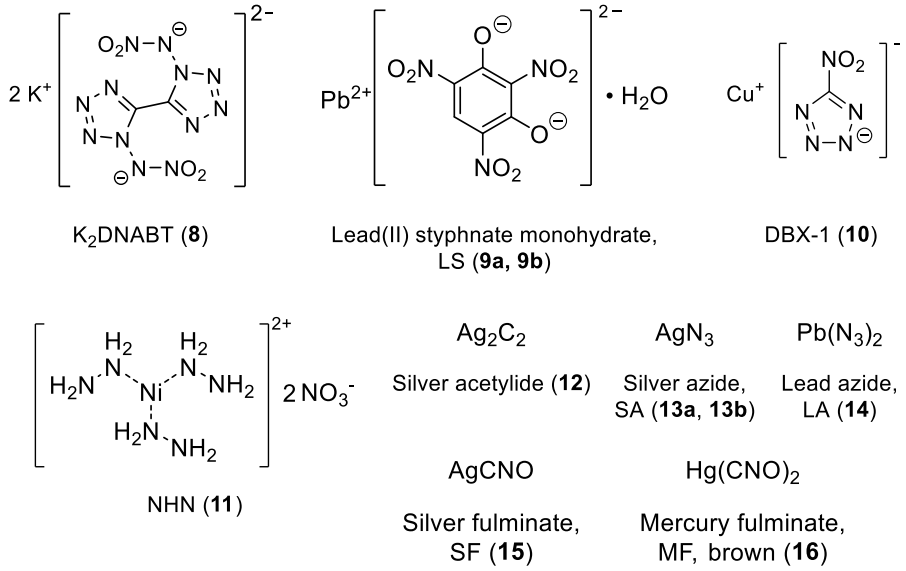

Chart 2. Synthesized primary explosives **8**–**16**.

The 1,1’-dinitramino-5,5’-bistetrazolate salt **8** was prepared from hydrazine and diethyl carbonate according to WO 2018209366 A2.[18] Dissolving an aqueous solution of styphnic acid in magnesium oxide and subsequent reaction with lead(II) nitrate yielded compound **9b**.[19] Compound **10** was obtained by conversion of sodium 5-nitrotetrazolate dihydrate into the copper(I) salt.[20] The nickel complex **11** was prepared by adding hydrazine hydrate to nickel nitrate.[21] Silver acetylide (**12**) was synthesized by

passing acetylene through silver nitrate solution in aqueous ammonia.[22] Silver azide (**13b**) was synthesized by a simple metathesis reaction starting from sodium azide and silver nitrate.[23] The fulminate salts **15** and **16** were obtained by dissolving the respective metal in nitric acid and then pouring the reaction mixture onto ethanol.[21,24]

2.2.2. Sensitivity Measurements

The ball drop experiments were carried out using the BIT-132 ball drop impact tester (OZM Research, Czech Republic)[25] following MIL-STD-1751 A (method 1016).[5] A steel ball (0.50–2.00 inch, 8.35–534.70 g) is rolled of a steel guidance and dropped onto the explosive compound with a certain spin. The sample layer was prepared as follows: The explosive compound was placed onto a steel target platform using a 30 mm^3 volumetric spoon. The sample was then spread out on the platform, resulting in a homogenous layer of 0.33 mm height (Figure 2).

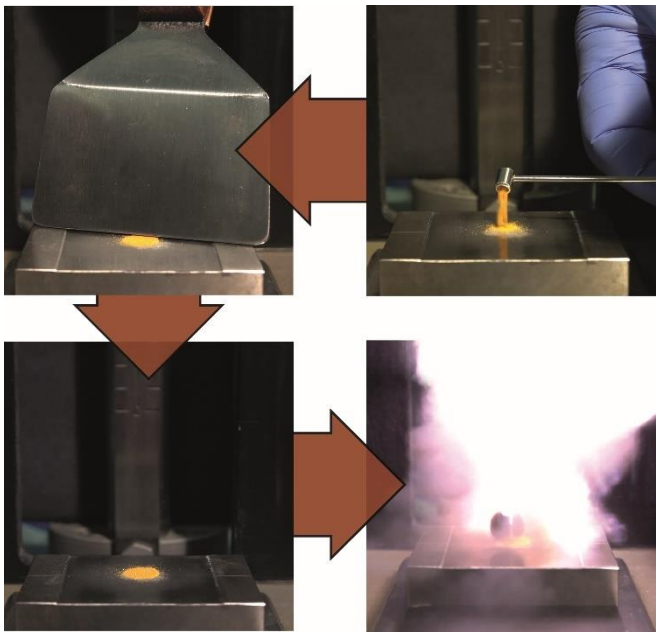

Figure 2. Stepwise sample preparation.

Steel balls with diameters of 0.50 inch (1.27 cm, 8.35 g) and 0.75 inch (1.91 cm, 28.20 g) were used. For every steel ball, a different steel ball guide was used to ensure a proper drop.[26] Any visual observation of decomposition was considered a positive result. After each trial, the remaining material was disposed of and the target block loaded with a freshly prepared layer. The steel balls were replaced for each substance. The impact energy was calculated from the product of the drop height, the mass of the steel ball used during the experiment and the gravitational constant. The initial drop height was chosen after several preliminary attempts, in which the height was determined at which the majority of the tests were positive. The probit analysis was used to evaluate the results.[9] The probability of ignition of each

compound was determined using 6 test heights, with 10–15 trials at each height. The probabilities obtained were expressed as probits and the linear regression between probits and natural logarithms of the impact energy was performed. The sensitivity curve was obtained by backward transformation of the regression line into the probability-impact energy coordinates. Details of the 1 of 6 method that was used when a probit analysis was impossible, can be found in the general methods in the Supporting Information. Additionally, the impact and friction sensitivities were determined according to the BAM (Bundesanstalt für Materialforschung und -prüfung) standard methods. The impact sensitivity tests were performed according to STANAG 4489[27] with a modified instruction[28] using a BAM drop hammer.[2] Steel guide rings and steel cylinders for BAM drop hammers were obtained from OZM Research, Czech Republic.[24] The impact energy was calculated as explained above for the ball drop device. Friction sensitivity tests were performed according to STANAG 4487[29] with a modified instruction[30] using a BAM friction tester.[2] Porcelain plates and pins were obtained from OZM Research, Czech Republic.[24] The friction force was calculated using the lever rule. The limiting values of the impact energy and friction force were determined in accordance with the method recommended by the UN for testing impact and friction sensitivities (1 of 6 method), according to ST/SG/AC.10/11/ Rev.6 (s. 13.4.2.3.3).[31]

2.3. Results and Discussion

A key factor influencing the results was the type of steel ball used for each measurement. For compounds **4**, **5**, **11**, and **16**, a smaller ball size at the same energy did not result in complete detonation or deflagration of the sample, and only a slight crackling was observed. This complicated the interpretation of a positive result by acoustic signals. It is assumed that the deflagration to detonation transition (DDT), shockwave sensitivity or critical diameter of each substance is an essential factor. This circumstance also influences any visual evaluation, since remaining substance does not necessarily indicate a negative test in every case. The use of larger steel balls solves the problem, since the larger surface area of the bigger steel ball enables a larger amount of material to react, making evaluation clearer. However, larger steel balls tend to mask the sound of the detonating sample due to the louder impact noise. In addition, the use of the larger steel ball dusts the solid that would remain after a negative test, making visual evaluation nearly impossible. Sensitivity measurements were carried out as described for each primary explosive. Standard deviations of the associated E_{50}, and $E_{16.6}$ values can be found in the Supporting Information (Table S1), together with plots of the results of each individual compound (Figure S1–S15). In addition, detailed data on the results of each substance can be found in the Tables S2–S16. In addition to primary explosives, some high explosives were also investigated. An evaluation with the probit method was not possible for any of these cases. In addition to the problems mentioned above with respect to the ignition of substances,

a strong grain size dependence was observed. PETN, RDX, and TKX-50 could be ignited only using the smallest grain sizes which were obtained after flash crystallization or sieving. Larger grain sizes showed lower impact sensitivities. In the case of FOX-7, no ignition was observed at all. Due to this behavior, we decided to investigate these substances in more detail in future work.

During the characterization of each metal azide (**13**, **14**), variations in the sensitivity were observed. A proper probit analysis leading to reliable sensitivity data was not possible. Extending the test setup, for example the number of test heights and the number of tests per selected height, is assumed to correct statistical variations in compounds **13** and **14**. In the case of silver fulminate (**15**), no probit evaluation was possible because a no-fire-level could not be determined. The Ball Drop Impact Sensitivity (BDIS) of these compounds was determined using the 1 of 6 method. The results of the sensitivity measurements are shown in Table 1 together with the sensitivity data determined using BAM standard methods. In order to compare the substances examined with probit analysis to those compounds for which it was not possible, the 16.6% ignition probability values of these substances were calculated. This corresponds approximately to the probability level represented by the 1 of 6 method. The probit method was successfully used for the evaluation of the BDIS of compounds **1**–**12** and **16**. The respective E_{50}, and $E_{16.6}$ values together with the sensitivity values according to BAM, as well as the particle size distributions are compiled in Table 1. The diagrams shown in Figures 3, 5, and 6 are combined according to their respective slopes. Figures 3 and 4 show the curves with the highest gradients. Compound **4b** was placed in Figure 4 to give a better comparison of the influence of the manufacturing process and the particle size of tetrazene. The improvised explosive HMTD (**1**) is the most sensitive compound investigated by the probit method ($E_{16.6}$ = 4 mJ). It is assumed that silver fulminate is even more sensitive, since a probit-based analysis was not possible. The $E_{16.6}$ level is even closer to the lowest measurement limit (1 of 6 = ≤ 4 mJ). However, this observation is only partly consistent with the sensitivity data according to BAM, as silver fulminate (**15**) has an unexpectedly high tolerance to impact (FS: 0.3 N (**1**), ≤ 0.1 N (**15**); IS: 1.5 J (**1**), 5 J (**15**)). Among the curves shown in Figure 3, K_2DNABT (**8**) has the highest $E_{16.6}$ value (25 mJ). This is in strong contrast to the extreme sensitivity data determined with the BAM standard methods (< 0.1 N, < 1 J). The same applies to TAT (**3**), which has a similar $E_{16.6}$ value (21 mJ) at very low friction and impact sensitivities according to BAM (FS: 0.3 N, IS: ≤ 1 J).

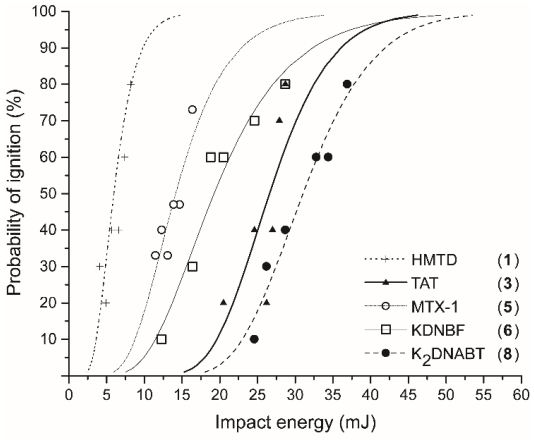

Figure 3. Probit curves of compounds **1**, **3**, **5**, **6**, and **8**.

Table 1. Sensitivity data of the compounds **1**–**16**.

Compound		Ball drop impact sensitivity [mJ]		BAM friction sensitivity	BAM impact sensitivity	Particle size dist. [µm]
		E_{50}	$E_{16.6}$	1 of 6 [N]	1 of 6 [J]	
HMTD	(**1**)	6	4	0.3	1.5	50–200
TATP	(**2**)	18	13	0.4	≤ 1	< 30
TAT	(**3**)	27	21	0.3	≤ 1	50–300
Tetrazene STANAG 4170	(**4a**)	10	5	2.5 (> 7[c])	1.5 (> 1[c])	< 30
Tetrazene	(**4b**)	33	21	2.5	1.5	400–1000
MTX-1	(**5**)	14	10	2	2	< 30
KDNBF	(**6**)	19	13	2	1.5	< 30
KDNP	(**7**)	56	40	12	3	< 30
K_2DNABT	(**8**)	31	25	≤ 0.1	≤ 1	500–1500
LS STANAG 4170	(**9a**)	28	19	1 (> 0.5[c])	7 (1.75[c])	40–140
LS	(**9b**)	22	15	0.45	8	< 30
DBX-1	(**10**)	39	21	≤ 0.1	≤ 1	< 30
NHN	(**11**)	175	134	15	20	< 30
Silver acetylide	(**12**)	29	14	≤ 0.1	≤ 1	50–150
AgN_3 STANAG 4170	(**13a**)	n.d.[a]	29[b]	≤ 0.1 (≤ 0.1[c])	≤ 1 (> 2.25[c])	< 10
AgN_3	(**13b**)	n.d.[a]	29[b]	≤ 0.1	3	< 30
$Pb(N_3)_2$ RD-1333	(**14**)	n.d.[a]	37[b]	≤ 0.1 (≤ 0.1[c])	4 (> 1.75[c])	< 30–50
AgCNO	(**15**)	n.d.[a]	≤ 4	≤ 0.1[c]	5	100–200
$Hg(CNO)_2$, brown	(**16**)	21	16	2.5	2.5	50–300

[a] No probit analysis possible. [b] Determined by 1 of 6 method. [c] Sensitivity data according to supplier.

In case of tetrazene (**4**), larger crystals show the same sensitivity toward friction (**4a**: FS: 2.5 N vs. **4b**: FS: 2.5 N), while in the case of lead styphnate monohydrate (**9**) the trend indicated by the ball drop impact tester was confirmed for the friction sensitivity (**9a**: FS: 1 N, $E_{16.6}$: 19 mJ vs. **9b**: FS: 0.45 N, $E_{16.6}$: 15 mJ). Identical sensitivity data were observed for both types of silver azide (**13a**, **13b**). This observation fits with expectations since both compounds have approximately the same particle size, whereby the commercial product **13a** consists of agglomerates of smaller particles (Figure 7).

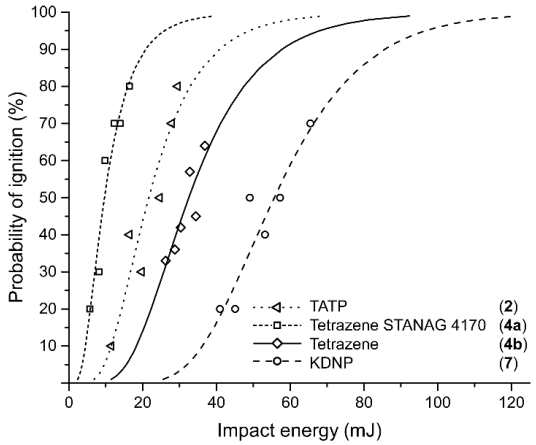

Figure 4. Probit curves of compounds **2**, **4a**, **4b**, and **7**.

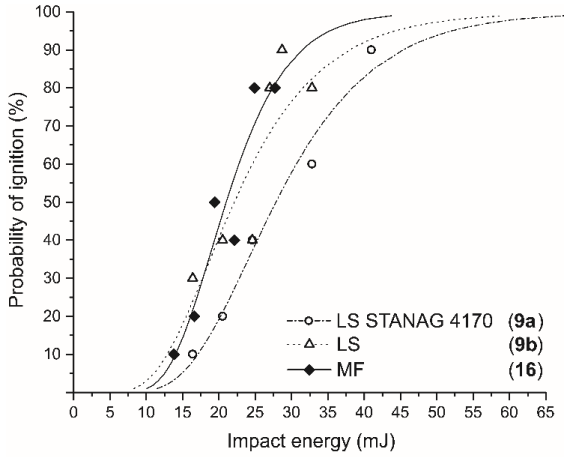

Figure 5. Probit curves of compounds **9a**, **9b**, and **16**.

With regard to the measured data (Table 1), however, these grain sizes do not seem to have any influence on the sensitivity toward mechanical manipulation. Nickel(II) hydrazine nitrate (**11**) turned out to be the most insensitive compound according to BAM (FS: 15 N, IS: 20 J). The data determined using the ball drop impact tester in this case agrees with the $E_{16.6}$ of 134 mJ. Regarding lead styphnate monohydrate (**9**) and the already mentioned silver fulminate (**15**), a significantly higher discrepancy between the ball drop impact sensitivities and impact sensitivities according to BAM was observed (**9a**: $E_{16.6}$: 19 mJ, IS: 7 J; **9b**: $E_{16.6}$: 15 mJ, IS: 8 J). It is assumed that grain size effects play a major role here. In addition, a comparison with literature values again reveals the problem of comparing sensitivity values. According to *Köhler*, lead styphnate monohydrate possesses an impact sensitivity of 2.5–5 J.[32,33] The United States Army Material Command reported an impact sensitivity of 3.4 J for the Picatinny Arsenal apparatus, as well as 0.17 J determined using the Bureau of Mines apparatus.[34] In both cases, no conclusions can be drawn about the measured particle size distribution, which is known to have a large influence on the results. Regarding the data by *Köhler*, no reference to the measuring instrument is given. This lack of a uniform specification of the measuring methodology also leaves open whether the results presented are

E_{50}, no-fire or BAM 1 of 6 values. A general relationship between both of the impact sensitivity testing methods was not found. It was generally observed that low BDIS values are accompanied by low friction sensitivity data (Figure 8). The only significant exception was KDNP (**7**). At low BDIS values, KDNP (**7**) shows a lower sensitivity to friction, which is comparable to that of NHN (**11**) (**7**: $E_{16.6}$: 40 mJ, FS: 12 N; **11**: $E_{16.6}$: 134 mJ, FS: 15 N).

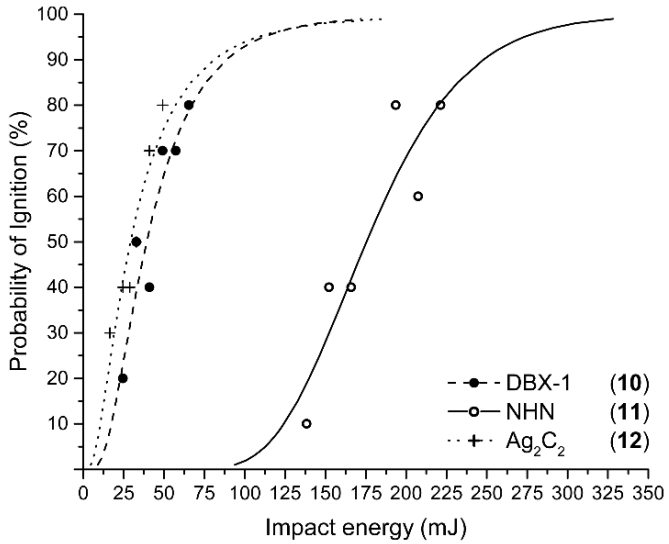

Figure 6. Probit curves determined for compounds **10**–**12**.

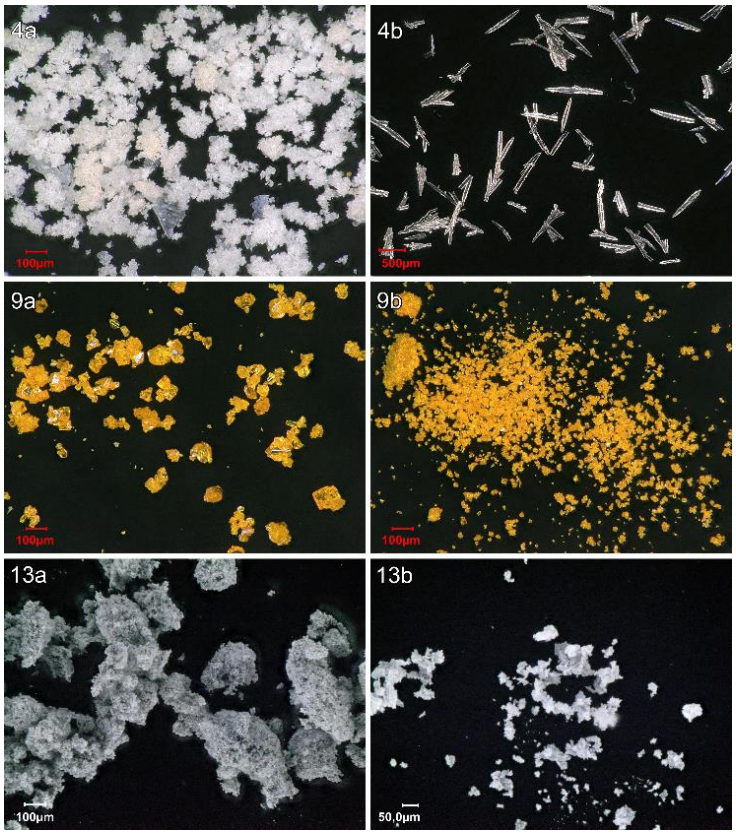

Figure 7. Different crystal shapes and particle size distributions of the compounds Tetrazene (**4**), Lead-styphnate Monohydrate (**9**), and Silver Azide (**13**).

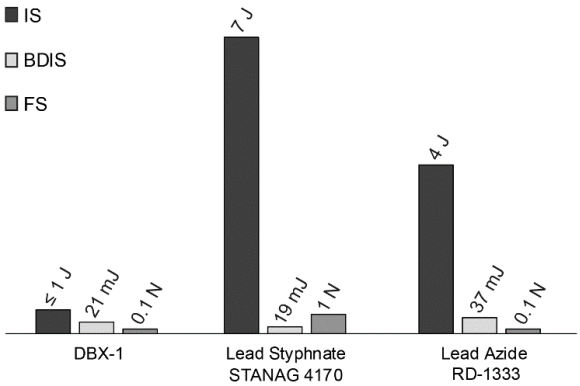

Figure 8. Comparison of the sensitivity data of compounds **9a** and **14**.

2.4. Conclusion

The BIT-132 Ball drop impact tester from OZM Research was used to evaluate the sensitivity of well-known, sensitive energetic materials. In addition, the BAM standard methods were used to determine sensitivities for all compounds. The sensitivity data obtained using the BIT-132 apparatus was evaluated using a probit analysis. In cases where this was not possible, the BAM 1 of 6 method was applied. As shown by the examples of lead styphnate and lead azide, it is impossible to correlate the most recent BIT results with the data obtained using the BAM drop hammer (1 of 6). This is a result of the different test set-ups and therefore different ignition types. A closer correlation between the sensitivity to friction and ball drop impact sensitivity was observed. It is assumed that a combination of friction and impact is exerted on the substance by the spin of a falling steel ball. Furthermore, it was found that there is a strong coherence between the particle size and the sensitivity toward BDIS of the compounds. Smaller particle sizes clearly showed more sensitivity, which is in strong contradiction to earlier assumptions that larger crystal sizes lead to drastically higher sensitivities. For the well-known explosives PETN, RDX, FOX-7, and TKX-50 no ignitions could be observed at certain grain sizes. So, the current BIT has limited suitability for characterization of secondary explosives. The authors would suggest the use of balls with a constant diameter and different densities. The 0.75 inch or the 1.00 inch ball, which were used in the set-up described in this work, are preferred for evaluating primary explosives. Since most of the above problems do not apply to the testing of primary explosives, the device is perfectly suitable for testing primary explosives.

2.5. Acknowledgements

Financial support of this work by the Ludwig-Maximilians-University of Munich (LMU), and the Office of Naval Research (ONR) under grant no. ONR.N00014-16-1-2062 is gratefully acknowledged. The authors would like to thank OZM Research for the cooperation on the development of explosive

equipment and testing devices. The authors would also like to thank Dr. Constantin Hoch for recording images with the microscope. In addition, the authors would like to thank Dr. Manuel Joas (DynITEC GmbH) for providing AgN_3 STANAG 4170, LS STANAG 4170, RD-1333, and Tetrazene STANAG 4170. We also would like to thank Dr. Davin Piercey and Mr. Maurus Völkl for their guidance during the synthesis of some of the primary explosives, as well as Mr. Maximilian Benz and Dr. Marc Bölter for the synthesis of several high explosives.

2.6. References

[1] M. H. Keshavarz, T. M. Klapötke, *The Properties of Energetic Materials, Sensitivity, Physical and Thermodynamic Properties*, 1st ed., De Gruyter, Berlin, Boston, **2018**.

[2] BAM, http://www.bam.de, (accessed August 2019).

[3] J. G. Reynolds, P. C. Hsu, G. A. Hust, S. A. Strout, H. K. Springer, *Propellants Explos. Pyrotech.* **2017**, *42*, 1303–1308.

[4] S. M. Walley, J. E. Field, R. A. Biers, W. G. Proud, D. M. Williamson, A. P. Jardine, *Propellants Explos. Pyrotech.* **2015**, *40*, 351–365.

[5] United States Military Standard 1751 A (MIL-STD-1751 A), Safety and performance tests for qualification of explosives (high explosives, propellants and pyrotechnics), Method 1016, **2001**.

[6] B. D. Pollock, R. F. Gentner, Impact Sensitivity of Wetted Primary Explosives as Determined by the Ball Drop Test, Picatinny Arsenal, Dover, NJ, **1972**.

[7] N. Szimhardt, M. H. H. Wurzenberger, L. Zeisel, M. S. Gruhne, M. Lommel, T. M. Klapötke, J. Stierstorfer, *Chem. – Eur. J.* **2018**, *24*, 1–13.

[8] N. Szimhardt, M. H. H. Wurzenberger, L. Zeisel, M. S. Gruhne, M. Lommel, J. Stierstorfer, *J. Mater. Chem. A* **2018**, *6*, 16257–16272.

[9] a) M. H. H. Wurzenberger, M. S. Gruhne, M. Lommel, N. Szimhardt, T. M. Klapötke, J. Stierstorfer, *Chem. – Asian J.* **2019**, *14*, 2018–2028; b) N. Szimhardt, M. H. H. Wurzenberger, P. Spiess, T. M. Klapötke, J. Stierstorfer, *Propellants Explos. Pyrotech.* **2018**, *43*, 1203–1209.

[10] C. I. Bliss, *Science* **1934**, *79*, 38–39.

[11] W. P. Schaefer, J. T. Fourkas, B. G. Tiemann, *J. Am. Chem. Soc.* **1985**, *107*, 2461–2463.

[12] O. Reany, M. Kapon, M. Botoshansky, E. Keinan, *Cryst. Growth Des.* **2001**, *9*, 3661–3670.

[13] E. Ott, E. Ohse, *Ber. Dtsch. Chem. Ges.* **1921**, *2*, 179–186.

[14] T. Urbański, *Chemistry and Technology of Explosives*, 3rd ed., Pergamon Press, Oxford, **1967**.

[15] J. W. Fronabarger, M. D. Williams, A. G. Stern, D. A. Parrish, *Cent. Eur. J. Energ. Mat.* **2016**, *13*, 33–52.

[16] A. K. S. Mehilal, S. Pawar, N. Skider, *J. Hazard. Mater.* **2002**, *90*, 221–227.

[17] J. W. Fronabarger, M. D. Williams, W. B. Sanborn, D. A. Parrish, M. Bichay, *Propellants Explos. Pyrotech.* **2011**, *36*, 459–470.

[18] E. L. Müller, T. M. Klapötke, J. Stierstorfer, M. F. Bölter, M. Völkl, DetNet South Africa (Pty.) Ltd., WO Patent 2018209366 A2, South Africa **2018**.

[19] T. Urbański, *Chemistry and Technology of Explosives*, 3rd ed., Pergamon Press, Oxford, **1967**, pp 213–215.

[20] J. W. Fronabarger, M. D. Williams, W. B. Sanborn, J. G. Bragg, D. A. Parrish, M. Bichay, *Propellants Explos. Pyrotech.* **2011**, *36*, 541–550.

[21] S. G. Zhu, Y. C. Wu, W. Y. Zhang, J. G. Mu, *Propellants Explos. Pyrotech.* **1997**, *22*, 317–320.

[22] R. Matyáš, J. Šelešovský, T. Musil, *J. Hazard. Mater.* **2012**, *213–214*, 236–241.

[23] T. Urbański, *Chemistry and Technology of Explosives*, 3rd ed., Pergamon Press, Oxford, **1967**, pp 182–184.

[24] T. Pasinszki, M. Krebsz, B. Hajgato, *Chem. Phys. Lett.* **2009**, *473*, 343–347.

[25] OZM, http://www.ozm.cz, (accessed August 2019).

[26] OZM Research: Ball Drop Impact Test BIT-132, Instruction Manual, Rev. No. 1/17, **2017**.

[27] NATO standardization agreement (STANAG) on explosives, impact sensitivity tests, no. 4489, 1st ed., Sept. 17, **1999**.

[28] WIWEB-Standardarbeitsanweisung 4-5.1.02, Ermittlung der Explosionsgefährlichkeit, hier der Schlagempfindlichkeit mit dem Fallhammer, Nov. 8, **2002**.

[29] NATO standardization agreement (STANAG) on explosive, friction sensitivity tests, no. 4487, 1st ed., Aug. 22, **2002**.

[30] WIWEB-Standardarbeitsanweisung 4-5.1.03, Ermittlung der Explosionsgefährlichkeit oder der Reibeempfindlichkeit mit dem Reibeapparat, Nov. 8, **2002**.

[31] UN Model Regulation: Recommendations on the Transport of Dangerous Goods-Manual of Tests and Criteria, section 13.4.2.3.3, **2015**.

[32] T. M. Klapötke, *Energetic Materials Encyclopedia*, 1st ed., De Gruyter, Berlin, Boston, **2018**, pp 278–279.

[33] R. Meyer, J. Köhler, A. Homburg, *Explosives*, 7th ed., Wiley-VCH, Weinheim, **2016**, pp. 206–207.

[34] AMC Pamphlet Engineering Design Handbook: Explosive Series Properties of Explosives of Military Interest, Headquarters, U. S. Army Materiel Command, January **1971**.

2.7. Supporting Information

2.7.1. Compound Overview

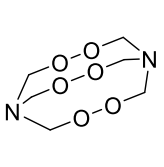

HMTD (**1**)

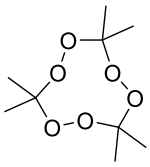

TATP (**2**)

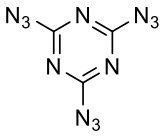

TAT (**3**)

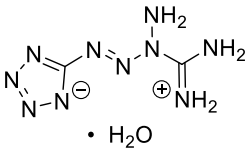

Tetrazene (**4a, 4b**)

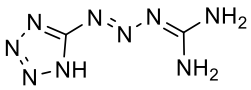

MTX-1 (**5**)

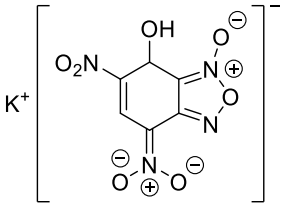

KDNBF (**6**)

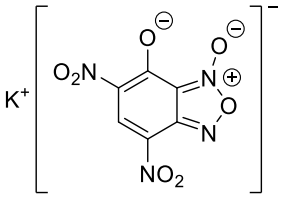

KDNP (**7**)

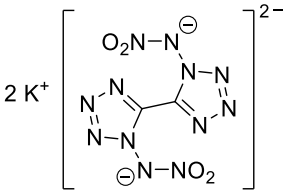

K_2DNABT (**8**)

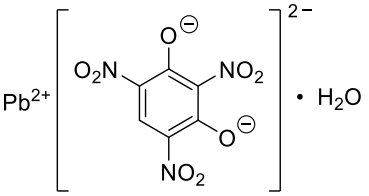

LS (**9a, 9b**)

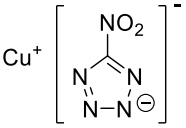

DBX-1 (**10**)

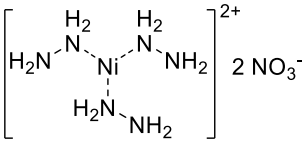

NHN (**11**)

Ag_2C_2

Silver acetylide (**12**)

AgN_3

SA (**13a**,**13b**)

$Pb(N_3)_2$

LA, RD-1333 (**14**)

AgCNO

SF (**15**)

$Hg(CNO)_2$

MF, brown (**16**)

2.7.2. Measurement Data and Graphical Illustration

Table S1. E_{50} and confidence limits together with the used ball size for every compound investigated by probit analysis.

Compound	Lower limit [mJ]	E_{50} [mJ]	Upper limit [mJ]	Ball size [inch]
1	5.016	5.951	6.820	0.50
2	17.761	21.662	26.210	0.50
3	24.167	26.596	31.496	0.50
4a	7.084	9.647	11.821	0.50
4b	16.884	22.104	25.617	0.50
5	12.561	14.149	20.328	0.50
6	16.083	19.241	22.517	0.50
7	49.908	55.663	74.668	0.50
8	28.357	31.036	34.482	0.50
9a	24.087	27.836	33.022	0.50
9b	16.883	22.104	25.617	0.50
10	27.298	39.243	49.678	0.50
11	155.900	175.405	194.883	0.75
12	18.465	29.180	41.987	0.50
16	18.552	20.991	24.009	0.75

HMTD (1)

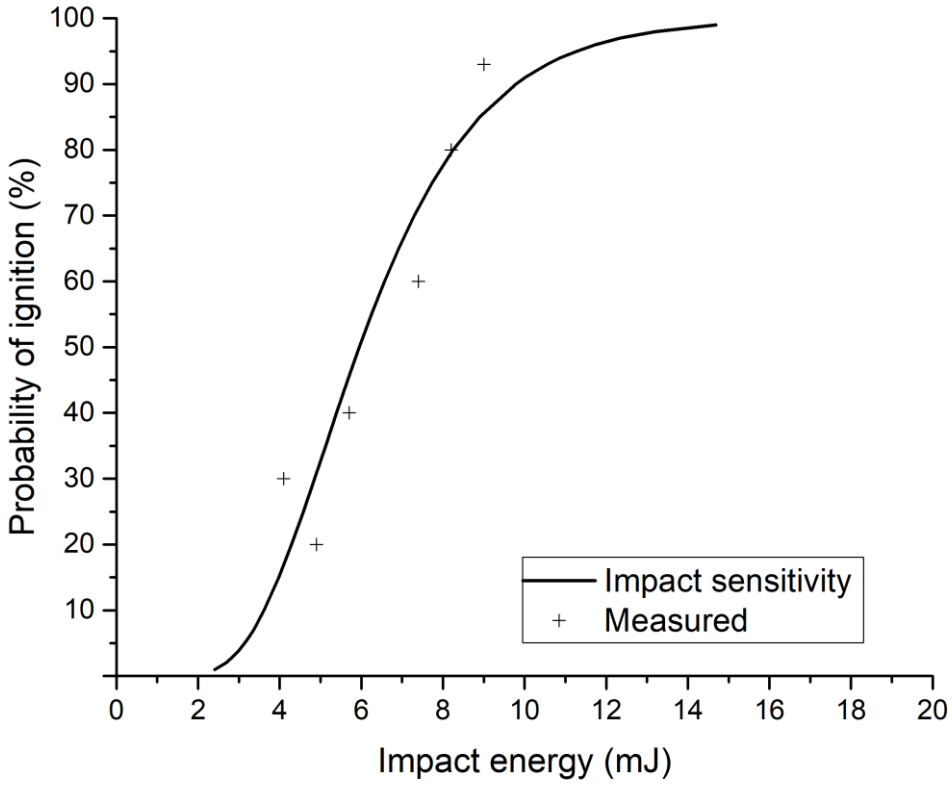

Figure S1. Probit of compound **1**.

Table S2. Measurement data of compound **1**.

Height [cm]	Energy [mJ]	Trials															Number of trials	Total number of positive trials	Positive trials [%]
		1	2	3	4	5	6	7	8	9	10	11	12	13	14	15			
10	**8.2**	1	0	1	1	0	1	1	1	1	1						10	**8**	**80**
5	**4.1**	0	0	0	0	0	1	0	0	1	1						10	**3**	**30**
7	**5.7**	0	0	0	0	1	0	0	1	1	1						10	**4**	**40**
11	**9.0**	1	1	1	1	1	1	1	1	1	1	0	1	1	1	1	15	**14**	**93**
9	**7.4**	1	1	0	1	0	1	1	0	1	0						10	**6**	**60**
6	**4.9**	0	0	0	0	1	0	0	1	0	0						10	**2**	**20**

1 = positive trial; 0 = negative trail.

TATP (2)

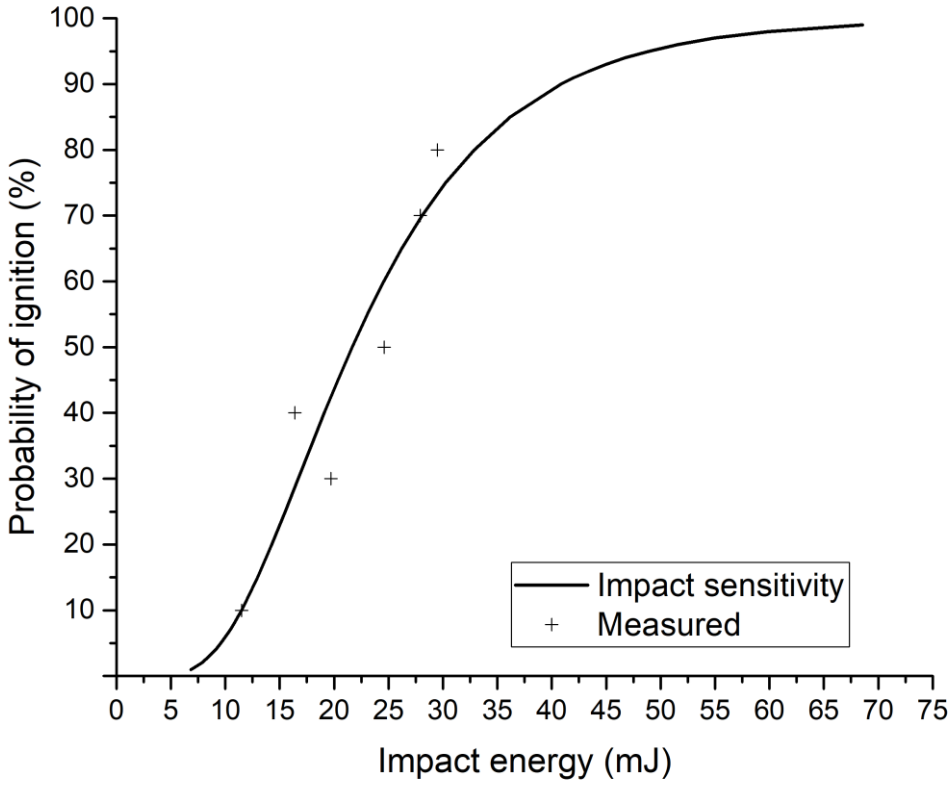

Figure S2. Probit plot of the organic peroxide **2**.

Table S3. Measurement data of compound **2**.

Height [cm]	Energy [mJ]	Trials															Number of trials	Total number of positive trials	Positive trials [%]
		1	2	3	4	5	6	7	8	9	10	11	12	13	14	15			
20	**16.4**	0	1	1	1	0	1	0	0	0	0						10	**4**	**40**
14	**11.5**	1	0	0	0	0	0	0	0	0	0						10	**1**	**10**
24	**19.7**	0	1	1	0	0	0	0	0	0	1						10	**3**	**30**
30	**24.6**	0	1	1	1	1	0	0	1	0	0						10	**5**	**50**
34	**27.9**	1	0	1	1	1	1	0	1	0	1						10	**7**	**70**
36	**29.5**	1	0	1	1	1	0	1	1	0	1	1	1	1	1	1	15	**12**	**80**

1 = positive trial; 0 = negative trail.

TAT (3)

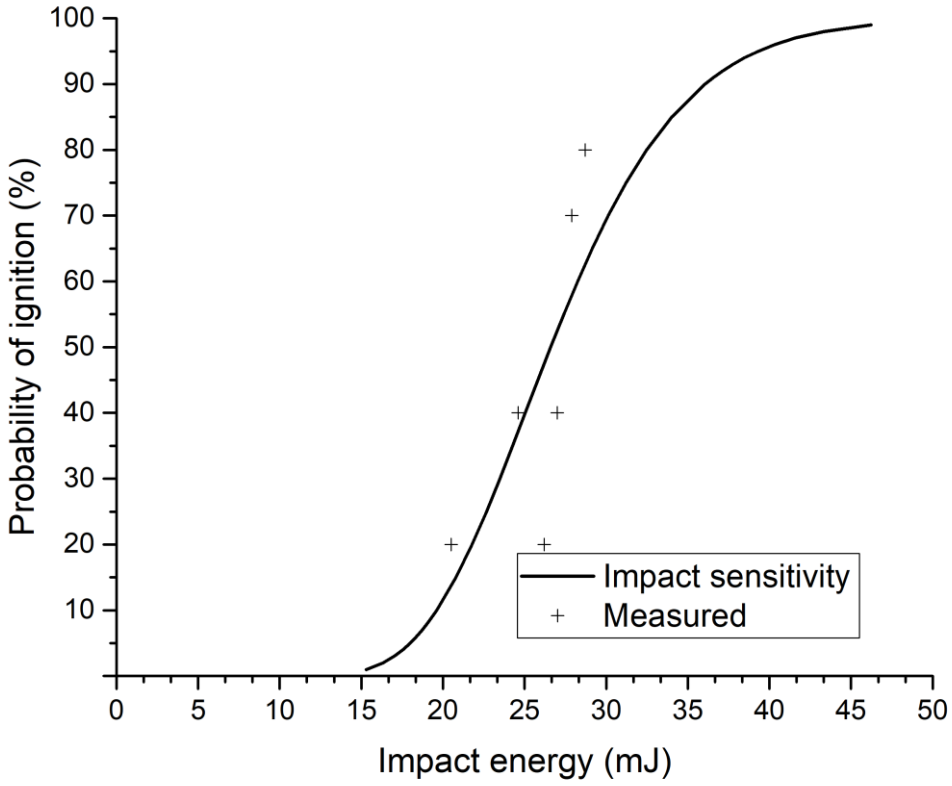

Figure S3. Probit plot of the azido compound **3**.

Table S4. Measurement data of compound **3**.

Height [cm]	Energy [mJ]	Trials										Number of trials	Total number of positive trials	Positive trials [%]
		1	2	3	4	5	6	7	8	9	10			
25	**20.5**	0	0	1	0	0	0	0	0	1	0	10	**2**	**20**
35	**28.7**	1	1	1	1	1	0	1	1	1	0	10	**8**	**80**
30	**24.6**	0	1	0	1	0	0	1	0	0	1	10	**4**	**40**
32	**26.2**	0	1	0	0	0	0	1	0	0	0	10	**2**	**20**
34	**27.9**	1	1	0	1	0	1	0	1	1	1	10	**7**	**70**
33	**27.0**	1	0	0	0	1	0	1	0	1	0	10	**4**	**40**

1 = positive trial; 0 = negative trail.

Tetrazene STANAG 4170 (4a)

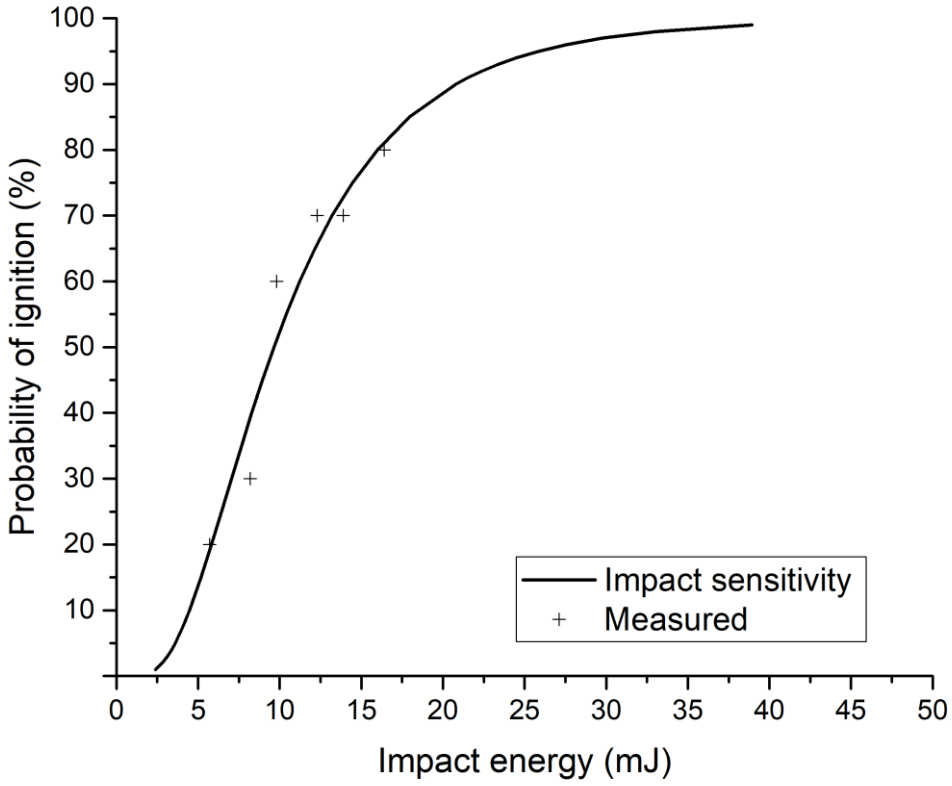

Figure S4. Probit of compound **4a**.

Table S5. Measurement data of compound **4a**.

Height [cm]	Energy [mJ]	Trials															Number of trials	Total number of positive trials	Positive trials [%]
		1	2	3	4	5	6	7	8	9	10	11	12	13	14	15			
10	**8.2**	0	0	0	0	1	1	0	1	0	0						10	**3**	**30**
20	**16.4**	1	1	1	1	1	1	1	1	1	1	0	1	0	0	1	15	**12**	**80**
15	**12.3**	1	1	1	1	1	0	0	1	0	1						10	**7**	**70**
12	**9.8**	1	0	0	1	1	1	1	0	0	1						10	**6**	**60**
7	**5.7**	0	0	0	0	0	0	0	0	1	1						10	**2**	**20**
17	**13.9**	0	1	1	1	1	1	0	1	0	1						10	**7**	**70**

1 = positive trial; 0 = negative trail.

Tetrazene (4b)

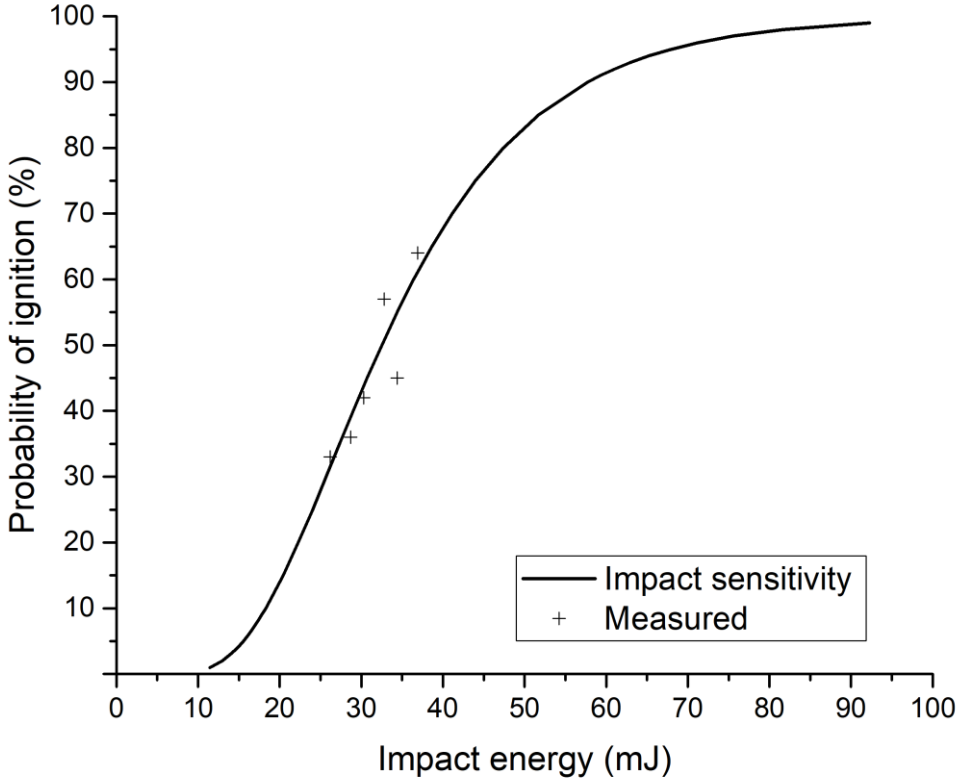

Figure S5. Probit analysis of compound **4b**.

Table S6. Measurement data of compound **4b**.

Height [cm]	Energy [mJ]	Trials															Number of trials	Total number of positive trials	Positive trials [%]
		1	2	3	4	5	6	7	8	9	10	11	12	13	14	15			
40	**32.8**	1	1	0	0	1	1	1	0	1	1	0	1	0	0		14	**8**	**57**
35	**28.7**	1	0	0	1	0	1	0	0	0	0	1					11	**4**	**36**
45	**36.9**	1	1	1	1	0	0	0	0	1	1	0	1	1	1		14	**9**	**64**
37	**30.3**	1	1	0	1	0	0	0	0	1	0	1	0				12	**5**	**42**
42	**34.4**	1	0	0	0	1	0	1	1	0	0	1					11	**5**	**45**
32	**26.2**	0	1	0	1	0	1	1	0	0	1	0	0	0	0	0	15	**5**	**33**

1 = positive trial; 0 = negative trail.

MTX-1 (5)

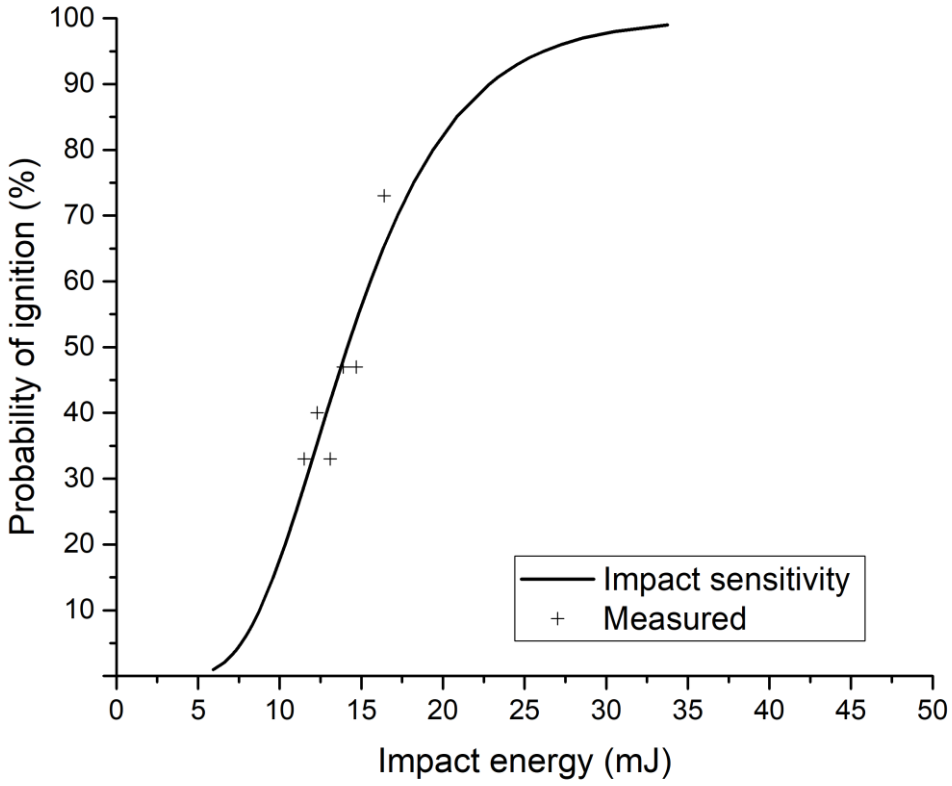

Figure S6. Probit analysis of compound **5**.

Table S7. Measurement data of compound **5**.

Height [cm]	Energy [mJ]	Trials															Number of trials	Total number of positive trials	Positive trials [%]
		1	2	3	4	5	6	7	8	9	10	11	12	13	14	15			
20	**16.4**	1	1	0	1	1	1	1	1	1	1	1	1	0	0	0	15	**11**	**73**
18	**14.7**	1	1	0	0	0	0	1	0	1	0	1	0	1	0	1	15	**7**	**47**
17	**13.9**	1	0	0	0	0	1	0	1	1	1	1	0	1	0	0	15	**7**	**47**
16	**13.1**	0	0	0	1	0	0	0	0	0	0	1	1	1	1	0	15	**5**	**33**
15	**12.3**	1	0	0	0	0	1	0	0	1	1	1	0	0	0	1	15	**6**	**40**
14	**11.5**	0	1	0	0	1	1	0	0	0	0	0	0	1	1	0	15	**5**	**33**

1 = positive trial; 0 = negative trail.

KDNBF (6)

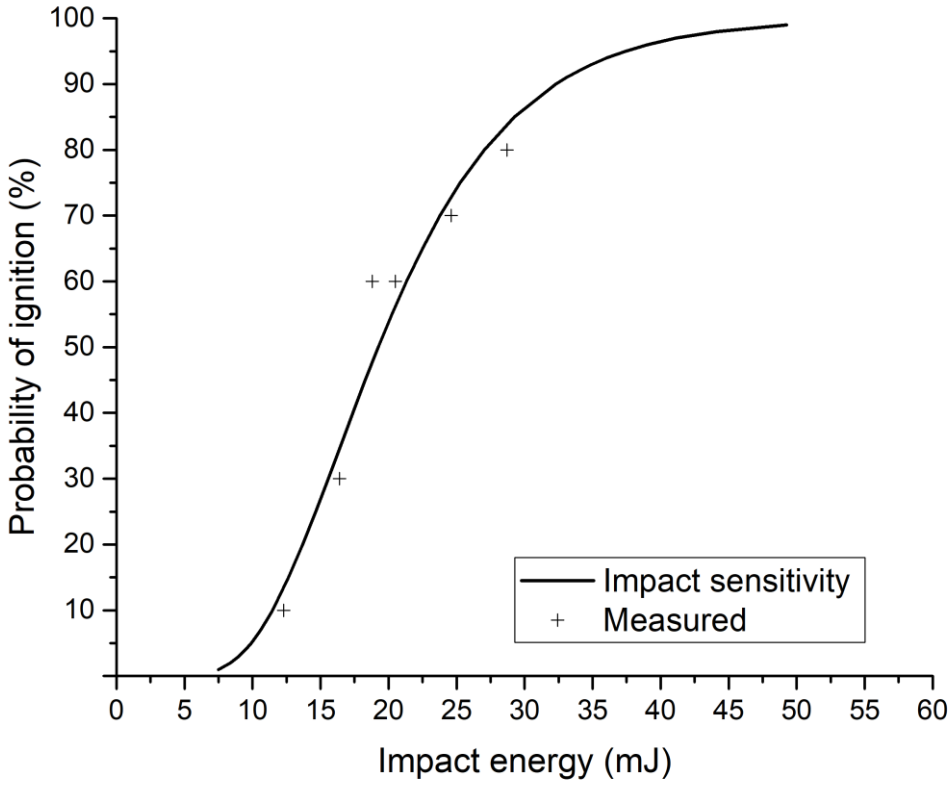

Figure S7. Probit of the potassium salt **6**.

Table S8. Measurement data of compound **6**.

Height [cm]	Energy [mJ]	Trials										Number of trials	Total number of positive trials	Positive trials [%]
		1	2	3	4	5	6	7	8	9	10			
20	**16.4**	0	0	1	1	0	0	1	0	0	0	10	**3**	**30**
25	**20.5**	0	0	1	1	0	1	1	1	0	1	10	**6**	**60**
23	**18.8**	0	1	1	1	1	1	0	0	0	1	10	**6**	**60**
30	**24.6**	1	1	1	1	0	1	1	0	0	1	10	**7**	**70**
35	**28.7**	0	1	0	1	1	1	1	1	1	1	10	**8**	**80**
15	**12.3**	0	0	0	0	0	0	0	1	0	0	10	**1**	**10**

1 = positive trial; 0 = negative trail.

KDNP (7)

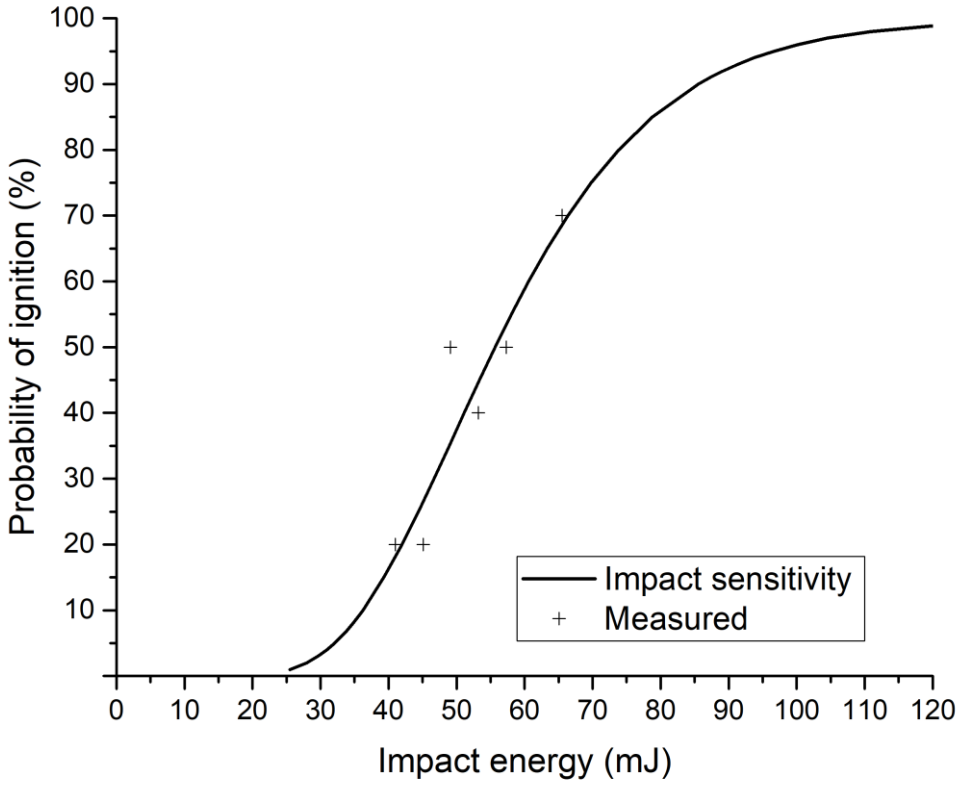

Figure S8. Probit analysis of the potassium salt **7**.

Table S9. Measurement data of compound **7**.

Height [cm]	Energy [mJ]	Trials															Number of trials	Total number of positive trials	Positive trials [%]
		1	2	3	4	5	6	7	8	9	10	11	12	13	14	15			
50	**41.0**	0	1	0	1	0	0	0	0	0	0						10	**2**	**20**
60	**49.1**	1	1	0	1	0	0	1	0	1	0						10	**5**	**50**
70	**57.3**	0	1	1	1	0	1	0	1	0	0						10	**5**	**50**
80	**65.5**	1	1	0	1	0	1	1	0	1	1						10	**7**	**70**
55	**45.1**	0	1	0	1	0	0	0	0	0	0	1	0	0	0	0	15	**3**	**20**
65	**53.2**	0	0	1	1	1	1	0	0	0	0						10	**4**	**40**

1 = positive trial; 0 = negative trail.

K_2DNABT (8)

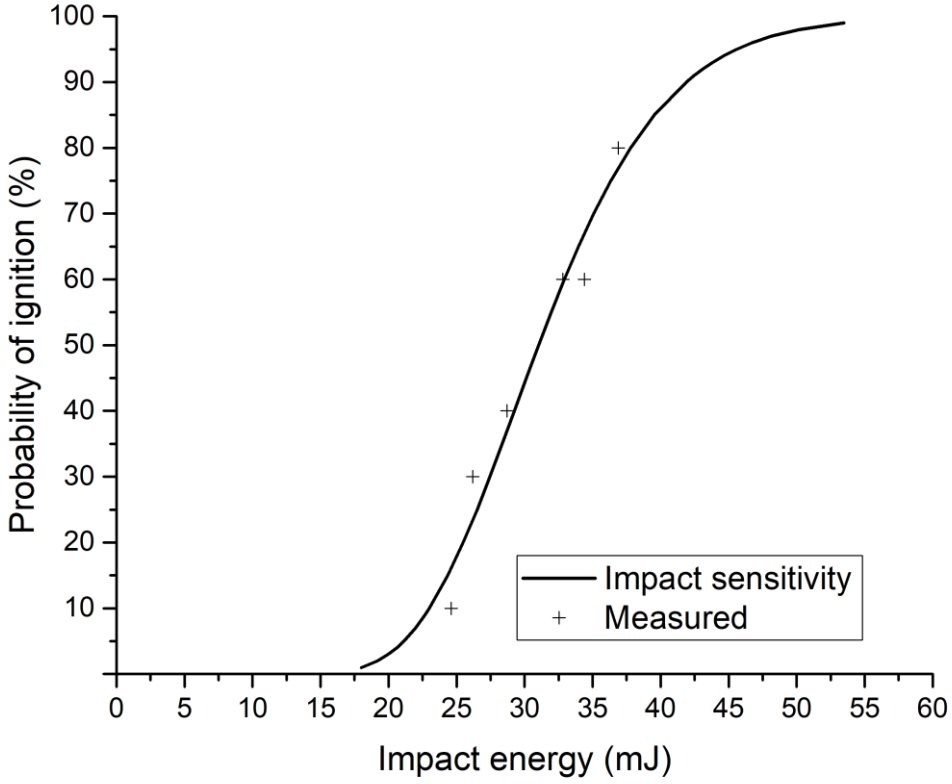

Figure S9. Probit plot of the dipotassium salt **8**.

Table S10. Measurement data of compound **8**.

Height [cm]	Energy [mJ]	Trials										Number of trials	Total number of positive trials	Positive trials [%]
		1	2	3	4	5	6	7	8	9	10			
30	**24.6**	0	0	0	1	0	0	0	0	0	0	10	**1**	**10**
35	**28.7**	1	0	1	0	0	0	1	0	0	1	10	**4**	**40**
32	**26.2**	0	0	1	0	0	0	1	1	0	0	10	**3**	**30**
40	**32.8**	1	0	1	1	1	1	0	1	0	0	10	**6**	**60**
45	**36.9**	1	1	1	1	0	1	1	1	1	0	10	**8**	**80**
42	**34.4**	1	1	1	1	0	0	1	0	1	0	10	**6**	**60**

1 = positive trial; 0 = negative trail.

Lead styphnate monohydrate, LS STANAG 4170 (9a)

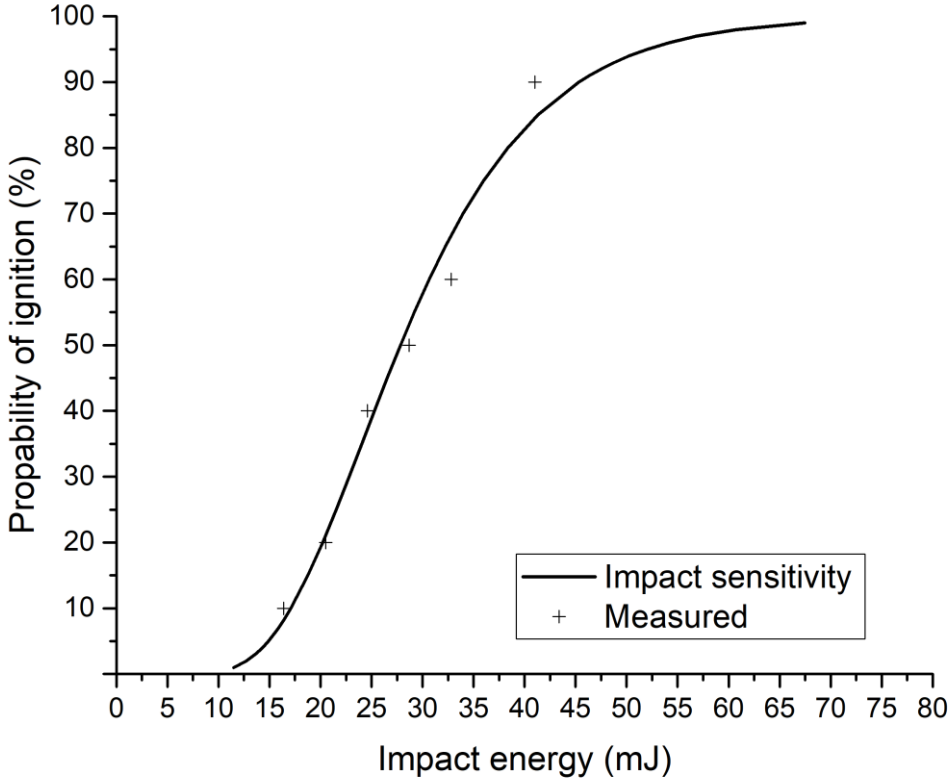

Figure S10. Probit plot of the lead salt **9a** provided by DynITEC GmbH.

Table S11. Measurement data of compound **9a**.

Height [cm]	Energy [mJ]	Trials										Number of trials	Total number of positive trials	Positive trials [%]
		1	2	3	4	5	6	7	8	9	10			
20	**16.4**	1	0	0	0	0	0	0	0	0	0	10	**1**	**10**
25	**20.5**	0	0	0	1	1	0	0	0	0	0	10	**2**	**20**
30	**24.6**	1	0	0	1	1	0	1	0	0	0	10	**4**	**40**
35	**28.7**	1	0	0	1	1	0	1	1	0	0	10	**5**	**50**
40	**32.8**	0	0	1	1	1	0	1	0	1	1	10	**6**	**60**
50	**41.0**	1	1	0	1	1	1	1	1	1	1	10	**9**	**90**

1 = positive trial; 0 = negative trail.

Lead styphnate monohydrate, LS (9b)

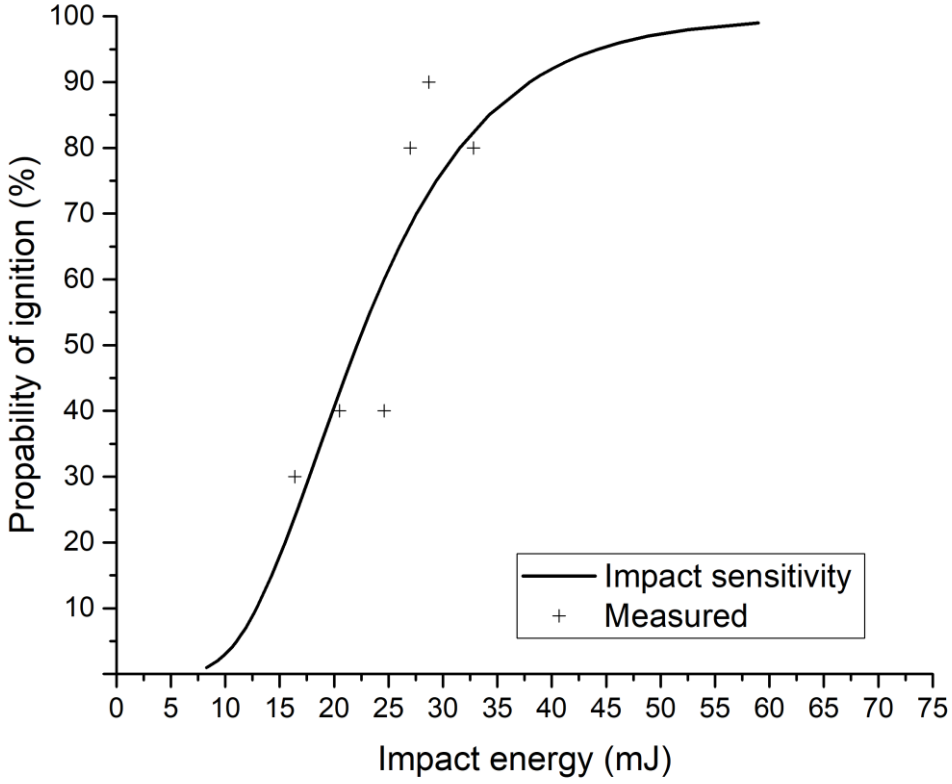

Figure S11. Probit plot of the lead salt **9b**.

Table S12. Measurement data of compound **9b**.

Height [cm]	Energy [mJ]	Trials										Number of trials	Total number of positive trials	Positive trials [%]
		1	2	3	4	5	6	7	8	9	10			
30	**24.6**	1	1	0	1	0	0	0	0	1	0	10	**4**	**40**
40	**32.8**	1	1	1	1	1	1	1	0	1	0	10	**8**	**80**
35	**28.7**	1	1	1	0	1	1	1	1	1	1	10	**9**	**90**
25	**20.5**	1	0	1	1	0	1	0	0	0	0	10	**4**	**40**
20	**16.4**	0	0	0	0	1	1	0	0	1	0	10	**3**	**30**
33	**27.0**	1	1	1	1	0	1	1	1	0	1	10	**8**	**80**

1 = positive trial; 0 = negative trail.

Copper(I) nitrotetrazolate, DBX-1 (10)

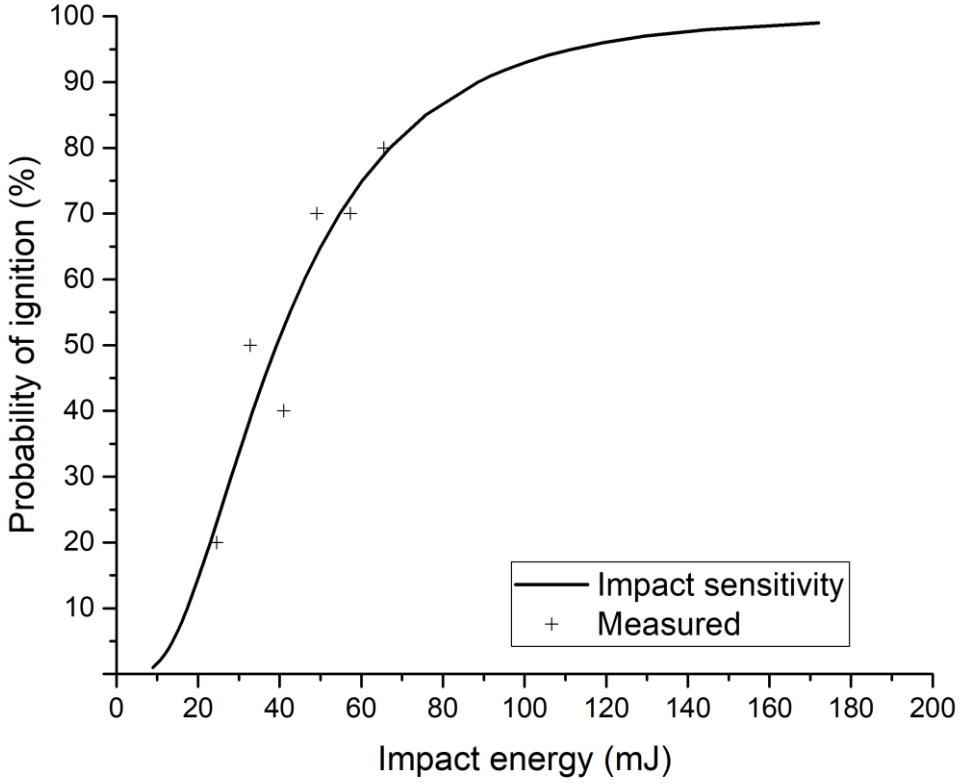

Figure S12. Probit plot of the copper(I) nitrotetrazolate **10**.

Table S13. Measurement data of compound **10**.

Height [cm]	Energy [mJ]	Trials										Number of trials	Total number of positive trials	Positive trials [%]
		1	2	3	4	5	6	7	8	9	10			
50	**41.0**	0	0	1	0	0	1	0	0	1	1	50	**4**	**40**
40	**32.8**	0	1	1	0	0	1	1	0	0	1	40	**5**	**50**
30	**24.6**	0	0	0	0	1	0	0	0	1	0	30	**2**	**20**
60	**49.1**	1	1	0	1	1	1	0	1	0	1	60	**7**	**70**
70	**57.3**	1	0	1	0	1	1	1	1	1	0	70	**7**	**70**
80	**65.5**	1	1	1	1	1	0	1	1	1	0	80	**8**	**80**

1 = positive trial; 0 = negative trail.

Nickel hydrazine nitrate, NHN (11)

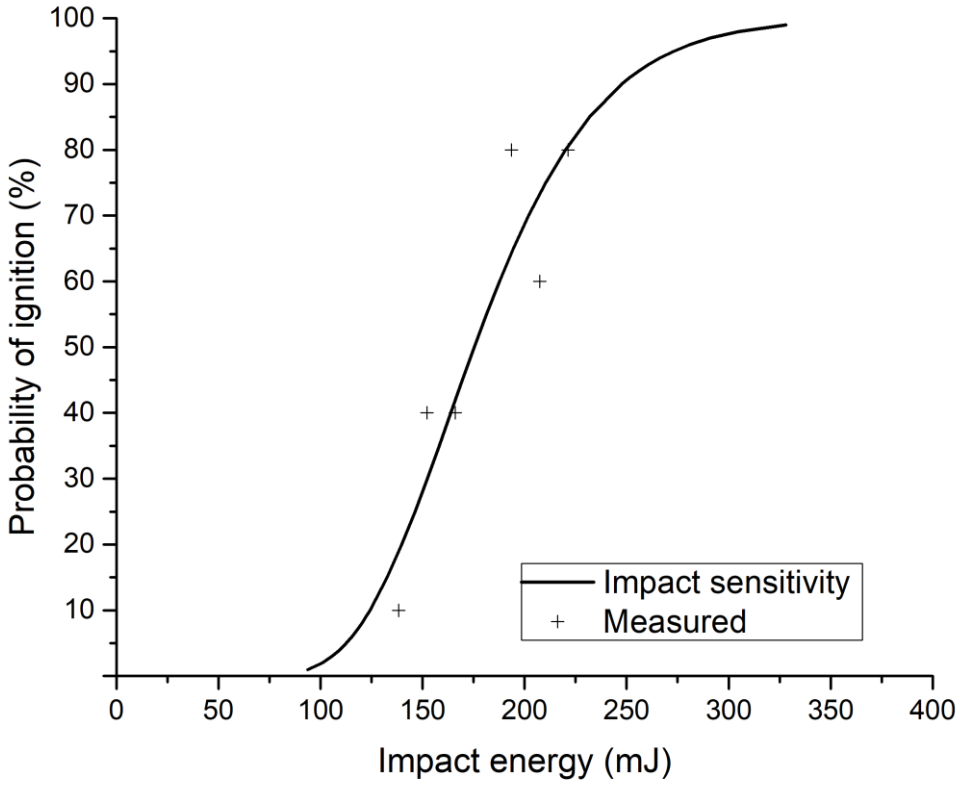

Figure S13. Probit plot of coordination compound **11**.

Table S14. Measurement data of compound **11**.

Height [cm]	Energy [mJ]	Trials										Number of trials	Total number of positive trials	Positive trials [%]
		1	2	3	4	5	6	7	8	9	10			
60	**166.0**	0	1	1	0	1	0	0	0	1	0	10	**4**	**40**
55	**152.2**	0	1	0	1	0	1	0	0	0	1	10	**4**	**40**
50	**138.3**	0	0	0	0	0	0	0	0	1	0	10	**1**	**10**
70	**193.6**	1	0	1	1	1	1	0	1	1	1	10	**8**	**80**
80	**221.3**	1	0	1	1	1	1	1	1	1	0	10	**8**	**80**
75	**207.5**	1	0	0	1	1	1	0	0	1	1	10	**6**	**60**

1 = positive trial; 0 = negative trail.

Silver Acetylide, Ag_2C_2 (12)

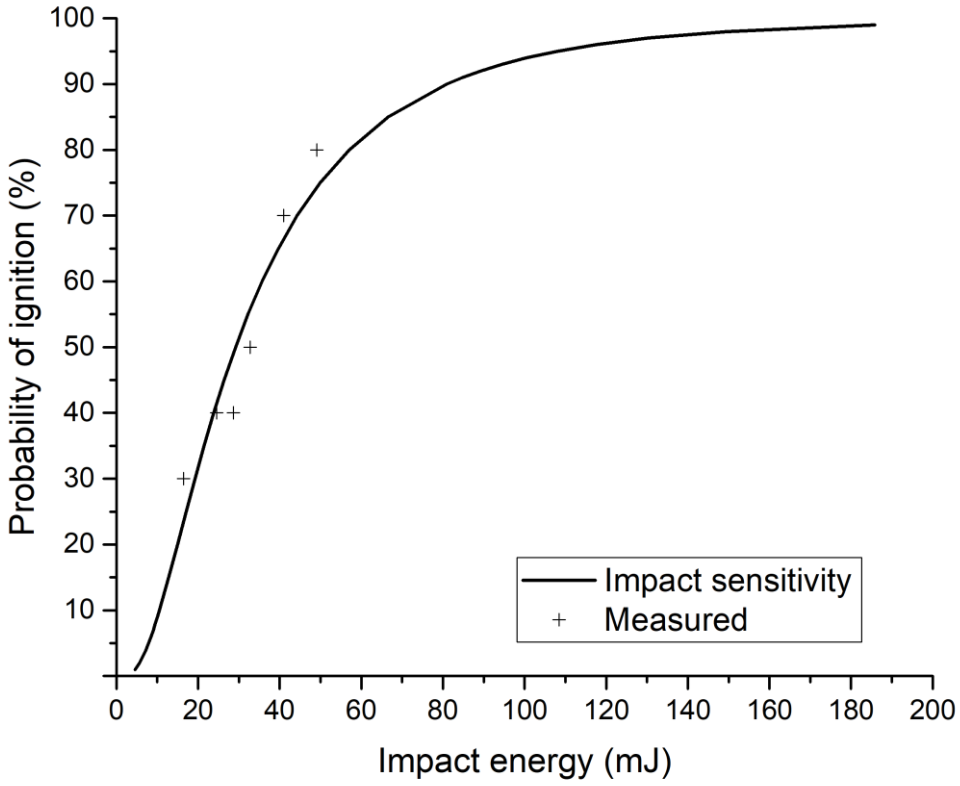

Figure S14. Probit plot of compound **12**.

Table S15. Measurement data of compound **12**.

Height [cm]	Energy [mJ]	Trials										Number of trials	Total number of positive trials	Positive trials [%]
		1	2	3	4	5	6	7	8	9	10			
30	**24.6**	1	1	0	1	0	0	0	0	0	1	10	**4**	**40**
20	**16.4**	0	0	0	0	0	0	1	1	1	0	10	**3**	**30**
35	**28.7**	1	0	0	0	1	0	1	0	1	0	10	**4**	**40**
40	**32.8**	0	0	0	1	1	1	0	1	0	1	10	**5**	**50**
50	**41.0**	1	0	1	1	1	1	0	0	1	1	10	**7**	**70**
60	**49.1**	0	1	1	1	1	1	0	1	1	1	10	**8**	**80**

1 = positive trial; 0 = negative trail.

Mercury fulminate, MF, brown (16)

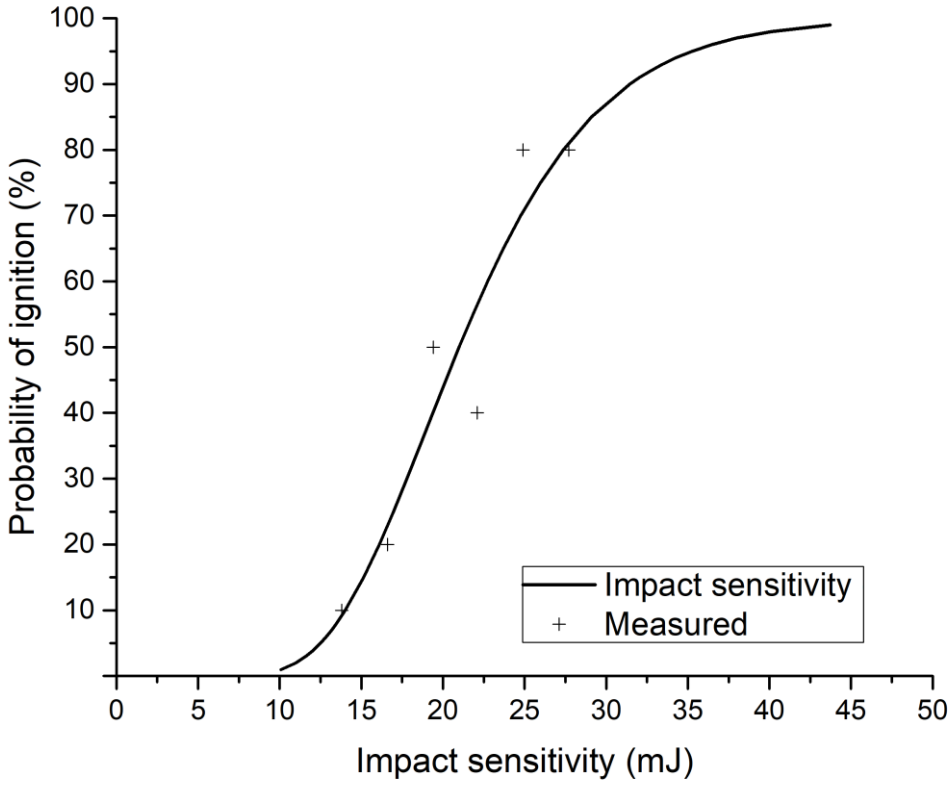

Figure S15. Probit plot of compound **16**.

Table S16. Measurement data of compound **16**.

Height [cm]	Energy [mJ]	Trials										Number of trials	Total number of positive trials	Positive trials [%]
		1	2	3	4	5	6	7	8	9	10			
10	**27.7**	1	1	1	1	0	0	1	1	1	1	10	**8**	**80**
5	**13.8**	0	0	0	1	0	0	0	0	0	0	10	**1**	**10**
6	**16.6**	0	0	0	0	0	0	1	1	0	0	10	**2**	**20**
7	**19.4**	0	1	0	0	0	1	1	0	1	1	10	**5**	**50**
8	**22.1**	0	1	0	0	1	1	1	0	0	0	10	**4**	**40**
9	**24.9**	1	1	1	1	1	1	1	0	1	0	10	**8**	**80**

1 = positive trial; 0 = negative trail.

2.7.3. Microscope Images and Particle Size Distributions

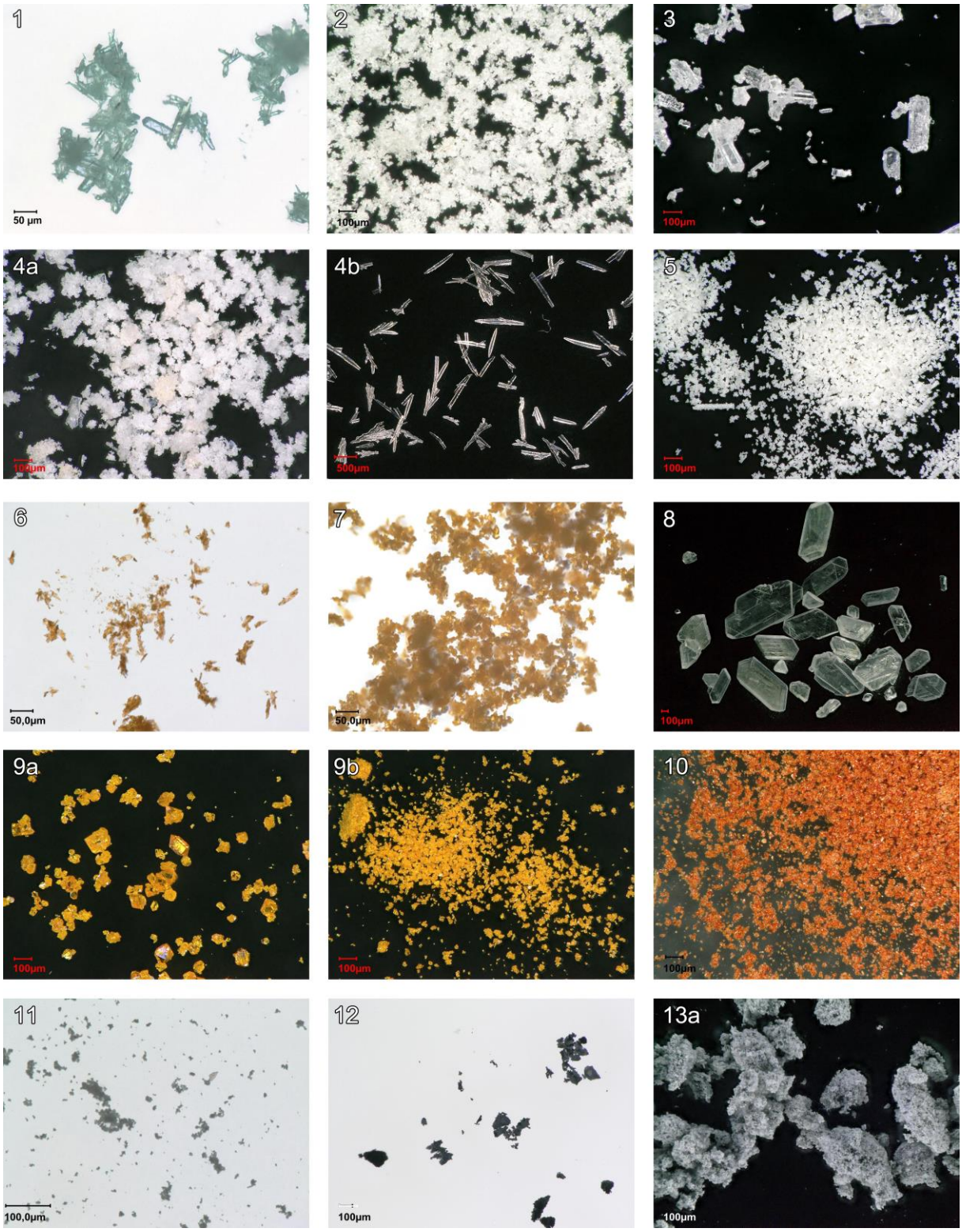

Figure S16. Microscope images of the compounds **1**–**13a**.

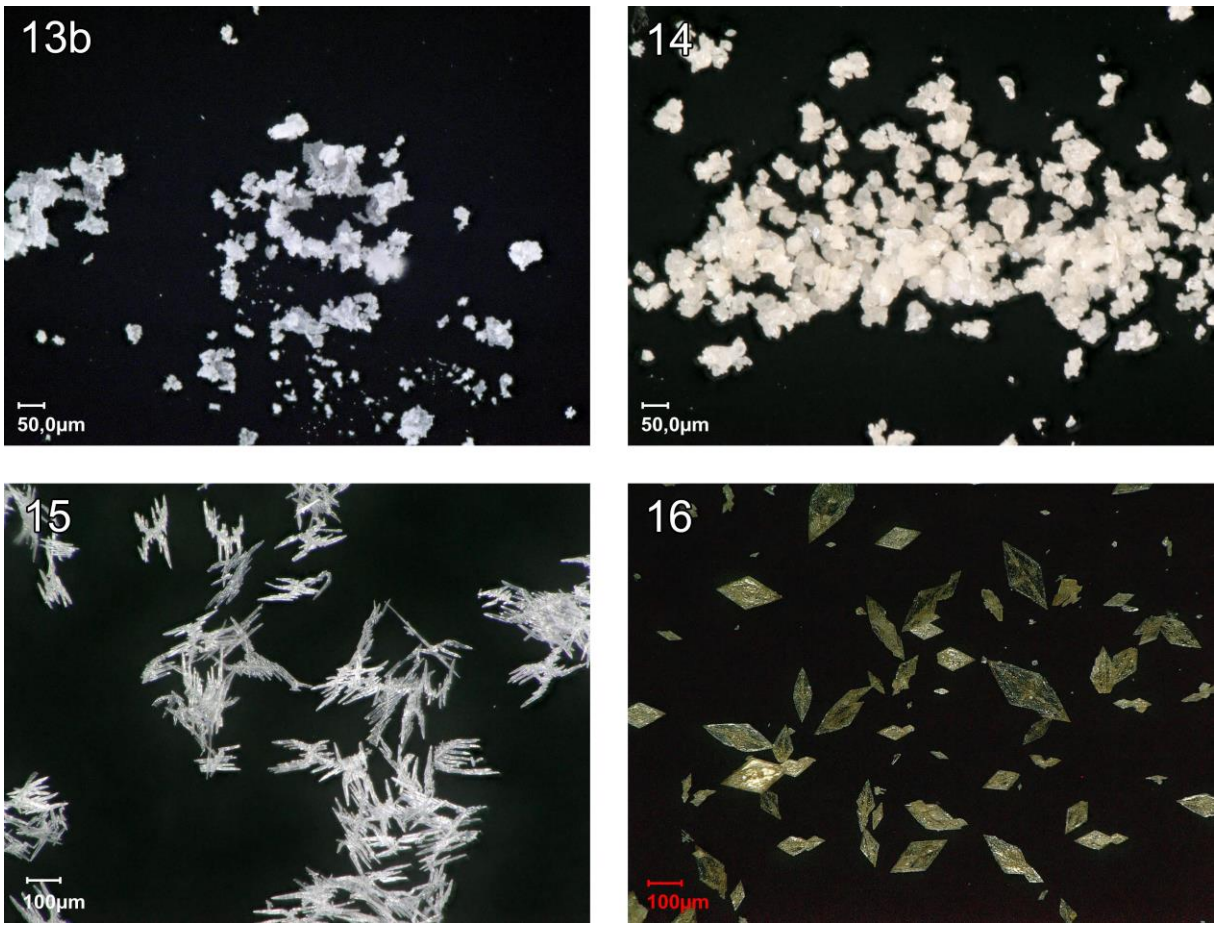

Figure S17. Microscope images of the compounds **13a**–**16**.

Table S17. Particle size distributions of the compounds **1**–**16**.

Compound	**1**	**2**	**3**	**4a**	**4b**
Grain size distribution [µm]	50–200	< 30	50–300	< 30	400–1000
Compound	**5**	**6**	**7**	**8**	**9a**
Grain size distribution [µm]	< 30	< 30	< 30	500–1500	40–140
Compound	**9b**	**10**	**11**	**12**	**13a**
Grain size distribution [µm]	< 30	< 30	< 30	50–150	< 10
Compound	**13b**	**14**	**15**	**16**	
Grain size distribution [µm]	< 30	< 30–50	100–200	50–300	

2.7.4. Experimental Part and General Methods

All chemicals and solvents were employed as received (Sigma-Aldrich, Fluka, Acros, ABCR). Determination of the carbon, hydrogen and nitrogen contents was carried out by combustion analysis using an Elementar Vario El (nitrogen contents determined are often lower than those calculated due to

their explosive behavior). Determination of the mercury content was carried out by ICP-OES analysis using a VARIAN-VISTA Simultaneous-Spectrometer (mercury contents determined are often lower due to absorption and amalgam formation). The images of the crystals and the particle size distributions were taken with a Keyence VHX-5000 digital microscope. Impact sensitivity tests were carried out according to STANAG 4489[1] with a modified instruction[2] using a BAM (Bundesanstalt für Materialforschung und -prüfung) drop hammer.[3] Steel guide rings and steel cylinders for BAM drop hammers were obtained from OZM Research, Czech Republic.[4] Friction sensitivity tests were performed according to STANAG 4487[5] with a modified instruction[6] using the BAM friction tester.[3] Porcelain plates and pins were obtained from OZM Research, Czech Republic.[4] The limiting values of impact energy and friction force were determined in conformity with the recommended UN method for testing impact and friction sensitivities (1-in-6 approach), according to ST/SG/AC.10/11Rev.6 (s. 13.4.2.3.3).[7] Ball drop impact sensitivity tests were determined on an OZM ball drop machine (BIT-132), following MIL-STD-1751A (method 1016) by dropping a free falling steel ball onto the explosive compound.[8] A sample was placed on a steel block using a 30 mm^3 volumetric spoon and spread into a 0.33 mm layer of substance. The steel ball guide was set to the desired height and the loaded impact block positioned underneath. By releasing the ball shield, a steel ball, with a defined weight, was allowed to fall onto the sample. Any visual observation of decomposition was regarded as a positive result. If no reaction occurred, the remaining substance was disposed, and the impact block loaded with a freshly prepared sample. The available steel balls are sized the following: 0.50 inch (8.35 g), 0.75 inch (28.20 g), 1.00 inch (66.84 g), 1.50 inch (225.60 g), and 2.00 inch (534.70 g). Two different measurement techniques were used during ball drop impact sensitivity measurements. The probit method, which is the primary method of evaluation, was applied in the following way: The probability of ignition of each compound was determined with 6 test heights, with 10–15 trials at each height. Probit evaluation was performed with IBM SPSS Statistics 25.0 using the number of positive trials per height as “Response Frequency”, the number of total shots as “Total Observed” variable and the impact energy as “Covariate”, transformed into the natural logarithm. The resulting energy levels with the corresponding probability values were plotted to generate the typical probit regression curve. The one out of six method, which was used in case of an impossible application of the probit method, was performed as follows: An initial drop height was chosen, at which an explosion of the sample could be ensured. The impact energy level (ball guide height) was now stepwise decreased until no more reaction was observed. At this point, testing was continued up to a total of six trials at that certain energy level. If an explosion occurred, the procedure was repeated by decreasing the drop height again. As soon as six trials at a fixed energy level emerged as negative, the next higher energy level, where at least one out of at least six trials resulted in an explosion, is determined as the limiting impact

energy. The impact energy of all drops was calculated as a product of the ball mass, the local gravitational field (9.81 m s^{-2}) and the drop height.

CAUTION! *All investigated compounds are energetic materials (most of the compounds lie in the range of primary explosives), which show increased sensitivities toward various stimuli (e.g., elevated temperatures, impact, friction, or electrostatic discharge). Therefore, proper security precautions (safety glasses, face shield, earthed equipment and shoes, leather coat, Kevlar gloves, Kevlar sleeves and ear plugs) have to be applied while synthesizing and handling the described compounds.*

Hexamethylene triperoxide diamine, HMTD (1):
Compound **1** was synthesized according to a literature procedure.[9] Hexamine (2.00 g, 14.3 mmol) was dissolved in a 30% solution of hydrogen peroxide (5.80 mL, 56.6 mmol) at 0 °C. Citric acid (2.84 g, 14.8 mmol) was added portion wise at 0 °C. Stirring was continued for 3 h, while keeping the temperature at 0 °C. The solution was warmed up to ambient temperature and compound **1** was afforded as a colorless solid after 12 h (2.10 g, 10.1 mmol, 71%).

EA ($C_6H_{12}N_2O_6$, 208.17) calcd.: C 34.62, H 5.81, N 13.46%; found: C 34.63, H 5.81, N 13.54%.

Triacetone triperoxide, TATP (2):
The organic peroxide was prepared according to a modified literature procedure.[10] A mixture of acetone (3.48 g, 60.0 mmol) and hydrogen peroxide (33%, 6.18 g, 60.0 mmol) was stirred at ice-bath temperature. Concentrated hydrochloric acid (37%, 7.68 g, 78.0 mmol) was added dropwise. After addition, the opaque solution was stirred for another 20 min at 0 °C and the foamy precipitate was filtered using a Buchner funnel. After washing with water, sodium carbonate solution (1% in water) and again several times with water, the product was obtained as a coke white powder and dried at room temperature overnight (1.71 g, 7.69 mmol, 38%).

EA ($C_9H_{18}O_6$, 222.24) calcd.: C 48.64, H 8.16%; found: C 48.71, H 7.98%.

2,4,6-Triazido-1,3,5-triazine, TAT (3):
The triazine (**3**) was prepared according to a modified literature procedure.[11] Acetone (24 mL) was added to a stirring solution of sodium azide (1.95 g, 30.0 mmol) in water (16 mL). Cyanuric chloride (1.84 g, 10.0 mmol) was added at once and the reaction mixture subsequently stirred at 50 °C. After 45 min the product started to precipitate in the form of small needles, and the mixture was stirred for another 20 min without heating. Vacuum filtration and washing with excess water yielded pure **3** in the form of colorless needles (1.88 g, 9.21 mmol, 92%).

EA (C_3N_{12}, 204.12) calcd.: C 17.65, N 82.35%; found: C 18.00, N 80.35%.

1-(5-Tetrazolyl)-3-guanyl tetrazene monohydrate, Tetrazene (4a,4b):
Compound **4a** qualified according to STANAG 4170 was supplied by DynITEC GmbH, Germany.[12] In addition, the compound (**4b**) was prepared by a modified procedure presented by Urbanski *et al*..[13] Aminoguanidine bicarbonate (10.21 g, 75.0 mmol) was dissolved in water (750 mL). Acetic acid (4.71 mL) was added and the mixture stirred at 60 °C for 20 min. After cooling down to 30 °C, sodium nitrite (8.28 g, 120 mmol) was added and after 67 h, compound **4b** was separated as pale-yellow crystalline needles (3.45 g, 18.3 mmol, 24%).

4b EA ($C_2H_8N_{10}O$, 188.16) calcd.: C 12.77, H 4.29, N 74.44%; found: C 13.05, H 3.99, N 74.17%.

1-[(2*E*)-3-(1*H*-Tetrazol-5-yl)triaz-2-en-1-ylidene]methanediamine, MTX-1 (5):
Compound (**5**) was synthesized according to a literature procedure.[14] A suspension of tetrazene (3.00 g, 25,5 mmol) in 1 M HNO_3 (150 mL) was reacted dropwise with a solution of sodium nitrite (1.82 g, 26.4 mmol) in water (15 mL) over a period of 10 min. After stirring for 4 h, a white precipitate was filtrated and washed with water (20 mL) for three times. The remaining solid was dried at 65 °C for 2 h to afford compound **5** as colorless crystals (2.25 g, 14.5 mmol, 57%).

EA ($C_2H_5N_9$, 155.13) calcd.: C 15.49, H 3.25, N 81.27%; found: C 15.53, H 3.05, N 78.46%.

Potassium dinitrobenzofuroxan, KDNBF (6):
Potassium 4,6-dinitrobenzofuroxan (**6**) was prepared in a modified two-step synthesis.[15] To a mixture of picryl chloride (2.50 g, 10.1 mmol) and sodium azide (0.78 g, 12.0 mmol), concentrated acetic acid (10 mL) was added dropwise. The solution was refluxed for 1.5 h and afterwards the reaction mixture was poured on iced water (40 mL). The formed precipitate was filtrated off and washed with water (25 mL). Recrystallization from chloroform (90 mL) afforded 4,6-dinitrobenzofuroxan (811 mg, 3.57 mmol, 35%). The precursor (786 mg, 3.48 mmol) was dissolved in water (8 mL) and heated to 60 °C. Potassium bicarbonate (350 mg, 3.50 mmol) was added portion wise until no further evolution of gas was detected. The orange precipitate was filtrated off and washed with water (5 mL) and acetone (5 mL) affording compound **6** as an orange solid (884 mg, 3.13 mmol, 90%)

EA ($C_6H_3KN_4O_7$, 282.21) calcd.: C 25.54, H 1.07, N 19.85%; found: C 25.76, H 1.10, N 19.85%.

Potassium 5,7-dinitro-[2,1,3]-benzoxadiazol-4-olate 3-oxide, KDNP (7):
The potassium salt **7** was prepared according to Fronabarger *et al*..[16] 3-bromo-2,4,6-trinitroanisole (3.00 g, 9.31 mmol) was dissolved in methanol (50 mL) and potassium azide (1.59 g, 19.6 mmol) was added to the solution. After refluxing for 1 h, the solution was allowed to cool down and the solvent was evaporated. Acetone (10 mL) was added and the solution filtrated. The filter cake was washed with

acetone (30 mL) and the combined organic layers were evaporated to dryness. Diethyl carbonate (50 mL, 0.42 mol) was added and the resulting solution refluxed for 2 h at 135 °C. After allowing the solution to slowly cool down to ambient temperature, an ice bath was used for further cooling for 30 min. Filtration and washing with 2-propanol afforded crude **7**. The brown solid was dissolved in 2-methoxyethanol (34 mL) at 100 °C, 2-propanol (135 mL) was added and the solution stirred for 5 min. The formed precipitate was filtrated off and washed with 2-propanol (20 mL). Drying at 65 °C for 48 h afforded KNDP (**7**) as a brown solid. (1.47 g, 5.25 mmol, 56%).

EA ($C_6HKN_4O_7$, 280.19) calcd.: C 25.72, H 0.36, N 20.00%; found: C 25.95, H 0.36, N 20.00%.

Dipotassium-1,1′-dinitramino-5,5′-bistetrazolate, K_2DNABT (8):
Dipotassium dinitraminobistetrazolate (**8**) was prepared according to WO 2018209366 in a 1.5 g scale.[17] The product was recrystallized form water under slow stirring.

EA ($C_2K_2N_{12}O_4$, 333.94) calcd.: C 7.19, N 50.28%; found: C 7.61, N 47.96%.

Lead(II) styphnate monohydrate, LS (9a, **9b):**
Lead styphnate (**9a**), fulfilling STANAG 4170 was provided by DynITEC GmbH, Germany.[12] Additionally, the lead salt of styphnic acid (**9b**) was prepared according to literature procedures.[18] Styphnic acid (1.20 g, 4.90 mmol) was suspended in water (20 mL). Magnesium oxide (0.23 mg, 5.60 mmol) was added and the mixture was allowed to warm up to 55 °C. After filtration, lead nitrate (1.87 g, 6.00 mmol) in water (6 mL) was added to the filtrate and compound **9b** started to precipitate immediately. The mixture was allowed to cool down to room temperature over a period of 30 min while stirring. Filtration and subsequent washing with water (20 mL) yielded lead styphnate monohydrate (1.76 g, 3.76 mmol, 77%)

9b EA ($C_6H_3N_3O_9Pb$, 468.30) calcd.: C 15.39, H 0.65, N 8.97%; found: C 15.57, H 0.78, N 8.87%.

Copper(I) 5-nitrotetrazolate, DBX-1, (10):
The compound was prepared according to a modified literature procedure.[19] A purified solution of sodium nitrotetrazolate dihydrate in water (1.73 g, 10.0 mmol, 40 mL) was added to a solution of copper(II)-chloride dihydrate in water (1.53 g, 9.00 mmol, 50 mL) at 80 °C under stirring. Seed crystals of authentic DBX-1 (0.16 g, 0.90 mmol) were added to the clear green solution. The temperature was further raised to 90 °C and a solution of sodium ascorbate in water (1.59 g, 9.00 mmol, 20 mL) was added dropwise and very slowly at a rate of 0.5 mL min^{-1}. The addition was paused after 4 mL of ascorbate solution and it was waited for the olive-brown precipitated to convert into a rust-red crystalline material settling down quickly when the stirring was briefly stopped. The remaining sodium ascorbate solution

was added at a rate of 2 mL min^{-1} and the hot suspension was stirred for another 10 min. The precipitate was washed by decantation and filtered using a Buchner funnel. After washing with 2-propanol two times (20 mL), the orange-red product was dried at 65 °C for 30 min (1.33 g, 7.46 mmol, 73%).

EA ($CCuN_5O_2$, 177.59) calcd.: C 6.76, H 0.00, N 39.44%, found: C 7.03, H 0.00, N 39.46%.

Nickel(II) hydrazine nitrate, NHN, (11):
The nickel complex **11** was prepared according to a literature procedure.[20] Nickel(II) nitrate hexahydrate (1.34 g, 4.62 mmol) was dissolved in water (10 mL) and heated to 65 °C. Hydrazine hydrate (1.4 mL, 29.75 mmol) and a solution of nickel(II) nitrate hexahydrate (1.34 g, 4.62 mmol) in water (10 mL) were simultaneously added over a period of 30 min. After stirring for 10 min at 65 °C the precipitate was filtrated off and washed with ethanol (20 mL). The nickel nitrate complex **11** was obtained as a purple solid (2.54 g, 9.11 mmol, 99%).

EA ($H_{12}N_8NiO_6$, 278.84) calcd.: H 4.34, N 40.19%; found: H 4.07, N 39.22%.

Silver acetylide, Ag_2C_2 (12):
The silver salt of acetylene (**12**) was obtained by a modified literature procedure.[21] Silver nitrate (7.48 g, 44.0 mmol) was dissolved in water (60 mL) and concentrated ammonia solution (60 mL) was added under stirring. Afterwards, acetylene gas, purified by concentrated sulfuric acid and half-concentrated solution of sodium hydroxide, was passed into the reaction mixture for 30 min. The reaction was stopped, the precipitate carefully separated and washed until the filtrate indicated a neutral pH-level. Silver acetylide (**12**) was received as a greyish amorphous solid (3.51 g, 14.6 mmol, 33%). The compound was dried in air and stored in a dark atmosphere due to its light sensitivity.

EA (C_2Ag_2, 239.76) calcd.: C 10.02%; found: C 10.02%.

Silver azide, SA (13a, 13b):
The azide **13a** was provided by DynITEC GmbH, Germany, qualified according to STANAG 4170.[12] Additionally, the azide (**13b**) was synthesized according to the standard procedures.[22] Silver nitrate (2.38 g, 14.0 mmol) in water (10 mL) was reacted dropwise with sodium azide (0.91 g, 14.0 mmol) in water (5 mL) at room temperature. The precipitate was filtered off, washed with water and dried in air, yielding silver azide (**13b**) as a light grey solid (2.05 g, 13.7 mmol, 98%).

13b EA (AgN_3, 149.89) calcd.: N 28.03%; found: N 28.15%.

Lead azide, LA, RD-1333 (14):

Lead azide (**14**), synthesized following MIL-L-46225C (RD-1333) was provided by DynITEC GmbH, Germany.[23]

Silver fulminate, SF (15):
The silver salt of the fulminic acid (**15**) was prepared according to Pasinszki *et al*..[24] Silver (432 mg, 4 mmol) was dissolved in a mixture of 65% nitric acid (5.6 mL, 124 mmol) and water (2.4 mL). The mixture was added to 96% ethanol (9.6 mL, 164 mmol) and the resulting solution was heated to reflux until a vigorous gas evaluation started. From that point on, the solution was allowed to cool to room temperature, stirring continued until the reaction had completely stopped. The suspension was washed by decanting with water until a neutral pH value was obtained. The resulting colorless solid was carefully filtrated off and dried at ambient temperature, yielding compound **15** (474 mg, 3 mmol, 75%).

EA (CAgNO, 149.89) calcd.: C 8.01, N 9.35%; found: C 8.46, N 9.54%.

Mercury fulminate, MF, brown (16):
The neat, brown modification of mercury fulminate (**16**) was prepared following a standard procedure.[21] During the whole reaction a major aspect was not to stir or shake any part of the reaction mixture. A 100 mL Erlenmeyer flask was charged with 65% nitric acid (30.0 ml, 667 mmol) and mercury (6.25 g, 24.9 mmol) was added. During the dissolution of mercury, a long-necked 800 mL beaker was charged with 96% ethanol (45.0 mL, 771 mmol) and directly after the completion of the reaction, the mixture was poured into the prepared beaker. The reaction started with a delay of several minutes, indicated by an evolution of white fumes. After 45 min the reaction was finished, the crystals were filtrated off and washed with water (100 mL) and ethanol (20 mL). Mercury fulminate (**16**) was obtained in the form of brownish needles (3.27 g, 11.5 mmol, 46%).

EA ($C_2HgN_2O_2$, 284.62) calcd.: Hg 70.48%; found: Hg 68.31%.

2.7.5. References

[1] NATO standardization agreement (STANAG) on explosives, impact sensitivity tests, no. 4489, 1st ed., Sept. 17, **1999**.

[2] WIWEB-Standardarbeitsanweisung 4-5.1.02, Ermittlung der Explosionsgefährlichkeit, hier der Schlagempfindlichkeit mit dem Fallhammer, Nov. 8, **2002**.

[3] BAM, http://www.bam.de, (accessed July 2019).

[4] OZM, http://www.ozm.cz, (accessed July 2019).

[5] NATO standardization agreement (STANAG) on explosive, friction sensitivity tests, no. 4487, 1st ed., Aug. 22, **2002**.

[6] WIWEB-Standardarbeitsanweisung 4-5.1.03, Ermittlung der Explosionsgefährlichkeit oder der Reibeempfindlichkeit mit dem Reibeapparat, Nov. 8, **2002**.

[7] UN Model Regulation: Recommendations on the Transport of Dangerous Goods – Manual of Tests and Criteria, section 13.4.2.3.3, **2015**.

[8] Military Standard 1751A (MIL-STD-1751A): safety and performance tests for qualification of explosives (high explosives, propellants and pyrotechnics), method 1016, Dec. 11, **2001**.

[9] W. P. Schaefer, J. T. Fourkas, B. G. Tiemann, *J. Am. Chem. Soc.* **1985**, *107*, 2461–2463.

[10] O. Reany, M. Kapon, M. Botoshansky, E. Keinan, *Cryst. Growth Des.* **2001**, *9*, 3661–3670.

[11] E. Ott, E. Ohse, *Ber. Dtsch. Chem. Ges.* **1921**, *2*, 179–186.

[12] NATO standardization agreement (STANAG) on the principles and methodology for the qualification of explosive materials for military use, no. 4170, 3rd ed., **2008**.

[13] T. Urbanski, *Chemistry and Technology of Explosives*, 3rd ed., Pergamon Press, Oxford, **1967**, pp 206–209.

[14] J. W. Fronabarger, M. D. Williams, A. G. Stern, D. A. Parrish, *Cent. Eur. J. Energ. Mat.* **2016**, *13*, 33–52.

[15] A. K. S. Mehilal, S. Pawar, N. Skider, *J. Hazard. Mater.* **2002**, *90*, 221–227.

[16] J. W. Fronabarger, M. D. Williams, W. B. Sanborn, D. A. Parrish, M. Bichay, *Propellants Explos. Pyrotech.* **2011**, *36*, 459–470.

[17] E. L. Müller, T. M. Klapötke, J. Stierstorfer, M. F. Bölter, M. Völkl, DetNet South Africa (Pty.) Ltd., WO Patent 2018209366A2, South Africa **2018**.

[18] T. Urbanski, *Chemistry and Technology of Explosives*, 3rd ed., Pergamon Press, Oxford, **1967**, pp 213–215.

[19] J. W. Fronabarger, M. D. Williams, W. B. Sanborn, J. G. Bragg, D. A. Parrish, M. Bichay, *Propellants Explos. Pyrotech.* **2011**, *36*, 541–550.

[20] S. G. Zhu, Y. C. Wu, W. Y. Zhang, J. G. Mu, *Propellants Explos. Pyrotech.* **1997**, *22*, 317–320.

[21] R. Matyáš, J. Šelešovský, T. Musil, *J. Hazard. Mater.* **2012**, *213–214*, 236–241.

[22] T. Urbanski, *Chemistry and Technology of Explosives*, 3rd ed., Pergamon Press, Oxford, **1967**, pp 182–184.

[23] United States Military Specification 46225C (MIL-L-46225C), lead azide RD-1333 (for use in ammunition), **1968**.

[24] T. Pasinszki, M. Krebsz, B. Hajgato, *Chem. Phys. Lett.* **2009**, *473*, 343–347.

3. Synthesis and Comparison of Copper(II) Complexes with Various *N*-Aminotetrazole Ligands Involving Trinitrophenol Anions

Maximilian H. H. Wurzenberger, Benjamin R. G. Bissinger, Marcus Lommel, Michael S. Gruhne, Norbert Szimhardt, and Jörg Stierstorfer

Adapted from *New Journal of Chemistry* **2019**, *43*, 18193–18202 with permission from the Centre National de la Recherche Scientifique (CNRS) and The Royal Society of Chemistry.

DOI: 10.1039/c9nj03937f

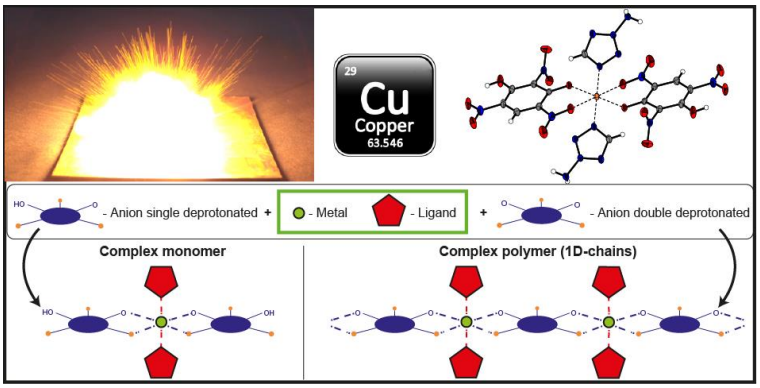

Abstract: Due to the ongoing research on lead-free energetic materials, two different ligand systems (1-amino-5*H*-tetrazole (1-AT), 2-amino-5*H*-tetrazole (2-AT), 1-amino-5-methyltetrazole (1-AMT), and 2-amino-5-methyltetrazole (2-AMT)) were applied for the synthesis of 12 new energetic coordination compounds (ECC) with copper(II) as the central metal. Different anions based on trinitrophenols (picric acid (HPA), styphnic acid (H_2TNR), and trinitrophloroglucinol (H_3TNPG)) were used for the specifical tuning of the energetic and physicochemical properties of the complexes. Through the choice of ligand, the characteristics of the resulting products can be easily adjusted either toward sensitive primary explosives usable for classical initiation setups or toward laser-ignitable explosives with decreased sensitivities. The ECC were extensively characterized by *e.g.*, X-ray diffraction (XRD), elemental analysis (EA), IR, differential thermal analysis (DTA), and UV-Vis. In addition, the most promising compounds were analyzed by TGA and in classical initiation tests using nitropenta (PETN). Furthermore, the sensitivities toward external stimuli (impact, friction, and electrostatic discharge) were determined by standard methods and the influence of the anions toward them was investigated. Compounds [Cu(TNR)(1-AMT)$_2$] and [Cu(HTNPG)(1-AMT)$_2$] both possess appropriate sensitivities as well as thermal stabilities above 200 °C and show promising results to be used as potential lead azide replacements. In addition, all ECC were irradiated with a near infrared light (NIR) laser diode leading to different responses.

3.1. Introduction

The energetic character of many nitroaromatic compounds derives from the oxidation of the carbon-backbone and the circumstance that these substances combine both the fuel (C–H backbone) and the oxidizer (nitro groups) within one molecule. As a result of this, selected polynitroaromatics can be used as explosives, most notably trinitrotoluene (TNT).[1] A close structural relative of TNT is picric acid (HPA, **1**) (Chart 1), which was discovered in the form of its potassium salt by Johann Glauber in 1742.[2]

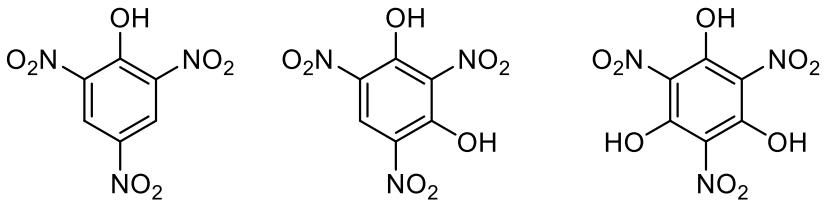

Chart 1. Trinitrophenols picric acid (**1**), styphnic acid (**2**) and trinitrophloroglucinol (**3**).

The compound was obtained *via* treatment of wool or horn with HNO_3 and has since been applied as a dye for silk, and, due to its intensely bitter taste and tinctorial power, as a replacement for hops in beer. However, it wasn't until more than 100 years later that German chemist Hermann Sprengel demonstrated that picric acid could be brought to detonation, and therefore filed the related patents. Following this, HPA replaced black powder in nearly all military applications.[2–4] Styphnic acid (H_2TNR, **2**) and 2,4,6-trinitrophloroglucinol (H_3TNPG, **3**) derive structurally from picric acid and have a wide history of military applications together with their metal salts. The most prominent is lead styphnate (LS), a rather sensitive and highly toxic primary explosive. Together with lead azide (LA), LS has been employed since the beginning of the 20th century and was originally developed as a replacement for mercury fulminate.[2,5] One major drawback of the highly acidic compounds **1–3** is their potential to corrode metal shells, along with the formation of the corresponding highly sensitive metal salts. This process significantly lowers the manageability of such explosives and is known to have caused fatal accidents.[6] With LA and LS still being the most predominantly used primary explosives *e.g.*, in small arms ammunition, people in frequent contact with firearms and commercial applications (mining, deconstruction works, *etc.*) are at high risk of chronic damage due to heavy metal poisoning. A recent study revealed elevated blood lead levels in regular visitors of shooting ranges, accredited to the discharge of lead upon firing a gun. The adverse health effects associated with shooting are especially critical to women and children, relating to the impact on future generations.[7] In order to reduce or even prevent the use of toxic explosives, scientists all around the world are focusing on the development of new substances with superior properties.[8–15] One very promising concept for replacing toxic primary explosives which has gained increasing attention in recent

years is focused on the laser ignition of energetic materials. By combining the right building blocks, this approach could ensure lifelong economic efficiency with environmentally friendly disposal management. At the same time, it can increase safety by allowing the application of less sensitive explosives.[16] 3D metal coordination compounds with trinitrophenolates of **1–3** as counter anions are known in the literature for only a few tetrazole derivatives, especially TNPG-based anions are rather uncommon. Copper(II) complexes have a unique position among these described compounds since in every single example the anions coordinate to the central metal and thus in almost all cases anhydrous compounds are obtained. Especially, the nitroaromatic complexes based on Mn(II), Co(II), Ni(II), and Zn(II) have a high tendency to incorporate aqua ligands, crystal water molecules or even both of them.[17–23] Another characteristic of styphnic acid and trinitrophloroglucinol is their ability to work either as singly or multiply deprotonated anions and it has also been shown that within one ligand system both cases can be obtained. A great advantage of the twofold deprotonation of trinitrophenols is their potential to bridge different metal centers. In contrast, abstraction of a single proton usually leads to complex monomers (Figure 1).[24] The linking of the anions allows the formation of polymeric structures with varying properties such as increased thermal stabilities.

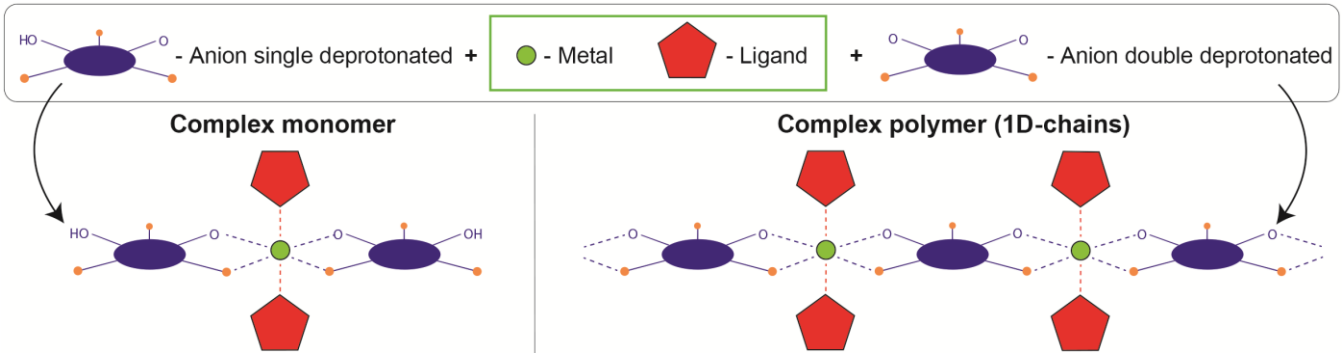

Figure 1. Schematic overview of the formation of either complex monomers (left) or polymeric structures (right) caused by the deprotonation level of the nitroaromatic anions.

Recently, our research group published several of the most powerful ECC available, based on 1-amino-5*H*-tetrazole (1-AT) and 2-amino-5*H*-tetrazole (2-AT), in combination with highly oxidizing anions such as perchlorate and nitrate.[25] Some of the most auspicious of these candidates combine excellent energetic properties with good thermal stabilities and low environmental toxicities, however, the highly endothermic aminotetrazole ligands and oxidizing anions induce extreme sensitivities to various mechanical stimuli. This diminishes their applicability as primary explosives in classical, as well as optical initiation systems. To manage the excessive energetic capacities and sensitivities of 1-AT and 2-AT based ECC, we replaced the common anions nitrate and perchlorate with nitroaromatic mono- and dianions of **1–3**. Furthermore, an additional methyl group was introduced at the 5-position of the ligands

(1-amino-5-methyltetrazole (1-AMT) and 2-amino-5-methyltetrazole (2-AMT)) to further stabilize the system by lowering the enthalpies of formation (Figure 2).

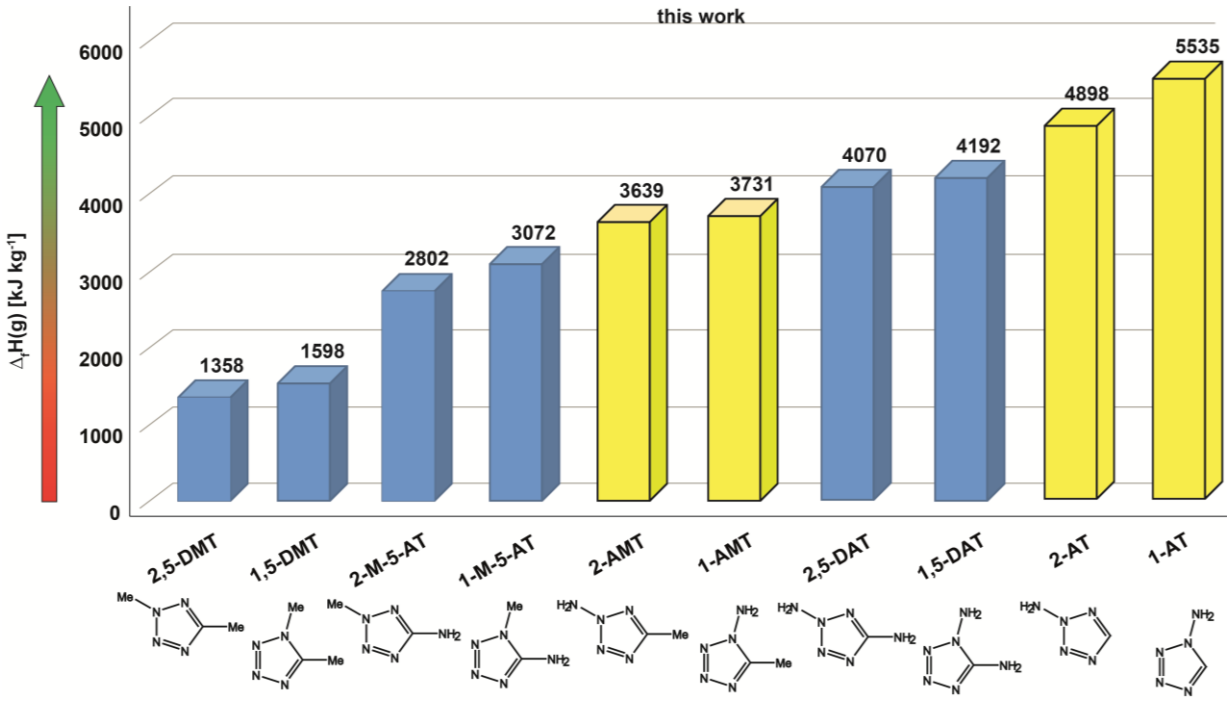

Figure 2. Comparing of the calculated enthalpies of formation for several *N*-substituted monotetrazoles showing decreased values for AMT ligands compared to AT. Gas phase enthalpies of formation were calculated using the atomization method ($\Delta_f H^0_{(g,\ M)} = H_{(M)} - \Sigma H^0_{(A)} + \Sigma \Delta_f H^0_{(A)}$) using Gaussian09 computed CBS-4M electronic enthalpies.

This extensive study describes the effect of various *N*-aminotetrazole ligands on nitroaromatic copper(II) complexes and their selective potential to be used as either laser ignitable explosives or as classical lead-free primary explosives for the initiation of PETN (nitropenta). Furthermore, the influence of the level of deprotonation as well as the number of hydroxy groups in the anions toward the properties of the ECC is compared.

3.2. Results and Discussion

3.2.1. Synthesis

1-AMT (**4b**) and 2-AMT (**5b**) were prepared in accordance with the synthesis[25] of **4a** and **5a** *via* nucleophilic amination of commercially available 5-methyl-1*H*-tetrazole with hydroxylamine-*O*-sulfonic acid under basic conditions, giving the isomers **4b** and **5b** in 33% and 25% yield, respectively (Scheme 1). Due to the positive inductive effect of the additional methyl group, which increases the nucleophilicity of the electron-poor heterocycle, the overall yield of the reaction could be increased compared to the amination of unsubstituted tetrazole (58% *vs.* 46%). In analogy to **4a**, 1-AMT can be obtained directly

and isomerically pure *via* a simple and scalable three-step reaction.[25] The synthesis is initiated by the condensation of benzaldehyde and hydrazine hydrate, followed by [3+1+1] cyclization with sodium azide and triethyl orthoacetate, which generates the 5-methyltetrazole-moiety (**4b_pro**). Cleavage under acidic conditions followed by water steam distillation furnishes the ligand **4b** in a relatively low yield of 18% (Scheme 2).

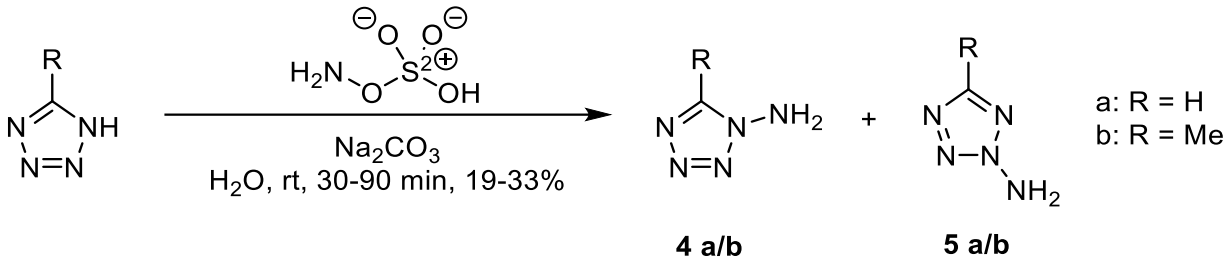

Scheme 1. Synthesis of aminotetrazole ligands **4** and **5** by amination of 1*H*-tetrazole with hydroxylamine-*O*-sulfonic acid (HOSA).

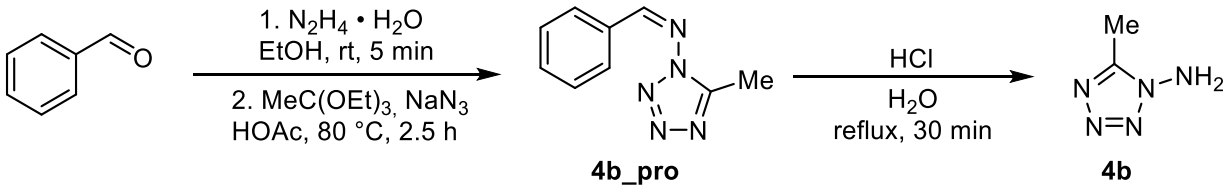

Scheme 2. Selective synthesis of 1-amino-5-methyltetrazole (1-AMT, **4b**).

The isomers **4b** and **5b** can easily be differentiated by IR (Figure S1) or by ^{1}H and ^{13}C NMR spectroscopy. Furthermore, proton coupled ^{15}N NMR measurements were performed for both compounds (Figures 3 and 4).

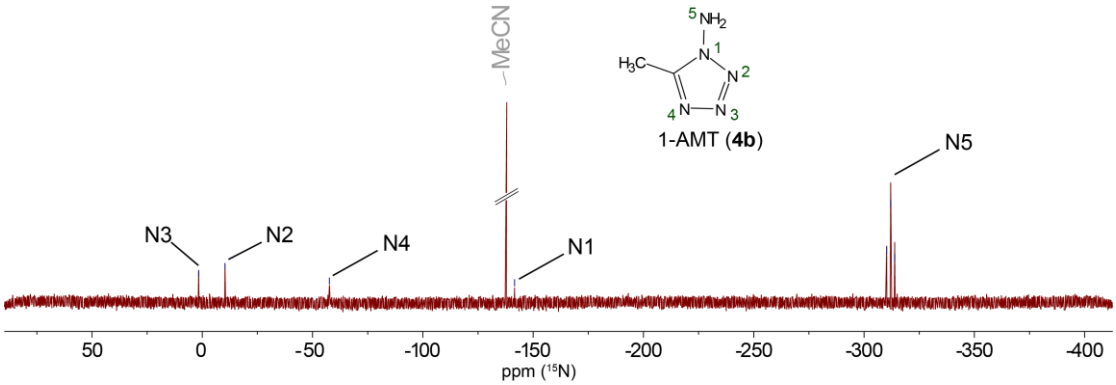

Figure 3. Proton coupled ^{15}N NMR spectra of **4b**.

The synthesis of ECC **6**–**17** starts with the *in situ* generation of the copper(II) salt of the required trinitrophenol, which is achieved by reaction of copper(II) carbonate with the respective acid **1**–**3** in aqueous medium at elevated temperatures. In the case of amino-5*H*-tetrazole derivates, each of the performed syntheses was carried out by slow addition of an aqueous solution of the ligand to the

respective solution of metal(II) salt at 80 °C (Schemes 3 and 4). After continuous stirring of the particular reaction mixture, the solutions were left for crystallization at room temperature. After a few days, the compounds were filtered off, washed with ethanol and dried in air. This synthetic strategy can easily be performed on a large scale and the products can be isolated almost quantitatively if the solvent of the reaction mixture is removed by rotary evaporation.

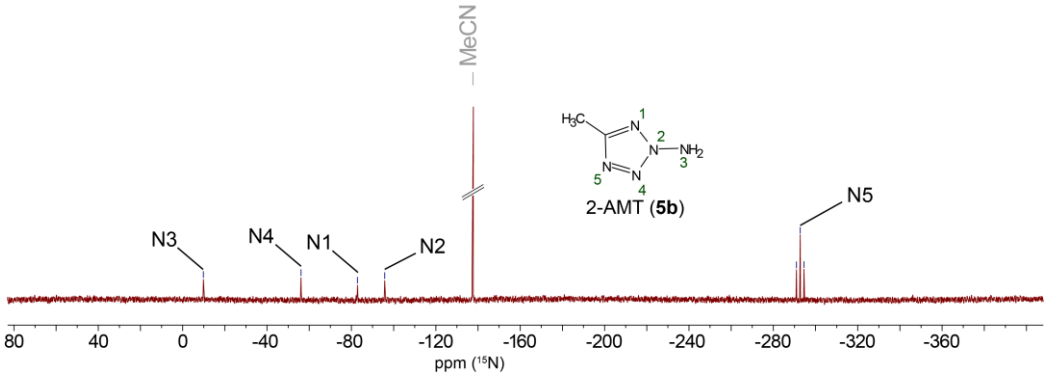

Figure 4. Proton coupled ^{15}N NMR spectra of **5b**.

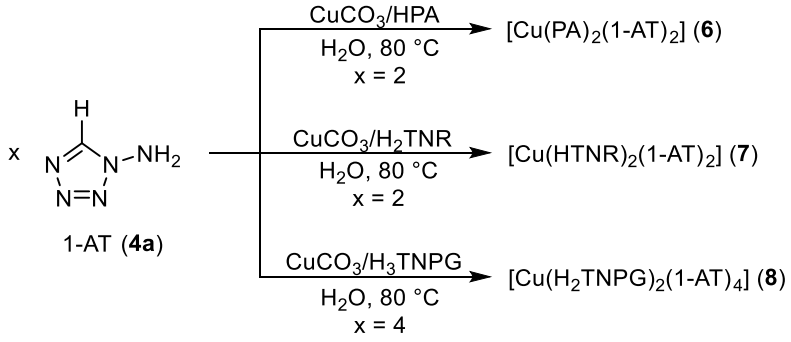

Scheme 3. Synthesis of copper(II) picrate, 3-hydroxy-2,4,6-trinitrophenolate and 3,5-dihydroxy-2,4,6-trinitrophenolate complexes **6**–**8** of 1-AT (**4a**).

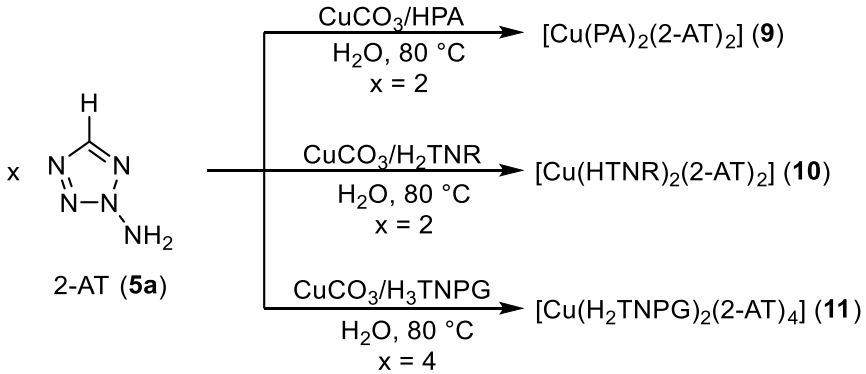

Scheme 4. Synthesis of the ECC **9**–**11** based on 2-amino-5*H*-tetrazole (2-AT, **5a**).

Synthesis of the analogous AMT-based complexes **12–17** proceeded identically (Schemes 5 and 6), the only noteworthy divergence being the immediate precipitation of green and brown solids during the synthesis of compounds **13** and **14a**, respectively. Both compounds form polymeric structures that arise

from the twofold deprotonation of the corresponding anions (**13**: styphnate, **14a**: 5-hydroxy-2,4,6-trinitroresorcinate) leading to bridging between different central metals, which significantly reduces their water solubility. All other isolated AMT-complexes were obtained after crystallization from the mother liquor within a few days. After formation, the products were filtered off, washed with ethanol and dried in air. Even though final products **13** and **14a** are formed of only one equivalent of the corresponding anions, for complete reaction of copper(II) carbonate twice the amount of free acid is required. Interestingly, the formation of a second (**14b**) and a third (**14c**) species during the reaction of copper(II) carbonate, trinitrophloroglucinol and 1-AMT was observed.

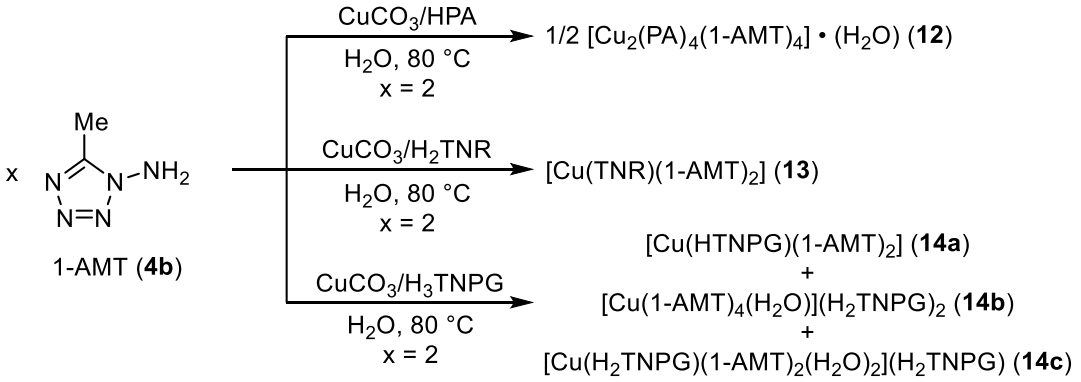

Scheme 5. Synthesis of copper(II) picrate (PA), styphnate (TNR) and 2,4,6-trinitrophloroglucinol-based (HTNPG/H_2TNPG) complexes of 1-amino-5-methyltetrazole (1-AMT, **4b**).

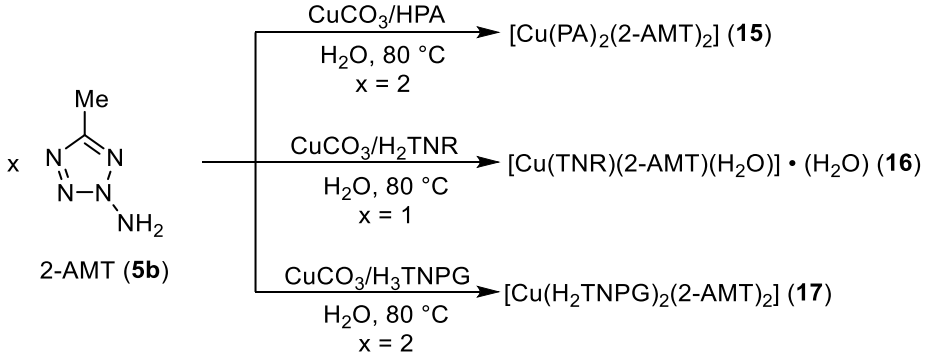

Scheme 6. Synthesis of ECC **15**–**17** based on 2-amino-5-methyltetrazole (2-AMT, **5b**).

Single crystal experiments reveal the composition of two different aqua complexes [Cu(1-AMT)$_4$(H_2O)](H_2TNPG)$_2$ (**14b**) and [Cu(H_2TNPG)(1-AMT)$_2$(H_2O)$_2$](H_2TNPG) (**14c**) with only singly deprotonated anions (3,5-dihydroxy-2,4,6-trinitrophenolate). The dark green needles of **14a** crystallized quickly from the filtrate and accumulated on the inner walls of the crystallization vessel. Contrary to **14a**, however, **14b** turned out to be extremely water-soluble, which prevented the execution of further analytical investigation, because sufficient amounts could not be isolated. Similar to **14b**, **14c** is highly water soluble and some single crystals could only be obtained after complete desiccation of the filtrate of **14a**. To the best of our knowledge, **14b** and **14c** are the first copper(II) complexes with non-coordinating

counter anions based on trinitrophenols of **1–3**. Compared to the anhydrous compounds **6–11** it becomes clear that the AMT ligands slightly increase the hydrophilicity of the formed products and thus the formation of complexes with aqua ligands (**14b** and **14c**), crystal water molecules (**12**) or even both of them (**16**) can partly be observed.

3.2.2. Crystal Structures

Nitrogen-rich ligand **4b** and its precursor **4b_pro**, as well as all ECC, were investigated by low-temperature single crystal X-ray diffraction. In contrast to their 1-amino isomers, 2-AT (**5a**) and 2-AMT (**5b**) were not able to be crystallized, even when subjected to liquid nitrogen. The crystal structure of ligand **4a** has already been published;[25] the results of the crystallographic analysis of **4b_pro** (Figure S4) are given in the Supporting Information, together with the measurement and refinement data of all experiments (Tables S1–S4). The crystal datasets were uploaded to the CSD database[26] and can be obtained free of charge with the CCDC 1934808 (**4_pro**), 1934810 (**4b**), 1934799 (**6**), 1934801 (**7**), 1934798 (**8**), 1934809 (**9**), 1934811 (**10**), 1934812 (**11**), 1934806 (**12**), 1934805 (**13**), 1934803 (**14a**), 1934807 (**14b**), 1934813 (**14c**), 1934800 (**15**), 1934802 (**16**), and 1934804 (**17**). All complexes, except side species **14b**, show octahedral coordination spheres around the copper(II) central cations with typical Jahn-Teller distortions along the axial O–Cu–O axes. In every structure, the ligands are solely coordinating through the N4 nitrogen atom of the tetrazole rings. In almost all compounds electrostatic intermolecular interactions can be observed, leading to specific orientations of the nitro groups of the phenolate anions. Normally the nitro groups of the trinitrophenols are aligned with the aromatic system, while nitro-nitro interactions between different anions twist one or two of the functional groups in the complexes. This perpendicular arrangement of nitro groups enables the electrostatic interaction of the vertical π-orbital with the oxygen atom of a second nitro group. The distances O_{Nitro}–$\pi(N)_{Nitro}$ in the crystal structures lie in the typical range of nitro-nitro interactions described in the literature.[27] Similar to **4a**,[25] tetrazole **4b** crystallizes in the orthorhombic space group $P2_12_12_1$ with four formula units per unit cell and a slightly lower calculated density of 1.420 g cm^{-3} at 143 K. This relatively significant difference in density arises from the presence of the methyl group in **4b**, preventing closer packing due to the increased steric hindrance (Figure 5). It crystallizes in the form of colorless blocks and all non-hydrogen atoms lie within a plane with torsion angles close to 0° (C1–N1–N2–N3 1.25(15)°, N5–N1–C1–C2−2.2(2)°, and N2–N1–C1–N4−1.13(16)°). The bond angles and lengths lie within the range of typical values for tetrazole compounds and differ only slightly from 1-AT. Picrate compounds **6** (green platelets) and **12** (green blocks) crystallize in similar monoclinic space groups $P2_1/c$ and $P2_1/n$ with calculated densities of 1.952 g cm^{-3} and 1.786 g cm^{-3} at 143 K, respectively. The slightly distorted octahedral coordination

spheres – **12** shows a stronger deviation than **6** – around the copper(II) central cations in both crystal structures show similar compositions. The central metals are surrounded by two monodentate tetrazole ligands and two chelating picrate anions. $[Cu(PA)_2(1\text{-}AT)_2]$ (**6**) represents a centrosymmetric unit in itself with *trans* coordinating 1-AT ligands, while in $[Cu_2(PA)_4(1\text{-}AMT)_4] \bullet H_2O$ (**12**) the pairs of ligand molecules and picrate anions each occupy adjacent coordination sites (Figure 6). The molecular unit of picrate **12** is a dimer consisting of two of the previously described asymmetric units and an additional crystal water molecule, where the coordinating picrate anions are facing each other in the center of the unit and are twisted against each other at angles of approximately 90°. Complexes **7** and **13**, based on 2,4,6-trinitroresorcinol, crystallize in the monoclinic and orthorhombic space groups $P2_1/c$ and $Pna2_1$ as green platelets and needles, respectively. Their calculated densities of 1.905 g cm^{-3} and 1.887 g cm^{-3} at 143 K vary only slightly. Except for the crystal water molecule, the compounds' chemical building blocks and the arrangement of those are comparable to those of the analogue picrate complexes **6** and **12**. ECC **7** forms complex monomers with a highly symmetrical structure, in which 1-AT and anionic 3-hydroxy-2,4,6-trinitrophenolate ligands oppose each other.

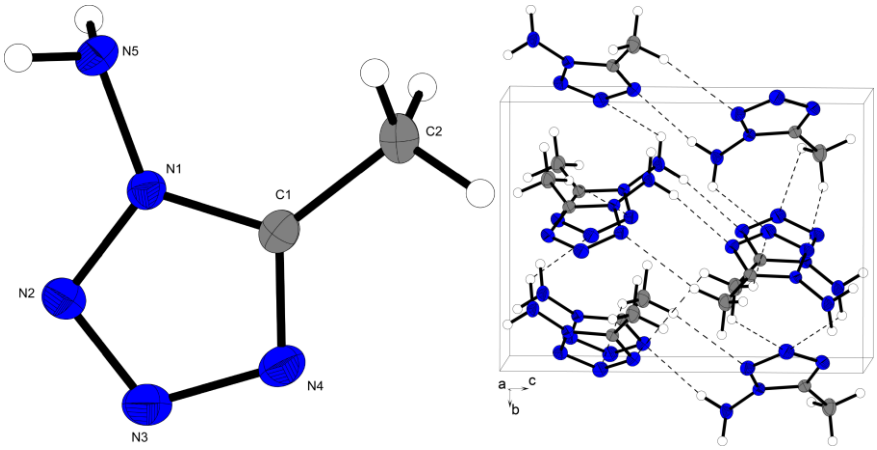

Figure 5. Molecular unit (left) and unit cell (right) of 1-AMT (**4b**). Thermal ellipsoids of nonhydrogen atoms in all structures are set to the 50% probability level. Selected bond lengths (Å): N1–N2 1.3482(16), N1–N5 1.3908(17), N1–C1 1.3341(18), N2–N3 1.2959(19), N3–N4 1.3648(19), N4–C1 1.3206(19); selected bond angles (°): N2–N1–N5 123.54(11), N2–N1–C1 109.92(12), N5–N1–C1 126.53(12), N3–N4–C1 106.14(12), N4–C1–C2 127.78(13).

In fact, both coordinating molecules of 1-AT lie in the same plane and are aligned perfectly parallel, the singly deprotonated anions span two parallel planes. In 1-AMT-based compound **13** the pairs of ligand molecules and styphnate anions again occupy adjacent coordination sites (Figure 7). The twofold deprotonation of styphnic acid in **13** leads to the formation of 1D-polymeric chains, in which each dianion bridges between two copper(II) centers. The monoanions existent in **7** are not suitable for linking between metal centers as they only possess a single coordination site, and thus two of them are required per formula unit.

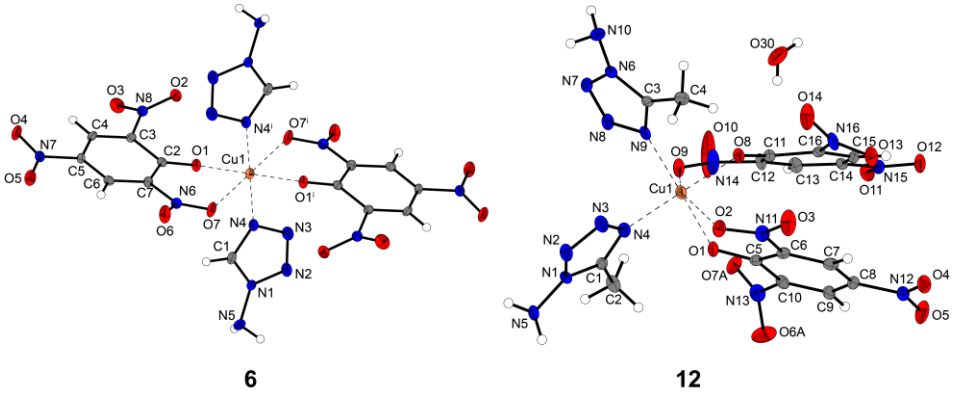

Figure 6. Molecular unit of [Cu(PA)$_2$(1-AT)$_2$] (**6**) (left) and segment of the unit cell of [Cu$_2$(PA)$_4$(1-AMT)$_4$] • H$_2$O (**12**) (right). Selected bond lengths (Å) of **6**: Cu1–O1 1.918(3), Cu1–O7 2.338(3), Cu1–N4 2.010(3); selected bond angles (°) of **6**: O1–Cu1–O7 78.92(10), O1–Cu1–N4 90.18(12), O7–Cu1–N4 86.01(11). Symmetry code of **6**: (i) 2−x, −y, 2−z. Selected bond lengths (Å) of **12**: Cu1–O2 2.467(3), Cu1–O8 1.946(3), Cu1–N4 1.972(3), Cu1–N9 1.995(3); selected bond angles (°) of **12**: O1–Cu1–O2 74.07(11), O1–Cu1–N4 90.31(13), O1–Cu1–N9 171.19(13), N4–Cu1–N9 89.82(14).

Comparing the styphnate complexes **7** and **13** with the analogous trinitrophloroglucinol-based compounds, it becomes clear that the complexation of the central metal is different in the case of **8** and almost identical for **14a**. They crystallize in the monoclinic space group $P2_1/n$ (**8**) as green-yellow rods and orthorhombic space group $Pna2_1$ (**14a**) as brown needles with calculated densities of 1.928 g cm^{-3} (173 K) and 1.891 g cm^{-3} (143 K), respectively. The crystal structure of **8** is composed of four neutral 1-AT ligands and two 3,5-dihydroxy-2,4,6-trinitrophenolate monoanions around octahedrally coordinated copper(II) centers. The singly deprotonated anions are monodentate and are building up the Jahn-Teller distortion along the axial O1–Cu–O1^{i} axis (Figure 8). All equatorial positions are occupied by tetrazole derivatives, which form hydrogen bonds with their amino function to nitro groups of the anions and tetrazole rings of neighbouring complex monomers. The primary species obtained from copper(II) carbonate, trinitrophloroglucinol and 1-AMT, [Cu(HTNPG)(1-AMT)$_2$] (**14a**), crystallizes isotypically to **13** with similar cell axes, density, and cell volume. Again, the double deprotonation leads to higher distortion and the formation of polymeric 1D chains. The coordination polymer is otherwise almost identical to **13**. The side species **14b** and **14c** both crystallize as green rods in monoclinic space groups ($P2_1/c$ and $P2_1/n$) with calculated densities of 1.798 g cm^{-3} (143 K) and 1.948 g cm^{-3} (111 K), respectively. While **14b** shows a rare square pyramidal coordination sphere around the copper(II) center, the coordination sphere of **14c** is a highly distorted octahedron. In contrast to **14a**, **14b** possesses non-coordinating anions and, similar to **8**, **11** and **17**, the TNPG-based monoanions are present as 3,5-dihydroxy-2,4,6-trinitrophenolates stacked on top of each other. They form hydrogen bonds to amino groups of neighbouring tetrazole ligands and typical nitro-nitro interactions between each other. The coordination sphere around the copper(II) central metal in **14b** is composed of one aqua and four ligand

molecules of 1-AMT (Figure 9). The water molecule represents the tip of the pyramid with a slightly longer Cu–O bond (2.230 Å) compared to the Cu–N bonds (1.997–2.005 Å). To minimise steric hindrance, pairs of opposing tetrazole ligands are arranged with the methyl groups facing in alternating directions and the two heterocycles are slightly angled, leading to a distorted plane of coordinating nitrogen atoms (N14–N4–N9–N19 23.7(1)°). The molecular unit of **14c** consists of one non-coordinating and one chelating monoanion, as well as two aqua and two tetrazole ligands. Interestingly, the Jahn-Teller distortion along the O2–Cu1–O10 axis shows one very long Cu–O bond (Cu1–O2 2.4665(14) Å), while the second is only slightly elongated (Cu1–O10 2.1604(16) Å).

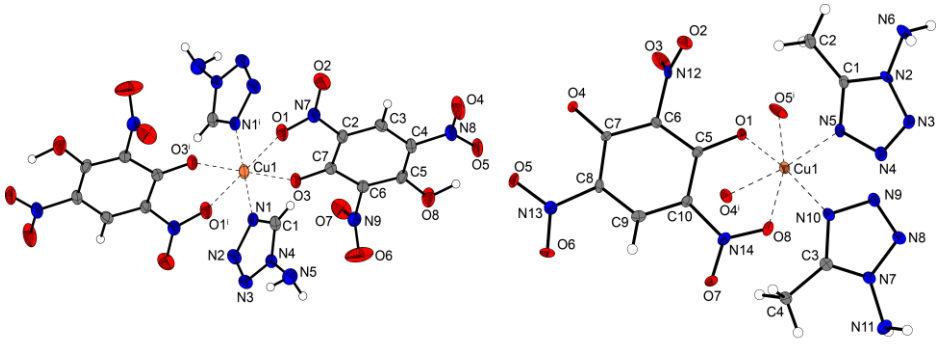

Figure 7. Molecular unit of [Cu(HTNR)$_2$(1-AT)$_2$] (**7**) (left) and the copper(II) coordination environment of [Cu(TNR)(1-AMT)$_2$] (**13**) (right). Selected bond lengths (Å) of **7**: Cu1–O1 2.316(3), Cu1–O3 1.962(2), Cu1–N1 1.998(3); selected bond angles (°) of **7**: O1–Cu1–O3 81.17(10), O1–Cu1–N1 87.63(12), O3–Cu1–N1 90.00(11). Symmetry code of **7**: (i) 2−x, 1−y, 1−z. Selected bond lengths (Å) of **13**: Cu1–O1 1.958(5), Cu1–O8 2.515(6), Cu1–N5 1.994(6), Cu1–N10 2.010(6); selected bond angles (°) of **13**: O1–Cu1–O8 72.54(16), O1–Cu1–N5 86.0(2), O1–Cu1–N10 167.1(2), N5–Cu1–N10 94.7(2). Symmetry code of **13**: (i) 1−x, 2−y, 0.5+z.

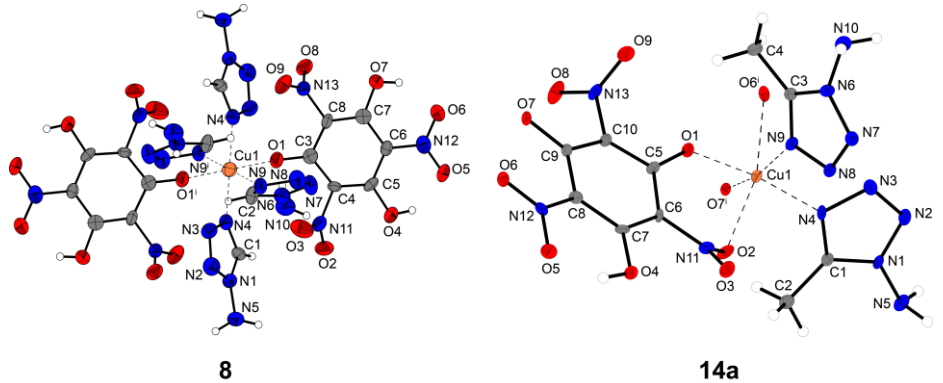

Figure 8. Molecular unit of [Cu(H$_2$TNPG)$_2$(1-AT)$_4$] (**8**) (left) and the copper(II) coordination environment of [Cu(HTNPG)(1-AMT)$_2$] (**14a**) (right). Selected bond lengths (Å) of **8**: Cu1–O1 2.348(4), Cu1–N4 2.015(5), Cu1–N9 1.986(5); selected bond angles (°) of **8**: O1–Cu1–N4 87.64(17), O1–Cu1–N9 96.28(17), N4–Cu1–N9 91.1(2). Symmetry code of **8**: (i) 1−x, 1−y, 1−z. Selected bond lengths (Å) of **14a**: Cu1–O1 1.933(4), Cu1–O2 2.252(5), Cu1–N4 1.985(6), Cu1–N9 2.007(6); selected bond angles (°) of **14a**: O1–Cu1–O2 81.56(18), O1–Cu1–N4 171.7(2), O1–Cu1–N9 90.8(2), N4–Cu1–N9 95.5(2). Symmetry code of **14a**: (i) 1−x, 1−y, −0.5+z.

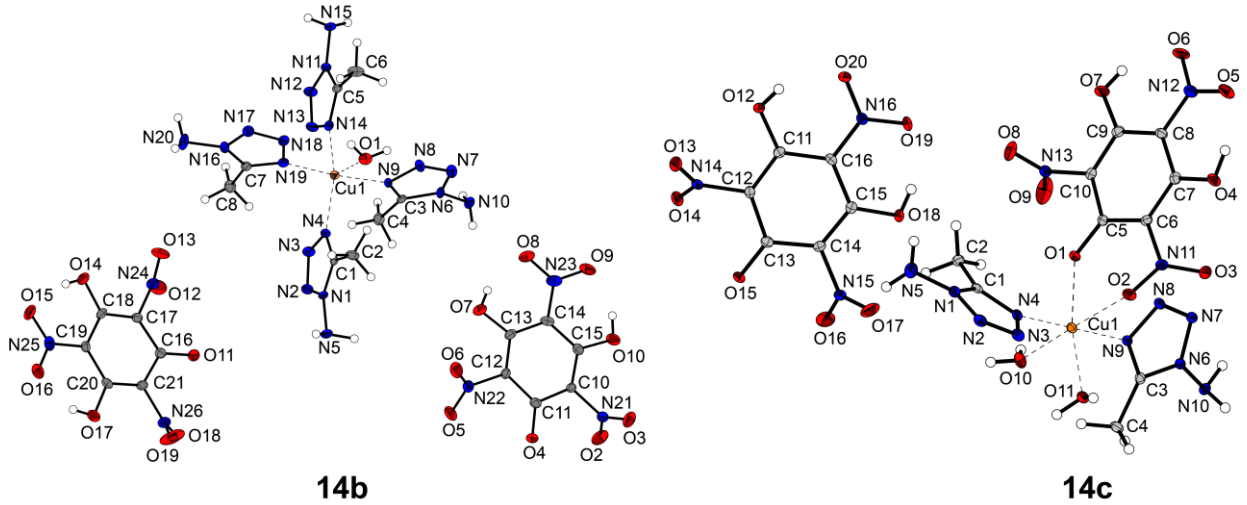

Figure 9. Molecular units of side species $[Cu(1\text{-}AMT)_4(H_2O)](H_2TNPG)_2$ (**14b**) (left) and $[Cu(H_2TNPG)(1\text{-}AMT)_2(H_2O)_2](H_2TNPG)$ (**14c**) (right). Selected bond lengths (Å) of **14b**: Cu1–O1 2.230(3), Cu1–N4 2.000(3), Cu1–N9 2.005(3), Cu1–N14 1.997(3), Cu1–N19 1.997(3); selected bond angles (°) of **14b**: O1–Cu1–N4 103.93(12), O1–Cu1–N9 87.27(12), N4–Cu1–N9 92.78(12), N4–Cu1–N14 149.23(11), N4–Cu1–N19 92.08(12), N9–Cu1–N19 174.14(12). Selected bond lengths (Å) of **14c**: Cu1–O1 1.9934(15), Cu1–O11 2.0671(17), Cu1–N4 1.9784(16), Cu1–N9 1.9856(16); selected bond angles (°) of **14c**: O1–Cu1–O2 74.84(6), O1–Cu1–O10 107.90(6), O1–Cu1–O11 163.97(6), O1–Cu1–N4 88.60(7), O1–Cu1–N9 91.36(7), N4–Cu1–N9 179.38(7).

Even though the coordination environments of the copper(II) centets of picrate complexes **9** and **15** are almost identical and show similar densities (**9**: 1.905 g cm^{-3} @ 173 K; **15**: 1.860 g cm^{-3} @ 143 K), they crystallize in fundamentally different space groups. $[Cu(PA)_2(2\text{-}AT)_2]$ (**9**) crystallizes as green needles in the monoclinic $P2_1/c$ and $[Cu(PA)_2(2\text{-}AMT)_2]$ (**15**) as green blocks in the triclinic space group $P\bar{1}$. The equatorial positions are occupied by deprotonated hydroxyl groups and two *trans* coordinating aminotetrazole ligands. In the case of 2-AT based complex **9**, the two heterocycles are aligned antiparallel, whereas, in complex **15**, the 2-AMT molecules are roughly mirrored in the equatorial plane. The axial positions are occupied by two nitro functions of the picrate anion (Figure 10). Whereas **9**, similar to picrate complex **6**, shows highly symmetric coordination of the ligands, compound **15** possesses a greater deviation from the perfect octahedron. It is the only AMT-based compound with methyl groups pointing in the same direction, leading to higher steric hindrance (N4–Cu1–N9 172.08(10)°) and thus lower symmetry. Styphnate compound **10** shows an almost identical composition to its 1-AT isomer **7** and crystallizes in the triclinic space group $P\bar{1}$ with a calculated density of 1.864 g cm^{-3} at 173 K in the form of green blocks. Its 5-methyltetrazole analogue **16** crystallizes as green rods in the monoclinic space group $P2_1/c$ with a calculated density of 1.949 g cm^{-3} at 143 K. The only similarity with its 1-AMT analogue **13** is the formation of polymer strands due to the twofold deprotonation of the anion. However, complex **16** only contains one neutral heterocycle and an additional aqua ligand, which are located *cis* to each other (Figure 11).

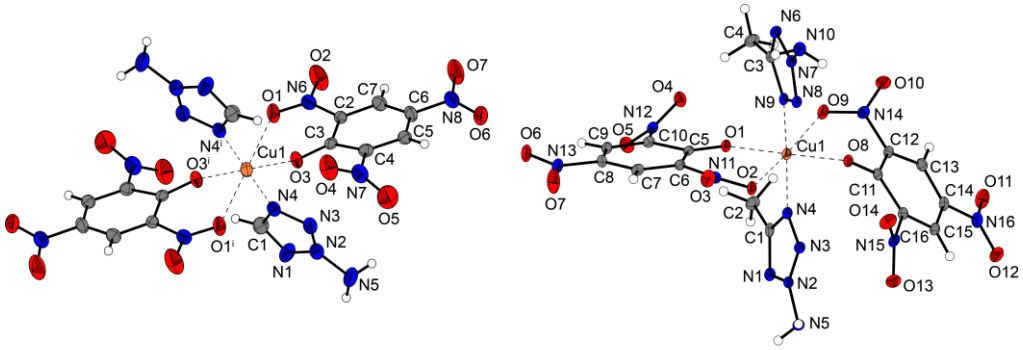

9 **15**

Figure 10. Molecular unit of $[Cu(PA)_2(2\text{-}AT)_2]$ (**9**) (left) and $[Cu(PA)_2(2\text{-}AMT)_2]$ (**15**) (right). Selected bond lengths (Å) of **9**: Cu1–O1 2.321(2), Cu1–O3 1.941(2), Cu1–N4 1.982(3); selected bond angles (°) of **9**: O1–Cu1–O3 80.03(9), O1–Cu1–N4 87.69(10), O3–Cu1–N4 92.42(10). Symmetry code of **9**: (i) −x, 1−y, 1−z. Selected bond lengths (Å) of **15**: Cu1–O1 1.933(2), Cu1–O2 2.335(2), Cu1–N4 2.003(2); selected bond angles (°) of **15**: O1–Cu1–O2 80.73(8), O1–Cu1–N4 89.67(9), O2–Cu1–N4 88.15(9).

Also, a molecule of crystal water is present in **16**, which is fixed inside the structure by four hydrogen bonds. 3,5-Dihydroxy-2,4,6-trinitrophenolate complexes **11** and **17** both crystallize as green blocks in the triclinic space group *P*−1 with similar calculated densities of 1.909 g cm^{-3} (173 K) and 1.939 g cm^{-3} (143 K), respectively. Again, **11** shows an identically constructed coordination sphere to 1-AT isomer **8** with four 2-AT ligands in the equatorial plane and monodentate H_2TNPG monoanions in axial positions. Compared to **11**, the octahedron in complex **17** consists only of two tetrazole ligands, and once again two H_2TNPG monoanions, which are in this case chelating (Figure 12). The presence of the anions as 3,5-dihydroxy-2,4,6-trinitrophenolate (like in **8**, **11**, **14b**, and **14c**) is preventing the bridging between different copper(II) centers.

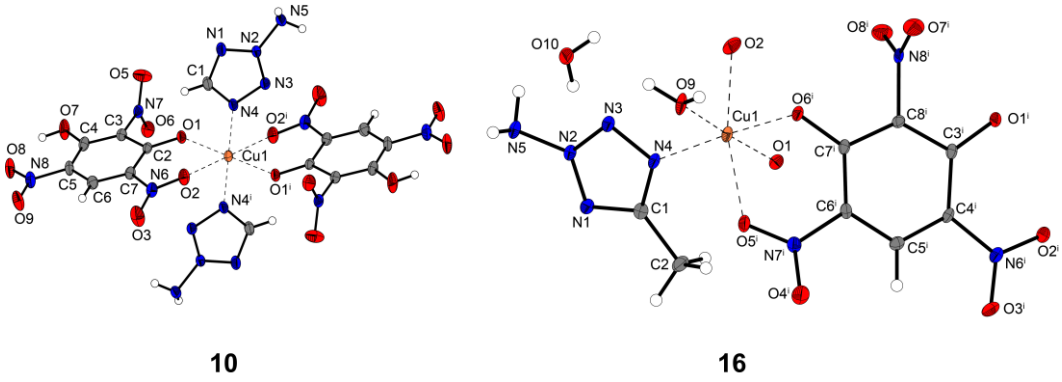

10 **16**

Figure 11. Molecular unit of $[Cu(HTNR)_2(2\text{-}AT)_2]$ (**10**) (left) and extended molecular unit of $[Cu(TNR)(2\text{-}AMT)(H_2O)] \bullet H_2O$ (**16**) (right). Selected bond lengths (Å) of **10**: Cu1–O1 1.9410(12), Cu1–O2 2.3932(13), Cu1–N4 1.9858(14); selected bond angles (°) of **10**: O1–Cu1–O2 78.44(5), O1–Cu1–N4 88.72(6), O2–Cu1–N4 88.65(5). Symmetry code of **10**: (i) −x, 2−y, −z. Selected bond lengths (Å) of **16**: Cu1–O1 1.941(2), Cu1–O2 2.284(2), Cu1–O9 1.968(2), Cu1–N4 2.005(2); selected bond angles (°) of **16**: O1–Cu1–O2 82.20(8), O1–Cu1–O9 176.78(9), O1–Cu1–N4 90.48(8), O2–Cu1–N4 92.83(9), O9–Cu1–N4 92.70(10). Symmetry code of **16**: (i) 1−x, −0.5+y, 0.5−z.

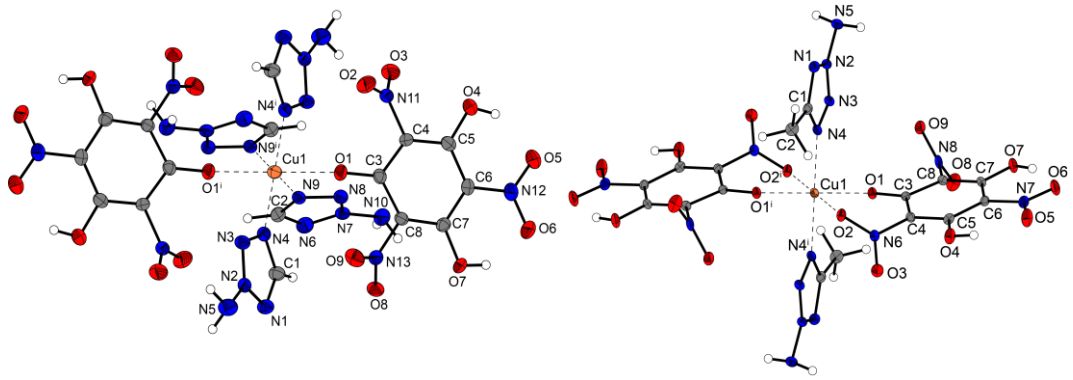

Figure 12. Molecular unit of $[Cu(H_2TNPG)_2(2\text{-}AT)_4]$ (**11**) (left) and $[Cu(H_2TNPG)_2(2\text{-}AMT)_2]$ (**17**) (right). Selected bond lengths (Å) of **11**: Cu1–O1 2.3614(18), Cu1–N4 2.007(2), Cu1–N9 2.0101(19); selected bond angles (°) of **11**: O1–Cu1–N4 88.38(7), O1–Cu1–N9 95.38(7), N4–Cu1–N9 89.16(9). Symmetry code of **11**: (i) 1−x, 1−y, −z. Selected bond lengths (Å) of **17**: Cu1–O1 1.9180(19), Cu1–O2 2.354(2), Cu1–N4 2.022(3); selected bond angles (°) of **17**: O1–Cu1–O2 81.50(9), O1–Cu1–N4 91.12(10), O2–Cu1–N4 92.03(10). Symmetry code of **17**: (i) −x, 1−y, −z.

3.2.3. Sensitivities and Thermal Stability

Ligands **4b** and **5b**, as well as energetic complexes **6–17**, with the exception of side-products **14b** and **14c**, were subjected to differential thermal analysis (DTA) by heating at a constant rate of β = 5 °C min^{-1} in the temperature range of 25–400 °C. Critical points, such as dehydration, loss of a coordinating ligand or decomposition, are listed in Table 1 and are given as onset temperatures. The DTA plots can be found in the Supporting Information (Figures S18–S24). All investigated compounds exhibit exothermic decomposition temperatures above 170 °C. Five of the examined ECC (**9**, **10**, **13**, **14a**, and **17**) even surpass a decomposition temperature of 200 °C. Styphnate **13**, the compound with the highest decomposition temperature of all investigated complexes (T_{exo} = 212 °C) derives its high thermal stability from its polymeric structure. A similar case can be observed in ECC **14a** (T_{exo} = 202 °C) with bridging trinitrophenolate anions. However, the relatively low decomposition temperature of the only other 2-AMT-based coordination polymer **16** (T_{exo} = 172 °C) can be explained by the presence of aqua ligands and crystal water molecules. The loss of both (T_{endo} = 122 °C and 160 °C) destabilizes the crystal structure, leading to a lower exothermic decomposition temperature. Comparison of the 1-AMT complexes to those featuring 5*H*-tetrazole ligands reveals higher exothermic stabilities for the methyltetrazole based compounds. In the case of the 2-amino isomers, it is the other way round. The ECC based on 2-AT are thermally more stable than the analogous 2-AMT complexes. Apart from **16**, an endothermic peak is only observed in the DTA plot of **11** and is caused by the evaporation of coordinating 2-AT ligands. More detailed investigations using thermal gravimetric analysis (TGA) reveals the loss of two tetrazole derivatives (≙18.4%) starting at 135 °C (Figure 13).

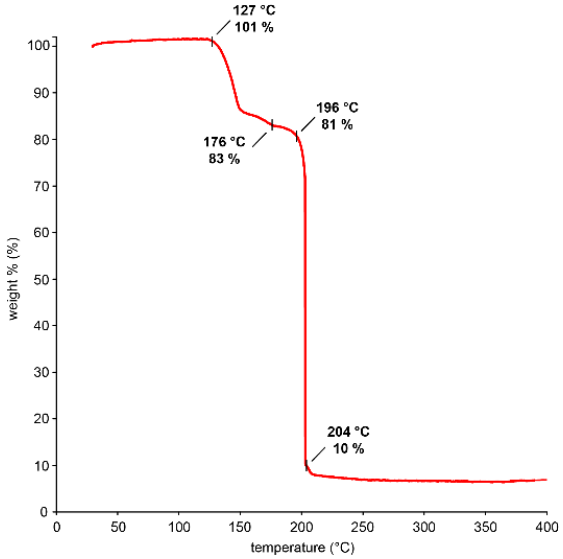

Figure 13. TGA plot of **11** showing the loss of two aminotetrazole ligands starting at 127 °C followed by the decomposition of the compound.

TGA measurements of ECC **6**, **8**, **11–13**, and **16** clearly show the loss of water molecules in **12** as well as in **16**, and no significant mass loss in the other measured compounds, which proves their thermal stability up to the corresponding exothermic decomposition points (Figure S17).

Table 1. Data of thermal stability measurements by DTA[a], as well as sensitivities toward various external stimuli and results of hot plate (HP) and hot needle (HN) experiments of **4a**–**5b** and **6**–**17**.

	$T_{endo.}$[b] [°C]	$T_{exo.}$[c] [°C]	*IS*[d] [J]	*FS*[e] [N]	*ESD*[f] [mJ]	*BDIS*[g] [mJ]	HP[h]	HN[h]
1-AT (**4a**)	-	182[23]	< 1[26]	64[26]	n.d.	n.d.	n.d.	n.d.
2-AT (**5a**)	-	197[23]	< 1[26]	36[26]	n.d.	n.d.	n.d.	n.d.
1-AMT (**5b**)	-	190	> 40	360	n.d.	n.d.	n.d.	n.d.
2-AMT (**5b**)	-	176	35	> 360	n.d.	n.d.	n.d.	n.d.
$[Cu(PA)_2(1\text{-}AT)_2]$ (**6**)	-	178	4	120	50	207	def.	def.
$[Cu(HTNR)_2(1\text{-}AT)_2]$ (**7**)	-	186	1.5	48	16	14	def.	def.
$[Cu(H_2TNPG)_2(1\text{-}AT)_4]$ (**8**)	-	193	3.5	20	90	14	def.	def.
$[Cu(PA)_2(2\text{-}AT)_2]$ (**9**)	-	203	3	128	60	> 207	def.	def.
$[Cu(HTNR)_2(2\text{-}AT)_2]$ (**10**)	-	206	3	48	20	55	def.	def.
$[Cu(H_2TNPG)_2(2\text{-}AT)_4]$ (**11**)	135	176	2	24	100	14	def.	def.
$[Cu_2(PA)_4(1\text{-}AMT)_4] \bullet H_2O$ (**12**)	-	190	2	168	88	> 207	def.	def.
$[Cu(TNR)(1\text{-}AMT)_2]$ (**13**)	-	212	2	16	6.3	10	def.	def.
$[Cu(HTNPG)(1\text{-}AMT)_2]$ (**14a**)	-	202	1	7	4.9	8	def.	det.
$[Cu(PA)_2(2\text{-}AMT)_2]$ (**15**)	-	176	2.5	108	37	> 207	def.	def.
$[Cu(TNR)(2\text{-}AMT)(H_2O)] \bullet H_2O$ (**16**)	122, 160	172	2.5	38	840	69	def.	def.
$[Cu(H_2TNPG)_2(2\text{-}AMT)_2]$ (**17**)	-	202	2	20	8.2	41	def.	def.
$Pb(N_3)_2$[29]	-	320–360	2.5–4.0	0.1–1.0	7.0	n.d.	n.d.	n.d.
PETN[29]	141–143	163–170	3.0–4.2	73	60	n.d.	n.d.	n.d.

[a] Onset temperatures at a heating rate of 5 °C min^{-1}. [b] Endothermic peak, which indicates melting, dehydration or loss of coordinating molecules. [c] Exothermic peak, which indicates decomposition. [d] Impact sensitivity according to the BAM drop hammer (method 1 of 6). [e] Friction sensitivity according to the BAM friction tester (method 1 of 6). [f] Electrostatic discharge sensitivity (OZM Electric XSpark10) (method 1 of 6). [g] Ball drop impact sensitivity determined with the 1 of 6 method in accordance with the MIL-STD 1751A (method 1016). [h] def.: deflagration, det.: detonation.

Due to the fact that the crystal morphology has a high effect on sensitivities as well as performance parameters (*e.g.*, a higher sensitivity against ESD with decreasing crystal size[30]), the compounds' grain size and habit were determined by light microscopy (Figures S5–S16). The sensitivities toward impact (IS) and friction (FS) of the compounds were determined according to BAM standard techniques (1 of 6) and they have been classified in accordance with the "UN Recommendations on the Transport of Dangerous Goods".[31] Furthermore, the electrostatic discharge sensitivity (ESD) of all isolated ECC was analyzed and all measurement data are summarized in Table 1. Comparing the free ligands, it becomes clear that the additional methyl group in 1-AMT and 2-AMT is drastically increasing the stability of the aminotetrazole derivatives against external stimuli. Concerning the impact sensitivity, all ECC show similar values against impact and, except **6** and **8** ("sensitive"), have to be classified as "very sensitive". In the case of FS, a clear trend is observable, revealing an increase of the sensitivity with the number of hydroxy groups of the anion (Figures 14 and S25–S27), leading to the general trend: PA (all friction "sensitive") < TNR ("very sensitive") ≤ TNPG ("very sensitive" or even "extremely sensitive" (**14a**)). Due to the more realistic conditions during ball drop impact sensitivity (BDIS) measurements, ECC **6**–**17** were all tested and show a similar trend in comparison to the determined FS. This confirms our previous findings[22] that the sensitivity against ball drop impact shows a higher correlation with FS than with IS. Interestingly, ECC **13** and **14a**, based on a less sensitive ligand, both show the most sensitive values against external stimuli. The multiple deprotonations of nitroaromatic anions lead not only to higher thermal stability but also to increased sensitivities. This concept can be used for the synthesis and design of sensitive but thermally stable primary explosives for classical initiation devices.

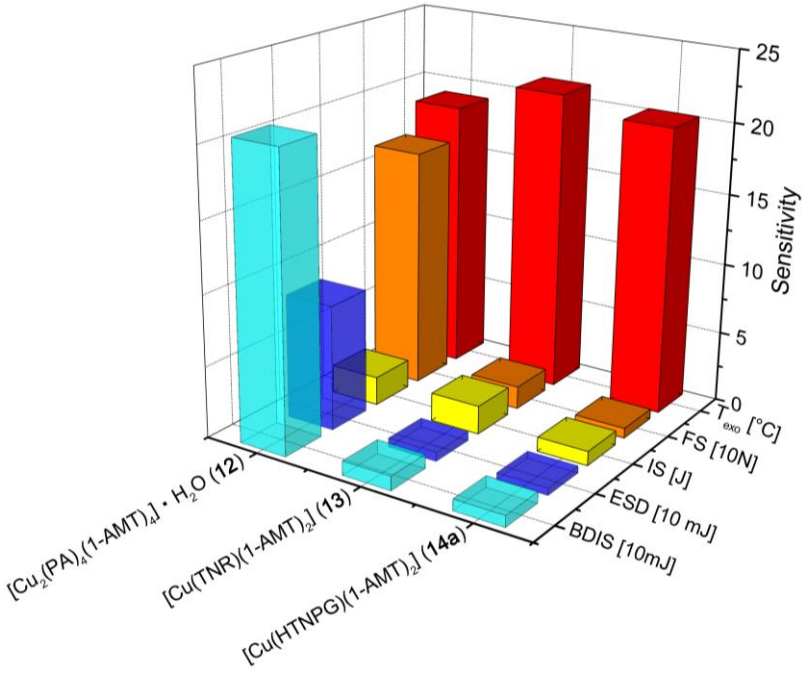

Figure 14. Comparing the sensitivities against external stimuli of the ECC **12**–**14a**.

3.2.4. Primary Explosive Suitability Evaluation

In order to get an insight into the compounds' behavior against fast heating with and without confinement, hot plate (HP) and hot needle (HN) tests were performed with all ECC (Figures 15 and S28–S41), except for side species **14b** and **14c**. The results are displayed in Table 1 and furthermore allow a preliminary evaluation of their applicability to be used for the initiation of energetic materials. The most promising compounds in these tests have been found to be the 1-AMT-based copper(II) styphnate (**13**) and 5-hydroxy-2,4,6-trinitroresorcinate (**14a**) complexes, which showed either sharp deflagrations or even detonations in this setup. For their potential use as lead-free primary explosives, both compounds were tested toward their capability of initiating pentaerythritol tetranitrate (PETN). Therefore, 200 mg of the booster explosive was loaded into a copper shell and the test substance was filled on top (Figure 16).

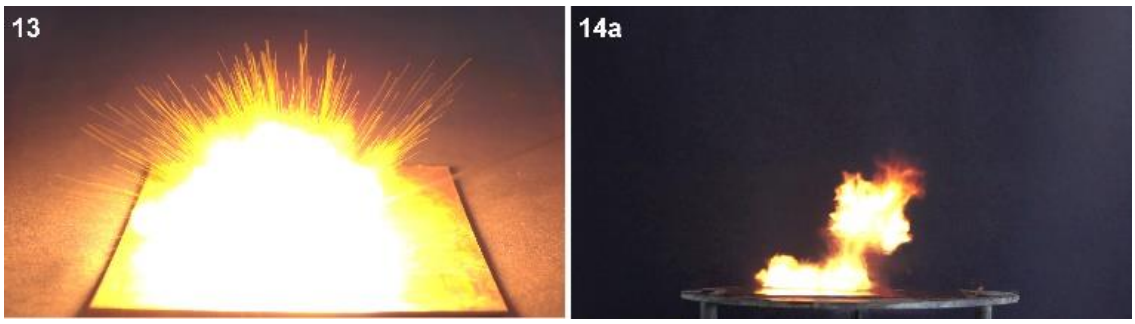

Figure 15. Moments of deflagration of **13** (left) during hot needle and **14a** (right) during hot plate test.

Figure 16. Schematic setup of PETN initiation capability test (left) as well as positive results of ECC **13** (middle) and **14a** (right).

More details on the test setup can be found in the General methods of the Supporting Information. Positive transfer of the detonation wave from the primary explosive toward PETN is indicated by a hole in the copper witness plate and fragmentation of the shell. Both compounds were able to initiate nitropenta; whereas **13** worked in our standard setup with pressed PETN, **14a** was only successful in combination with uncompressed PETN (Figure 16). Due to the known fact that unconfined PETN requires much lower energies than the compressed one,[30] **13** is the more powerful primary explosive compared to **14a**. Additionally, **13** shows a 10 °C higher thermal stability and is slightly less sensitive toward all tested external stimuli (IS, FS, ESD, and BDIS) making its manageability safer.

3.2.5. Laser Initiation Experiments

The most tremendous benefits of laser initiation over classical ignition methods (thermal or mechanical) are the applicability of less sensitive compounds and the resulting lower risk of unintended ignition.[16] Therefore, this research area has gained increasing interest within the energetic material community and a lot of investigations were performed.[17,20,32–34] All complexes, except **14b** and **14c**, were irradiated with an InGaAs laser diode working in single-pulsed mode. Details of the applied test setup can be found in the Supporting Information. All examined ECC showed a reaction toward the laser irradiation, differing in the intensity of the outcome (Table 2 and Figures S42–S53). The most interesting compounds in this investigation are the ones showing both decreased impact and friction sensitivities (≥3 J, ≥48 N), which are close to the values of PETN.[29]

Table 2. Results of the laser initiation experiments.[a]

E_{max} [mJ]	0.17	0.20	0.24	3.00	25.5	30.0	36.0
6	dec.	dec.	-	-	-	-	dec.
7	def.	-	-	-	det.	-	-
8	def.	-	-	def.	-	-	-
9	dec.	dec.	-	-	-	-	dec.
10	def.	def.	-	-	def.	-	-
11	def.	-	-	-	-	def.	det.
12	-	-	-	-	-	dec.	dec.
13	-	-	-	-	dec.	-	dec.
14a	neg.	-	dec.	-	-	dec.	-
15	-	dec.	-	-	-	-	dec.
16	-	-	-	dec.	-	dec.	-
17	dec.	dec.	-	-	-	-	-

[a] -: not tested; neg.: no reaction; dec.: decomposition; def.: deflagration; det.: detonation. Operating parameters: voltage U = 4 V; wavelength λ = 915 nm; current I = 7–9 A; pulse length τ = 0.1–15 ms; theoretical maximal output power P_{max} = 45 W; theoretical energy E_{max} = 0.17–36.0 mJ.

These values pose slightly increased sensitivities toward mechanical stimuli but still allow safe handling of the material. Interestingly, all complexes based on AMT ligands solely exhibit decomposition or no reaction at all, regardless of the energy they are irradiated with. In the case of the aminotetrazole compounds, the picrates display the same outcome, whereas the HTNR- and H_2TNPG-based ECC deflagrate at lower energies or can even be detonated (**7** and **11**) when irradiated with higher values. Comparing the more sensitive compounds (**7**, **8**, **11**, **13**, **14a**, and **17**), it becomes clear that the most sensitive ones (**13**, **14a**, and **17**) and also the most energetic ones in classical initiation tests (**13** and **14a**) show lower performance in this setup, which is not in accordance with our previous findings.[17,20,22]

3.2.6. UV-Vis Spectroscopy

UV-Vis spectra in the solid state were recorded for the examined ECC **6–17**, except **14b** and **14c**, in the range of 350–1000 nm (Figures S54–S57), to reveal any possible correlation between the absorption intensity and wavelength of the laser diode. The discovered optical properties of the complexes are summarized in Table 3. All ECC show characteristic transitions in the near infrared, visible and UV regions, as well as moderate to very strong absorption at a laser wavelength of 915 nm. The observed absorptions can mainly be assigned to the d–d transitions of the copper(II) centers. In accordance with previous investigations, the positive reaction toward laser irradiation could be explained by the imaginable formation of several hot spots within the compounds caused by photothermal excitation after irradiation.[16] Interestingly, there is no trend between the absorption intensity at the laser wavelength and the resulting outcome of the irradiation.

Table 3. Summary of the discovered optical properties of the examined ECC **6**–**17**.

Compound	M	Color	$\lambda_{d\text{-}d}$[a]	$\lambda_{915}/\lambda_{d\text{-}d}$[b]
6	Cu(II)	green	405	0.45
7	Cu(II)	green	410	0.65
8	Cu(II)	green-yellow	356	0.35
9	Cu(II)	green	424	0.43
10	Cu(II)	green	412	0.52
11	Cu(II)	green	437	0.56
12	Cu(II)	green	431	0.64
13	Cu(II)	green	459	0.57
14a	Cu(II)	brown	409	0.53
15	Cu(II)	green	426	0.68
16	Cu(II)	green	610	0.97
17	Cu(II)	green	388	0.40

[a] Absorption intensity maximum wavelength in the observed range of 350–1000 nm, which can be assigned to electron d–d transitions. [b] Quotient of the absorption intensity at the laser wavelength and the intensity at the d–d absorption wavelength

3.3. Conclusion

In this extensive study, the nitrogen-rich ligands 1-amino- (**4a**, 1-AT) and 2-amino-5*H*-tetrazole (**5a**, 2-AT) as well as 1-amino- (**4b**, 1-AMT) and 2-amino-5-methyltetrazole (**5b**, 2-AMT) were successfully applied for the synthesis of new copper(II) complexes. It could be demonstrated that ligands **4b** and **5b** tend to form complexes with higher thermal stability and lower sensitivity. The crystal structures of 16 (12 main products, 2 side species, one ligand, and one precursor) compounds were elucidated by low-temperature single crystal X-ray diffraction and compared in detail. Especially the use of anions based on trinitrophloroglucinol offers a wide range of different complexes with various as well as interesting coordination modes. Furthermore, like styphnic acid, it allows the formation of polymeric structures

through the multiple deprotonation of its hydroxy groups, which is accompanied by an increase in thermal stability. Interestingly, the ECC based on the more energetic and more sensitive AT-ligands show better stabilities against external stimuli, such as impact and friction, than the analogous compounds containing AMT derivatives. Whereas complexes **13** and **14a** were able to successfully initiate nitropenta, **7**, **8**, **10**, and **11** show promising results during the laser ignition experiments. Due to their deflagrations at already 0.17 mJ they are interesting candidates for future laser ignition devices, while **13** and **14a** could be potential replacements for lead azide in classic initiation devices. The low performances of the AMT complexes when irradiated with NIR wavelengths indicate that systems based on copper(II) and nitroaromatic anions with these are not very suitable for laser initiation or need substantially higher energies.

3.4. Acknowledgements

Financial support of this work from the Ludwig-Maximilians-University of Munich (LMU). The authors would like to thank Prof. Dr. Thomas M. Klapötke for his scientific support as well as for providing his research facilities and, furthermore, Prof. Dr. Konstantin Karaghiosoff for measuring the ^{15}N NMR spectra. Mr. Andreas Bartonek and Mrs. Jasmin Lechner are given thanks for their great contribution to this work.

3.5. References

[1] T. M. Klapötke, *Chemistry of High-Energy Materials*, 4th ed., De Gruyter, Berlin, Boston, **2017**.

[2] J. Akhavan, *The Chemistry of Explosives*, 2nd ed., Royal Society of Chemistry, Cambridge, **2004**.

[3] H. Sprengel, *The Discovery of Picric Acid (Melinite, Lyddite) ''As a Powerful Explosive'' and of Cumulative Detonation with its Bearing on wet Gun Cotton*, 2nd ed., Eyre & Spottiswoode, London, **1903**.

[4] H. Sprengel, British Patent 921, UK **1871**.

[5] J. S. Wallace, *Chemical Analysis of Firearms, Ammunition, and Gunshot Residue*, 1st ed., CRC Press, Boca Raton, **2008**.

[6] J. P. Agrawal, R. D. Hodgson, *Organic Chemistry of Explosives*, 1st ed., John Wiley & Sons, Hoboken, **2007**.

[7] M. A. S. Laidlaw, G. Filippelli, H. Mielke, B. Gulson, A. S. Ball, *Environ. Health* **2017**, *16*, 34/1–34/15.

[8] R. V. Kent, T. P. Vaid, J. A. Boissonnault, A. J. Matzger, *Dalton Trans.* **2019**, *48*, 7509–7513.

[9] Y. Liu, G. Zhao, Y. Tang, J. Zhang, L. Hu, G. H. Imler, D. A. Parrish, J. M. Shreeve, *J. Mater. Chem. A* **2019**, *7*, 7875–7884.

[10] E. C. Johnson, E. J. Bukowski, J. J. Sabatini, R. C. Sausa, E. F. C. Byrd, M. A. Garner, D. E. Chavez, *ChemPlusChem* **2019**, *84*, 319–322.

[11] Q. Sun, X. Li, Q. Lin, M. Lu, *J. Mater. Chem. A* **2019**, *7*, 4611–4618.

[12] A. A. Larin, N. V. Muravyev, A. N. Pivkina, K. Y. Suponitsky, I. V. Ananyev, D. V. Khakimov, L. L. Fershtat, N. N. Makhova, *Chem. – Eur. J.* **2019**, *25*, 4225–4233.

[13] R. Haiges, K. O. Christe, *Dalton Trans.* **2015**, *44*, 10166–10176.

[14] J.-G. Xu, X.-Z. Li, H.-F. Wu, F.-K. Zheng, J. Chen, G.-C. Guo, *Cryst. Growth Des.* **2019**, *19*, 3934–3944.

[15] J.-G. Xu, C. Sun, M.-J. Zhang, B.-W. Liu, X.-Z. Li, J. Lu, S.-H.Wang, F.-K. Zheng, G.-C. Guo, *Chem. Mater.* **2017**, *29*, 9725–9733.

[16] S. R. Ahmad, M. Cartwright, *Laser Ignition of Energetic Materials*, 1st ed., John Wiley & Sons, Ltd., Hoboken, **2015**.

[17] N. Szimhardt, M. H. H. Wurzenberger, A. Beringer, L. J. Daumann, J. Stierstorfer, *J. Mater. Chem. A* **2017**, *5*, 23753–23765.

[18] Y. Cui, T. L. Zhang, J. G. Zhang, L. Yang, J. Zhang, X. Hu, *Propellants Explos. Pyrotech.* **2008**, *33*, 437–442.

[19] Y. Cui, J. G. Zhang, T. L. Zhang, L. Yang, Y. Zhang, Y. J. Shu, *Chin. J. Chem.* **2008**, *26*, 2029–2034.

[20] N. Szimhardt, M. H. H. Wurzenberger, T. M. Klapötke, J. T. Lechner, H. Reichherzer, C. C. Unger, J. Stierstorfer, *J. Mater. Chem. A* **2018**, *6*, 6565–6577.

[21] Y.-G. Bi, Y.-A. Feng, Y. Li, B.-D. Wu, T.-L. Zhang, *J. Coord. Chem.* **2015**, *68*, 181–194.

[22] M. H. H. Wurzenberger, M. S. Gruhne, M. Lommel, N. Szimhardt, T. M. Klapötke, J. Stierstorfer, *Chem. – Asian J.* **2019**, *14*, 2018–2028.

[23] Y. Cui, J. G. Zhang, T. L. Zhang, L. Yang, J. Zhang, X. Hu, *J. Hazard. Mater.* **2008**, *160*, 45–50.

[24] N. Szimhardt, M. H. H. Wurzenberger, L. Zeisel, M. S. Gruhne, M. Lommel, T. M. Klapötke, J. Stierstorfer, *Chem. – Eur. J.* **2019**, *25*, 1963–1974.

[25] N. Szimhardt, M. H. H. Wurzenberger, L. Zeisel, M. S. Gruhne, M. Lommel, J. Stierstorfer, *J. Mater. Chem. A* **2018**, *6*, 16257–16272.

[26] Crystallographic data for the structures has been deposited with the Cambridge Crystallographic Data Centre. Copies of the data can be obtained free of charge on application to The Director, CCDC, 12 Union Road, Cambridge CB2 1EZ, UK (Fax: int.code_(1223)336-033; e-mail for inquiry: fileserv@ccdc.cam.ac.uk; e-mail for deposition: (deposit@ccdc.cam.ac.uk)).

[27] M. Daszkiewicz, *CrystEngComm* **2013**, *15*, 10427–10430.

[28] T. M. Klapötke, D. G. Piercey, J. Stierstorfer, *Dalton Trans.* **2012**, *41*, 9451–9459.

[29] T. M. Klapötke, *Energetic Materials Encyclopedia*, 1st ed., De Gruyter, Berlin, Boston, **2018**.

[30] R. Matyáš, J. Pachman, *Primary Explosives*, 1st ed., Springer, Berlin, **2013**.

[31] Impact: insensitive > 40 J, less sensitive ≥ 35 J, sensitive ≥ 4 J, very sensitive ≤ 3 J; friction: insensitive > 360 N, less sensitive = 360 N, sensitive < 360 N and > 80 N, very sensitive ≤ 80 N, extremely sensitive ≤ 10 N. According to the UN Recommendations on the Transport of Dangerous Goods, 5th ed., **2009**.

[32] D. E. Chavez, S. K. Hanson, R. J. Scharff, J. M. Veauthier, T. W. Myers, Triad National SecurityLLC, US Patent 20160031767 A1, USA **2015**.

[33] S. I. Gerasimov, M. A. Ilyushin, I. V. Shugalei, A. V. Smirnov, Z. V. Kapitonenko, *Russ. J. Gen. Chem.* **2017**, *87*, 3156–3159.

[34] W. Guo, L. Wu, N. He, S. Chen, W. Zhang, R. Shen, Y. Ye, *Laser Part. Beams* **2018**, *36*, 29–40.

3.6. Supporting Information

3.6.1. Compound Overview

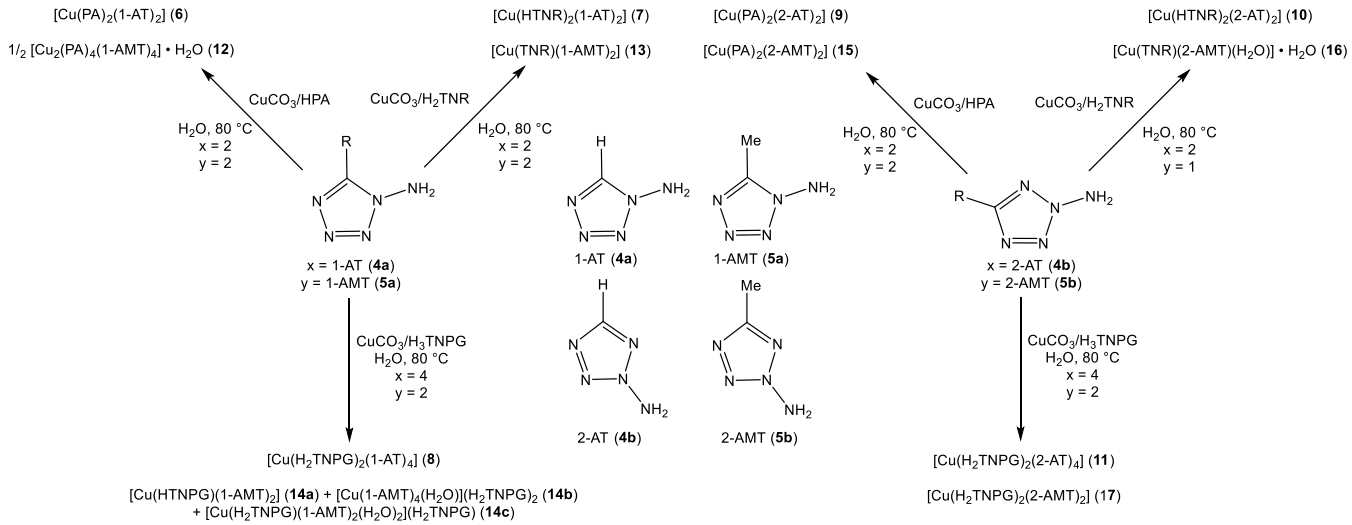

3.6.2. IR Spectroscopy of 4b, 5b, and 6–17

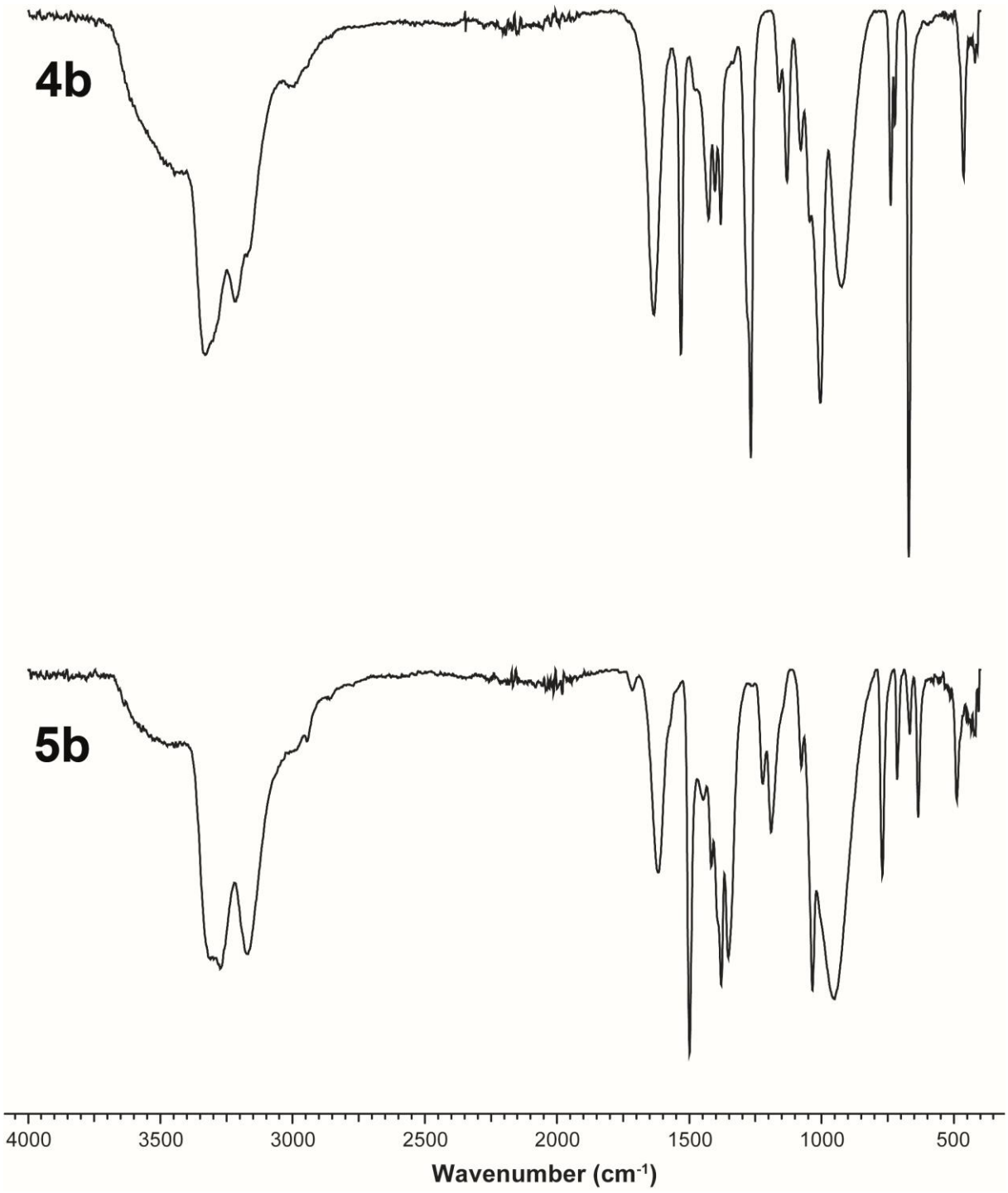

Figure S1. Infrared spectra of nitrogen-rich compounds **4b** and **5b**.

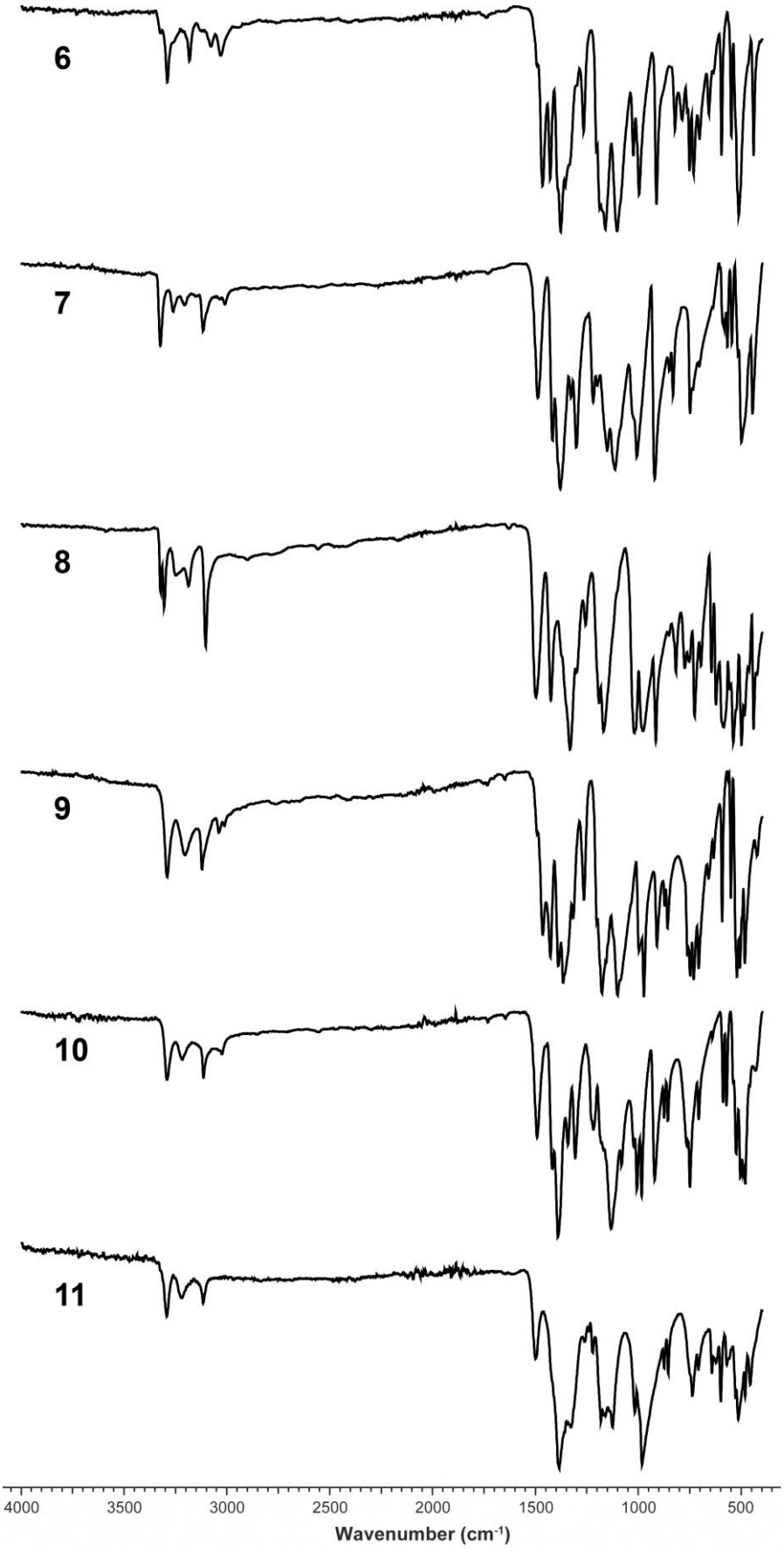

Figure S2. IR spectra of **6**–**11**.

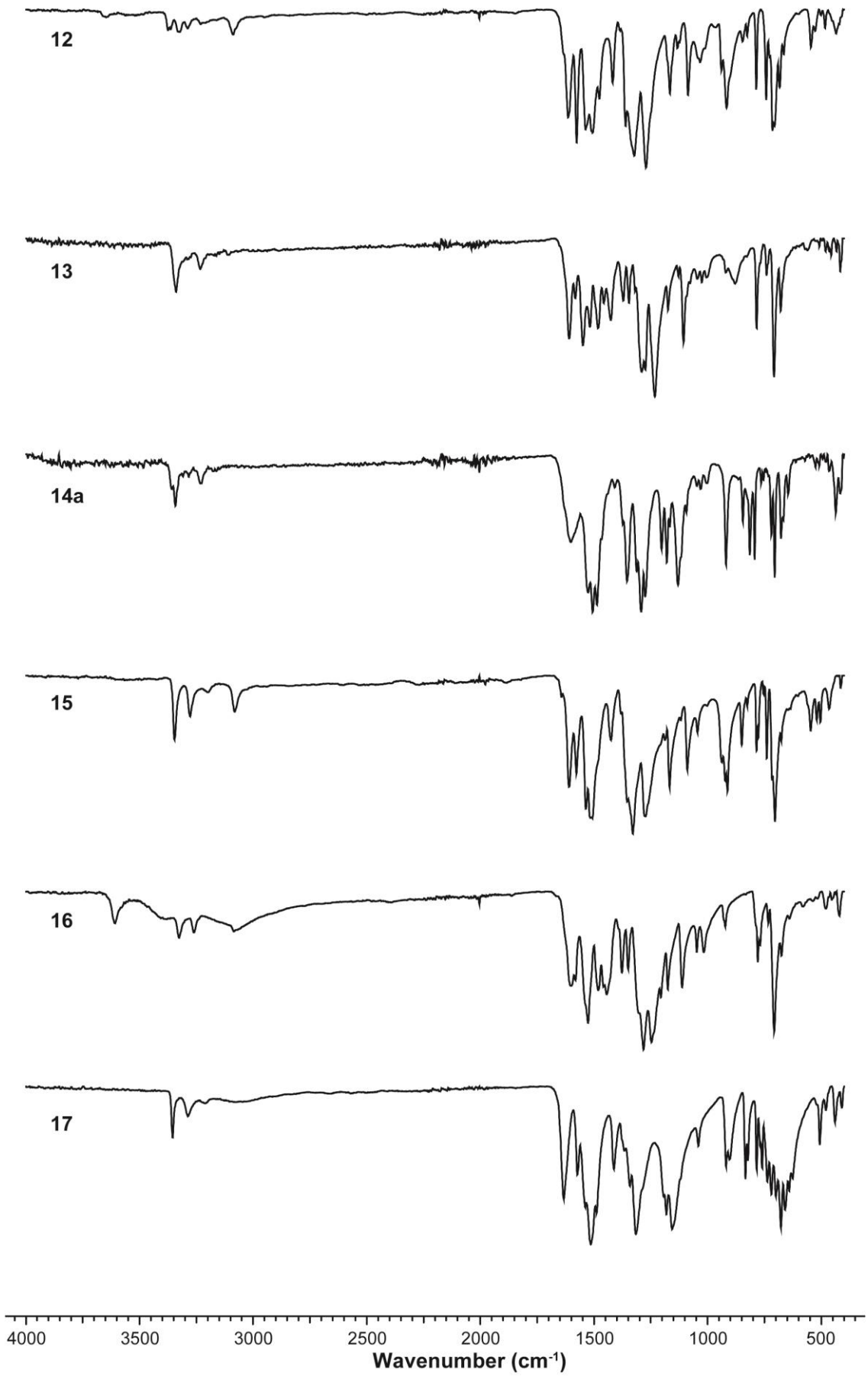

Figure S3. Infrared spectra of **12**–**14a** and **15**–**17**.

3.6.3. X-ray Diffraction and Microscope Images

For all crystalline compounds, an Oxford Xcalibur3 diffractometer with a CCD area detector or Bruker D8 Venture TXS diffractometer equipped with a multilayer monochromator, a Photon 2 detector and a rotating-anode generator were employed for data collection using Mo-*K*α radiation (λ = 0.7107 Å). On the Oxford device, data collection and reduction were carried out using the CRYSALISPRO software.[1] On the Bruker diffractometer, the data were collected with the Bruker Instrument Service v3.0.21, the data reduction was performed using the SAINT V8.18C software (Bruker AXS Inc., 2011). The structures were solved by direct methods (SIR-92,[2] SIR-97[3] or SHELXS-97[4]) and refined by full-matrix least-squares on *F*2 (SHELXL[4]) and finally checked using the PLATON software[5] integrated in the WinGX[6] software suite. The non-hydrogen atoms were refined anisotropically. The absorptions were corrected by a SCALE3 ABSPACK or SADABS Bruker APEX3 multiscan method.[7,8] All DIAMOND2 plots are shown with thermal ellipsoids at the 50% probability level and hydrogen atoms are shown as small spheres of arbitrary radius. X-ray powder experiments were performed on a Gunier diffractometer (Huber G644) with Mo-*K*α1 radiation (λ = 0.7093 Å, quartz monochromator) in Lindemann capillaries (0.7 mm diameter). The angle calibration was performed with electronic grade germanium. In the 2θ range between 4 and 34° with an increment of 0.04°, 750 data points were collected with a counting rate of 10 s for each increment. The Rietveld parameters were analyzed with the program FullProf.[9]

Table S1. Crystallographic data of **4b_pro**, **4b**, **6**, and **7**.

	4b_pro	**4b**	**6**	**7**
Formula	$C_9H_9N_5$	$C_2H_5N_5$	$C_{14}H_{10}CuN_{16}O_{14}$	$C_{14}H_{10}CuN_{16}O_{16}$
FW [g mol^{-1}]	187.21	99.11	689.92	721.92
Crystal system	monoclinic	orthorhombic	monoclinic	monoclinic
Space Group	$P2_1/n$	$P2_12_12_1$	$P2_1/c$	$P2_1/c$
Color / Habit	yellow block	colorless block	green platelet	green block
Size [mm]	0.34 x 0.50 x 0.50	0.24 x 0.25 x 0.53	0.05 x 0.10 x 0.25	0.10 x 0.15 x 0.20
a [Å]	11.5832(8)	5.7191(4)	7.8960(6)	5.8896(3)
b [Å]	7.4944(4)	7.7483(5)	21.2750(15)	19.8705(9)
c [Å]	11.9045(8)	10.4586(7)	7.0280(7)	10.7979(6)
α [°]	90	90	90	90
β [°]	118.862(9)	90	95.995(8)	94.962(6)
γ [°]	90	90	90	90
V [Å^3]	905.05(13)	463.46(5)	1174.16(17)	1258.94(11)
Z	4	4	2	2
$\rho_{calc.}$ [g cm^{-3}]	1.374	1.420	1.952	1.905
μ [mm^{-1}]	0.092	0.107	1.042	0.982
F(000)	392	208	694	726
$\lambda_{MoK\alpha}$ [Å]	0.71073	0.71073	0.71069	0.71073
T [K]	129	143	143	173
θ Min–Max [°]	3.4, 32.2	4.4, 32.4	4.1, 26.0	4.2, 26.0
Dataset	−17: 16; −10: 10; −17: 17	−8: 8; −9: 11; −14: 15	−9: 9; −24: 26; −8: 8	−7: 7; −24: 24; −13: 13
Reflections collected	9657	4787	7938	9810
Independent refl.	2995	1534	2306	2459
R_{int}	0.022	0.027	0.074	0.063
Observed reflections	2511	1360	1495	1771
Parameters	127	84	213	230
R_1 (obs)[a]	0.0432	0.0362	0.0498	0.0537
wR_2 (all data)[b]	0.1293	0.0925	0.1052	0.1220
GooF[c]	1.07	1.05	1.03	1.10
Resd. Dens. [e Å^{-3}]	−0.24, 0.43	−0.18, 0.13	−0.47, 0.61	−0.32, 0.81
Absorption correction	multi-scan	multi-scan	multi-scan	multi-scan
CCDC	1934808	1934810	1934799	1934801

[a] $R_1 = \Sigma||F_0|- |F_c||/ \Sigma|F_0|$; [b] $wR_2 = [\Sigma[w(F_0^2-F_c^2)^2]/\Sigma[w(F_0)^2]]^{1/2}$; $w = [\sigma c^2(F_0^2)+(xP)^2+yP]^{-1}$ and $P = (F_0^2+2F_c^2)/3$; [c] GooF = $\{\Sigma[w(F_o^2-F_c^2)^2]/(n-p)\}^{1/2}$ (n = number of reflections; p = total number of parameters).

Table S2. Crystallographic data of **8**–**11**.

	8	**9**	**10**	**11**
Formula	$C_{16}H_{16}CuN_{26}O_{18}$	$C_{14}H_{10}CuN_{16}O_{14}$	$C_{14}H_{10}N_{16}O_{16}$	$C_{16}H_{16}CuN_{26}O_{18}$
FW [g mol^{-1}]	924.09	689.92	721.93	924.10
Crystal system	monoclinic	monoclinic	triclinic	triclinic
Space Group	$P2_1/n$	$P2_1/c$	$P\bar{1}$	$P\bar{1}$
Color / Habit	green-yellow rod	green needle	green block	green block
Size [mm]	0.09 x 0.11 x 0.44	0.05 x 0.10 x 0.55	0.16 x 0.32 x 0.37	0.13 x 0.23 x 0.26
a [Å]	10.5340(11)	13.0030(8)	6.2297(4)	8.6130(7)
b [Å]	8.9870(9)	13.5073(11)	8.8060(6)	9.2780(9)
c [Å]	17.0430(15)	6.8287(5)	12.0376(7)	11.6430(12)
α [°]	90	90	79.309(5)	106.515(9)
β [°]	99.395(8)	93.619(6)	89.906(5)	101.929(7)
γ [°]	90	90	82.408(5)	107.829(8)
V [Å^3]	1591.8(3)	1202.55(15)	643.04(7)	804.01(16)
Z	2	2	1	1
$\rho_{calc.}$ [g cm^{-3}]	1.928	1.905	1.864	1.909
μ [mm^{-1}]	0.813	1.017	0.961	0.805
F(000)	934	694	363	467
$\lambda_{MoK\alpha}$ [Å]	0.71069	0.71073	0.71073	0.71069
T [K]	173	173	173	173
θ Min–Max [°]	4.3, 26.0	4.2, 26.0	4.3, 26.4	4.3, 26.0
Dataset	−12: 9; −10:11; −21: 20	−16: 15; −16: 16; −8: 8	−7: 7; −11: 10; −15: 15	−10: 10; −11: 10; −14: 11
Reflections collected	10227	9343	4991	6244
Independent refl.	3104	2359	2612	3143
R_{int}	0.115	0.080	0.020	0.030
Observed reflections	1570	1648	2390	2592
Parameters	295	221	234	295
R_1 (obs)[a]	0.0713	0.0441	0.0291	0.0363
wR_2 (all data)[b]	0.1260	0.0875	0.0701	0.0868
GooF[c]	1.02	1.02	1.09	1.10
Resd. Dens. [e Å^{-3}]	−0.53, 0.87	−0.47, 0.39	−0.30, 0.31	−0.32, 0.40
Absorption correction	multi-scan	multi-scan	multi-scan	multi-scan
CCDC	1934798	1934809	1934811	1934812

[a] $R_1 = \Sigma||F_0|- |F_c||/ \Sigma|F_0|$; [b] $wR_2 = [\Sigma[w(F_0^2-F_c^2)^2]/\Sigma[w(F_0)^2]]^{1/2}$; $w = [\sigma c^2(F_0^2)+(xP)^2+yP]^{-1}$ and $P = (F_0^2+2F_c^2)/3$; [c] GooF = $\{\Sigma[w(F_o^2-F_c^2)^2]/(n-p)\}^{1/2}$ (n = number of reflections; p = total number of parameters).

Table S3. Crystallographic data of **12**–**14b**.

	12	**13**	**14a**	**14b**
Formula	$C_{32}H_{30}CuN_{32}O_{29}$	$C_{10}H_{11}CuN_{13}O_8$	$C_{10}H_{11}CuN_{13}O_9$	$C_{20}H_{26}CuN_{26}O_{19}$
FW [g mol^{-1}]	1453.96	504.86	520.86	998.21
Crystal system	monoclinic	orthorhombic	orthorhombic	monoclinic
Space Group	$P2_1/n$	$Pna2_1$	$Pna2_1$	$P2_1/c$
Color / Habit	green block	green needle	brown needle	green rod
Size [mm]	0.17 x 0.21 x 0.38	0.02 x 0.05 x 0.54	0.03 x 0.05 x 0.46	0.08 x 0.12 x 0.31
a [Å]	16.5743(8)	14.6007(14)	15.2566(9)	6.8633(3)
b [Å]	15.0908(7)	15.0584(14)	14.7433(7)	16.3608(8)
c [Å]	22.2088(10)	8.0850(7)	8.1350(5)	32.863(2)
α [°]	90	90	90	90
β [°]	103.280(4)	90	90	92.152(5)
γ [°]	90	90	90	90
V [Å^3]	5406.3(4)	1777.6(3)	1829.83(18)	3687.6(3)
Z	4	4	4	4
$\rho_{calc.}$ [g cm^{-3}]	1.786	1.887	1.891	1.798
μ [mm^{-1}]	0.911	1.309	1.279	0.711
F(000)	2944	1020	1052	2036
$\lambda_{MoK\alpha}$ [Å]	0.71073	0.71069	0.71073	0.71073
T [K]	143	143	143	143
θ Min–Max [°]	4.2, 26.0	4.3, 29.4	4.2, 32.3	4.2, 26.4
Dataset	−18: 20; −18: 16; −18: 27	−19: 19; −11: 20; −10: 11	−22: 22; −21: 22; −11: 12	−8: 8; −20: 20; −31: 41
Reflections collected	29193	13583	17850	20880
Independent refl.	10570	4360	5814	7501
R_{int}	0.073	0.095	0.121	0.066
Observed reflections	6322	2894	3397	4672
Parameters	911	299	304	655
R_1 (obs)[a]	0.0550	0.0580	0.0668	0.0513
wR_2 (all data)[b]	0.1305	0.0847	0.1062	0.1182
GooF[c]	1.04	1.03	0.99	1.02
Resd. Dens. [e Å^{-3}]	−0.59, 0.73	−0.57, 0.64	−0.79, 0.74	−0.44, 0.71
Absorption correction	multi-scan	multi-scan	multi-scan	multi-scan
CCDC	1934806	1934805	1934803	1934807

[a] $R_1 = \Sigma||F_0|- |F_c||/ \Sigma|F_0|$; [b] $wR_2 = [\Sigma[w(F_0^2-F_c^2)^2]/\Sigma[w(F_0)^2]]^{1/2}$; $w = [\sigma c^2(F_0^2)+(xP)^2+yP]^{-1}$ and $P = (F_0^2+2F_c^2)/3$; [c] GooF = $\{\Sigma[w(F_o^2-F_c^2)^2]/(n-p)\}^{1/2}$ (n = number of reflections; p = total number of parameters).

Table S4. Crystallographic data of **14c** and **15**–**17**.

	14c	**15**	**16**	**17**
Formula	$C_{16}H_{18}CuN_{16}O_{20}$	$C_{16}H_{14}CuN_{16}O_{14}$	$C_8H_{10}CuN_8O_{10}$	$C_{16}H_{14}CuN_{16}O_{18}$
FW [g mol^{-1}]	818.00	717.97	441.78	781.98
Crystal system	monoclinic	triclinic	monoclinic	triclinic
Space Group	$P2_1/n$	$P\bar{1}$	$P2_1/c$	$P\bar{1}$
Color / Habit	green rod	green block	green rod	green block
Size [mm]	0.02 x 0.03 x 0.10	0.08 x 0.13 x 0.22	0.11 x 0.14 x 0.50	0.07 x 0.17 x 0.19
a [Å]	19.3734(7)	7.7928(6)	11.7176(5)	8.0087(9)
b [Å]	7.3825(3)	11.1366(9)	8.0996(3)	8.7623(10)
c [Å]	20.6095(8)	15.8638(12)	16.7581(9)	11.2661(9)
α [°]	90	73.445(7)	90	69.572(9)
β [°]	108.836(1)	81.065(6)	108.825(5)	78.715(8)
γ [°]	90	77.470(7)	90	64.890(11)
V [Å^3]	2789.80(19)	1281.80(18)	1505.40(13)	669.80(14)
Z	4	2	4	1
$\rho_{calc.}$ [g cm^{-3}]	1.948	1.860	1.949	1.939
μ [mm^{-1}]	0.909	0.958	1.531	0.936
F(000)	1660	726	892	395
$\lambda_{MoK\alpha}$ [Å]	0.71073	0.71073	0.71073	0.71073
T [K]	111	143	143	143
θ Min–Max [°]	3.0, 26.4	4.1, 26.0	4.3, 26.0	4.1, 26.4
Dataset	−24: 24; −9: 9; −25: 25	−9: 9; −13: 10; −19: 18	−12: 14; −9: 9; −20: 19	−9: 9; −10: 10; −14: 13
Reflections collected	44649	10367	11264	4191
Independent refl.	5708	5012	9243	2712
R_{int}	0.044	0.040	0.035	0.035
Observed reflections	4968	3881	2494	2184
Parameters	528	442	269	249
R_1 (obs)[a]	0.0321	0.0434	0.0321	0.0432
wR_2 (all data)[b]	0.0759	0.1063	0.0805	0.0950
GooF[c]	1.06	1.04	1.06	1.05
Resd. Dens. [e Å^{-3}]	−0.44, 0.40	−0.60, 0.38	−0.36, 0.41	−0.42, 0.55
Absorption correction	multi-scan	multi-scan	multi-scan	multi-scan
CCDC	1934813	1934800	1934802	1934804

[a] $R_1 = \Sigma||F_0|- |F_c||/ \Sigma|F_0|$; [b] $wR_2 = [\Sigma[w(F_0^2-F_c^2)^2]/\Sigma[w(F_0)^2]]^{1/2}$; $w = [\sigma c^2(F_0^2)+(xP)^2+yP]^{-1}$ and $P = (F_0^2+2F_c^2)/3$; [c] GooF = $\{\Sigma[w(F_o^2-F_c^2)^2]/(n-p)\}^{1/2}$ (n = number of reflections; p = total number of parameters).

The intermediate **4_pro** crystallizes as a yellow block in the monoclinic space Group $P2_1/n$ with four formula units per cell and a calculated density of 1.374 g cm^{-3} at 129 K. All non-hydrogen atoms lie within a plane and the structure is stabilized through several intermolecular interactions such as π-π stacking between benzyl groups as well as hydrogen bonding between methyl functions and tetrazole rings (Figure 1).

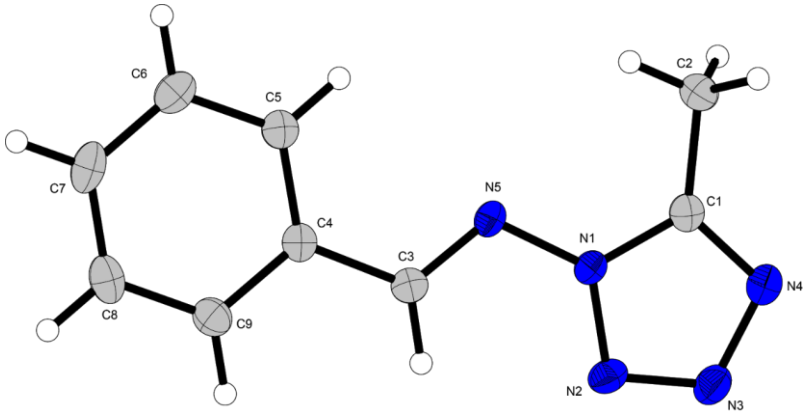

Figure S4. Molecular unit of 1-benzylidene-1-amino-5-methyltetrazole (**4_pro**). Selected bond lengths (Å): N1–N2 1.3564(12), N1–N5 1.3798(14), N1–C1 1.3494(15), N2–N3 1.2948(16), N3–N4 1.3697(13), N4–C1 1.3187(14), N5–C3 1.2824(14), C1–C2 1.4768(14), C3–C4 1.4613(16); selected bond angles (°): N2–N1–N5 125.99(9), N2–N1–C1 109.38(9), N5–N1–C1 124.60(8), N1–N2–N3 105.30(9), N2–N3–N4 111.57(9), N3–N4–C1 105.90(10), N1–N5–C3 115.79(8), N1–C1–N4 107.85(8), N1–C1–C2 124.39(10), N4–C1–C2 127.77(11), N5–C3–C4 120.10(8).

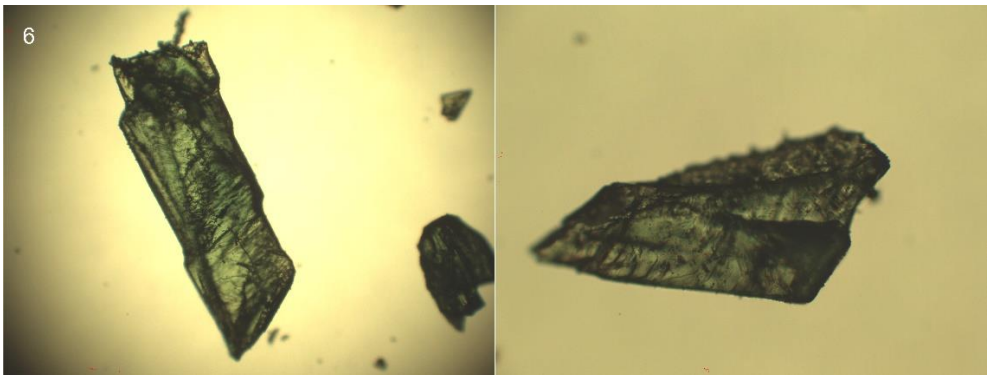

Figure S5. Microscope images of complex **6** (left: fourfold magnitude; right: tenfold magnitude).

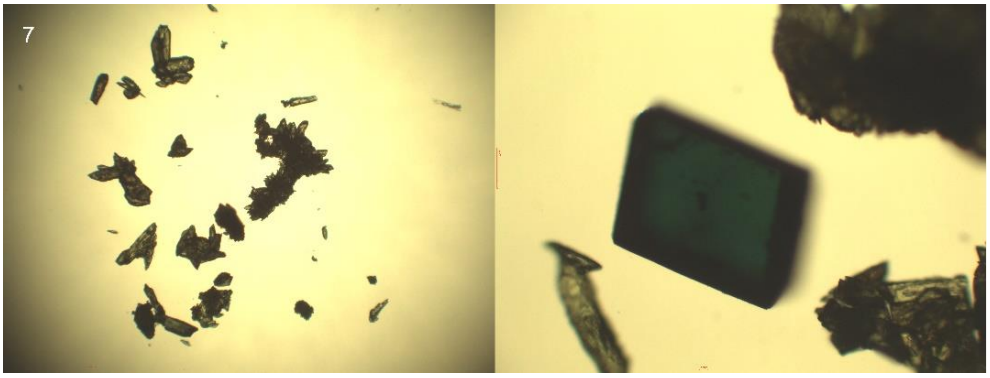

Figure S6. Microscope images of compound **7** (left: fourfold magnitude; right: tenfold magnitude).

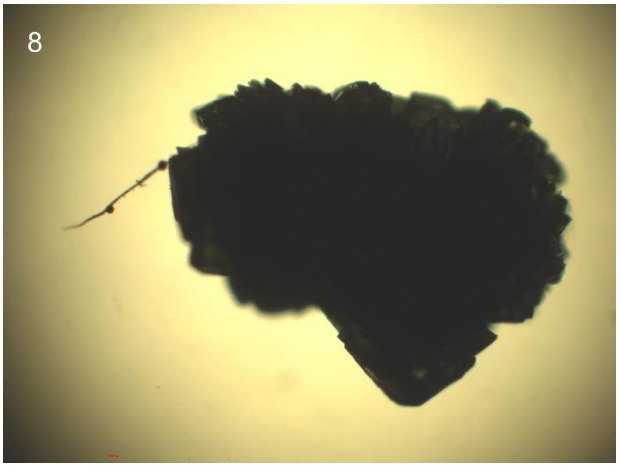

Figure S7. Microscope image of complex **8** (fourfold magnitude).

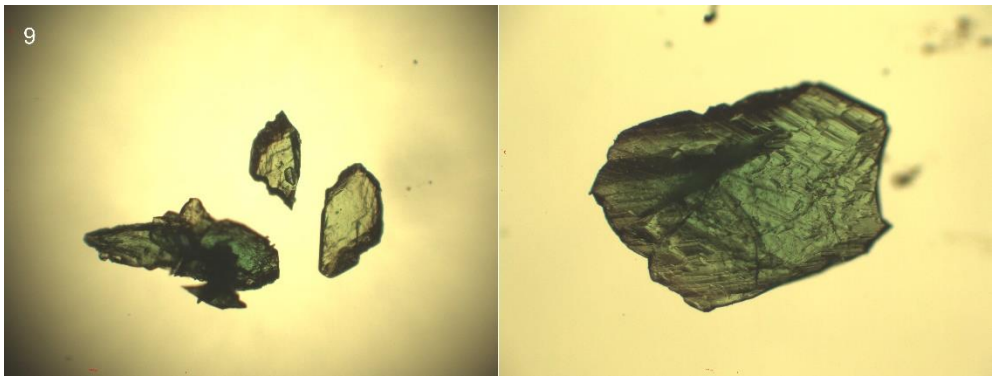

Figure S8. Microscope images of complex **9** (left: fourfold magnitude; right: tenfold magnitude).

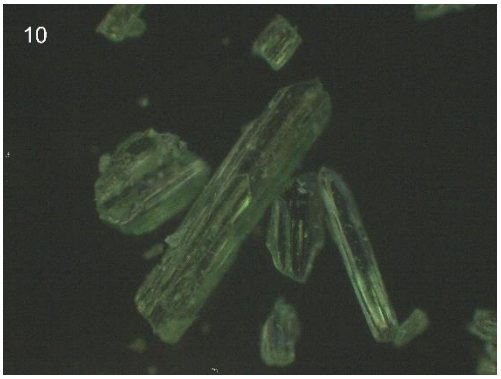

Figure S9. Microscope image of coordination compound **10** (fourfold magnitude).

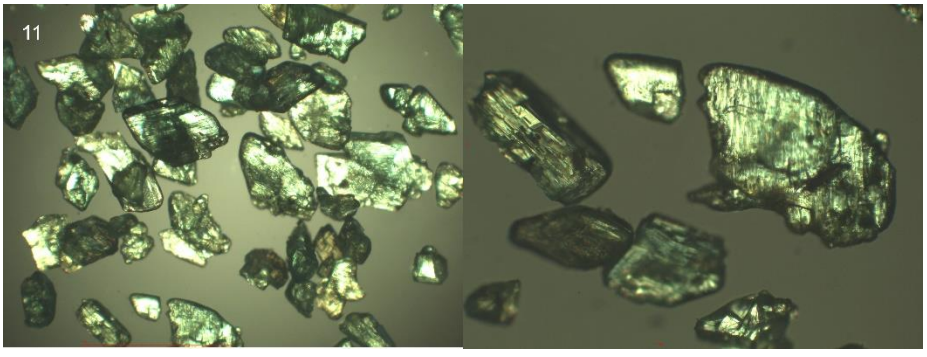

Figure S10. Microscope images of complex **11** (fourfold magnitude).

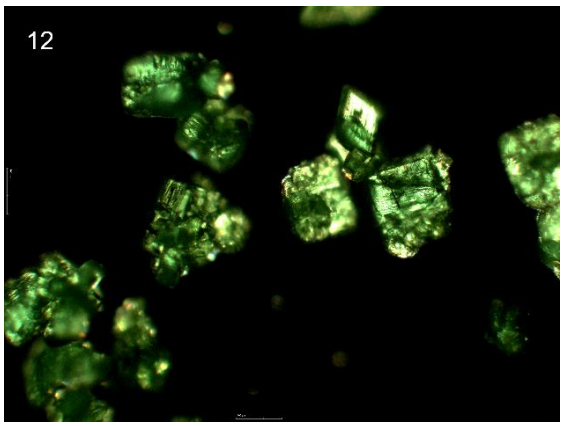

Figure S11. Microscope image of complex **12** (tenfold magnification).

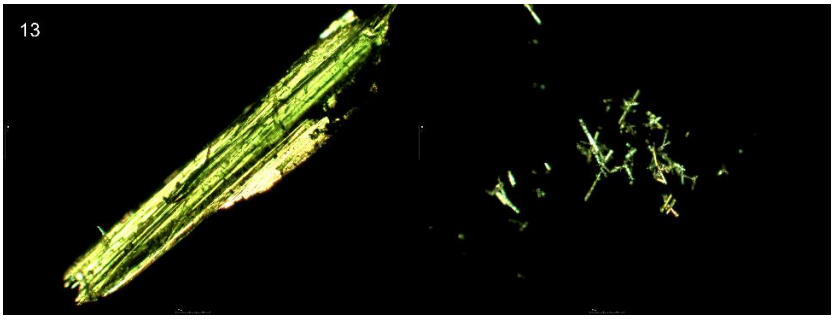

Figure S12. Microscope image of complex **13** (tenfold magnification).

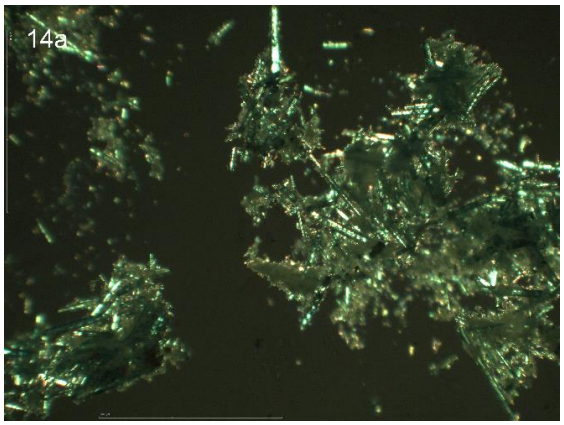

Figure S13. Microscope image of complex **14a** (fourfold magnification).

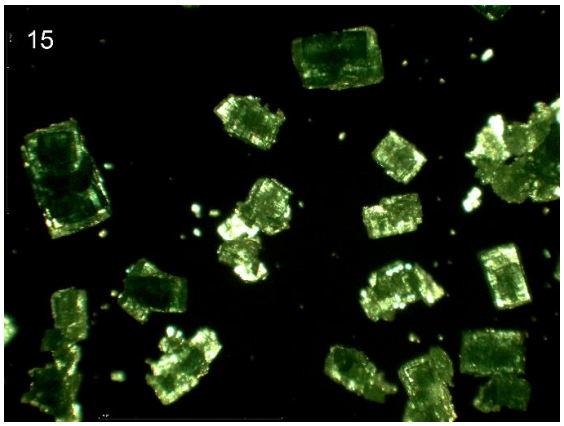

Figure S14. Microscope image of complex **15** (fourfold magnification).

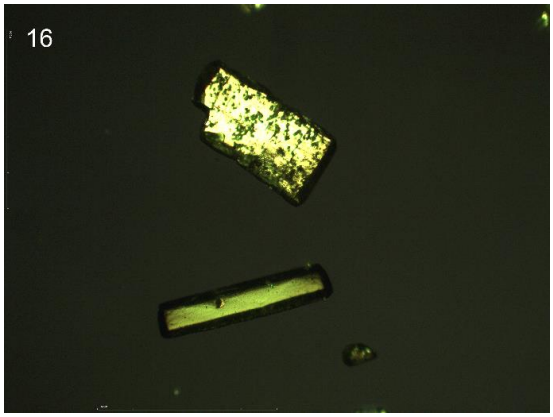

Figure S15. Microscope image of complex **16** (fourfold magnification).

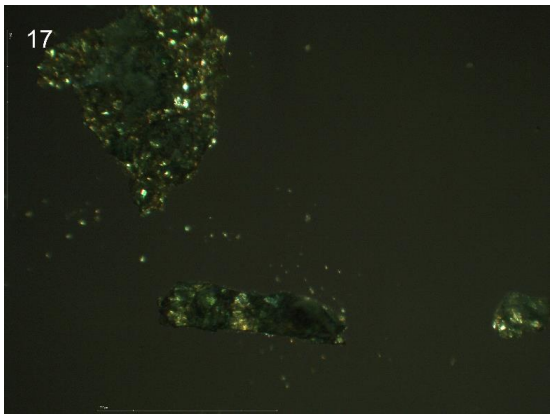

Figure S16. Microscope image of complex **17** (fourfold magnification).

3.6.4. TGA Plots of 6, 8, 11–13, and 16

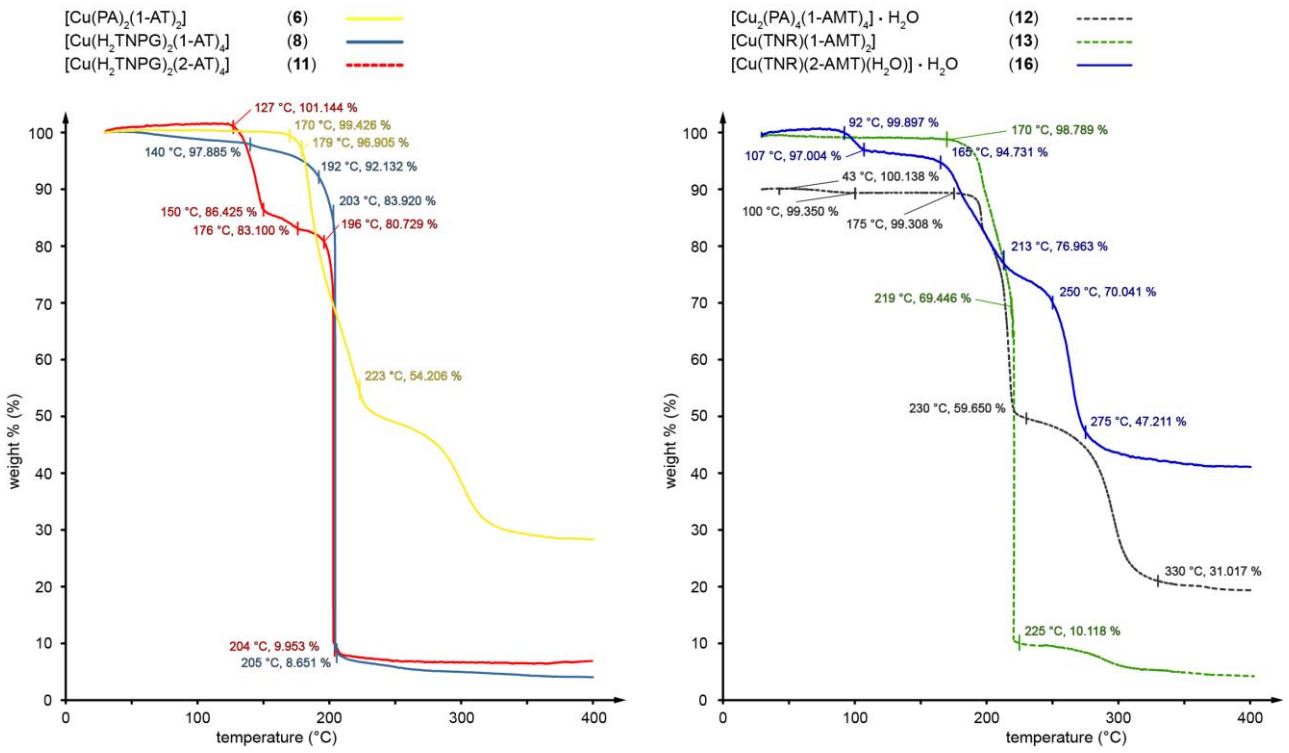

Figure S17. TGA plots of **6**, **8 11**–**13**, and **16**.

3.6.5. DTA Plots of 4b, 5b, and 6–17

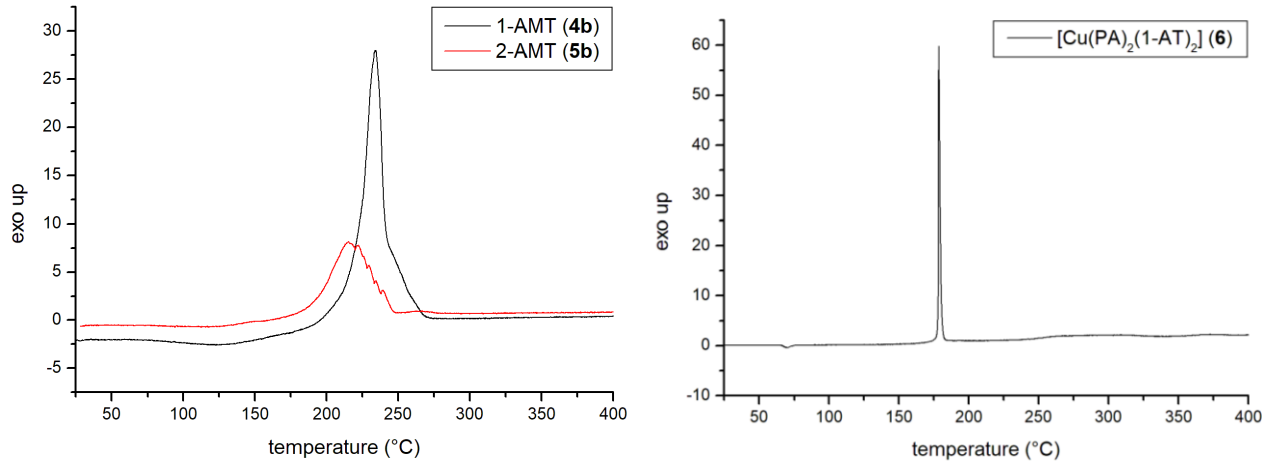

Figure S18. DTA plots of **4b**, **5b**, and **6**.

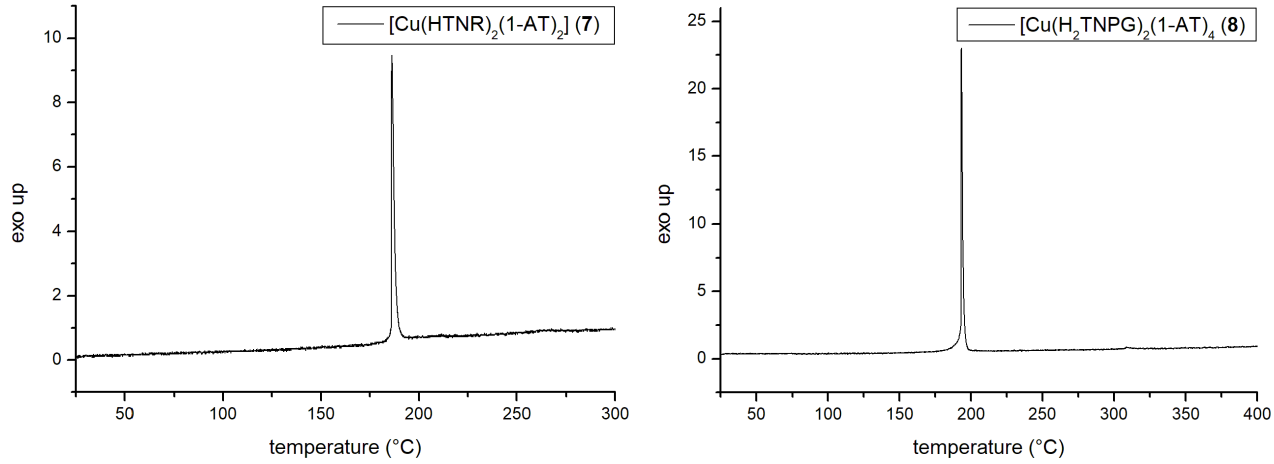

Figure S19. DTA plots of **7** and **8**.

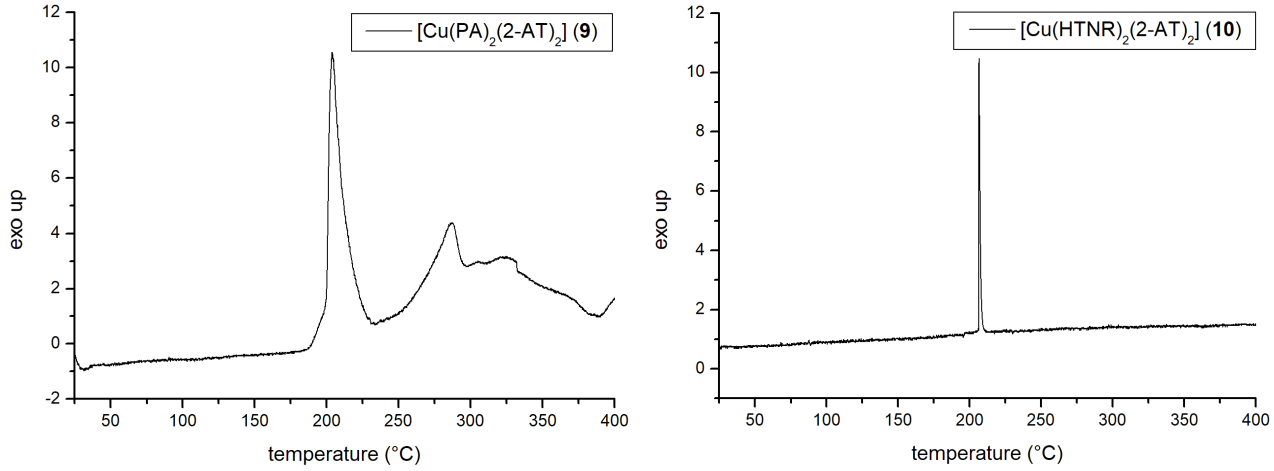

Figure S20. DTA plots of **9** and **10**.

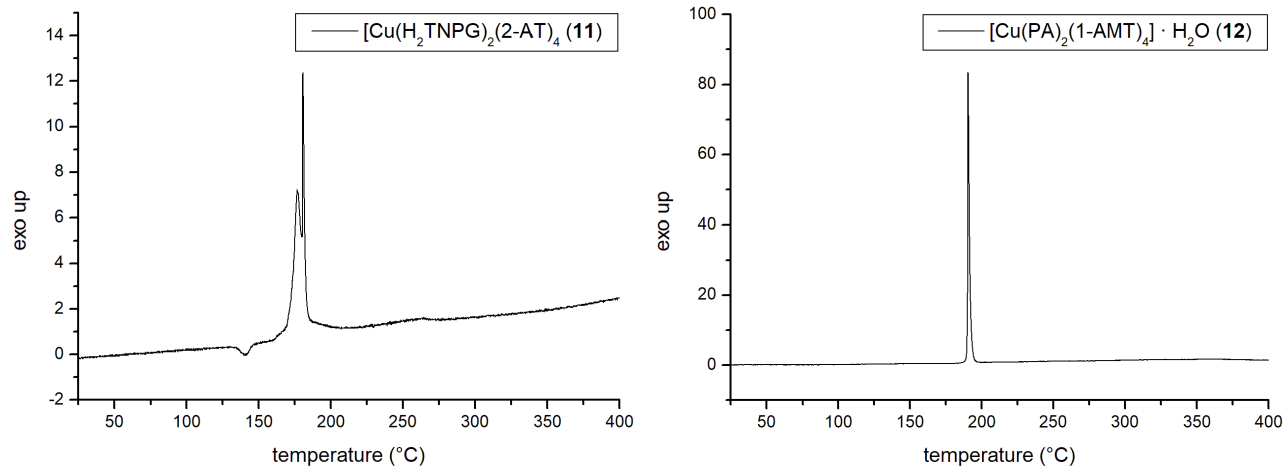

Figure S21. DTA plots of **11** and **12**.

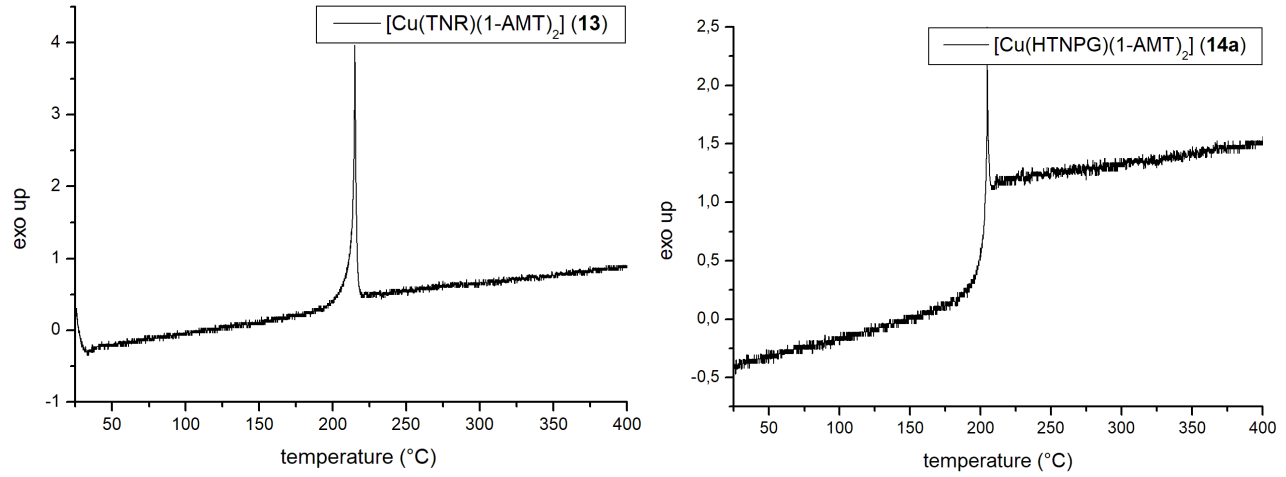

Figure S22. DTA plots of **13** and **14a**.

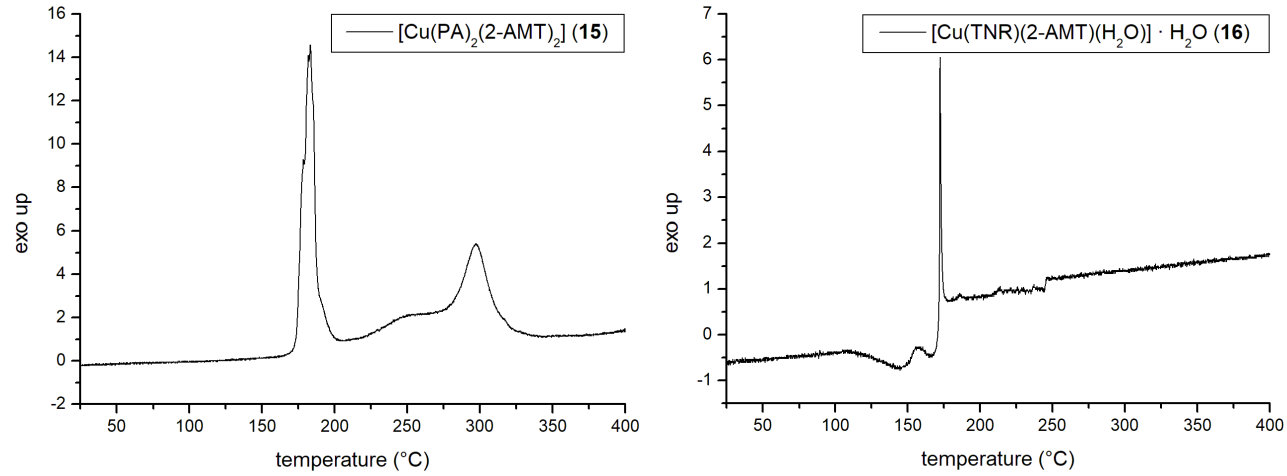

Figure S23. DTA plots of **15** and **16**.

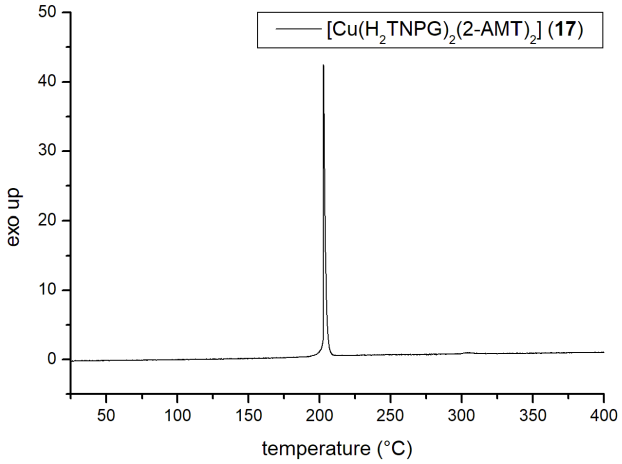

Figure S24. DTA plot of **17**.

3.6.6. Column Diagrams of the Complexes 6–17

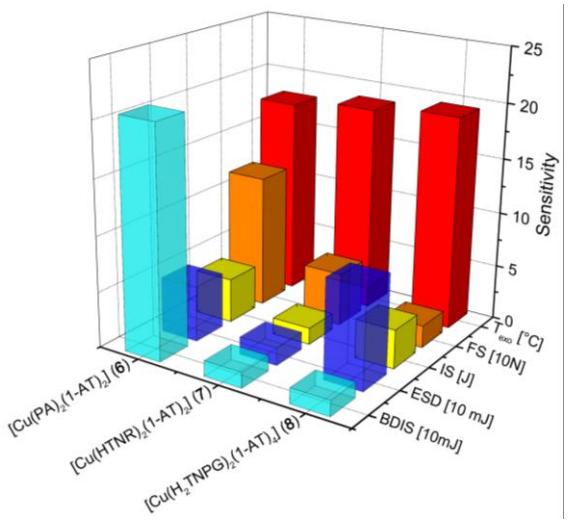

Figure S25. Stabilities of the investigated 1-AT complexes **6**–**8**.

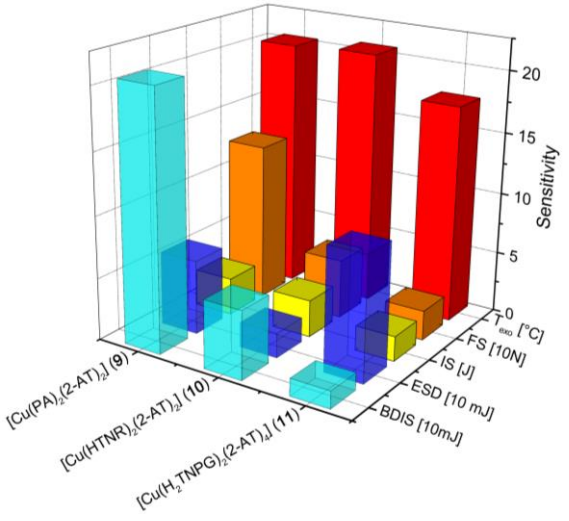

Figure S26. Stabilities of the investigated 2-AT complexes **9**–**11**.

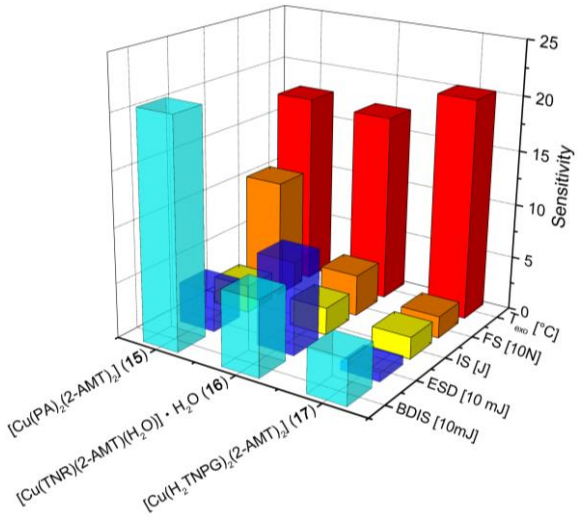

Figure S27. Stabilities of the investigated 2-AMT complexes **15**–**17**.

3.6.7. Hot Plate and Hot Needle Tests

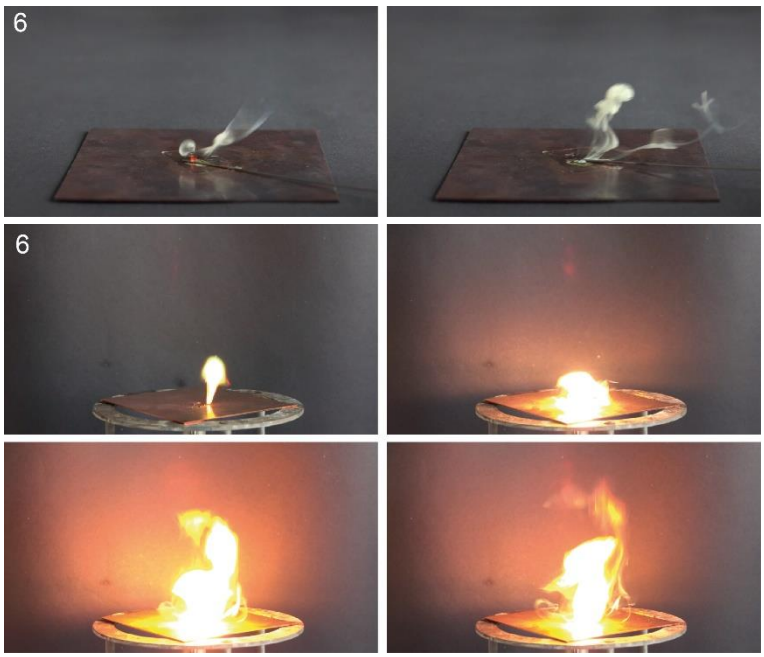

Figure S28. Hot needle and hot plate tests of complex **6** shown as a sequence.

Figure S29. Hot needle test of coordination compound **7** shown as a sequence.

Figure S30. Hot plate test of coordination compound **7** shown as a sequence.

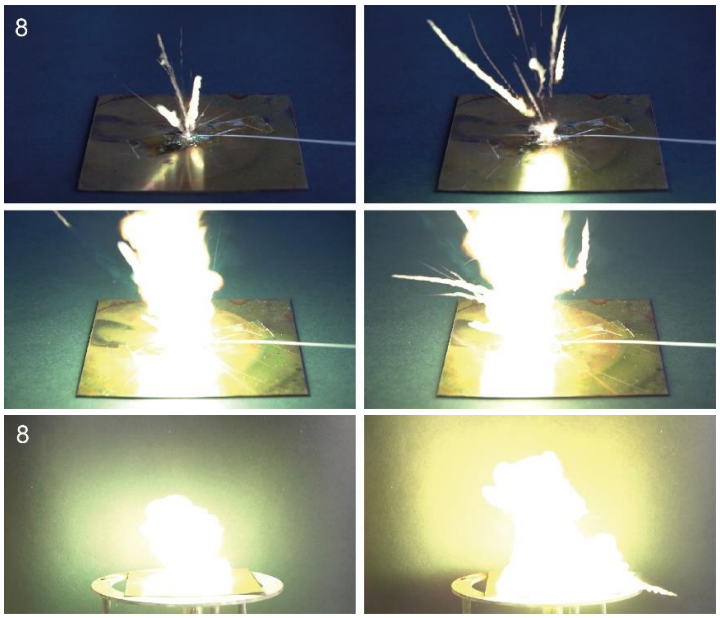

Figure S31. Hot needle and hot plate tests of complex **8** shown as a sequence.

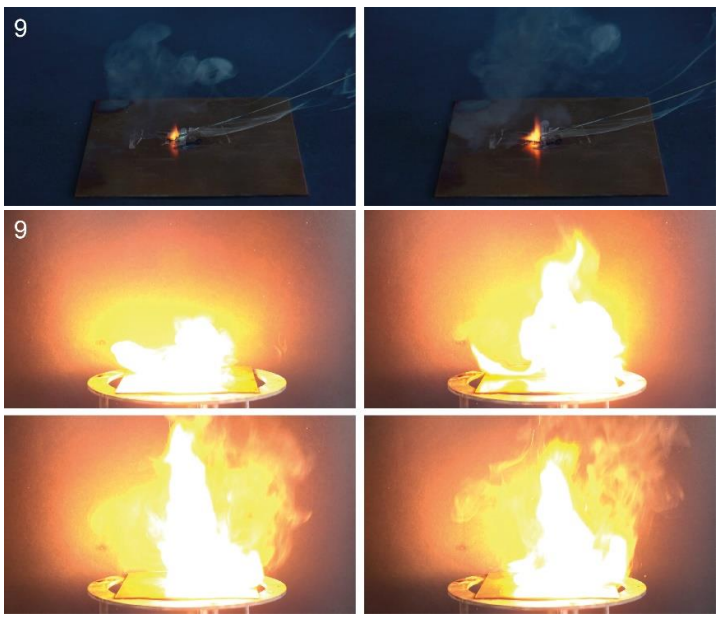

Figure S32. Deflagration of coordination compound **9** during the hot needle and hot plate tests, shown as a sequence.

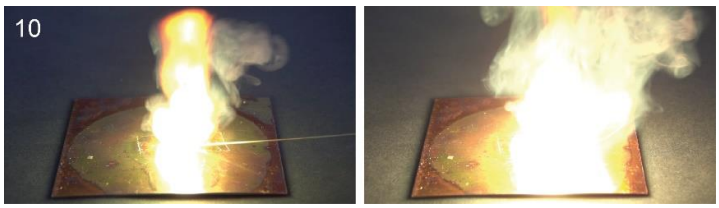

Figure S33. Initiation of complex **10** shown as a sequence during the hot needle test.

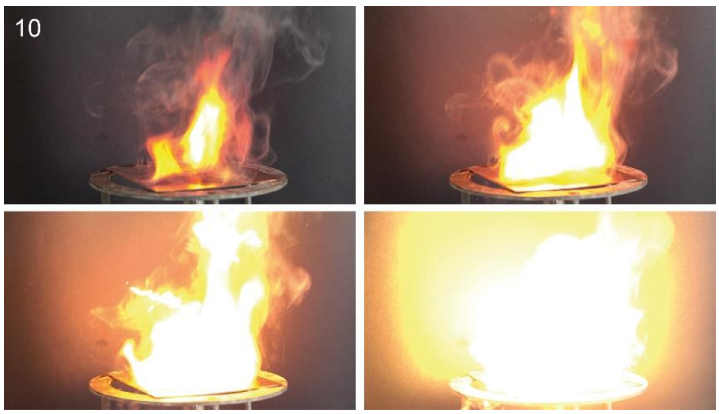

Figure S34. Hot plate test of complex **10** shown as a sequence.

Figure S35. Hot needle and hot plate tests of ECC **11** shown as sequences.

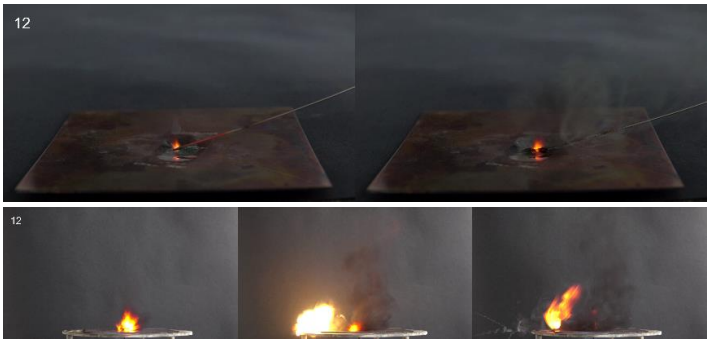

Figure S36. Initiation of the picrate complex **12** shown as sequences during the hot needle and hot plate tests.

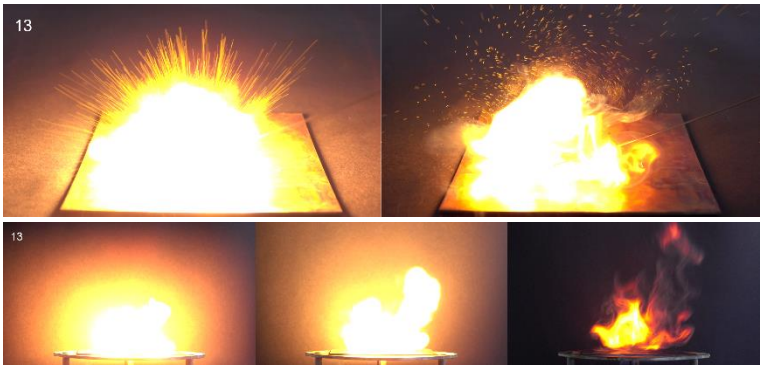

Figure S37. Deflagrations of the coordination compound **13** shown as sequences during the hot needle and hot plate tests.

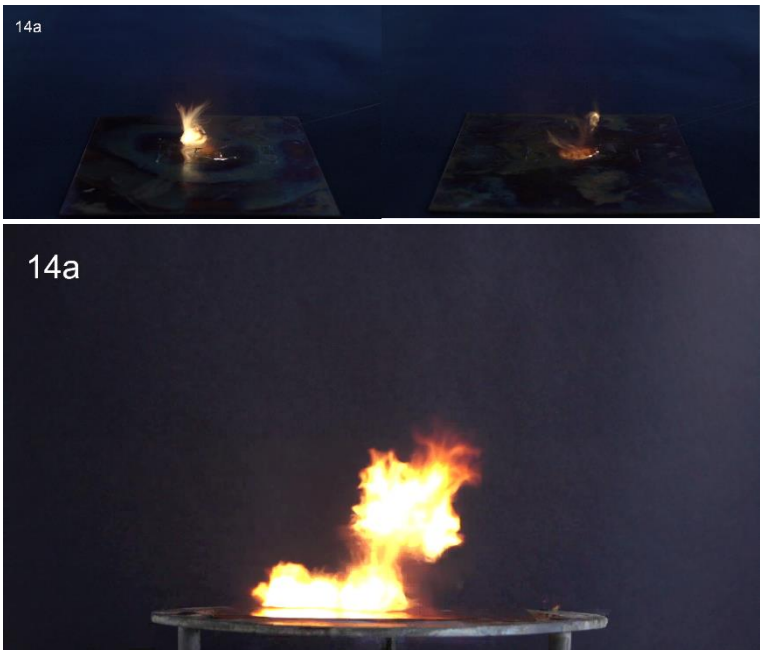

Figure S38. Detonation of coordination compound **14a** shown as sequence during the hot needle test, as well as moment of deflagration during the hot plate test.

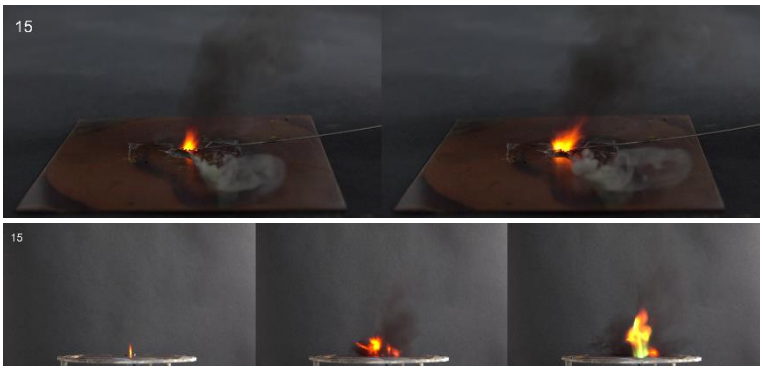

Figure S39. Deflagrations of picrate complex **15** during hot plate and hot needle tests, shown as sequences.

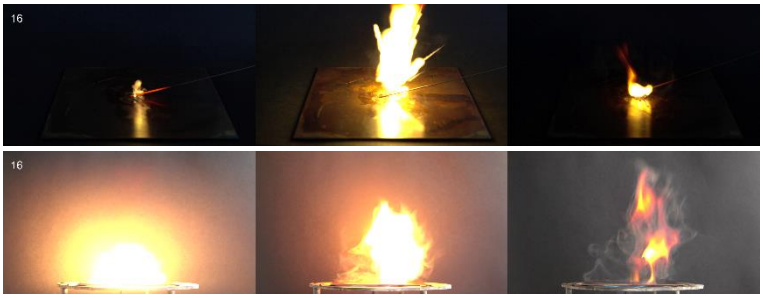

Figure S40. Deflagrations of styphnate **16** in hot plate and hot needle experiments, shown as sequences.

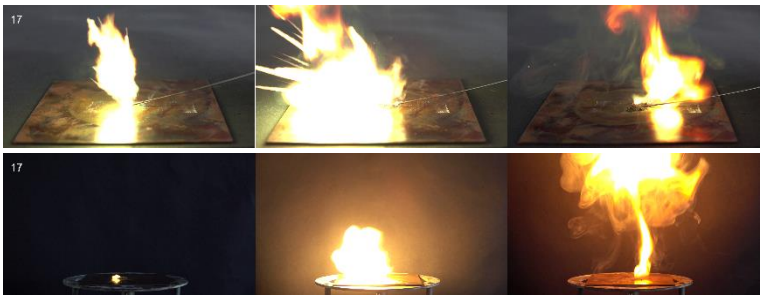

Figure S41. Deflagration of complex **17** during the hot needle and hot plate tests, shown as sequences.

3.6.8. Laser Ignition Tests

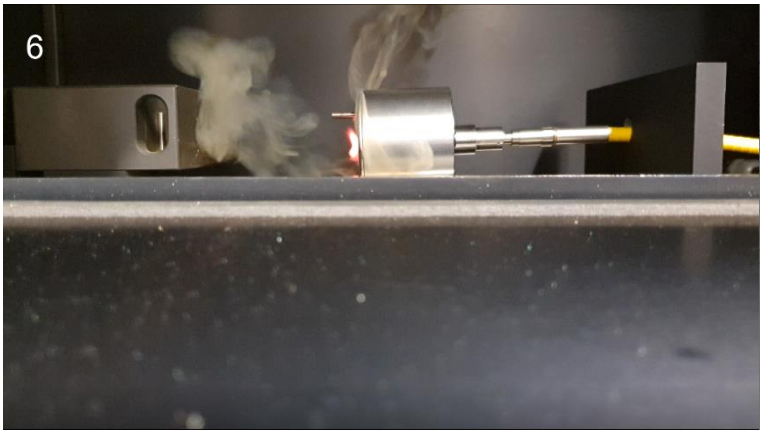

Figure S42. Decomposition of **6** during the laser initiation test.

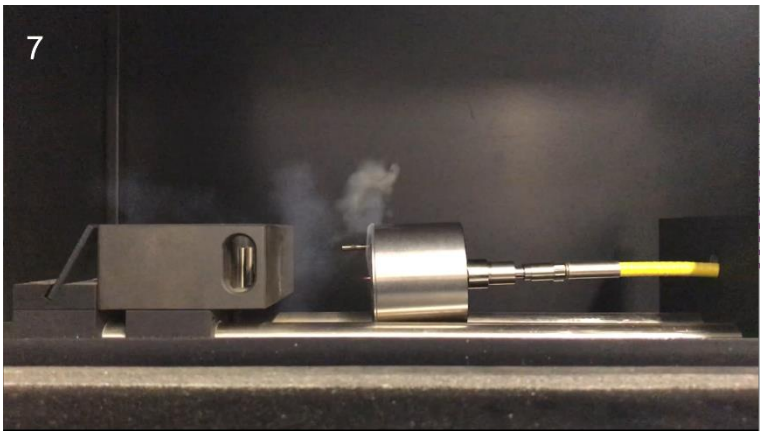

Figure S43. Deflagration of **7** induced by laser irradiation.

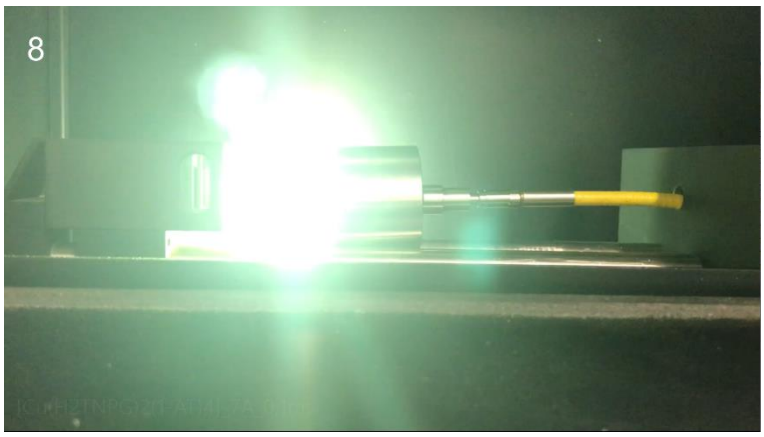

Figure S44. Moment of deflagration of 1-AT trinitrophloroglucinate complex **8**.

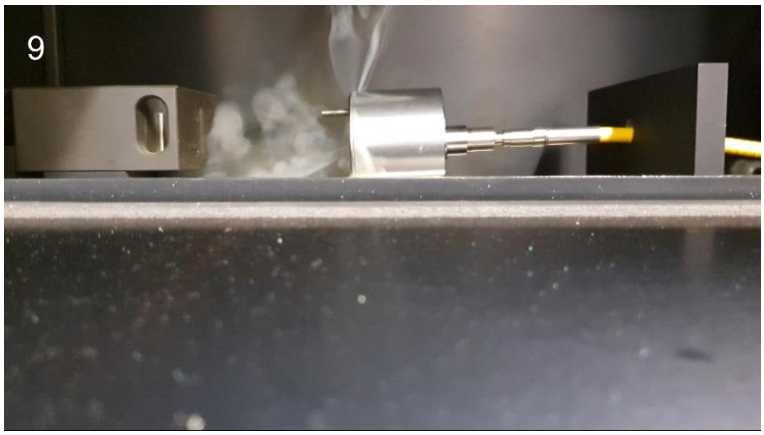

Figure S45. Decomposition of complex **9** during the laser initiation experiment.

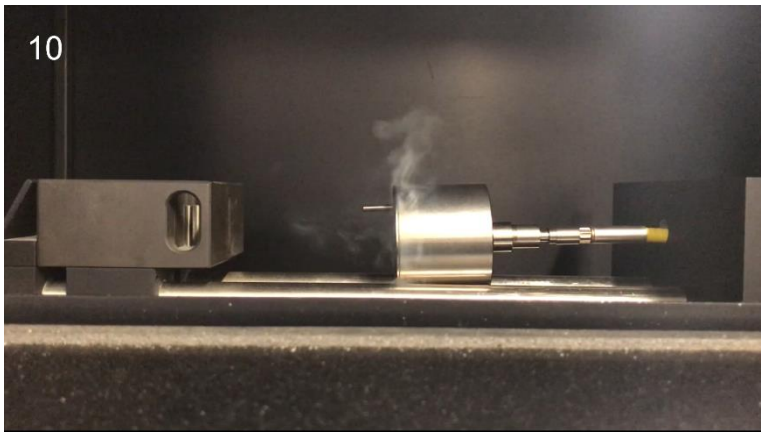

Figure S46. Deflagration of the copper(II) styphnate complex **10**.

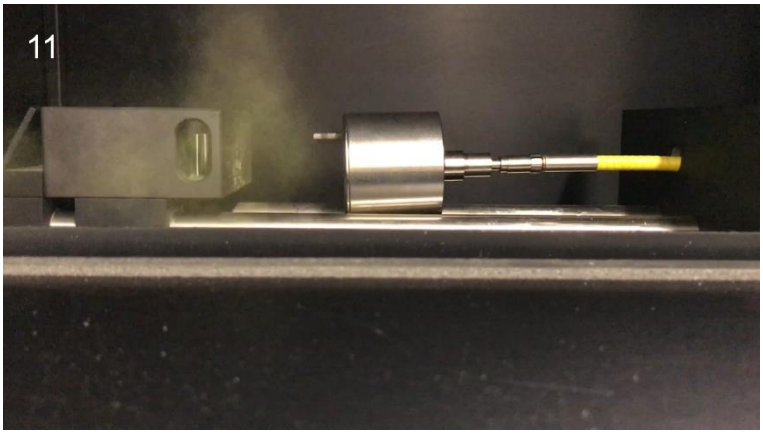

Figure S47. Moment of detonation of 2-AT trinitrophloroglucinate complex **11**.

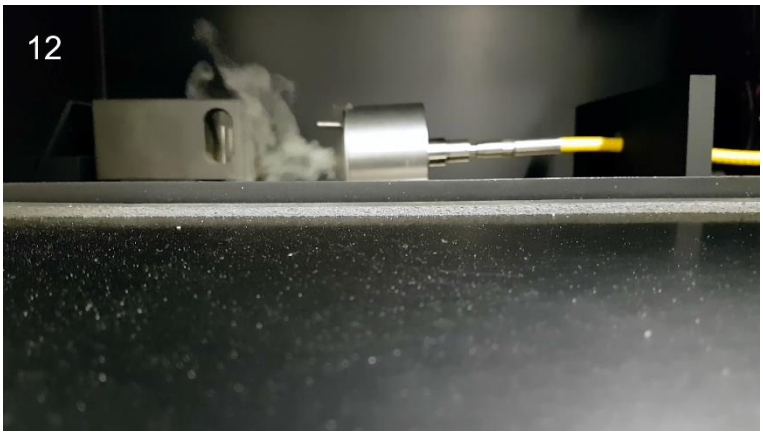

Figure S48. Decomposition of compound **12** in the laser irradiation experiment.

Figure S49. Decomposition of ECC **13** in the laser irradiation experiment.

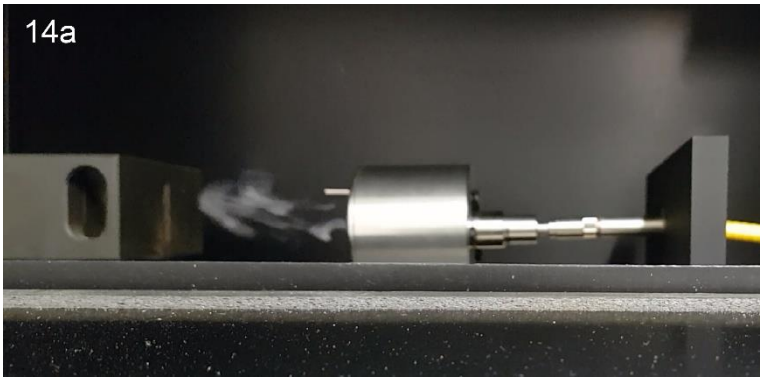

Figure S50. Decomposition of compound **14a** induced by laser irradiation.

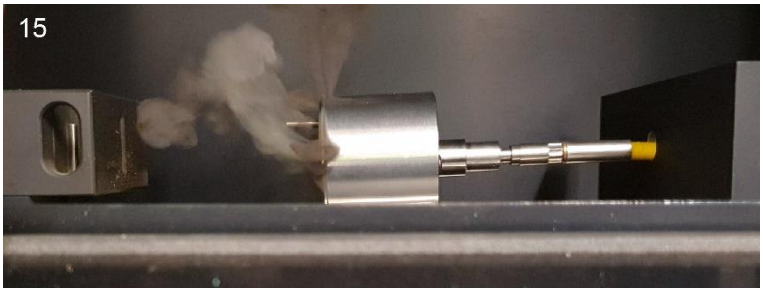

Figure S51. Decomposition of coordination compound **15** after irradiation with a NIR laser.

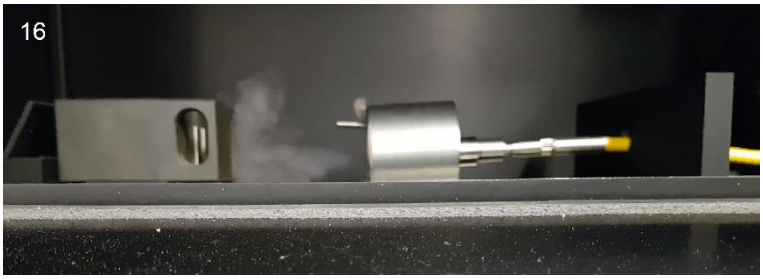

Figure S52. Decomposition of complex **16** in the laser irradiation experiment.

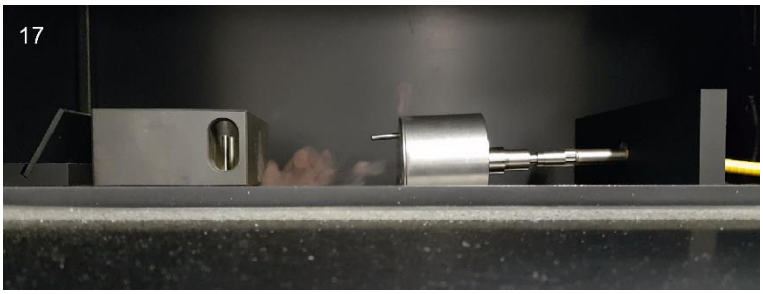

Figure S53. Decomposition of compound **17** in the laser irradiation experiment.

3.6.10. UV-Vis Spectra of 6–14a and 15–17

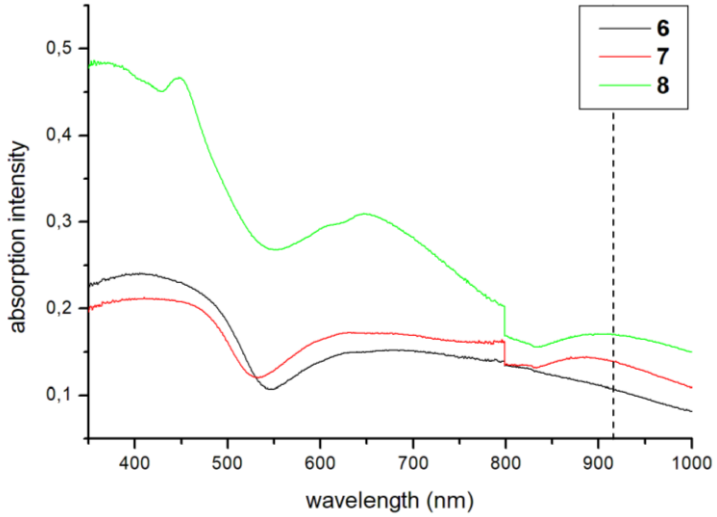

Figure S54. UV-Vis spectra in the solid state of coordination compounds **6**–**8** together with the laser wavelength.

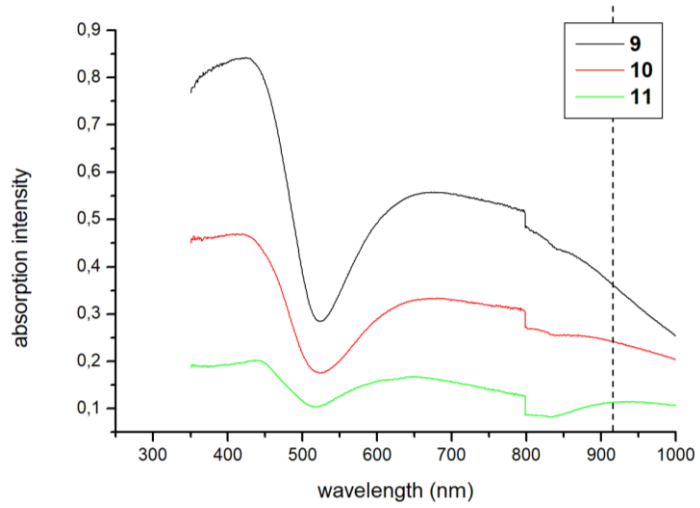

Figure S55. UV-Vis spectra in the solid state of coordination compounds **9**–**11** together with the laser wavelength.

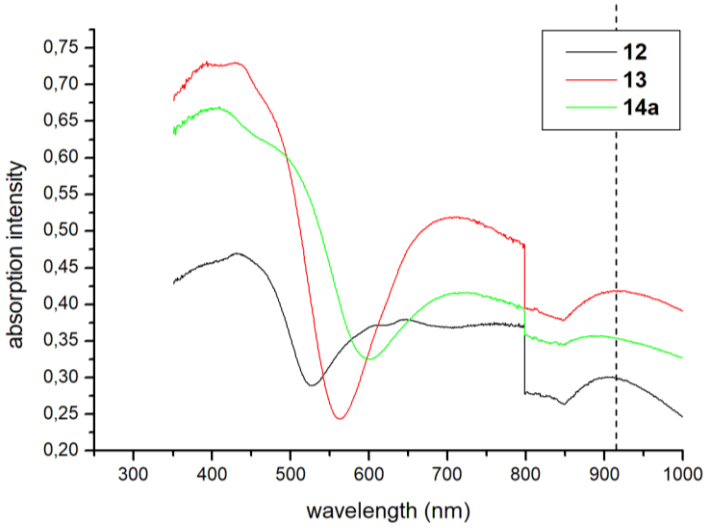

Figure S56. UV-Vis spectra in the solid state of coordination compounds **12**–**14a** together with the laser wavelength.

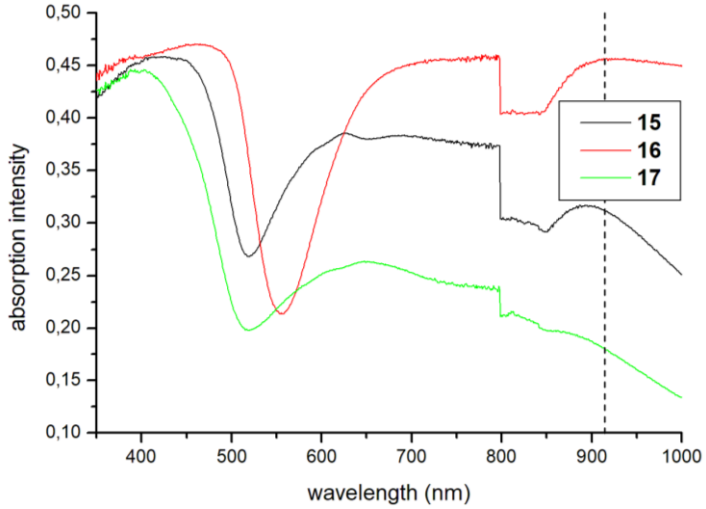

Figure S57. UV-Vis spectra in the solid state of coordination compounds **15**–**17** together with the laser wavelength.

3.6.10. Experimental Part and General Methods

All chemicals and solvents were employed as received (Sigma-Aldrich, Fluka, Acros, ABCR). ^{1}H, ^{13}C, and ^{15}N spectra were recorded at ambient temperature using a JEOL Bruker 400, Eclipse 270, JEOL EX 400 or a JEOL Eclipse 400 instrument. The chemical shifts quoted in ppm in the text refer to typical standards such as tetramethylsilane (^{1}H, ^{13}C) and nitromethane (^{15}N) in d_6-DMSO, d-$CHCl_3$ or d_3-MeCN as the solvents. Endothermic and exothermic events of the described compounds, which indicate melting, evaporation or decomposition, are given as the extrapolated onset temperatures. The samples were measured in a range of 25–400 °C at a heating rate of 5 °C min^{-1} through differential thermal analysis (DTA) with an OZM Research DTA 552-Ex instrument and partly by thermal gravimetric analysis (TGA) with a PerkinElmer TGA4000. Infrared spectra were measured with pure samples on a Perkin-Elmer BXII FT-IR system with a Smith DuraSampler IR II diamond ATR. Determination of the carbon, hydrogen and nitrogen contents was carried out by combustion analysis using an Elementar Vario El (nitrogen values determined are often lower than those calculated due to their explosive behavior). UV-Vis spectra were recorded in the solid state using a Varian Cary 500 spectrometer in the wavelength range of 350–1000 nm. The step in the absorption intensity at 800 nm is caused by a detector change. Impact sensitivity tests were carried out according to STANAG 4489[10] with a modified instruction[11] using a BAM (Bundesanstalt für Materialforschung und -prüfung) drop hammer.[12,13] Ball drop impact sensitivities were determined on an OZM ball drop machine (BIT-132) following MIL-STD-1751A (method 1016) by dropping a free-falling steel ball onto the explosive compound.[14] A sample of approximately 30 mg was placed on a steel block and spread into a 0.33 mm layer of substance. The steel ball guide was set to the desired height and the loaded impact block positioned underneath. By releasing the ball shield, a 0.500-inch steel ball, weighing 8.35 g, was allowed to fall onto the sample. Any visual observation of decomposition was regarded as a positive result. If no reaction occurred, the remaining substance was disposed, and the impact block loaded with a freshly prepared sample. The limiting impact energy was determined in conformity with the recommended UN method for testing impact and friction sensitivities (1-in-6 approach), according to ST/SG/AC.10/11/Rev.6 (s. 13.4.2.3.3).[15] The impact energy was calculated as the product of the weight of the steel ball and its fall height. An initial drop height was chosen, at which an explosion of the sample could be ensured. The impact energy level (ball guide height) was now stepwise decreased until no reaction was observed. At this point, testing was continued up to a total of six trials at that certain energy level. If an explosion occurred, the procedure was repeated by decreasing the drop height. As soon as six trials at a fixed energy level emerged as negative, the next higher energy level, where at least one out of at least six trials resulted in an explosion, is determined as the limiting impact energy. Friction sensitivity tests were carried out according to STANAG 4487[16] with

a modified instruction[17] using the BAM friction tester. The classification of the tested compounds results from the "UN Recommendations on the Transport of Dangerous Goods".[18] Additionally, all compounds were tested to determine the sensitivity toward electrical discharge using the OZM Electric Spark Tester ESD 2010 EN or OZM Electric Spark XSpark10 device.[11] Hot plate and hot needle tests were performed in order to classify the initiation capability of selected complexes. The samples were fixed on a copper plate underneath adhesive tape and initiated by a red-hot needle. Strong deflagration or detonation of the compound usually indicates a valuable primary explosive. The safe and straightforward hot plate test only shows the behavior of the unconfined sample toward fast heating on a copper plate. It does not necessarily allow any conclusions on a compound´s capability as a suitable primary explosive. Initiation capability tests of the newly investigated complexes toward pentaerythritol tetranitrate (PETN) were carried out in a copper shell with a diameter of 7 mm and length of 88 mm filled with 200 mg of sieved secondary explosive (grain size < 100 µm). First, the secondary explosive was pressed with a weight of 8 kg, then the primary explosive to be investigated was subsequently filled on top of the main charge and pressed with the same pressure force. The shell was sealed by an insulator, placed in a retaining ring, which was soldered to a copper witness plate with a thickness of 1 mm and finally initiated by a type A electric igniter. A positive test is indicated by a hole in the copper plate and fragmentation of the shell caused by a deflagration-to-detonation transition (DDT) of PETN. The laser initiation experiments were performed with a 45 W InGaAs laser diode operating in the single-pulsed mode. The diode is attached to an optical fibre with a core diameter of 400 µm and a cladding diameter of 480 µm. The optical fibre is connected via a SMA type connecter directly to the laser and to a collimator. This collimator is coupled to an optical lens, which was positioned in its focal distance (f = 29.9 mm) to the sample. The lens is shielded from the explosive by a sapphire glass. Approximately 25 mg of the carefully pestled complex to be investigated was filled into a transparent plastic cap (PC), pressed with a pressure force of 1 kN and sealed by a UV-curing adhesive. The confined samples were irradiated at a wavelength of 915 nm, a voltage of 4 V, currents of 7–9 A and varying pulse lengths (0.1 ms–15 ms). The combined currents and pulse lengths result in energy output of about 0.17 mJ up to 36 mJ.

The obtained coordination compounds were washed with cold ethanol when stated, dried overnight in air and used for analytics without further purification.

CAUTION! *All investigated compounds are potentially explosive energetic materials (the majority of the compounds lie in the range of primary explosives), which show partly increased sensitivities toward various stimuli (e.g., elevated temperatures, impact, friction or electrostatic discharge). Therefore, proper security precautions (safety glasses, face shield, earthed equipment and shoes, leather jacket,*

Kevlar gloves, Kevlar sleeves and ear plugs) have to be worn while synthesizing and handling the described compounds. Especially the very sensitive compounds ***14a*** *must be handled with great care!*

Procedure for the preparation of 1-amino-5*H*-tetrazole (4a) and 2-amino-5*H*-tetrazole (5a):

Selective 1-amino-5*H*-tetrazole (4a) synthesis:
Hydrazine monohydrate (46.2 mL, 940 mmol) was dissolved in 200 ml ethanol and the mixture cooled to 0 °C with an ice bath. Under vigorous stirring benzaldehyde (24 mL, 236 mmol) was added dropwise over a time period of 5 minutes. After complete addition, the resulting mixture was further stirred for 1 min at this temperature before quenching with water (300 mL). The milky white aqueous phase was extracted with dichloromethane (3 x 300 mL) and the combined organic phases dried over $MgSO_4$. The solvent was removed under reduced pressure yielding benzhydrazone in form of a yellow, odorous oil (20.8 g, 193 mmol, 82%). ^{1}H NMR ($CHCl_3$-*d*, 25 °C, ppm) δ: 7.71 (s, 1H, NC-*H*), 7.54–7.49 (m, 2H, C_{aromat}-*H*), 7.36–7.23 (m, 3H, C_{aromat}-*H*), 5.48 (s, 2H, -NH_2). Benzhydrazone (20.8 g, 193 mmol) was dissolved in triethyl orthoformate (60 mL, 364 mmol) and subsequently further reacted with sodium azide (16.0 g, 246 mmol). While stirring, glacial acetic acid (100 mL) was added dropwise and the resulting reaction mixture heated to 80 °C for 2.5 h. During the reaction, a color change from yellow to orange and finally red could be observed. After complete reaction, the warm mixture was poured into water (200 mL) and stirred overnight. The yellow precipitate formed was filtrated, washed with a small amount of water and dried overnight in air yielding 1-benzylideneaminotetrazole (13.2 g, 76.2 mmol, 40%). ^{1}H NMR ($CHCl_3$-*d*, 25 °C, ppm) δ: 9.37 (s, 1H, N_4C-*H*), 8.87 (s, 1H, NC-*H*), 7.96–7.84 (m, 2H, C_{aromat}-*H*), 7.67–7.47 (m, 3H, C_{aromat}-*H*). Under vigorous stirring, concentrated hydrochloric acid (150 mL) was added to 1-benzylideneaminotetrazole (13.2 g, 76.2 mmol) and water (200 mL). The suspension obtained was refluxed for 30 min resulting in a clear yellow solution. The cleaved benzaldehyde was removed together with the solvent in vacuo at 80 °C and the residues checked by TLC upon reaction completion. The received yellow-white residue was neutralized with a saturated solution of $NaHCO_3$ and extracted with EtOAc (3 x 400 mL). The combined organic phases were dried over $MgSO_4$ and the solvent removed under reduced pressure, yielding 1-amino-5*H*-tetrazole (**4a**, 6.40 g, 75.2 mmol, 99%) in form of a yellow liquid.

Amination of 1,5*H*-tetrazole:
The performed synthesis of the two isomers was carried out analogous to our previous reported procedure.[20] 1,5*H*-Tetrazole (14.0 g, 200 mmol) was dissolved in water (150 mL) and treated with Na_2CO_3 (23.2 g, 219 mmol). The resulting solution was heated to 75 °C, followed by the dropwise addition of hydroxylamine-*O*-sulfonic acid (27.2 g, 240 mmol) in water (120 mL). In the meantime, the

pH value of the solution was maintained between 7 and 8 by periodic addition of a saturated solution of $NaHCO_3$. The reaction mixture was refluxed for 30 min followed by the evaporation of approximately half of the solvent under reduced pressure. After continuously extracting the remaining solution with ethyl acetate for two days, the evaporation of the extract gave a viscous oil containing both isomers **4a** and **5a**. The isomers were separated by column chromatography (SiO_2, ethyl acetate/ dichloromethane 5:1, R_f = 0.71, 0.47) yielding highly pure 2-amino-5*H*-tetrazole (**5a**, 3.17 g, 37.2 mmol, 19%) and 1-amino-5*H*-tetrazole (**4a**, 4.54 g, 53.4 mmol, 27%) as colorless liquids.

1-Amino-5*H*-tetrazole (4a)
DTA (5 °C min^{-1}): 182 °C (exothermic); IR (ATR, cm^{-1}): ῦ = 3326 (m), 3197 (m), 3144 (m), 1626 (m), 1491 (w), 1430 (w), 1342 (w), 1273 (w), 1185 (s), 1098 (vs), 962 (s), 871 (s), 723 (m), 695 (m), 643 (vs); ^{1}H NMR (DMSO-d_6, 25 °C, ppm) δ: 9.24 (s, 1H, C-*H*), 7.10 (s, 2H, -NH_2); ^{13}C NMR (DMSO-d_6, 25 °C, ppm) δ: 143.4 (-*C*N_4); ^{15}N NMR (MeCN-d_3, 25 °C, ppm) δ: 6.8 (N3), −10.0 (N2), −53.8 (N4, d, $^2J_{N\text{-}H}$ = 11.2 Hz), −138.0 (N1, d, $^2J_{N\text{-}H}$ = 8.4 Hz), −308.4 (N5, t, $J_{N\text{-}H}$ = 73.1 Hz); EA: (CH_3N_5, 85.07) calcd.: C 14.12, H 3.55, N 82.33%; found: C 14.60, H 3.63, N 82.16%.

2-Amino-5*H*-tetrazole (5a)
DTA (5 °C min^{-1}): 197 °C (exothermic); IR (ATR, cm^{-1}): ῦ = 3314 (m), 3144 (m), 3128 (m), 3083 (w), 3012 (w), 2978 (w), 1685 (w), 1613 (m), 1488 (m), 1451 (m), 1434 (m), 1388 (w), 1374 (w), 1361 (w), 1285 (s), 1259 (w), 1218 (m), 1174 (s), 1141 (s), 1111 (s), 1103 (s), 1064 (m), 1024 (s), 992 (s), 975 (s), 928 (s), 876 (s), 803 (w), 797 (w), 745 (m), 722 (m), 704 (s), 680 (m), 666 (vs), 644 (m); ^{1}H NMR (DMSO-d_6, 25 °C, ppm) δ: 8.72 (s, 1H, C-*H*), 8.03 (s, 2H, -NH_2); ^{13}C NMR (DMSO-d_6, 25 °C, ppm) δ: 151.8 (-*C*N_4); ^{15}N NMR (MeCN-d_3, 25 °C, ppm) δ: −11.2 (N3), −53.9 (N4, d, $^2J_{N\text{-}H}$ = 12.2 Hz), −78.9 (N1, d, $^2J_{N\text{-}H}$ = 14.5 Hz), −92.6 (N2, d, $^2J_{N\text{-}H}$ = 7.9 Hz), −289.6 (N5, t, $J_{N\text{-}H}$ = 72.5 Hz); EA: (CH_3N_5, 85.07) calcd.: C 14.12, H 3.55, N 82.33%; found: C 14.45, H 3.58, N 82.26%.

Selective 1-amino-5-methyl-tetrazole (4b) synthesis:
Hydrazine monohydrate (200 mL, 4.07 mol) was dissolved in ethanol (800 mL) and cooled down to 0 °C. While stirring, benzaldehyde (100 mL, 0.98 mol) was added dropwise over 5 min. After complete addition, the solution was stirred for another minute before adding water (1000 mL). The reaction mixture was extracted with dichloromethane (3x600 mL). The crude product was distilled under heating in vacuo to yield pure benzhydrazone (40.2 g, 0.33 mol, 33%) as a colorless oil. ^{1}H NMR ($CHCl_3$-*d*, 25 °C, ppm) δ: 7.71 (s, 1H, NC-*H*), 7.54–7.49 (m, 2H, C_{aromat}-*H*), 7.36–7.23 (m, 3H, C_{aromat}-*H*), 5.48 (s, 2H, -NH_2). To a dispersion of benzhydrazone (40.0 g, 0.33 mol), NaN_3 (28.3 g, 0.43 mol) and triethyl orthoacetate (119.4 g, 0.73 mol) glacial acetic acid (180 mL) was added dropwise while stirring. The solution was heated to 80 °C, stirred for 2.5 h and then poured into water (1000 mL). After 2 days an orange solid was

filtered off and recrystallized from ethanol to yield 1-benzylidene-1-amino-5-methyltetrazole (12.2 g, 0.07 mmol, 21%) as a colorless solid. ^{1}H NMR (DMSO-d_6, 25 °C, ppm) δ: 9.41 (s, 1H, NC-*H*), 8.04 (d, 2H, C_{aromat}-*H*), 7.64 (t, 1H, C_{aromat}-*H*), 7.58 (t, 2H, C_{aromat}-*H*, 2.63 (s, 3H, -CH_3); ^{13}C NMR (DMSO-d_6, 25 °C, ppm) δ: 158.6 (H*C*=N), 150.1 (N*C*N), 133.1 (C_{aromat}-H), 131.6 (C_{quart}), 129.3 (C_{aromat}-H), 129.2 (C_{aromat}-H), 8.3 (-*C*H$_3$). 3 M hydrochloric acid (250 mL) was added and the reaction mixture water steam distilled to yield 1-amino-5-methyltetrazole (6.3 g, 0.06 mol, 18%) as a brown solid

Amination of 5-methyltetrazole:

The performed synthesis of the two isomers was carried out similar to the amination of unsubstituted tetrazole. To a dispersion of sodium carbonate (31.9 g, 301 mmol) in water (150 mL) in a 1000 mL round-bottom flask, 5-methyltetrazole (12.0 g, 143 mmol) was added while stirring. The resulting solution was heated to 75 °C and hydroxylamine-*O*-sulfonic acid (38.7 g, 342 mmol) dissolved in water (50 mL) was added dropwise over the course of 35 min. During the entirety of the addition the pH of the solution was kept between 7–8, utilizing a saturated solution of sodium bicarbonate. Upon completion of the addition, the reaction mixture was stirred at elevated temperature for another 1 h. The mixture was allowed to cool to room temperature and was subsequently continuously extracted with ethyl acetate (3 × 200 mL) for time periods of 48 h, 24 h and 3 h. The combined organic phases were dried with sodium sulfate and the solvent was removed under reduced pressure. Purification by flash column chromatography (1:1 EtOAc/isohexane) yielded 1-amino-5-methyltetrazole (**4b**, 4.58 g, 46.2 mmol, 33%) and 2-amino-5-methyltetrazole (**5b**, 3.58 g, 36.1 mmol, 25%) as light-yellow oils.

1-Amino-5-methyl-tetrazole (4b)

DTA (5 °C min^{-1}): 220 °C (exothermic); IR (ATR, cm^{-1}): ῦ = 3273 (m), 3169 (m), 1715 (w), 1617 (m), 1499 (s), 1417 (m), 1379 (s), 1353 (s), 1222 (m), 1191 (m), 1076 (m), 1034 (s), 951 (s), 770 (s), 714 (s), 666 (s), 634 (s), 577 (s), 558 (s), 550 (s), 533 (s), 521 (s), 514 (s), 489 (vs), 464 (vs), 450 (vs), 434 (vs), 418 (vs), 406 (vs); ^{1}H NMR (DMSO-d_6, 25 °C, ppm) δ: 6.83 (s, 2H, -NH_2), 2.42 (s, 3H, -CH_3); ^{13}C NMR (DMSO-d_6, 25 °C, ppm) δ: 151.0 (-*C*N$_4$), 8.0 (-*C*H$_3$); ^{15}N NMR (MeCN-d_3, 25 °C, ppm) δ: 1.7 (N3), −10.3 (N2), −57.6 (N4), −141.6 (N1) −312.1 (N5, t, J_{N-H} = 73.6 Hz); EA: ($C_2H_5N_5$, 99.10) calcd.: C 24.24, H 5.09, N 70.67%; found: C 23.56, H 5.13, N 66.98%. BAM drop hammer: > 40 J; friction tester: 360 N (at grain size 100–500 µm).

2-Amino-5-methyl-tetrazole (5b)

DTA (5 °C min^{-1}): 184 °C (exothermic); IR (ATR, cm^{-1}): ῦ = 3273 (m), 3169 (m), 1715 (w), 1617 (m), 1499 (s), 1417 (m), 1379 (s), 1353 (s), 1222 (m), 1191 (m), 1076 (m), 1034 (s), 951 (s), 770 (s), 714 (s), 666 (s), 634 (s), 577 (s), 558 (s), 550 (s), 533 (s), 521 (s), 514 (s), 489 (vs), 464 (vs), 450 (vs), 434 (vs), 418 (vs), 406 (vs); ^{1}H NMR (DMSO-d_6, 25 °C, ppm) δ: 7.86 (s, 2H, -NH_2), 2.37 (s, 3H, -CH_3); ^{13}C NMR

(DMSO-d_6, 25 °C, ppm) δ: 160.2 (-*C*N_4), 10.7 (-*C*H_3); ^{15}N NMR (MeCN-d_3, 25 °C, ppm) δ: −9.8 (N3), −56.1 (N4), −82.9 (N1), −95.8 (N2), −292.7 (N5, t, J_{N-H} = 72.4 Hz); EA: ($C_2H_5N_5$, 99.10) calcd.: C 24.24, H 5.09, N 70.67%; found: C 24.64, H 4.85, N 70.31%. BAM drop hammer: 35 J; friction tester: > 360 N (at grain size 100–500 μm).

General procedure for the preparation of the copper(II) 1-AT picrate (PA), 2,4,6-trinitro-3-hydroxyphenolate (HTNR), 2,4,6-trinitro-3,5-dihydroxyphenolate (H_2TNPG) complexes (6–8):
Copper(II) carbonate (**6**: 61.8 mg, 0.50 mmol; **7**: 30.9 mg, 0.25 mmol; **8**: 15.5 mg, 0.125 mmol) and the corresponding trinitrobenzene derivative based acid (**1**: 229 mg, 1.00 mmol; **2**: 123 mg, 0.50 mmol; **3**: 65.2 mg, 0.25 mmol) were combined and dissolved in distilled water (5 mL) at 80 °C. After obtaining a clear solution, the ligand (**6**: 85.0 mg, 1.00 mmol; **7**: 42.5 mg, 0.50 mmol; **8**: 42.5 mg, 0.50 mmol) was added, the reaction mixture mechanically stirred for one minute at this temperature and finally left for crystallization. After crystallization, the complexes were filtered off, washed with cold ethanol and dried in air.

[Cu(PA)$_2$(1-AT)$_2$] (6)
Coordination compound **6** could be isolated within 6 days in the form of green single crystals suitable for X-ray determination. Yield: 163 mg (0.24 mmol, 47%).

DTA (5 °C min^{-1}): 178 °C (exothermic); IR (ATR, cm^{-1}): ῡ = 3363 (w), 3331 (m), 3229 (w), 3131 (w), 3086 (w), 1634 (w), 1608 (s), 1573 (s), 1525 (vs), 1504 (s), 1419 (m), 1361 (s), 1345 (vs), 1320 (vs), 1266 (vs), 1191 (s), 1165 (s), 1085 (vs), 1000 (s), 968 (vw), 944 (m), 933 (m), 915 (m), 887 (s), 845 (s), 825 (s), 786 (m), 741 (m), 707 (s), 639 (s), 608 (vs), 590 (s), 576 (w), 549 (w), 526 (w), 449 (m), 431 (m); EA: ($C_{14}H_{10}CuN_{16}O_{14}$, 689.88): calcd.: C 24.37, H 1.46, N 32.49%; found: C 24.28, H 1.49, N 32.22%; BAM drop hammer: 4 J; friction tester: 120 N; ESD: 46 mJ (at grain size > 100 μm (ESD) and 500–1000 μm (IS, FS).

[Cu(HTNR)$_2$(1-AT)$_2$] (7)
Yellow-green blocks suitable for X-ray diffraction of the copper(II) styphnate complex **7** were obtained in less than one day. Yield: 141 mg (0.20 mmol, 80%).

DTA (5 °C min^{-1}): 186 °C (exothermic); IR (ATR, cm^{-1}): ῡ = 3363 (m), 3304 (w), 3252 (w), 3166 (m), 3067 (w), 2953 (w), 1629 (m), 1562 (s), 1526 (vs), 1477 (s), 1454 (s), 1376 (s), 1357 (m), 1311 (s), 1276 (vs), 1175 (s), 1093 (vs), 1026 (s), 1009 (s), 931 (s), 918 (s), 888 (s), 826 (m), 782 (m), 775 (m), 759 (s), 739 (s), 711 (s), 695 (vs), 644 (vs); EA: ($C_{14}H_{10}CuN_{16}O_{16}$, 721.88): calcd.: C 23.29, H 1.40, N 31.05%; found: C 23.49, H 1.57, N 30.83%; BAM drop hammer: 1.5 J; friction tester: 48 N; ESD: 16 mJ (at grain size 500–1000 μm).

[Cu(H$_2$TNPG)$_2$(1-AT)$_4$] (8)
Within 6 days, complex **8** emerged in the form of green-yellowish rods suitable for X-ray determination. Yield: 90.2 mg (0.10 mmol, 78%).

DTA (5 °C min^{-1}): 193 °C (exothermic); IR (ATR, cm^{-1}): ῡ = 3362 (m), 3346 (w), 3293 (w), 3233 (m), 3155 (w), 2994 (w), 2860 (w), 2638 (s), 1640 (s), 1569 (vs), 1484 (m), 1454 (m), 1410 (s), 1349 (vs), 1329 (vs), 1188 (m), 1147 (vw), 1088 (w), 1027 (w), 995 (m), 955 (w), 937 (w), 910 (vs), 882 (vs), 833 (w), 812 (w), 786 (m), 777 (vw), 747 (vw), 733 (vw), 695 (w), 680 (w), 660 (w), 639 (vw); EA: ($C_{16}H_{16}CuN_{26}O_{18}$, 924.09): calcd.: C 20.80, H 1.75, N 39.41%; found: C 20.84, H 1.88, N 38.05%; BAM drop hammer: 3.5 J; friction tester: 20 N; ESD: 90 mJ (at grain size 100–500 μm).

General procedure for the preparation of the copper(II) 2-AT picrate (PA), 2,4,6-trinitro-3-hydroxyphenolate (HTNR), 2,4,6-trinitro-3,5-dihydroxyphenolate (H$_2$TNPG) complexes (9–11):
Copper(II) carbonate (**9**–**11**: 30.9 mg, 0.25 mmol) and the corresponding trinitrobenzene derivative based acid (**1**: 115 mg, 0.50 mmol; **2**: 123 mg, 0.50 mmol; **3**: 131 mg, 0.50 mmol) were mechanically stirred in H_2O (5 mL) at 80 °C. After a clear solution was obtained, the reaction mixture was treated under stirring with 2-amino-5*H*-tetrazole (**5a**, **9**/**10**: 42.5 mg, 0.50 mmol; **11**: 85.0 mg, 1.00 mmol) and finally left for crystallization. After crystallization, the complexes were filtered off, washed with cold ethanol and dried in air.

[Cu(PA)$_2$(2-AT)$_2$] (9)
Within five days, compound **9** was obtained in the form of green needles suitable for X-ray determination. Yield: 163 mg (0.24 mmol, 95%).

DTA (5 °C min^{-1}): 203 °C (exothermic); IR (ATR, cm^{-1}): ῡ = 3347 (m), 3271 (w), 3164 (w), 3097 (w), 3072 (w), 1632 (w), 1607 (m), 1575 (vs), 1532 (s), 1520 (s), 1507 (s), 1480 (s), 1422 (m), 1361 (m), 1338 (vs), 1309 (s), 1265 (s), 1167 (s), 1139 (s), 1083 (m), 1048 (m), 1028 (m), 935 (m), 926 (s), 914 (s), 894 (s), 845 (m), 825 (w), 785 (m), 743 (m), 707 (s), 691 (s), 680 (m), 554 (w), 521 (w); EA ($C_{14}H_{10}CuN_{16}O_{14}$, 689.92): calcd.: C 24.37, H 1.46, N 32.49%; found: C 24.28, H 1.71, N 32.08%; BAM drop hammer: 3 J; friction tester: 128 N; ESD: 60 mJ (at grain size 100–500 μm).

[Cu(HTNR)$_2$(2-AT)$_2$] (10)
The copper(II) styphnate complex **10** could be isolated within one day in the form of green blocks suitable for X-ray diffraction. Yield: 95.3 mg (0.13 mmol, 53%).

DTA (5 °C min^{-1}): 206 °C (exothermic); IR (ATR, cm^{-1}): ῡ = 3333 (m), 3262 (w), 3165 (m), 3080 (w), 1633 (m), 1563 (s), 1538 (vs), 1491 (s), 1458 (s), 1375 (m), 1339 (s), 1328 (s), 1293 (vs), 1245 (s), 1189 (s), 1175 (s), 1153 (s), 1093 (s), 1050 (m), 1033 (s), 944 (s), 932 (s), 891 (s), 828 (m), 779 (m), 764 (m),

732 (m), 719 (s), 700 (vs), 686 (vs), 677 (vs), 657 (s), 628 (s); EA: ($C_{14}H_{10}CuN_{16}O_{16}$, 721.88): calcd.: C 23.29, H 1.40, N 31.05%; found: C 23.35, H 1.51, N 30.84%; BAM drop hammer: 3 J; friction tester: 48 N; ESD: 20 mJ (at grain size 100–500 μm).

[Cu(H_2TNPG)$_2$(2-AT)$_4$] (11)
After several days, complex **11** emerged in the form of green blocks suitable for X-ray determination. Yield: 80.4 mg (0.09 mmol, 35%).

DTA (5 °C min^{-1}): 135 °C (endothermic), 176 °C (exothermic); IR (ATR, cm^{-1}): ῦ = 3335 (m), 3268 (m), 3175 (m), 3144 (m), 3120 (w), 1634 (s), 1564 (m), 1495 (s), 1477 (s), 1327 (vs), 1317 (vs), 1303 (vs), 1252 (w), 1226 (m), 1176 (s), 1138 (vs), 1103 (s), 1044 (m), 1024 (m), 947 (s), 909 (s), 899 (s), 828 (m), 816 (s), 786 (s), 765 (s), 751 (m), 724 (s), 696 (s), 690 (s); EA: ($C_{16}H_{16}CuN_{26}O_{18}$, 924.10): calcd.: C 20.80, H 1.75, N 39.41%; found: C 20.73, H 1.75, N 38.87%; BAM drop hammer: 2 J; friction tester: 24 N; ESD: 100 mJ (at grain size 100–500 μm).

General procedure for the preparation of the copper(II) 1-AMT picrate (PA), styphnate (TNR), 2,4,6-trinitro-5-hydroxyresorcinate (HTNPG) complexes (12–14):
Copper(II) carbonate (124 mg, 1.00 mmol) and the corresponding trinitrobenzene derivative based acid (**1**: 458 mg, 2.00 mmol; **2**: 245 mg, 1.00 mmol; **3**: 279 mg, 1.00 mmol) were combined and dissolved in distilled water (5 mL) at 80 °C. After obtaining a clear solution, the ligand (198 mg, 2.00 mmol) was added and the reaction mixture mechanically stirred for one minute at this temperature.

[Cu$_2$(PA)$_4$(1-AMT)$_4$] • (H_2O) (12)
Copper(II) picrate compound **12** was isolated after the solvent was removed under reduced pressure as dark green, crystalline powder (585 mg, 0.40 mmol, 80%).

DTA onset (5 °C min^{-1}): 190 °C (exothermic); IR (ATR, cm^{-1}): ῦ = 3649 (w), 3375 (w), 3363 (w), 3323 (w), 3288 (w), 3231 (w), 3088 (w), 1614 (s), 1576 (s), 1537 (s), 1506 (s), 1477 (m), 1418 (m), 1387 (w), 1361 (s), 1323 (vs), 1271 (vs), 1166 (m), 1133 (w), 1123 (w), 1086 (m), 1033 (m), 1012 (m), 939 (m), 916 (s), 846 (w), 826 (w), 786 (m), 742 (s), 727 (m), 715 (s), 706 (s), 683 (m), 665 (m), 545 (m), 527 (w), 502 (w), 483 (w), 435 (m), 420 (w); EA: ($C_{32}H_{30}Cu_2N_{32}O_{29}$, 1453.96): calcd.: C 26.44, H 2.08, N 30.83%, found: C 26.18, H 1.95, N 30.55%; BAM drop hammer: 2 J; friction tester: 168 N; ESD: 88.4 mJ (at grain size: 100–500 μm).

[Cu(TNR)(1-AMT)$_2$] (13)
After addition of ligand **4b** styphnate complex **13** started precipitating as a green solid, which was filtered off. The reaction solution was left for crystallization, yielding another amount of [Cu(TNR)(1-AMT)$_2$] in the form of green needles (320 mg, 0.634 mmol, 63%).

DTA onset (5 °C min^{-1}): 212 °C (exothermic); IR (ATR, cm^{-1}): ῡ = 3339 (m), 3233 (w), 2180 (vw), 1609 (s), 1582 (m), 1549 (s), 1518 (m), 1482 (m), 1457 (m), 1426 (m), 1371 (m), 1346 (m), 1319 (m), 1290 (s), 1274 (s), 1233 (vs), 1174 (m), 1129 (w), 1106 (s), 1078 (m), 1045 (w), 1026 (m), 1005 (w), 920 (w), 880 (m), 828 (w), 784 (s), 768 (w), 741 (w), 708 (vs), 679 (m), 612 (w), 571 (w), 561 (w), 508 (w), 481 (w), 464 (w), 456 (w), 433 (w), 416 (m); EA: ($C_{10}H_{11}CuN_{13}O_8$, 504.86): calcd.: C 23.79, H 2.20, N 36.07%, found: C 23.95, H 2.12, N 35.69%; BAM drop hammer: 2 J; friction tester: 16 N; ESD: 6.3 mJ, ball drop: 10 mJ (at grain size: 100–500 µm).

[Cu(HTNPG)(1-AMT)$_2$] (14a)
Copper(II) 2,4,6-trinitro-5-hydroxyresorcinate complex **14a** precipitated as brown solid (389 mg, 0.747 mmol, 75%).

DTA onset (5 °C min^{-1}): 202 °C (exothermic); IR (ATR, cm^{-1}): ῡ = 3357 (w), 3342 (m), 3309 (w), 3283 (w), 3233 (w), 3228 (w), 2005 (w), 1602 (m), 1526 (s), 1506 (vs), 1487 (vs), 1467 (m), 1408 (w), 1373 (m), 1354 (s), 1312 (s), 1292 (vs), 1275 (vs), 1203 (s), 1180 (s), 1166 (m), 1130 (s), 1094 (m), 1047 (w), 1031 (w), 919 (s), 864 (w), 845 (m), 814 (s), 793 (s), 764 (w), 754 (w), 720 (m), 705 (s), 677 (m), 667 (m), 645 (w), 464 (w), 436 (m), 416 (m); EA: ($C_{10}H_{11}CuN_{13}O_9$, 520.86): calcd.: C 23.06, H 2.13, N 34.96%, found: C23.29, H 2.05, N 34.73%; BAM drop hammer: 1 J; friction tester: 7 N; ESD: 4.9 mJ, ball drop: 8 mJ (at grain size: 100–500 µm).

General procedure for the preparation of the copper(II) 2-AMT picrate (PA), styphnate (TNR), 2,4,6-trinitro-3,5-dihydroxyphenolate (H_2TNPG) complexes (15–17):
Copper(II) carbonate (**15**–**17**: 247 mg, 2.00 mmol) and the corresponding trinitrobenzene derivative based acid (**1**: 916 mg, 4.00 mmol; **2**: 490 mg, 2.00 mmol; **3**: 1.12 g, 4.00 mmol) were mechanically stirred in H_2O (5 mL) at 80 °C. After a clear solution was obtained, the reaction mixture was treated under stirring with 2-amino-5-methyltetrazole (**5b**, **15**/**17**: 396 mg, 4.00 mmol; **16**: 298 mg, 2.00 mmol). The reaction mixtures were stirred for another 15 min, before the solvent was evaporated and the products were obtained as crystalline solids.

[Cu(PA)$_2$(2-AMT)$_2$] (15)
Picrate complex **15** was obtained as a dark green, crystalline solid (1.06 g, 1.48 mmol, 74%).

DTA onset (5 °C min^{-1}): 176 °C (exothermic); IR (ATR, cm^{-1}): ῡ = 3361 (w), 3350 (m), 3289 (w), 3203 (w), 3135 (w), 3083 (w), 1873 (vw), 1639 (w), 1607 (s), 1579 (s), 1515 (vs), 1463 (m), 1423 (m), 1335 (vs), 1278 (vs), 1186 (m), 1167 (s), 1117 (w), 1091 (s), 1044 (m), 936 (m), 918 (s), 892 (s), 848 (m), 826 (m), 794 (m), 784 (m), 770 (m), 740 (s), 717 (s), 700 (vs), 673 (m), 646 (m), 632 (m), 547 (m), 533 (m), 522 (m), 508 (m), 480 (m), 426 (w), 412 (m); EA: ($C_{16}H_{14}CuN_{16}O_{14}$, 717.97): calcd.: C 26.77, H 1.97,

N 31.22%, found: C 26.64, H 1.87, N 30.79%; BAM drop hammer: 2.5 J; friction tester: 108 N; ESD: 37 mJ (at grain size: 100–500 µm).

[Cu(TNR)(2-AMT)(H_2O)] • (H_2O) (16)
The final product was obtained as a green, crystalline solid, however IR spectroscopy revealed impurities. Recrystallization from water gave pure **16** (190 mg, 0.430 mmol, 22%) in the form of green rods.

DTA onset (5 °C min^{-1}): 122 °C (endothermic), 160 °C (endothermic), 172 °C (exothermic); IR (ATR, cm^{-1}): ῡ = 3608 (w), 3326 (m), 3261 (w), 3085 (w), 2005 (vw), 1599 (m), 1582 (m), 1526 (s), 1481 (s), 1458 (s), 1444 (s), 1377 (m), 1350 (m), 1282 (vs), 1247 (vs), 1206 (s), 1175 (s), 1112 (s), 1047 (m), 1017 (m), 923 (m), 779 (m), 769 (m), 733 (m), 707 (vs), 675 (s), 639 (m), 578 (m), 516 (m), 478 (m), 465 (m), 446 (s), 436 (s), 419 (s); EA: ($C_8H_{10}CuN_8O_{10}$, 441.78): calcd.: C 21.75, H 2.28, N 25.37%, found: C 21.91, H 2.19, N 25.32%; BAM drop hammer: 2,5 J; friction tester: 38 N; ESD: 840 mJ (at grain size: 100–500 µm).

[Cu(H_2TNPG)$_2$(2-AMT)$_2$] (17)
Copper(II) 2,4,6-trinitro-3,5-dihydroxyphenolate **17** was isolated as green, crystalline solid (900 mg, 1.15 mmol, 58%).

DTA onset (5 °C min^{-1}): 202 °C (exothermic); IR (ATR, cm^{-1}): ῡ = 3354 (m), 3286 (w), 3211 (w), 3086 (w), 1634 (s), 1573 (m), 1539 (s), 1514 (vs), 1488 (s), 1413 (m), 1366 (m), 1342 (s), 1316 (vs), 1193 (s), 1182 (s), 1156 (vs), 1041 (m), 919 (m), 903 (m), 834 (s), 823 (m), 784 (s), 769 (m), 760 (s), 737 (s), 720 (s), 700 (s), 678 (vs), 659 (s), 641 (s), 626 (s), 506 (m), 479 (m), 440 (m), 410 (m); EA ($C_{16}H_{14}CuN_{16}O_{18}$, 781.98): calcd.: C 24.58, H 1.80, N 28.66%, found: C 24.61, H 1.76, N 28.45%; BAM drop hammer: 2 J; friction tester: 20 N; ESD: 8.2 mJ (at grain size: 500–100 µm).

3.6.11. References

[1] *CrysAlisPro*, Oxford Diffraction Ltd., version 171.33.41, **2009**.

[2] A. Altomare, G. Cascarano, C. Giacovazzo, A. Guagliardi, *J. Appl. Crystallogr.* **1993**, *26*, 343–350.

[3] a) A. Altomare, G. Cascarano, C. Giacovazzo, A. Guagliardi, A. G. G. Moliterni, M. C. Burla, G. Polidori, M. Camalli, R. Spagna, *SIR97*, **1997**; b) A. Altomare, M. C. Burla, M. Camalli, G. L. Cascarano, C. Giacovazzo, A. Guagliardi, A. G. G. Moliterni, G. Polidori, R. Spagna, *J. Appl. Crystallogr.* **1999**, *32*, 115–119.

[4] a) G. M. Sheldrick, *SHELXL-97*, University of Göttingen, Germany, **1997**; b) G. M. Sheldrick, *Acta Crystallogr. Sect. A* **2008**, *64*, 112–122.

[5] A. L. Spek, *PLATON*, Utrecht University, The Netherlands, **1999**.

[6] L. J. Farrugia, *J. Appl. Cryst.* **2012**, *45*, 849–854.

[7] Empirical absorption correction using spherical harmonics, implemented in SCALE3 ABSPACK scaling algorithm (CrysAlisPro Oxford Diffraction Ltd., Version 171.33.41, **2009**).

[8] *APEX3*. Bruker AXS Inc., Madison, Wisconsin, USA.

[9] J. R. Rodriguez-Carvajal, Abstracts of the Satellite Meeting on Powder Diffration of XV Congress of the IUCr, Toulouse, France, **1990**.

[10] NATO standardization agreement (STANAG) on explosives, impact sensitivity tests, no. 4489, 1st ed., Sept. 17, **1999**.

[11] WIWEB-Standardarbeitsanweisung 4-5.1.02, Ermittlung der Explosionsgefährlichkeit, hier der Schlagempfindlichkeit mit dem Fallhammer, Nov. 8, **2002**.

[12] http://www.ozm.cz, (accessed April 2019).

[13] http://www.bam.de, (accessed April 2019).

[14] Military Standard 1751A (MIL-STD-1751A): safety and performance tests for qualification of explosives (high explosives, propellants and pyrotechnics), method 1016, Dec. 11, **2001**.

[15] UN Model Regulation: Recommendations on the Transport of Dangerous Goods – Manual of Tests and Criteria, section 13.4.2.3.3, **2015**.

[16] NATO standardization agreement (STANAG) on explosive, friction sensitivity tests, no. 4487, 1st ed., Aug. 22, **2002**.

[17] WIWEB-Standardarbeitsanweisung 4-5.1.03, Ermittlung der Explosionsgefährlichkeit oder der Reibeempfindlichkeit mit dem Reibeapparat, Nov. 8, **2002**.

[18] Impact: insensitive > 40 J, less sensitive ≥ 35 J, sensitive ≥ 4 J, very sensitive ≤ 3 J; Friction: insensitive > 360 N, less sensitive = 360 N, sensitive < 360 N and > 80 N, very sensitive ≤ 80 N, extremely sensitive ≤ 10 N. According to the UN Recommendations on the Transport of Dangerous Goods, 5th ed., **2009**.

[19] N. Szimhardt, M. H. H. Wurzenberger, L. Zeisel, M. S. Gruhne, M. Lommel, J. Stierstorfer, *J. Mater. Chem. A* **2018**, *6*, 16257–16272.

4. Comparison of 1-Ethyl-5*H*-tetrazole and 1-Azidoethyl-5*H*-tetrazole as Ligands in Energetic Transition Metal Complexes

Maximilian H. H. Wurzenberger, Michael S. Gruhne, Marcus Lommel, Norbert Szimhardt, Thomas M. Klapötke, and Jörg Stierstorfer

Published in *Chemistry – an Asian Journal* **2019**, *14*, 2018–2028.

DOI: 10.1002/asia.201900269

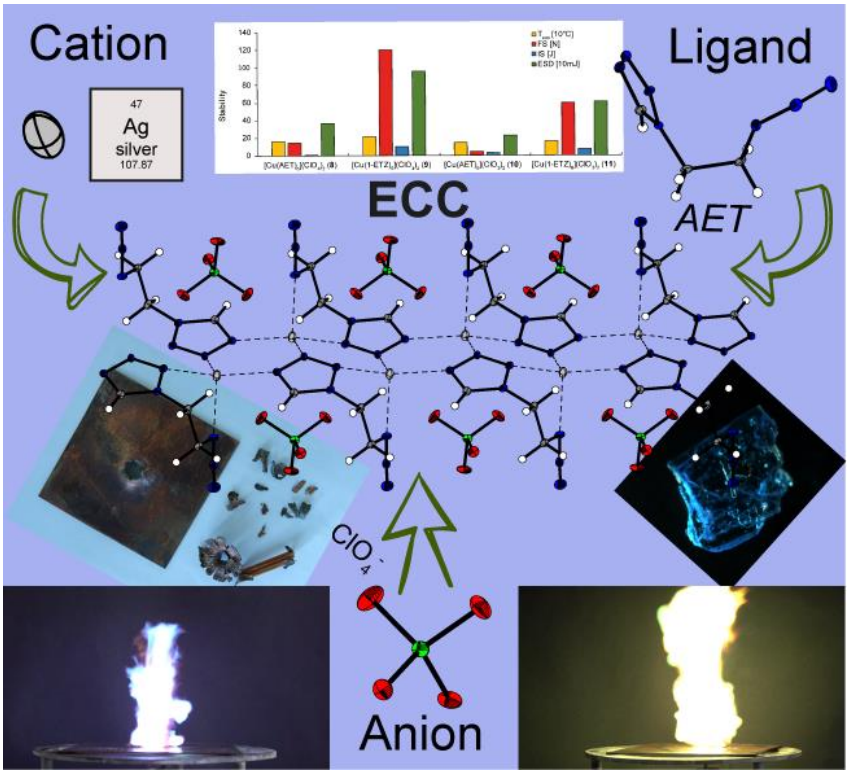

Abstract: Energetic coordination compounds (ECC) based on 3d or 4d transition metals show promising characteristics to be used as potential replacements for highly toxic lead-containing primary explosives. Herein we report the synthesis of 12 new ECC based on 1-azidoethyl-5*H*-tetrazole (AET) or 1-ethyl-5*H*-tetrazole (1-ETZ) as nitrogen-rich ligands as well as various central metals (Cu^{2+}, Fe^{2+}, Zn^{2+}, Ag^{+}) and anions such as perchlorate and nitrate. The influence of the increased endothermicity by adding an additional azide group was studied by comparing analogous ECC based on AET and 1-ETZ. Furthermore, the compounds were extensively analyzed by XRD, IR, EA, solid-state UV-Vis, and DTA as well as their sensitivities toward impact and friction were determined with BAM standard techniques, together with their sensitivity against electrostatic discharge. The sensitivities were compared with the one toward ball drop impact measurements. Classical initiation tests (nitropenta filled detonators) and ignition by laser irradiation highly prove the potential use of the most promising compounds in lead-free initiation systems.

4.1. Introduction

Ever since the discovery of the azide anion by Curtius in 1890,[1] the ongoing azide chemistry has fascinated several generations of chemists. Today almost every single element from the periodic table has been combined to build up covalent and ionic azides. The combination of simple main-group and transition metals with the azide anion has provided one high point in this chemistry together with the well-deserved reputation for the explosive behavior.[2] Among easily available and industrial useful ionic azides, lead azide (LA) and sodium azide are the most prominent examples. Nowadays, NaN_3, as the cheapest azide source, is indispensable in many chemical transformations like substitutions or addition reactions in synthetic organic chemistry. Additionally, sodium azide was also found in previous airbag systems.[3] Covalently bonded and ionic azides, in particular, heavy metal azides, are known as thermally decomposable and, in part, explosive classes of compounds. LA is one of the most commonly used primary explosives in both industrial and military applications. However, alternatives, so-called green primary explosives, are in great demand to prevent the considerable, highly toxic lead contamination in military training grounds. Over 95% of all missile launches, shooting, and explosions within the police forces or military are done exclusively for training purposes in "friendly" areas,[4] leading to an ongoing research for new and more eco-friendly energetic materials.[5–10] Since the discovery of phenyl azide in 1864,[11] azido organic compounds have attracted the attention of chemists due to their unique characteristics. The initial postulation of Curtius and Hantzsch for the structural determination of organic azides suggested a cyclic 1*H*-triazirine structure. Later, however, this hypothesis was rapidly revised in favor of the linear structure (Scheme 1).[1,12–14] The chemical diversity of many organic azides can be explained on the basis of the physicochemical properties by a consideration of the polar mesomeric structures.[15,16]

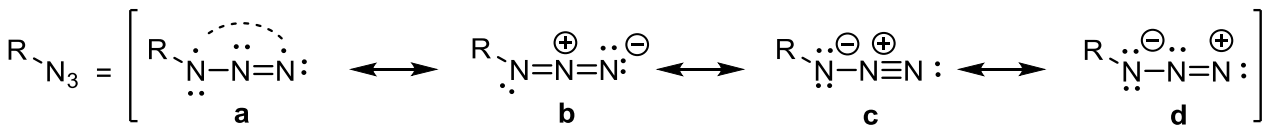

Scheme 1. Mesomeric structures of covalent bonded azide.

The mesomeric structures **c** and **d**, proposed by Pauling,[17,18] compellingly explain the reactivity in 1,3-dipolar cycloadditions and the decomposition of azides to form nitrenes under the elimination of nitrogen gas. The reactivity of the azide functionality in terms of nucleophilicity (nucleophilic attack of N1) and electrophilicity (nucleophilic attack on N3) can be deduced from the basis of structure **d**. From a thermodynamic standpoint, the azide group is a structural fragment, which shows a high positive heat of formation and adding about 364 kJ mol^{-1} of endothermicity to a hydrocarbon compound.[19] Additionally,

the azide groups exhibit an environmentally friendly balance, as nitrogen gas is produced as an exclusive smokeless combustion product. Therefore, organic azides are potential candidates for the use in high energetic materials like binders, hypergolic ionic liquids, plasticizers and additives (Figure 1).[2,20–23]

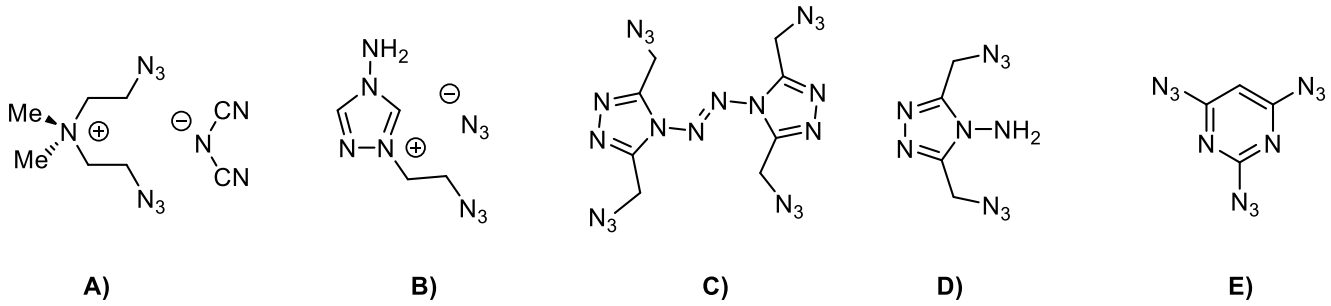

Figure 1. Representative examples for energetic organic compounds: hypergolic ionic liquids (bis(2-azidoethyl)dimethylammonium dicyanamide (**A**) and 1-(2-azidoethyl)-4-amino-1,2,4-triazolium azide (**B**)), energetic plasticizers (3,3',5,5'-tetra(azidomethyl)-4,4'-azo-1,2,4-triazole (**C**) and 4-amino-3,5-di(azidomethyl)-1,2,4-triazole (**D**)), or an energetic additive in nanotubes (2,4,6-triazidopyrimidine (**E**)).

Due to the smokeless gas evolution, the major application nowadays is found in gas generators. Besides these utilizations of organic azides, the use in primary explosives is especially promising. Nitrogen-rich molecules are considered as prime candidates for "green" energetic materials[24–27] since the main combustion product is molecular dinitrogen and the materials exhibit desirable performance characteristics in high explosives due to their high positive heat of formation.

In this paper, we demonstrate the increasing performance of ECC by solely substituting one proton of the alkyl rest of 1-ethyl-5*H*-tetrazole with an azide group. The AET based transition metal complexes were both investigated toward their usability as lead-free primary and laser ignitable explosives. In addition, they were compared to their analogous ECC with unsubstituted 1-ETZ as nitrogen-rich ligand.

4.2. Results and Discussion

4.2.1. Synthesis

Over three decades ago, the synthesis of 1-azidoethyl-5*H*-tetrazole was published for the first time by Gaponik *et al.*.[28] The only reported complex is based on copper(II) chloride as metal salt and was only investigated for its crystal structure.[29] For synthesizing ligand **1** a two-step reaction, starting from a simple and cheap feedstock was performed (Scheme 2). The first target molecule was 1-azidoethylamine hydrochloride, which is less volatile than the neutral compound and for which several syntheses are already reported in the literature.[30,31] 2-Chloroethylamine hydrochloride was reacted with sodium azide in water to form the intermediate in quantitative yield.

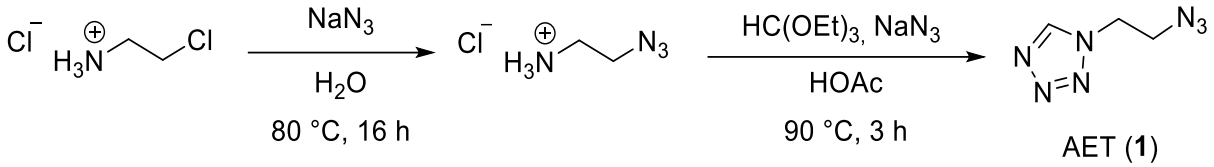

Scheme 2. Synthesis of 1-azidoethyl-5*H*-tetrazole (**1**) starting from 2-chloroethylamine hydrochloride.

The crude hydrochloride salt was converted in a [3+1+1] cyclization to the corresponding substituted alkyl tetrazole **1** by applying an excess of triethyl orthoformate and sodium azide in glacial acetic acid at elevated temperature. For the isolation of the nitrogen-rich ligand, the crude was filtrated, extracted with ethyl acetate and subjected to column chromatography leading to a yellowish oil in acceptable 33% yield over two steps. The physical state of **1** can be explained by previous reports showing the liquefying effect of the azidoethyl functionality.[2] With 1-ethyl-5*H*-tetrazole (**2**), another ethyl-substituted 5*H*-tetrazole derivative is used for the synthesis of nitrogen-rich ECC in this work. The ligand can be obtained via the same selective pathway (Scheme 3) as mentioned above.[28]

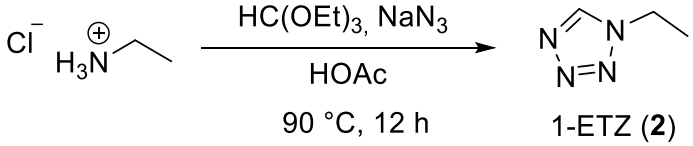

Scheme 3. Selective route for the synthesis of 1-ethyl-5*H*-tetrazole (**2**).

The [3+1+1] ring closure reaction again is performed, using triethyl orthoformate, sodium azide, and glacial acetic acid at 80 °C for 12 h. After filtration and extraction using ethyl acetate, the product was received in a satisfying yield of 75%. Both tetrazole derivatives can easily be characterized by IR spectroscopy (Figure S1), proton and carbon NMR spectroscopy. Additionally, two dimensional ^{1}H-^{15}N-NMR HMBC or proton-coupled ^{15}N NMR spectroscopy can be performed (Figures 2 and 3). As mentioned, a large number of complexes based on various mono-tetrazoles (*e.g.*, 1-methyl- or 1-amino-5*H*-tetrazole) have been described in the literature, either having insufficient power or are way too sensitive for practical use.[32,33] In order to maximize the performance, ligand **1** is applied in the formation of new transition metal complexes, whereas the use of ligand **2** is a promising opportunity for reaching the middle course between both demands. The absence of acidic protons in both ligands allows their inclusion in neutral metal coordination compounds with oxidizing anions like nitrates, perchlorates, picrates (PA), styphnates (TNR) or 2,4,6-trinitro-3,5-dihydroxyphenolates (H_2TNPG). The selective integration of these anions in combination with one of the two ligands and different metal(I) or metal(II) cations, results in energetic coordination compounds with adjustable sensitivities and performance parameters. The formation of the coordination compounds **3**–**9** was achieved through the combination of

ethanolic solutions of the relevant metal(I) or metal(II) salts and the ligand in stoichiometric amounts at r.t. or elevated temperatures in case of compound **3** (Schemes 4 and 5).

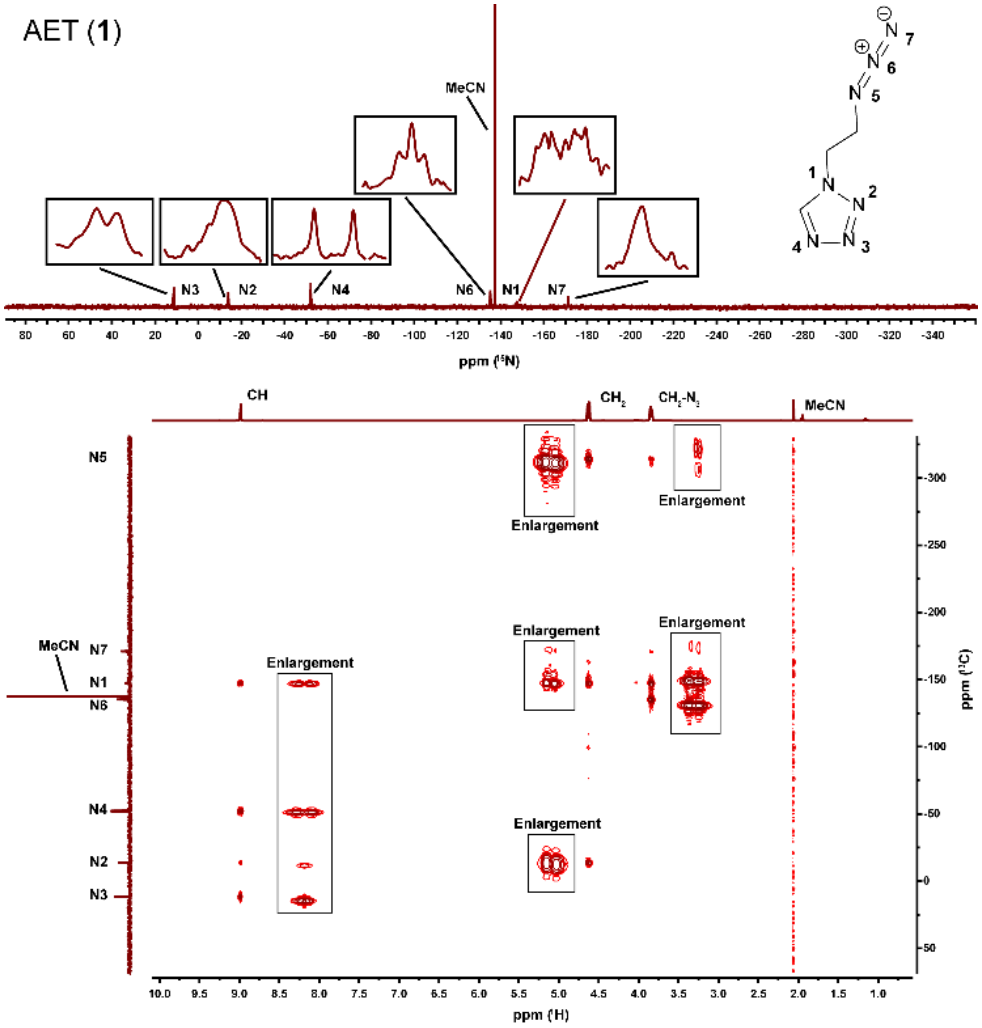

Figure 2. Proton coupled ^{15}N NMR spectra and two dimensional ^{1}H-^{15}N-HMBC NMR spectra of **1**. ^{15}N NMR (MeCN-d_3, 25 °C, ppm) δ: 11.4 (N3, d, $^{2}J_{N\text{-}H}$ = 3.0), −13.9 (N2), −52.2 (N4, d, $^{2}J_{N\text{-}H}$ = 12.1 Hz), −135.2 (N6, t, $^{2}J_{N\text{-}H}$ = 3.3 Hz), −147.4 (N1, d, $^{2}J_{N\text{-}H}$ = 7.3 Hz), −171.1 (N7).

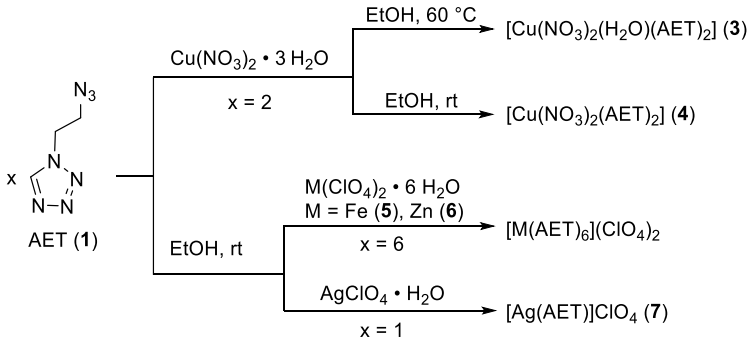

Scheme 4. Synthesis of the nitrato complexes **3** and **4** together with the perchlorate complexes **5**–**7**.

Water and ethanol as solvent were chosen because of their non-toxic character and the good solubility of the ligand and the metal salts. Except coordination compound **3**, every complex crystallized without

inclusion of water molecules. Complex **4** has only been obtained as a side species of **3**, making a further characterization impossible. Copper(II) chlorate complexes based on ligand **1** and **2** have been synthesized analogously to our recently published work (Scheme 6).[34] Due to the commercial unavailability of the copper(II) starting materials of the compounds **12**–**14**, an acid-base reaction had to be applied, starting from the respective 2,4,6-trinitrophenol derivatives and copper(II) carbonate in water at 70 °C. Filtration and treating with ligand **1** yielded the respective coordination compound (Scheme 7).

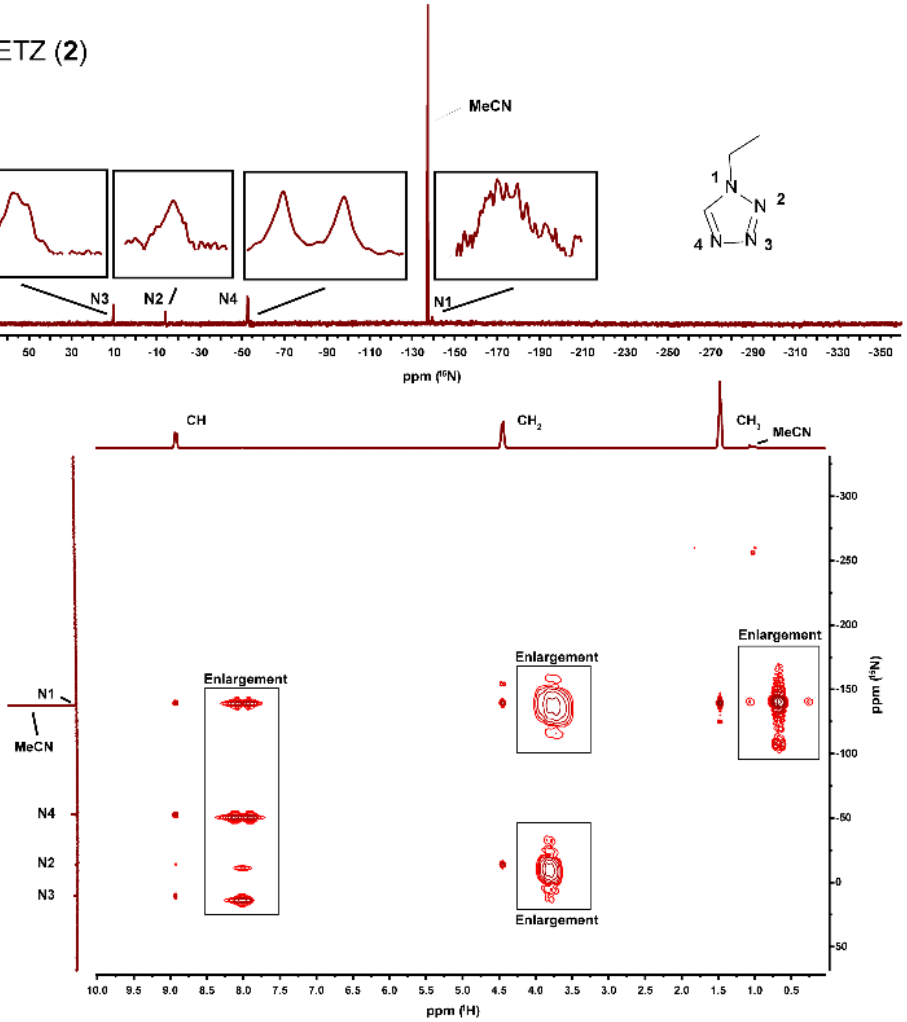

Figure 3. Proton coupled ^{15}N NMR spectra and two dimensional ^{1}H-^{15}N-HMBC NMR spectra of **2**. ^{15}N NMR (MeCN-d_3, 25 °C, ppm) δ: 10.4 (N3), −14.1 (N2), −52.8 (N4, d, $^{2}J_{N\text{-}H}$ = 12.2 Hz), −139.5 (N1).

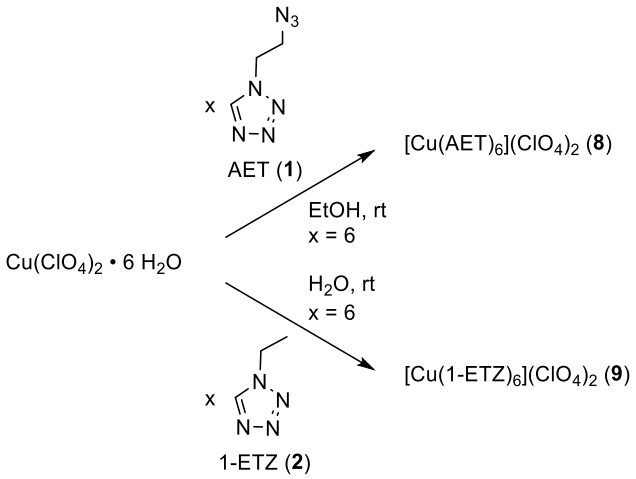

Scheme 5. Synthesis of the copper(II) perchlorate complexes **8** and **9**.

Potential precipitates during the addition of the ligand are dissolved by dropwise addition of water. Single crystals suitable for X-Ray diffraction were obtained directly from the mother liquor within a day. The filtration step after the acid-base reaction toward **12**–**14** turned out to be indispensable for elemental analysis pure products because traces of unreacted copper(II) carbonate cannot be removed by washing with cold ethanol after crystallization.

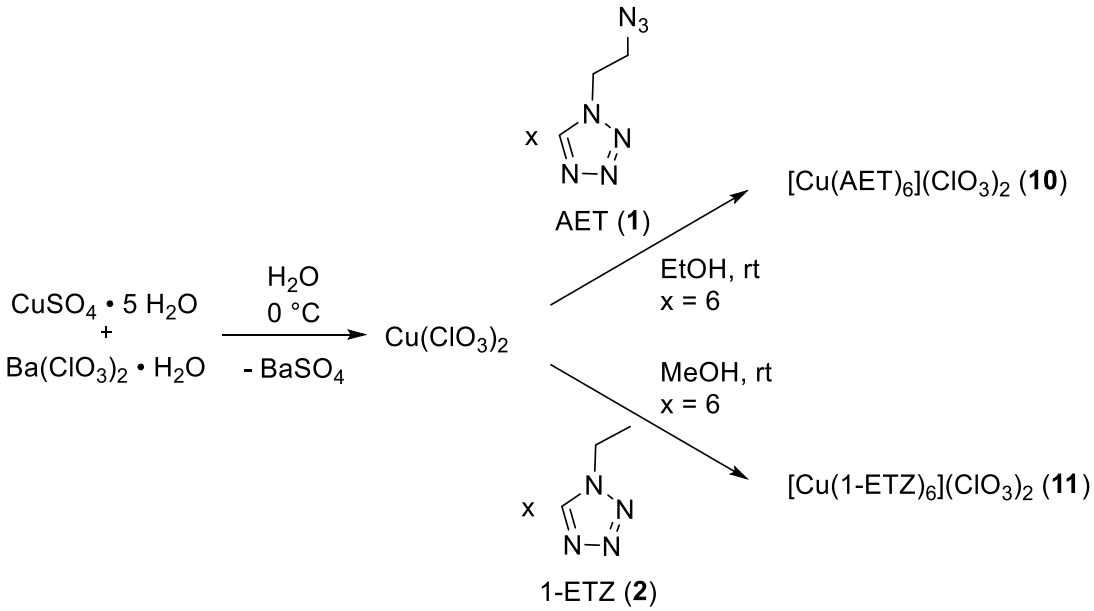

Scheme 6. Synthesis of the chlorate complexes **10** and **11**.

All coordination compounds were obtained directly from the mother liquor and crystallized in satisfactory yields (38–87%). The crystalline materials were filtered off, washed with small amounts of ice-cold ethanol and dried in air overnight. Single crystals suitable for X-ray diffraction of every compound except **5**, **8**, **9** and **10** were also obtained directly from the mother liquor. Crystals of the remaining coordination compounds were obtained after recrystallization from water.

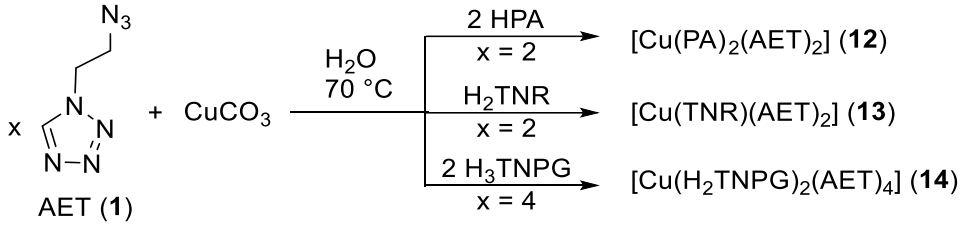

Scheme 7. Synthesis of the nitroaromatic coordination compounds **12**–**14**.

4.2.2. Crystal Structures

The crystal structures of the ligands 1-azidoethyl-5*H*-tetrazole (**1**) and 1-ethyl-5*H*-tetrazole (**2**) are not described in the literature. Due to their liquid state at r.t. and very low melting points, single crystals of those molecules were not obtained. Therefore, single-crystal X-ray diffraction studies of all complexes were performed. Details on the crystal structures of compound **9** and **11** together with the measurement and refinement data of all complexes are given in the Supporting Information (Tables S1–3 and Figures S5–7). The crystal datasets were uploaded to the CSD database[35] and can be obtained free of charge with the CCDC 1898402 (**3**), 1898401 (**4**), 1898397 (**5**), 1898400 (**7**), 1898399 (**9**), 1898541 (**11**), 1898395 (**12**), 1898398 (**13**), 1898396 (**14**). All metal(II) (per)chlorate complexes show octahedral coordination spheres around the central metals built up by six molecules of ligand **1** or **2** (Figures 5, S5 and S6). Unfortunately, compounds **6**, **8** and **10** could only be measured at r.t. and are therefore highly disordered. Finalization of the datasets was impossible, but the measurements allowed an insight into the complexes' composition, which were confirmed by elemental analysis and IR spectroscopy (Figures S2–4). In all complexes, except compound **7**, both tetrazole derivatives coordinate to the central metals exclusively through their heterocyclic N4 nitrogen atoms. ECC **3** shows a rather uncommon sevenfold-bonded copper(II) cation (Figure 4) and complex **7**, with Ag−N bond lengths between 2.323(3) and 2.538(3) Å, possesses distorted tetrahedrally coordinated silver ions. The copper(II) nitrato complex (**3**) crystallizes in the form of blue plates in the triclinic space group *P*−1 with two formula units per unit cell and a calculated density of 1.834 g cm^{-3} at 143 K. The sevenfold coordination environment of the copper(II) center consists of two chelating nitrato, one aqua, and two AET ligands. The nitrates are functioning as bidentate nitrato-ligands, resulting in a longer (2.734 Å) and a shorter (1.971 Å) Cu−O bond. Overall, the unusual amount of five ligands together with the extended sevenfolded coordination sphere results in three clearly longer Cu−O bonds (O2–Cu1 2.734(5) Å, O5–Cu1 2.734(5) Å, O7–Cu1 2.337(5) Å), including the aqua ligand. The anhydrous nitrato complex **4** crystallizes in the form of blue blocks in the monoclinic space group $P2_1/c$ with two formula units per unit cell. The calculated density is 1.895 g cm^{-3} at 173 K. The closed octahedral coordination sphere again includes two chelating nitrato and two AET ligands (Figure 4). The nitrato ligands are located in the equatorial and axial positions, whereas ligand **1**

exclusively occupies equatorial positions. In consequence of the bidentate character of the nitrate, the bond angles are highly distorted from the ideal bond angle of 90°. A comparison of the complexes **3** and **4** shows, that the addition of a water ligand leads to a simple extension of the coordination sphere from a sixfold highly symmetric complex to a sevenfolded coordinated complex without any symmetry. In case of an extended coordination sphere, it is not surprising that in complex **3** the bond distances between the coordinating ligands and the copper(II) center are longer than the bond distances reported for the water-free compound **4**. Additionally, the torsion angle between the oxygens of one nitrate ligand is shortened from 53.54° (**4**) to 52.15° (**3**). The formation of a sevenfolded coordination sphere is a behavior, already observed for 1*H*-substituted tetrazole derivatives in copper(II) nitrato complexes with similar bond lengths around the central metal.[33]

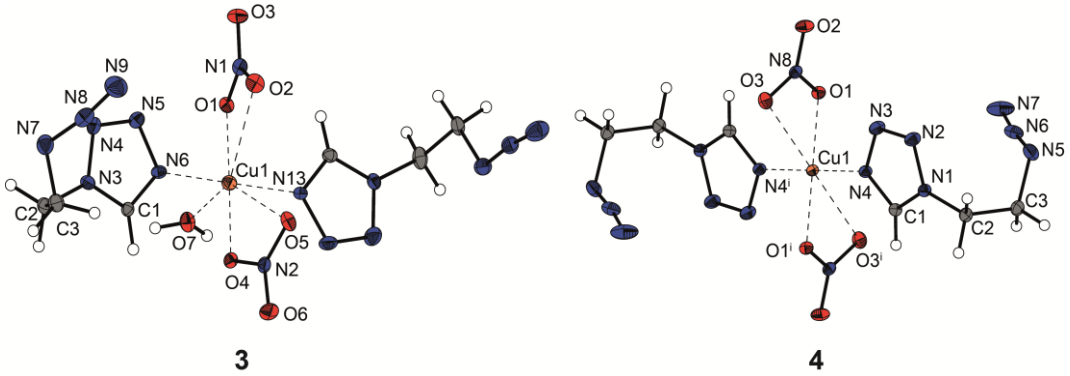

Figure 4. Molecular units of $[Cu(NO_3)_2(H_2O)(AET)_2]$ (**3**) and $[Cu(NO_3)_2(AET)_2]$ (**4**). Selected bond lengths (Å) of **3**: Cu1–N6 1.997(5), Cu1–N13 1.981(5); selected bond angles (°) of **3**: O1–Cu1–O2 52.15(15), O1–Cu1–O4 178.70(16), O1–Cu1–O5 127.78(15), O1–Cu1–N6 91.55(19), O1–Cu1–N13 88.86(19), O2–Cu1–O4 127.13(15), O2–Cu1–O5 78.29(14), O4–Cu1–O5 51.98(15), O4–Cu1–N13 92.32(19), O5–Cu1–O7 137.21(17), O5–Cu1–N6 98.24(17), O5–Cu1–N13 79.86(17), O7–Cu1–N6 92.5(2), O7–Cu1–N13 89.6(2), N6–Cu1–N13 177.85(19). Selected bond lengths (Å) of **4**: Cu–O1 1.9837(14), Cu1–O3 2.6497(18), Cu1–N4 1.971(2); selected bond angles (°) of **4**: O1–Cu1–O3 53.54(6), O1–Cu1–N4 89.96(7), O1–Cu1–$O1^i$ 180.00, O1–Cu1–$O3^i$ 126.46(6); symmetry code of **4**: (i) 1−x, 2−y, 1−z.

The metal(II) perchlorate complexes **5**, **6**, and **8** all crystallize isotypically in the monoclinic space group $P2_1/c$ with similar cell parameters and densities. Unfortunately, compounds **6** and **8** could only be measured at r.t. and therefore the ethyl azide moieties are highly disordered. The unit cell of **5** is built up by two formula units and possesses a calculated density of 1.648 g cm^{-3} at 128 K. The iron(II) central atom is surrounded by six molecules of ligand **1** (Figure 5) with similar Fe1−N bond lengths. Both perchlorate anions are non-coordinating. The silver(I) complex **7** crystallizes in the form of colorless needles in the triclinic space group $P\bar{1}$ and consists of two formula units per unit cell. With a calculated density of 2.470 g cm^{-3} at 173 K, the complex possesses the highest one of all compounds (Figure 6). In contrast to all other complexes based on AET, the ligand coordinates with four different coordination

sides, in particular, the nitrogen atoms N2, N3, N4, and N5. This is resulting in the formation of one-dimensional polymeric chains (Figure 7). For the first time, the azide functionality of the ligand **1** is involved in the coordination bonding, with an astonishing long bond of Ag1–N5 (2.538 Å). With its bond angles ($N3^{ii}$–Ag–$N4^{i}$ = 122.84°, N2–Ag1–N5 = 77.31°), the tetrahedral formed by compound **7** strongly differs from the perfect angles of 109.47°. This deviation can be explained by the perchlorate anions located above and underneath the layers of silver ions and their interaction with these.

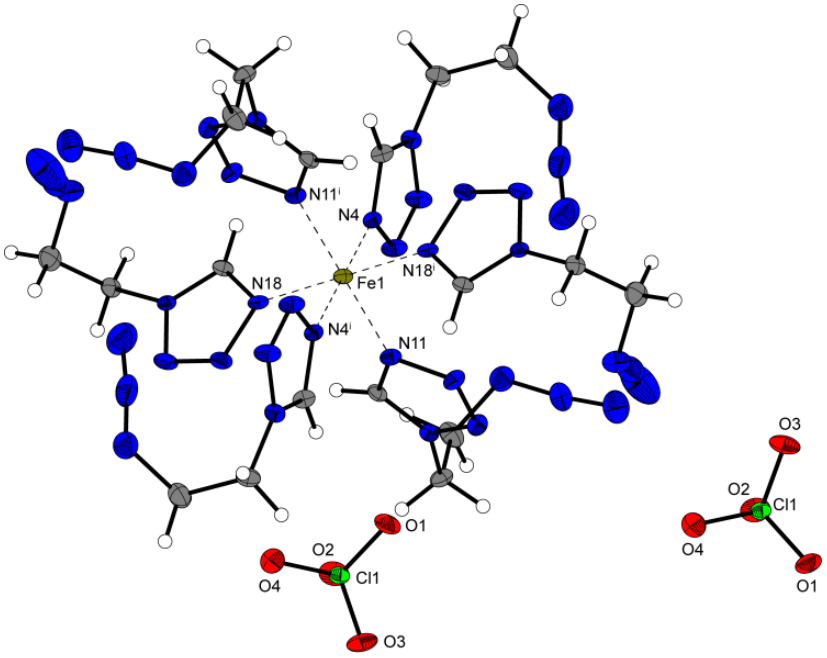

Figure 5. Molecular unit of $[Fe(AET)_6](ClO_4)_2$ (**5**). Selected bond lengths (Å): Fe1–N4 1.990(4), Fe1–N11 1.996(4), Fe–N18 1.977(5); selected bond angles (°): N11–Fe1–$N11^{i}$ 180.00, N4–Fe1–N11 89.17(16), N18–Fe1–$N18^{i}$ 180.00, N4–Fe1–$N18^{i}$ 89.96(16), N4–Fe1–$N4^{i}$ 180.00, N11–Fe1–N18 89.41(18); symmetry code: −x, −y, −z.

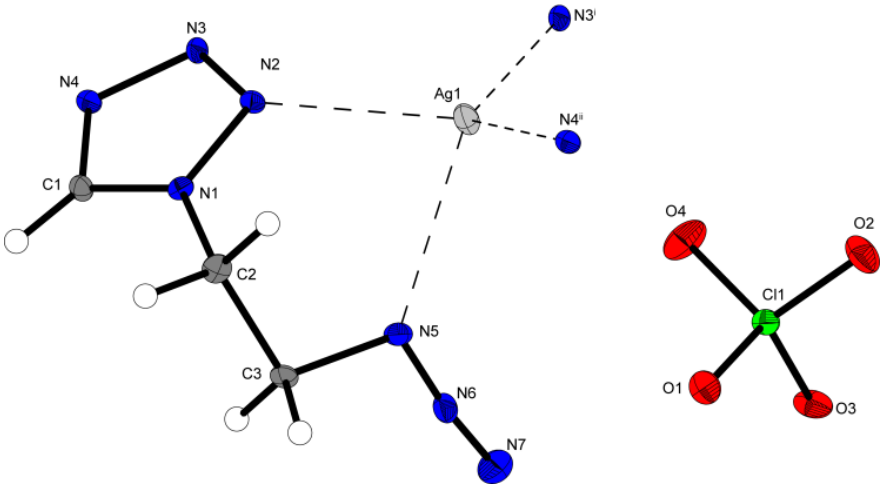

Figure 6. Coordination environment of $[Ag(AET)](ClO_4)$ (**7**). Selected bond lengths (Å): Ag1–N2 2.420(3), Ag1–$N4^{i}$ 2.323(3), Ag1–$N3^{ii}$ 2.331(3); selected bond angles (°): N2–Ag1–$N4^{i}$ 122.84(10), N2–Ag1–$N3^{ii}$ 111.68(11), $N4^{i}$–Ag1–N5 86.06(11), $N3^{ii}$–Ag1–N5 133.85(10); symmetry codes: (i) −x, 1−y,1−z; (ii) 1+x, y, z.

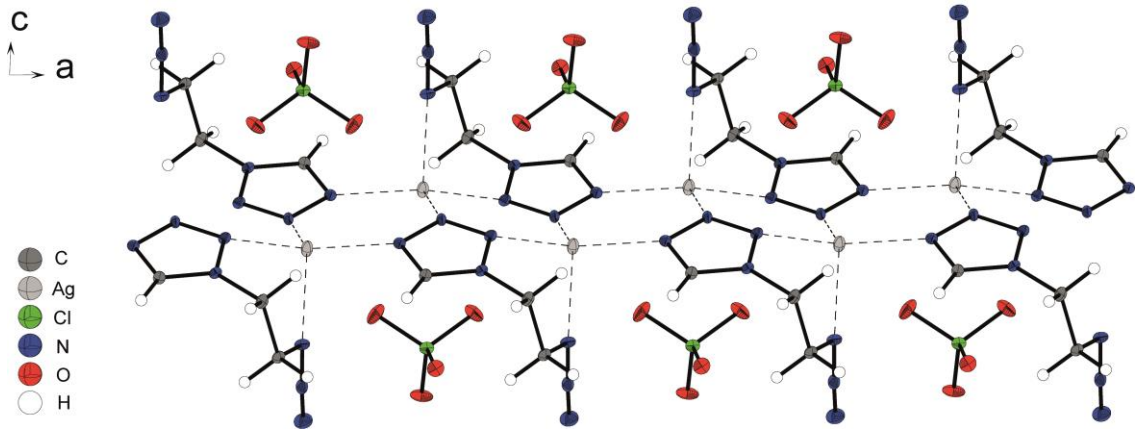

Figure 7. Segment of the polymeric chain of **7**, formed by tetrazole rings linking between three different silver atoms.

The coordination compound **12** crystallizes in the form of green plates in the monoclinic space group $P2_1/c$ with two formula units per unit cell. The complex possesses a calculated density of 1.815 g cm^{-3} at 143 K. The coordination sphere is built up by two equatorial arranged AET ligands and two molecules of picrate (Figure 8). The anions are acting as bidentate ligands, coordinating over the deprotonated hydroxy group and by another oxygen atom of one of the nitro groups. The latter occupy axial positions leading to a typical Jahn-Teller distortion along the O2–Cu1–O2^{i} axis.

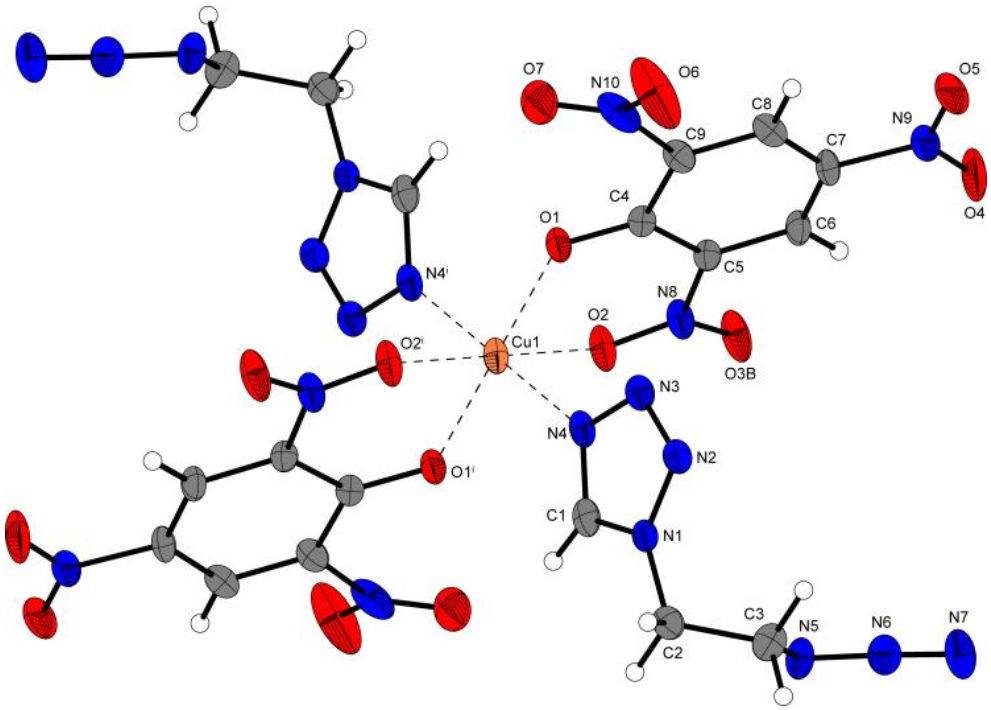

Figure 8. Molecular unit of [Cu(PA)$_2$(AET)$_2$] (**12**). Selected bond lengths (Å): Cu1–O1 1.931(4), Cu1–O2 2.334(3), Cu1–N4 1.997(4); selected bond angles (°): O1–Cu1–O1^{i} 180.00, O1–Cu1–O2 79.35(14), O1–Cu1–N4 91.62(17); symmetry code: (i) −x, 1−y, −z.

The styphnate complex **13** shows a similar density (1.803 g cm^{-3} at 143 K) to compound **12** and crystallizes in the triclinic space group $P\bar{1}$ with two formula units per unit cell (Figure 9).

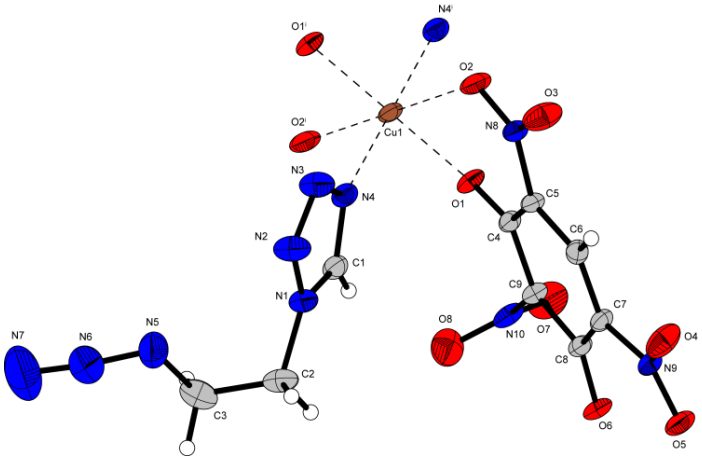

Figure 9. Coordination environment of [Cu(TNR)(AET)$_2$] (**13**). Selected bond lengths (Å): Cu1–O1 1.9266(16), Cu1–O2 2.3431(17), Cu1–N4 2.0115(19); selected bond angles (°): O1–Cu1–O1^{i} 180.00, O1–Cu1–O2 80.65(7), O1–Cu1–N4 88.92(7); symmetry code: (i) 2−x, −y, 2−z.

Both hydroxy groups of styphnic acid are deprotonated leading to the formation of a trinitroresorcinate anion, which is coordinating to two different copper(II) cations by chelating each with one nitro and one phenolate oxygen. The Jahn-Teller distortion along the O2–Cu1–O2^{i} is formed by two weaker bonded nitro groups of two different anions. Similar to silver complex **7**, **13** forms one-dimensional polymeric chains, which are however not caused by bridging ligands but by the fourfold coordinating anion (Figure S7). Coordination compound **14** crystallizes in the triclinic space group *P*−1 with only one formula unit per unit cell and a calculated density of 1.766 g cm^{-3} at 143 K. In contrast to nitroaromatic compound **13**, the anions are only single deprotonated and solely coordinating with the phenolate group (Figure 10). The remaining equatorial positions are occupied by four instead of two molecules of ligand **1**. Again, the Jahn-Teller distortion can be observed along the O–Cu–O axis.

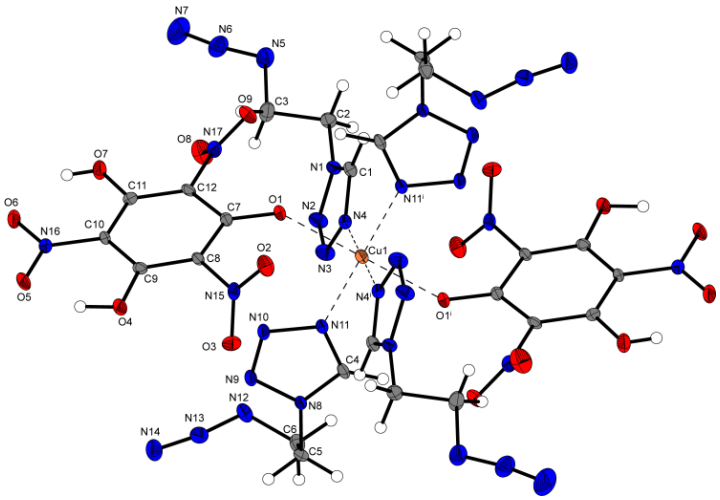

Figure 10. Unit cell of coordination compound [Cu(H$_2$TNPG)$_2$(AET)$_4$] (**14**). Selected bond lengths (Å): Cu1–O1 2.345(2), Cu1–N4 2.027(3), Cu1–N11 1.983(3); selected bond angles (°): O1–Cu1–N4 89.97(11), O1–Cu1–N11 95.31(11), O1–Cu1–O1^{i} 180.00, N4–Cu1–N11 89.59(11); symmetry code: (i) 1−x, −y, 1−z.

4.2.3. Sensitivities and Thermal Stability

The behavior of all compounds, except the side-product **4**, was investigated in differential thermal analysis (DTA). The measurements were performed in the range from 25–400 °C at a heating rate of β = 5 °C min^{-1}. Critical points are given as onset temperatures. The observed endothermic events (melting, dehydration or loss of coordinating ligand), as well as exothermic events, are listed in Table 1. DTA plots of the compounds **1**–**3** and **5**–**14** are available in Figures S12–15 in the Supporting Information.

Table 1. Overview of the compounds' thermal stability,[a] sensitivities toward various external stimuli and results of hot plate (HP) and hot needle (HN) tests compared to lead azide.

	$T_{endo.}$[b] [°C]	$T_{exo.}$[c] [°C]	*IS*[d] [J]	*FS*[e] [N]	*ESD*[f] [mJ]	*BDIS*[g] [mJ]	HP[h]	HN[h]
AET (**1**)	-	193	9	> 360	n.d.	n.d.	n.d.	n.d.
1-ETZ (**2**)	-	208	> 40	> 360	n.d.	n.d.	n.d.	n.d.
$[Cu(NO_3)_2(H_2O)(AET)_2]$ (**3**)	94, 121	152	10	108	840	n.d.	def.	def.
$[Fe(AET)_6](ClO_4)_2$ (**5**)	-	151	3	3.75	65.0	< 4	det.	det.
$[Zn(AET)_6](ClO_4)_2$ (**6**)	159	196	15	40	368	20	def.	def.
$[Ag(AET)]ClO_4$ (**7**)	-	165	< 1	0.6	65.0	< 4	det.	det.
$[Cu(AET)_6](ClO_4)_2$ (**8**)	135	158	< 1	15	368	12	def.	det.
$[Cu(1\text{-}ETZ)_6](ClO_4)_2$ (**9**)	172	210	10	120	960	n.d.	def.	def.
$[Cu(AET)_6](ClO_3)_2$ (**10**)	77	146	2.5	4	226	29	def.	det.
$[Cu(1\text{-}ETZ)_6](ClO_3)_2$ (**11**)	111	158	7	60	608	n.d.	def.	def.
$[Cu(PA)_2(AET)_2]$ (**12**)	-	183	3	252	226	> 200	def.	def.
$[Cu(TNR)(AET)_2]$ (**13**)	-	177	< 1	240	123	> 200	def.	def.
$[Cu(H_2TNPG)_2(AET)_4]$ (**14**)	-	121	1.5	84	608	> 200	def.	def.
$Pb(N_3)_2$[37]		320–360	2.5–4.0	0.1–1.0	7.0	n.d.	n.d.	n.d.

[a] Onset temperature at a heating rate of 5 °C min^{-1} measured by DTA; [b] Endothermic peak, which indicates melting, vaporization, dehydration, or loss of aqua ligands; [c] Exothermic peak, which indicates decomposition. [d] Impact sensitivity according to the BAM drop hammer (method 1 of 6). [e] Friction sensitivity according to the BAM friction tester (method 1 of 6). [f] Electrostatic discharge sensitivity (OZM Electric Spark XSpark10). [g] Ball drop impact sensitivity determined with the 1 of 6 method in accordance with the MIL-STD 1751A (method 1016). [h] def.: deflagration; det.: detonation.

The exothermic decomposition temperature reported for ligand **1** is in accordance with our findings, whereas for ligand **2** no data is available.[28] The exothermic decomposition temperatures of most of the investigated compounds are above 150 °C, except **10** (T_{exo} = 146 °C) and **14** (T_{exo} = 121 °C). The relatively low thermal stabilities of the nitrato compound **3** (T_{exo} = 152 °C), as well as the chlorate complexes, are a known issue, resulting from the metal salt, the coordination compounds are based on and is already reported in the literature.[32,33] Besides its low point of exothermic decomposition, the nitrato complex (**3**) is the only compound showing two endothermic signals (T_{endo1} = 94 °C, T_{endo2} = 121 °C), indicating melting, followed by the loss of coordinating aqua ligand (proofed by TGA). Other endothermic events of compounds **6** and **8**–**11** can also be assigned to their respective melting points, which were also observed during heating of the respective compounds in hot plate tests. In order to examine the endothermic events more closely, some of the compounds were further investigated by

thermal gravimetric analysis (Figure S15). Except **3**, none of the compounds based on ligand **1** showed significant loss of mass until their exothermic decomposition points. Copper(II) complexes comprising 1-ETZ (**2**) show similar to the methyl-substituted analogous compounds evaporation of the ligand before their exothermic decomposition.[32] In the row of 2,4,6-trinitroaromatic based copper(II) complexes, the thermal stability decreases with increasing number of hydroxy groups, with **14** (T_{exo} = 121 °C) showing the lowest stability of all investigated compounds. The highest exothermic decomposition temperature was observed for the copper(II) perchlorate complex **9** (T_{exo} = 210 °C), based on ligand **2**, showing an exothermic signal 52 °C higher than the analogous coordination compound based on ligand **1** (**8**: T_{exo} = 158 °C). The same can be observed for the two comparable chlorate complexes (Figure 11). This trend is confirmed, looking at the temperatures evaluated for the respective ligand (**1**: T_{exo} = 193 °C; **2**: T_{exo} = 208 °C) and is guessed to be caused by the azido function of ligand **1**.

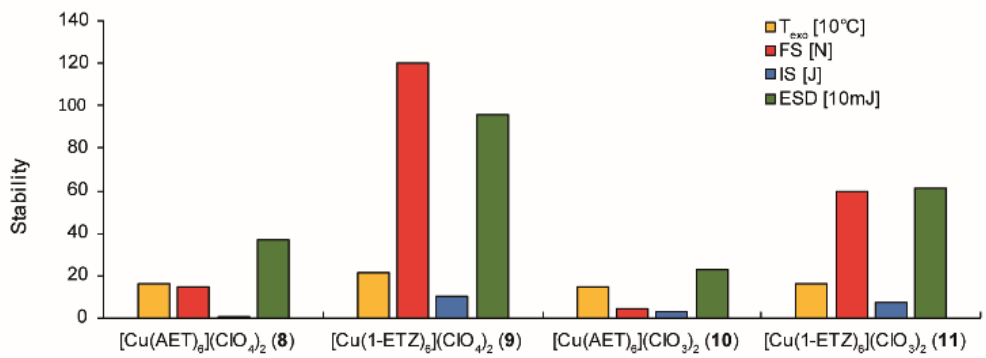

Figure 11. Comparison of the sensitivities and thermal stability of the chlorate and perchlorate complexes based on the ligands **1** and **2**, confirming the lower stability of chlorate compounds toward external stimuli.

A general trend within the row of the investigated 3d perchlorate coordination compounds shows higher exothermic decomposition temperatures with an increasing atomic number (Fe^{2+} < Cu^{2+} < Zn^{2+}), which is in conflict (Cu^{2+}-based complexes being less stable than Fe^{2+}) with our prior findings for 1*H*-substiuted tetrazoles (Figure 11).[32] Interestingly, compounds **6** and **9** even show slightly higher exothermic decomposition temperatures (T_{exo} = 196 °C and 210 °C, respectively) than the corresponding ligand. The sensitivities toward impact (IS) and friction (FS) were assessed according to BAM standard methods (1 of 6) together with the electrostatic discharge sensitivity (ESD) for all compounds. In addition, all complexes have been categorized in accordance with the "UN Recommendations on the Transport of Dangerous Goods" using the determined sensitivities.[36] An overview of the sensitivities is given in Table 1. Because sensitivity data are highly affected by the crystal morphology, the compounds' grain size and habitus were investigated using light microscopy. The data are represented in the Supporting Information (Figures S8–11). The free ligand **2** is the only investigated compound to be ranked as insensitive with its high stability toward friction and impact. In contrast to that, ligand **1** has to be classified as sensitive

because of its sensitivity of 9 J toward impact, whereas it is insensitive toward friction. No measurements regarding electrostatic discharge could be performed due to the physical state of both ligands. The highest stability toward impact of all ECC (15 J, sensitive) is possessed by the only zinc coordination compound **6**, which has to be considered as very sensitive because of its friction sensitivity. Comparing the perchlorate complexes reveals, that all have to be considered as very sensitive (**6**, **8**) or even extremely sensitive (**5**, **7**), except compound **9**, which is stated as sensitive, also possessing the highest stability toward friction of all investigated perchlorates. The sensitivity toward impact of the ECC based on perchlorate and AET increases in the following order: Zn^{2+} (15 J) < Fe^{2+} (3 J) < Cu^{2+} (<1 J) ≈ Ag^{+} (<1 J) and in the following order against friction: Zn^{2+} (40 N) < Cu^{2+} (15 N) < Fe^{2+} (3.75 N) < Ag^{+} (0.6 N) (Figure 12). Again these results contradict earlier observations.[32,33]

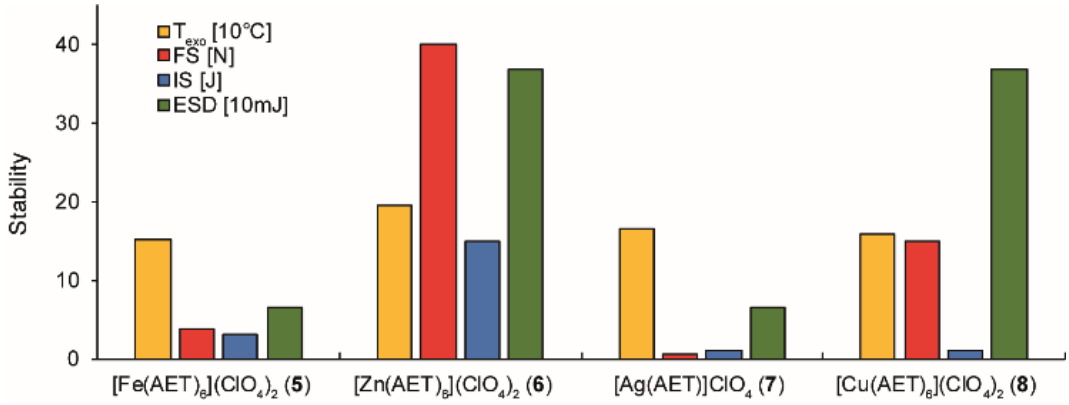

Figure 12. Comparison of the thermal stabilities together with the sensitivities toward various stimuli of the perchlorate coordination compounds **5**–**8**, showing that the silver compound is the most sensitive and the zinc one is the most insensitive one.

Compounds **8**–**11** show comparable trends to external stimuli as in thermal experiments. Complexes based on ligand **1** are more sensitive (**8** and **10** are both ranked as extremely sensitive) than those of compound **2** (both sensitive) and the copper(II) chlorate complexes are less stable (**11**) or at least show similar sensitivities (**10**) compared to the analogous perchlorate ones (Figure 11), which is in accordance to our previous findings.[34] The nitroaromatic derivatives **12**–**14** possess one of the highest stabilities of all complexes toward friction, but due to their sensitivities toward impact, they are all ranked as very sensitive (Figure S17). Because of the realistic terms of testing, sensitivity toward ball drop impact (BDIS) was also determined for the most sensitive complexes **5**–**8**, and **10** (Figure S18). Due to the high discrepancy of **12**–**14** regarding the sensitivities toward impact and friction according to BAM standard methods, ball drop experiments were carried out for those compounds too. In the case of the perchlorate complexes it becomes clear that low stability to friction (**7** < **5** < **8** < **6**) is accompanied by a higher sensitivity to BDIS (**7** ~ **5** < **8** <**6**) and that the impact sensitivity in the drop hammer experiments (**7** ~ **8** < **5** << **6**) is less significant. The same trend can be observed for the nitroaromatic compounds **12**–**14**.

4.2.4. Primary Explosive Suitability Evaluation and Laser Initiation

For an insight into the behavior toward fast heating with and without confinement and for gaining an overall insight in their applicability as a primary explosive, hot plate and hot needle tests were performed for every investigated coordination compound (Table 1, Figures 13 and S19–30). Except the chlorate and perchlorate complexes **5**, **7**, **8**, and **10**, which at least showed detonations during one of the tests, every other compound only deflagrated.

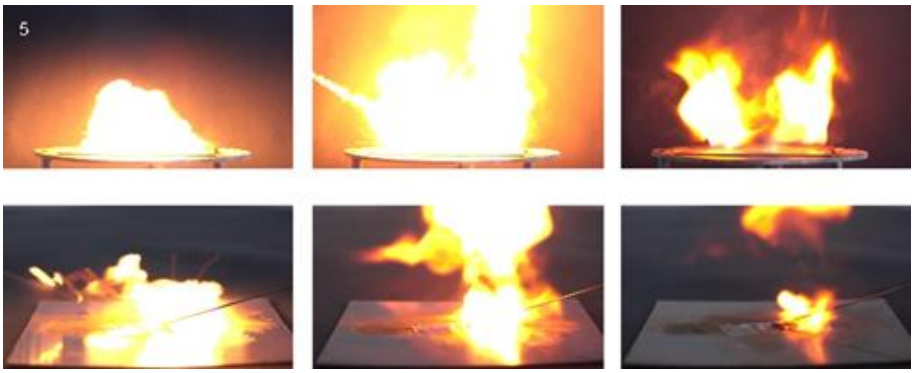

Figure 13. Hot plate test (top) and hot needle test (bottom) of the iron(II) perchlorate complex **5**, shown as a sequence.

The most promising compounds were tested in initiation capability tests with nitropenta (PETN) as the main charge. Further information on the test setup can be found in the General Methods of the Supporting Information. Positive tests, indicated by a hole in the copper witness plate and fragmentation of the shell, caused by a positive deflagration-to-detonation transition (DDT) toward the secondary explosive, were observed for **5** and **7**. [Ag(AET)]ClO_4 (**7**) is representing one of the rare ECC with silver as central metal being able to initiate PETN (Figure 14). Tests concerning the copper(II) and zinc(II) perchlorate compounds **6** and **8** did in our test not result in a positive DDT.

Figure 14. Positive results of the initiation capability tests toward PETN of compounds **5** and **7**.

Nowadays used primary explosives like LA or LS suffer, besides their toxicity, from their high sensitivity toward mechanical stimuli.[25] In classical initiation devices, which are based on mechanical stimuli, these properties are mandatory, but with the ability to be initiated by laser irradiation they are no longer

required. This circumstance is responsible for the great interest that the field has gained in recent years.[38,39] Possible industrial applications like optical detonators or laser ignitable ammunition are already under current research.[40,41] Based on latest results concerning the laser ignition of ECC, this work focused only on the colored compounds **3**, **5** and **8**–**14**.[33] Further information for the applied setup can be found in the Supporting Information. All complexes showed reaction toward laser irradiation (Table 2), which strongly differed by the applied ligand and anion system. As already recognized during hot plate and hot needle tests, coordination compounds based on the more energetic ligand **1** tend way more likely to show detonations than compounds based on ligand **2**. The use of nitrate or aromatic anions is leading to deflagrations only, whereas, in case of ligand **1**, the use of chlorates and perchlorates leads to detonations (Figures 15 and S31–37).

Table 2. Results of the laser initiation experiments.[a]

Compound	0.17 mJ	25.5 mJ	30 mJ	111 mJ
3	-	-	def.	-
5	-	def.	det.	-
8	def.	det.	-	-
9	-	-	dec.	-
10	det.	det.	-	-
11	-	-	dec.	-
12	-	-	-	dec.
13	-	-	dec.	-
14	-	dec.	-	-

[a] -: not tested; dec.: decomposition; def.: deflagration; det.: detonation. Operating parameters: current I = 7–12 A; voltage U = 4 V; theoretical maximal output power P_{max} = 45 W; theoretical energy E_{max} = 0.17–111 mJ; wavelength λ = 915 nm; pulse length τ = 0.1–20 ms.

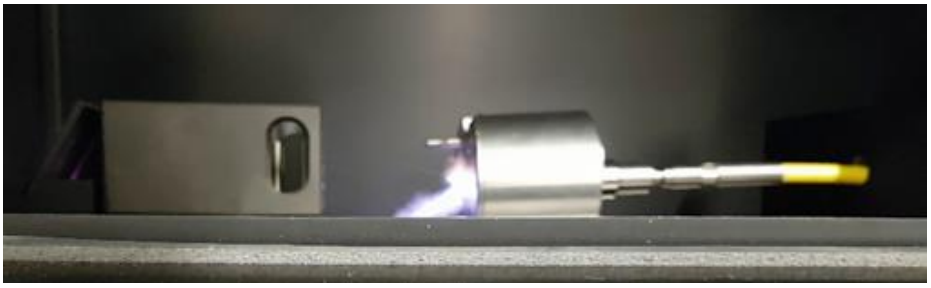

Figure 15. Detonation of the copper(II) perchlorate complex **8** during laser initiation test.

4.2.5. UV-Vis Spectroscopy

Regarding the mechanism of laser initiation, UV-Vis spectra (Figures S38 and S39) of all tested compounds were recorded in the solid-state and analyzed in detail at the laser operating wavelength of 915 nm. A summary of the optical properties of the measured compounds is given in Table S4. The observed absorption in the near infrared, visible and ultra-violet region results from the d-d transitions, based on the respective central metal and its interaction with the ligand and anion. Nevertheless, the process of initiation via laser irradiation (*e.g.*, thermal, electrochemical) has still not been understood

completely and is therefore of high importance and strongly investigated.[42,43] All complexes show moderate absorption behavior at the laser wavelength of 915 nm. This could be a possible explanation for the ignitability via laser irradiation since the colorless zinc and silver perchlorate compounds **6** and **7** could not be ignited. Besides the absorption in the desired area, other factors are important concerning laser initiation, like the corresponding metal or its electron configuration. Therefore, future studies should aim at the initiation process, in particular, the influence of the complexes' structure and the mechanism behind the initiation.

4.3. Conclusion

The nitrogen-rich ligands 1-azidoethyl-5*H*-tetrazole (**1**, AET) and 1-ethyl-5*H*-tetrazole (**2**, 1-ETZ), which can be synthesized in straightforward, green and cost-effective manners were successfully applied in coordination compounds and analyzed by two dimensional ^{1}H-^{15}N-HMBC NMR. Copper, iron, zinc, and silver salts of common anions like perchlorate or nitrate were used together with rather unusual ones like picrate, styphnate, trinitrophloroglucinate or chlorate. All of the synthesized coordination compounds, except byproduct **4**, were characterized in detail. By introducing the azide function into the ligand system, the performance of the ECC can be significantly increased. While the sensitivities of compounds **9** and **11** (based on 1-ETZ (**2**)) lie in the range of secondary explosives, most of the ECC based on ligand **1** are primary explosives. The iron (**5**) and silver (**7**) perchlorate compounds were both positive tested to initiate PETN. Especially **5** with its manageable sensitivities and nontoxic central metal could be a candidate of future interest. During laser ignition experiments coordination compound **5** as well as the copper compounds **8** and **10** showed detonations at energies between 0.17 and 30.0 mJ making them promising candidates as green laser ignitable explosives. The comparison of the impact sensitivities determined by drop hammer and ball drop reveals a higher similarity of the BDIS to FS than IS.

4.4. Acknowledgements

Financial support of this work by the Ludwig-Maximilian-University of Munich (LMU). The authors would like to thank Prof. Dr. Konstantin Karaghiosoff for the measurement of various ^{15}N NMR spectra, Mrs. Antonia Stadler for proofreading and Mr. Valentin Bockmair as well as Mr. Philipp Spieß for their great contribution to this work.

4.5. References

[1] T. Curtius, *Ber. Dtsch. Chem. Ges.* **1890**, *23*, 3033–3041.

[2] S. Schneider, T. Hawkins, M. Rosander, J. Mills, A. Brand, L. Hudgens, G. Warmoth, A. Vij, *Inorg. Chem.* **2008**, *47*, 3617–3624.

[3] J. Haase, *Organic Azides: Syntheses and Applications*, 1st ed., Wiley, Hoboken, **2010**, pp. 29–48.

[4] T. M. Klapötke, N. Mehta, *Propellants Explos. Pyrotech.* **2014**, *39*, 7–8.

[5] J. C. Bennion, N. Chowdhury, J. W. Kampf, A. J. Matzger, *Angew. Chem. Int. Ed.* **2016**, *55*, 13118–13121.

[6] S. I. Gerasimov, M. A. Ilyushin, I. V. Shugalei, A. V. Smirnov, Z. V. Kapitonenko, *Russ. J. Gen. Chem.* **2017**, *87*, 3156–3159.

[7] H. Wei, J. Zhang, J. M. Shreeve, *Chem. – Asian J.* **2015**, *10*, 1130–1132.

[8] D. E. Chavez, D. A. Parrish, L. Mitchell, G. H. Imler, *Angew. Chem. Int. Ed.* **2017**, *56*, 3575–3578.

[9] C. Qi, R. Zhang, X. Zhang, Y. Li, Y. Wang, S. Pang, *Chem. – Asian J.* **2011**, *6*, 1456–1462.

[10] K. O. Christe, D. A. Dixon, M. Vasiliu, R. Haiges, B. Hu, *Propellants Explos. Pyrotech.* **2019**, *44*, 263– 266.

[11] P. Griess, *J. Chem. Soc.* **1865**, *18*, 268–272.

[12] A. Hantzsch, *Ber. Dtsch. Chem. Ges.* **1933**, *66*, 1349–1354.

[13] M. N. Glukhovtsev, R. D. Bach, L. Laiter, *Int. J. Quantum Chem.* **1997**, *62*, 373–384.

[14] T. Curtius, *J. Prakt. Chem.* **1894**, *50*, 275–294.

[15] G. L′Abbé, *Chem. Rev.* **1969**, *69*, 345–363.

[16] E. F. V. Scriven, K. Turnbull, *Chem. Rev.* **1988**, *88*, 297–368.

[17] L. O. Brockway, L. Pauling, *Proc. Natl. Acad. Sci. USA* **1933**, *19*, 860–867.

[18] L. Pauling, L. O. Brockway, *J. Am. Chem. Soc.* **1937**, *59*, 13–20.

[19] M. A. Petrie, J. A. Sheehy, J. A. Boatz, G. Rasul, G. K. Surya Prakash, G. A. Olah, K. O. Christe, *J. Am. Chem. Soc.* **1997**, *119*, 8802–8808.

[20] Y. Tang, J. M. Shreeve, *Chem. – Eur. J.* **2015**, *21*, 7285–7291.

[21] D. Kumari, K. D. B. Yamajala, H. Singh, R. R. Sanghavi, N. A. Shri, K. Raju, S. Banerjee, *Propellants Explos. Pyrotech.* **2013**, *38*, 805–809.

[22] C. Ye, H. Gao, J. A. Boatz, G. W. Drake, B. Twamley, J. M. Shreeve, *Angew. Chem. Int. Ed.* **2006**, *45*, 7262–7265.

[23] Y.-H. Joo, H. Gao, Y. Zhang, J. M. Shreeve, *Inorg. Chem.* **2010**, *49*, 3282–3288.

[24] Y. H. Ding, S. Inagaki, *Chem. Lett.* **2003**, *32*, 304–305.

[25] T. M. Klapötke, *High Energy Density Materials*, 1st ed., Springer, Berlin, **2007**, pp. 85–122.

[26] J. Giles, *Nature* **2004**, *427*, 580–581.

[27] R. P. Singh, R. D. Verma, D. T. Meshri, J. M. Shreeve, *Angew. Chem. Int. Ed.* **2006**, *45*, 3584–3601.

[28] P. N. Gaponik, V. P. Karavai, Yu. V. Grigor′ev, *Khim. Geterotsikl. Soedin.* **1985**, *11*, 1521–1524.

[29] D. O. Ivashkevich, A. S. Lyakhov, P. N. Gaponik, A. N. Bogatikov, A. A. Govorova, *Acta Crystallogr. Sect. E* **2001**, *57*, m335–m337.

[30] Y. Guo, H. Liu, M. Xu, *Hecheng Huaxue* **2011**, *19*, 299–303.

[31] A. Riechers, A. Grauer, S. Ritter, B. Sperl, T. Berg, B. König, *J. Mol. Recognit.* **2010**, *23*, 329–334.

[32] N. Szimhardt, M. H. H. Wurzenberger, A. Beringer, L. J. Dauman, J. Stierstorfer, *J. Mater. Chem. A* **2017**, *5*, 23753–23765.

[33] N. Szimhardt, M. H. H. Wurzenberger, L. Zeisel, M. S. Gruhne, M. Lommel, J. Stierstorfer, *J. Mater. Chem. A* **2018**, *6*, 16257–16272.

[34] M. H. H. Wurzenberger, N. Szimhardt, J. Stierstorfer, *J. Am. Chem. Soc.* **2018**, *140*, 3206–3209.

[35] CCDC 1898402 (**3**), 1898401 (**4**), 1898397 (**5**), 1898400 (**7**), 1898399 (**9**), 1898541 (**11**), 1898395 (**12**), 1898398 (**13**), 1898396 (**14**) contain the supplementary crystallographic data for this paper. These data can be obtained free of charge from The Cambridge Crystallographic Data Centre.

[36] Impact: insensitive > 40 J, less sensitive ≥ 35 J, sensitive ≥ 4 J, very sensitive ≤ 3 J; Friction: insensitive > 360 N, less sensitive = 360 N, sensitive < 360 N and > 80 N, very sensitive ≤ 80 N, extremely sensitive ≤ 10 N. According to the UN Recommendations on the Transport of Dangerous Goods, 5th ed., **2009**.

[37] T. M. Klapötke, *Energetic Materials Encyclopedia*, 1st ed., De Gruyter, Berlin, Boston, **2018**, pp. 275–277.

[38] T. W. Myers, J. A. Bjorgaard, K. E. Brown, D. E. Chavez, S. K. Hanson, R. J. Scharff, S. Tretiak, J. M. Veauthier, *J. Am. Chem. Soc.* **2016**, *138*, 4685–4692.

[39] T. W. Myers, K. E. Brown, D. E. Chavez, R. J. Scharff, J. M. Veauthier, *Inorg. Chem.* **2017**, *56*, 2297–2303.

[40] R. Schirra, H. Zöllner, *Proc. Int. Pyrotech. Semin.* **2016**, *42*, 422–428.

[41] H. Lebreton, D. Cazajous, S. Larue, *Proc. Int. Pyrotech. Semin.* **2015**, *41*, 1–6.

[42] S. R. Ahmad, M. Cartwright, *Laser Ignition of Energetic Materials*, Wiley, Hoboken, **2015**, pp. 17–29.

[43] E. D. Aluker, A. G. Krechetov, A. Y. Mitrofanov, D. R. Nurmukhametov, M. M. Kukja, *J. Phys. Chem. C* **2011**, *115*, 6893–6901.

4.6. Supporting Information

4.6.1. Compounds Overview

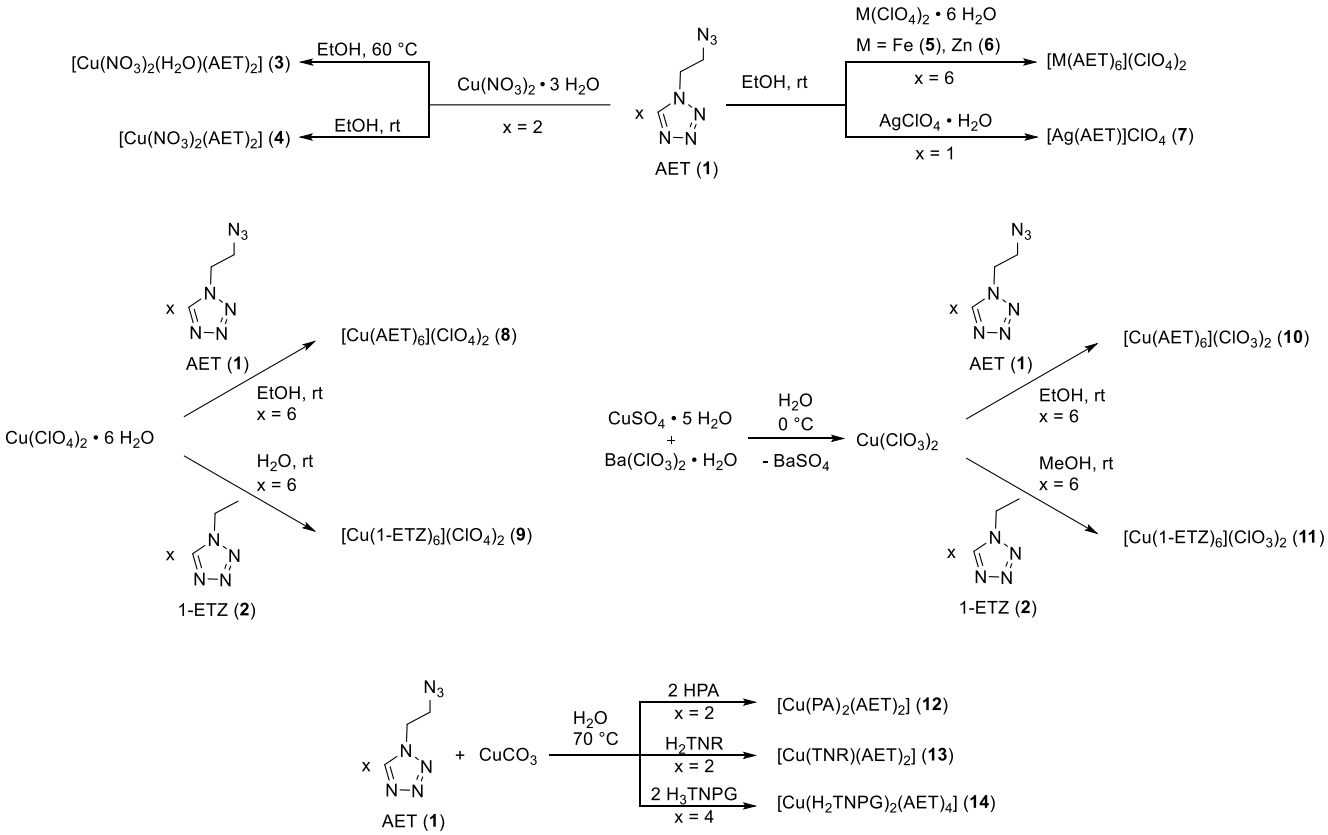

4.6.2. IR Spectroscopy of 1–3, and 5–14

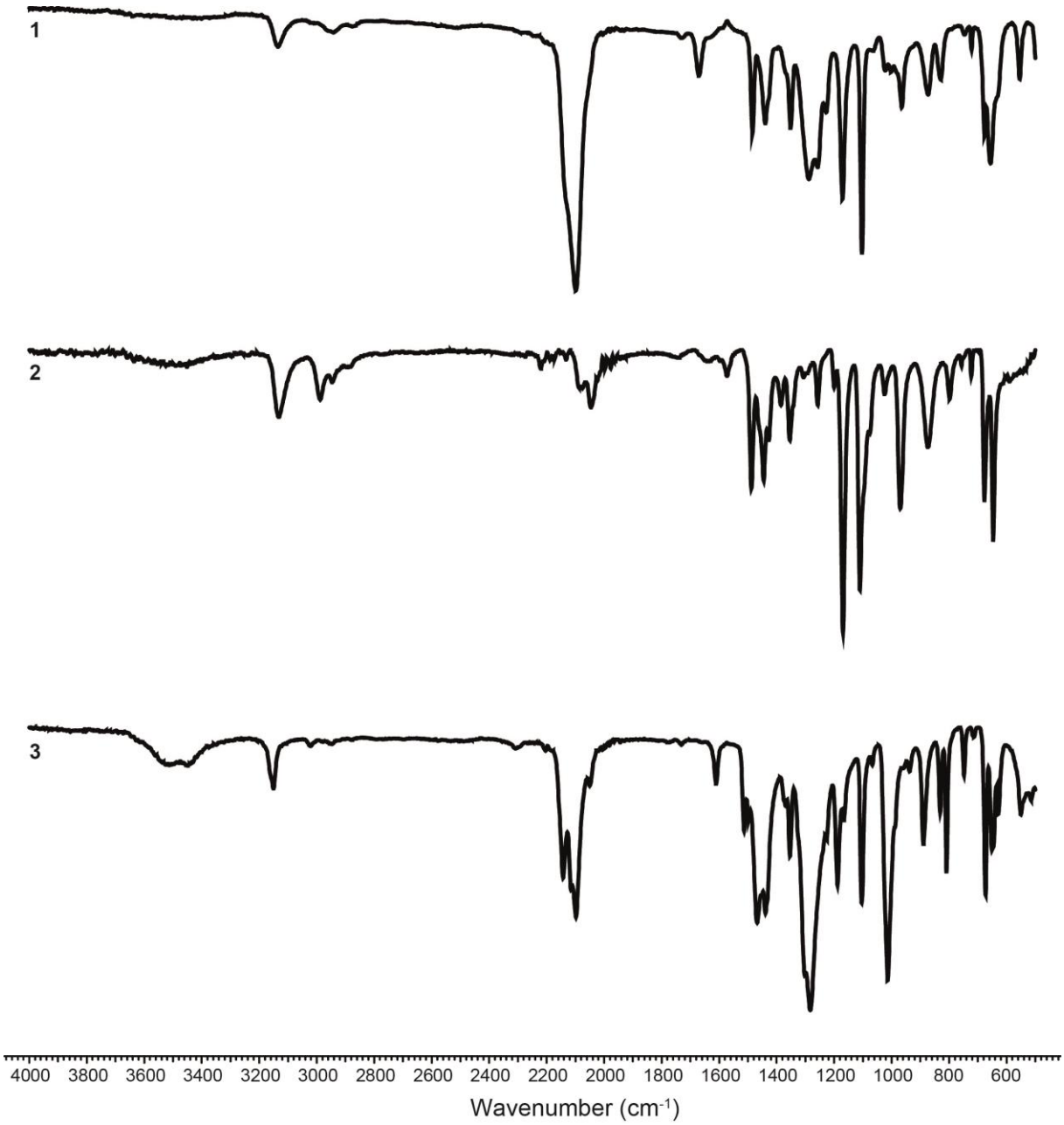

Figure S1. Infrared spectra of compounds **1**–**3**.

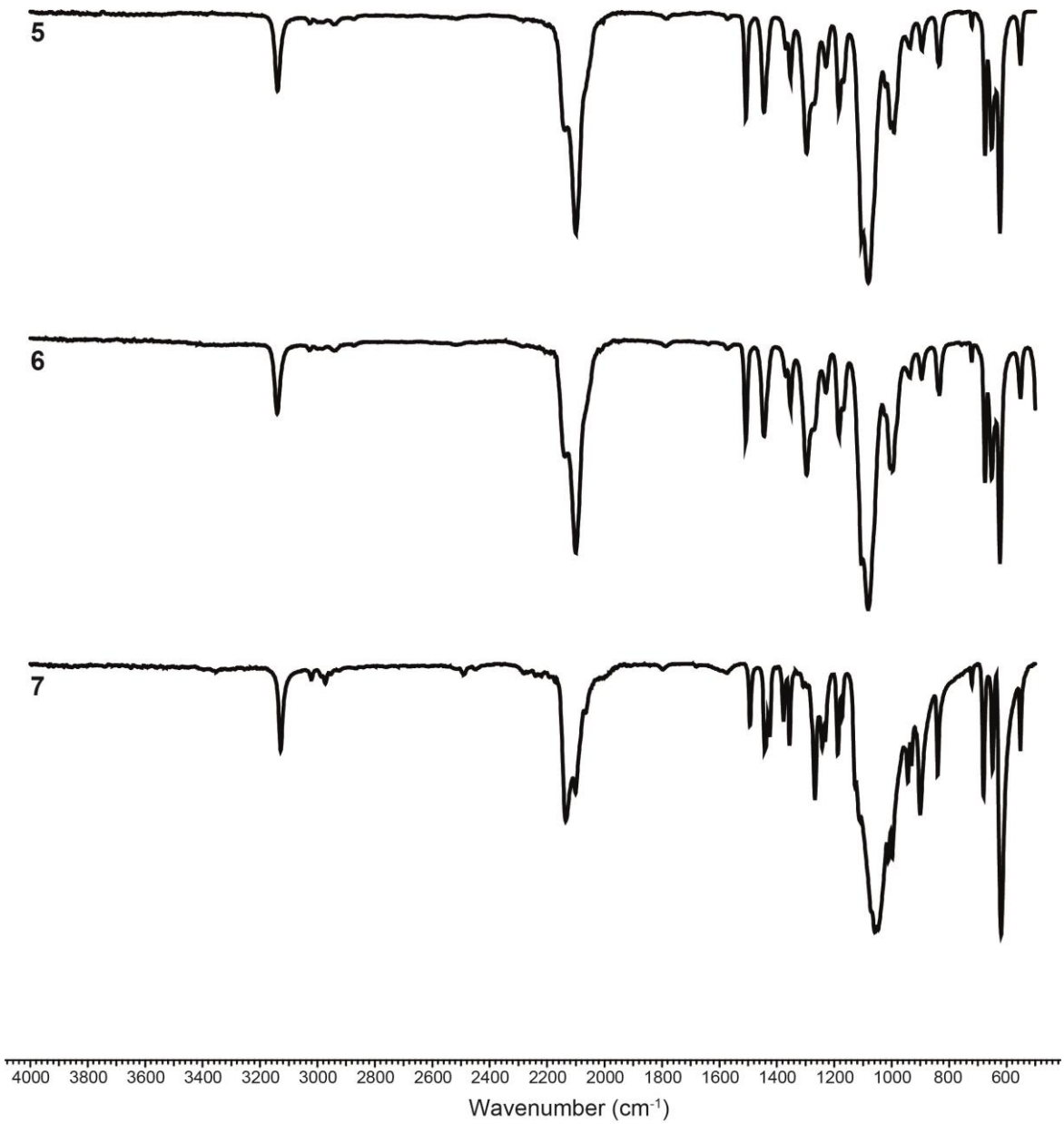

Figure S2. Infrared spectra of the iron(II) **5**, zinc(II) **6**, and silver(I) **7** complexes.

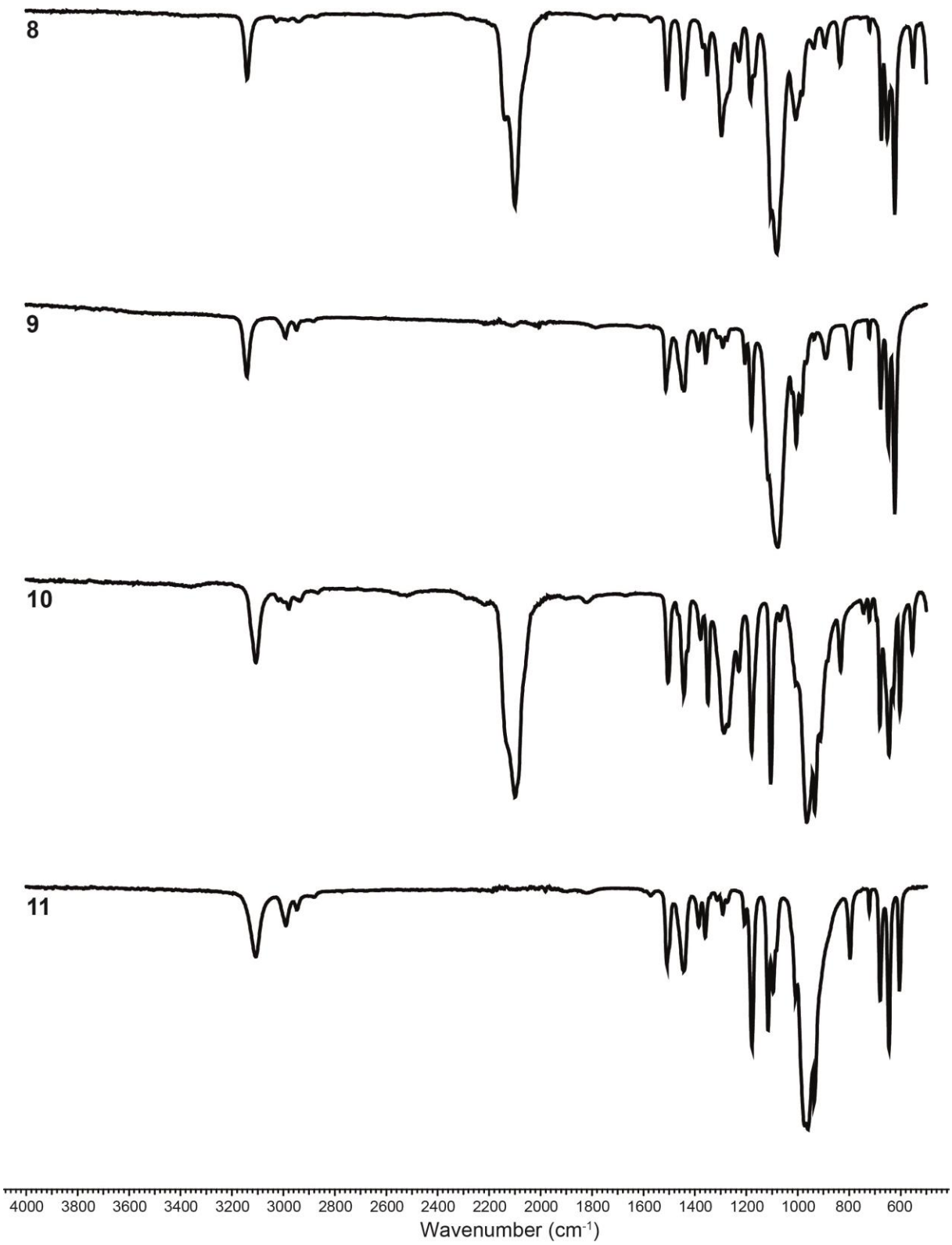

Figure S3. Infrared spectra of chlorate and perchlorate coordination compounds **8**–**11**.

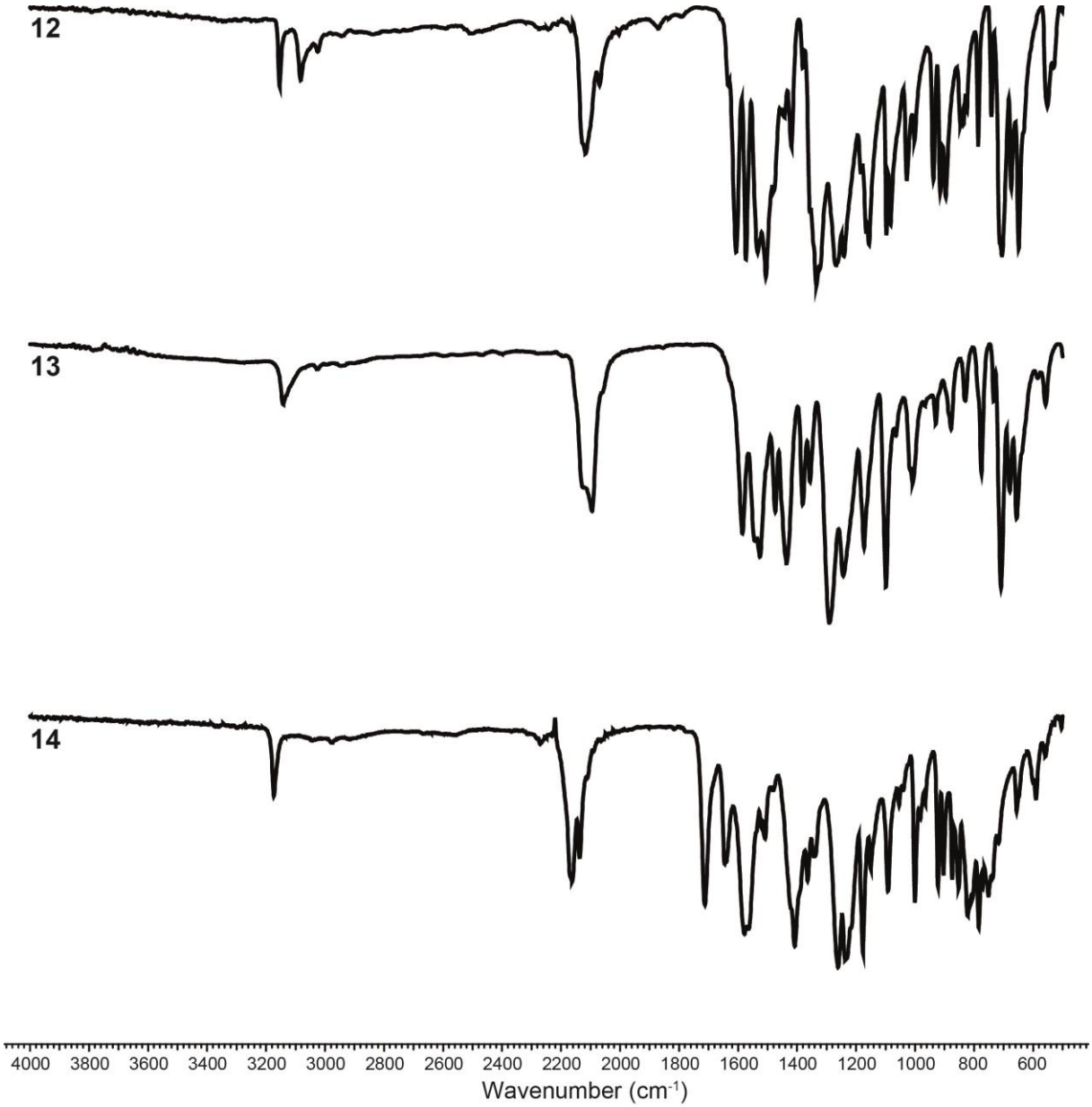

Figure S4. Infrared spectra of the nitroaromatic complexes **12**–**14**.

4.6.3. X-ray Diffraction and Microscope Images

For all crystalline compounds, an Oxford Xcalibur3 diffractometer with a CCD area detector or Bruker D8 Venture TXS diffractometer equipped with a multilayer monochromator, a Photon 2 detector and a rotating-anode generator were employed for data collection using Mo-Kα radiation (λ = 0.7107 Å). On the Oxford device, data collection and reduction were carried out using the CRYSALISPRO software.[1] On the Bruker diffractometer, the data were collected with the Bruker Instrument Service v3.0.21, the data reduction was performed using the SAINT V8.18C software (Bruker AXS Inc., 2011). The structures were solved by direct methods (SIR-92,[2] SIR-97[3] or SHELXS-97[4]) and refined by full-matrix least-squares on F2 (SHELXL[4]) and finally checked using the PLATON software[5] integrated in the WinGX[6]

software suite. The non-hydrogen atoms were refined anisotropically and the hydrogen atoms were located and freely refined. The absorptions were corrected by a SCALE3 ABSPACK or SADABS Bruker APEX3 multiscan method.[7,8] All DIAMOND2 plots are shown with thermal ellipsoids at the 50% probability level and hydrogen atoms are shown as small spheres of arbitrary radius.

Table S1. Crystallographic data of **3**–**5**.

	3	**4**	**5**
Formula	$C_6H_{12}CuN_{16}O_7$	$C_6H_{10}CuN_{16}O_6$	$C_{18}H_{30}Cl_2FeN_{42}O_8$
FW [g mol^{-1}]	483.86	465.84	1089.59
Crystal system	triclinic	monoclinic	monoclinic
Space Group	*P*−1	$P2_1/c$	$P2_1/c$
Color / Habit	blue block	blue block	colorless platelet
Size [mm]	0.05 x 0.10 x 0.20	0.05 x 0.23 x 0.41	0.04 x 0.17 x 0.29
a [Å]	7.2147(10)	13.5068(9)	12.8715(15)
b [Å]	9.8636(13)	6.6047(3)	17.6468(18)
c [Å]	13.186(2)	9.7789(7)	10.3064(10)
α [°]	72.220(13)	90	90
β [°]	78.695(13)	110.604(7)	110.293(11)
γ [°]	86.484(11)	90	90
V [Å^3]	876.2(2)	816.56(10)	2195.7(4)
Z	2	2	2
$\rho_{calc.}$ [g cm^{-3}]	1.834	1.895	1.648
μ [mm^{-1}]	1.323	1.412	0.561
F(000)	490	470	1112
$\lambda_{MoK\alpha}$ [Å]	0.71069	0.71073	0.71073
T [K]	143	143	128
θ Min–Max [°]	4.2, 26.0	4.2, 26.0	4.4, 26.4
Dataset	−8: 8; −11: 12; −16: 15	−16: 16; −7: 8; −12: 11	−12: 16; −22: 21; −12: 12
Reflections collected	6673	6457	12644
Independent refl.	3416	1602	4468
R_{int}	0.096	0.040	0.108
Observed reflections	1816	1360	2222
Parameters	279	133	322
R_1 (obs)[a]	0.0614	0.0309	0.0723
wR_2 (all data)[b]	0.1173	0.0765	0.1638
GooF[c]	0.84	1.05	0.99
Resd. Dens. [e Å^{-3}]	−0.43, 0.60	−0.25, 0.41	−0.58, 1.01
Absorption correction	multi-scan	multi-scan	multi-scan
CCDC	1898402	1898401	1898397

[a] $R_1 = \Sigma||F_0|- |F_c||/ \Sigma|F_0|$; [b] $wR_2 = [\Sigma[w(F_0^2-F_c^2)^2]/\Sigma[w(F_0)^2]]^{1/2}$; $w = [\sigma c^2(F_0^2)+(xP)^2+yP]^{-1}$ and $P = (F_0^2+2F_c^2)/3$; [c] GooF = $\{\Sigma[w(F_o^2-F_c^2)^2]/(n-p)\}^{1/2}$ (n = number of reflections; p = total number of parameters).

Table S2. Crystallographic data of **7**, **9**, and **11**.

	7	**9**	**11**
Formula	$C_3H_5AgClN_7O_4$	$C_{18}H_{36}Cl_2CuN_{24}O_8$	$C_{18}H_{36}Cl_2CuN_{24}O_6$
FW [g mol^{-1}]	346.46	851.15	819.15
Crystal system	triclinic	triclinic	trigonal
Space Group	*P*−1	*P*−1	*R*−3
Color / Habit	colorless needle	blue plate	blue block
Size [mm]	0.06 x 0.08 x 0.28	0.11 x 0.50 x 0.50	0.04 x 0.06 x 0.10
a [Å]	6.3384(6)	10.0781(5)	10.5921(3)
b [Å]	7.1649(6)	15.8073(8)	10.5921(3)
c [Å]	10.7216(10)	18.4505(9)	29.6787(15)
α [°]	78.832(7)	72.526(4)	90
β [°]	83.609(8)	78.495(4)	90
γ [°]	77.891(7)	83.803(4)	120
V [Å^3]	465.79(7)	2743.7(2)	2883.6(3)
Z	2	3	3
$\rho_{calc.}$ [g cm^{-3}]	2.470	1.545	1.415
μ [mm^{-1}]	2.466	0.820	0.773
F(000)	336	1317	1269
$\lambda_{MoK\alpha}$ [Å]	0.71073	0.71073	0.71073
T [K]	143	127	296
θ Min–Max [°]	4.4, 26.0	3.4, 26.4	3.5, 25.0
Dataset	−7: 7; −8: 11; −13: 11	−12: 11; −11: 19; −20: 23	−12: 12; −12: 12; −35: 35
Reflections collected	3379	15109	9088
Independent refl.	1822	11062	1132
R_{int}	0.037	0.030	0.033
Observed reflections	1613	7347	954
Parameters	145	764	79
R_1 (obs)[a]	0.0280	0.0521	0.0813
wR_2 (all data)[b]	0.0594	0.1230	0.2569
GooF[c]	1.02	1.05	1.05
Resd. Dens. [e Å^{-3}]	−0.68, 0.53	−0.45, 0.52	−0.31, 0.61
Absorption correction	multi-scan	multi-scan	multi-scan
CCDC	1898400	1898399	1898541

[a] $R_1 = \Sigma||F_0|- |F_c||/ \Sigma|F_0|$; [b] $wR_2 = [\Sigma[w(F_0^2-F_c^2)^2]/\Sigma[w(F_0)^2]]^{1/2}$; $w = [\sigma c^2(F_0^2)+(xP)^2+yP]^{-1}$ and $P = (F_0^2+2F_c^2)/3$; [c] GooF = $\{\Sigma[w(F_o^2-F_c^2)^2]/(n-p)\}^{1/2}$ (n = number of reflections; p = total number of parameters).

Table S3. Crystallographic data of **12**–**14**.

	12	**13**	**14**
Formula	$C_{18}H_{14}CuN_{20}O_{14}$	$C_{12}H_{11}CuN_{17}O_8$	$C_{24}H_{24}CuN_{34}O_{18}$
FW [g mol^{-1}]	798.04	584.93	1140.31
Crystal system	monoclinic	triclinic	triclinic
Space Group	$P2_1/c$	$P\bar{1}$	$P\bar{1}$
Color / Habit	green plate	yellow-green block	green plate
Size [mm]	0.04 x 0.23 x 0.35	0.07 x 0.20 x 0.30	0.03 x 0.16 x 0.30
a [Å]	10.3199(19)	9.5735(4)	9.0161(9)
b [Å]	17.4689(12)	10.8581(4)	11.1883(9)
c [Å]	8.1071(7)	11.4077(5)	12.0818(12)
α [°]	90	68.645(4)	72.386(8)
β [°]	92.536(9)	78.203(4)	82.174(8)
γ [°]	90	81.504(4)	67.389(8)
V [Å^3]	1460.1(3)	1077.59(8)	1072.05(19)
Z	2	2	1
$\rho_{calc.}$ [g cm^{-3}]	1.815	1.803	1.766
μ [mm^{-1}]	0.855	1.098	0.627
F(000)	806	590	579
$\lambda_{MoK\alpha}$ [Å]	0.71073	0.71073	0.71073
T [K]	143	143	143
θ Min–Max [°]	4.3, 26.4	4.1, 32.4	4.3, 26.4
Dataset	−11: 12; −21: 21; −10: 10	−13: 14; −15: 15; −17: 17	−9: 11; −13: 11; −15: 9
Reflections collected	11560	22857	6375
Independent refl.	2964	7196	4332
R_{int}	0.104	0.046	0.041
Observed reflections	1665	5128	2953
Parameters	251	420	357
R_1 (obs)[a]	0.0676	0.0451	0.0590
wR_2 (all data)[b]	0.1585	0.1065	0.1127
GooF[c]	1.01	1.04	1.04
Resd. Dens. [e Å^{-3}]	−0.42, 0.72	−0.54, 0.51	−0.61, 0.65
Absorption correction	multi-scan	multi-scan	multi-scan
CCDC	1898395	1898398	1898396

[a] $R_1 = \Sigma||F_0|- |F_c||/ \Sigma|F_0|$; [b] $wR_2 = [\Sigma[w(F_0^2-F_c^2)^2]/\Sigma[w(F_0)^2]]^{1/2}$; $w = [\sigma c^2(F_0^2)+(xP)^2+yP]^{-1}$ and $P = (F_0^2+2F_c^2)/3$; [c] GooF = $\{\Sigma[w(F_o^2-F_c^2)^2]/(n-p)\}^{1/2}$ (n = number of reflections; p = total number of parameters).

Copper(II) perchlorate compound **9** crystallizes in the triclinic space group $P\bar{1}$ with three formula units per unit cell and a calculated density of 1.545 g cm^{-3} at 127 K. The copper(II) cation is coordinated by six molecules of 1-ETZ (**2**) and the perchlorate anions are non-coordinating (Figure S5). The coordination sphere shows a typical Jahn-Teller distortion along the N12–Cu1–N24 axis with only small deviations from the perfect octahedral angles. Complex **11** crystallizes in the trigonal space group $R\bar{3}$ with three formula units per unit cell and possesses a calculated density of 1.415 g cm^{-3} at 296 K. Similar to compound **9**, the molecular unit contains one copper(II) cation coordinated by six molecules of 1-ETZ (**2**) and two non-coordinating anions (Figure S6). Interestingly, the octahedral coordination sphere does not show any Jahn-Teller distortion at all with identical Cu–N bond lengths.

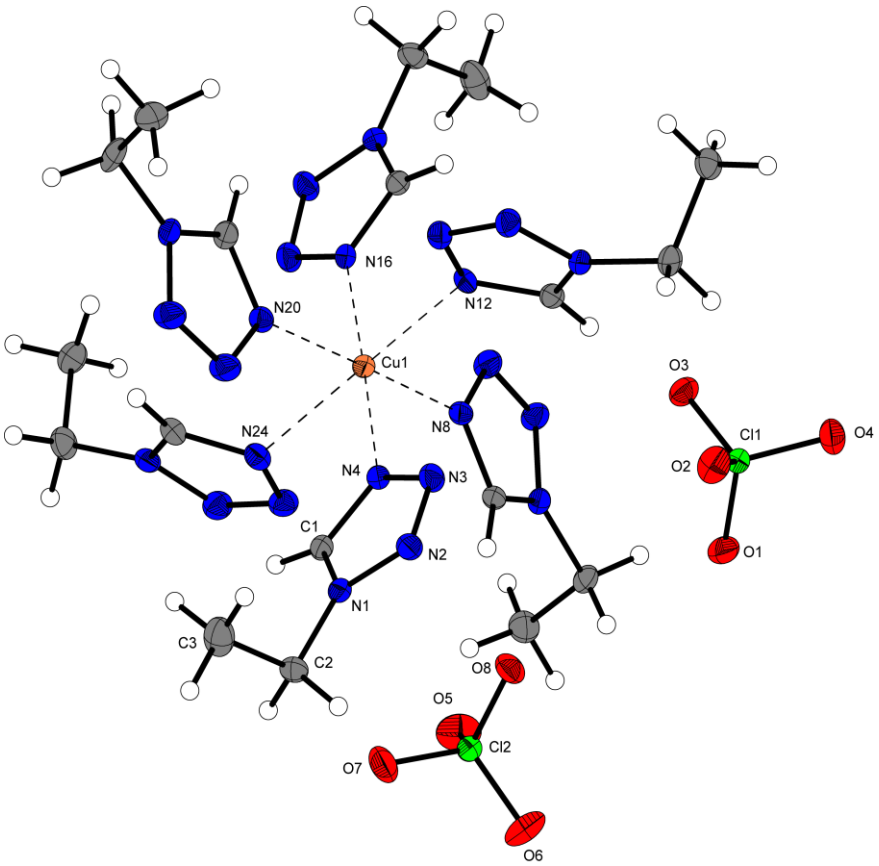

Figure S5. Molecular unit of $[Cu(1\text{-}ETZ)_6](ClO_4)_2$ (**9**). Selected bond lengths (Å): Cu1–N4 2.033(3), Cu1–N8 2.040(3), Cu1–N12 2.335(3); selected bond angles (°): N4–Cu1–N8 92.42(12), N4–Cu1–N12 90.62(11), N4–Cu1–N16 178.38(12), N4–Cu1–N20 89.18(12).

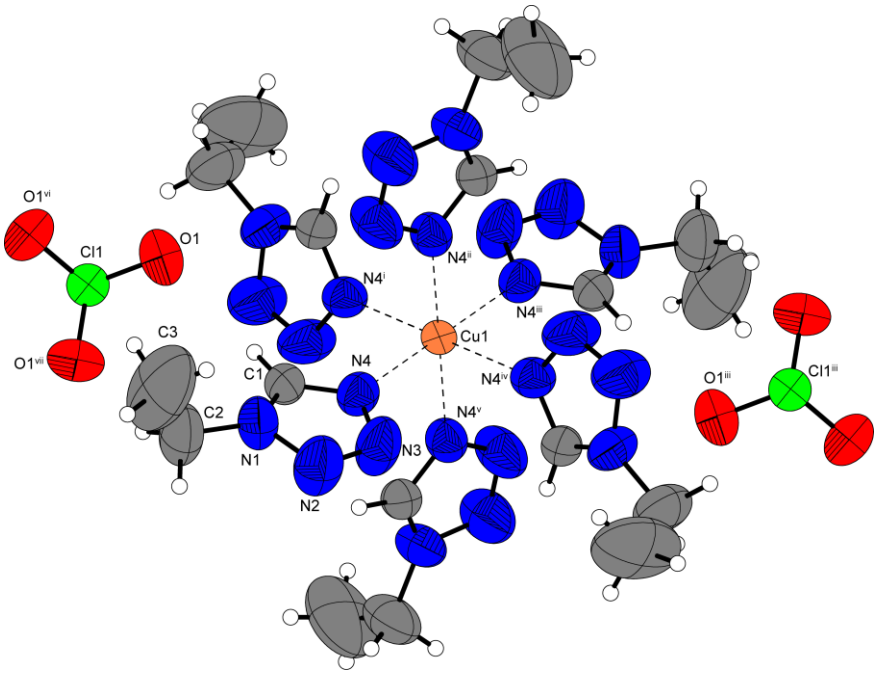

Figure S6. Molecular unit of $[Cu(1\text{-}ETZ)_6](ClO_3)_2$ (**11**). Selected bond length (Å): Cu1–N4 2.138(5); selected bond angles (°): N4–Cu1–$N4^{ii}$ 90.4(2), N4–Cu1–N^{v} 89.6(2), $N4^{ii}$–Cu1–$N4^{iii}$ 90.4(3); Symmetry codes: (i) 1−y, x−y, z; (ii) 1−x+y, 1−x, z; (iii) y, x−y, z; (iv) −x+y, −x, z; (v) −x, −y, −z (vi) y, −x+y, −z (vii) x−y, x, −z.

The bridging anions in compound **13** are leading to the formation of one-dimensional polymeric chains with altering layers of styphnate rings along the b-axis (Figure S7). Interestingly the coordinating nitro groups are within the plane of the benzene ring, whereas the non-coordinating one is perpendicular to it. One of the ligand molecules is highly disordered, which only allows an isotropic refinement of it.

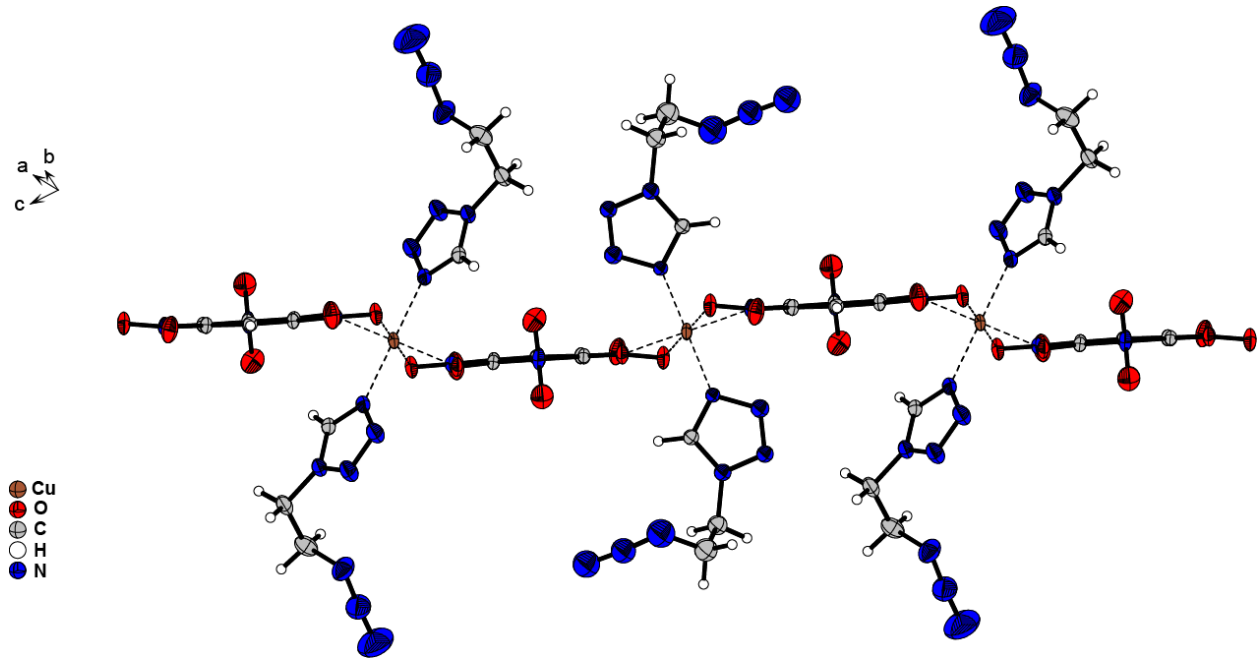

Figure S7. Segment of the polymeric chain of **13**, formed by double-chelating styphnate anions linking between two different copper cations.

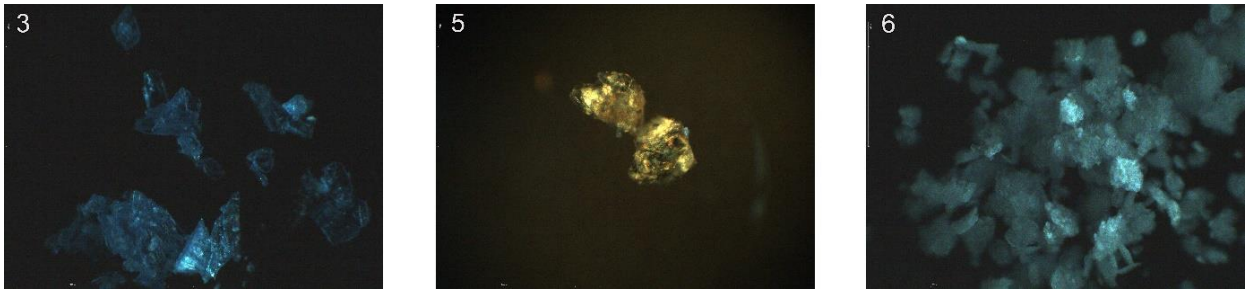

Figure S8. Microscope images of **3**, **5**, and **6** (fourfold magnitude).

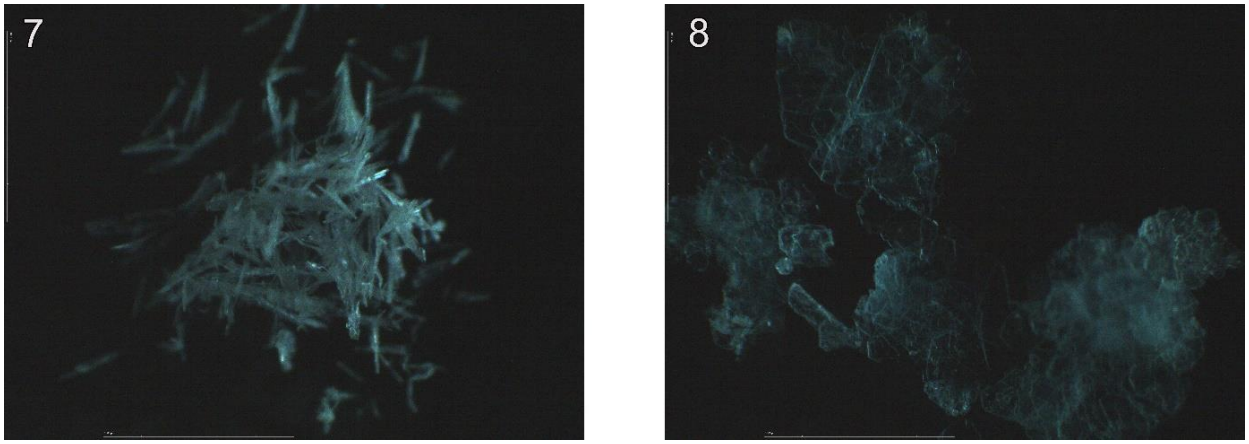

Figure S9. Microscope images of **7** and **8** (fourfold magnitude).

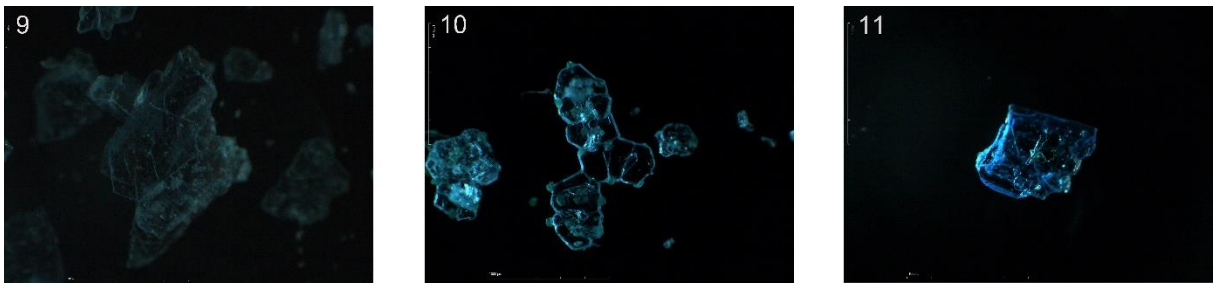

Figure S10. Microscope images of **9**–**11** (fourfold magnitude).

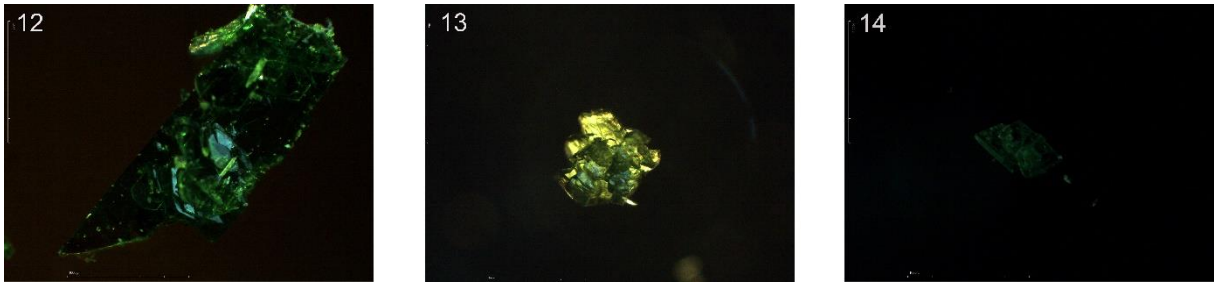

Figure S11. Microscope images of **12**–**14** (fourfold magnitude).

4.6.4. DTA Plots of 1–3, 5–14

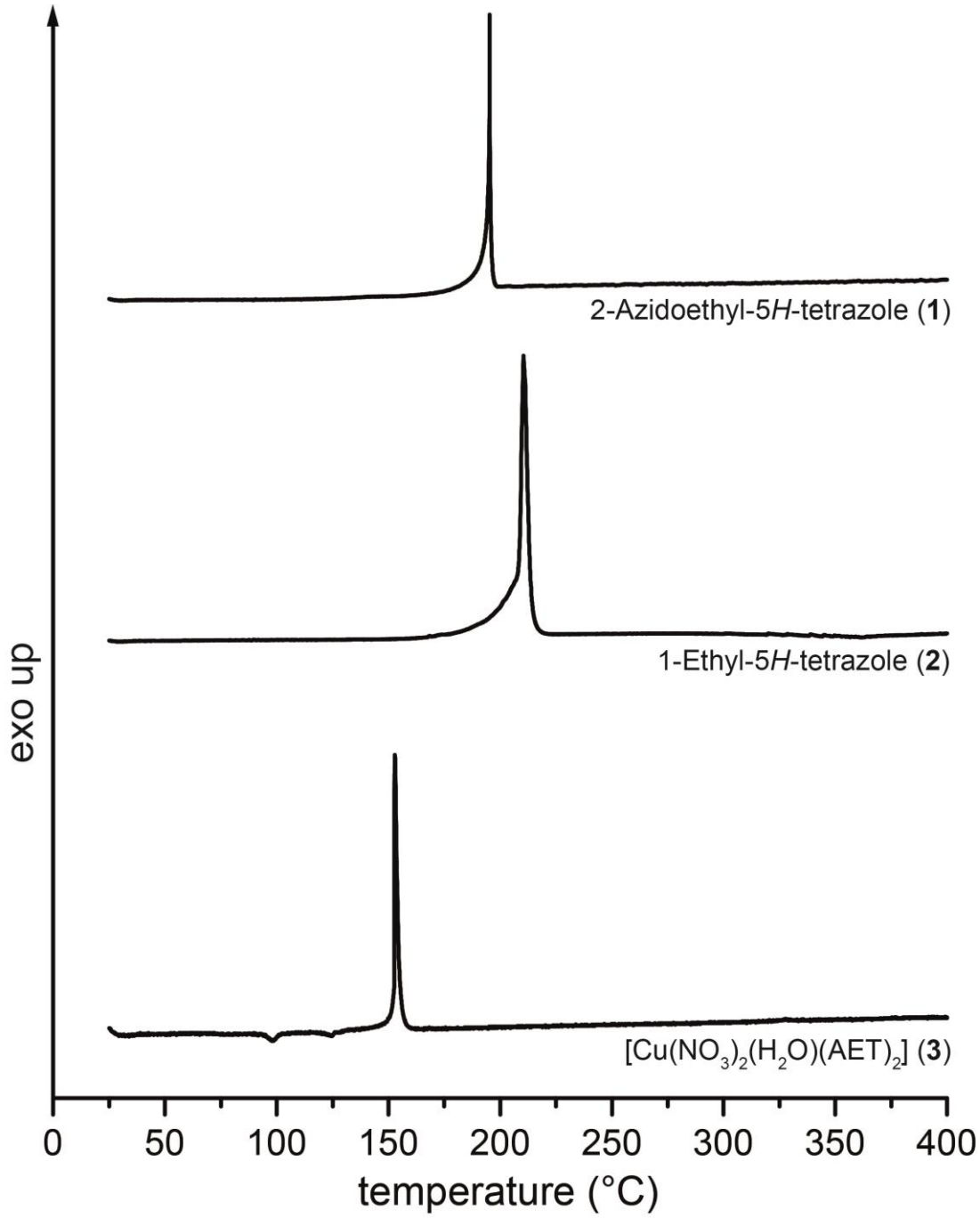

Figure S12. DTA plots of the ligands **1** and **2** together with the complex **3**.

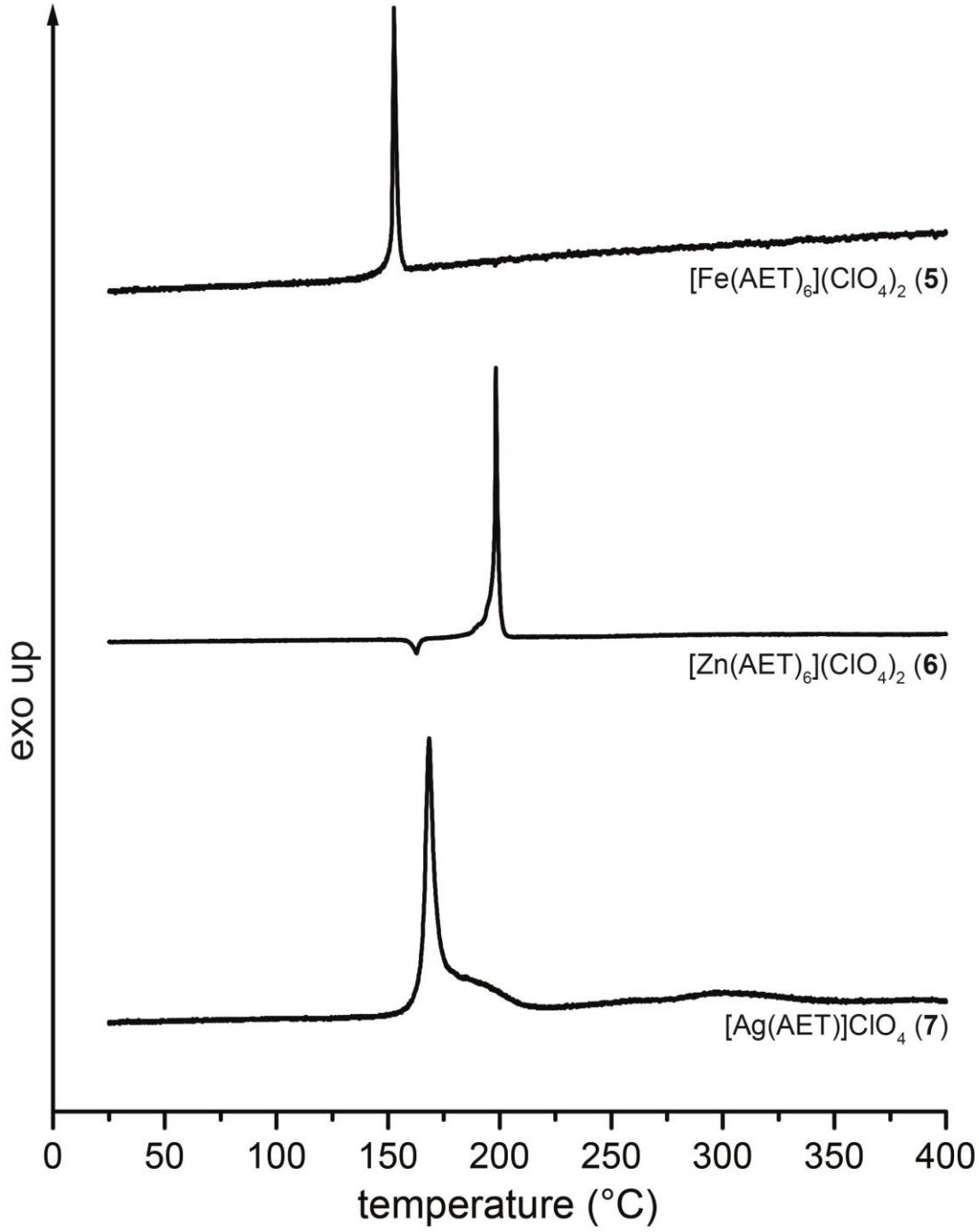

Figure S13. Differential thermal analysis of the perchlorate compounds **5**–**7**.

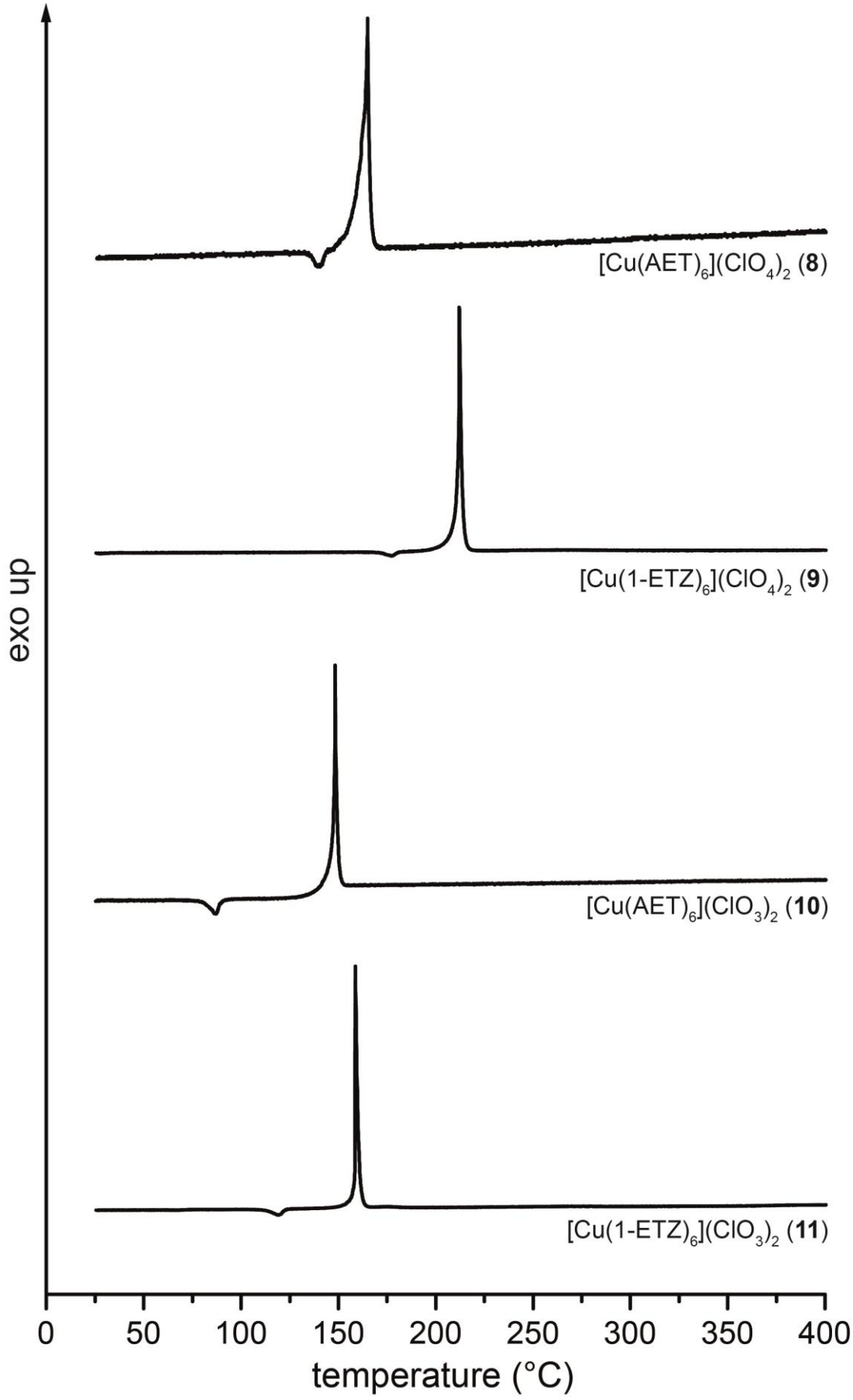

Figure S14. Differential thermal analysis plots of the coordination compounds **8**–**11**.

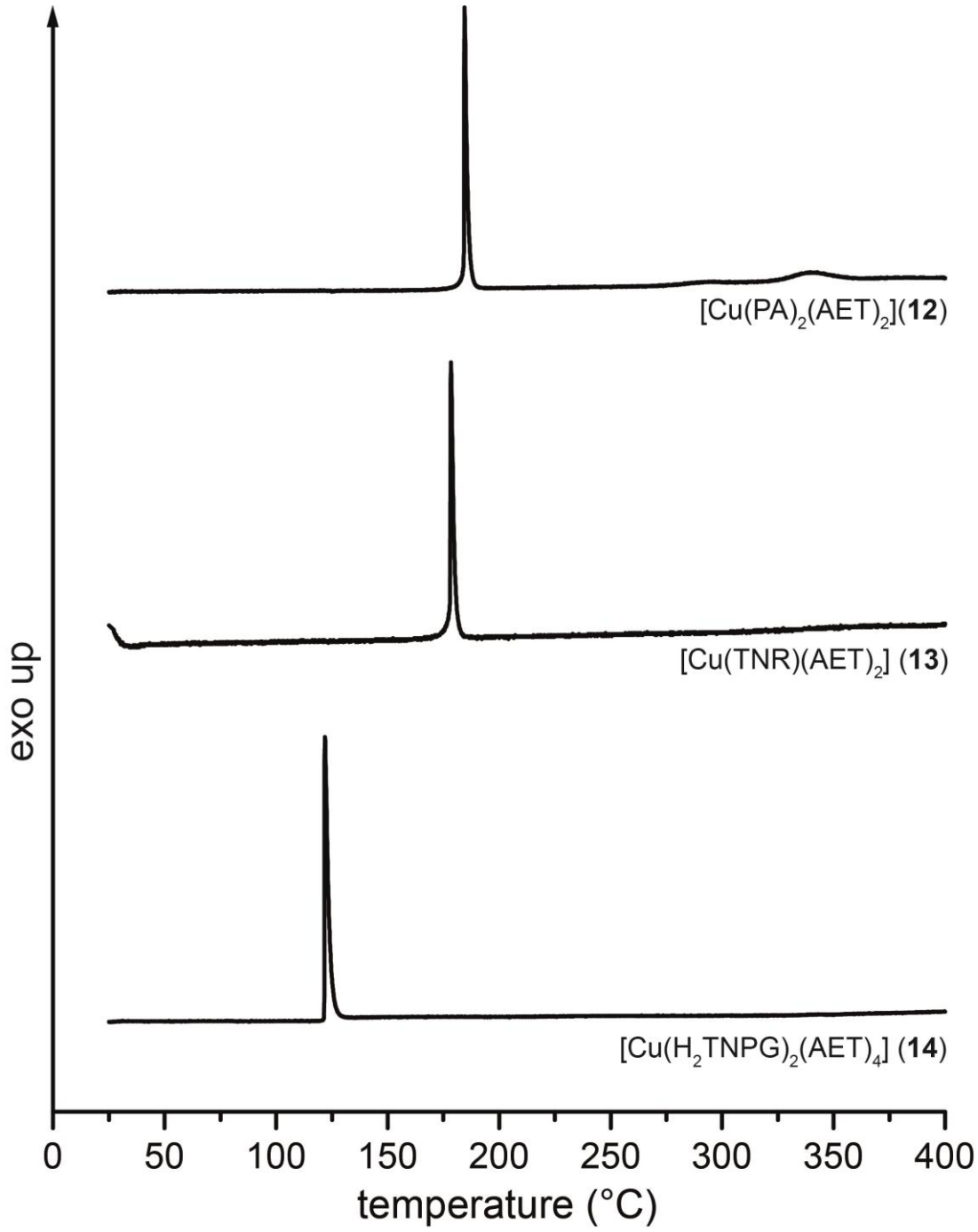

Figure S15. DTA plots of **12**–**14**.

4.6.5. TGA Plots of 1, 3, 5–6, and 8–9

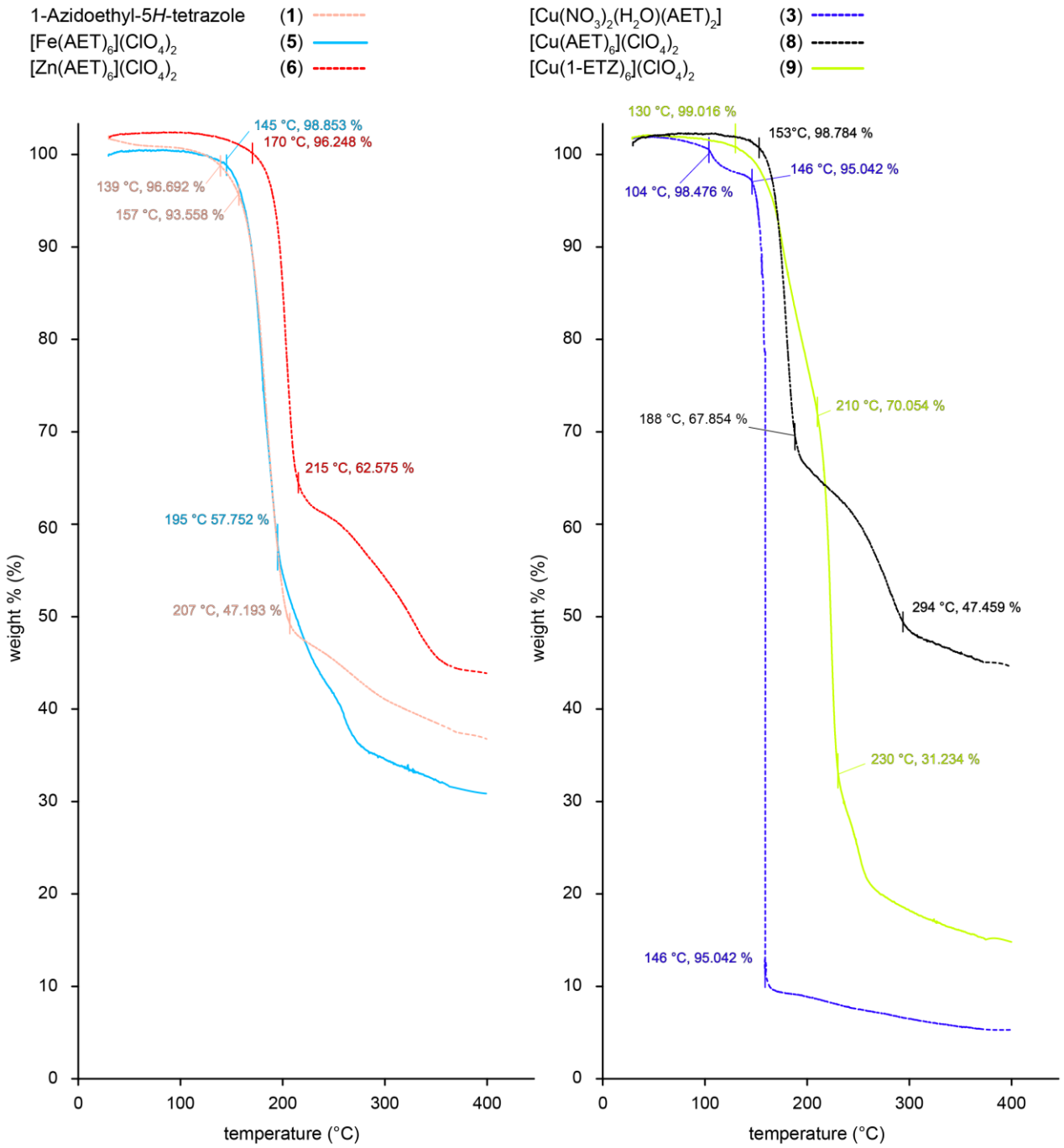

Figure S16. TGA plots of the ligand **1** and the complexes **3**, **5**–**6**, **8**, and **9**.

4.6.6. Column Diagrams of the Complexes 5–8, 10, and 12–14

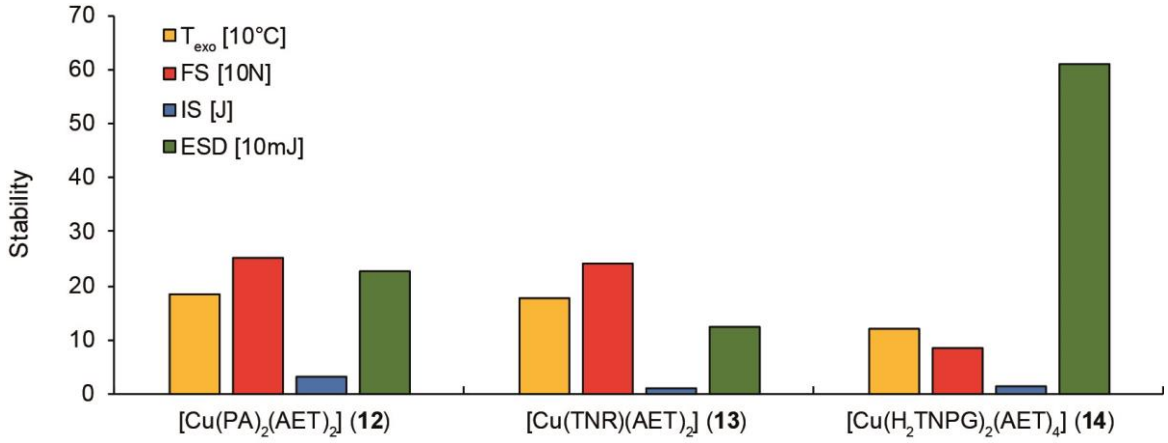

Figure S17. Comparison of the stabilities of complex compounds **12**–**14**.

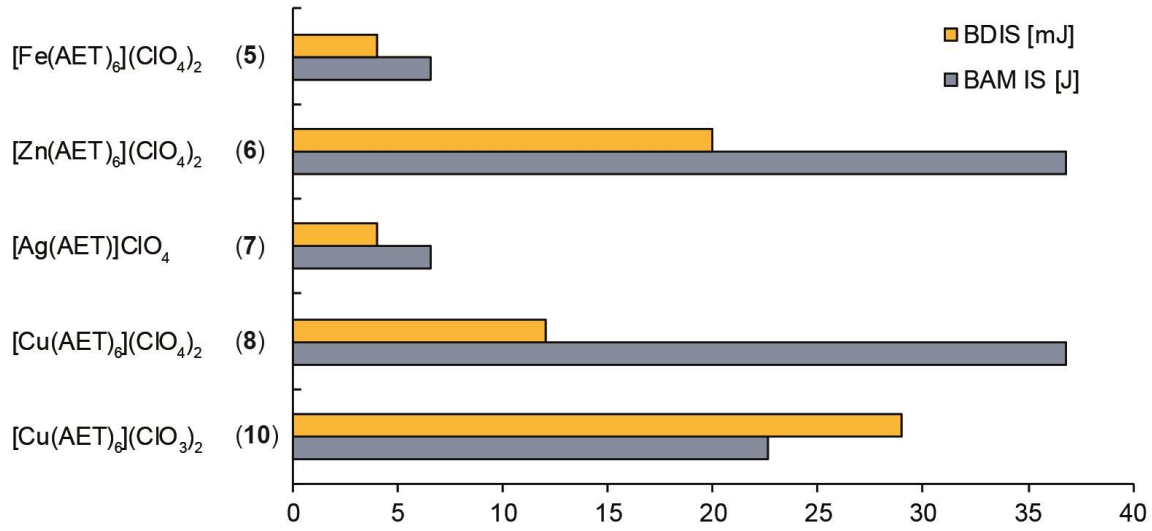

Figure S18. Impact sensitivities of compounds **5**–**8** and **10** determined with BAM drop hammer and ball drop impact tester.

4.6.7. Hot Plate and Hot Needle Tests

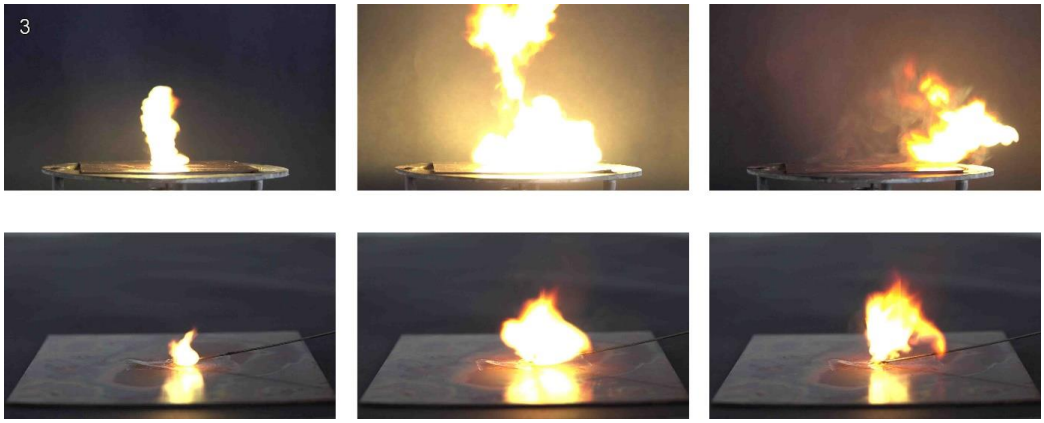

Figure S19. Hot plate and hot needle tests of complex **3** shown as a sequence.

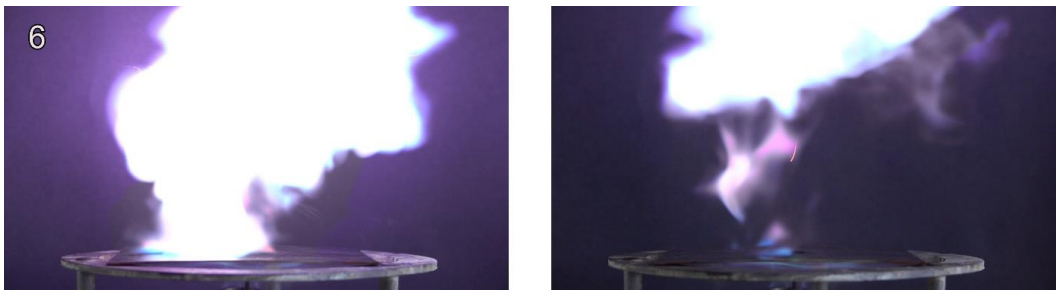

Figure S20. Hot plate test of complex **6** shown as a sequence.

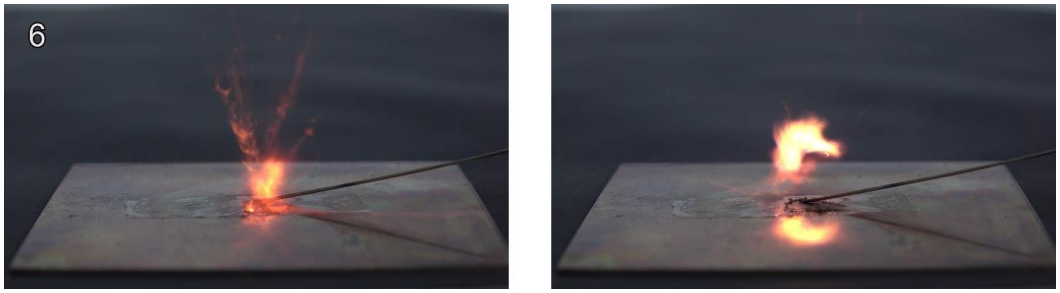

Figure S21. Hot needle test of complex **6** shown as a sequence.

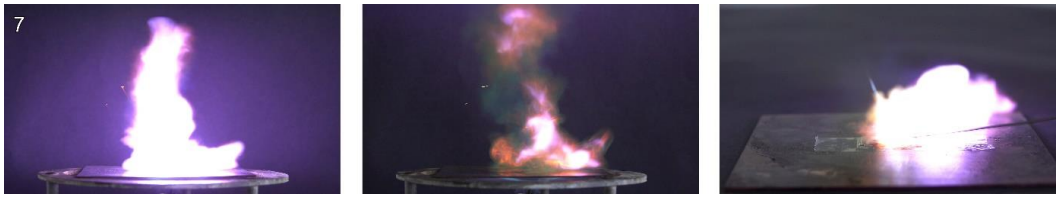

Figure S22. Hot plate (left & middle) and hot needle test (right) of complex **7**.

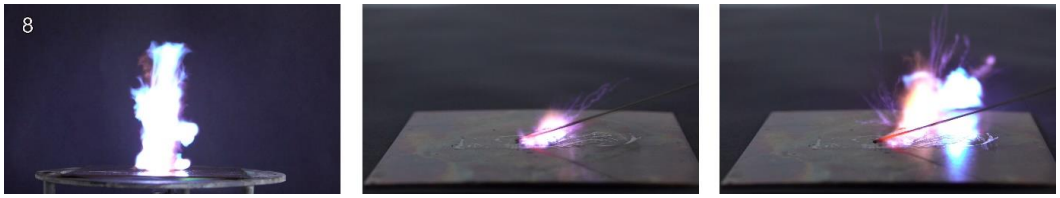

Figure S23. Deflagration (left) and detonation (right & middle) of the copper(II) perchlorate complex **8** during hot plate und hot needle test.

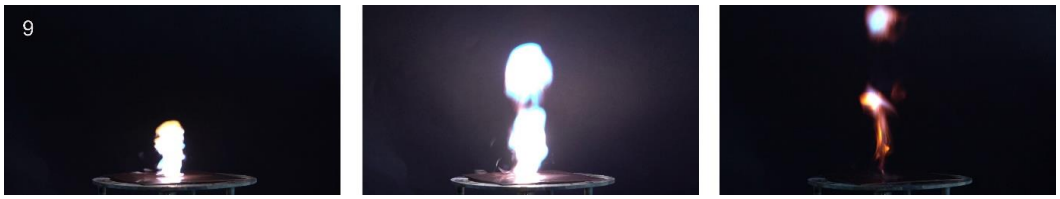

Figure S24. Deflagration of the copper(II) perchlorate complex **9** during hot plate test.

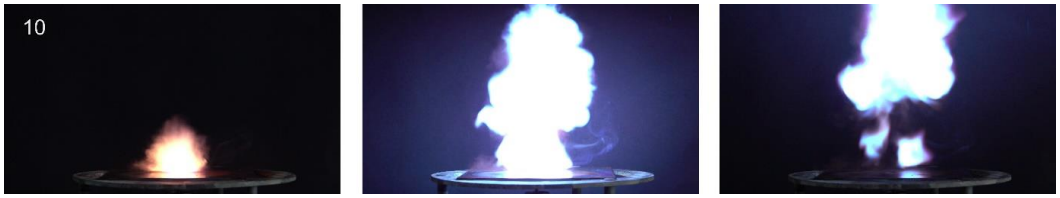

Figure S25. Hot plate test of complex **10** shown as a sequence.

Figure S26. Hot needle test of complex **10** shown as a sequence.

Figure S27. Deflagration of compound **11** during hot plate test shown as a sequence.

Figure S28. Deflagration of the picrate complex **12** during hot plate und hot needle tests.

Figure S29. Deflagration of styphnate compound **13** during hot plate and hot needle test.

Figure S30. Deflagration of compound **14** during a hot plate test.

4.6.8. Laser Ignition Tests of 3, 5, 7, 9, 10, and 12–14

Figure S31. Deflagration of compound **3** during laser initiation test.

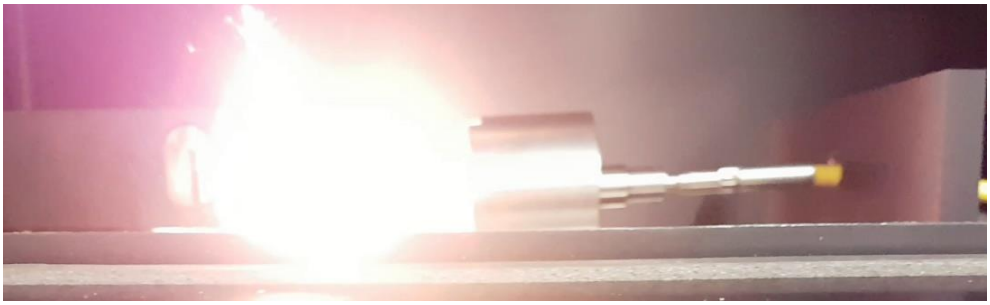

Figure S32. Moment of detonation of iron(II) perchlorate complex **5**

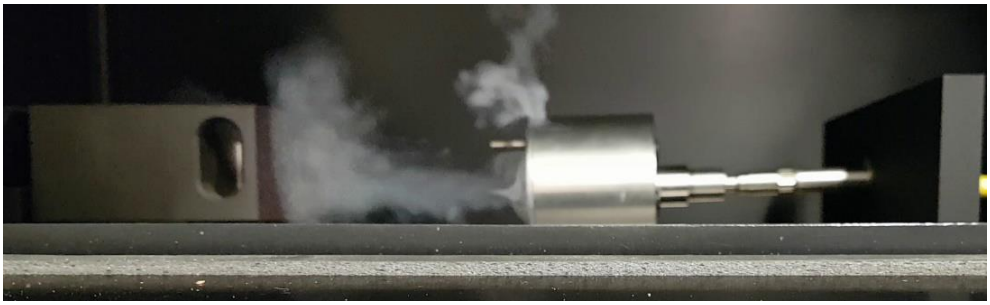

Figure S33. Decomposition of copper complex **9** during the laser initiation experiment.

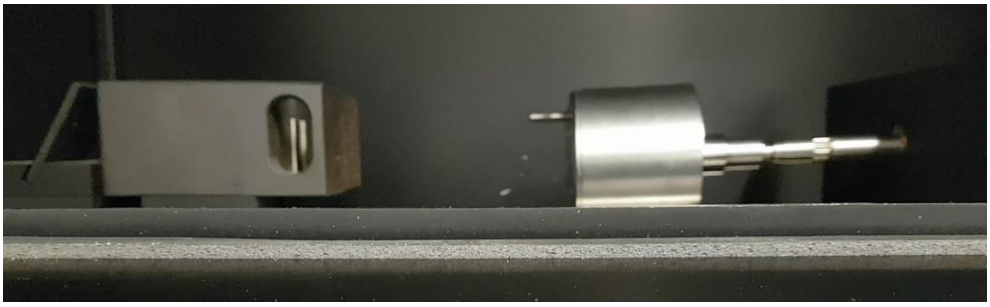

Figure S34. Detonation of the chlorate complex **10** during the laser irradiation experiment.

Figure S35. Decomposition of **12** in reaction to laser irradiation.

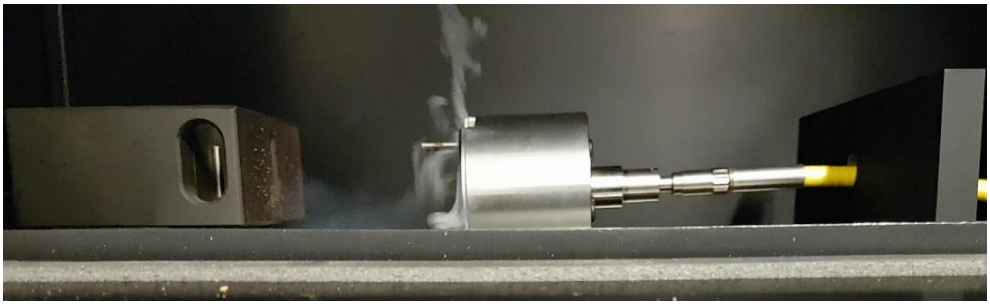

Figure S36. Decomposition of styphnate compound **13** during laser initiation test.

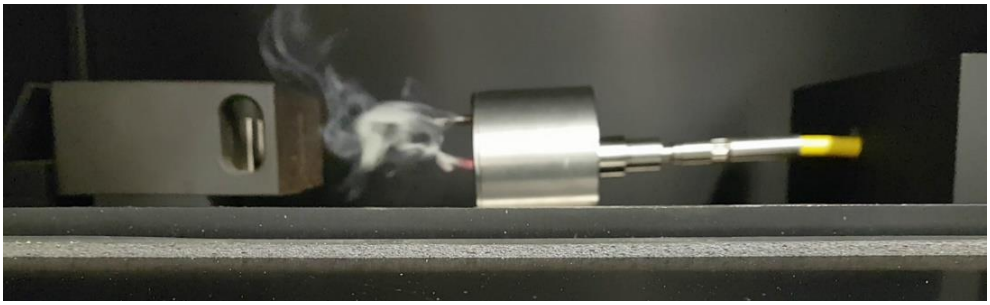

Figure S37. Decomposition of compound **14** during laser initiation test.

4.6.9. UV-Vis Spectra and Optical Properties of 3, 5–9, and 12–14

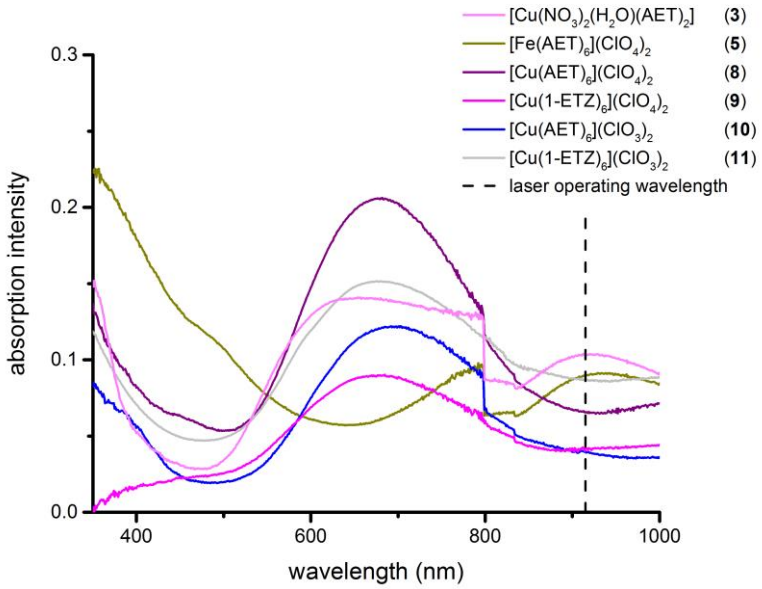

Figure S38. UV-Vis spectra of **3**, **5**, and **8**–**11** recorded in the solid state.

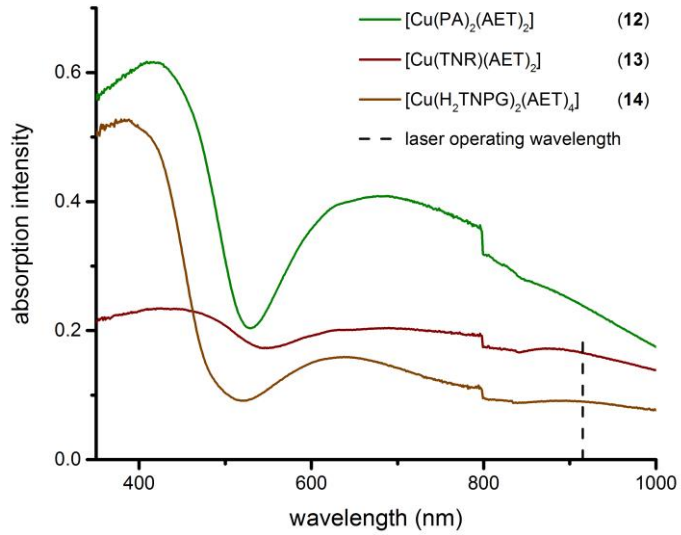

Figure S39. Solid state UV-Vis spectra of coordination compounds **12**–**14**.

Table S4. Optical properties measured for the coordination compounds **3**, **5**, and **8**–**14**.

Compound	M	Color	$\lambda_{d\text{-}d}$[a]	$\lambda_{915}/\lambda_{d\text{-}d}$[b]
3	Cu^{II}	blue	654	0.74
5	Fe^{II} (hs)	yellowish	786	0.95
8	Cu^{II}	blue	682	0.31
9	Cu^{II}	blue	685	0.47
10	Cu^{II}	blue	698	0.32
11	Cu^{II}	blue	669	0.58
12	Cu^{II}	green	690	0.58
13	Cu^{II}	green	690	0.81
14	Cu^{II}	green	638	0.57

[a] Absorption intensity maximum wavelength, which can be assigned to electron d-d transitions in the measured range of 350–1000 nm. [b] Quotient of the absorption intensity at the laser wavelength and the intensity at the d-d absorption wavelength.

4.6.10. Experimental Part and General Methods

All chemicals and solvents were employed as received (Sigma-Aldrich, Fluka, Acros, ABCR). ^{1}H, ^{13}C and ^{15}N spectra were recorded at ambient temperature using a JEOL Bruker 400, Eclipse 270, JEOL EX 400 or a JEOL Eclipse 400 instrument. The chemical shifts quoted in ppm in the text refer to typical standards such as tetramethylsilane (^{1}H, ^{13}C) and nitromethane (^{15}N) in d_6-DMSO or d_3-MeCN as the solvents. The ^{1}H-^{15}N-HMBC NMR spectra were measured with a data matrix of 1024 x 256, an applied zero filling of 2048 x 4096, 32 scans per round, a relaxation delay of 1 second, an acquisition time of 0.3 seconds at a concentration of 140 mg/mL and an overall measurement time of approx. 3 h. Endothermic and exothermic events of the described compounds, which indicate melting, evaporation or decomposition, are given as the extrapolated onset temperatures. The samples were measured in a range of 25–400 °C at a heating rate of 5 °C min^{-1} through differential thermal analysis (DTA) with an OZM Research DTA 552-Ex instrument and in some cases additional by thermal gravimetric analysis (TGA) with a PerkinElmer TGA4000. Infrared spectra were measured with pure samples on a Perkin-Elmer BXII FT-IR system with a Smith DuraSampler IR II diamond ATR. Determination of the carbon, hydrogen and nitrogen contents was carried out by combustion analysis using an Elementar Vario El (nitrogen values determined are often lower than the calculated ones' due to their explosive behavior). UV-Vis spectra were recorded in the solid state using a Varian Cary 500 spectrometer in the wavelength range of 350–1000 nm. The step in the absorption intensity at 800 nm is caused by a detector change. Impact sensitivity tests were carried out according to STANAG 4489[9] with a modified instruction[10] using a BAM (Bundesanstalt für Materialforschung und -prüfung) drop hammer.[11,12] Ball drop impact sensitivity tests were determined for selected compounds on an OZM ball drop machine (BIT-132), following MIL-STD-1751A (method 1016) by dropping a free falling steel ball onto the explosive compound.[13] A sample of approximately 30 mg was placed on a steel block and spread into a 0.33 mm layer of substance. The steel ball guide was set to the desired height and the loaded impact block positioned underneath. By

releasing the ball shield, a 0.500-inch steel ball, weighing 8.35 g, was allowed to fall onto the sample. Any visual observation of decomposition was regarded as a positive result. If no reaction occurred, the remaining substance was disposed, and the impact block loaded with a freshly prepared sample. The limiting impact energy was determined in conformity with the recommended UN method for testing impact and friction sensitivities (1-in-6 approach), according to ST/SG/AC.10/11Rev.6 (s. 13.4.2.3.3).[14] The impact energy was calculated as the product of the weight of the steel ball and its fall height. An initial drop height was chosen, at which an explosion of the sample could be ensured. The impact energy level (ball guide height) was now stepwise decreased until no reaction was observed. At this point, testing was continued up to a total of six trials at that certain energy level. If an explosion occurred, the procedure was repeated by decreasing the drop height. As soon as six trials at a fixed energy level emerged as negative, the next higher energy level, where at least one out of at least six trials resulted in an explosion, is determined as the limiting impact energy. Friction sensitivity tests were carried out according to STANAG 4487[15] with a modified instruction[16] using the BAM friction tester. The classification of the tested compounds results from the "UN Recommendations on the Transport of Dangerous Goods".[17] Additionally all compounds were tested upon the sensitivity toward electrical discharge using the OZM Electric Spark XSpark10 device.[12] Hot plate and hot needle tests were performed in order to classify the initiation capability of selected complexes. The samples were fixed on a copper plate underneath adhesive tape and initiated by a red-hot needle. Strong deflagration or detonation of the compound usually indicates a valuable primary explosive. The safe and straightforward hot plate test only shows the behavior of the unconfined sample toward fast heating on a copper plate. It does not necessarily allow any conclusions on a compound's capability as a suitable primary explosive. Initiation capability tests of the newly investigated complexes toward pentaerythritol tetranitrate (PETN) were carried out in a copper shell with a diameter of 7 mm and a length of 88 mm filled with 200 mg of sieved PETN (grain size < 100 µm). First, nitropenta was pressed with a weight of 8 kg, then the primary explosive to be investigated was subsequently filled on top of the main charge and pressed with the same pressure force. The shell was sealed by an insulator, placed in a retaining ring, which was soldered to a copper witness plate with a thickness of 1 mm and finally initiated by a type A electric igniter. A positive test is indicated by a hole in the copper plate and fragmentation of the shell caused by a deflagration-to-detonation transition (DDT) of PETN. The laser initiation experiments were performed with a 45 W InGaAs laser diode operating in the single-pulsed mode. The diode is attached to an optical fiber with a core diameter of 400 µm and a cladding diameter of 480 µm. The optical fiber is connected via a SMA type connecter directly to the laser and to a collimator. This collimator is coupled to an optical lens, which was positioned in its focal distance (f = 29.9 mm) to the sample. The lens is shielded from the explosive by a sapphire glass.

Approximately 15 mg of the carefully pestled compound to be investigated was filled into a transparent plastic cap (PC), pressed with a pressure force of 1 kN and sealed by a UV-curing adhesive. The confined samples were irradiated at a wavelength of 915 nm, a voltage of 4 V, a current of 7–12 A and pulse lengths of 0.1–20 ms. The combined currents and pulse lengths result in an energy output of 0.17 –111 mJ.

The obtained coordination compounds were washed with cold ethanol when stated, dried overnight in air and used for analytics without further purification.

CAUTION! *All investigated compounds are energetic materials (some of the compounds are primary explosives!), which show partly increased sensitivities toward various stimuli (e.g., elevated temperatures, impact, friction or electrostatic discharge). Therefore, proper security precautions (safety glasses, face shield, earthed equipment and shoes, leather jacket, Kevlar gloves, Kevlar sleeves and ear plugs) have to be worn while synthesizing and handling the described compounds. Especially the very sensitive compounds **5**, **7**, **8**, and **10** must be handled with great care!*

Procedure for the preparation of 1-azidoethyl-5*H*-tetrazole (1):
The nitrogen-rich compound **1** was synthesized following a modified literature procedure.[18] 2-Chloroethylamine hydrochloride (11.6 g, 100 mmol) and sodium azide (13.0 g, 200 mmol) were dissolved in water (200 mL) and the mixture was then heated to 80 °C for 14 h. The solvent was removed under reduced pressure, yielding the crude product of 1-azidoethylamine hydrochloride as a white solid in quantitative yield. The crude was suspended in triethyl orthoformate (26 mL, 210 mmol) and sodium azide (9.40 g, 144 mmol) and glacial acetic acid (50 mL) was added dropwise. The resulting mixture was heated to 90 °C for 3 h, cooled down and filtrated. After the evaporation of the solvent, the residue was dissolved in water (200 mL) and extracted with ethyl acetate (3x, 300 mL). The combined organic layers were dried using magnesium sulfate and the solvent was removed under reduced pressure. The reddish crude product was subjected to column chromatography (silica, ethyl acetate, R_f = 0.69) yielding 1-azidoethyl-5*H*-tetrazole (4.63 g, 33.3 mmol, 33% over two steps) as a yellow liquid.

DTA (5 °C min^{-1}) onset: 193 °C (exothermic); IR (ATR, cm^{-1}): $\tilde{\nu}$ = 3135 (w), 2099 (vs), 1730 (w), 1670 (w), 1484 (m), 1439 (m), 1352 (m), 1288 (s), 1257 (m), 1228 (m), 1171 (s), 1103 (s), 1022 (w), 1002 (w), 965 (m), 873 (m), 829 (w), 746 (vw), 722 (w), 677 (m), 656 (m), 554 (w), 486 (m); ^{1}H NMR (DMSO-d_6, 25 °C, ppm) δ: 9.45 (s, 1H, C*H*), 4.67 (t, $^3J_{H-H}$ = 7.3 Hz, 2H, CH_2), 3.88 (t, $^3J_{H-H}$ = 7.3 Hz, 2H, CH_2); ^{13}C NMR (DMSO-d_6, 25 °C, ppm) δ: 144.3 (-*C*N$_4$), 49.5 (-*C*H$_2$), 47.1 (-CH_2); ^{15}N NMR (MeCN-d_3, 25 °C, ppm) δ: 11.4 (N3, d, $^2J_{N-H}$ = 3.0), −13.9 (N2), −52.2 (N4, d, $^2J_{N-H}$ = 12.1 Hz), −135.2 (N6, t, $^2J_{N-H}$ = 3.3 Hz), −147.4 (N1, d, $^2J_{N-H}$ = 7.3 Hz), −171.1 (N7); EA ($C_3H_5N_7$, 139.12) calcd.: C 25.90, H 3.62, N 70.48%; found: C 26.27, H 3.58, N 70.03%; BAM drop hammer: 9 J; friction tester: > 360 N.

Procedure for the preparation of 1-ethyl-5*H*-tetrazole (2):

Selective 1-ethyl-5*H*-tetrazole synthesis:
The synthesis of **2** was carried out according to a modified literature procedure.[18] An aqueous solution of ethylamine in water (70%, 5.40 g, 120 mmol) was added to triethyl orthoformate (26.5 g, 179 mmol) and subsequently further reacted with sodium azide (9.30 g, 143 mmol). Glacial acetic acid (100 mL) was added and the reaction mixture was heated to 90 °C for 12 h, cooled down and filtrated. After evaporation of the solvent, the residue was dissolved in water (200 mL) and extracted with ethyl acetate (3x, 300 mL). The combined organic layers were dried using magnesium sulfate. After removing the solvent under reduced pressure, 1-ethyl-5*H*-tetrazole (8.05 g, 90.3 mmol, 75%) was yielded as a slightly brown liquid.

Substitution of ethyl bromide:
The nitrogen-rich ligand (**2**) was obtained, following a literature procedure for the synthesis of 1-substituted tetrazole derivatives using an alkyl halide.[19] 1*H*-Tetrazole (5.00 g, 71.4 mmol) was dissolved in acetone (50.0 mL) and ethyl bromide (5.33 mL, 71.4 mmol) as well as triethylamine (9.89 mL, 71.4 mmol) were added. The solution was heated to reflux for 2 h. The formed solid was separated and washed using acetone (10 mL). A concentrated solution of sodium hydroxide (5 mL) in water was added to the combined organic layers and filtrated off. After the separation of the layers and subsequent drying using magnesium sulfate, the solvent was removed under reduced pressure. Fractional distillation (1.5 mbar, 95 °C) of the remaining oil yielded 1-ethyl-5*H*-tetrazole 1.84 g (18.8 mmol, 26%) as well as 2-ethyl-5*H*-tetrazole (the yield of the second isomer was not determined) as colorless liquids.

DTA (5 °C min^{-1}) onset: 208 °C (exothermic); IR (ATR, cm^{-1}): $\tilde{\nu}$ = 3132 (w), 2988 (w), 2947 (w), 2886 (vw), 2221 (vw), 2046 (w), 1648 (vw), 1573 (vw), 1488 (m), 1445 (m), 1427 (m), 1385 (w), 1354 (m), 1306 (vw), 1257 (w), 1200 (w), 1169 (vs), 1110 (s), 1076 (w), 1024 (w), 970 (m), 874 (m), 798 (w), 757 (vw), 723 (vw), 677 (m), 647 (s); ^{1}H NMR (DMSO-d_6, 25 °C, ppm) δ: 9.39 (s, 1H, C*H*), 4.47 (q, $^{3}J_{H\text{-}H}$ = 5.6 Hz, 2H, CH_2), 1.46 (t, $^{3}J_{H\text{-}H}$ = 5.6 Hz, 3H, CH_3); ^{13}C NMR (DMSO-d_6, 25 °C, ppm) δ: 143.9 (-CN_4), 43.3 (CH_2), 15.2 (CH_2); ^{15}N NMR (MeCN-d_3, 25 °C, ppm) δ: 10.4 (N3), −14.1 (N2), −52.8 (N4, d, $^{2}J_{N\text{-}H}$ = 12.2 Hz), −139.5 (N1); EA: ($C_3H_6N_6$, 98.11) calcd.: C 36.73, H 6.16, N 57.11%; found: C 36.56, H 5.89, N 57.15%; BAM drop hammer: > 40 J; friction tester: > 360 N.

[Cu(NO$_3$)$_2$(H$_2$O)(AET)$_2$] (3)
A solution of 1-azidoethyl-5*H*-tetrazole (**1**, 209 mg, 1.5 mmol) in ethanol (2 mL) was added to an ethanolic solution (3 mL) of copper(II) nitrate trihydrate (181 mg, 0.75 mmol). After the addition, for complete dissolution the resulting suspension was heated to 60 °C for 5 min and left for crystallization at

ambient temperatures. After four days blue blocks, suitable for X-ray diffraction were obtained. Yield: 282 mg (0.58 mmol, 78%).

DTA (5 °C min^{-1}) onset: 94 °C (endothermic), 121 °C (endothermic), 152 °C (exothermic); IR (ATR, cm^{-1}): $\tilde{\nu}$ = 3518 (w), 3440 (w), 3151 (w), 2143 (m), 2115 (m), 2098 (s), 2050 (w), 1611 (w), 1513 (m), 1496 (m), 1468 (s), 1452 (s), 1439 (s), 1354 (m), 1302 (s), 1283 (vs), 1226 (m), 1188 (m), 1167 (m), 1104 (s), 1067 (w), 1014 (s), 960 (w), 916 (vw), 889 (m), 831 (m), 809 (m), 748 (w), 713 (vw), 673 (s); UV-Vis spectrum: λ_{max} = 654 nm; EA ($C_6H_{12}CuN_{16}O_7$, 483.81) calcd.: C 14.90, H 2.50, N 46.32%; found: C 15.11, H 2.20, N 46.50%; BAM drop hammer: 10 J; friction tester: 108 N; ESD: 840 mJ (at grain size 100–500 µm)

$[Cu(NO_3)_2(AET)_2]$ (4)
The ligand (**1**, 209 mg, 1.5 mmol) was dissolved in ethanol (2 mL) and added to an ethanolic solution (3 mL) of copper(II) nitrate trihydrate (181 mg, 0.75 mmol). After the addition, crystallization was observed resulting in blue blocks, suitable for X-ray diffraction, consisting of the coordination compounds **3** and **4**.

General procedure for the preparation of metal(I) and metal(II) (AET) perchlorate complexes (5–8):
The nitrogen-rich ligand **1** (**5**, **6**, **8**, 209 mg, 1.50 mmol; **7**, 139 mg, 1.0 mmol) dissolved in ethanol (2 ml) was added to an ethanolic solution (3 mL) of the corresponding metal(I) (**7**: $AgClO_4$ (225 mg, 1.0 mmol)) or metal(II) perchlorate salt (**5**: $Fe(ClO_4)_2 \cdot 6\ H_2O$ (63.7 mg, 0.25 mmol), **6**: $Zn(ClO_4)_2 \cdot 6\ H_2O$ (93.1 mg, 0.25 mmol), **8**: $Cu(ClO_4)_2 \cdot 6\ H_2O$ (92.6 mg, 0.25 mmol)). The reaction mixtures were mechanically stirred for one minute at ambient temperature and left for crystallization. In case of complex compound **5**, a white precipitate was formed after the full addition of the ligand, which was dissolved by adding water and heating to 60 °C.

$[Fe(AET)_6](ClO_4)_2$ (5)
After four days, slightly yellow crystals of the iron(II) complex **5** were isolated. Yield: 278 mg (0.26 mmol, 51%).

DTA (5 °C min^{-1}) onset: 151 °C (exothermic); IR (ATR, cm^{-1}): $\tilde{\nu}$ = 3139 (w), 2100 (s), 1508 (m), 1445 (m), 1369 (w), 1353 (w), 1296 (m), 1229 (w), 1183 (m), 1105 (s), 1082 (vs), 1022 (w), 1004 (m), 992 (m), 937 (w), 895 (w), 834 (w), 721 (vw), 675 (m), 652 (m), 623 (s), 551 (w); UV-Vis spectrum: λ_{max} = 786 nm; EA ($C_{18}H_{30}Cl_2FeN_{42}O_8$, 1089.47) calcd.: C 19.84, H 2.78, N 54.00%; found: C 19.96, H 2.62, N 53.77%; BAM drop hammer: 3 J; friction tester: 3.75 N; ESD: 65 mJ; ball drop impact tester: < 4 mJ (at grain size 100–500 µm).

[Zn(AET)$_6$](ClO$_4$)$_2$ (6)
Directly after the addition of the ligand **1**, the zinc perchlorate complex (**6**) was isolated in the form of colorless plates. Yield: 282 mg (0.26 mmol, 51%).

DTA (5 °C min^{-1}) onset: 159 °C (endothermic), 196 °C (exothermic); IR (ATR, cm^{-1}): $\tilde{\nu}$ = 3140 (w), 2100 (s), 1508 (m), 1444 (m), 1369 (w), 1353 (w), 1296 (m), 1229 (w), 1184 (m), 1169 (w), 1106 (s), 1082 (vs), 1005 (m), 996 (m), 937 (w), 896 (w), 834 (w), 722 (vw), 675 (m), 652 (m), 623 (s), 551 (w), 493 (m), 481 (w); EA ($C_{18}H_{30}Cl_2N_{42}O_8Zn$, 1099.01) calcd.: C 19.67, H 2.75, N 53.53%; found: C 19.90, H 2.59, N 53.55%; BAM drop hammer: 15 J; friction tester: 40 N; ESD: 368 mJ; ball drop impact tester: 20 mJ (at grain size < 100 µm).

[Ag(AET)]ClO$_4$ (7)
Colorless needles suitable for X-ray diffraction were formed within a few hours. Yield: 300 mg (0.87 mmol, 87%).

DTA (5 °C min^{-1}) onset: 165 °C (exothermic); IR (ATR, cm^{-1}): $\tilde{\nu}$ = 3128 (m), 2136 (m), 2101 (m), 1494 (w), 1442 (m), 1425 (w), 1377 (w), 1356 (m), 1267 (m), 1242 (m), 1232 (w), 1188 (m), 1173 (w), 1128 (m), 1112 (m), 1071 (vs), 1059 (vs), 1048 (vs), 1012 (s), 998 (s), 944 (m), 931 (m), 901 (m), 840 (m), 680 (m), 649 (m), 619 (vs), 552 (m); EA ($C_3H_5AgClN_7O_4$, 346.44) calcd.: C 10.40, H 1.45, N 28.30%; found: C 10.61, H 1.41, N 28.01%; BAM drop hammer: < 1 J; friction tester: 0.6 N; ESD: 65 mJ; ball drop impact tester: < 4 mJ (at grain size < 100 µm).

[Cu(AET)$_6$](ClO$_4$)$_2$ (8)
After the addition of the ligand **1**, the coordination compound **8** was isolated after three days in the form of blue plates. Yield: 150 mg (0.14 mmol, 56%).

DTA (5 °C min^{-1}) onset: 134 °C (endothermic), 158 °C (exothermic); IR (ATR, cm^{-1}): $\tilde{\nu}$ = 3141 (w), 2100 (s), 1509 (m), 1445 (m), 1369 (w), 1353 (w), 1297 (m), 1229 (w), 1184 (m), 1105 (s), 1082 (vs), 1007 (m), 983 (m), 938 (w), 895 (w), 834 (w), 721 (vw), 675 (m), 652 (m), 623 (s), 551 (w), 493 (m); UV-Vis spectrum: λ_{max} = 682 nm; EA ($C_{18}H_{30}Cl_2CuN_{42}O_8$, 1097.17) calcd.: C 19.71, H 2.76, N 53.62%; found: C 19.72, H 2.62, N 53.36%; BAM drop hammer: < 1 J; friction tester: 15 N; ESD: 368 mJ; ball drop impact tester: 12 mJ (at grain size 100–500 µm).

[Cu(1-ETZ)$_6$](ClO$_4$)$_2$ (9)
To an ethanolic solution (1 mL) of the nitrogen-rich compound **2** (294 mg, 3.00 mmol), a solution of copper(II) perchlorate hexahydrate was added dropwise (185 mg, 0.50 mmol). After five minutes, coordination compound **9** was isolated in the form of blue plates. Yield: 162 mg (0.19 mmol, 38%).

DTA (5 °C min^{-1}) onset: 172 °C (endothermic), 210 °C (exothermic); IR (ATR, cm^{-1}): $\tilde{\nu}$ = 3142 (m), 2992 (w), 2949 (w), 2884 (vw), 2105 (vw), 2006 (w), 1786 (w), 1616 (w), 1513 (m), 1441 (m), 1386 (w), 1357 (w), 1312 (w), 1291 (w), 1276 (w), 1206 (w), 1180 (m), 1116 (s), 1077 (vs), 1022 (m), 1006 (m), 986 (m), 936 (w), 892 (w), 797 (w), 722 (w), 678 (m), 648 (m), 623 (s), 423 (vw); UV-Vis spectrum: λ_{max} = 685 nm; EA ($C_{18}H_{36}Cl_2CuN_{24}O_8$, 851.09) calcd.: C 25.40, H 4.26, N 39.50%; found: C 39.22, H 4.06, N 39.22%; BAM drop hammer: 10 J; friction tester: 120 N; ESD 960 mJ (at grain size > 1000 µm).

General procedure for the preparation of metal(II) chlorate complexes (10, and 11):
Copper(II) chlorate was obtained by combining solutions of barium(II) chlorate monohydrate (304 mg, 1.00 mmol) and copper(II) sulfate pentahydrate (250 mg, 1.00 mmol). After mechanically stirring for 5 min and cooling in an ice bath for another 5 min, the precipitated barium(II) sulfate was filtrated off using a syringe filter. The filtrate was evaporated under reduced pressure, the remaining solid was dissolved in 2 mL of the desired solvent (**10**: ethanol, **11**: methanol) and the ligand dissolved in 2 mL of alcoholic solvent was added in stoichiometric amounts.

$[Cu(AET)_6](ClO_3)_2$ (10)
Single crystals of **10** were obtained within a day in form of blue blocks. Yield: 504 mg (0.46 mmol, 46%).

DTA (5 °C min^{-1}) onset: 77 °C (endothermic), 146 °C (exothermic); IR (ATR, cm^{-1}): $\tilde{\nu}$ = 3107 (m), 3019 (vw), 2979 (w), 2936 (vw), 2866 (vw), 2515 (vw), 2285 (vw), 2220 (w), 2099 (s), 1900 (vw), 1818 (vw), 1505 (m), 1442 (m), 1429 (w), 1378 (w), 1349 (m), 1286 (s), 1271 (s), 1229 (m), 1179 (s), 1105 (s), 1008 (m), 965 (vs), 934 (vs), 913 (s), 884 (m), 833 (m), 745 (w), 722 (w), 694 (w), 681 (s), 645 (s), 630 (m), 603 (m), 555 (w), 478 (s), 427 (vw); UV-Vis spectrum: λ_{max} = 698 nm; EA ($C_{18}H_{30}Cl_2CuN_{42}O_6$, 1065.17) calcd.: C 20.30, H 2.84, N 55.23%; found: C 20.08, H 2.81, N 54.41%; BAM drop hammer: 2.5 J; friction tester: 4 N; ESD 226 mJ; ball drop impact tester: 29 mJ (at grain size 500–1000 µm).

$[Cu(1\text{-}ETZ)_6](ClO_3)_2$ (11)
Crystals suitable for X-ray diffraction of **11** were obtained after 24 h as blue blocks. Yield: 350 mg (0.70 mmol, 70%).

DTA (5 °C min^{-1}) onset: 111 °C (endothermic), 158 °C (exothermic); IR (ATR, cm^{-1}): $\tilde{\nu}$ = 3107 (w), 2990 (w), 2947 (vw), 2881 (vw), 1813 (vw), 1572 (vw), 1509 (m), 1442 (m), 1385 (w), 1360 (w), 1313 (vw), 1291 (w), 1274 (vw), 1207 (w), 1178 (s), 1115 (m), 1096 (m), 1083 (w), 1008 (m), 974 (vs), 961 (vs), 936 (s), 796 (w), 722 (w), 680 (m), 645 (s), 605 (m); UV-Vis spectrum: λ_{max} = 669 nm; EA ($C_{18}H_{36}Cl_2CuN_{24}O_6$, 819.10) calcd.: C 26.39, H 4.43, N 41.04%; found: C 26.49, H 4.20, N 40.71%; BAM drop hammer: 7 J; friction tester: 60 N; ESD 608 mJ (at grain size > 1000 µm).

General procedure for the preparation of copper(II) picrate (PA), styphnate (TNR) and trinitrophloroglucinate (TNPG) complexes 12–14:

Copper(II) carbonate (124 mg, 1 mmol) and the corresponding 1,3,5-trinitrophenol derivative based acid (**12**: HPA (458 mg, 2 mmol), **13**: H_2TNR (245 mg, 1 mmol), **14**: H_3TNPG (131 mg, 2 mmol)) were mechanically stirred in water (5 mL) at 70 °C. After an almost clear solution was obtained, the reaction mixture was filtrated using a syringe filter and treated with 1-aziodoethyl-5*H*-tetrazole (**1**) in stochiometric amount under stirring and finally left for crystallization. Precipitates formed during the addition of the ligand were dissolved by addition of water.

[Cu(PA)$_2$(AET)$_2$] (12)

The copper(II) picrate complex **12** could be obtained within three days in the form of green plates suitable for X-ray determination. Yield: 632 mg (0.79 mmol, 79%).

DTA (5 °C min^{-1}) onset: 183 °C (exothermic); IR (ATR, cm^{-1}): $\tilde{\nu}$ = 3154 (m), 3083 (m), 3024 (w), 2941 (w), 2590 (vw), 2504 (vw), 2272 (vw), 2228 (vw), 2130 (m), 2120 (m), 2070 (w), 2024 (vw), 2014 (vw), 1870 (vw), 1791 (vw), 1750 (vw), 1634 (m), 1608 (vs), 1574 (vs), 1537 (vs), 1522 (s), 1506 (vs), 1477 (s), 1444 (m), 1419 (m), 1381 (w), 1358 (s), 1335 (vs), 1324 (vs), 1269 (vs), 1243 (s), 1183 (s), 1167 (s), 1157 (s), 1097 (vs), 1084 (s), 1028 (s), 1002 (m), 938 (s), 915 (s), 898 (s), 847 (m), 835 (m), 824 (m), 786 (s), 741 (m), 713 (s), 708 (s), 675 (s), 649 (s), 552 (m); UV-Vis spectrum: λ_{max} = 690 nm; EA ($C_{18}H_{14}CuN_{20}O_{14}$, 797.98) calcd.: C 27.09, H 1.77, N 35.11%; found: C 27.22, H 1.60, N 35.23%; BAM drop hammer: 3 J; friction tester: 252 N; ESD: 226 mJ; ball drop impact tester: > 200 mJ (at grain size > 1000 µm).

[Cu(TNR)(AET)$_2$] (13)

The copper(II) styphnate complex **13** was received within two days in form of green blocks suitable for X-ray diffraction. Yield: 437 mg (0.75 mmol, 75%).

DTA (5 °C min^{-1}) onset: 177 °C (exothermic); IR (ATR, cm^{-1}): $\tilde{\nu}$ = 3142 (w), 3026 (vw), 2946 (vw), 2599 (vw), 2473 (vw), 2401 (vw), 2124 (m), 2095 (m), 1585 (s), 1543 (s), 1540 (s), 1526 (s), 1474 (s), 1436 (s), 1381 (m), 1356 (m), 1290 (vs), 1244 (s), 1173 (s), 1099 (s), 1065 (m), 1018 (m), 1008 (m), 967 (w), 930 (w), 878 (m), 830 (w), 775 (m), 734 (w), 709 (s), 679 (m), 656 (s), 584 (w), 558 (w), 488 (w), 466 (vw), 453 (w), 440 (w), 423 (m); UV-Vis spectrum: λ_{max} = 690 nm; EA ($C_{12}H_{11}CuN_{17}O_{18}$, 584.88) calcd.: C 24.64, H 1.90, N 40.71%; found: C 24.89, H 1.85, N 40.10%; BAM drop hammer: < 1 J; friction tester: 240 N; ESD: 123 mJ; ball drop impact tester: > 200 mJ (at grain size 100–500 µm).

[Cu(H_2TNPG)$_2$(AET)$_4$] (14)

Crystals of compound **14** were isolated in form of green plates suitable for X-Ray diffraction within one day. Yield: 568.3 mg (0.5 mmol, 50%).

DTA (5 °C min^{-1}) onset: 121 °C (exothermic); IR (ATR, cm^{-1}): $\tilde{\nu}$ = 3150 (m), 3015 (vw), 2949 (w), 2885 (vw), 2222 (w), 2110 (s), 2084 (m), 2057 (w), 2035 (w), 1647 (s), 1578 (m), 1573 (m), 1509 (s), 1495 (s), 1451 (m), 1437 (m), 1409 (w), 1334 (vs), 1289 (s), 1263 (m), 1183 (vs), 1158 (vs), 1137 (s), 1096 (vs), 1069 (s), 1009 (s), 970 (m), 955 (w), 915 (s), 896 (m), 879 (m), 834 (s), 815 (s), 785 (s), 762 (s), 731 (s), 714 (s), 692(s), 679 (s), 658 (s); UV-Vis spectrum: λ_{max} = 638 nm; EA ($C_{24}H_{24}CuN_{34}O_{18}$, 1140.22) calcd.: C 25.28, H 2.12, N 41.77%; found: C 25.35, H 2.06, N 41.77%; BAM drop hammer: 1.5 J; friction tester: 84 N; ESD: 608 mJ; ball drop impact tester: > 200 mJ (at grain size 500–1000 µm).

4.6.11. References

[1] *CrysAlisPro*, Oxford Diffraction Ltd., version 171.33.41, **2009**.

[2] A. Altomare, G. Cascarano, C. Giacovazzo, A. Guagliardi, *J. Appl. Crystallogr.* **1993**, *26*, 343–350.

[3] a) A. Altomare, G. Cascarano, C. Giacovazzo, A. Guagliardi, A. G. G. Moliterni, M. C. Burla, G. Polidori, M. Camalli, R. Spagna, *SIR97*, **1997**; b) A. Altomare, M. C. Burla, M. Camalli, G. L. Cascarano, C. Giacovazzo, A. Guagliardi, A. G. G. Moliterni, G. Polidori, R. Spagna, *J. Appl. Crystallogr.* **1999**, *32*, 115–119.

[4] a) G. M. Sheldrick, *SHELXL-97*, University of Göttingen, Germany, **1997**; b) G. M. Sheldrick, *Acta Crystallogr. Sect. A* **2008**, *64*, 112–122.

[5] A. L. Spek, *PLATON*, Utrecht University, The Netherlands, **1999**.

[6] L. J. Farrugia, *J. Appl. Cryst.* **2012**, *45*, 849–854.

[7] Empirical absorption correction using spherical harmonics, implemented in SCALE3 ABSPACK scaling algorithm (CrysAlisPro Oxford Diffraction Ltd., Version 171.33.41, **2009**).

[8] *APEX3*. Bruker AXS Inc., Madison, Wisconsin, USA.

[9] NATO standardization agreement (STANAG) on explosives, impact sensitivity tests, no. 4489, 1st ed., Sept. 17, **1999**.

[10] WIWEB-Standardarbeitsanweisung 4-5.1.02, Ermittlung der Explosionsgefährlichkeit, hier der Schlagempfindlichkeit mit dem Fallhammer, Nov. 8, **2002**.

[11] http://www.ozm.cz, (accessed April 2019).

[12] http://www.bam.de, (accessed April 2019).

[13] Military Standard 1751A (MIL-STD-1751A): safety and performance tests for qualification of explosives (high explosives, propellants and pyrotechnics), method 1016, Dec. 11, **2001**.

[14] UN Model Regulation: Recommendations on the Transport of Dangerous Goods – Manual of Tests and Criteria, section 13.4.2.3.3, **2015**.

[15] NATO standardization agreement (STANAG) on explosive, friction sensitivity tests, no. 4487, 1st ed., Aug. 22, **2002**.

[16] WIWEB-Standardarbeitsanweisung 4-5.1.03, Ermittlung der Explosionsgefährlichkeit oder der Reibeempfindlichkeit mit dem Reibeapparat, Nov. 8, **2002**.

[17] Impact: insensitive > 40 J, less sensitive ≥ 35 J, sensitive ≥ 4 J, very sensitive ≤ 3 J; Friction: insensitive > 360 N, less sensitive = 360 N, sensitive < 360 N and > 80 N, very sensitive ≤ 80 N, extremely sensitive ≤ 10 N. According to the UN Recommendations on the Transport of Dangerous Goods, 5th ed., **2009**.

[18] P. N. Gaponik, V. P. Karavai, Yu. V. Grigor'ev, *Chem. Heterocycl. Compd.* **1985**, *21*, 1255–1258.

[19] P. N. Gaponik, M. M. Degtyarik, A. S. Lyakhov, V. E. Matulis, O. A. Ivashkevich, M. Quesada, J. Reedijk, *Inorg. Chim. Acta* **2005**, *358*, 3949–3957.

5. Comparison of 1-Propyl-5*H*-tetrazole and 1-Azidopropyl-5*H*-tetrazole as Ligands for Laser Ignitable Energetic Materials

Maximilian H. H. Wurzenberger, Simon M. J. Endraß, Marcus Lommel, Thomas M. Klapötke, and Jörg Stierstorfer

Reprinted (adapted) with permission from *ACS Applied Energy Materials* **2020**, *3*, 3798–3806.

DOI: 10.1021/acsaem.0c00229

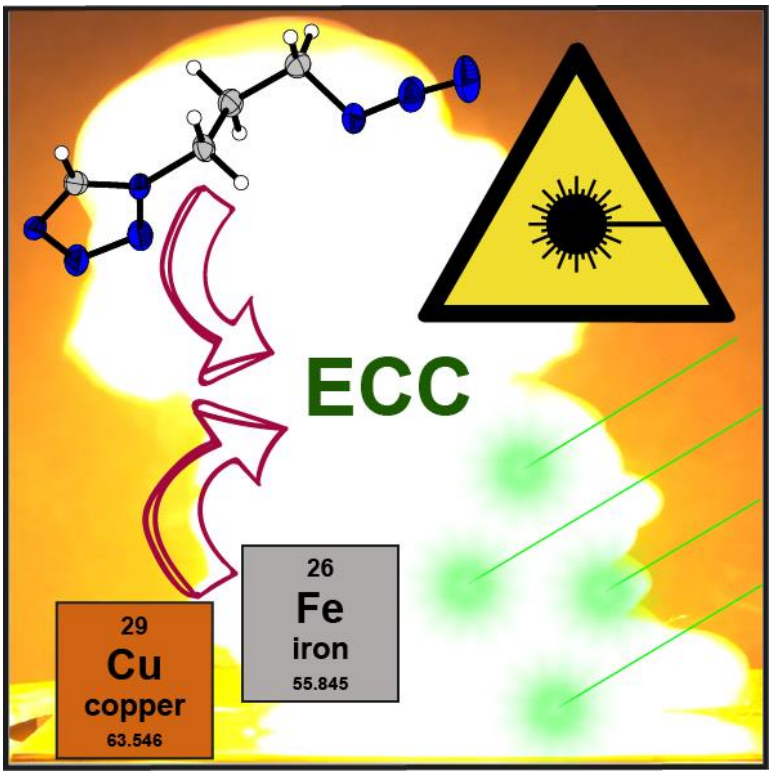

Abstract: Laser ignitable explosives are potential candidates in future applications for replacing toxic and very sensitive primary explosives, which are used in current devices. In this study, the literature unknown ligand 1-azidopropyl-5*H*-tetrazole (APT, **1**) was synthesized for the first time and applied in energetic coordination compounds (ECC). The complexes are based on different 3d transition metals (Mn^{2+}, Fe^{2+}, Cu^{2+}, and Zn^{2+}) as well as various oxidizing anions (NO_3^-, ClO_4^-, and ClO_3^-) and were tested toward their capability as laser ignitable explosives. Furthermore, analogous complexes based on the literature known ligand 1-propyl-5*H*-tetrazole (PT, **2**) were investigated for comparing the influence of the additional azide group toward the performance of the ECC. Toxicity measurements using *Vibrio fischeri* and the decreased sensitivities prove their usability as safer laser ignitable explosive with lower toxicities compared to currently used explosives.

5.1. Introduction

Since Theodore Maiman invented the first practical laser in 1960, they have become nowadays ubiquitous and indispensable in countless areas of daily life. They can be found in simple light pointers, readers of optical storage media, and all the way to laser scalpels.[1] A rather unconventional application are laser ignition systems, which could be used in new combustion engines with higher efficiency or in next-generation rocket engines. The latter one would prevent the utilization of highly toxic hydrazine and dinitrogen tetroxide and allows the usage of "green" nonhypergolic propellants, which are getting initiated when irradiated with a laser diode.[2,3] Lasers are already being used for the initiation or ignition of energetic materials and are attracting increasing attention in this field of research (Figure 1).[4–7]

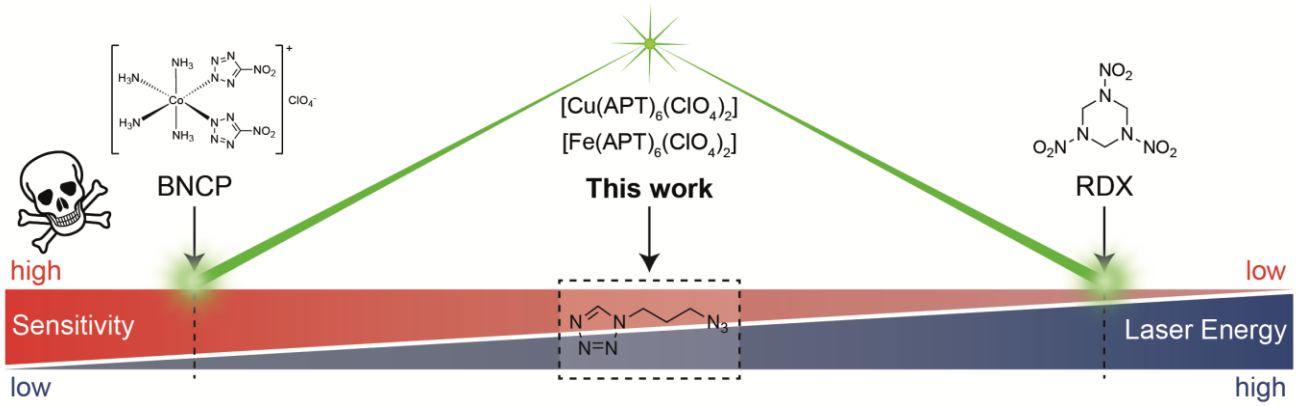

Figure 1. Conflict between sensitivities and ignitability of explosives. Well-balanced laser ignitable compounds (**6** and **7**) from this work can be placed in between.

In general, a lot of research from scientists all around the world is undertaken to improve the disadvantages of conventional initiator systems, such as introducing less toxic materials.[8–11] In contrast to traditional initiation methods (spark, friction, heat, etc.), laser ignition and initiation is probably the most beneficial method of all, since the isolation of the energetic material from electric impulses excludes unintended initiation in most cases. Further advantages over classical initiation methods are the very short function times (<1 ms) and the possible application of less sensitive and lead-free ignition charges, which increase the safety and handling of these compounds significantly. The investigation of energetic transition metal complexes for their initiation abilities started with pentaammine(5-cyano-2*H*-tetrazolate)cobalt(III) perchlorate (CP) and its promising replacement tetraammine-*cis*-bis(5-nitro-2*H*-tetrazolato-N^2)cobalt(III) perchlorate (BNCP).[12,13] Since then, various coordination compounds with varying ligands and metal centers have been synthesized and tested in applications of laser irradiation.[14–16] To overcome the toxicities and the high sensitivities of CP and BNCP, the ligand 1-azidopropyl-5*H*-tetrazole (APT, **1**) has been synthesized and used as nitrogen-rich ligand for laser ignitable ECC with decreased sensitivities.

5.2. Results and Discussion

5.2.1. Synthesis

For the synthesis of the new ligand 1-azidopropyl-5*H*-tetrazole (**1**), a simple two-step synthesis was performed similar to that of 1-azidoethyl-5*H*-tetrazole (Scheme 1).[17]

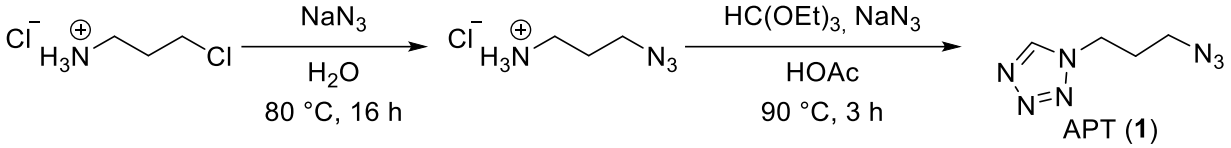

Scheme 1. Synthesis of 1-azidopropyl-5*H*-tetrazole (**1**).

The starting material 3-chloropropylamine hydrochloride is a cheap commercially available molecule, which can be reacted in nearly quantitative yields to the corresponding azide with an excess of NaN_3. A [3+1+1] cyclization of the intermediate together with triethyl orthoformate and sodium azide in acetic acid is leading to the target molecule in a good overall yield of 60% over two steps. APT can also be synthesized in a one-pot reaction, avoiding the isolation and purification of the intermediate. The second heterocyclic ligand, 1-propyl-5*H*-tetrazole (**2**), was synthesized based on a modified literature procedure by the substitution of 1-bromopropane with 1,5*H*-tetrazole.[18] The deprotonation of 1,5*H*-tetrazole with triethylamine and following reaction with the bromoalkane led to the formation of an isomeric mixture of PT and 2-PT in an overall yield of 70% (Scheme 2). Isomeric pure PT was obtained after column chromatography with ethyl acetate (31%).

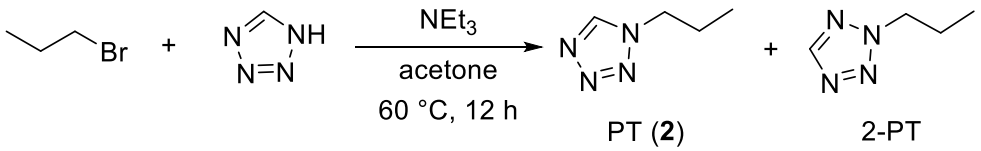

Scheme 2. Synthesis of 1-propyl-5*H*-tetrazole (**2**)

The successful synthesis of **1** and **2** can easily be proven by infrared (IR) (Figure S1) as well as proton and carbon NMR spectroscopy. Also, two-dimensional ^{1}H-^{15}N-HMBC or proton-coupled ^{15}N NMR are particularly suitable (Figures 2 and 3). In the case of APT (**1**), it is important to perform both types of measurements. Normally, ^{1}H-^{15}N-HMBC is much faster and more sensitive compared to normal proton-coupled ^{15}N NMR; on the other hand, the terminal nitrogen of the azide group is almost invisible with this method (Figure 2, bottom). Because of the absence of acidic protons in **1** and **2**, they both can be used as neutral ligands in coordination compounds. By the combination of different oxidizing anions (nitrate, chlorate, and perchlorate) with various 3d transition metal cations (Mn^{2+}, Fe^{2+}, Cu^{2+}, and Zn^{2+}), the characteristics and performances of the resulting ECC can be tuned toward the desired properties.

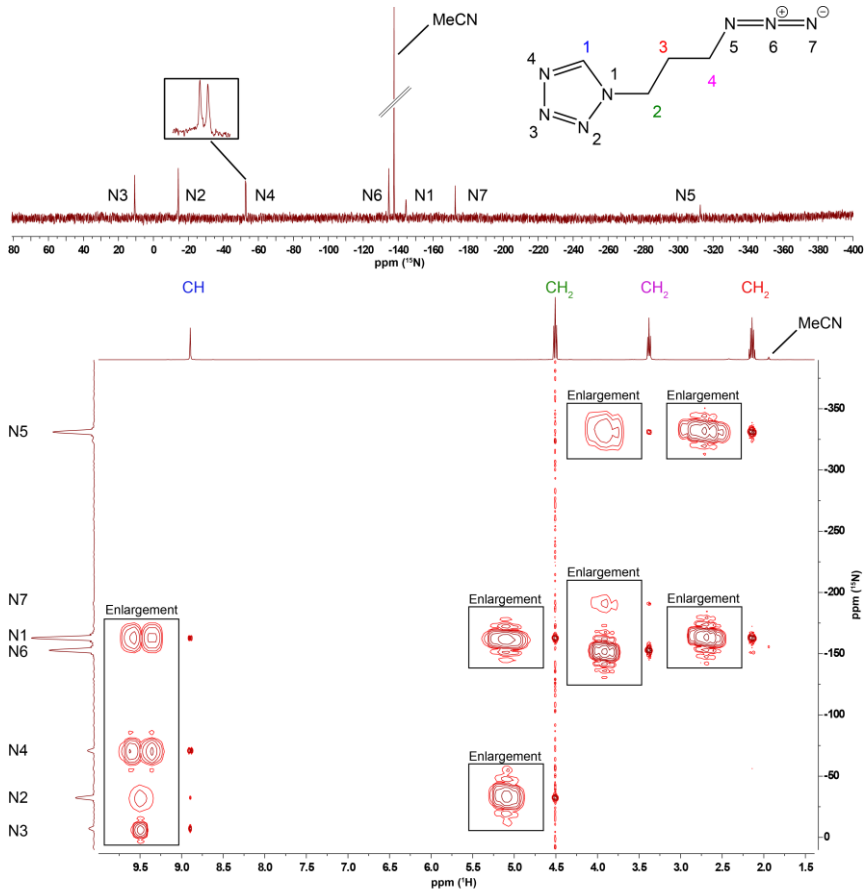

Figure 2. Proton coupled ^{15}N NMR spectra (top) and two dimensional ^{1}H-^{15}N-HMBC NMR spectra (bottom) of **1**. ^{15}N NMR (MeCN-d_3, 25 °C): δ = 10.7 (N3, s), −14.2 (N2, s), −52.8 (N4, d, $J_{N–H}$ = 11.9 Hz), −134.6 (N6, s), −144.4 (N1, s), −172.6 (N7, s), −312.7 ppm (N5, s).

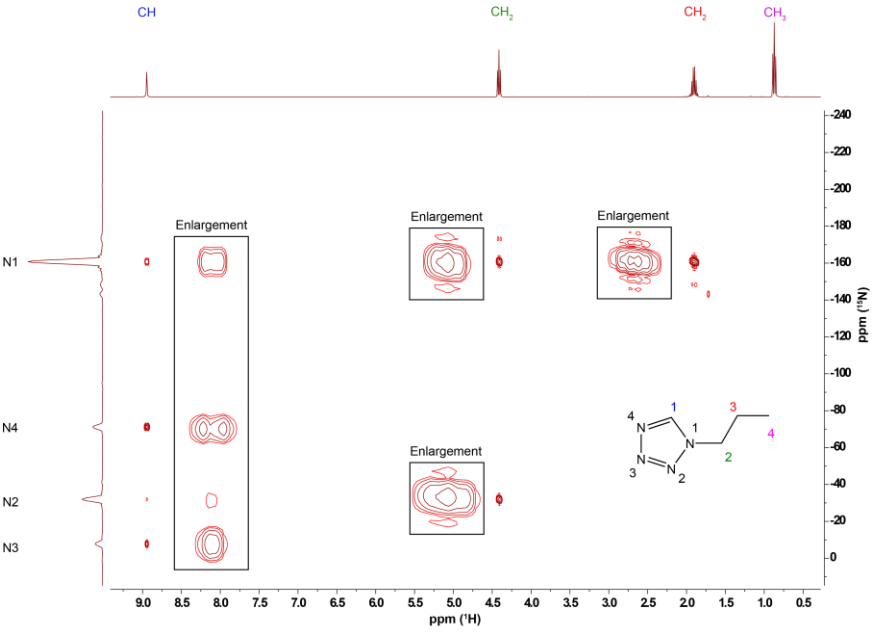

Figure 3. Two dimensional ^{1}H-^{15}N-HMBC NMR spectra of **2**.

For the synthesis of ECC **3**–**12**, ethanolic solutions of **1** or **2** were combined with the respective metal(II) salts, dissolved either in ethanol (**3** and **4**) or acetonitrile (**5**–**12**) (Schemes 3 and 4). The reaction mixtures

were stirred for 10 min at ambient (**10**–**12**) or elevated (**4**–**9**) temperatures and left in air for crystallization. At room temperature, the reaction of copper(II) nitrate with APT produced two different complexes. It was possible to pick crystals of an anhydrous compound ($[Cu(NO_3)_2(APT)_2]$, **3**) and a monohydrate species ($[Cu(NO_3)_2(H_2O)(APT)_2]$, **4**) out of one reaction vessel. The latter one was able to be synthesized specifically when increasing the reaction temperature to 60 °C.

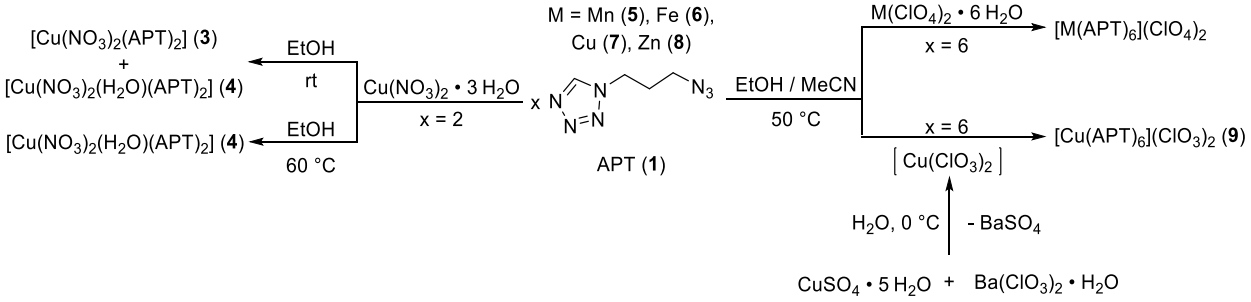

Scheme 3. Synthesis of ECC **3**–**9** based on ligand **1**.

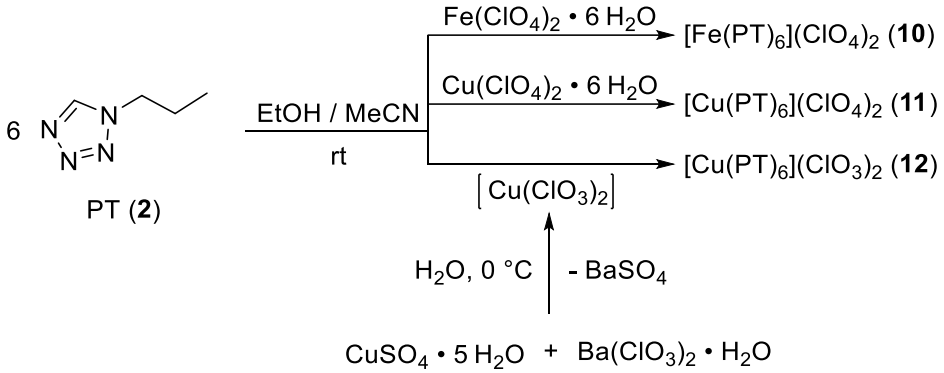

Scheme 4. Synthesis of ECC **10**–**12** based on ligand **2**.

While the metal(II) perchlorate salts for coordination compounds **5**–**8**, **10**, and **11** are commercially available, copper(II) chlorate for the syntheses of **9** and **12** was obtained by a simple metathesis reaction. All complexes were obtained within days up to several weeks (10 weeks for complex **12**) as crystalline materials in very low to very good yields (12–84%).

5.2.2. Crystal Structures

The crystal structures of $[Fe(PT)_6](ClO_4)_2$ (**10**) and $[Cu(PT)_6](ClO_4)_2$ (**11**) are already known in the literature, and therefore no low-temperature single-crystal X-ray diffraction experiments were performed on those.[19,21] All other compounds were measured, but similar to the already mentioned difficulties for determining the structure of **10**, the crystals of the chlorate and perchlorate compounds are highly intergrown, and cutting of them led to the introduction of many defects. Only in the case of manganese(II) perchlorate complex **5** one good single crystal of sufficient size for finalizing the data set was obtained.

In all other cases, except copper(II) nitrate species **3** and **4**, the measurements only allowed an insight into the compositions of the compounds. They all show an octahedral coordination sphere around the central metals consisting of six tetrazole ligands and non-coordinating anions. The structures' compositions were verified by elemental analysis and IR spectra (Figures S1–S3). The measurement and refinement data of complexes **3**–**5** are given in the Supporting Information (Table S1), and the data sets were uploaded to the CSD database (CCDC 1980874 (**3**), 1980875 (**4**), and 1980876 (**5**)). The ligands are exclusively coordinating through their heterocyclic N4 nitrogen atoms in all structures. The side species **3** crystallizes in the triclinic space group *P*−1 with two formula units per unit cell and a calculated density of 1.732 g cm^{-3} at 134 K. The octahedral coordination sphere around the copper atom is built up by two chelating nitrato and two APT ligands (Figure 4).

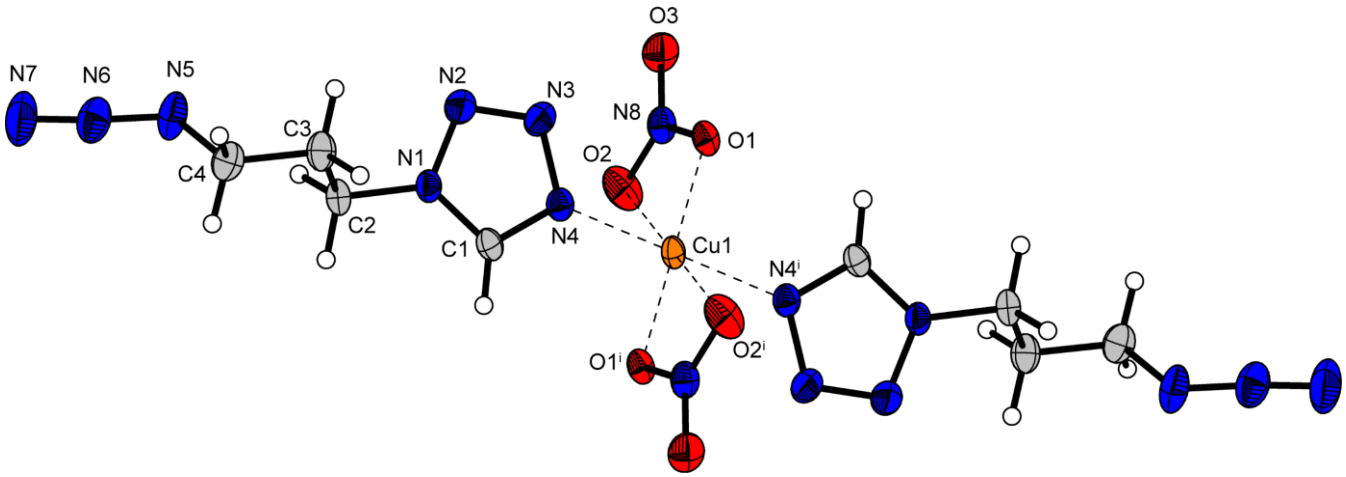

Figure 4. Molecular unit of side species [Cu(NO$_3$)$_2$(APT)$_2$] (**3**). Selected bond lengths (Å): Cu1–O1 1.974(2), Cu1–O2 2.625(3), Cu1–N4 1.988(3); selected bond angles (°): O1–Cu1–O2 53.90(7), O1–Cu1–N4 90.24(10), O1–Cu1–O1^{i} 180.00, O1–Cu1–O2^{i} 126.10(7); symmetry code: 2−x, −y, −z.

Because of the typical Jahn-Teller distortion along the O2–Cu1–O2^{i} axis and the sterical hindrance of the anionic ligands, there is a strong deviation of the perfect octahedron. The monohydrate of **3**, complex **4**, shows a similar density (1.713 g cm^{-3} (134 K)) and crystallizes in the monoclinic space group *I*2/*a* with four formula units per unit cell. The addition of the aqua ligand leads to a simple extension of the coordination sphere from an octahedron to a rather uncommon capped trigonal-prismatic molecular geometry around the copper central metal (Figure 5). Similar to compound **3**, the manganese(II) perchlorate complex **5** crystallizes in the triclinic space group *P*−1 and possesses a relatively low density of 1.534 g cm^{-3} at 131 K with two formula units per unit cell. The complex is built up by six APT ligands around the central metal with similar Mn–N bond lengths (2.239(2)–2.264(2) Å) and two non-coordinating perchlorate anions (Figure 6).

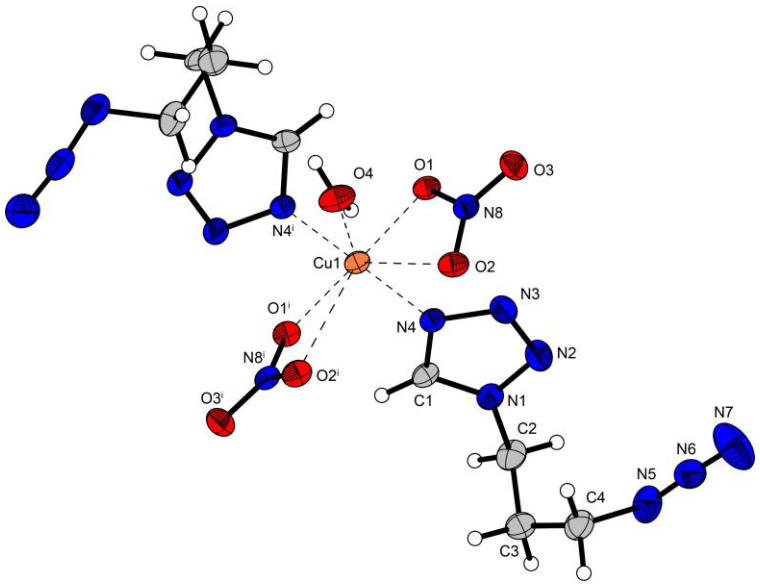

Figure 5. Molecular unit of $[Cu(NO_3)_2(H_2O)(APT)_2]$ (**4**). Selected bond lengths (Å): Cu1–O1 1.9830(12), Cu1–O2 2.7675(12), Cu1–O4 2.348(2), Cu1–N4 1.9865(14); selected bond angles (°): O1–Cu1–O2 51.42(4), O1–Cu1–O4 88.56(3), O1–Cu1–N4 91.81(5), O1–Cu1–$O1^i$ 177.12(5), O1–Cu1–$O2^i$ 131.41(4), O2–Cu1–O4 138.81(3); symmetry code: 0.5−x, y, −z.

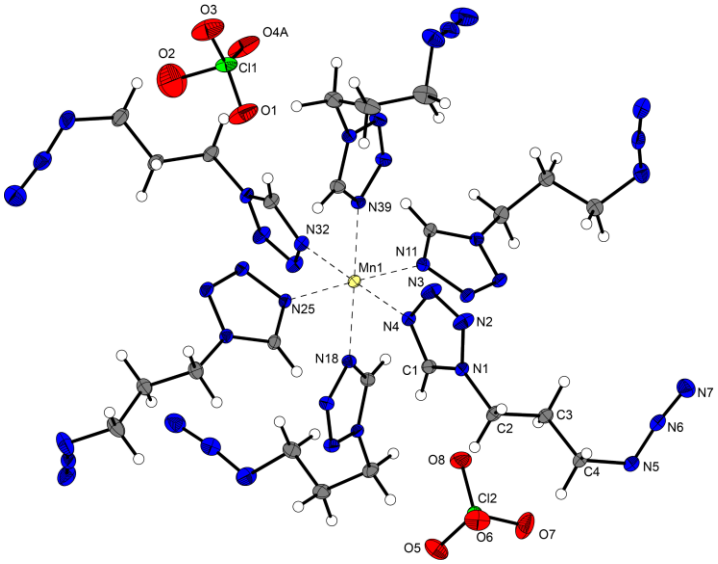

Figure 6. Molecular unit of $[Mn(APT)_6](ClO_4)_2$ (**5**). Selected bond lengths (Å): Mn1–N4 2.249(2), Mn1–N11 2.239(2), Mn–N18 2.264(2), Mn1–N25 2.249(2), Mn1–N32 2.239(2), Mn–N39 2.254(2); selected bond angles (°): N4–Mn1–N11 89.75(8), N4–Mn1–N18 87.61(8), N4–Mn1–N25 90.05(8), N4–Mn1–N32 178.86(9).

5.2.3. Sensitivities and Thermal Stability

All compounds, except side species **3**, were investigated by differential thermal analysis (DTA), and additionally, thermal gravimetric analyses (TGA) were performed to further examine the critical onset temperatures (*e.g.*, melting or dehydration as well as exothermic decomposition) from the DTA experiments (Figures 7 and S4–S8). All values from the DTA experiments are given in Table 1 together

with the compounds' stability against various external stimuli, such as impact, friction, and electrostatic discharge.

Table 1. Thermal stability[a] and sensitivities to external stimuli of compounds **1**, **2**, and **4**–**12** compared to the ones of lead azide and PETN.[21]

	$T_{endo.}$[b] [°C]	$T_{exo.}$[c] [°C]	*IS*[d] [J]	*FS*[e] [N]	*ESD*[f] [mJ]
APT (**1**)	-	195	> 40	> 360	n.d.
PT (**2**)	-	206	> 40	> 360	n.d.
$[Cu(NO_3)_2(H_2O)(APT)_2]$ (**4**)	70	155	> 40	96	422
$[Mn(APT)_6](ClO_4)_2$ (**5**)	122	208	4.5	60	368
$[Fe(APT)_6](ClO_4)_2$ (**6**)	-	146	2.5	28	317
$[Cu(APT)_6](ClO_4)_2$ (**7**)	115	165	2.5	32	368
$[Zn(APT)_6](ClO_4)_2$ (**8**)	-	183	9.0	80	422
$[Cu(APT)_6](ClO_3)_2$ (**9**)	65	151	2.5	24	> 1500
$[Fe(PT)_6](ClO_4)_2$ (**10**)	-	202	25	192	1220
$[Cu(PT)_6](ClO_4)_2$ (**11**)	174	209	30	240	> 1500
$[Cu(PT)_6](ClO_3)_2$ (**12**)	111	152	> 40	168	960
PETN	141–143	180–210	3.0–4.2	60–80	60
$Pb(N_3)_2$	-	320–360	2.5–4.0	0.1–1.0	7.0

[a] DTA onset temperatures at a heating rate of 5 °C min^{-1}. [b] Endothermic peak indicating melting or dehydration. [c] Exothermic peak indicating decomposition. [d] Impact sensitivity according to the BAM drop hammer (method 1 of 6). [e] Friction sensitivity according to the BAM friction tester (method 1 of 6). [f] Electrostatic discharge sensitivity (OZM Electric Spark XSpark10; method 1 of 6).

Comparing the values of the pure nitrogen-rich ligands, it becomes clear that both are insensitive against impact as well as friction (> 40 J; > 360 N) and that the azide substituent has only a slightly destabilizing effect toward heat resistance (**1**: 195 °C; **2**: 206 °C). Because of the liquid state of both molecules, it was not possible to perform ESD measurements. All ECC, except **6**, show exothermic decomposition temperatures above 150 °C whereas complexes **5** and **11** even exceed the ones of their corresponding ligands (208 and 209 °C, respectively). In the row of perchlorate complexes, the temperature stability is increasing in the following order: $Fe^{2+} < Cu^{2+} < Zn^{2+} < Mn^{2+}$, which is in accordance with previous findings.[17] Comparing analogous complexes based on the different ligands APT and PT, the clear trend of higher stability for compounds based on **2** is observable. While the free nitrogen-rich molecules only show a difference of 11 °C, the iron(II) and copper(II) perchlorate composed complexes deviate 56 and 44 °C, respectively. Whereas the metal centers in **6** and **7** seem to catalyze the decomposition of the azide-containing ligand, the relatively low stability of the chlorate complexes **9** and **12** can be attributed to the anion, which is known in the literature.[16] The endothermic event in ECC **4** can be assigned to the loss of the aqua ligand, which is also confirmed by TGA (Figure 7). All other complexes do not show alterations in weight at the endothermic events, revealing the presence of melting points. Especially remarkable is the high temperature difference between melting and decomposition of compounds **5** and **9** with values of 86 °C, making them potential melt castable explosives. The sensitivities of all compounds toward impact (IS) and friction (FS) were determined according to BAM standard methods (1 of 6) together with

the electrostatic discharge sensitivity (ESD). In addition, the compounds have been classified in accordance with the "UN Recommendations on the Transport of Dangerous Goods" by using the determined sensitivities.[22] Whereas nitrate complex **4** is insensitive against impact and sensitive against friction, all other APT-based ECC show increased sensitivities. Except for zinc(II) compound **8** (9.0 J), their impact sensitivity is in the range of lead azide as well as PETN, and therefore they have to be classified as very sensitive (**6**, **7**, **9**) or sensitive (**5**). Compared to the primary explosive $Pb(N_3)_2$, they all possess higher stability against friction close to the values of PETN. Their safer handling is finally proven by their ESD sensitivities, which are all above the ones of lead azide and nitropenta. The absence of the azide function in complexes **10**–**12** is significantly increasing the stability compared to the APT-based analogues, which is leading to their classification as sensitive materials.

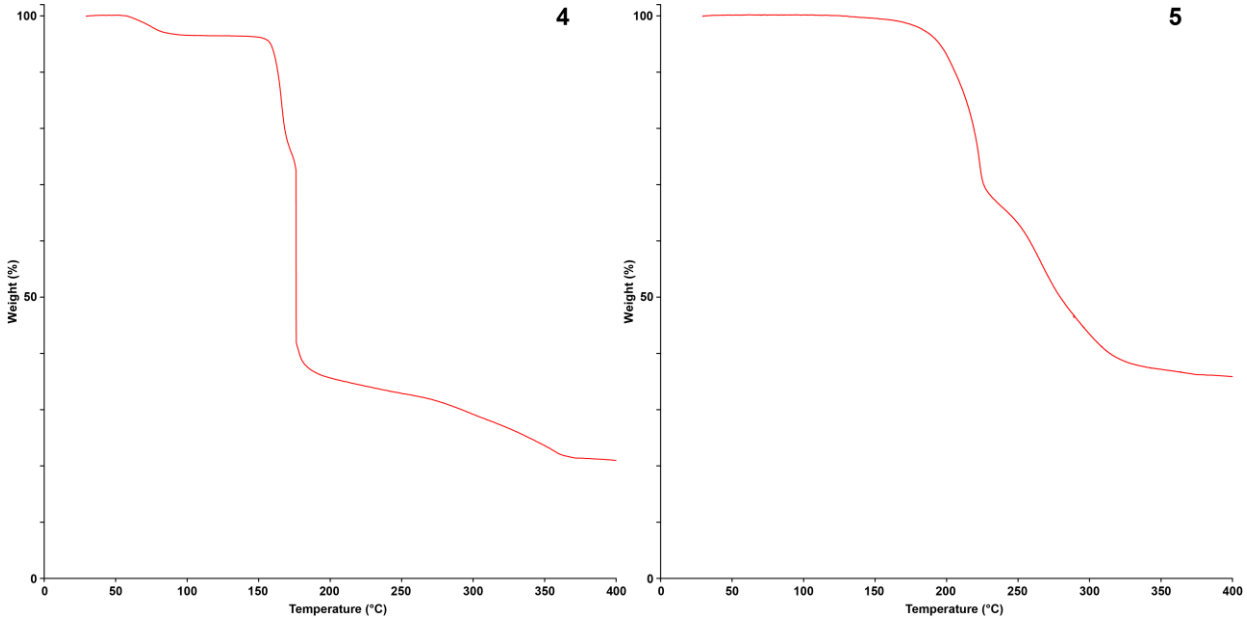

Figure 7. TGA plots of ECC **4** and **5** revealing the loss of the aqua ligand in $[Cu(NO_3)_2(H_2O)(APT)_2]$ (**4**) and the presence of melting point in $[Mn(APT)_6](ClO_4)_2$ (**5**).

5.2.4. Energetic Performance and Laser Initiation

To get an insight into the compounds' energetic performance, hot plate (HP) and hot needle (HN) tests were performed. While the HP test only reveals the behavior of the unconfined samples against fast heating on a copper plate, the ECC are fixed under adhesive tape during HN tests. All PT-based complexes only decomposed in both setups, whereas the azide compounds showed deflagrations with varying intensity depending on the combination of central metal and anion (Figures 8 and S9–S13). The weakest output possesses nitrate compound **4** followed by the (per)chlorate ECC **5**, **8**, and **9**. A very strong deflagration is shown by the iron(II) compound **6**.

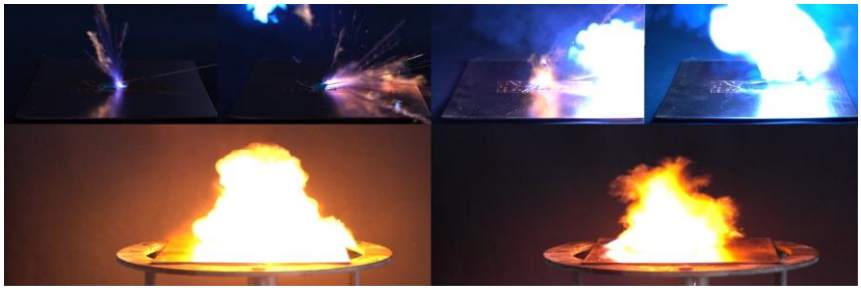

Figure 8. Top: HN test of copper(II) perchlorate complex **7** shown as a sequence. Bottom: deflagration of iron (**6**, left) and copper (**7**, right) compounds during the HP test.

For testing the usability of the ECC as laser ignitable explosives, they were irradiated with a 45 W InGaAs laser diode working in the single-pulsed mode and a wavelength of 915 nm. Approximately 25 mg of all colored compounds (colorless substances **5**, **8**, and **10** cannot be ignited in our setup) was filled in transparent plastic caps, pressed with a pressure force of 1 kN, and sealed with a UV-curing adhesive. The samples were placed in the focal distance (f = 29.9 mm) of an optical lens, which was linked to a collimator. The collimator itself was coupled via a SMA type connector and an optical fiber (core diameter of 400 µm and cladding diameter of 480 µm) to the laser diode. The confined samples were irradiated with a voltage of 4 V and a varying current (7–20 A) as well as pulse length (1–20 ms), which together resulted in an energy output of 2.00–68.0 mJ. All tested compounds showed a reaction to the laser irradiation (Table 2) varying in the strength of the output (Figures 9 and S14–S17). While copper(II) chlorate and perchlorate complexes of APT already show a deflagration at very low energies (2 mJ), iron compound **6** must be irradiated with higher power for the same output. ECC **7** can even be detonated with further increased energy levels. Nitrate compound **4** has in common with perchlorate complexes **11** and **12** that they only decompose under the generation of smoke when initiated with a laser pulse. They even show the same output with energies above 150 mJ. The ECC initiated in the laser experiments were investigated in solid state UV-Vis measurements concerning a possible correlation between the absorption of the complexes at the laser wavelength and their laser ignitability (Figure 10). The optical properties are summarized in Table 3 and clearly show typical d-d transitions of the corresponding 3d transition metal. All measured ECC show moderate absorptions in the range of the operating laser wavelength.

Table 2. Outcome of the laser initiation experiments at different energy levels.[a]

E_{max} [mJ]	2.00	25.5	30.0	51.0	68.0
$[Cu(NO_3)_2(H_2O)(APT)_2]$ (**4**)	-	-	dec.	dec.	dec.
$[Fe(APT)_6](ClO_4)_2$ (**6**)	-	dec.	def.	def.	-
$[Cu(APT)_6](ClO_4)_2$ (**7**)	def.	-	def.	det.	-
$[Cu(APT)_6](ClO_3)_2$ (**9**)	def.	-	def.	-	def.
$[Cu(PT)_6](ClO_4)_2$ (**11**)	-	-	dec.	dec.	dec.
$[Cu(PT)_6](ClO_3)_2$ (**12**)	-	-	dec.	dec.	dec.

[a] -: not tested, dec.: decomposition, def.: deflagration, det.: detonation. Operating parameters: voltage U = 4 V; wavelength λ = 915 nm; current I = 7–20 A; pulse length τ = 1–20 ms; theoretical maximal output power P_{max} = 45 W; theoretical energy E_{max} = 2.00–68.0 mJ.

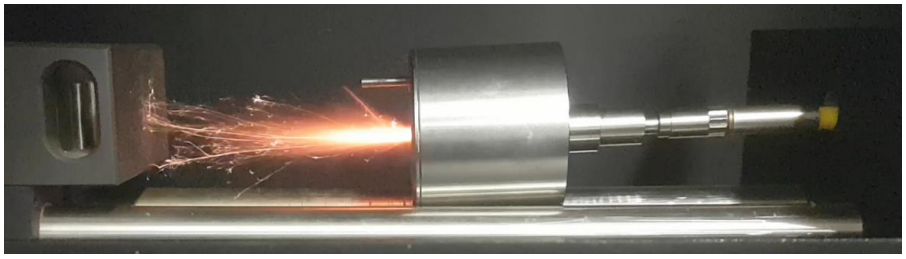

Figure 9. Deflagration of $[Fe(APT)_6](ClO_4)_2$ (**6**) during the laser experiments.

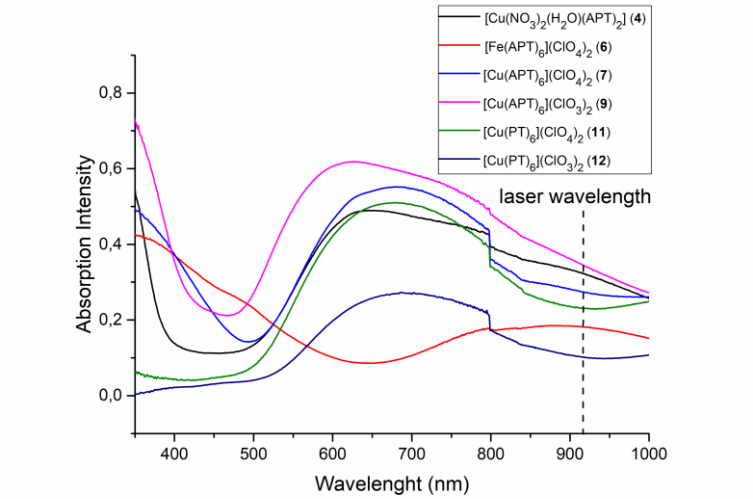

Figure 10. Solid state UV-Vis spectra of ECC tested in the laser ignition experiments. The spectra have only qualitative character, and the step at 800 nm is caused by a detector change.

It is noticeable that there is no observable difference between the complexes which showed a positive outcome in the laser initiation experiments (**6**, **7**, **9**) and those that were tested negative (**4**, **11**, **12**). But in fact, **6**, **7**, and **9** are more sensitive compared to the other compounds. This and the fact that the colorless compounds **5**, **8**, and **10** do not show any reaction in the setup lead to the explanation that the initiation ability by a laser not only depends on the absorption at the relevant wavelength but also on other factors like the metal center surrounding and sensitivities toward mechanical stimuli. In accordance with previous results, the formation of several hot spots by photothermal excitation when irradiated is assumed and a certain energetic character is necessary for the deflagration or detonation of the ECC.[23,24]

5.2.1. Toxicity

The toxicities of the uncoordinated free ligand 1-azidopropyl-5*H*-tetrazole (**1**) and iron(II) perchlorate complex **6** were investigated by using the common luminescence bacteria inhibition test in aqueous media.[25] Details of the measurements are given in the Supporting Information. With values of 0.28 g L^{-1} for the free tetrazole **1** and 0.84 g L^{-1} for the iron(II) perchlorate complex **6**, both compounds have to be considered as toxic. The toxicity of APT (**1**) is comparable to the ones of commonly used secondary explosive RDX (EC_{50} (30 min) = 0.24 g L^{-1}),[26] whereas ECC **6** is 3 times less toxic.

5.3. Conclusion

For the first time in the literature, it was possible to synthesize the nitrogen-rich molecule 1-azidopropyl-5*H*-tetrazole (**1**, APT). It was successfully applied as ligand in energetic coordination compounds. The synthesis can be performed in a straightforward, green as well as cost-effective approach and furthermore avoids the isolation of intermediate species. ^{1}H-^{15}N-HMBC NMR proved to be very useful for assigning all tetrazole nitrogens. For the comparison with **1**, the literature-known ligand 1-propyl-5*H*-tetrazole (**2**, PT) and three complexes consisting of it were synthesized and compared to the APT analogues. All investigated ECC are based on less or nontoxic 3d transition metals (Mn, Fe, Cu, and Zn) and oxidizing anions like nitrate, chlorate, or perchlorate. All synthesized complexes, except side product **3**, were comprehensively characterized, and especially their energetic character was investigated in detail. Compared to commonly used primary explosives such as lead azide, they possess higher stability against friction, which allows safer handling of those compounds. With the ignitability of the complexes **6** and **7** based on iron(II) and copper(II) perchlorate in single-pulsed laser experiments making them to possible candidates for future laser explosive applications, avoiding the use of lead-containing and very dangerous primary explosives.

5.4. Acknowledgements

We gratefully acknowledge the financial support of this work by the Ludwig-Maximilians-University (LMU), the Office of Naval Research (ONR) under Grant ONR N00014-19-1-2078, and the Strategic Environmental Research and Development Program (SERDP) under Contract W912HQ19C0033. The authors also thank Prof. Dr. Konstantin Karaghiosoff for the measurement of the ^{15}N NMR spectra, Mrs. Cornelia Unger for toxicity assessments, Mrs. Antonia Stadler for proofreading, and Mrs. Marina Schönherr for her great contribution to this work.

5.5. References

[1] T. H. Maiman, *Nature* **1960**, *187*, 493–494.

[2] C. Manfletti, *J. Propul. Power* **2014**, *30*, 952–961.

[3] M. Weinrotter, H. Kopecek, E. Wintner, *Laser Phys.* **2005**, *15*, 947–953.

[4] A. Y. Zhilin, M. A. Ilyushin, I. V. Tselinskii, A. S. Brykov, *Russ. J. Appl. Chem.* **2001**, *74*, 99–102.

[5] T. W. Myers, J. A. Bjorgaard, K. E. Brown, D. E. Chavez, S. K. Hanson, R. J. Scharff, S. Tretiak, J. M. Veauthier, *J. Am. Chem. Soc.* **2016**, *138*, 4685–4692.

[6] H. Zhang, L. Wu, P. Hu, W. Guo, W. Zhang, Y. Ye, R. Shen, *Opt. Laser Technol.* **2019**, *120*, 105709.

[7] T. Wang, Q. Zhang, H. Deng, L. Shang, D. Chen, Y. Li, S. Zhu, H. Li, *ACS Appl. Mater. Interfaces* **2019**, *11*, 41523–41530.

[8] J. Zhang, J. Zhang, G. H. Imler, D. A. Parrish, J. M. Shreeve, *ACS Appl. Energy Mater.* **2019**, *2*, 7628–7634.

[9] R. V. Kent, T. P. Vaid, J. A. Boissonnault, A. J. Matzger, *Dalton Trans.* **2019**, *48*, 7509–7513.

[10] A. F. Baxter, I. Martin, K. O. Christe, R. Haiges, *J. Am. Chem. Soc.* **2018**, *140*, 15089–15098.

[11] Y. Tang, C. He, G. H. Imler, D. A. Parrish, J. M. Shreeve, *ACS Appl. Energy Mater.* **2019**, *2*, 2263–2267.

[12] S. C. Kunz, F. J. Salas, Diode laser ignition of high explosives and pyrotechnics. *Proceedings of the 13th International Pyrotechnics Seminar* **1988**, 505–523.

[13] J. A. Merson, F. J. Salas, J. G. Harlan, The development of a laser ignited deflagration-to-detonation (DDT) detonators and pyrotechnic actuators. *Proceedings of the 19th International Pyrotechnics Seminar* **1994**, 191–206.

[14] T. W. Myers, K. E. Brown, D. E. Chavez, R. J. Scharff, J. M. Veauthier, *Eur. J. Inorg. Chem.* **2016**, *2016*, 3178–3183.

[15] A. V. Smirnov, M. A. Ilyushin, I. V. Tselinskii, *Russ. J. Appl. Chem.* **2004**, *77*, 794–796.

[16] M. H. H. Wurzenberger, N. Szimhardt, J. Stierstorfer, *J. Am. Chem. Soc.* **2018**, *140*, 3206–3209.

[17] M. H. H. Wurzenberger, M. S. Gruhne, M. Lommel, N. Szimhardt, T. M. Klapötke, J. Stierstorfer, *Chem. – Asian J.* **2019**, *14*, 2018–2028.

[18] P. N. Gaponik, M. M. Degtyarik, A. S. Lyakhov, V. E. Matulis, O. A. Ivashkevich, M. Quesada, J. Reedijk, *Inorg. Chim. Acta* **2005**, *358*, 3949–3957.

[19] L. Wiehl, *Acta Crystallogr. Sect. B* **1993**, *49*, 289–303.

[20] A. M. Mills, A. L. Spek, A. F. Stassen, J. G. Haasnoot, J. Reedijk, Private Communication CCDC 637921, **2007**.

[21] T. M. Klapötke, *Energetic Materials Encyclopedia*, 1st ed., De Gruyter, Berlin, **2018**.

[22] Impact: insensitive > 40 J, less sensitive ≥ 35 J, sensitive ≥ 4 J, very sensitive ≤ 3 J; Friction: insensitive > 360 N, less sensitive = 360 N, sensitive < 360 N and > 80 N, very sensitive ≤ 80 N, extremely sensitive ≤ 10 N. According to the UN Recommendations on the Transport of Dangerous Goods, 5th ed., **2009**.

[23] M. H. H. Wurzenberger, B. R. G. Bissinger, M. Lommel, M. S. Gruhne, N. Szimhardt, J. Stierstorfer, *New J. Chem.* **2019**, *43*, 18193–18202.

[24] N. Szimhardt, M. H. H. Wurzenberger, T. M. Klapötke, J. T. Lechner, H. Reichherzer, C. C. Unger, J. Stierstorfer, *J. Mater. Chem. A* **2018**, *6*, 6565–6577.

[25] G. I. Sunahara, S. Dodard, M. Sarrazin, L. Paquet, G. Ampleman, S. Thiboutot, J. Hawari, A. Y. Renoux, *Ecotoxicol. Environ. Saf.* **1998**, *39*, 185–194.

[26] D. Fischer, T. M. Klapötke, M. Reymann, J. Stierstorfer, *Chem. – Eur. J.* **2014**, *20*, 6401–6411.

5.6. Supporting Information

5.6.1. Compounds Overview

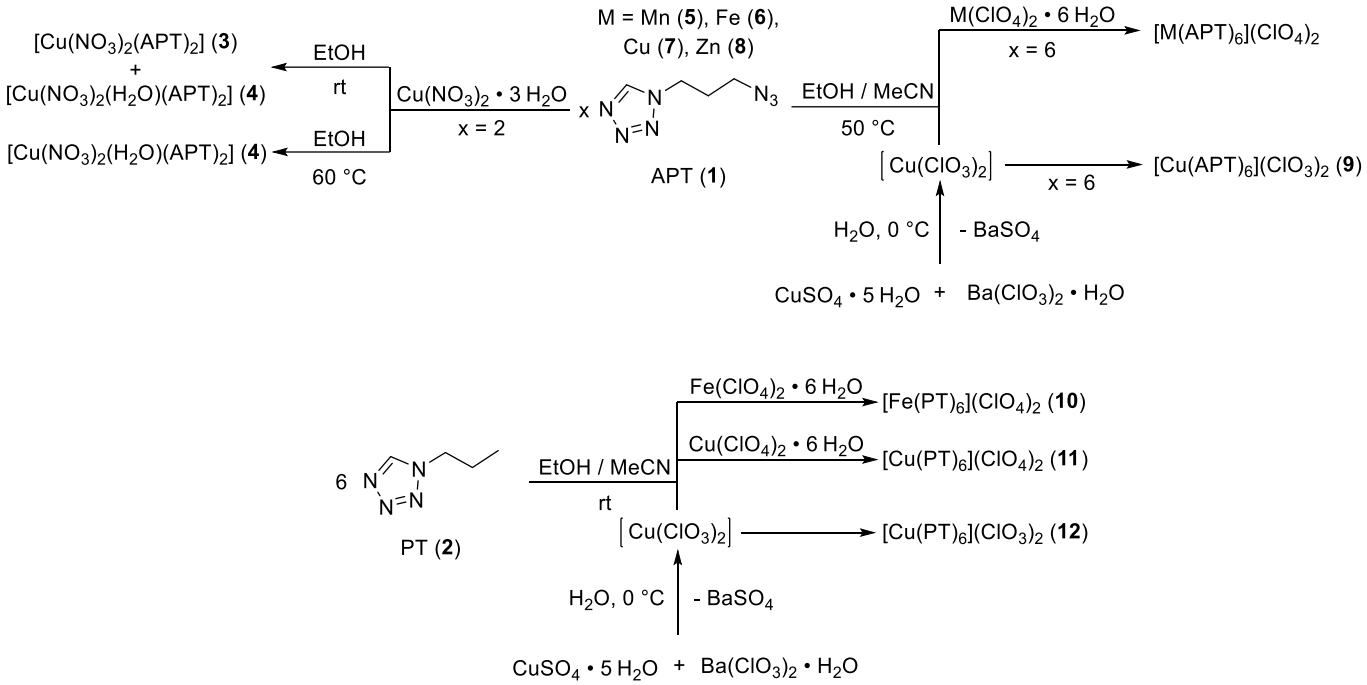

5.6.2. IR Spectroscopy of 1, 2, and 4–12

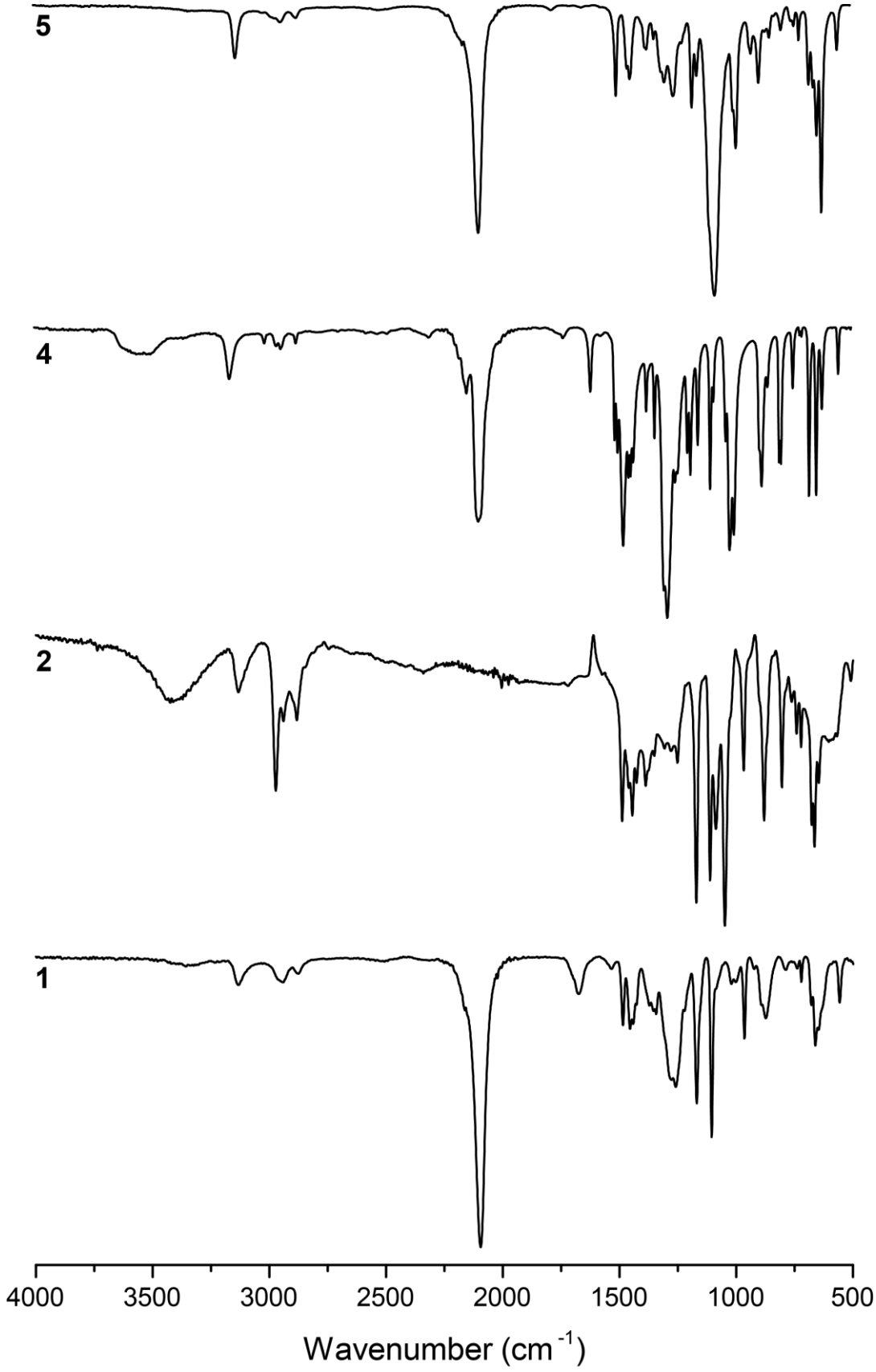

Figure S1. Infrared spectra of compounds **1**, **2**, **4**, and **5**.

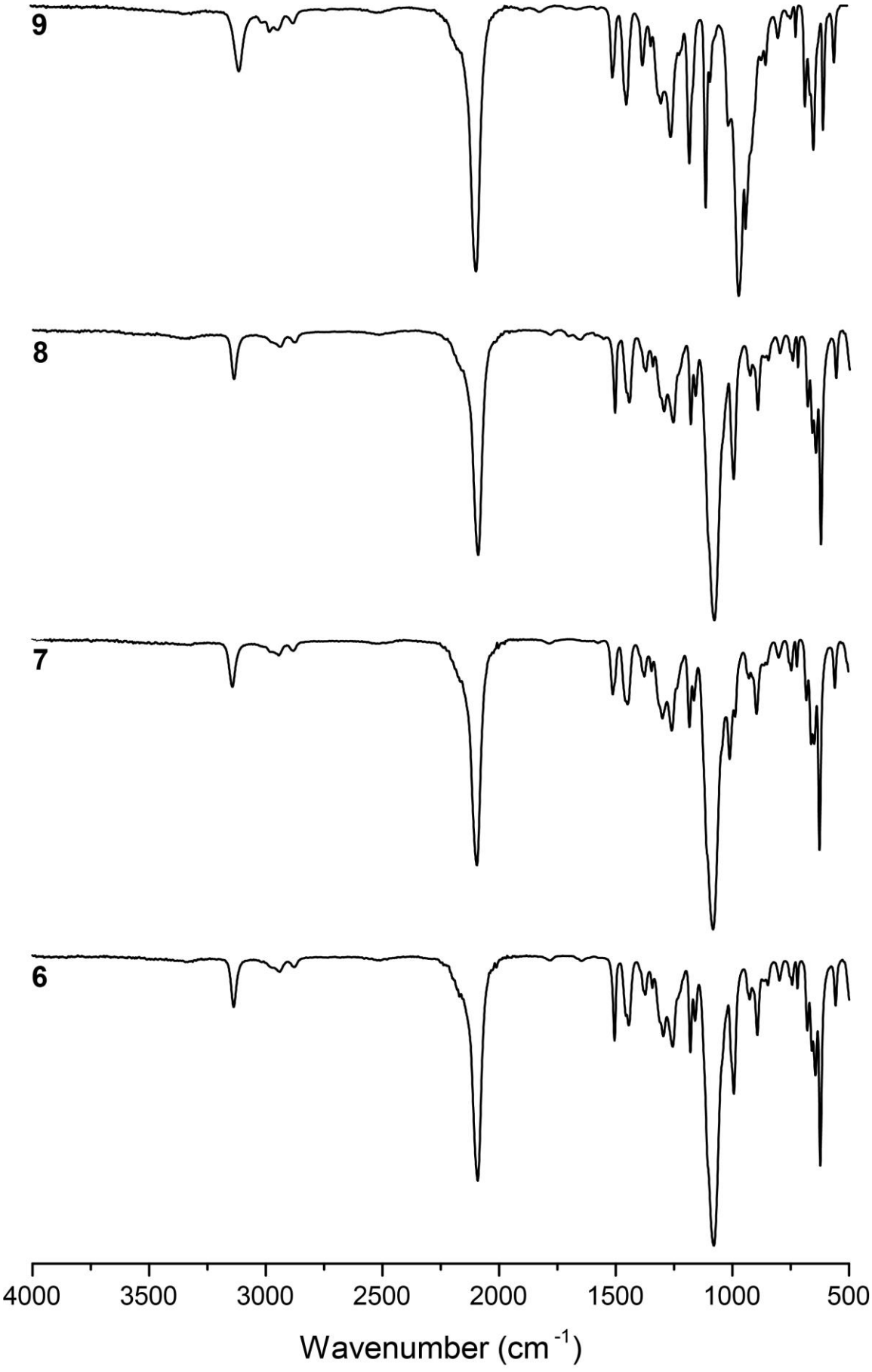

Figure S2. Infrared spectra of (per)chlorate complexes **6**–**9**.

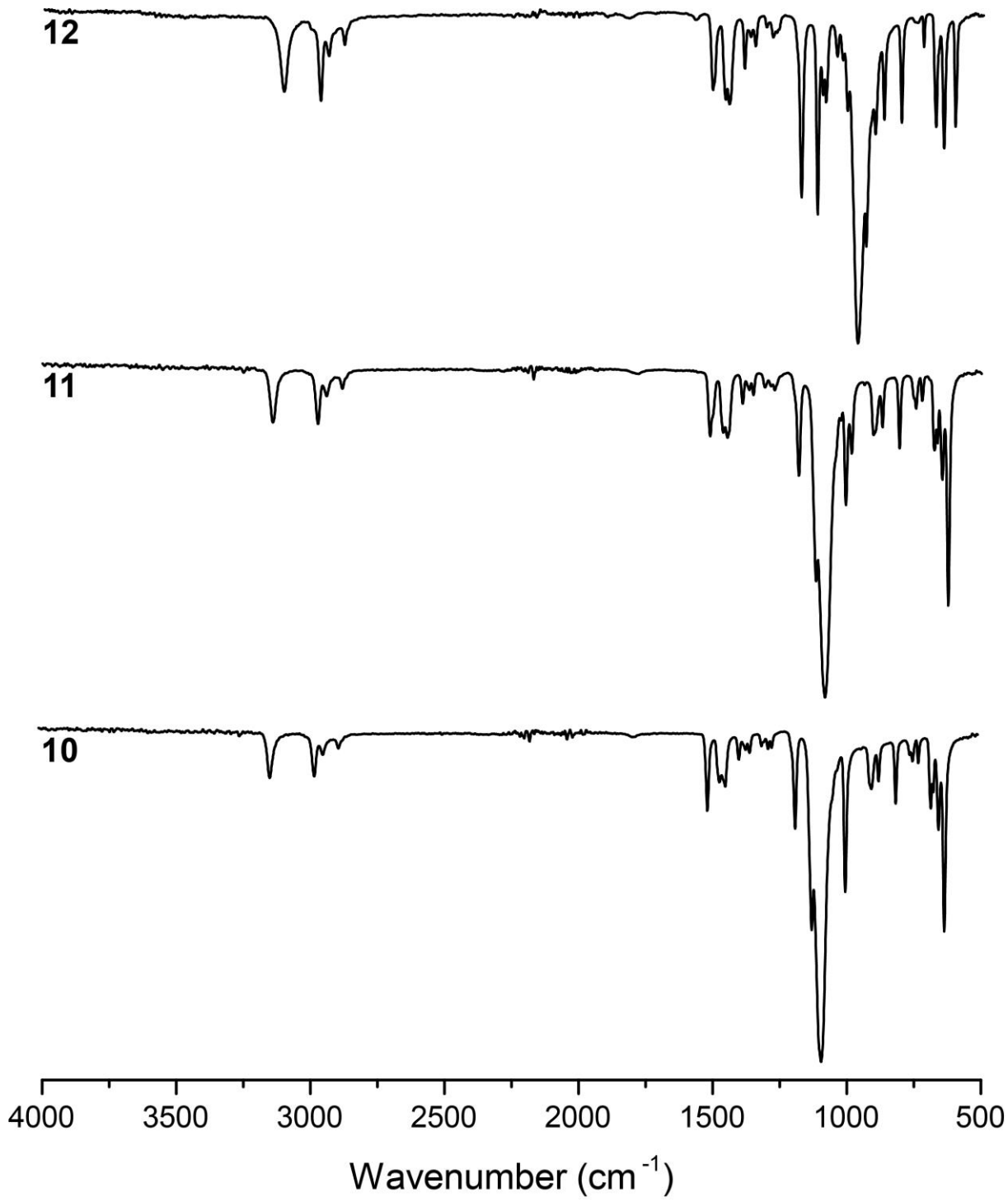

Figure S3. Infrared spectra of PT complexes **10**–**12**.

5.6.3. X-ray Diffraction

For all crystalline compounds, an Oxford Xcalibur3 diffractometer with a CCD area detector using Mo-*K*α radiation (λ = 0.7107 Å). Data collection and reduction were carried out using the CRYSALISPRO software.[1] The structures were solved by direct methods (SIR-92,[2] SIR-97,[3] or SHELXS-97[4]) and refined by full-matrix least-squares on *F*2 (SHELXL[5,6]) and finally checked using the PLATON software[7]

integrated in the WinGX[8] software suite. The non-hydrogen atoms were refined anisotropically and the hydrogen atoms were located and freely refined. The absorptions were corrected by a SCALE3 ABSPACK or SADABS Bruker APEX3 multiscan method.[9,10] All DIAMOND2 plots are shown with thermal ellipsoids at the 50% probability level and hydrogen atoms are shown as small spheres of arbitrary radius.

Table S1. Crystallographic data of **3**–**5**.

	3	**4**	**5**
Formula	$C_8H_{14}CuN_{16}O_6$	$C_8H_{16}CuN_{16}O_7$	$C_{24}H_{42}Cl_2MnN_{42}O_8$
FW [g mol^{-1}]	493.89	511.91	1172.83
Crystal system	triclinic	monoclinic	triclinic
Space Group	*P*−1	*I*2/*a*	*P*−1
Color / Habit	blue plate	blue platelet	colorless block
Size [mm]	0.10 x 0.25 x 0.50	0.05 x 0.47 x 0.50	0.10 x 0.37 x 0.50
a [Å]	6.7490(5)	10.3228(7)	11.1513(3)
b [Å]	9.4686(5)	6.9582(4)	13.4062(7)
c [Å]	15.1899(14)	28.0173(16)	18.1394(6)
α [°]	100.567(6)	90	70.851(4)
β [°]	95.373(7)	99.518(6)	83.359(2)
γ [°]	93.398(5)	90	84.320(3)
V [Å^3]	947.13(12)	1984.7(2)	2539.15(18)
Z	2	4	2
$\rho_{calc.}$ [g cm^{-3}]	1.732	1.713	1.534
μ [mm^{-1}]	1.222	1.174	0.454
F(000)	502	1044	1206
$\lambda_{MoK\alpha}$ [Å]	0.71073	0.71073	0.71073
T [K]	134	134	131
θ Min–Max [°]	3.5, 26.4	3.5, 26.4	3.3, 26.4
Dataset	−8: 7; −11: 11; −18: 14	−12: 12; −8: 7; −34: 34	−13: 13; −13: 16; −22: 22
Reflections collected	7471	5915	21685
Independent refl.	3865	2032	10352
R_{int}	0.041	0.020	0.031
Observed reflections	2950	1804	7586
Parameters	283	150	704
R_1 (obs)[a]	0.0434	0.0254	0.0497
wR_2 (all data)[b]	0.1085	0.0696	0.1380
GooF[c]	1.03	1.07	1.03
Resd. Dens. [e Å^{-3}]	−0.66, 0.72	−0.25, 0.43	−0.80, 1.07
Absorption correction	multi-scan	multi-scan	multi-scan
CCDC	1980874	1980875	1980876

[a] $R_1 = \Sigma||F_0|- |F_c||/ \Sigma|F_0|$; [b] $wR_2 = [\Sigma[w(F_0^2-F_c^2)^2]/\Sigma[w(F_0)^2]]^{1/2}$; $w = [\sigma c^2(F_0^2)+(xP)^2+yP]^{-1}$ and $P = (F_0^2+2F_c^2)/3$; [c] GooF = $\{\Sigma[w(F_o^2-F_c^2)^2]/(n-p)\}^{1/2}$ (n = number of reflections; p = total number of parameters).

5.6.4. DTA Plots of 1, 2, and 4–12

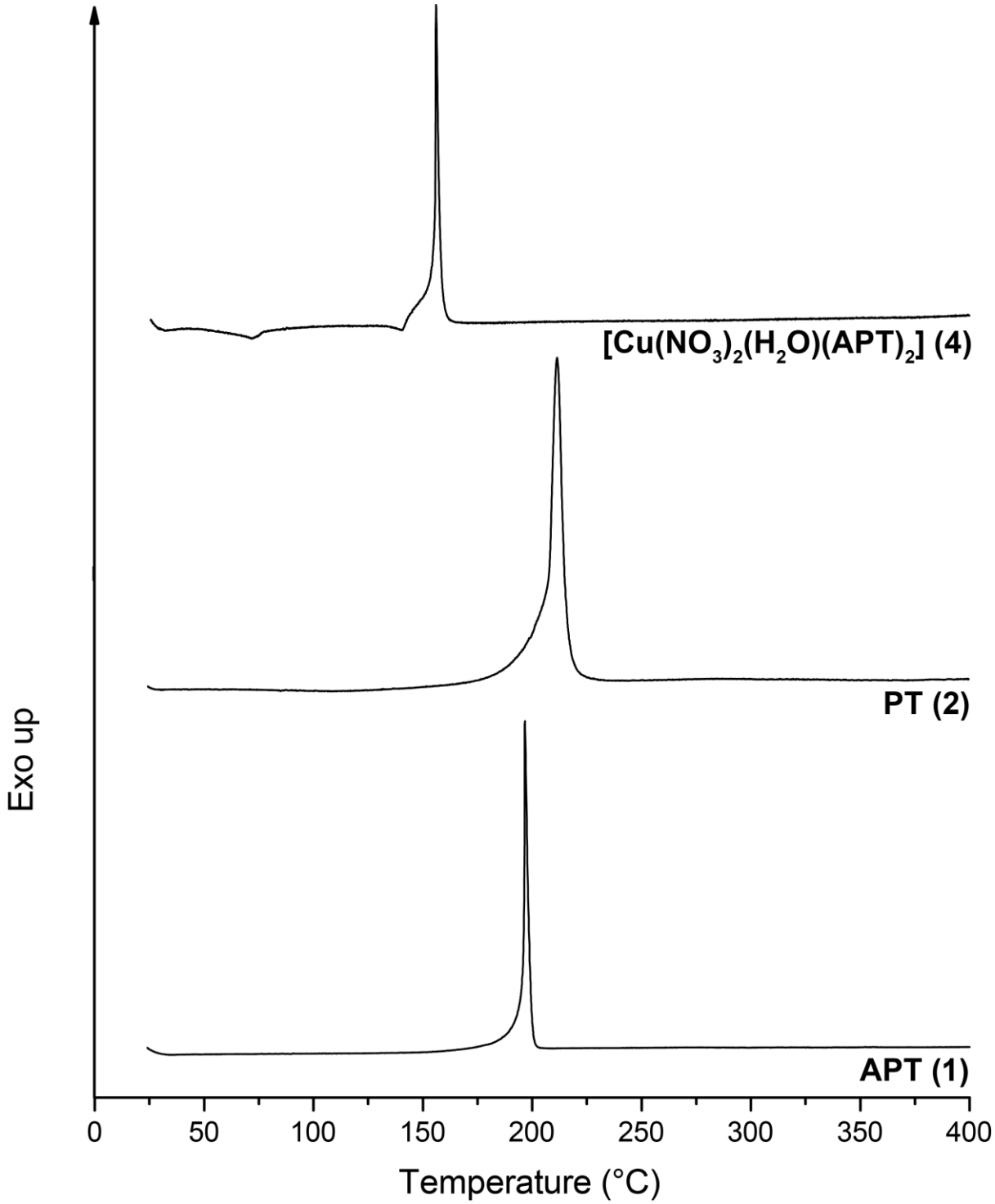

Figure S4. DTA plots of the ligands **1** and **2** together with nitrate complex **4**.

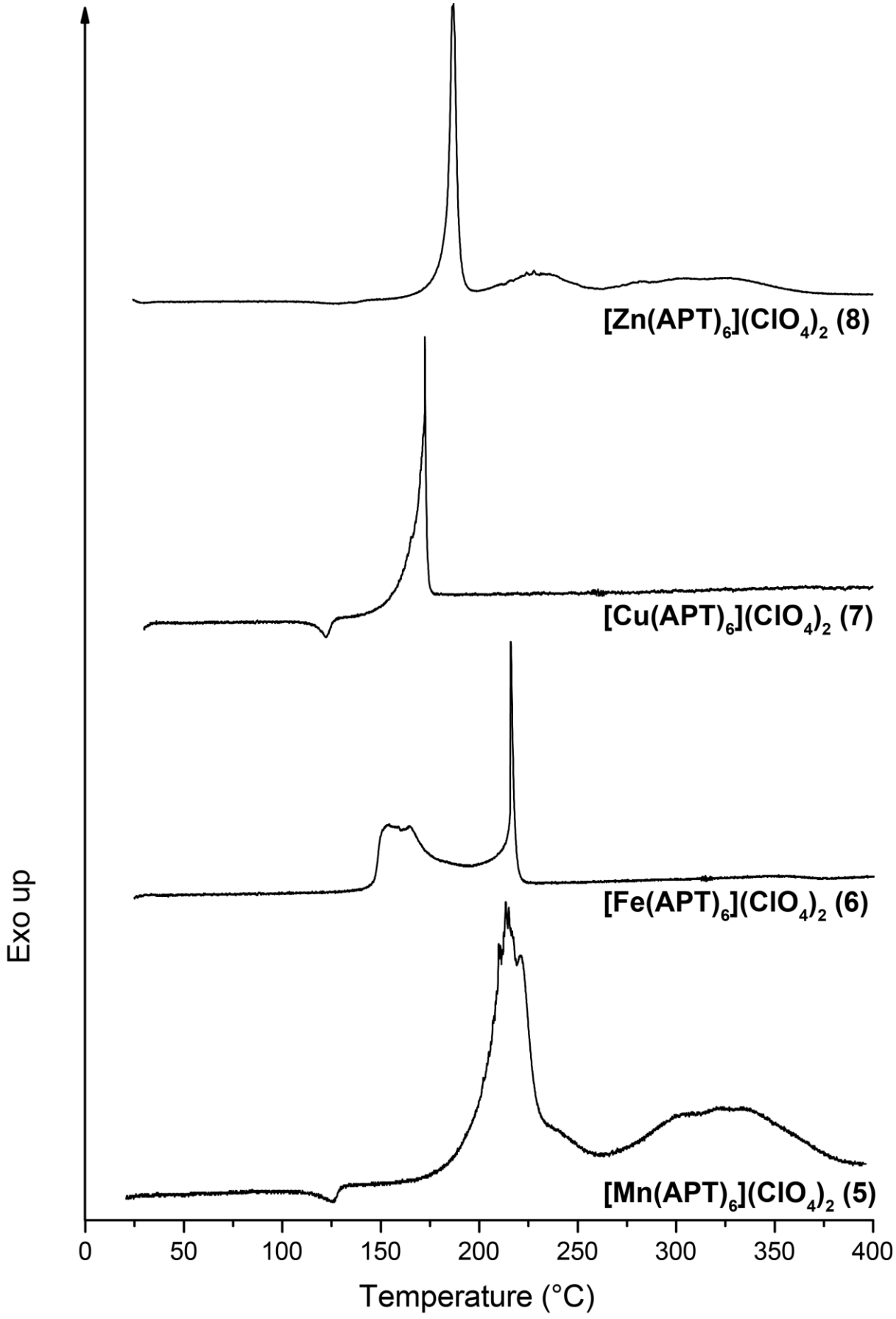

Figure S5. Differential thermal analysis of perchlorate ECC **5**–**8**.

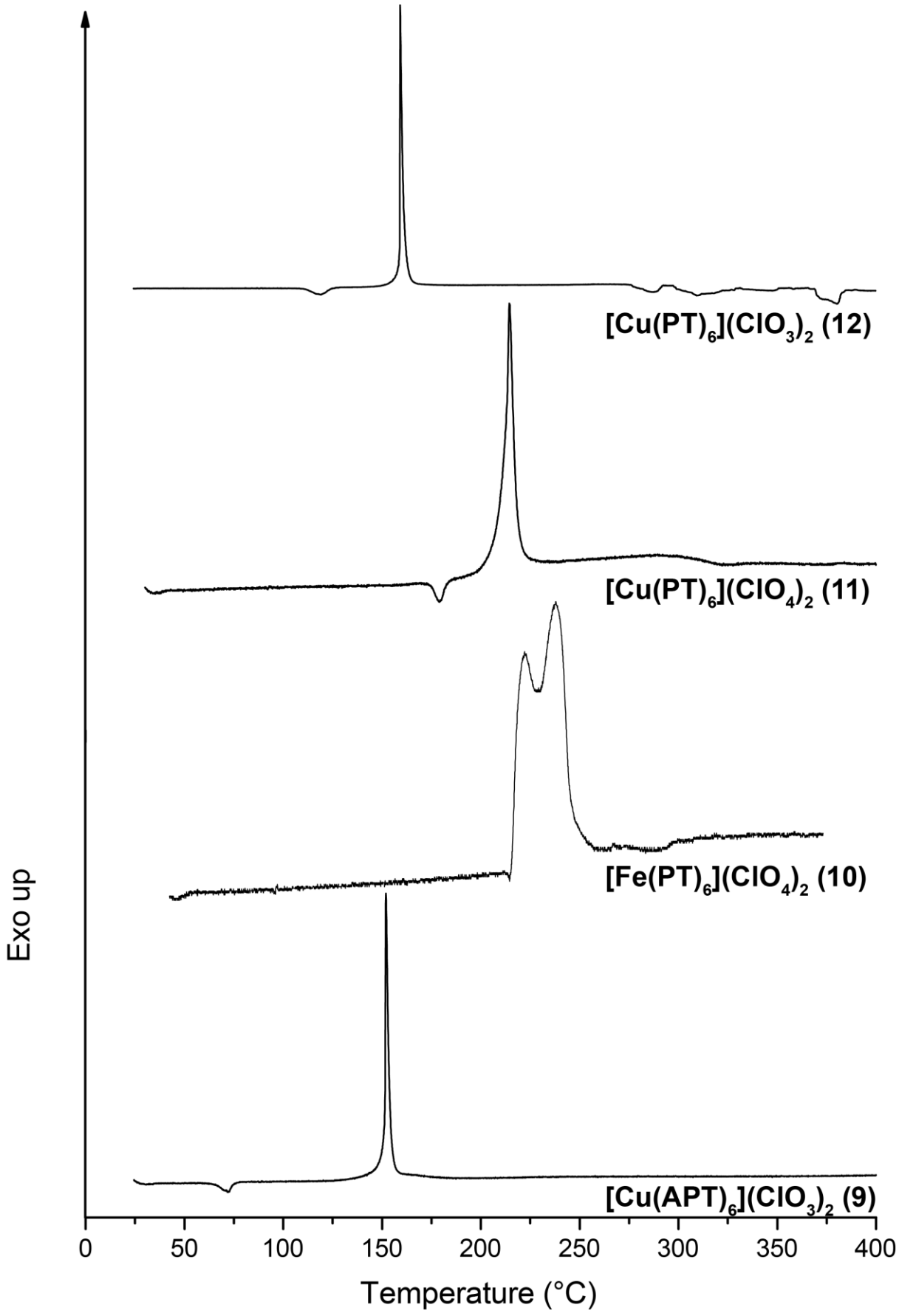

Figure S6. DTA plots of coordination compounds **9**–**12**.

5.6.5. TGA Plots of 6–12

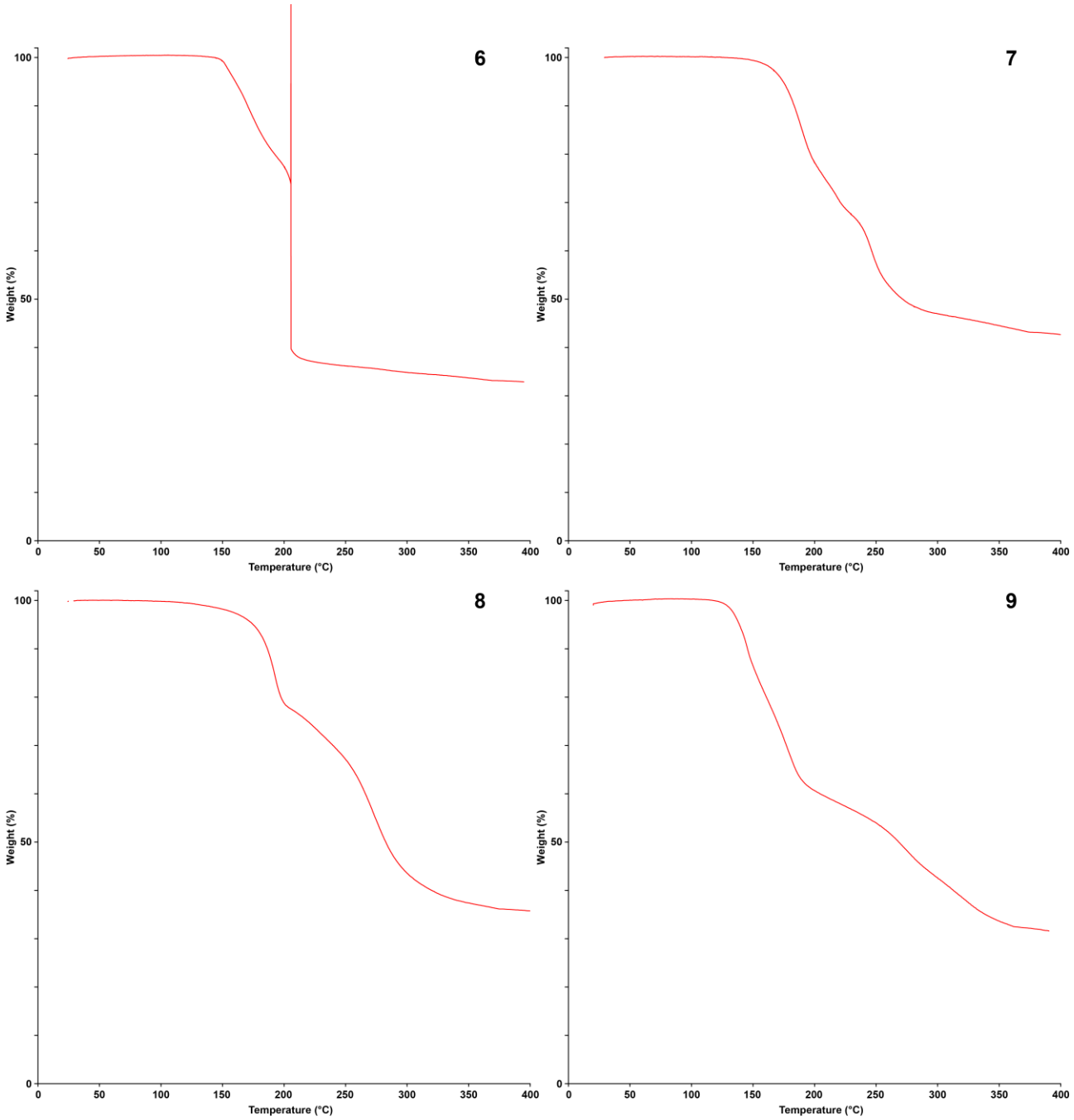

Figure S7. TGA plots of ECC **6**–**9**.

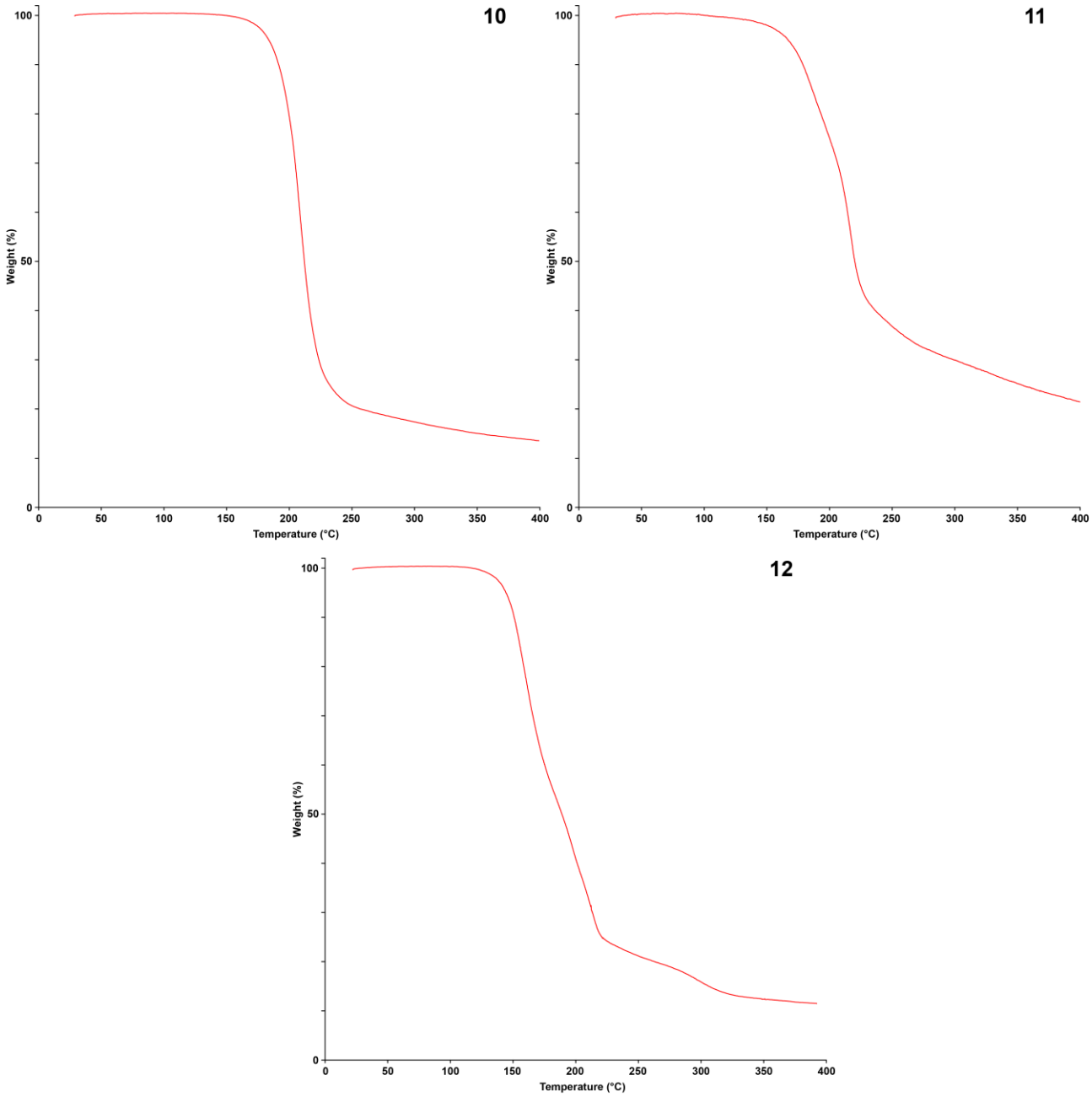

Figure S8. TGA plots of PT based complexes **10**–**12**.

5.6.6. Hot Plate and Hot Needle Tests

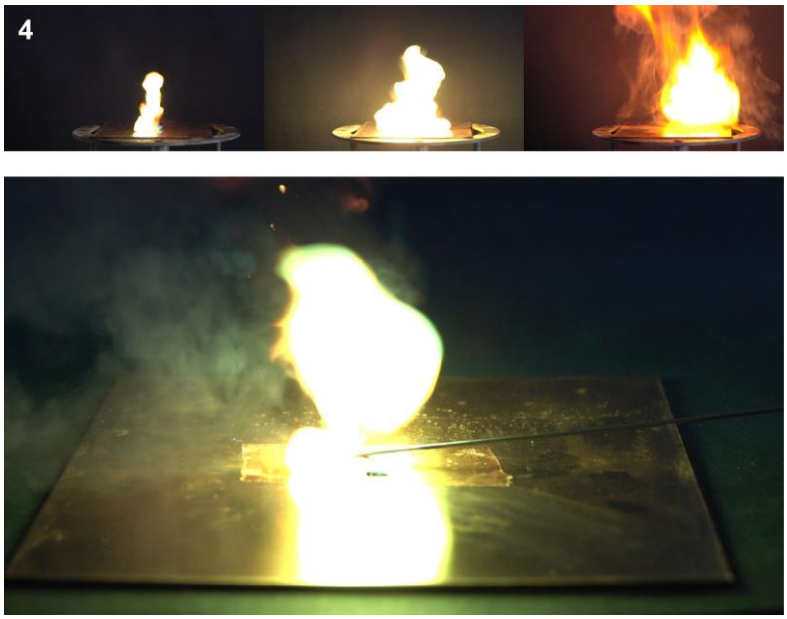

Figure S9. Hot plate test shown as a sequence (top) and hot needle test (bottom) of complex **4**.

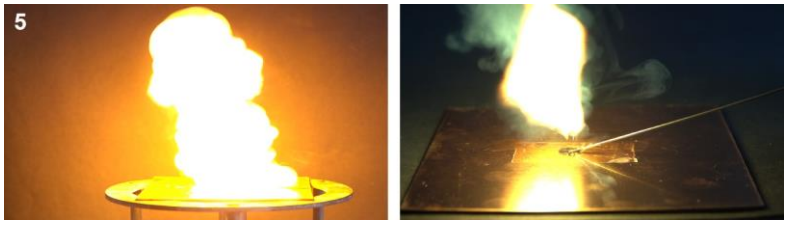

Figure S10. Hot plate (left) and hot needle test (right) of complex **5**.

Figure S11. Hot plate test (left) and initiation during hot needle test (right) of complex **6**.

Figure S12. Hot plate test shown as a sequence (top) and hot needle test (bottom) of compound **8**.

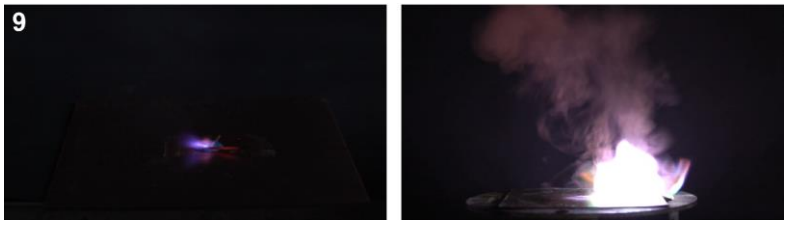

Figure S13. Initiation of copper(II) chlorate complex **9** during hot needle (left) und hot plate test (right).

5.6.7. Laser Initiation Tests of 4, 9, 11, and 12

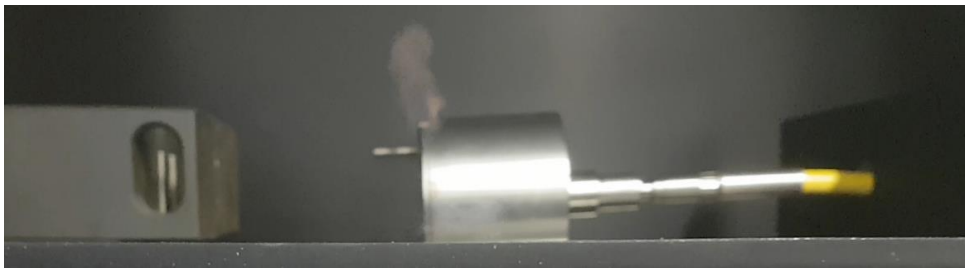

Figure S14. Moment of decomposition of nitrate complex **4**.

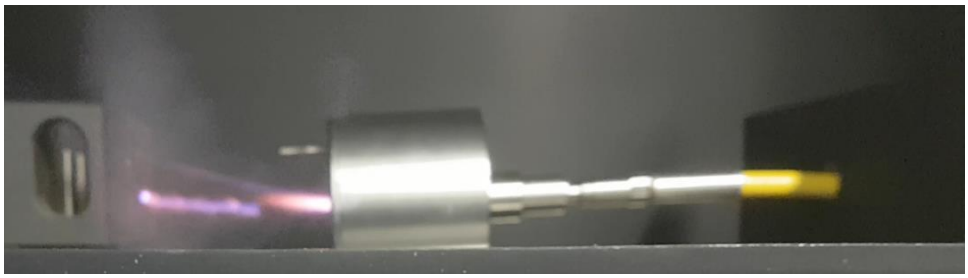

Figure S15. Deflagration of copper(II) chlorate compound **9** during the laser experiment.

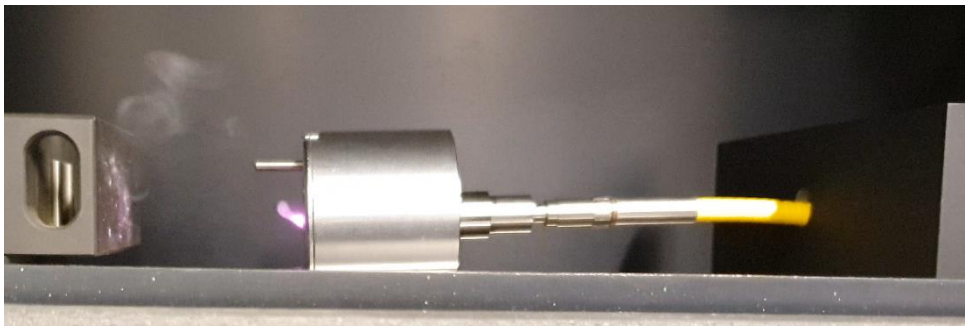

Figure S16. Decomposition of copper(II) perchlorate complex **11**.

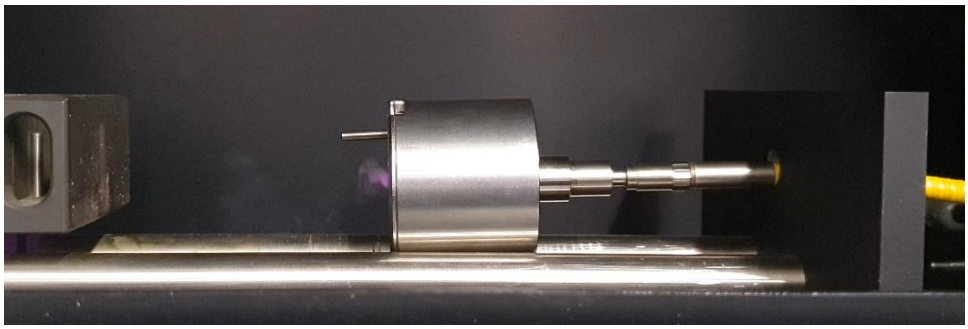

Figure S17. Decomposition of **12** when irradiated with a laser.

5.6.8. Experimental Part and General Methods

All chemicals and solvents were employed as received (Sigma-Aldrich, Fluka, Acros, ABCR). ^{1}H, ^{13}C and ^{15}N spectra were recorded at ambient temperature using a JEOL Bruker 400, Eclipse 270, JEOL EX 400 or a JEOL Eclipse 400 instrument. The chemical shifts quoted in ppm in the text refer to typical standards such as tetramethylsilane (^{1}H, ^{13}C) and nitromethane (^{15}N) in d_6-DMSO or d_3-MeCN as the solvents. The ^{1}H-^{15}N-HMBC NMR spectra were measured with a data matrix of 1024 x 256, an applied zero filling of 2048 x 4096, 32 scans per round, a relaxation delay of 1 second, an acquisition time of 0.3 seconds at a concentration of 140 mg/mL and an overall measurement time of approx. 3 h. Endothermic and exothermic events of the described compounds, which indicate melting, evaporation or decomposition, are given as the extrapolated onset temperatures. The samples were measured in a range of 25–400 °C at a heating rate of 5 °C min^{-1} through differential thermal analysis (DTA) with an OZM Research DTA 552-Ex instrument and in some cases additional by thermal gravimetric analysis (TGA) with a PerkinElmer TGA4000. Infrared spectra were measured with pure samples on a Perkin-Elmer BXII FT-IR system with a Smith DuraSampler IR II diamond ATR. Determination of the carbon, hydrogen and nitrogen contents was carried out by combustion analysis using an Elementar Vario El (nitrogen values determined are often lower than the calculated ones' due to their explosive behavior). UV-Vis spectra were recorded in the solid state using a Varian Cary 500 spectrometer in the wavelength range of 350–1000 nm. The step in the absorption intensity at 800 nm is caused by a detector change. Impact sensitivity tests were carried out according to STANAG 4489[11] with a modified instruction[12] using a BAM (Bundesanstalt für Materialforschung und -prüfung) drop hammer.[13,14] Friction sensitivity tests were carried out according to STANAG 4487[15] with a modified instruction[16] using the BAM friction tester. The classification of the tested compounds results from the "UN Recommendations on the Transport of Dangerous Goods".[17] Additionally all compounds were tested upon the sensitivity toward electrical discharge using the OZM Electric Spark XSpark10 device.[12] Hot plate and hot needle tests were performed in order to classify the initiation capability of selected complexes. The samples were fixed on a copper plate underneath adhesive tape and initiated by a red-hot needle. Strong deflagration or detonation of the compound usually indicates a valuable primary explosive. The safe and straightforward hot plate test only shows the behavior of the unconfined sample toward fast heating on a copper plate. It does not necessarily allow any conclusions on a compound's capability as a suitable primary explosive. The laser initiation experiments were performed with a 45 W InGaAs laser diode operating in the single-pulsed mode. The diode is attached to an optical fiber with a core diameter of 400 μm and a cladding diameter of 480 μm. The optical fiber is connected via a SMA type connecter directly to the laser and to a collimator. This collimator is coupled to an optical lens, which was positioned in its focal distance (*f* =

29.9 mm) to the sample. The lens is shielded from the explosive by a sapphire glass. Approximately 25 mg of the carefully pestled compound to be investigated was filled into a transparent plastic cap (PC), pressed with a pressure force of 1 kN and sealed by a UV-curing adhesive. The confined samples were irradiated at a wavelength of 915 nm, a voltage of 4 V, a current of 7–20 A and pulse lengths of 0.1–20 ms. The combined currents and pulse lengths result in an energy output of 2.00 –68.0 mJ. The luminescent marine bacterium of the strain *Vibrio fischeri* NRRL-B-11177, which is a representative for other aquatic organisms and hence a valuable indicator in case of groundwater contamination, were used as part of the commercially available bioassay system LUMIStox. The half-maximal effective concentration (EC_{50}) of both compounds was measured after 30 min of incubation time. This toxicological parameter is determined as the concentration at which the bioluminescence of the bacterial strain is decreased by 50% after a certain exposure time and then compared to the primary luminescence of the sample before being treated. Compounds can be classified according to their EC_{50} (30 min) as very toxic (< 0.10 g L^{-1}), toxic (0.10–1.00 g L^{-1}) or non-toxic (> 1.00 g L^{-1}).

The obtained coordination compounds were washed with cold acetonitrile when stated, dried overnight in air and used for analytics without further purification.

CAUTION! *All investigated compounds are energetic materials, which show partly increased sensitivities toward various stimuli (e.g., elevated temperatures, impact, friction or electrostatic discharge). Therefore, proper security precautions (safety glasses, face shield, earthed equipment and shoes, leather jacket, Kevlar gloves, Kevlar sleeves and ear plugs) have to be worn while synthesizing and handling the described compounds.*

Procedure for the preparation of 1-azidopropyl-5*H*-tetrazole (1, APT):
3-Chloropropylamine hydrochloride (13.0 g, 100 mmol) as well as sodium azide (13.0 g, 200 mmol) were dissolved in 200 mL H_2O and the mixture was stirred at 80 °C for 20 h. The solvent was removed and crude 3-azidopropylamine hydrochloride (^{1}H NMR (DMSO-d_6, 25 °C, ppm) δ: 4.96 (s, 3H, N*H*3), 3.46 (t, 2H, C*H*2), 2.78 (t, 2H, C*H*2), 1.79 (tt, 2H, C*H*2)) was received together with remaining NaN_3 and NaCl as white solid. The solids were suspended in triethyl orthoformate (26.0 mL, 200 mmol) and sodium azide (9.40 g, 144 mmol) was added. Glacial acetic acid (50 mL) was added dropwise over 30 min and the reaction mixture was refluxed at 100 °C for 16 h. After cooling down to room temperature, inorganic salts were filtered off and the solvent was removed in vacuo. Sodium hydroxide (32% solution) was added up to a slightly basic pH value and the product was extracted with acetonitrile (3 x 300 mL). The collected organic phases were dried over $MgSO_4$, the solvent removed and the product subjected to column

chromatography (EtOAc) yielding 1-azidopropyl-5*H*-tetrazole (**1**, 9.12 g, 60.0 mmol, 60% over two steps) as a yellowish oil.

DTA (5 °C min^{-1}) onset: 195 °C (exothermic); IR (ATR, cm^{-1}): $\tilde{\nu}$ = 3132 (vw), 2943 (vw), 2876 (vw), 2162 (w), 2095 (vs), 1674 (w), 1485 (w), 1455 (w), 1442 (w), 1427 (w), 1372 (w), 1355 (w), 1343 (w), 1259 (m), 1222 (w), 1169 (m), 1105 (s), 1020 (vw), 965 (w), 892 (w), 873 (w), 787 (vw), 739 (vw), 721 (vw), 677 (w), 661 (m), 647 (w), 556 (w), 461 (w); ^{1}H NMR (DMSO-d_6, 25 °C, ppm) δ: 9.42 (s, 1H, C*H*), 4.53 (t, 2H, CH_2), 3.41 (t, 2H, CH_2), 2.10 (q, 2H, CH_2); ^{13}C NMR (DMSO-d_6, 25 °C, ppm) δ: 144.0 (*C*N_4), 47.7 (*C*H_2), 45.0 (CH_2), 28.4 (CH_2); ^{15}N NMR (MeCN-d_3, 25 °C, ppm) δ: 10.7 (N3, s), −14.2 (N2, s), −52.8 (N4, d, $J_{N–H}$ = 11.9 Hz), −134.6 (N6, s), −144.4 (N1, s), −172.6 (N7, s), −312.7 ppm (N5, s); EA ($C_4H_7N_7$, 153.15) calcd.: C 31.37, H 4.61, N 64.02%; found: C 31.42, H 4.23, N 63.93%; BAM drop hammer: > 40 J; friction tester: > 360 N.

Procedure for the preparation of 1-propyl-5*H*-tetrazole (2, PT):
1,5*H*-Tetrazole (9.11 g, 130 mmol) and triethylamine (18.1 mL, 130 mmol) were dissolved in acetone (130 mL). 1-Bromopropane (11.8 mL, 130 mmol) was added and the solution was stirred under reflux for 24 h at 70 °C. Half of the solvent was evaporated under reduced pressure and the suspension was chilled on an ice bath until no further precipitation was observed. The suspension was then filtered, and the filtrate was evaporated in vacuo. The obtained orange oil was purified by column chromatography (SiO_2, EtOAc). 1-Propyl-5*H*-tetrazole (**2**, 4.50 g, 40.1 mmol, 31%) and 2-propyl-5*H*-tetrazole (5.64 g, 50.3 mmol, 39%) were received in form of yellow oils.

DTA (5 °C min^{-1}) onset: 206 °C (exothermic); IR (ATR, cm^{-1}): $\tilde{\nu}$ = 3418 (m), 3132 (m), 2972 (s), 2939 (m), 2882 (m), 1488 (s), 1459 (m), 1444 (s), 1426 (m), 1387 (m), 1350 (m), 1306 (m), 1278 (m), 1251 (m), 1170 (vs), 1111 (s), 1087 (s), 1048 (vs), 967 (m), 880 (s), 803 (m), 761 (w), 741 (m), 721 (m), 676 (s), 663 (s), 645 (m), 595 (m), 508 (w), 429 (w); ^{1}H NMR (acetonitrile-d_3, 25 °C, ppm) δ: 9.16 (s, 1H, C*H*), 4.63 (t, 2H, CH_2), 2.17–2.08 (m, 2H, CH_2), 1.09 (t, 3H, CH_3); ^{13}C NMR (acetonitrile-d_3, 25 °C, ppm) δ: 144.3 (CN_4), 50.5 (CH_2), 23.7 (CH_2), 11.0 (CH_3); EA: ($C_4H_8N_4$, 112.14) calcd.: C 42.84, H 7.19, N 49.96%; found: C 42.28, H 6.69, N 49.77%; BAM drop hammer: > 40 J; friction tester: > 360 N.

[$Cu(NO_3)_2(H_2O)(APT)_2$] (4)
A solution of 1-azidoproyl-5*H*-tetrazole (**1**, 306 mg, 2.00 mmol) in acetonitrile (2 mL) was added dropwise to an ethanolic solution (3 mL) of copper(II) nitrate trihydrate (242 mg, 1.00 mmol). The resulting reaction mixture was heated to 60 °C for 5 min under stirring and blue crystals of **4** suitable for X-ray diffraction were obtained within one week. Yield: 366 mg (0.72 mmol, 72%).

DTA (5 °C min^{-1}) onset: 70 °C (endothermic), 155 °C (exothermic); IR (ATR, cm^{-1}): $\tilde{\nu}$ = 3562 (vw), 3502 (vw), 3164 (w), 3014 (vw), 2945 (vw), 2879 (vw), 2148 (w), 2097 (s), 1617 (w), 1513 (m), 1500 (m), 1476 (s), 1454 (m), 1445 (m), 1434 (m), 1378 (w), 1342 (m), 1301 (vs), 1287 (vs), 1254 (m), 1244 (m), 1202 (m), 1188 (m), 1157 (m), 1104 (m), 1091 (w), 1037 (m), 1020 (s), 1002 (s), 883 (m), 858 (w), 808 (m), 800 (m), 750 (w), 680 (m), 649 (m), 625 (w), 555 (w); UV-Vis spectrum: λ_{max} = 350 nm; EA ($C_8H_{16}CuN_{16}O_7$, 511.87) calcd.: C 18.77, H 3.15, N 43.78% ; found: C 18.83, H 2.85, N 43.42%; BAM drop hammer: > 40 J; friction tester: 96 N; ESD: 422 mJ (at grain size 100–500 µm)

General procedure for the preparation of metal(II) perchlorate complexes 5–8:
The nitrogen-rich ligand **1** (230 mg, 1.50 mmol) was dissolved in acetonitrile (2 ml) and added dropwise to an ethanolic solution (2 mL) of the corresponding metal(II) perchlorate salt (**5**: $Mn(ClO_4)_2 \cdot 6\ H_2O$ (90.5 mg, 0.25 mmol), **6**: $Fe(ClO_4)_2 \cdot 6\ H_2O$ (90.7 mg, 0.25 mmol), **7**: $Cu(ClO_4)_2 \cdot 6\ H_2O$ (92.6 mg, 0.25 mmol), **8**: $Zn(ClO_4)_2 \cdot 6\ H_2O$ (93.1 mg, 0.25 mmol)). The resulting reaction mixtures were mechanically stirred for 5 min at 50 °C and left for crystallization in air.

$[Mn(APT)_6](ClO_4)_2$ (5)
Within two weeks colorless crystals of complex **5** suitable for X-ray diffraction were obtained. Yield: 46.0 mg (0.04 mmol, 16%).

DTA (5 °C min^{-1}) onset: 122 °C (endothermic), 208 °C (exothermic); IR (ATR, cm^{-1}): $\tilde{\nu}$ = 3135 (w), 2942 (vw), 2875 (vw), 2162 (w), 2093 (s), 1503 (m), 1456 (w), 1445 (w), 1380 (w), 1373 (w), 1342 (w), 1296 (w), 1258 (m), 1178 (m), 1158 (w), 1080 (vs), 1003 (m), 989 (m), 926 (w), 892 (w), 847 (w), 797 (vw), 743 (vw), 721 (w), 678 (w), 659 (w), 643 (m), 623 (s), 557 (w); EA ($C_{24}H_{42}Cl_2MnN_{42}O_8$, 1172.73) calcd.: C 24.58, H 3.61, N 50.16%; found: C 24.85, H 3.61, N 48.32%; BAM drop hammer: 4.5 J; friction tester: 60 N; ESD: 368 mJ (at grain size 500–1000 µm).

$[Fe(APT)_6](ClO_4)_2$ (6)
After five days, slightly yellow crystals of the iron(II) complex **6** were isolated. Yield: 212 mg (0.18 mmol, 72%).

DTA (5 °C min^{-1}) onset: 146 °C (exothermic); IR (ATR, cm^{-1}): $\tilde{\nu}$ = 3137 (w), 2940 (vw), 2878 (vw), 2091 (s), 1504 (w), 1456 (w), 1444 (w), 1373 (w), 1343 (w), 1295 (w), 1255 (m), 1179 (m), 1159 (w), 1079 (vs), 993 (m), 925 (w), 892 (w), 847 (w), 797 (vw), 743 (w), 721 (w), 678 (w), 659 (m), 643 (m), 623 (s), 557 (w), 494 (w); UV-Vis spectrum: λ_{max} = 350 nm; EA ($C_{24}H_{42}Cl_2FeN_{42}O_8$, 1173.63) calcd.: C 24.56, H 3.61, N 50.13%; found: C 24.65, H 3.45, N 49.85%; BAM drop hammer: 2.5 J; friction tester: 28 N; ESD: 317 mJ (at grain size 100–500 µm).

[Cu(APT)$_6$](ClO$_4$)$_2$ (7)
Product **5** was obtained within one week in form of blue crystals. Yield: 248 mg (0.21 mmol, 84%).

DTA (5 °C min^{-1}) onset: 115 °C (endothermic), 165 °C (exothermic); IR (ATR, cm^{-1}): $\tilde{\nu}$ = 3139 (w), 2941 (vw), 2878 (vw), 2091 (s), 1509 (w), 1445 (w), 1373 (w), 1343 (w), 1296 (w), 1256 (m), 1180 (m), 1161 (w), 1079 (vs), 1008 (m), 984 (w), 925 (w), 892 (w), 798 (vw), 744 (w), 720 (vw), 678 (w), 658 (m), 645 (m), 622 (s), 556 (w), 494 (w), 463 (w); UV-Vis spectrum: λ_{max} = 680 nm; EA ($C_{24}H_{42}Cl_2CuN_{42}O_8$, 1181.33) calcd.: C 24.40, H 3.58, N 49.80%; found: C 24.35, H 3.70, N 49.72%; BAM drop hammer: 2.5 J; friction tester: 32 N; ESD: 368 mJ (at grain size 500–1000 µm).

[Zn(APT)$_6$](ClO$_4$)$_2$ (8)
Zinc(II) compound **8** was obtained as colorless crystals within 9 days. Yield: 165 mg (0.14 mmol, 56%).

DTA (5 °C min^{-1}) onset: 183 °C (exothermic); IR (ATR, cm^{-1}): $\tilde{\nu}$ = 3138 (w), 2943 (vw), 2877 (vw), 2092 (s), 1505 (w), 1444 (w), 1373 (w), 1343 (w), 1295 (w), 1255 (m), 1180 (m), 1159 (w), 1079 (vs), 997 (m), 925 (w), 893 (w), 847 (w), 798 (vw), 743 (w), 721 (w), 679 (w), 659 (m), 644 (m), 622 (s), 557 (w), 494 (w), 461 (vw), 405 (vw); EA ($C_{24}H_{42}Cl_2N_{42}O_8Zn$, 1183.17) calcd.: C 24.36, H 3.58, N 49.72%; found: C 24.50, H 3.61, N 49.45%; BAM drop hammer: 9 J ; friction tester: 80 N, ESD: 422 mJ (at grain size 500–1000 µm).

General procedure for the preparation of metal(II) perchlorate complexes 10 and 11:
1-PT **2** (673 mg, 6.00 mmol) was dissolved in acetonitrile (2 ml) and added dropwise to an ethanolic solution (2 mL) of the corresponding metal(II) perchlorate salt at room temperature (**10**: Fe(ClO$_4$)$_2$ • 6 H$_2$O (363 mg, 1.00 mmol), **12**: Cu(ClO$_4$)$_2$ • 6 H$_2$O (371 mg, 1.00 mmol)). The resulting reaction mixtures were stirred for 5 min at ambient conditions and left for crystallization in air.

[Fe(PT)$_6$](ClO$_4$)$_2$ (10)
Coordination compound **10** was isolated after two weeks in the form of colorless crystals. Yield: 107 mg (0.12 mmol, 12%).

DTA (5 °C min^{-1}) onset: 202 °C (exothermic); IR (ATR, cm^{-1}): $\tilde{\nu}$ = 3138 (w), 2972 (w), 2941 (vw), 2882 (vw), 1507 (w), 1462 (w), 1440 (w), 1389 (vw), 1364 (vw), 1349 (vw), 1305 (vw), 1280 (vw), 1267 (vw), 1179 (m), 1118 (s), 1083 (vs), 992 (m), 895 (w), 868 (w), 804 (w), 752 (vw), 742 (w), 721 (w), 673 (w), 664 (w), 645 (m), 623 (s), 472 (vw); EA ($C_{24}H_{48}Cl_2FeN_{24}O_8$, 927.55) calcd.: C 31.08, H 5.22, N 36.24%; found: C 31.31, H 4.95, N 36.26%; BAM drop hammer: 25 J ; friction tester: 192 N; ESD: 1220 mJ (at grain size 100–500 µm).

[Cu(PT)$_6$](ClO$_4$)$_2$ (11)

Blue crystals of copper(II) compound **11** were obtained within 10 days. Yield: 424 mg (0.45 mmol, 45%).

DTA (5 °C min^{-1}) onset: 174 °C (endothermic), 209 °C (exothermic); IR (ATR, cm^{-1}): $\tilde{\nu}$ = 3142 (w), 2973 (w), 2941 (w), 2882 (vw), 1511 (w), 1462 (w), 1446 (w), 1389 (w), 1365 (vw), 1349 (w), 1306 (vw), 1283 (vw), 1270 (vw), 1180 (m), 1116 (s), 1083 (vs), 1024 (w), 1005 (m), 983 (w), 901 (w), 868 (w), 804 (w), 743 (w), 720 (w), 674 (w), 663 (w), 645 (m), 623 (s), 475 (vw); UV-Vis spectrum: λ_{max} = 678 nm; EA: ($C_{24}H_{48}Cl_2CuN_{24}O_8$, 935.25) calcd.: C 30.82, H 5.17, N 35.92%; found: C 30.74, H 4.87, N 36.03%; BAM drop hammer: 30 J; friction tester: 240 N; ESD > 1500 mJ (at grain size > 1000 μm).

General procedure for the preparation of metal(II)chlorate complexes 9 and 12:
$Ba(ClO_3)_2 \cdot H_2O$ (322 mg, 1.00 mmol) was dissolved in 5 mL of water, $CuSO_4 \cdot 5\,H_2O$ (250 mg, 1.00 mmol) was added and the solution was stirred for 5 min. The resulting suspension was cooled to 0 °C and filtered off. The filtrate was evaporated in vacuo, copper(II) chlorate dissolved in ethanol and the corresponding ligand (**1** (919 mg, 6.00 mmol); **2** (673 mg, 6.00 mmol)) in acetonitrile (2 mL) added. The resulting reaction mixtures were stirred for 5 min at ambient (**12**) or elevated (**9**) temperatures and left for crystallization in air.

$[Cu(APT)_6](ClO_3)_2$ (9)
Blue crystals of **9** were obtained within one week. Yield: 932 mg (0.81 mmol, 81%).

DTA (5 °C min^{-1}) onset: 65 °C (endothermic), 151 °C (exothermic); IR (ATR, cm^{-1}): $\tilde{\nu}$ = 3108 (w), 2977 (vw), 2940 (vw), 2876 (vw), 2173 (w), 2091 (vs), 1507 (w), 1447 (m), 1378 (w), 1342 (w), 1299 (m), 1257 (m), 1176 (m), 1106 (s), 1089 (w), 1010 (m), 965 (vs), 935 (s), 850 (w), 797 (w), 721 (w), 681 (m), 659 (m), 645 (m), 604 (m), 557 (w); UV-Vis spectrum: λ_{max} = 350 nm; EA: ($C_{24}H_{42}Cl_2CuN_{42}O_6$, 1149.34) calcd.: C 25.08, H 3.68, N 51.19%; found: C 25.29, H 3.61, N 50.63%; BAM drop hammer: 2.5 J; friction tester: 24 N; ESD > 1500 mJ (at grain size 500–1000 μm).

$[Cu(1\text{-}PT)_6](ClO_3)_2$ (12)
Ocean blue crystals of **12** formed after 10 weeks and were filtered off and washed with cold ethanol. Yield: 327 mg (0.36 mmol, 36%).

DTA (5 °C min^{-1}) onset: 111 °C (endothermic), 152 °C (exothermic); IR (ATR, cm^{-1}): $\tilde{\nu}$ = 3107 (w), 2970 (w), 2940 (w), 2881 (w), 1571 (vw), 1508 (w), 1461 (w), 1447 (w), 1389 (w), 1367 (vw), 1349 (w), 1307 (vw), 1283 (vw), 1262 (vw), 1178 (m), 1118 (s), 1098 (w), 1087 (w), 1044 (w), 1023 (w), 1006 (m), 968 (vs), 937 (s), 902 (m), 869 (m), 804 (m), 721 (w), 676 (m); UV-Vis spectrum: λ_{max} = 686 nm; EA: ($C_{24}H_{48}Cl_2CuN_{24}O_6$, 903.26) calcd.: C 31.91 H 5.36 N 37.22%; found: C 31.89 H 5.40 N 37.38%; BAM drop hammer: > 40 J; friction tester: 168 N; ESD 960 mJ (at grain size > 1000 μm).

5.6.9. References

[1] *CrysAlisPro*, Oxford Diffraction Ltd., version 171.33.41, **2009**.

[2] A. Altomare, G. Cascarano, C. Giacovazzo, A. Guagliardi, *J. Appl. Crystallogr.* **1993**, *26*, 343–350.

[3] A. Altomare, G. Cascarano, C. Giacovazzo, A. Guagliardi, A. G. G. Moliterni, M. C. Burla, G. Polidori, M. Camalli, R. Spagna, *SIR97*, **1997**.

[4] A. Altomare, M. C. Burla, M. Camalli, G. L. Cascarano, C. Giacovazzo, A. Guagliardi, A. G. G. Moliterni, G. Polidori, R. Spagna, *J. Appl. Crystallogr.* **1999**, *32*, 115–119.

[5] G. M. Sheldrick, *SHELXL-97*, University of Göttingen, Germany, **1997**.

[6] G. M. Sheldrick, *Acta Crystallogr. Sect. A* **2008**, *64*, 112–122.

[7] A. L. Spek, *PLATON*, Utrecht University, The Netherlands, **1999**.

[8] L. J. Farrugia, *J. Appl. Cryst.* **2012**, *45*, 849–854.

[9] Empirical absorption correction using spherical harmonics, implemented in SCALE3 ABSPACK scaling algorithm (CrysAlisPro Oxford Diffraction Ltd., Version 171.33.41, **2009**).

[10] *APEX3*. Bruker AXS Inc., Madison, Wisconsin, USA.

[11] NATO standardization agreement (STANAG) on explosives, impact sensitivity tests, no. 4489, 1st ed., Sept. 17, **1999**.

[12] WIWEB-Standardarbeitsanweisung 4-5.1.02, Ermittlung der Explosionsgefährlichkeit, hier der Schlagempfindlichkeit mit dem Fallhammer, Nov. 8, **2002**.

[13] http://www.ozm.cz, (accessed April 2019).

[14] http://www.bam.de, (accessed April 2019).

[15] NATO standardization agreement (STANAG) on explosive, friction sensitivity tests, no. 4487, 1st ed., Aug. 22, **2002**.

[16] WIWEB-Standardarbeitsanweisung 4-5.1.03, Ermittlung der Explosionsgefährlichkeit oder der Reibeempfindlichkeit mit dem Reibeapparat, Nov. 8, **2002**.

[17] Impact: insensitive > 40 J, less sensitive ≥ 35 J, sensitive ≥ 4 J, very sensitive ≤ 3 J; Friction: insensitive > 360 N, less sensitive = 360 N, sensitive < 360 N and > 80 N, very sensitive ≤ 80 N, extremely sensitive ≤ 10 N. According to the UN Recommendations on the Transport of Dangerous Goods, 5th ed., **2009**.

6. Closing the Gap: Synthesis of Three Isomeric *N*,*N*-Ditetrazolylmethane Ligands and their Coordination Proficiency in Adaptable Laser Responsive Copper(II) and Sensitive Silver(I) Complexes

Maximilian H. H. Wurzenberger, Vanessa Braun, Marcus Lommel, Thomas M. Klapötke, and Jörg Stierstorfer

Reprinted (adapted) with permission from *Inorganic Chemistry* **2020**, *59*, 10938–10952.

DOI: 10.1021/acs.inorgchem.0c01403

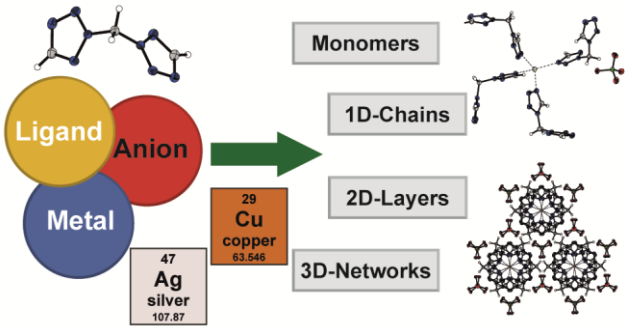

Abstract: *N*,*N*-Substituted ditetrazolylalkanes are widely used molecules in the field of coordination chemistry and are known with different alkyl chain lengths. The missing fragment within this row is presented by the elementary methylene-bridged ditetrazoles. The three different isomers (di(tetrazol-1-yl)methane (1,1-dtm, **1**), (tetrazol-1-yl)(tetrazol-2-yl)methane (1,2-dtm, **2**), and di(tetrazol-2-yl)methane (2,2-dtm, **3**)) were synthesized in a convenient one-step reaction. All of them were successfully incorporated as neutral ligands in 15 new energetic coordination compounds (ECC) based on Cu^{2+} and Ag^{+} as well as different anions (nitrate, picrate (PA), styphnate (TNR), trinitrophloroglucinate (TNPG), and perchlorate) revealing an extraordinary coordination behavior of the ligands compared to other 5*H*-ditetrazolylalkanes. All compounds were extensively characterized using single-crystal X-ray diffraction experiments, infrared spectroscopy (IR), elemental analysis (EA), and differential thermal analysis (DTA). Furthermore, the sensitivities were determined using standard techniques, and Hirshfeld surface calculations of the ligands were applied to explain their significant divergences to external stimuli. The ECC possess very good exothermic decomposition temperatures up to 242 °C. The ignition of all colored complexes was tested in laser experiments, and two copper(II) perchlorate compounds showed promising results in classic initiation capability tests using pentaerythritol tetranitrate (PETN).

6.1. Introduction

Since the discovery of tetrazoles by Baldin in 1885, its derivatives continue to attract the attention of chemists, and there is still a growing worldwide research interest in this field of nitrogen-rich chemistry.[1] The scope of tetrazole-based compounds is manifold and ranges from medicinal chemistry to molecular electronics to energetic materials.[2] However, it took until 1985 for the very first 5*H*-ditetrazolylalkane to be synthesized by Gaponik *et al.*, namely 1,2-di(tetrazol-1-yl)ethane (dte; Chart 1B).[3] Another 15 years later the first-ever complex based on this class of molecules (i-dtp; Chart 1B) was reported in the literature.[4] Since then the chemistry of 5*H*-ditetrazolylalkanes rapidly grew, and due to the resulting unique properties, they were incorporated as neutral ligands in myriad numbers of transition metal complexes.[5] In general, the *N*1,*N*1-substituted ligands can be easily and isomerically pure obtained by [3+1+1] cyclization reactions starting from the corresponding diamino compounds.[3] They are reported for chain lengths with 2–10 and 12 carbon atoms and can all be incorporated as neutral ligands in coordination compounds. Most of them were used in combination with iron(II) tetrafluoroborate, perchlorate, or hexafluorophosphate as spin-crossover systems in magnetic studies.[6] It is a known fact that the yields during the ligand syntheses drastically drop for compounds with an odd-numbered chain length between the two tetrazole substituents.[7] Another approach for synthesizing *N*-substituted ditetrazolylalkanes deals with the reaction of the corresponding dihaloalkanes with tetrazolates. This synthetic pathway results in an isomeric mixture of the symmetrically *N*1,*N*1- and *N*2,*N*2- as well as asymmetrically *N*1,*N*2-substituted molecules (Chart 1 A). Although this technique further increases the variability of possible ligands and new coordination compounds, it is rather uncommon in the literature.[8]

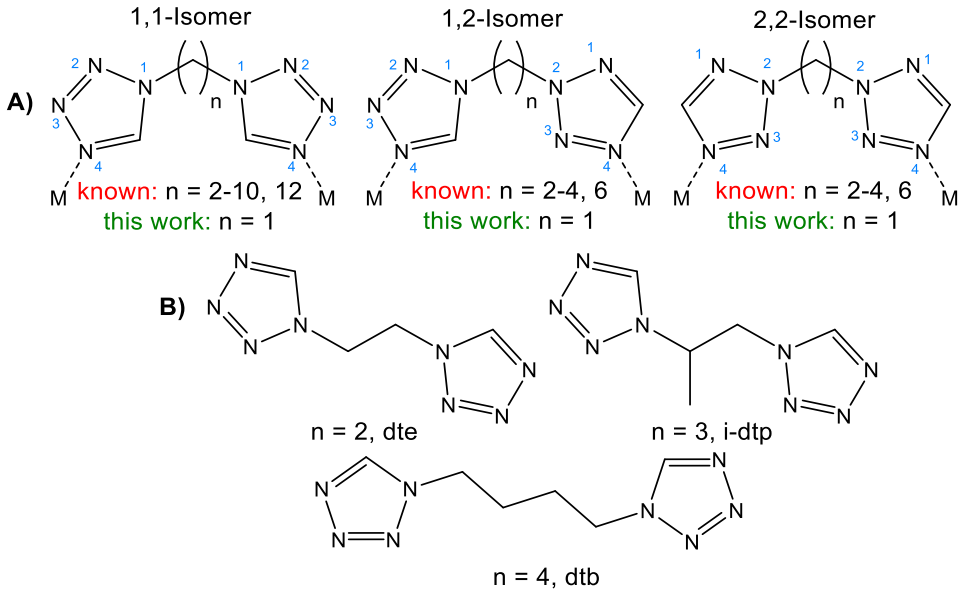

Chart 1. A) Literature known 5*H*-ditetrazolylalkanes and their bridging behavior in transition metal complexes and B) most commonly used ligands.[9]

As already mentioned, complexes based on 5*H*-ditetrazolylalkane ligands are known for a variety of different transition metals as well as anions and are discussed for diverse applications, especially as spin crossover materials or molecular magnetics.[10] However, it should not be forgotten that these tetrazoles occasionally show high heat of formations and are potential energetic materials. As expected, the heat of formation increases with shorter alkane bridges, which is shown in Figure 1.

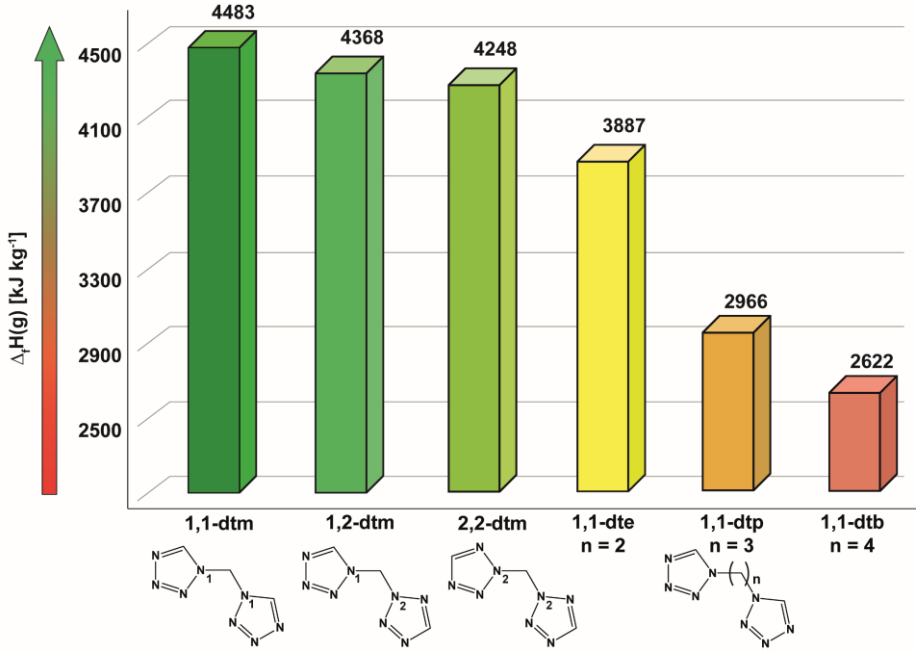

Figure 1. Overview of several calculated gas phase enthalpies of formation for *N*,*N*-disubstituted ditetrazoles showing increased values for the ditetrazolylmethane ligands. Enthalpies of formation were calculated using the atomization method ($\Delta_f H^0_{(g,M)} = H_{(M)} - \Sigma H^0_{(A)} + \Sigma \Delta_f H^0_{(A)}$) using Gaussian09 computed CBS-4 M electronic enthalpies.

Especially their transition metal complexes based on (per)chlorates and azides can easily be applied as explosives, making their use in the nonenergy field more difficult or even dangerous.[11] Lead azide (LA) and lead styphnate (LS) are still dominating the field of primary explosives in both military and industrial applications. Due to their high toxicity, both were added to the candidate list of authorization (substances of very high concern, Annex XIV) for the REACH (Registration, Evaluation, Authorization and Restriction of Chemicals) regulations in 2011.[12] In addition, executed firing and missile trainings in "friendly" areas are leading to a strong demand for less toxic primary explosives to reduce the contamination with lead.[13] In recent years, the concept of energetic coordination compounds (ECC) has received increasing attention. It allows easy tuning of the energetic performance as well as other properties, (*e.g.*, optical or thermal) of the products by simply exchanging one of the building blocks.[14] The evolving requirements for energetic materials, such as reduced toxicity, safer handling, and easy synthesis, have highly influenced the research of scientists around the world.[15] For closing the gap in this highly suitable class of ligands, we report on the first synthesis of methylene bridged *N*,*N*-substituted

ditetrazoles. These ligands, consisting of the shortest possible alkyl chain, were successfully incorporated in new ECC and show a fascinating coordination diversity. Due to the increased heat of formations compared to other ditetrazoles, they allow the enormous increase of the energetic performance of the resulting complexes. Following the concept of energetic coordination compounds, the sensitivities and properties of ECC can be easily adjusted by exchanging either the anions or central metals.

6.2. Results and Discussion

6.2.1. Synthesis and Analysis of the Pure Ligands

As already mentioned above, there are two common methods for the syntheses of *N*-substituted ditetrazolylalkanes either starting from the corresponding diamine (also hydrochlorides) or dihaloalkanes. Analogous to the synthesis of 1,3-di(tetrazol-1-yl)propane, no product could be obtained during the selective regioisomeric reaction toward **1** staring from methylenediamine dihydrochloride (Scheme 1).[16]

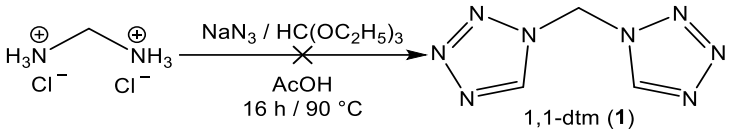

Scheme 1. Failed attempt for the selective synthesis of **1**.

Therefore, dibromomethane was reacted with *in situ* generated triethylammonium tetrazolate according to a slightly modified literature procedure.[17] This nucleophilic substitution reaction is leading to an isomeric mixture of **1**–**3** in an overall yield of 28% (Scheme 2).

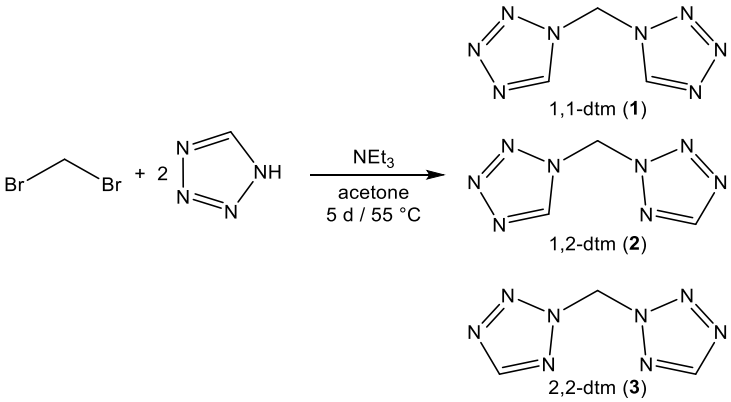

Scheme 2. Synthesis of isomers **1**–**3** starting from dibromomethane, 1,5*H*-tetrazole, and triethylamine.

The relatively low amount of product could be explained by the steric hindrance of two tetrazole rings bounded to the same carbon atom, also extending the reaction time to 5 days. It was not possible to increase the yields when using diiodomethane instead of dibromomethane or switching to synthetic protocols based on phase-transfer catalyst or different bases (NaOH, KOH). The three different isomers

can be easily separated by flash column chromatography on silica gel using a gradient of pentane and ethyl acetate. The pure compounds were obtained in differing yields of 7% (**1**), 12% (**2**), and 9% (**3**). The different isomers can easily be distinguished by IR spectroscopy (Figure S1) as well as ^{1}H and ^{13}C NMR spectroscopy. Also, the very useful two-dimensional ^{1}H-^{15}N-HMBC method was applied, which drastically decreases the measurement time compared to normal ^{15}N NMR spectroscopy (Figures 2–4).

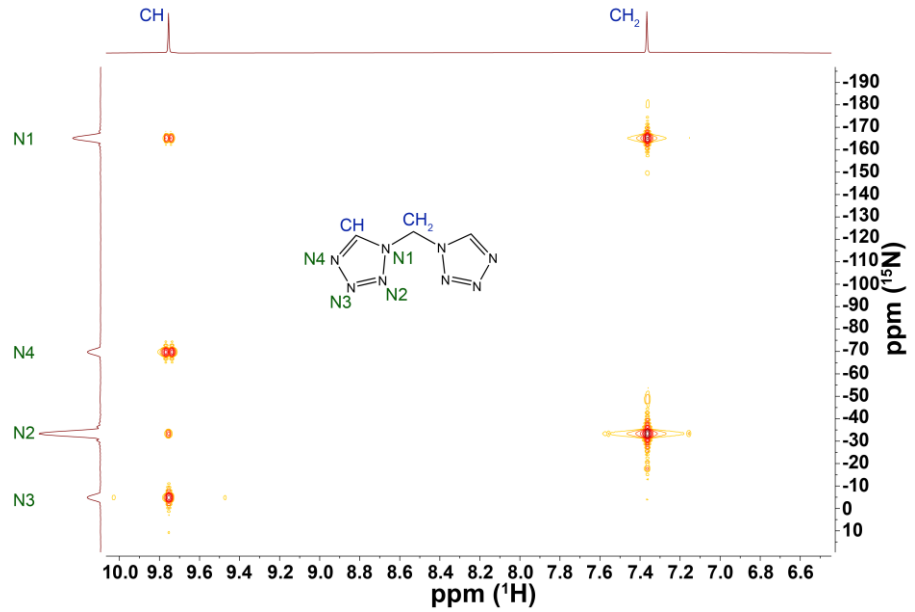

Figure 2. Two-dimensional ^{1}H-^{15}N-HMBC NMR spectra of **1** (DMSO-d_6, 25 °C): δ = −4.7 (N3), −33.2 (N2), −69.6 (N4), −165.1 ppm (N1).

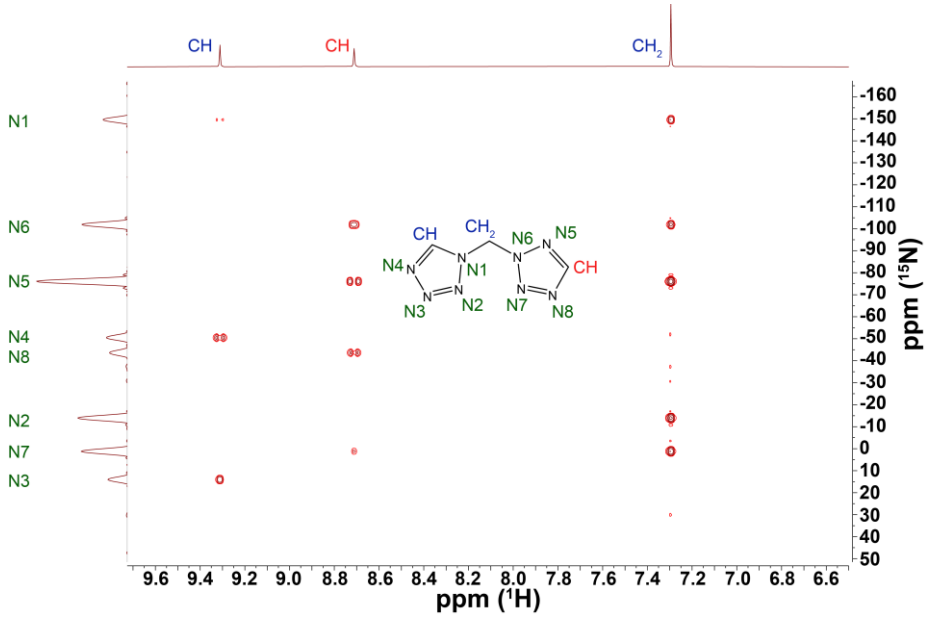

Figure 3. Two-dimensional ^{1}H-^{15}N-HMBC NMR spectra of **2** (MeCN-d_3, 25 °C): δ = 14.2 (N3), 1.3 (N7), −14.0 (N2), −43.7 (N8), −50.4 (N4), −76.2 (N5), −102.0 (N6), −149.7 ppm (N1).

The free ligands **1**–**3** crystallize in monoclinic ($P2_1/c$; **1**) or orthorhombic space groups ($Fdd2$; **2** and **3**) with comparable densities (1.605 g cm^{-3} (**2**) < 1.632 g cm^{-3} (**3**) < 1.637 g cm^{-3} (**1**)).

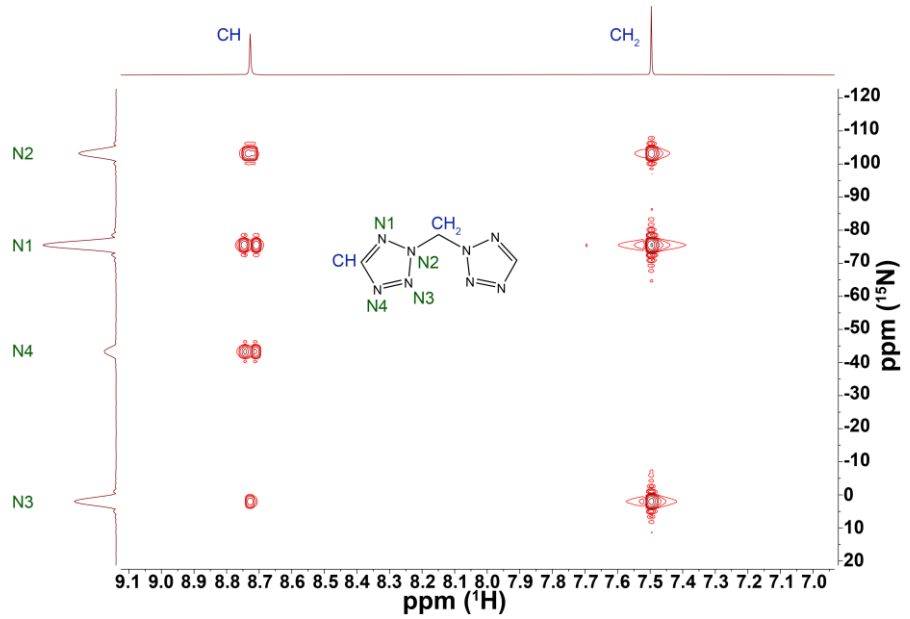

Figure 4. Two-dimensional ^{1}H-^{15}N-HMBC NMR spectra of **3** (MeCN-d_3, 25 °C): δ = 2.1 (N3), −43.3 (N4), −75.4 (N1), −103.2 ppm (N2).

The bond lengths are in the typical range of *N*,*N*′-substituted ditetrazoles, and all angles around the methylene bridges are close to the one of a perfect tetrahedron (Figure 5).[4]

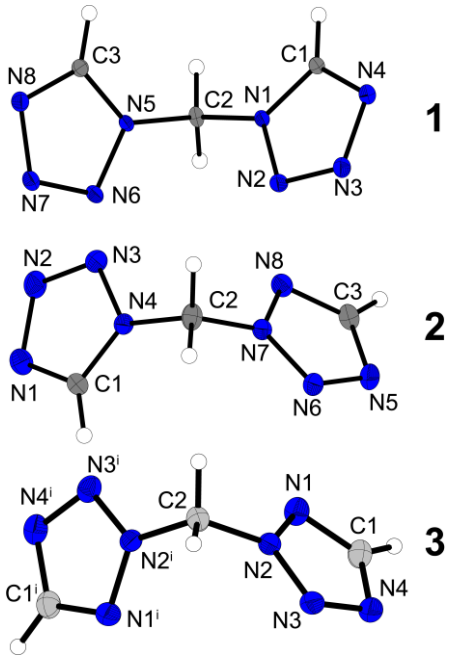

Figure 5. Crystal structures of **1**–**3**. Thermal ellipsoids of non-hydrogen atoms in all structures are set to the 50% probability level. Selected bond lengths of **1** (Å): N1–N2 1.3502(15), N1–C1 1.3377(19), N1–C2 1.4546(19). Selected bond angles of **1** (°): N2–N1–C1 108.47(11), N2–N1–C2 121.24(11), N1–C2–N5 111.27(11). Selected bond lengths of **2** (Å): N3–N4 1.347(3), N4–C1 1.328(4), N4–C2 1.453(3). Selected bond angles of **2** (°): N3–N4–C1 108.5(2), N3–N4–C2 120.1(2), N4–C2–N7 110.2(2). Selected bond lengths of **3** (Å): N1–N2 1.327(2), N1–C1 1.320(2), N2–C2 1.451(2). Selected bond angles of **3** (°): N1–N2–N3 114.24(13), N1–N2–C2 122.99(12), N2–C2–N2^{i} 110.07(19). Symmetry code of **3**: (i) −x, 1−y, z.

Comparing the onset temperatures of the three ligands **1**–**3** during DTA experiments, it becomes clear that **3** is the thermally most stable one (184 °C), followed by **1** (152 °C) and **2** (138 °C). They all show an endothermic event, which can be attributed to their melting points (proven by TGA measurements (Figure 6), whereas **1** decomposes immediately afterward.

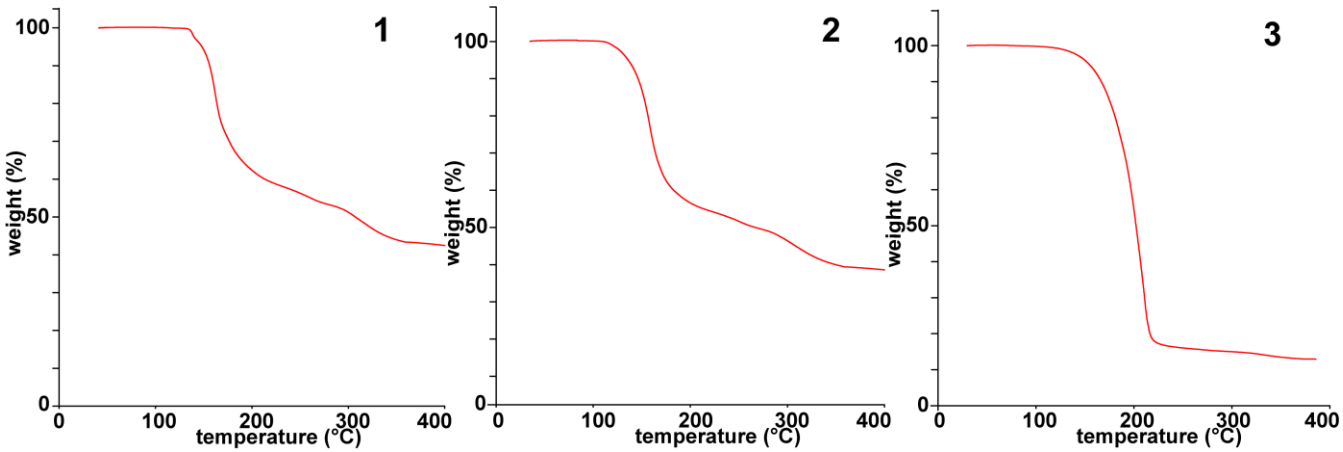

Figure 6. TGA plots of the dtm ligands revealing their stability up to the corresponding exothermic decomposition temperatures.

The same trend for the decomposition temperatures can also be observed in all ECC when comparing the ones based on the same central metals and anions. Interestingly, coordination to metal centers yields in most cases to a significant increase of the resulting decomposition temperatures. The sensitivities toward both, impact and friction, of the free ligands increase in the following order: **1** (8 J, > 360 N) < **2** (2 J, 168 N) < **3** (1.5 J, 84 N). Hirshfeld surface and fingerprint analysis supports the trend of increasing sensitivity. In all three ligands, strong attracting intermolecular N–H bonds are present, explaining the overall stability of the high nitrogen containing molecules (Figure 7). **3** bears a decreased amount of N–H interactions in the crystal and increased repulsive N–N and H–H interactions. The resulting decrease in intermolecular hydrogen bonding is a known cause for destabilization.[18] Ligand **2**, whose sensitivity lies between the ones of **1** and **3**, shows a very similar distribution of attracting (N–H) and repulsive (N–N, H–H) interactions as **1**, according to fingerprint analysis. Nevertheless, the slightly higher sensitivity is explained by the distribution of present H–H bonds. Even though the amount of repulsive H–H interactions remains nearly the same, they are now promoted as the hydrogen atoms are approaching at a closer distance, pictured by an H–H-spike to the lower left of the fingerprint plot (Figure 7, red surface). With regard to temperature stability, the compounds behave contradictory to the Hirshfeld analysis, and no explanation can be given so far. For a better comparison with known explosives, important detonation parameters of **1**–**3** were calculated using the EXPLO5 code and compared with the ones of TNT (Table 1).[19] Compound **2** shows interesting properties as a melt-cast explosive.

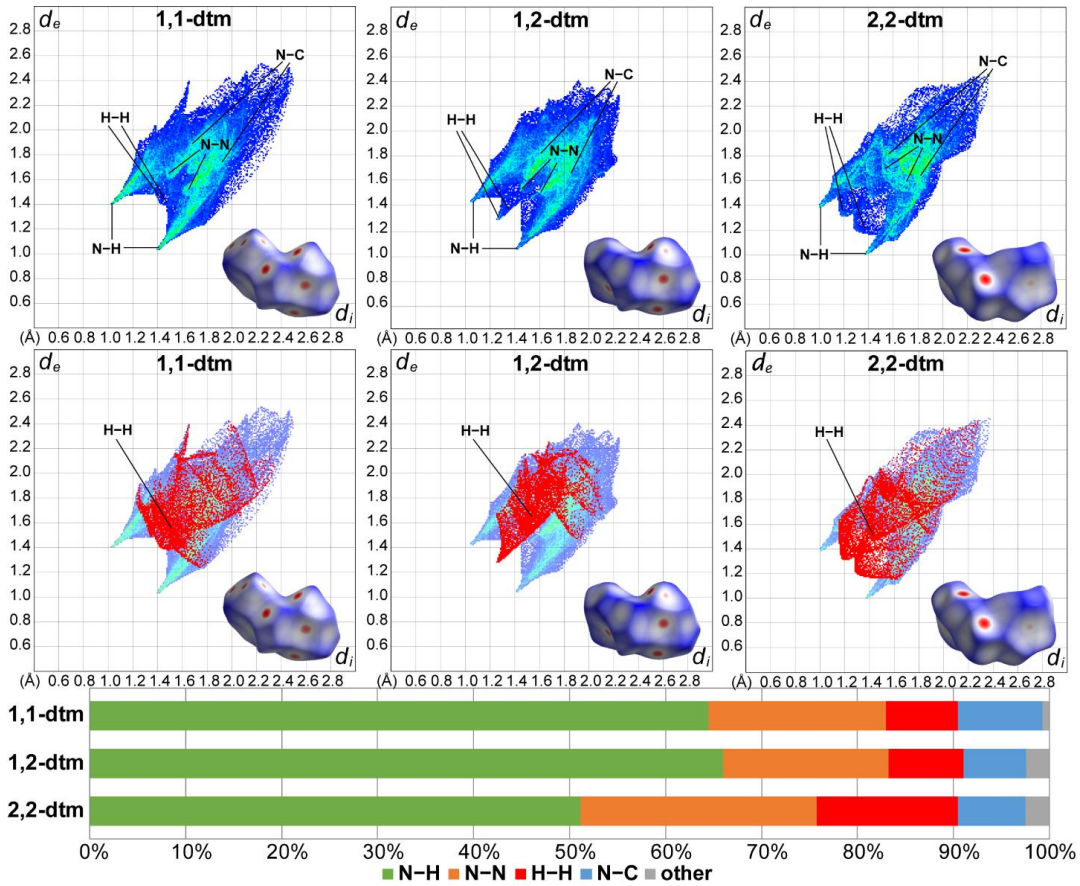

Figure 7. Two-dimensional fingerprint plots of the free ligands **1**–**3** together with their Hirshfeld surfaces. The atomic contacts percentage contribution to the Hirshfeld surface can be obtained from the bar chart.

Table 1. EXPLO5 6.05.02 values of **1**–**3** compared to TNT

	1	**2**	**3**	TNT
$\rho^{[a]}$ [g cm^{-3}]	1.59	1.57	1.59	1.65
$\Omega_{CO2}{}^{[b]}$ [%]	−84.14	−84.14	−84.14	−73.96
$\Delta_f H°^{[c]}$ [kJ mol^{-1}]	621	599	588	−261
$\Delta_f U°^{[d]}$ [kJ kg^{-1}]	4178	4035	3962	−171
$-\Delta_{ex} H°^{[e]}$ [kJ kg^{-1}]	4076	3938	3866	−4427
T_{det} [K]	2850	2793	2752	3222
$P_{CJ}{}^{[f]}$ [GPa]	20.9	19.9	20.5	1.94
$V_{det}{}^{[g]}$ [m s^{-1}]	7829	7672	7749	6824
$V_0{}^{[h]}$ [L kg^{-1}]	776	777	775	633

[a] Measured X-ray densities converted to RT. [b] Oxygen balance (Ω=(xO−2yC−1/2zH)M/1600). [c] Calculated enthalpy of formation at 298.15 K. [d] Calculated energy of formation at 298.15 K. [e] Heat of explosion. [f] Detonation pressure. [g] Detonation velocity. [h] Volume of detonation gases (assuming only gaseous products).

6.2.2. Synthesis of the Coordination Compounds

In general, the 5*H*-ditetrazolyl ligands in transition metal complexes show a bridging character leading to the formation of polymeric structures. There are only a few coordination compounds reported in the literature where they act as terminal ligands, either in the presence of bridging anions or in mixed systems, containing both bridging and terminal ligands.[20] During the synthesis of ECC based on the different

isomers **1**–**3**, it becomes clear that the nitrogen-rich molecules are often present as terminal ligands. Therefore, the first attempts were performed with 4 (silver(I) complexes) or 6 (copper(II) complexes) equiv. of ligand, and after determining the compositions, the compounds were synthesized using the exact ratio of metal salt to ligand. Except for Ag^{+} and Cu^{2+}, perchlorate salts of the eco-friendly Mn^{2+}, Fe^{2+}, and Zn^{2+} cations were used for the syntheses of coordination compounds, but in all cases only starting material could be obtained. For synthesizing silver complexes **4**–**8**, both starting materials were dissolved in a mixture of water/acetonitrile and stirred for 5 min at room temperature after combining both solutions (Scheme 3).

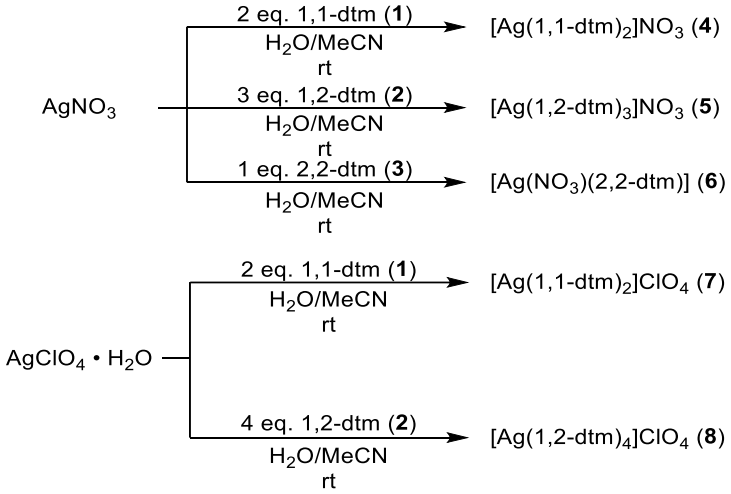

Scheme 3. Synthesis of silver nitrate and perchlorate complexes **4**–**8**.

While standing in air the compounds started to crystallize within minutes to 1 day. The attempted synthesis of a silver(I) perchlorate complex based on 2,2-dtm led to the decomposition of the starting materials, which also occurred in the dark. In the case of the copper(II) complexes **9**–**18**, it is highly important to use the right solvents and reaction temperatures, to prevent the formation of aqua species (**9**–**12**) or amorph compounds with an unclear composition (**13**–**18**) (Schemes 4 and 5). **9** is the only copper(II) nitrate-based ECC, which could be isolated without any starting material residues or side species.

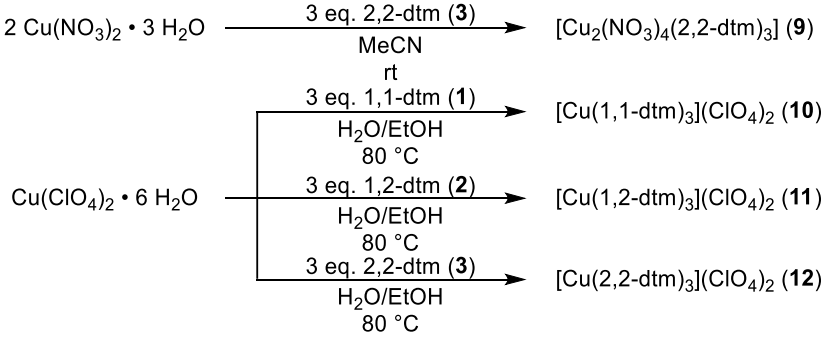

Scheme 4. Synthesis of copper(II) nitrate and perchlorate complexes **9**–**12**.

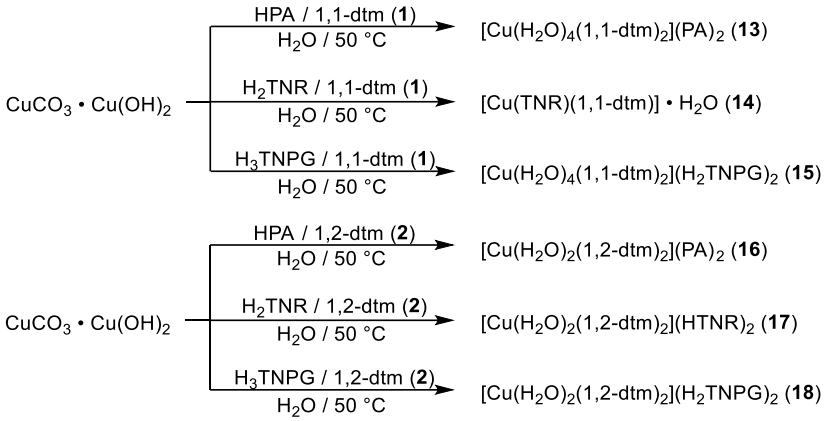

Scheme 5. Synthesis of trinitroaromatic complexes **13**–**18**.

It crystallized from the reaction solution within 5 days after combining the dissolved metal salt and ligand. When reacting the ditetrazoles with copper(II) perchlorate in water, different aqua complexes were obtained. Changing the solvents to organic ones allows the precipitation of the anhydrous compounds. Single crystals were obtained from the mother liquors after filtration. Complexes **10**–**12** can also be crystallized within 1 h when using ethanol as solvent at 80 °C and adding water dropwise until the precipitates are completely dissolved. For the first step of the syntheses of nitroaromatic complexes **13**–**18**, basic copper(II) carbonate was reacted with 2 equiv. of the corresponding acid to ensure complete conversion. Even in the case of ECC **14** with the presence of a double-deprotonated anion, 2 equiv. of styphnic acid had to be used. The dissolved ligands were added dropwise at elevated temperatures to the *in situ* synthesized copper(II) trinitrophenolates, and the corresponding complexes were obtained as single crystals within some hours. Due to the low yields of **3** during the ligand synthesis and the high water content of the nitroaromatic complexes, no ECC based on this combination were attempted. Some of the complexes **13**–**18** show endothermic events during DTA measurements. Drying these compounds at 100 °C overnight resulted in anhydrous powders, which rapidly incorporate water again under ambient conditions.

6.2.3. Crystal Structures of the ECC

All ECC were investigated by single-crystal X-ray diffraction experiments. The details of the crystal structures of compounds **15**, **17**, and **18**, as well as the measurements and refinement data of all structures, can be found in the Supporting Information (Tables S1–S5 and Figures S5 and S6).[21] The bond lengths as well as angles of the coordinating ditetrazoles in all complexes are comparable to the ones of the free ligands and are therefore not further discussed. The nitrogen-rich molecules solely bind via the N4 atoms of their heterocycles and, interestingly, in some cases only coordinate with one of the two tetrazole substituents. Whereas all silver complexes, except **6**, show a 4-fold coordination around the central metal,

the copper(II) compounds, except nitrate ECC **9**, possess an octahedral coordination sphere. The three silver nitrate complexes (**4**–**6**) all show different compositions with varying metal to ligand ratios explaining the differences in their density. While **4** crystallizes in the triclinic space group *P*−1 with a density of 2.112 g cm^{-3} (131 K), **5** and **6** are present in orthorhombic (*Pna*2$_1$) and monoclinic (*Ia*) space groups, respectively. With the highest ligand content, **5** also possesses the lowest density (1.886 g cm^{-3} @ 108 K), whereas it is the other way around for **6** showing the highest density (2.404 g cm^{-3} @ 122 K) of all compounds. The molecular unit of ECC **4** consists of one silver cation, two coordinating ligands, and a nonbinding nitrate anion (Figure 8).

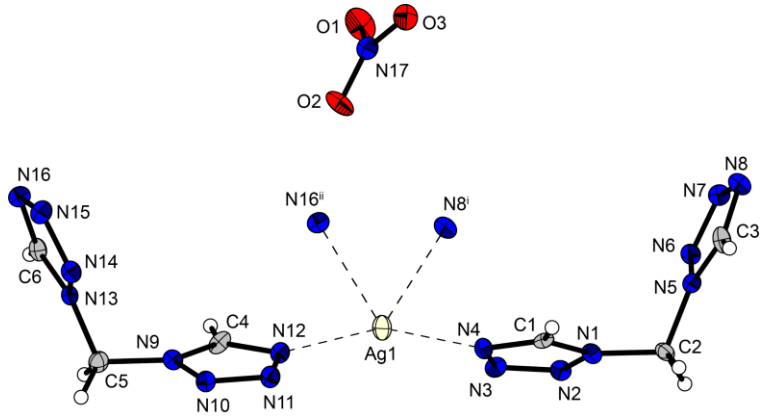

Figure 8. Silver(I) coordination environment of nitrate complex **4**. Selected bond lengths (Å): Ag1–N4 2.254(4), Ag1–N16^{ii} 2.593(4). Selected bond angles (°): N4–Ag1–N8^{i} 84.83(12), N8^{i}–Ag1–N16^{ii} 78.86(13). Symmetry codes: (i) −x, 1−y, −z; (ii) 1−x, −y, 1−z.

The 4-fold coordination sphere around the central metal is caused by the bridging of the ligands between the same cations, leading to the formation of polymeric chains. The geometry can be described as an extended linear coordination. The N4–Ag1–N12 axis with Ag–N bond lengths of 2.254(4) Å gets bent by the elongated bounding (2.593(4) Å) of two more nitrogen atoms from linking ligands to an angle of 157.21(13)°. Like **4**, the silver cation in complex **5** is 4-fold coordinated by tetrazole rings, and the anion is not coordinating. In contrast, the geometry can be described as a strongly distorted tetrahedron with a smaller deviation of the Ag–N bond lengths (2.261(3)–2.386(3) Å). The three different ligands present in the unit cell, all show a diverse coordination behavior. Whereas one of them is binding with both heterocycles to two different silver cations, the other two are only single coordinating, one with the 1*N*- and the second with the 2*N*-substituted ring (Figure 9). The linking of one ligand, in turn, leads to the formation of a polymeric structure in the form of a chain. Like in coordination compound **4**, the geometry around the silver cation in complex **6** can be described as an extended linear structure. The ligand is connecting two central metals (Ag1–N4 2.231(5) Å and Ag1–N8^{ii} 2.211(7) Å), and the elongated bounding of three oxygen atoms (2.542(5)–2.734(5) Å) is bending the N4–Ag1–N8^{ii} axis to 148.89(19)°, which is even stronger than in compound **4**. Interestingly, in this structure the nitrato anion is not only

chelating one cation but also bridging to another one, leading to an uncommon 5-fold coordination sphere around the silver(I) central metal (Figure 10).

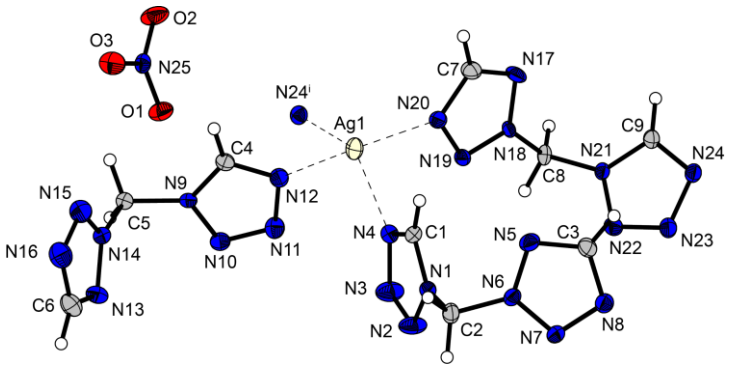

Figure 9. Silver(I) coordination environment of nitrate complex **5**. Selected bond lengths (Å): Ag1–N4 2.386(3), Ag1–N12 2.336(3), Ag1–N20 2.261(3). Selected bond angles (°): N4–Ag1–N12 108.62(9), N4–Ag1–N20 99.66(9), N12–Ag1–N20 114.87(10), N20–Ag1–N24^{i} 135.69(10). Symmetry code: (i) 1−x, −y, −0.5+z.

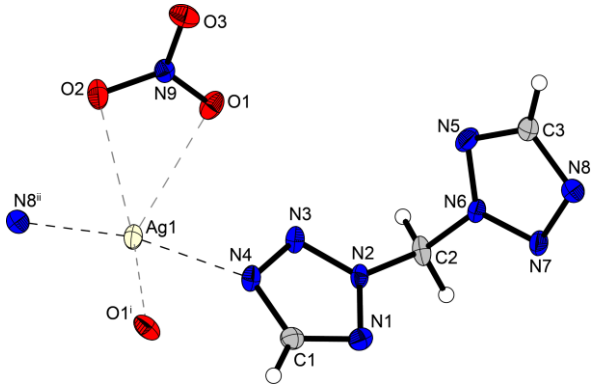

Figure 10. Silver(I) coordination environment of nitrate complex **6**. Selected bond lengths (Å): Ag1–O1 2.712(5), Ag1–O1^{i} 2.542(5), Ag1–O2 2.734(5). Selected bond angles (°): O1–Ag1–O2 46.80(15), O1–Ag1–N4 78.82(16), O2–Ag1–N4 123.89(15). Symmetry codes: (i) 0.5+x, −y, z; (ii) x, y, −1+z.

The double linking of the two different ligands is building a 2D-polymeric network (Figure 11).

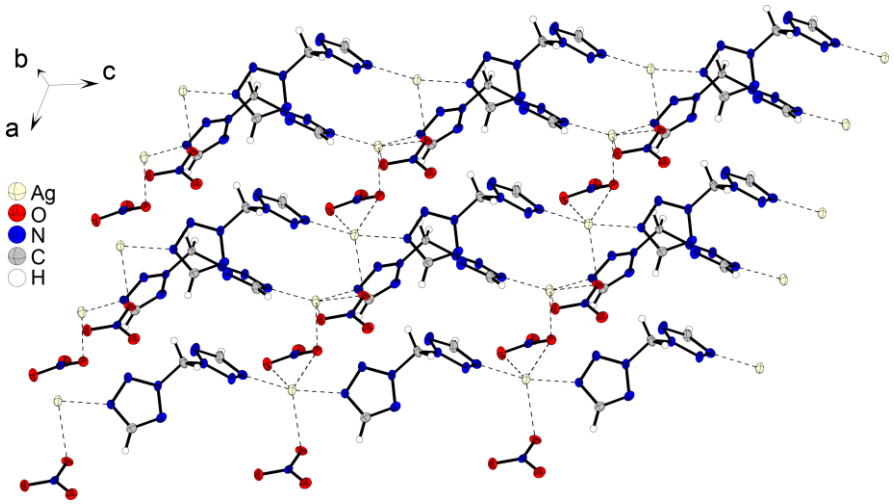

Figure 11. Polymeric structures of **6**.

The perchlorate complexes **7** and **8** show similar coordination geometries to the one of **4**. The linear structures are highly deviating from the ideal 180° by the elongated bonding of additional tetrazole ligands. Whereas the ligands in **7** are both bridging and leading to the formation of polymeric chains, the four ligands in **8** are solely coordinating with one of their rings building up complex monomers (Figure 12).

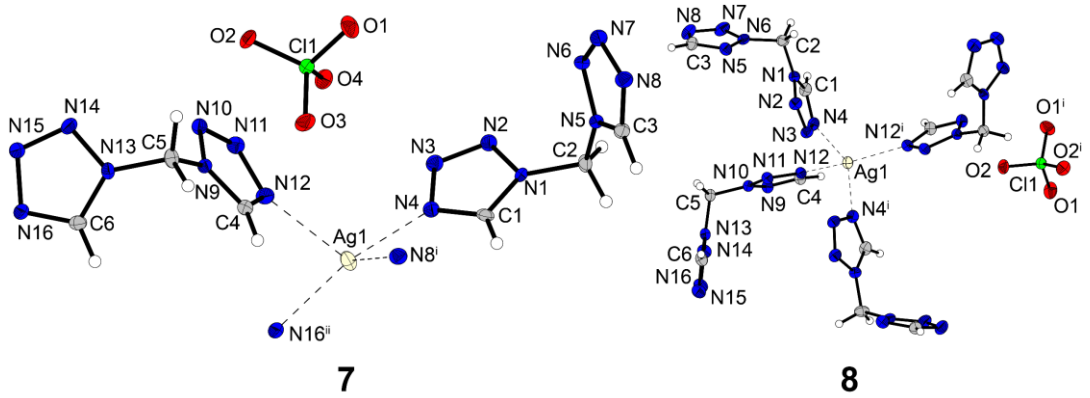

Figure 12. Coordination environment of perchlorate compound **7** and molecular unit of **8**. Selected bond lengths of **7** (Å): Ag1–N4 2.260(2), Ag1–N12 2.581(2), Ag1–N8^{i} 2.612(2), Ag1–N16^{ii} 2.259(2). Selected bond angles of **7** (°): N4–Ag1–N12 114.85(8), N4–Ag1–N8^{i} 83.40(8), N4–Ag1–N16^{ii} 153.50(8). Symmetry codes of **7**: (i) 1−x, −y, 1−z; (ii) −x, 1−y, −z. Selected bond lengths of **8** (Å): Ag1–N4 2.419(2), Ag1–N12 2.3036(19). Selected bond angles of **8** (°): N4–Ag1–N12 95.66(7), N4–Ag1–N4^{i} 99.92(7), N12–Ag1–N12^{i} 145.79(8). Symmetry code of **8**: (i) 0.5−x, y, 0.5−z.

Again, the different composition of the ligand/metal ratio is highly influencing the density. **7** crystallizes with a density of 2.190 g cm^{-3} at 128 K in the triclinic space group *P*−1. The higher ligand content in **8**, which is crystallizing in the monoclinic space group *P*2/*n*, causes a lower density of 1.901 g cm^{-3} at 111 K. Copper(II) nitrate complex **9** crystallizes as blue blocks in the monoclinic space group *I*2/*a* with four formula units per unit cell and a calculated density of 1.945 g cm^{-3} at 109 K. The molecular unit is composed of a dimer of central metals bridged by one ligand. Each of the two copper(II) cations is further connected by a pair of ligands to the next dimeric unit, leading to the formation of polymeric chains. Apart from the three coordination sides occupied by nitrogen atoms, the coordination sphere is completed by two chelating nitrato ligands. The resulting molecular geometry around the copper central metal is a strongly disordered pentagonal bipyramid, which is very uncommon for copper(II) (Figure 13). The copper(II) perchlorate complexes **10**–**12** all show the same composition of their molecular units with three coordinating ligands, each linking between two copper(II) centers and two non-coordinating anions (Figures 14–16). Complexes **10** and **11** crystallize in monoclinic space groups (*C*2/*c* and *P*2$_1$/*n*, respectively), and **12** is present in the hexagonal space group *P*6$_3$/*m* (**12a**) as well as the trigonal one *P*−3*c*1 (**12b**). While the ECC possess the same compositions, they highly differ in their polymeric structure because of the different bridging modes of the ligands.

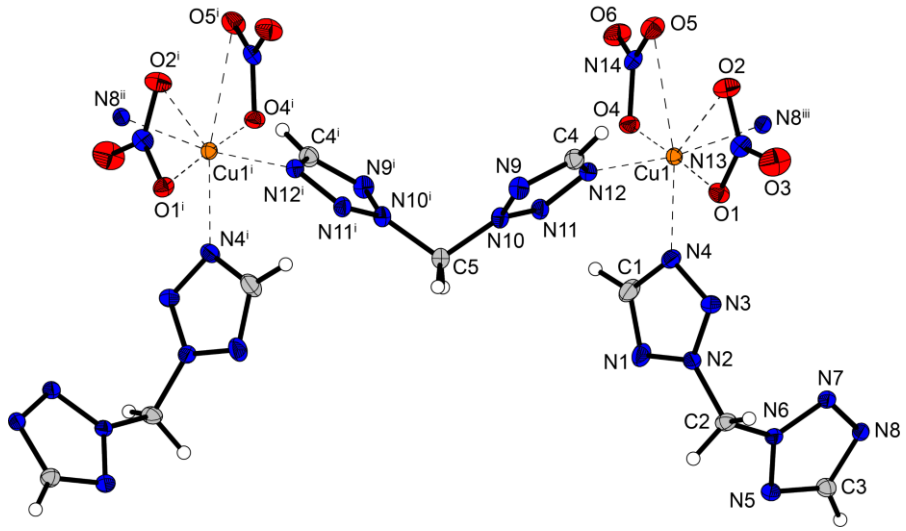

Figure 13. Copper(II) coordination environment of dimeric compound **9**. Selected bond lengths (Å): Cu1–O1 1.9927(14), Cu1–O2 2.7352(16), Cu1–O4 1.9570(14), Cu1–N4 2.2444(16), Cu1–N12 2.0286(16). Selected bond angles (°): O1–Cu1–O2 52.05(5), O1–Cu1–O4 177.48(6), O1–Cu1–O5 130.04(5), O1–Cu1–N4 89.27(6), O1–Cu1–N12 85.95(6), O1–Cu1–N8^{iii} 90.03(6). Symmetry codes: (i) 0.5−x, y, 1−z; (ii) −0.5+x, −y, 1+z; (iii) 1−x, −y, −z.

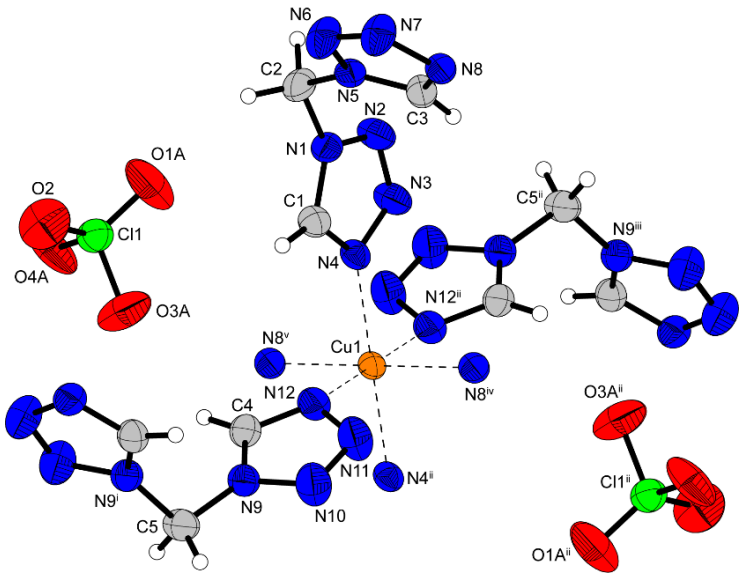

Figure 14. Extended molecular structure of copper(II) perchlorate complex **10**. Selected bond lengths (Å): Cu1–N4 2.0378(19), Cu1–N12 2.313(2), Cu1–N8^{iv} 2.071(2). Selected bond angles (°): N4–Cu1–N12 91.30(8), N4–Cu1–N4^{ii} 180.00, N4–Cu1–N8^{iv} 91.66(8). Symmetry codes: (i) −x, y, 0.5−z; (ii) 0.5−x, 0.5−y, 1−z; (iii) 0.5+x, 0.5−y, 0.5+z; (iv) −x, 1−y, 1−z; (v) 0.5+x, −0.5+y, z.

10 and **11** are forming similar 3D networks by the connection of one central metal to four other ones. In **10**, pairs of equatorial ligands are bridging between the same two copper(II) cations building up polymeric chains. Each ligand in the axial position is linking to another chain, and the strands are twisted at around 90° to each other leading to the formation of 3D-polymeric structures. A similar case can be observed in **11** with the only exception that pairs of one axial and one equatorial ligand are building up chains and the remaining equatorial ligands are responsible for the further linking.

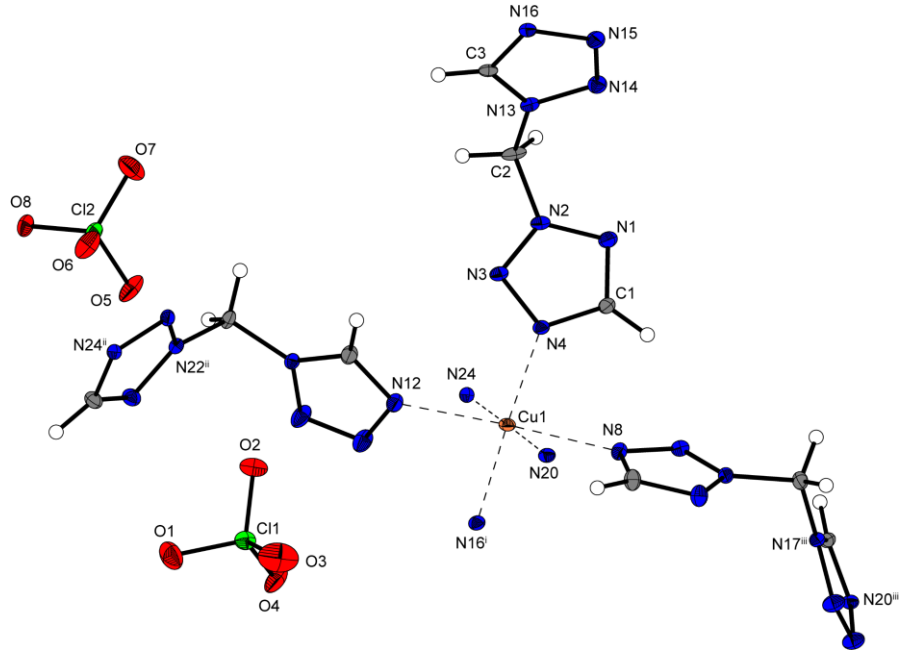

Figure 15. Extended molecular structure of copper(II) perchlorate complex **11**. Selected bond lengths (Å): Cu1–N4 2.0084(18), Cu1–N8 2.445(2), Cu1–N24 2.0398(18). Selected bond angles (°): N4–Cu1–N8 89.59(7), N4–Cu1–N12 92.93(7), N8–Cu1–N12 177.15(6). Symmetry codes: (i) 0.5+x, 0.5−y, 0.5+z; (ii) −x, 1−y, 1−z; (iii) 1−x, −y, 1−z.

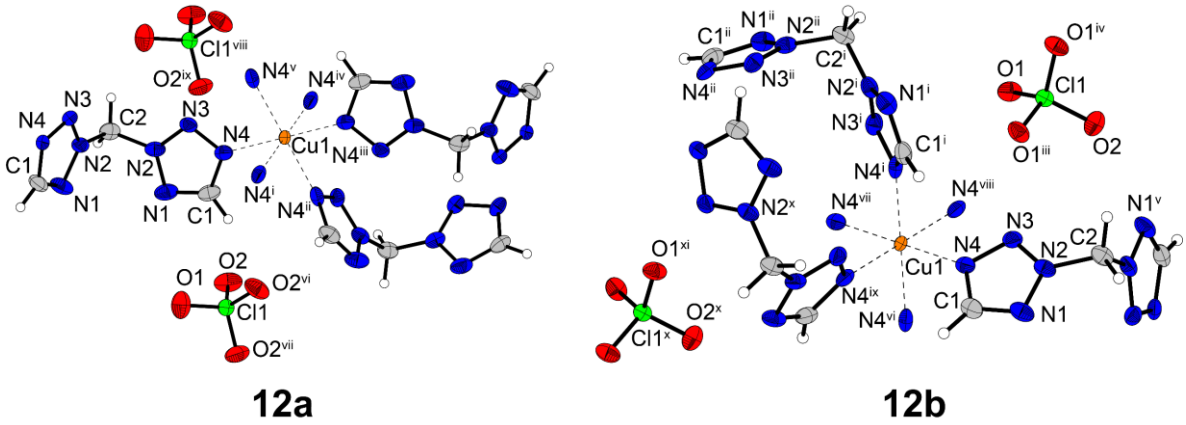

Figure 16. Copper(II) coordination environments of the two different polymorphs of **12**. Selected bond length of **12a** (Å): Cu1–N4 2.131(3). Selected bond angles of **12a** (°): N4–Cu1–N4^{i} 88.37(11), N4–Cu1–N4^{iii} 180.00, N4–Cu1–N4^{iv} 91.63(11). Symmetry codes of **12a**: (i) −y, x−y, z; (ii) x−y, x, −z; (iii) −x, −y, −z; (iv) y, −x+y, −z; (v) −x+y, −x, z; (vi) −x+y, −1−x, z; (vii) −1−y, −1+x−y, z; (viii) x, 1+y, z; (ix) −1−y, x−y, z. Selected bond length of **12b** (Å): Cu1–N4 2.133(2). Selected bond angles of **12b** (°): N4–Cu1–N4^{vi} 90.86(11), N4–Cu1–N4^{vii} 180.00, N4^{vi}–Cu1–N4^{vii} 89.14(11). Symmetry codes of **12b**: (i) y, −x+y, −z; (ii) x, x−y, −0.5+z; (iii) 1−x+y, 1−x, z; (iv) 1−y, x−y, z; (v) y, x, 0.5−z; (vi) −y, x−y, z; (vii) −x, −y, −z; (viii) −x+y, −x, z; (ix) x−y, x, −z; (x) −x+y, y, −0.5+z; (xi) −y, 1−x, −0.5+z.

Whereas **10** and **11** are forming higher polymeric structures, both polymorphs of **12** are present as 1D chains. In **12a** as well as **12b**, three ligands are bridging between the same two copper(II) cations facilitating the formation of single strands. The only difference in the structures is the arrangement of the two tetrazole rings within the ligand molecules. Whereby in **12a** the carbon atoms are pointing in the

same direction, they are opposite in **12b**. This affects the copper-copper distances within the chains (**12a**: ~8.3 Å; **12b**: ~7.5 Å) and is therefore also influencing the compounds' densities (**12a**: 1.913 g cm^{-3}; **12b**: 2.003 g cm^{-3}). In both cases, the polymeric chains are conjoined over hydrogen bonds and the interaction with the perchlorate anions (Figure 17).

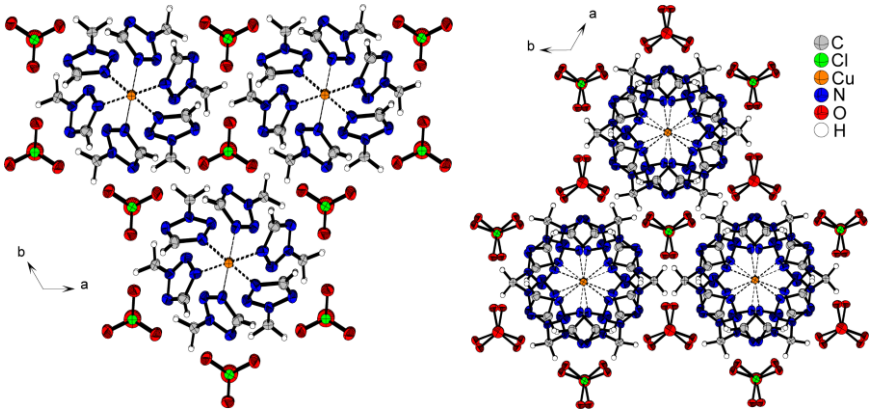

Figure 17. Polymeric structures of **12a** with parallel and **12b** with antiparallel arranged tetrazole rings viewed along the *c* axis.

The nitroaromatic complexes **13** and **15** based on **1** show a similar buildup. In both cases, the copper(II) central metals are coordinated by four aqua and two ditetrazole ligands, which are only binding with one of their heterocycles. The complex monomers are completed by two non-coordinating and single-deprotonated anions (Figures 18 and S5).

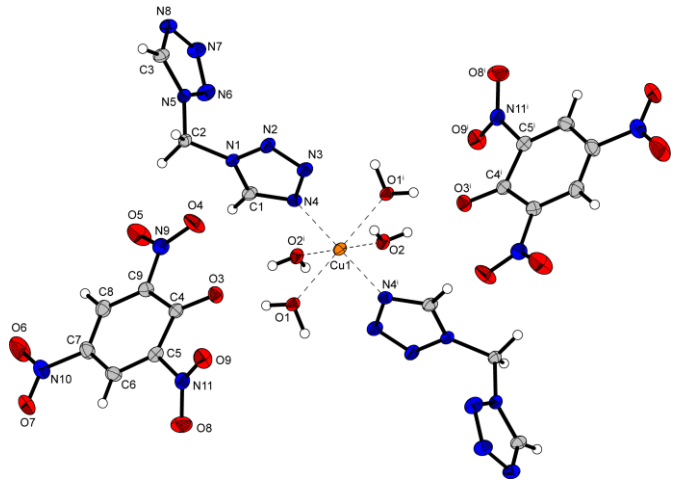

Figure 18. Molecular unit of picrate complex **13**. Selected bond lengths (Å): Cu1–O1 2.3139(18), Cu1–O2 2.003(2), Cu1–N4 2.002(2). Selected bond angles (°): O1–Cu1–O2 92.46(7), O1–Cu1–N4 85.98(7), O1–Cu1–O1^{i} 180.00. Symmetry code: (i) 1−x, −y, −z.

Each anion is forming hydrogen bonds to two of the aqua ligands. In contrast to **13** and **15**, a double-deprotonated anion and bridging ligand is present in **14**. This is leading on the one side to a chelating effect and on the other side also to a linking of the styphnate between two copper(II) cations. The molecular unit is completed by an additional crystal water molecule (Figure 19).

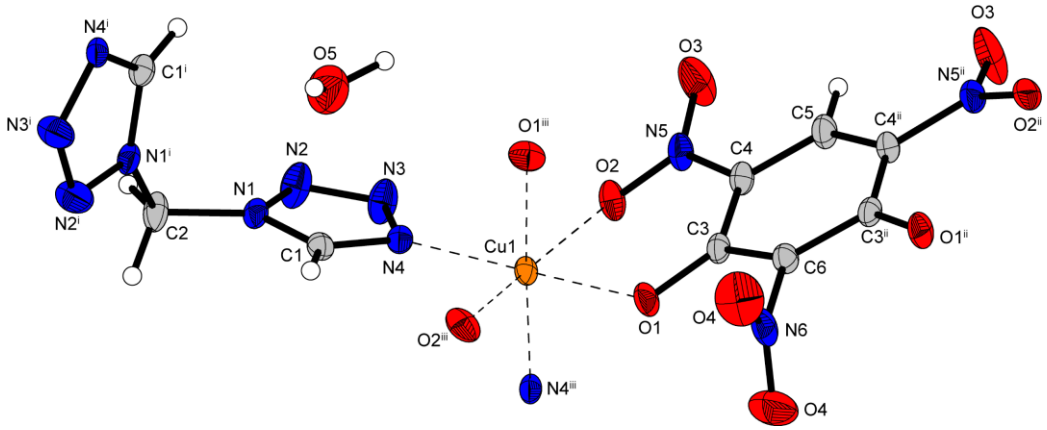

Figure 19. Copper(II) coordination environments of styphnate compound **14**. Selected bond lengths (Å): Cu1–O1 1.9380(15), Cu1–O2 2.2690(15), Cu1–N4 2.0084(17). Selected bond angles (°): O1–Cu1–O2 82.43(6), O1–Cu1–N4 177.66(7), O2–Cu1–N4 99.16(6). Symmetry codes: (i) 1.75−x, 0.75–y, z; (ii) 0.25−x, y, 0.25−z; (iii) 0.75−x, 0.75−y, z.

The bridging of tetrazole and styphnate ligands is leading to the formation of polymeric chains. The crystal water molecules are embedded within holes of the chain and show interactions with non-coordinating nitro groups twisted from the ring plane (Figure 20).

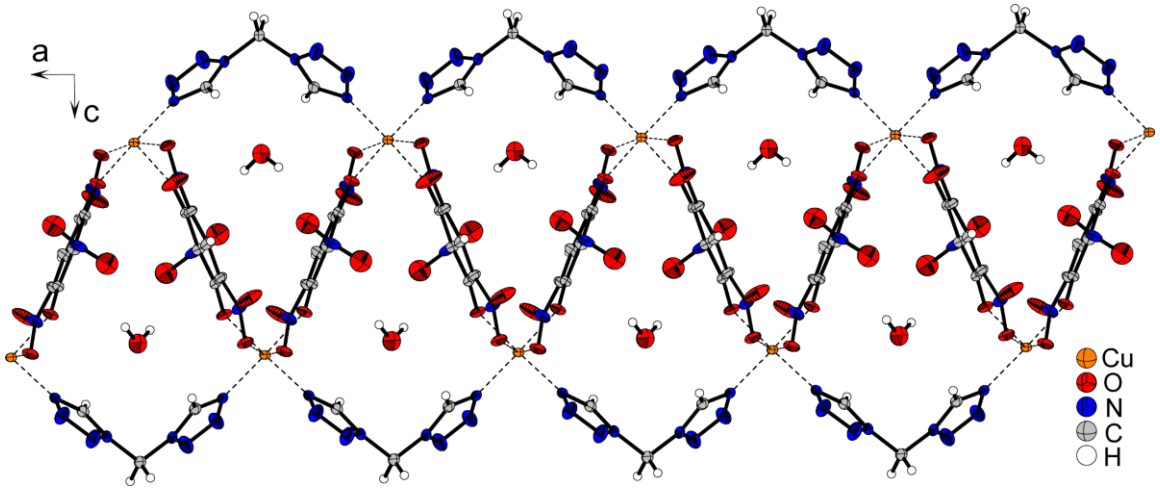

Figure 20. Polymeric structure of **15** view along the *b* axis.

The polymeric structure is also increasing the density of **14** (1.973 g cm^{-3} @ 103 K) compared to **13** and **15** (1.757 g cm^{-3} @ 119 K and 1.810 g cm^{-3} @ 122 K, respectively). Complexes **16**–**18** crystallize in triclinic (*P*−1 (**16**)) or monoclinic (*C*2/*c* (**17**) and *P*2$_1$/*n* (**18**)) space groups and show a similar buildup. The molecular units consist of one central atom with two aqua as well as two bridging ligands of **2** and two single-deprotonated, non-coordinating anions (Figures 21, S6, and S7). The main difference of the three complexes is the level of Jahn-Teller distortion along the N5^{ii}–Cu–N5^{iii} (**16**), O1–Cu–O1^{i} (**17**), and N4–Cu–N4^{i} (**18**) axis. Like **13** and **15**, the anions in **16**–**18** are forming hydrogen bonds to the aqua ligands. The bridging of the ligands is reducing the number of water molecules and leading to the formation of polymeric chains in all three structures (Figure 22).

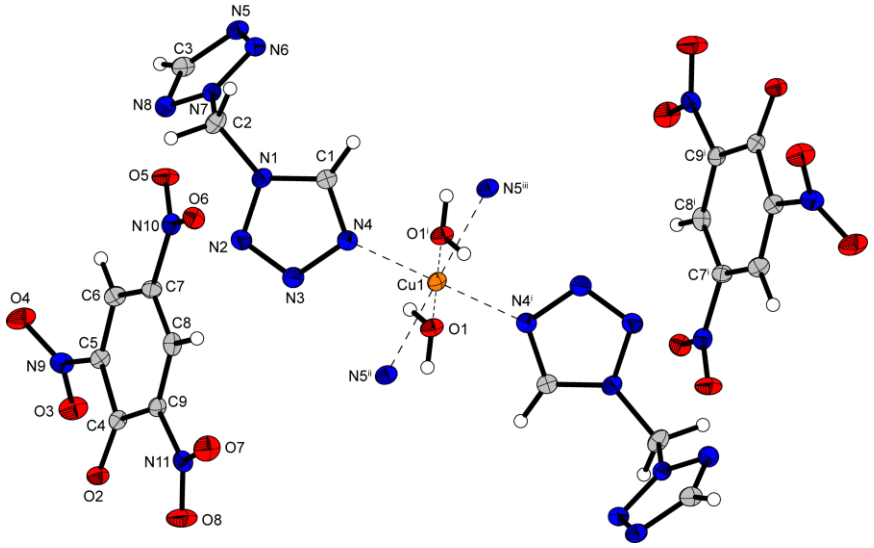

Figure 21. Copper(II) coordination environment of complex **16**. Selected bond lengths (Å): Cu1–O1 1.9778(19), Cu1–N4 2.015(3), Cu1–N5^{ii} 2.362(3). Selected bond angles (°): O1–Cu1–N4 90.41(9), O1–Cu1–N5^{iii} 91.53(9), N4–Cu1–N5^{iii} 89.61(11). Symmetry codes: (i) 2−x, 1−y, −z; (ii) 1+x, y, z; (iii) 1−x, 1−y, −z.

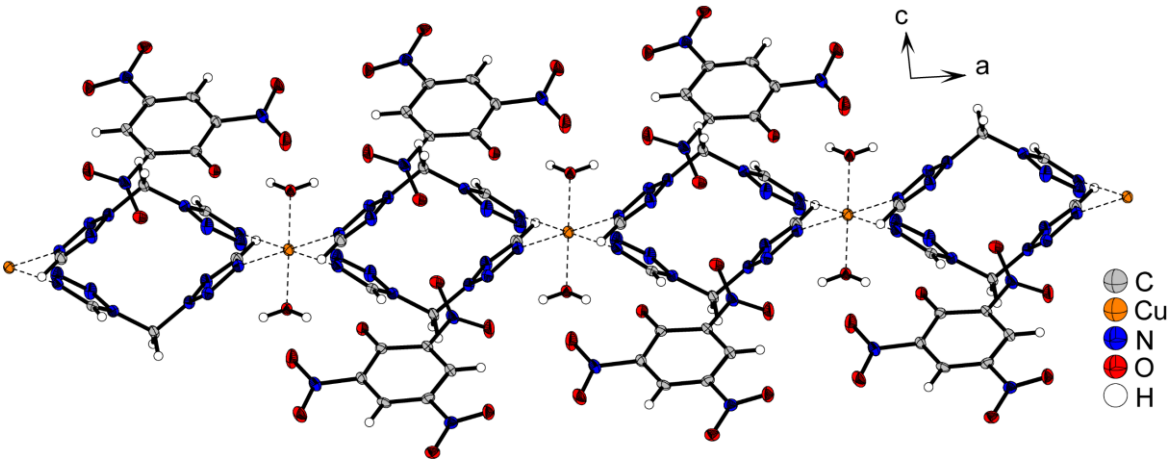

Figure 22. Polymeric structure of **16** viewed along the *b* axis.

6.2.4. Thermal Stability and Sensitivity Measurements

The three ligands and all complexes were examined with respect to their thermal behavior in differential thermal analysis (DTA), and their stability against external stimuli (impact (IS), friction (FS), electrostatic discharge (ESD), and ball drop impact (BDIS) sensitivities) was determined. All values are summarized in Table 2 together with the compounds' outcome in the hot needle and hot plate tests. The DTA experiments were performed with a heating rate of $\beta = 5$ °C min^{-1} in the range of 35–400 °C, and the critical points, such as melting, dehydration, or exothermic decomposition, are given as onset temperatures. Except for **4**, **5**, and **18**, all complexes show a higher thermal stability than the respective ligand. The highest decomposition temperatures are achieved by copper(II) perchlorate complexes **10**–**12** as well as styphnate compound **14**, which all exceed 200 °C and **12** is even close to 250 °C (242 °C).

Table 2. Summary of the compounds' thermal stability,[a] sensitivities toward various external stimuli and results of hot plate (HP) and hot needle (HN) tests compared to LA.[22]

	$T_{endo.}$[b] [°C]	$T_{exo.}$[c] [°C]	*IS*[d] [J]	*FS*[e] [N]	*ESD*[f] [mJ]	*BDIS*[g] [mJ]	HP[h]	HN[h]
1,1-dtm (**1**)	145	152	8	> 360	480	n.d.	n.d.	n.d.
1,2-dtm (**2**)	96	138	2	168	181	n.d.	n.d.	n.d.
2,2-dtm (**3**)	58	184	1.5	84	160	n.d.	n.d.	n.d.
$[Ag(1,1\text{-dtm})_2]NO_3$ (**4**)	132	136	4	144	450	> 200	def.	dec.
$[Ag(1,2\text{-dtm})_3]NO_3$ (**5**)	113	124	2	108	540	124	def.	def.
$[Ag(NO_3)(2,2\text{-dtm})]$ (**6**)	166	186	3	36	380	124	def.	def.
$[Ag(1,1\text{-dtm})_2]ClO_4$ (**7**)	-	163	≤ 1	30	1080	28	def.	def.
$[Ag(1,2\text{-dtm})_4]ClO_4$ (**8**)	132	140	≤ 1	50	226	20	def.	def.
$[Cu_2(NO_3)_4(2,2\text{-dtm})_3]$ (**9**)	-	198	1.5	30	> 1500	16	def.	def.
$[Cu(1,1\text{-dtm})_3](ClO_4)_2$ (**10**)	-	230	≤ 1	0.75	42	12	def.	def.
$[Cu(1,2\text{-dtm})_3](ClO_4)_2$ (**11**)	-	215	1.5	1	47	≤ 4	det.	det.
$[Cu(2,2\text{-dtm})_3](ClO_4)_2$ (**12**)	-	242	≤ 1	0.75	37	≤ 4	det.	def.
$[Cu(H_2O)_4(1,1\text{-dtm})_2](PA)_2$ (**13**)	108	185	6	> 360	840	> 200	dec.	dec.
$[Cu(TNR)(1,1\text{-dtm})] \cdot H_2O$ (**14**)	-	236	2	192	188	66	def.	dec.
$[Cu(H_2O)_4(1,1\text{-dtm})_2](H_2TNPG)_2$ (**15**)	74	196	4	48	960	16	def.	dec.
$[Cu(H_2O)_2(1,2\text{-dtm})_2](PA)_2$ (**16**)	122	159	1	> 360	750	> 200	dec.	dec.
$[Cu(H_2O)_2(1,2\text{-dtm})_2](HTNR)_2$ (**17**)	132	156	7	144	1500	> 200	def.	dec.
$[Cu(H_2O)_2(1,2\text{-dtm})_2](H_2TNPG)_2$ (**18**)	-	136	1.5	128	1350	> 200	def.	dec.
$Pb(N_3)_2$	-	320–360	2.5–4	0.1–1.0	7	37	det.	det.

[a] Onset temperature at a heating rate of 5 °C min^{-1} measured by DTA. [b] Endothermic peak, which indicates melting, dehydration, or loss of aqua ligands. [c] Exothermic peak, which indicates decomposition. [d] Impact sensitivity according to the BAM drop hammer (method 1 of 6). [e] Friction sensitivity according to the BAM friction tester (method 1 of 6). [f] Electrostatic discharge sensitivity (OZM Electric Spark XSpark10; method 1 of 6). [g] Ball drop impact sensitivity determined with the 1 of 6 method in accordance with the MIL-STD 1751A (method 1016). [h] Abbreviations: dec.: decomposition; def.: deflagration; det.: detonation.

Silver nitrate complexes **4** and **5** possess the lowest thermal stability (136 and 124 °C, respectively) as well as **18** with 136 °C (Figure 23). Interestingly, no endothermic event can be observed for the water containing compounds **14** and **18**. Therefore, they were further investigated using thermal gravimetric analysis (TGA).

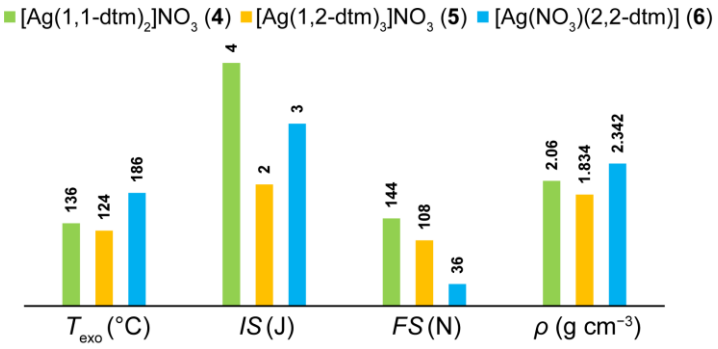

Figure 23. Comparison of the sensitivities and thermal stability of the silver nitrate complexes as well as dependency of the densities (recalculated to room temperature) on ligand content.

The measurements clearly reveal the slow evaporation of the crystal water molecule in **14** before the compound decomposes, whereas in **18** no evaporation can be detected (Figure 24).

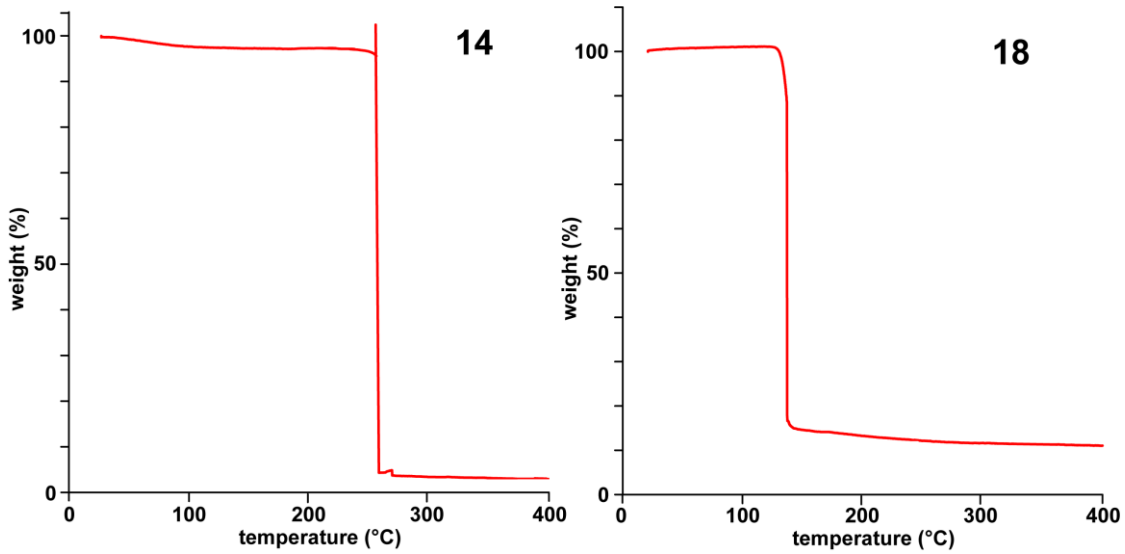

Figure 24. TGA plots of compounds **14** and **18**.

This and the relatively low decomposition temperature (136 °C) lead to the assumption that the complex stability immediately breaks down when the aqua ligands start to evaporate. The determined sensitivities have been used to classify the compounds in accordance with the "UN Recommendations on the Transport of Dangerous Goods".[23] In general, all complexes must be ranked as sensitive (**4**, **13**, **15**, and **17**) or very sensitive toward impact, and the only two coordination compounds which are insensitive toward friction are the picrate complexes **13** and **16**. Except for **15** (very sensitive), all other trinitrophenolates can be classified as sensitive toward friction. While the copper(II) perchlorate complexes **10**–**12** are extremely sensitive toward friction (0.75–1 N), **9** and all silver compounds can be categorized as sensitive (**4** and **5**) or very sensitive (**6**–**9**). Comparing the BDIS, which gives more realistic test conditions,[22b] it becomes clear that especially the perchlorate ECC but also compounds **9** and **15** are even more sensitive than LA.

6.2.5. Energetic Performance and Initiation Tests

For getting insight into the energetic behavior of the compounds, hot plate (HP) and hot needle (HN) tests of all complexes were performed (Table 2, Figures 25 and S12–S17). While the HP test only shows the performance of the unconfined samples during fast heating, the HN test allows an insight of their confined manners and therefore their potential use as primary explosives. All nitroaromatic compounds show decompositions or weak deflagrations during both tests, which is not surprising due to the presence of aqua ligands or crystal water molecules. Remarkably, all silver complexes possess only poor energetic performances with rather weak deflagrations or even decompositions (**4**) during the experiments. In contrast, the copper(II) perchlorate ECC show detonations or strong deflagrations, which makes them possible candidates for the initiation of secondary or booster explosives. Therefore, the three complexes **10**–**12** were investigated in classical initiation capability tests with PETN (nitropenta) as the main charge.

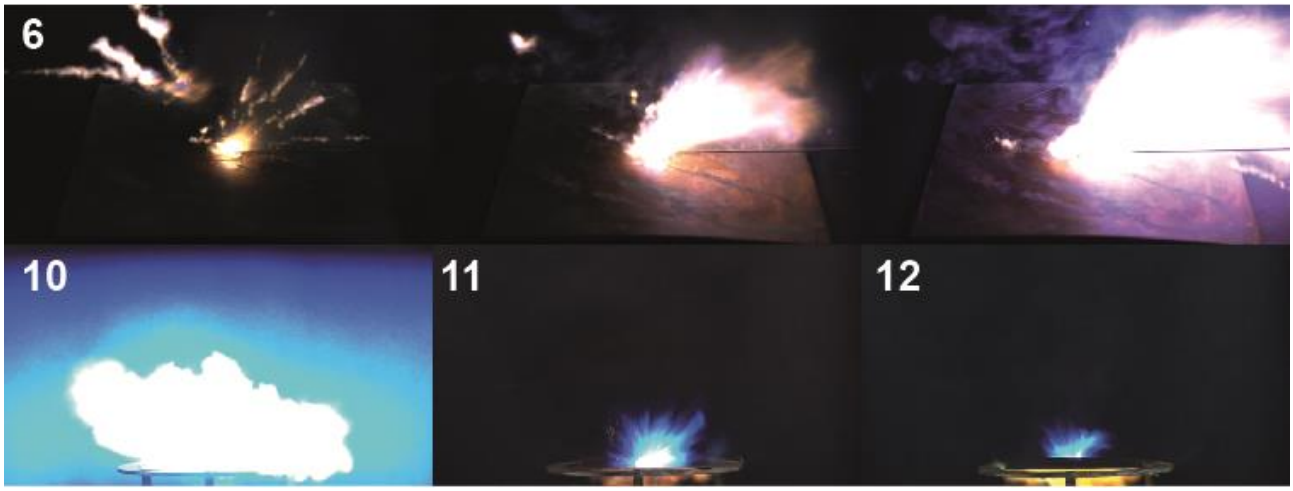

Figure 25. Top: HN test of nitrate compound **6** shown as a sequence; bottom: moments of deflagration (**10**) or detonation (**11** and **12**) of copper(II) perchlorate complexes during the HP tests.

Details on the setup can be found in the Supporting Information. Compounds **11** and **12** were able to cause a positive deflagration-to-detonation transition (DDT) toward the booster explosive, which is indicated by a hole in the copper witness plate and fragmentation of the shell (Figure 26).

Figure 26. Positive results of the initiation capability tests toward PETN of compounds **11** (left) and **12** (right).

In contrast, no positive results were achieved (even in the case of using unpressed PETN) when **10** was applied as primary explosive. Furthermore, all colored ECC **9**–**18** were tested in laser ignition experiments using an InGaAs laser diode working in the single-pulsed mode. The results are in accordance with our previous findings, and details of the test setup are given in the Supporting Information.[24] All nitroaromatic complexes solely show decomposition when irradiated associated with the generation of smoke (Figure 27). The application of a 20 mJ beam on **9** leads to a strong deflagration, whereas the perchlorate complexes **10**–**12** show very strong detonations with an energy input of only 0.2 mJ. Compound **10** detonated violently resulting in the destruction of the sapphire glass, which usually protects the laser lens.

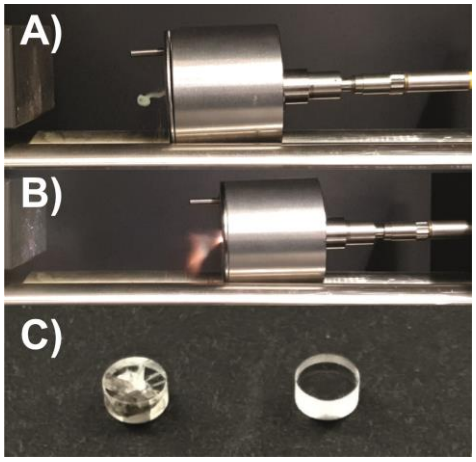

Figure 27. Results of the laser initiation tests: A) decomposition of picrate complex **13**; B) moment of deflagration of nitrate compound **9**; and C) comparison of destroyed (left) sapphire glass with a new one (right) after detonation of **10**.

6.3. Conclusion

For the first time the nitrogen-rich compounds di(tetrazol-1-yl)methane (1,1-dtm, **1**), (tetrazol-1-yl)(tetrazol-2-yl)methane (1,2-dtm, **2**), and di(tetrazol-2-yl)methane (2,2-dtm, **3**) were synthesized by the reaction of triethylammonium 5*H*-tetrazolate with dibromomethane in a one-step reaction and exhaustively characterized, *e.g.*, using two-dimensional ^{1}H-^{15}N-HMBC NMR spectroscopy, X-ray studies (**2**: 1.605 g cm^{-3}, *Fdd*2) < **3**: 1.632 g cm^{-3}, *Fdd*2 < (**1**) 1.637 g cm^{-3}, $P2_1/c$), and Hirshfeld surface calculations. The coordination behavior of the three ligands was studied in detail leading to 15 new energetic coordination compounds (ECC) based on silver(I) and copper(II) as well as different oxidizing anions (nitrate, perchlorate, picrate, styphnate, and trinitrophloroglucinate). The appropriate selection of central metal, anion, and dtm isomer allowed the accurate tuning of the compounds' properties. The combination of the ligands with copper(II) perchlorate results in the formation of powerful and thermally highly stable primary explosives with very efficient performance. Especially ECC **11** and **12** show very good initiation capabilities of PETN. The utilization of nitrate as a building block is increasing the stability toward external stimuli and in the case of **9** allows its use as a laser ignitable explosive with decreased sensitivities. Interestingly, in most cases, complex formation improves thermal stability compared to pure ligands. The crystal structures reveal a high degree of diversity for the coordination of the three different isomers. Due to the potential bridging character of the ligands, most of the complexes form polymeric structures with differing dimensionality. However, especially compared to other 5*H*-ditetrazolyl ligands, **1**–**3** have comparatively often a terminal coordination behavior, which is highly influencing the polymeric structures and even leading in some cases to the formation of complex monomers. Moreover, exceptional coordination spheres, like a 5-fold bounding to silver(I) in complex **6** or a distorted pentagonal bipyramidal geometry around Cu^{2+} in ECC **9**, can be observed.

6.4. Acknowledgements

Financial support of this work by Ludwig-Maximilians-University (LMU), the Office of Naval Research (ONR) under grant no. ONR N00014-19-1-2078, and the Strategic Environmental Research and Development Program (SERDP) under contract no. W912HQ19C0033 is gratefully acknowledged. The authors would also like to thank Prof. Dr. Konstantin Karaghiosoff for the measurement of the two-dimensional ^{1}H-^{15}N-HMBC NMR spectra and Mr. Sebastian Hagenrainer for his great contribution to this work.

6.5. References

[1] (a) R. N. Butler, *Compr. Heterocycl. Chem.* **1984**, *5*, 791–838; (b) V. A. Ostrovskii, G. I. Koldobskii, R. E. Trifonov, *Compr. Heterocycl. Chem. III.* **2008**, *6*, 257–423.

[2] V. A. Ostrovskii, E. A. Popova, R. E. Trifonov, *Adv. Heterocycl. Chem.* **2017**, *123*, 1–62.

[3] P. N. Gaponik, V. P. Karavai, Yu. V. Grigor'ev, *Khim. Geterotsikl. Soedin.* **1985**, *11*, 1521–1524.

[4] P. J. van Koningsbruggen, Y. Garcia, O. Kahn, L. Fournes, H. Kooijman, A. L. Spek, J. G. Haasnoot, J. Moscovici, K. Provost, A. Michalowicz, F. Renz, P. Gütlich, *Inorg. Chem.* **2000**, *39*, 1891–1900.

[5] J.-H. Yu, K. Mereiter, N. Hassan, C. Feldgitscher, W. Linert, *Cryst. Growth Des.* **2008**, *8*, 1535–1540.

[6] (a) J. Schweifer, P. Weinberger, K. Mereiter, M. Boca, C. Reichl, G. Wiesinger, G. Hilscher, P. J. van Koningsbruggen, H. Kooijman, M. Grunert, W. Linert, *Inorg. Chim. Acta* **2002**, *339*, 297–306; (b) A. Absmeier, M. Bartel, C. Carbonera, G. N. L. Jameson, P. Weinberger, A. Caneschi, K. Mereiter, J.-F. Létard, W. Linert, *Chem. – Eur. J.* **2006**, *12*, 2235–2243; (c) C. M. Grunert, J. Schweifer, P. Weinberger, W. Linert, *Inorg. Chem.* **2004**, *43*, 155–165.

[7] A. Absmeier, M. Bartel, C. Carbonera, G. N. L. Jameson, F. Werner, M. Reissner, A. Caneschi, J.-F. Létard, W. Linert, *Eur. J. Inorg. Chem.* **2007**, *2007*, 3047–3054.

[8] (a) A. Białońska, R. Bronisz, *Inorg. Chem.* **2010**, *49*, 4534–4542; (b) R. Bronisz, *Inorg. Chim. Acta* **2002**, *340*, 215–220; (c) A. Białońska, R. Bronisz, *Inorg. Chem.* **2012**, *51*, 12630–12637; (d) R. Bronisz, *Inorg. Chim. Acta* **2004**, *357*, 396–404.

[9] (a) P. J. van Koningsbruggen, Y. Garcia, H. Kooijman, A. L. Spek, J. G. Haasnoot, O. Kahn, J. Linares, E. Codjovi, F. Varret, *J. Chem. Soc. Dalton Trans.* **2001**, *4*, 466–471; (b) C. Baldé, M. S. Sylla, C. Desplanches, G. Chastanet, *Polyhedron* **2019**, *159*, 84–92.

[10] (a) P. J. van Koningsbruggen, Y. Garcia, G. Bravic, D. Chasseau, O. Kahn, *Inorg. Chim. Acta* **2001**, *326*, 101–105; (b) P.-P. Liu, A.-L. Cheng, N. Liu, W.-W. Sun, E.-Q. Gao, *Chem. Mater.* **2007**, *19*, 2724–2726; (c) P.-P. Liu, Y.-Q. Wang, C.-Y. Tian, H.-Q. Peng, E.-Q. Gao, *J. Mol. Struct.* **2009**, *920*, 459–465; (d) C. Knoll, D. Müller, M. Seifried, G. Giester, J. M. Welch, W. Artner, K. Hradil, M. Reissnere, P. Weinberger, *Dalton Trans.* **2018**, *47*, 5553–5557.

[11] (a) J.-G. Xu, X.-Z. Li, H.-F. Wu, F.-K. Zheng, J. Chen, G.-C. Guo, *Cryst. Growth Des.* **2019**, *19*, 3934–3944; (b) M. Joas, U. Deisenroth, DE Patent 102016120539 A1 20180503, Germany **2018**; (c) M. H. H. Wurzenberger, N. Szimhardt, J. Stierstorfer, *J. Am. Chem. Soc.* **2018**, *140*, 3206–3209; (d) J.-G. Xu, S.-J. Lin, X.-Z. Li, H.-F. Wu, J. Lu, W.-F. Wang, J. Chen, F.-K. Zheng, G.-C. Guo, *Chem. Eng. J.* **2020**, *390*, 124587.

[12] https://echa.europa.eu/de/candidate-list-table, (accessed June 2020).

[13] T. M. Klapötke, N. Mehta, *Propellants Explos. Pyrotech.* **2014**, *39*, 7–8.

[14] (a) T. W. Myers, J. A. Bjorgaard, K. E. Brown, D. E. Chavez, S. K. Hanson, R. J. Scharff, S. Tretiak, J. M. Veauthier, *J. Am. Chem. Soc.* **2016**, *138*, 4685–4692; (b) Q. Sun, X. Li, Q. Lin, M. Lu, *J. Mater. Chem. A* **2019**, *7*, 4611–4618; (c) Q. Zhang, J. M. Shreeve, *Angew. Chem. Int. Ed.* **2014**, *53*, 2540–2542; (d) M. A. Ilyushin, A. A. Kotomin, S. A. Dushenok, *Russ. J. Phys. Chem. B* **2019**, *13*, 119–138.

[15] (a) K. B. Landenberger, O. Bolton, A. J. Matzger, *J. Am. Chem. Soc.* **2015**, *137*, 5074–5079; (b) A. A. Larin, N. V. Muravyev, A. N. Pivkina, K. Yu Suponitsky, I. V. Ananyev, D. V. Khakimov, L. L. Fershtat, N. N. Makhova, *Chem. – Eur. J.* **2019**, *25*, 4225–4233; (c) L. M. Barton, J. T. Edwards, E. C. Johnson, E. J. Bukowski, R. C. Sausa, E. F. C. Byrd, J. A. Orlicki, J. J. Sabatini, P. S. Baran, *J. Am. Chem. Soc.* **2019**, *141*, 12531–12535; (d) A. F. Baxter, I. Martin, K. O. Christe, R. Haiges, *J. Am. Chem. Soc.* **2018**, *140*, 15089–15098.

[16] D. Müller, C. Knoll, B. Stöger, W. Artner, M. Reissner, P. Weinberger, *Eur. J. Inorg. Chem.* **2013**, *2013*, 984–991.

[17] N. Szimhardt, M. H. H. Wurzenberger, T. M. Klapötke, J. T. Lechner, H. Reichherzer, C. C. Unger, J. Stierstorfer, *J. Mater. Chem. A* **2018**, *6*, 6565–6577.

[18] (a) J. Zhang, Q. Zhang, T. T. Vo, D. A. Parrish, J. M. Shreeve, *J. Am. Chem. Soc.* **2015**, *137*, 1697–1704; (b) Y. Liu, G. Zhao, Q. Yu, Y. Tang, G. H. Imler, D. A. Parrish, J. M. Shreeve, *J. Org. Chem.* **2019**, *84*, 16019–16026.

[19] M. Sućeska, *EXPLO5*, Version 6.05.02; Zagreb, **2018**.

[20] (a) E.-Q. Gao, P.-P. Liu, Y.-Q. Wang, Q. Yue, Q.-L. Wang, *Chem. – Eur. J.* **2009**, *15*, 1217–1226; (b) M. Quesada, H. Kooijman, P. Gamez, J. Sánchez Costa, P. J. van Koningsbruggen, P. Weinberger, M. Reissner, A. L. Spek, J. G. Haasnoot, J. Reedijk, *Dalton Trans.* **2007**, *6*, 5434–5440; (c) M. H. H. Wurzenberger, N. Szimhardt, J. Stierstorfer, *Inorg. Chem.* **2018**, *57*, 7940–7949; (d) P.-P. Liu, A.-L. Cheng, Q. Yue, N. Liu, W.-W. Sun, E.-Q. Gao, *Cryst. Growth Des.* **2008**, *8*, 1668–1673.

[21] CCDC 1988649 (**1**), 1988643 (**2**), 1988633 (**3**), 1988648 (**4**), 1988639 (**5**), 1988636 (**6**), 1988647 (**7**), 1988642 (**8**), 1988637 (**9**), 1988644 (**10**), 1988651 (**11**), 1988640 (**12a**), 1988638 (**12b**), 1988650 (**13**), 1988641 (**14**), 1988634 (**15**), 1988635 (**16**), 1988646 (**17**), and 1988645 (**18**) contain the supplementary crystallographic data for this paper. These data are provided free of charge by The Cambridge Crystallographic Data Centre.

[22] (a) T. M. Klapötke, *Energetic Materials Encyclopedia*, 1st ed., De Gruyter, Berlin,Boston, **2018**; (b) M. S. Gruhne, M. Lommel, M. H. H. Wurzenberger, N. Szimhardt, T. M. Klapötke, J. Stierstorfer, *Propellants Explos. Pyrotech.* **2020**, *45*, 147–153.

[23] Impact: insensitive > 40 J, less sensitive ≥ 35 J, sensitive ≥ 4 J, very sensitive ≤ 3 J. Friction: insensitive > 360 N, less sensitive = 360 N, sensitive < 360 N and > 80 N, very sensitive ≤ 80 N, extremely sensitive ≤ 10 N. According to the UN Recommendations on the Transport of Dangerous Goods, 5th ed., **2009**.

[24] M. H. H. Wurzenberger, M. S. Gruhne, M. Lommel, N. Szimhardt, T. M. Klapötke, J. Stierstorfer, *Chem. – Asian J.* **2019**, *14*, 2018–2028.

6.6. Supporting Information

6.6.1. Experimental Part and General Methods

All chemicals and solvents were employed as received (Sigma-Aldrich, Fluka, Acros, ABCR). ^{1}H, ^{13}C and ^{15}N spectra were recorded at ambient temperature using a JEOL Bruker 400, Eclipse 270, JEOL EX 400 or a JEOL Eclipse 400 instrument. The chemical shifts quoted in ppm in the text refer to typical standards such as tetramethylsilane (^{1}H, ^{13}C) and nitromethane (^{15}N) in d_6-DMSO or d_3-MeCN as the solvents. The ^{1}H-^{15}N-HMBC NMR spectra were measured with a data matrix of 1024 x 256, an applied zero filling of 2048 x 4096, 32 scans per round, a relaxation delay of 1 second, an acquisition time of 0.3 seconds at a concentration of 140 mg/mL and an overall measurement time of approx. 3 h. Exothermic events of the described compounds, which indicate decomposition, are given as the extrapolated onset temperatures. The samples were measured in a range of 25–300 °C at a heating rate of 5 °C min^{-1} through differential thermal analysis (DTA) with an OZM Research DTA 552-Ex instrument and in some cases additional by thermal gravimetric analysis (TGA) with a PerkinElmer TGA4000. Infrared spectra were measured with pure samples on a Perkin-Elmer BXII FT-IR system with a Smith DuraSampler IR II diamond ATR. Determination of the carbon, hydrogen and nitrogen contents was carried out by combustion analysis using an Elementar Vario El (nitrogen values determined are often lower than the calculated ones due to their explosive behavior). Impact sensitivity tests were carried out according to STANAG 4489[1] with a modified instruction[2] using a BAM (Bundesanstalt für Materialforschung und -prüfung) drop hammer.[3,4] Ball drop impact sensitivity tests were determined for selected compounds on an OZM ball drop machine (BIT-132), following MIL-STD-1751A (method 1016) by dropping a free falling steel ball onto the explosive compound.[5] A sample of approximately 30 mg was placed on a steel block and spread into a 0.33 mm layer of substance. The steel ball guide was set to the desired height and the loaded impact block positioned underneath. By releasing the ball shield, a 0.500-inch steel ball, weighing 8.35 g, was allowed to fall onto the sample. Any visual observation of decomposition was regarded as a positive result. If no reaction occurred, the remaining substance was disposed, and the impact block loaded with a freshly prepared sample. The limiting impact energy was determined in conformity with the recommended UN method for testing impact and friction sensitivities (1-in-6

approach), according to ST/SG/AC.10/11Rev.6 (s. 13.4.2.3.3).[6] The impact energy was calculated as the product of the weight of the steel ball and its fall height. An initial drop height was chosen, at which an explosion of the sample could be ensured. The impact energy level (ball guide height) was now stepwise decreased until no reaction was observed. At this point, testing was continued up to a total of six trials at that certain energy level. If an explosion occurred, the procedure was repeated by decreasing the drop height. As soon as six trials at a fixed energy level emerged as negative, the next higher energy level, where at least one out of at least six trials resulted in an explosion, is determined as the limiting impact energy. Friction sensitivity tests were carried out according to STANAG 4487[7] with a modified instruction[8] using the BAM friction tester. The classification of the tested compounds results from the "UN Recommendations on the Transport of Dangerous Goods".[9] Additionally all compounds were tested upon the sensitivity toward electrical discharge using the OZM Electric Spark XSpark10 device.[3] Hot plate and hot needle tests were performed in order to classify the initiation capability of selected complexes. The samples were fixed on a copper plate underneath adhesive tape and initiated by a red-hot needle. Strong deflagration or detonation of the compound usually indicates a valuable primary explosive. The safe and straightforward hot plate test only shows the behavior of the unconfined sample toward fast heating on a copper plate. It does not necessarily allow any conclusions on a compound´s capability as a suitable primary explosive. Initiation capability tests of the newly investigated complexes toward pentaerythritol tetranitrate (PETN) were carried out in a copper shell with a diameter of 7 mm and a length of 88 mm filled with 200 mg of sieved PETN (grain size < 100 µm). First, nitropenta was pressed with a weight of 8 kg, then the primary explosive to be investigated was subsequently filled loosely on top of the main charge. The shell was sealed by an insulator, placed in a retaining ring, which was soldered to a copper witness plate with a thickness of 1 mm and finally initiated by a type A electric igniter. A positive test is indicated by a hole in the copper plate and fragmentation of the shell caused by a deflagration-to-detonation transition (DDT) of PETN. The laser initiation experiments were performed with a 45 W InGaAs laser diode operating in the single-pulsed mode. The diode is attached to an optical fiber with a core diameter of 400 µm and a cladding diameter of 480 µm. The optical fiber is connected via a SMA type connecter directly to the laser and to a collimator. This collimator is coupled to an optical lens, which was positioned in its focal distance (f = 29.9 mm) to the sample. The lens is shielded from the explosive by a sapphire glass. Approximately 15 mg of the carefully pestled compound to be investigated was filled into a transparent plastic cap (PC), pressed with a pressure force of 1 kN and sealed by a UV-curing adhesive. The confined samples were irradiated at a wavelength of 915 nm, a voltage of 4 V, a current of 8 A and pulse lengths of 0.1–10 ms. The combined currents and pulse lengths result in an energy output of 0.20 –20 mJ. Hirshfeld surfaces and the corresponding two-dimensional fingerprint plots were

generated with CrystalExplorer v17.5, using Tanto.[10] The images in the top of Figure 7 show fingerprint plots of the Hirshfeld surfaces. The blue color represents a low amount of contact populations whereas a red color represents high contact populations. In the bottom images, hydrogen interactions are highlighted in red. The Hirshfeld surfaces in the lower right corners show shorter atom contacts in red and longer contacts as blue and white areas. The di axis corresponds to the distance measured from the surface to the nearest atom inside of the surface, the de axis shows the distance from the surface to the nearest atom outside the surface.[11]

The obtained coordination compounds were washed with cold ethanol and acetonitrile when stated, dried overnight in air and used for analytics without further purification.

CAUTION! *All investigated compounds are highly energetic materials, which show increased sensitivities toward various stimuli (e.g., elevated temperatures, impact, friction or electrostatic discharge). Therefore, proper security precautions (safety glasses, face shield, earthed equipment and shoes, leather jacket, Kevlar gloves, Kevlar sleeves and ear plugs) have to be worn while synthesizing and handling the described compounds.*

Procedure for the preparation of the ditetrazolylmethane ligands

Triethylamine (114 mmol, 15.8 mL) was added to a suspension of 1,5*H*-tetrazole (114 mmol, 8.00 g) in acetone (40 mL) under continuous stirring. A solution of dibromomethane (57.0 mmol, 4.00 mL) in acetone (40 mL) was added and the resulting mixture was stirred at 60 °C for 5 days. After filtration, the solvent was evaporated under reduced pressure and the resulting orange oil was purified by column chromatography (SiO_2, gradient ethyl acetate/pentane 10:1.5, 10:1, 10:0.5, and ethyl acetate/methanol 10:1) yielding the isomers. 1,1-dtm (R_f(EtOAc) = 0.38) was obtained as colorless needles (3.78 mmol, 5.88 g, 7%), 1,2-dtm (R_f(EtOAc) = 0.70) as colorless blocks (7.47 mmol, 1.14 g, 13%) and 2,2-dtm (R_f(iHex/EtOAc 1:1) = 0.59) as yellowish crystals (5.33 mmol, 0.81 g, 9%).

1,1-dtm

DTA (5 °C min^{-1}) onset: 145 °C (endothermic), 152 °C (exothermic); IR (ATR, cm^{-1}): $\tilde{\nu}$ = 3147 (m), 3133 (m), 3023 (w), 2981 (w), 1763 (vw), 1491 (m), 1469 (m), 1443 (m), 1436 (m), 1425 (m), 1379 (w), 1314 (m), 1290 (w), 1225 (w), 1174 (vs), 1138 (m), 1094 (s), 1031 (w), 1015 (m), 979 (m), 960 (w), 949 (m), 884 (s), 783 (s), 737 (s), 715 (s), 650 (s), 582 (w); ^{1}H NMR (DMSO-d_6, 25 °C, ppm) δ: 9.75 (s, 2H, C*H*), 7.30 (s, 2H, CH_2); ^{13}C NMR (DMSO-d_6, 25 °C, ppm) δ: 144.8 (-*C*N_4), 56.0 (-*C*H_2); ^{1}H-^{15}N NMR (DMSO-d_6, 25 °C, ppm) δ: −4.7 (N3), −33.2 (N2), −69.6 (N4), −165.1 ppm (N1); EA ($C_3H_4N_8$, 152.12) calcd.: C 23.69, H 2.65, N 73.66%; found: C 23.94, H 2.51, N 73.43%; BAM drop hammer: 8 J; friction tester: > 360 N; ESD: 480 mJ (at grain size > 1000 µm).

1,2-dtm

DTA (5 °C min^{-1}) onset: 96 °C (endothermic), 138 °C (exothermic); IR (ATR, cm^{-1}): $\tilde{\nu}$ = 3157 (w), 3143 (m), 3033 (w), 2923 (w), 1478 (m), 1456 (w), 1439 (w), 1427 (m), 1379 (w), 1366 (m), 1288 (m), 1191 (w), 1170 (s), 1134 (m), 1118 (m), 1099 (m), 1032 (m), 1017 (m), 1007 (m), 966 (w), 948 (m), 889 (m), 881 (m), 794 (s), 742 (vs), 718 (m), 703 (m), 671 (s), 650 (m); ^{1}H NMR (DMSO-d_6, 25 °C, ppm) δ: 9.84 (s, 1H, C*H*), 9.14 (s, 1H, C*H*), 7.57 (s, 2H, CH_2); ^{13}C NMR (DMSO-d_6, 25 °C, ppm) δ: 154.3 (-*C*N_4), 145.0 (-*C*N_4), 60.1 (-*C*H_2); ^{1}H-^{15}N NMR (MeCN-d_3, 25 °C, ppm) δ: 14.2 (N3), 1.3 (N7), −14.0 (N2), −43.7 (N8), −50.4 (N4), −76.2 (N5), −102.0 (N6), −149.7 ppm (N1); EA ($C_3H_4N_8$, 152.12) calcd.: C 23.69, H 2.65, N 73.66%; found: 23.96, H 2.65, N 73.48%; BAM drop hammer: 2 J; friction tester: 168 N; ESD: 181 mJ (at grain size 500–1000 µm).

2,2-dtm

DTA (5 °C min^{-1}) onset: 58 °C (endothermic), 184 °C (exothermic); IR (ATR, cm^{-1}): $\tilde{\nu}$ = 3148 (w), 3047 (w), 2992 (vw), 1455 (w), 1429 (w), 1381 (m), 1354 (s), 1283 (s), 1201 (w), 1182 (m), 1121 (m), 1100 (w), 1019 (vs), 998 (s), 951 (m), 890 (m), 795 (s), 753 (vs), 706 (s), 670 (vs); ^{1}H NMR (DMSO-d_6, 25 °C, ppm) δ: 9.16 (s, 2H, C*H*), 7.83 (s, 2H, CH_2); ^{13}C NMR (DMSO-d_6, 25 °C, ppm) δ: 154.3 (-*C*N_4), 64.0 (-*C*H_2); ^{1}H-^{15}N NMR (MeCN-d_3, 25 °C, ppm) δ: 2.1 (N3), −43.3 (N4), −75.4 (N1), −103.2 ppm (N2); EA ($C_3H_4N_8$, 152.12) calcd.: C 23.69, H 2.65, N 73.66%; found: C 23.88, H 2.57, N 73.50%; BAM drop hammer: 1.5 J; friction tester: 84 N; ESD: 160 mJ (at grain size 500–1000 µm).

General procedure for the preparation of silver(I) complexes 4–8

The silver(I) salts (0.50 mmol, $AgClO_4$ • H_2O: 113 mg; $AgNO_3$: 84.9 mg, 1 eq.) and the respective amounts of ligand (**4**: 1.00 mmol, 152 mg, 2 eq. (1,1-dtm); **5**: 1.50 mmol, 228 mg, 3 eq. (1,2-dtm); **6**: 0.50 mmol, 76.1 mg, 1 eq. (2,2-dtm); **7**: 1.00 mmol, 152 mg, 2 eq. (1,1-dtm); **8**: 2.00 mmol, 304 mg, 4 eq. (1,2-dtm)) were each dissolved in mixture (3 mL) of water and acetonitrile (2/1). The ligand solution was added dropwise to the dissolved silver salt under stirring at room temperature. The complexes started crystallizing while standing in air within minutes or one day. The compounds were filtered off before a complete evaporation of the solvent and were washed with cold acetonitrile.

[Ag(1,1-dtm)$_2$]NO_3 (4)

ECC **4** was obtained in the form of colorless needle-shaped crystals. Yield: 204 mg (0.43 mmol, 86%).

DTA (5 °C min^{-1}) onset: 132 °C (endothermic), 136 °C (exothermic); IR (ATR, cm^{-1}): $\tilde{\nu}$ = 3151 (w), 3106 (w), 3020 (w), 2975 (w), 1501 (w), 1477 (m), 1451 (w), 1440 (w), 1431 (w), 1400 (m), 1338 (s), 1317 (s), 1299 (m), 1277 (m), 1228 (m), 1171 (vs), 1142 (m), 1105 (s), 1095 (s), 1047 (w), 1032 (w), 1011 (w), 981 (m), 973 (w), 953 (m), 891 (m), 884 (m), 829 (w), 787 (m), 776 (m), 736 (s), 713 (m), 648

(m); EA ($C_6H_8AgN_{17}O_3$, 474.11) calcd.: C 15.20, H 1.70, N 50.22%; found: C 15.60, H 1.75, N 51.15%; BAM drop hammer: 4 J; friction tester: 144 N; ESD: 450 mJ; ball drop impact tester: > 200 mJ (at grain size 100–500 µm).

[Ag(1,2-dtm)$_3$]NO$_3$ (5)
Complex **5** was received as colorless platelets. Yield: 229 mg (0.37 mmol, 74%).

DTA (5 °C min^{-1}) onset: 113 °C (endothermic), 124 °C (exothermic); IR (ATR, cm^{-1}): $\tilde{\nu}$ = 3169 (w), 3146 (w), 3132 (w), 3056 (w), 3040 (w), 2990 (w), 1492 (m), 1441 (w), 1435 (w), 1359 (s), 1341 (s), 1320 (s), 1293 (m), 1282 (s), 1247 (w), 1202 (m), 1183 (s), 1173 (m), 1120 (m), 1113 (m), 1095 (s), 1039 (w), 1026 (m), 1014 (m), 1002 (m), 971 (m), 950 (m), 913 (w), 892 (m), 888 (m), 878 (w), 833 (w), 792 (s), 744 (vs), 713 (m), 708 (m), 701 (w), 670 (s), 649 (w), 641 (m); EA ($C_9H_{12}AgN_{25}O_3$, 626.24) calcd.: C 17.26, H 1.93, N 55.92%; found: C 16.90, H 1.98, N 55.38%; BAM drop hammer: 2 J; friction tester: 108 N; ESD: 540 mJ; ball drop impact tester: 124 mJ (at grain size 100–500 µm).

[Ag(NO$_3$)(2,2-dtm)] (6)
Nitrato complex **6** crystallized in the form of colorless blocks. Yield: 108 mg (0.34 mmol, 68%).

DTA (5 °C min^{-1}) onset: 166 °C (endothermic), 186 °C (exothermic); IR (ATR, cm^{-1}): $\tilde{\nu}$ = 3158 (w), 3148 (w), 3038 (w), 2983 (w), 1457 (w), 1431 (m), 1409 (m), 1381 (m), 1359 (s), 1309 (vs), 1286 (vs), 1207 (m), 1193 (s), 1139 (w), 1121 (s), 1035 (s), 1013 (m), 957 (m), 919 (m), 911 (m), 824 (m), 795 (m), 756 (s), 713 (w), 702 (m), 672 (s); EA ($C_3H_4AgN_9O_3$, 321.99) calcd.: C 11.19, H 1.25, N 39.15%; found: C 11.21, H 1.31, N 38.40%; BAM drop hammer: 3 J; friction tester: 36 N; ESD: 380 mJ; ball drop impact tester: 124 mJ (at grain size 100–500 µm).

[Ag(1,1-dtm)$_2$]ClO$_4$ (7)
Perchlorate compound **7** was obtained as colorless block-like crystals. Yield: 207 mg (0.41 mmol, 82%).

DTA (5 °C min^{-1}) onset: 163 °C (exothermic); IR (ATR, cm^{-1}): $\tilde{\nu}$ = 3153 (w), 3146 (w), 3121 (w), 3051 (vw), 3038 (vw), 2994 (w), 1500 (m), 1475 (m), 1450 (w), 1438 (w), 1426 (w), 1390 (w), 1371 (w), 1319 (w), 1300 (w), 1230 (vw), 1175 (s), 1139 (w), 1108 (s), 1088 (vs), 1028 (w), 1008 (m), 979 (w), 970 (m), 951 (w), 938 (w), 886 (m), 783 (s), 766 (w), 741 (m), 731 (s), 712 (m), 649 (m), 623 (s); EA ($C_6H_8AgClN_{16}O_4$, 511.56) calcd.: C 14.09, H 1.58, N 43.81%; found: C 14.25, H 1.54, N 43.59%; BAM drop hammer: < 1 J; friction tester: 30 N; ESD: 1080 mJ; ball drop impact tester: 28 mJ (at grain size 100–500 µm).

[Ag(1,2-dtm)$_4$]ClO$_4$ (8)
Silver perchlorate complex **8** crystallized as colorless rods. Yield: 329 mg (0.40 mmol, 81%).

DTA (5 °C min^{-1}) onset: 132 °C (endothermic), 140 °C (exothermic); IR (ATR, cm^{-1}): $\tilde{\nu}$ = 3137 (w), 3045 (w), 2995 (vw), 1479 (w), 1439 (w), 1427 (m), 1382 (w), 1359 (m), 1298 (w), 1289 (w), 1283 (w), 1201 (w), 1192 (w), 1170 (m), 1124 (m), 1109 (s), 1093 (vs), 1085 (vs), 1037 (m), 1027 (m), 1016 (m), 1003 (m), 964 (w), 946 (m), 889 (m), 793 (s), 773 (w), 741 (vs), 714 (w), 707 (w), 698 (w), 670 (s), 648 (m), 622 (s); EA ($C_{12}H_{16}AgClN_{32}O_4$, 815.80) calcd.: C 17.67, H 1.98, N 54.94%; found: C 17.49, H 1.83, N 55.65%; BAM drop hammer: < 1 J; friction tester: 50 N; ESD: 226 mJ; ball drop impact tester: 20 mJ (at grain size 100–500 µm).

$[Cu_2(NO_3)_4(2,2\text{-dtm})_3]$ (9)

Copper(II) nitrate trihydrate (1.70 mmol, 411 mg, 1.0 eq.) and 2,2-dtm (2.55 mmol, 388 mg, 1.5 equiv.) were each dissolved in acetonitrile (2 mL). The dissolved ligand was added dropwise to the copper(II) nitrate solution under stirring at 50 °C and left to crystallize at room temperature. ECC **9** crystallized in form of dodger blue crystals after 5 days. Yield: 266 mg (0.32 mmol, 38%).

DTA (5 °C min^{-1}) onset: 198 °C (exothermic); IR (ATR, cm^{-1}): $\tilde{\nu}$ = 3194 (vw), 3164 (w), 3147 (w), 3057 (w), 3034 (w), 2996 (w), 2982 (vw), 1519 (m), 1482 (s), 1472 (s), 1427 (m), 1390 (m), 1367 (m), 1353 (m), 1316 (vs), 1299 (s), 1292 (s), 1279 (vs), 1204 (s), 1145 (m), 1128 (s), 1048 (m), 1037 (m), 1012 (s), 963 (m), 912 (m), 894 (m), 884 (w), 801 (s), 763 (vs), 749 (m), 705 (m), 671 (vs), 408 (w); EA ($C_9H_{12}Cu_2N_{28}O_{12}$, 831.47) calcd.: C 13.00, H 1.45, N 47.17%; found: C 13.42, H 1.51, N 47.36%; BAM drop hammer: 1.5 J; friction tester: 30 N; ESD: > 1500 mJ; ball drop impact tester: 16 mJ (at grain size 100–500 µm).

General procedure for the preparation of copper(II) perchlorate complexes 10–12

Copper(II) perchlorate hexahydrate (0.5 mmol, 185 mg, 1 eq.) was dissolved in ethanol and heated to 80 °C. It is highly important to use the right solvents and reaction temperatures, to prevent the formation of aqua species. While stirring, an ethanolic solution of the respective ligand (1.5 mmol, 228 mg, 3 eq) was added dropwise, which lead to the precipitation of the complexes. The powders were filtered off and washed with cold acetonitrile.

For obtaining the ECC as single-crystals suitable for X-ray diffraction, water was added dropwise to the hot ethanolic suspensions until a complete dissolution occurred at 80 °C. After cooling and standing in air the compounds crystallized within 30 min.

$[Cu(1,1\text{-dtm})_3](ClO_4)_2$ (10)

Complex compound **10** precipitated as light blue powder. Yield: 266 mg (0.37 mmol, 74%).

DTA (5 °C min^{-1}) onset: 230 °C (exothermic); IR (ATR, cm^{-1}): $\tilde{\nu}$ = 3132 (w), 3040 (w), 2996 (vw), 1511 (w), 1492 (m), 1460 (w), 1451 (w), 1446 (w), 1435 (w), 1371 (w), 1311 (vw), 1230 (w), 1198 (m), 1184 (m), 1150 (w), 1099 (vs), 1074 (vs), 1026 (m), 1006 (m), 986 (m), 962 (m), 952 (m), 938 (w), 894 (m), 881 (m), 783 (s), 736 (s), 714 (s), 646 (s), 620 (vs); EA ($C_9H_{12}Cl_2CuN_{24}O_8$, 718.80) calcd.: C 15.04, H 1.68, N 46.77%; found: C 15.04, H 1.68, N 46.21%; BAM drop hammer: < 1 J; friction tester: 0.75 N; ESD: 42 mJ; ball drop impact tester: 12 mJ (at grain size < 100 µm).

$[Cu(1,2\text{-dtm})_3](ClO_4)_2$ (11)
ECC **11** was received in the form of a light blue precipitate. Yield: 280 mg (0.39 mmol, 78%).

DTA (5 °C min^{-1}) onset: 215 °C (exothermic); IR (ATR, cm^{-1}): $\tilde{\nu}$ = 3159 (w), 3136 (w), 3111 (w), 3062 (vw), 3042 (w), 3006 (vw), 2991 (vw), 1513 (w), 1501 (w), 1492 (w), 1458 (w), 1448 (w), 1425 (m), 1397 (vw), 1379 (w), 1367 (m), 1307 (w), 1297 (w), 1183 (m), 1147 (m), 1075 (vs), 1049 (s), 1040 (s), 1029 (s), 1016 (m), 996 (m), 985 (m), 951 (m), 927 (w), 899 (m), 883 (w), 797 (s), 765 (m), 748 (s), 712 (w), 702 (w), 672 (s), 643 (m), 621 (vs), 549 (vw); EA ($C_9H_{12}Cl_2CuN_{24}O_8$, 718.80) calcd.: C 15.04, H 1.68, N 46.77%; found: C 15.08, H 1.87, N 46.95%; BAM drop hammer: 1.5 J; friction tester: 1 N; ESD: 47 mJ; ball drop impact tester: < 4 mJ (at grain size < 100 µm).

$[Cu(2,2\text{-dtm})_3](ClO_4)_2$ (12)
The blue precipitate mainly contained the trigonal species **12b** (Yield: 316 mg (0.44 mmol, 88%)), while during the crystallization the complex was mostly obtained in its hexagonal form **12a** as aquamarine blocks (Yield: 280 mg (0.39 mmol, 78%)). Both products contain impurities of the other species.

DTA (5 °C min^{-1}) onset: 242 °C (exothermic); IR **12a** (ATR, cm^{-1}): $\tilde{\nu}$ = 3164 (w), 3053 (w), 2997 (w), 1471 (w), 1434 (w), 1366 (m), 1350 (w), 1305 (w), 1203 (w), 1192 (m), 1145 (m), 1076 (vs), 1051 (s), 1036 (s), 1023 (m), 1013 (m), 962 (m), 936 (vw), 887 (m), 798 (m), 763 (m), 704 (m), 673 (s), 621 (vs), 526 (w), 506 (vw), 406 (w); IR **12b** (ATR, cm^{-1}): $\tilde{\nu}$ = 3139 (m), 3046 (m), 2991 (w), 2930 (vw), 1819 (vw), 1472 (w), 1435 (w), 1396 (vw), 1371 (w), 1351 (m), 1307 (w), 1278 (m), 1197 (m), 1150 (m), 1073 (vs), 1047 (vs), 972 (m), 935 (w), 910 (s), 789 (m), 747 (s), 706 (m), 677 (s), 622 (vs), 462 (vw), 403 (w); EA ($C_9H_{12}Cl_2CuN_{24}O_8$, 718.80) calcd.: C 15.04, H 1.68, N 46.77%; found: C 15.29, H 1.68, N 46.66%; BAM drop hammer: < 1 J; friction tester: 0.75 N; ESD: 37 mJ; ball drop impact tester: < 4 mJ (at grain size < 100 µm).

General procedure for the preparation of trinitroaromatic complexes 13–18
Basic copper(II) carbonate (0.25 mmol, 111 mg, 1 eq.) and the respective acid (1.00 mmol, picric acid (HPA): 229 mg; styphnic acid (H_2TNR) 245 mg; trinitrophloroglucinol (H_3TNR): 261 mg, 2 eq.) were reacted in 5 mL H_2O at 50 °C. Afterwards aqueous solutions of the corresponding ligands (**13**/**15**:

1.00 mmol, 152 mg, 2 eq. (1,1-dtm); **14**: 0.50 mmol, 76.1 mg, 1 eq. (1,1-dtm); **16**–**18**: 1.00 mmol, 152 mg, 2 eq. (1,2-dtm)) were added dropwise. The resulting reaction solutions were stirred at 50–60 °C until a complete dissolution occurred, and the complexes started crystallizing while standing in air within some hours. They were filtered off and washed with cold ethanol.

$[Cu(H_2O)_4(1,1\text{-dtm})_2](PA)_2$ (13)
Complex **13** was received as lawn green needles. Yield: 307 mg (0.34 mmol, 69%).

DTA (5 °C min^{-1}) onset: 108 °C (endothermic), 185 °C (exothermic); IR (ATR, cm^{-1}): $\tilde{\nu}$ = 3417 (m), 3365 (m), 3346 (m), 3287 (m), 3276 (m), 3235 (m), 3202 (m), 3163 (s), 3130 (s), 3072 (m), 3048 (s), 3000 (m), 1627 (m), 1606 (s), 1584 (m), 1568 (s), 1539 (s), 1532 (s), 1512 (vs), 1482 (s), 1457 (m), 1437 (m), 1429 (m), 1363 (s), 1338 (vs), 1309 (s), 1271 (s), 1221 (m), 1198 (m), 1181 (s), 1157 (s), 1100 (s), 1083 (m), 1031 (m), 1008 (m), 992 (m), 967 (m), 944 (m), 930 (m), 912 (m), 894 (m), 869 (m), 836 (m), 817 (m), 788 (s), 781 (s), 757 (m), 744 (vs), 714 (s), 676 (m), 643 (s), 598 (m), 547 (m), 522 (m); EA ($C_{18}H_{20}CuN_{22}O_{18}$, 896.04) calcd.: C 24.13, H 2.25, N 34.39%; found: C 24.31, H 2.26, N 34.44%; BAM drop hammer: 6 J; friction tester: > 360 N; ESD: 840 mJ; ball drop impact tester: > 200 mJ (at grain size 100–500 µm).

$[Cu(TNR)(1,1\text{-dtm})] \cdot H_2O$ (14)
Styphnate compound **14** crystallized in the form of dark green blocks. Yield: 228 mg (0.48 mmol, 96%).

DTA (5 °C min^{-1}) onset: 236 °C (exothermic); IR (ATR, cm^{-1}): $\tilde{\nu}$ = 3656 (w), 3562 (vw), 3121 (w), 3017 (w), 2976 (w), 1607 (m), 1582 (m), 1538 (s), 1521 (s), 1495 (m), 1488 (m), 1473 (m), 1440 (s), 1428 (s), 1371 (m), 1287 (vs), 1225 (vs), 1188 (vs), 1172 (s), 1144 (s), 1107 (s), 1097 (s), 1021 (m), 1004 (m), 958 (m), 925 (w), 908 (m), 775 (m), 746 (m), 734 (w), 708 (vs), 647 (s), 460 (w), 417 (w); EA ($C_9H_7CuN_{11}O_9$, 476.77) calcd.: C 22.67, H 1.48, N 32.32%; found: C 22.70, H 1.41, N 32.41%; BAM drop hammer: 2 J; friction tester: 192 N; ESD: 188 mJ; ball drop impact tester: 66 mJ (at grain size 100–500 µm).

$[Cu(H_2O)_4(1,1\text{-dtm})_2](H_2TNPG)_2$ (15)
ECC **15** was obtained as forest green crystals. Yield: 392 mg (0.41 mmol, 82%).

DTA (5 °C min^{-1}) onset: 74 °C (endothermic), 196 °C (exothermic); IR (ATR, cm^{-1}): $\tilde{\nu}$ = 3154 (m), 3136 (m), 3041 (w), 2998 (w), 1644 (s), 1615 (w), 1555 (s), 1505 (vs), 1489 (vs), 1454 (s), 1439 (m), 1416 (m), 1356 (s), 1330 (vs), 1298 (m), 1217 (m), 1205 (s), 1183 (vs), 1157 (vs), 1148 (vs), 1134 (s), 1098 (s), 1087 (vs), 1033 (m), 1022 (s), 1011 (m), 1001 (m), 966 (m), 916 (m), 898 (s), 883 (m), 839 (s), 816 (m), 777 (s), 753 (s), 743 (s), 713 (s), 690 (vs), 652 (s), 644 (s), 620 (s), 523 (w), 497 (w), 467 (m), 412 (w); EA ($C_{18}H_{20}CuN_{22}O_{22}$, 960.04) calcd.: C 22.52, H 2.10, N 32.10%; found: C 22.76, H 1.63, N 32.19%;

BAM drop hammer: 4 J; friction tester: 48 N; ESD: 960 mJ; ball drop impact tester: 16 mJ (at grain size 100–500 µm).

[Cu(H$_2$O)$_2$(1,2-dtm)$_2$](PA)$_2$ (16)
Complex **16** was received as yellow-green crystals. Yield: 231 mg (0.27 mmol, 54%).

DTA (5 °C min^{-1}) onset: 122 °C (endothermic), 159 °C (exothermic); IR (ATR, cm^{-1}): $\tilde{\nu}$ = 3455 (w), 3149 (w), 3072 (m), 3060 (m), 3006 (w), 2986 (w), 1630 (s), 1609 (s), 1570 (s), 1552 (s), 1514 (s), 1485 (m), 1474 (m), 1453 (w), 1429 (m), 1367 (s), 1337 (vs), 1311 (s), 1300 (s), 1264 (vs), 1210 (m), 1193 (s), 1167 (m), 1164 (m), 1137 (w), 1124 (m), 1086 (s), 1037 (m), 1018 (w), 1005 (m), 999 (w), 948 (m), 926 (m), 914 (m), 895 (m), 794 (m), 788 (s), 747 (vs), 724 (s), 712 (s), 701 (s), 670 (s), 650 (m), 553 (m), 522 (m), 442 (w); EA ($C_{18}H_{16}CuN_{22}O_{16}$, 860.01) calcd.: C 25.14, H 1.88, N 35.83%; found: C 24.99, H 1.83, N 35.83%; BAM drop hammer: 1 J; friction tester: > 360 N; ESD: 750 mJ; ball drop impact tester: > 200 mJ (at grain size 100–500 µm).

[Cu(H$_2$O)$_2$(1,2-dtm)$_2$](HTNR)$_2$ (17)
Complex compound **17** was received in the form of chocolate brown blocks. Yield: 173 mg (0.19 mmol, 39%).

DTA (5 °C min^{-1}) onset: 132 °C (endothermic), 156 °C (exothermic); IR (ATR, cm^{-1}): $\tilde{\nu}$ = 3509 (w), 3315 (m), 3230 (w), 3161 (m), 3063 (m), 3010 (w), 2999 (w), 2984 (w), 1634 (s), 1582 (s), 1541 (s), 1507 (s), 1489 (s), 1441 (s), 1378 (s), 1342 (s), 1299 (vs), 1252 (vs), 1187 (vs), 1171 (s), 1134 (s), 1094 (vs), 1047 (m), 1029 (m), 1008 (m), 953 (m), 927 (m), 902 (m), 820 (m), 783 (s), 753 (s), 728 (s), 714 (s), 704 (s), 690 (s), 670 (vs), 651 (s), 600 (m), 518 (m), 493 (m); EA ($C_{18}H_{16}CuN_{22}O_{18}$, 892.01) calcd.: C 24.24, H 1.81, N 34.55%; found: C 24.42, H 1.81, N 34.51%; BAM drop hammer: 7 J; friction tester: 144 N; ESD: 1500 mJ; ball drop impact tester: > 200 mJ (at grain size 100–500 µm).

[Cu(H$_2$O)$_2$(1,2-dtm)$_2$](H$_2$TNPG)$_2$ (18)
ECC **18** was obtained as lime green crystals. Yield: 368 mg (0.40 mmol, 80%).

DTA (5 °C min^{-1}) onset: 136 °C (exothermic); IR (ATR, cm^{-1}): $\tilde{\nu}$ = 3540 (m), 3146 (w), 3104 (m), 3042 (m), 2998 (m), 1640 (s), 1635 (s), 1568 (s), 1538 (m), 1505 (s), 1485 (vs), 1456 (s), 1414 (m), 1361 (s), 1338 (s), 1321 (s), 1293 (s), 1212 (s), 1186 (s), 1179 (s), 1153 (s), 1125 (vs), 1096 (s), 1035 (m), 1016 (m), 1009 (m), 995 (m), 918 (m), 902 (m), 831 (m), 819 (m), 786 (s), 768 (s), 753 (s), 742 (s), 715 (s), 700 (s), 682 (m), 671 (s), 664 (s), 645 (s), 615 (m), 574 (m), 561 (m); EA ($C_{18}H_{16}CuN_{22}O_{20}$, 924.01) calcd.: C 23.40, H 1.75, N 33.35%; found: C 23.39, H 1.80, N 33.09%; BAM drop hammer: 1.5 J; friction tester: 128 N; ESD: 1350 mJ; ball drop impact tester: > 200 mJ (at grain size 100–500 µm).

6.6.2. IR Spectroscopy

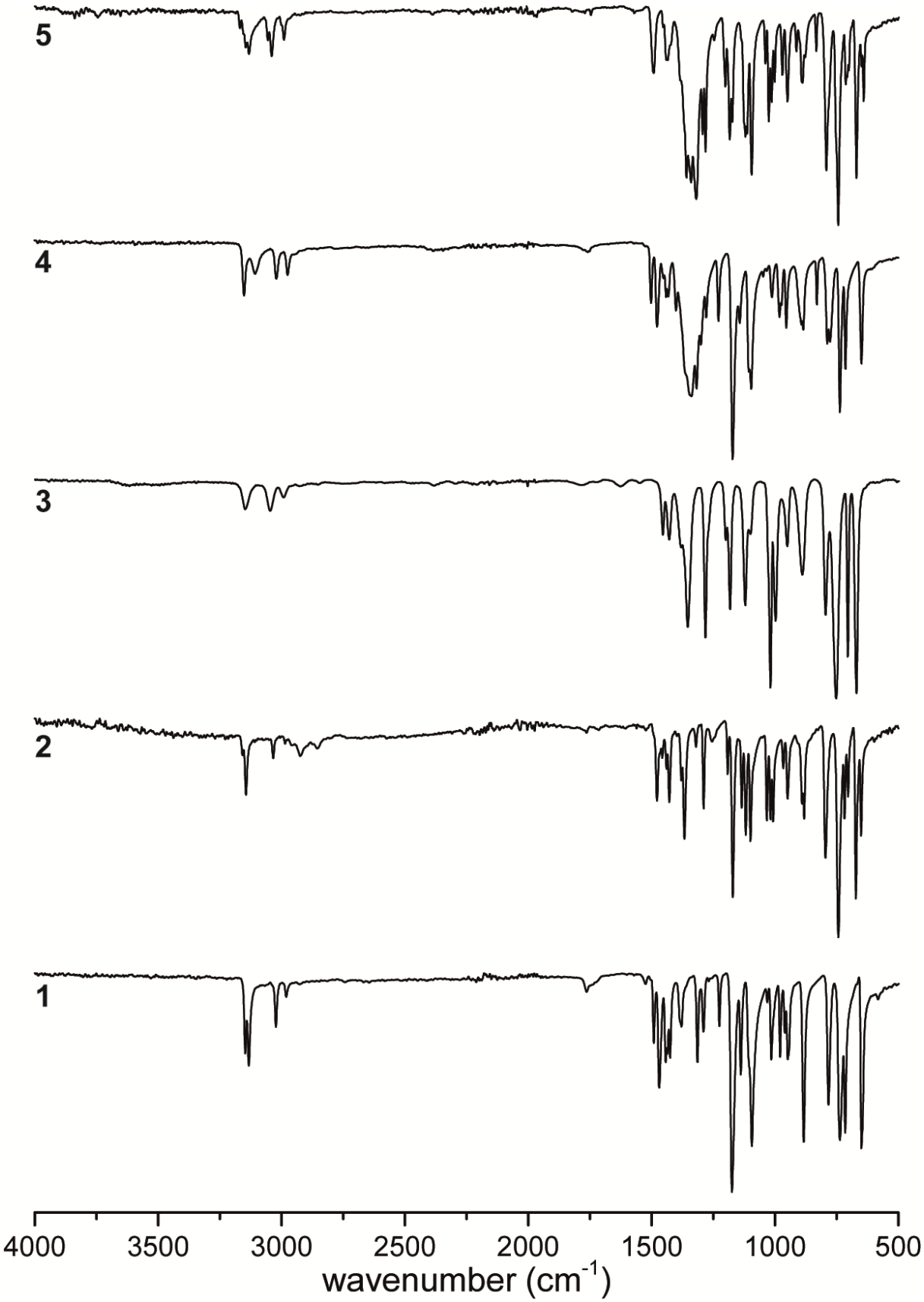

Figure S1. Infrared spectra of compounds **1**–**5**.

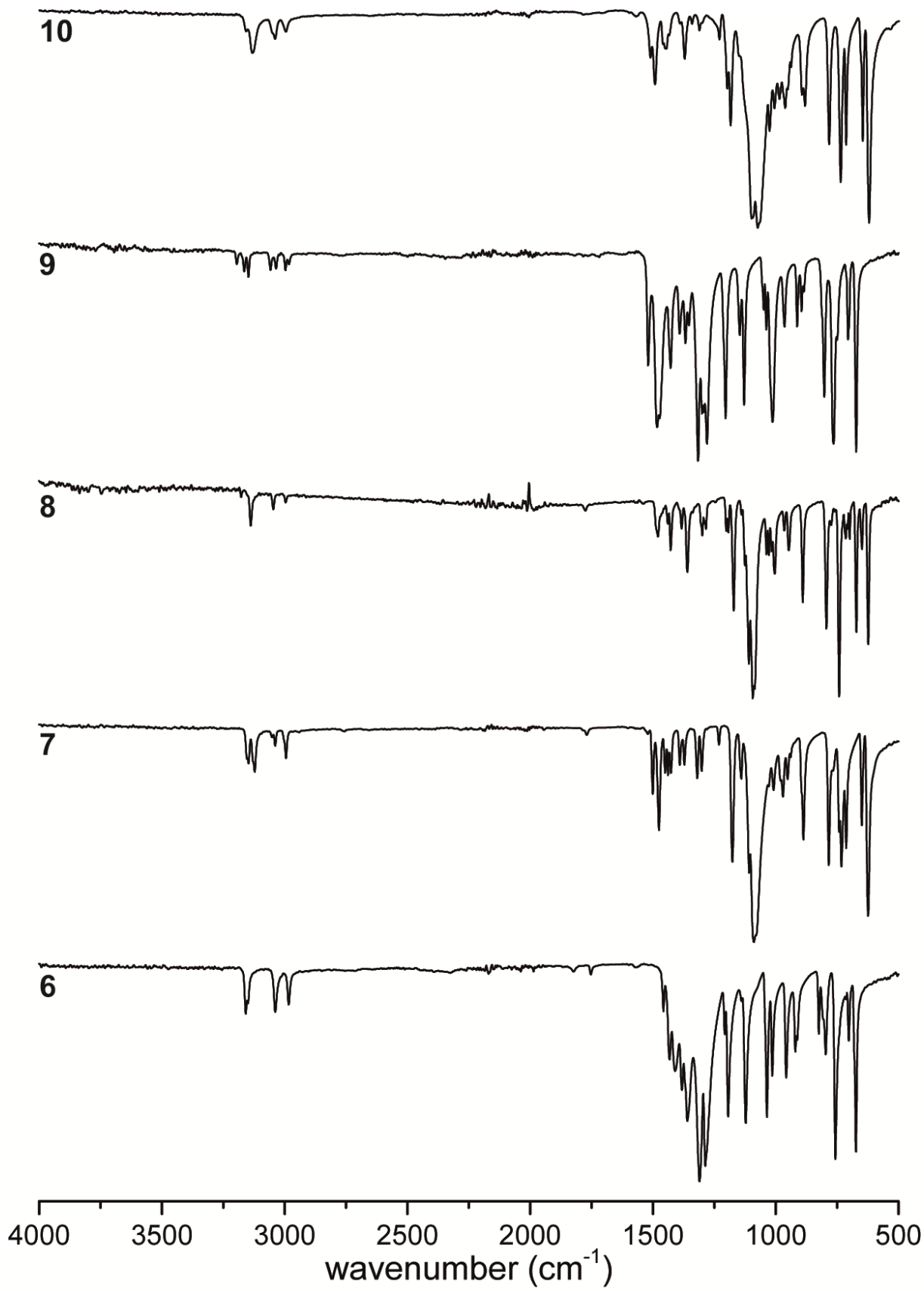

Figure S2. Infrared spectra of complexes **6**–**10**.

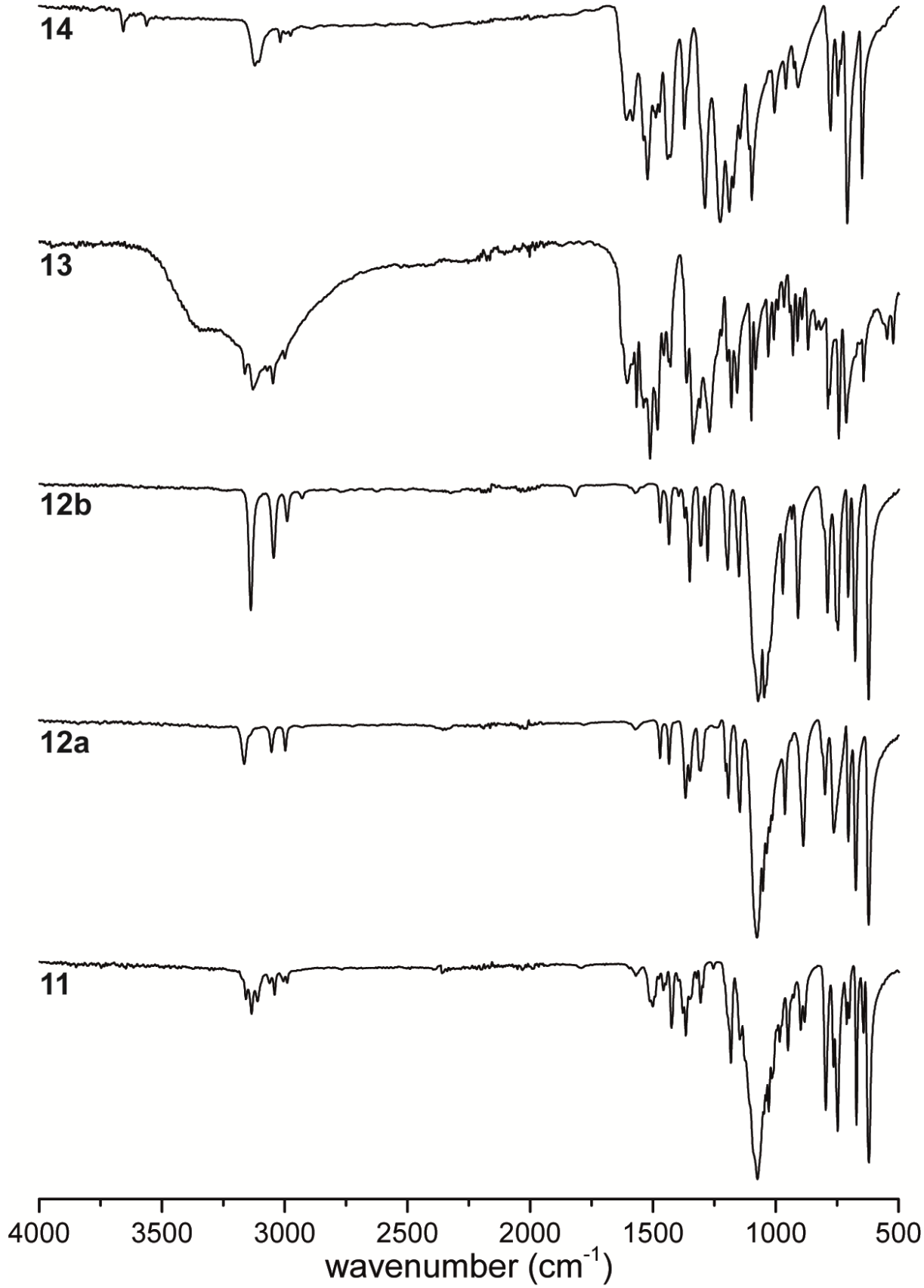

Figure S3. Infrared spectra of ECC **11**–**14**.

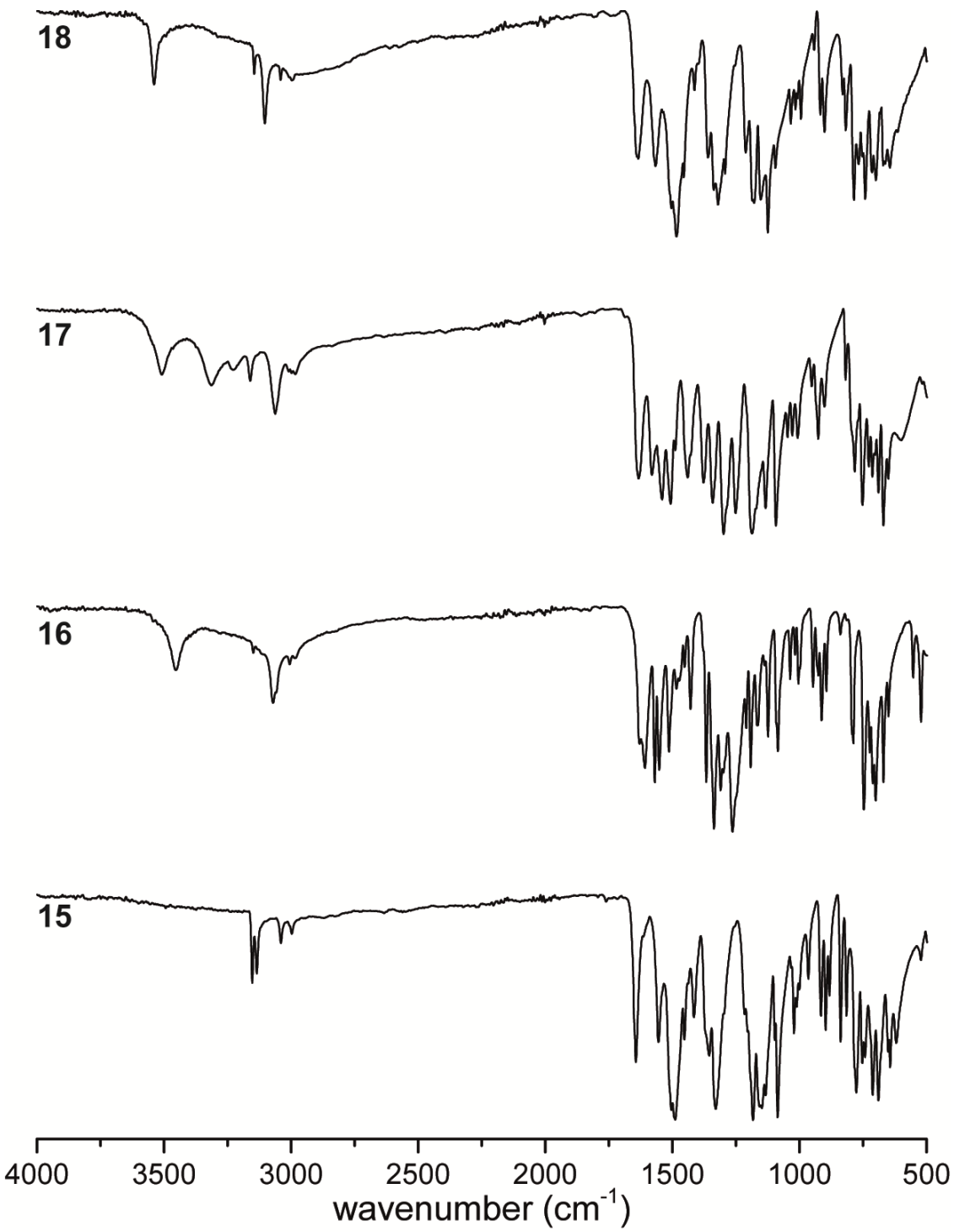

Figure S4. Infrared spectra of compounds **15**–**18**.

6.6.3. X-ray Diffraction

For all crystalline compounds, an Oxford Xcalibur3 diffractometer with a CCD area detector or Bruker D8 Venture TXS diffractometer equipped with a multilayer monochromator, a Photon 2 detector and a rotating-anode generator were employed for data collection using Mo-*K*α radiation (λ = 0.71073 Å). On the Oxford device, data collection and reduction were carried out using the CRYSALISPRO software.[12] On

the Bruker diffractometer, the data were collected with the Bruker Instrument Service v3.0.21, the data reduction was performed using the SAINT V8.18C software (Bruker AXS Inc., 2011). The structures were solved by direct methods (SIR-92,[13] SIR-97,[14] or SHELXS-97[15]) and refined by full-matrix least-squares on *F*2 (SHELXL[15]) and finally checked using the PLATON software[16] integrated in the WinGX[17] software suite. The non-hydrogen atoms were refined anisotropically and the hydrogen atoms were located and freely refined. The absorptions were corrected by a SCALE3 ABSPACK or SADABS Bruker APEX3 multiscan method.[18,19] All DIAMOND2 plots are shown with thermal ellipsoids at the 50% probability level and hydrogen atoms are shown as small spheres of arbitrary radius.

Table S1. Crystallographic data of **1**–**4**.

	1	**2**	**3**	**4**
Formula	$C_3H_4N_8$	$C_3H_4N_8$	$C_3H_4N_8$	$C_6H_8AgN_{17}O_3$
FW [g mol^{-1}]	152.14	152.14	152.14	474.16
Crystal system	monoclinic	orthorhombic	orthorhombic	triclinic
Space Group	$P2_1/c$	$Fdd2$	$Fdd2$	$P\bar{1}$
Color / Habit	colorless rod	colorless block	colorless block	colorless needle
Size [mm]	0.03 x 0.04 x 0.10	0.24 x 0.27 x 0.40	0.15 x 0.20 x 0.50	0.04 x 0.08 x 0.50
a [Å]	10.1121(5)	12.2896(13)	9.9615(5)	5.1440(4)
b [Å]	5.2180(2)	39.396(4)	13.9350(8)	10.8619(9)
c [Å]	12.1615(6)	5.2035(6)	8.9230(6)	13.7886(13)
α [°]	90	90	90	78.685(7)
β [°]	105.888(2)	90	90	83.864(7)
γ [°]	90	90	90	81.923(7)
V [Å^3]	617.19(5)	2519.3(5)	1238.63(13)	745.45(11)
Z	4	16	8	2
$\rho_{calc.}$ [g cm^{-3}]	1.637	1.605	1.632	2.112
μ [mm^{-1}]	0.126	0.123	0.125	1.412
F(000)	312	1248	624	468
$\lambda_{MoK\alpha}$ [Å]	0.71073	0.71073	0.71073	0.71073
T [K]	100	143	123	131
θ Min–Max [°]	3.5, 26.0	4.3, 26.0	3.4, 26.4	2.2, 26.4
Dataset	−12: 12; −6: 6; −14: 14	−14: 14; −31: 48; −6: 6	−9: 12; −13: 17; −8: 11	−6: 6; −13: 11; −15: 17
Reflections collected	5454	4892	1862	4108
Independent refl.	1212	1233	595	3018
R_{int}	0.030	0.048	0.018	0.036
Observed reflections	1080	1114	586	2434
Parameters	100	100	51	244
R_1 (obs)[a]	0.0324	0.0360	0.0218	0.0443
wR_2 (all data)[b]	0.0810	0.0857	0.0506	0.0783
GooF[c]	1.09	1.08	1.07	1.00
Resd. Dens. [e Å^{-3}]	−0.22, 0.18	−0.22, 0.21	−0.15, 0.12	−0.92, 0.70
Absorption correction	multi-scan	multi-scan	multi-scan	multi-scan
CCDC	1988649	1988643	1988633	1988648

[a] $R_1 = \Sigma||F_0|- |F_c||/ \Sigma|F_0|$; [b] $wR_2 = [\Sigma[w(F_0^2-F_c^2)^2]/\Sigma[w(F_0)^2]]^{1/2}$; $w = [\sigma c^2(F_0^2)+(xP)^2+yP]^{-1}$ and $P = (F_0^2+2F_c^2)/3$; [c] GooF = $\{\Sigma[w(F_o^2-F_c^2)^2]/(n-p)\}^{1/2}$ (n = number of reflections; p = total number of parameters).

Table S2. Crystallographic data of **5**–**8**.

	5	**6**	**7**	**8**
Formula	$C_9H_{12}AgN_{25}O_3$	$C_3H_4AgN_9O_3$	$C_6H_8AgClN_{16}O_4$	$C_{12}H_{16}AgClN_{32}O_4$
FW [g mol^{-1}]	626.31	322.02	511.60	815.89
Crystal system	orthorhombic	monoclinic	triclinic	monoclinic
Space Group	*Pna*2$_1$	*Ia*	*P*−1	*P*2/*n*
Color / Habit	colorless platelet	colorless block	colorless block	colorless rod
Size [mm]	0.01 x 0.03 x 0.09	0.20 x 0.20 x 0.50	0.11 x 0.26 x 0.42	0.01 x 0.01 x 0.10
a [Å]	20.7288(11)	7.1009(3)	5.1744(3)	15.9202(6)
b [Å]	5.3514(3)	13.4805(5)	10.3376(6)	5.3427(2)
c [Å]	19.8800(11)	9.8789(4)	15.2952(8)	16.7636(6)
α [°]	90	90	75.203(5)	90
β [°]	90	109.790(5)	83.560(4)	91.547(1)
γ [°]	90	90	79.510(5)	90
V [Å^3]	2205.3(2)	889.80(7)	775.94(8)	1425.34(9)
Z	4	4	2	2
$\rho_{calc.}$ [g cm^{-3}]	1.886	2.404	2.190	1.901
μ [mm^{-1}]	0.990	2.280	1.535	0.890
F(000)	1248	624	504	816
$\lambda_{MoK\alpha}$ [Å]	0.71073	0.71073	0.71073	0.71073
T [K]	108	122	128	111
θ Min–Max [°]	3.6, 26.4	2.7, 26.4	2.1, 26.4	3.5, 26.4
Dataset	−25: 25; −6: 6; −24: 24	−8: 8; −13: 16; −12: 11	−6: 6; −12: 6; −19: 15	−18: 19; −6: 6; −20: 20
Reflections collected	33839	3255	4299	14616
Independent refl.	4503	1462	3138	2896
R_{int}	0.037	0.020	0.024	0.036
Observed reflections	4301	1437	2760	2600
Parameters	343	146	253	227
R_1 (obs)[a]	0.0193	0.0283	0.0291	0.0278
wR_2 (all data)[b]	0.0386	0.0721	0.0623	0.0535
GooF[c]	1.07	1.06	1.00	1.09
Resd. Dens. [e Å^{-3}]	−0.38, 0.23	−0.80, 0.45	−0.53, 0.76	−0.45, 0.40
Absorption correction	multi-scan	multi-scan	multi-scan	multi-scan
CCDC	1988639	1988636	1988647	1988642

[a] $R_1 = \Sigma||F_0|- |F_c||/ \Sigma|F_0|$; [b] $wR_2 = [\Sigma[w(F_0^2-F_c^2)^2]/\Sigma[w(F_0)^2]]^{1/2}$; $w = [\sigma c^2(F_0^2)+(xP)^2+yP]^{-1}$ and $P = (F_0^2+2F_c^2)/3$; [c] GooF = $\{\Sigma[w(F_o^2-F_c^2)^2]/(n-p)\}^{1/2}$ (n = number of reflections; p = total number of parameters).

Table S3. Crystallographic data of **9**–**12a**.

	9	**10**	**11**	**12a**
Formula	$C_9H_{12}Cu_2N_{28}O_{12}$	$C_9H_{12}Cl_2CuN_{24}O_8$	$C_9H_{12}Cl_2CuN_{24}O_8$	$C_9H_{12}Cl_2CuN_{24}O_8$
FW [g mol^{-1}]	831.55	718.87	718.87	718.87
Crystal system	monoclinic	monoclinic	monoclinic	hexagonal
Space Group	*I*2/*a*	*C*2/*c*	$P2_1/n$	$P6_3/m$
Color / Habit	blue block	blue block	blue block	blue hexagon
Size [mm]	0.25 x 0.37 x 0.47	0.02 x 0.03 x 0.06	0.17 x 0.25 x 0.50	0.14 x 0.38 x 0.44
a [Å]	11.1692(4)	11.6488(5)	13.7258(7)	9.3331(3)
b [Å]	19.2892(6)	11.7668(4)	11.2957(5)	9.3331(3)
c [Å]	13.7786(5)	18.1722(7)	16.6108(8)	16.5449(8)
α [°]	90	90	90	90
β [°]	106.958(3)	100.644(1)	104.145(4)	90
γ [°]	90	90	90	120
V [Å^3]	2839.45(18)	2447.99(16)	2497.3(2)	1248.09(12)
Z	4	4	4	2
$\rho_{calc.}$ [g cm^{-3}]	1.945	1.951	1.912	1.913
μ [mm^{-1}]	1.607	1.205	1.182	1.182
F(000)	1664	1444	1444	722
$\lambda_{MoK\alpha}$ [Å]	0.71073	0.71073	0.71073	0.71073
T [K]	109	298	143	119
θ Min–Max [°]	2.2, 26.4	3.1, 26.4	4.2, 26.0	2.5, 26.3
Dataset	−13: 12; −14: 24; −17: 16	−14: 12; −14: 14; −22: 22	−15: 16; −13: 13; −20: 20	−10: 11; −11: 11; −20: 18
Reflections collected	9362	12901	19149	7763
Independent refl.	2910	2512	4882	884
R_{int}	0.023	0.030	0.034	0.038
Observed reflections	2615	2125	4088	815
Parameters	231	229	397	69
R_1 (obs)[a]	0.0250	0.0308	0.0310	0.0363
wR_2 (all data)[b]	0.0650	0.0792	0.0828	0.0844
GooF[c]	1.05	1.09	1.06	1.22
Resd. Dens. [e Å^{-3}]	−0.38, 0.44	−0.31, 0.34	−0.40, 0.41	−0.33, 0.45
Absorption correction	multi-scan	multi-scan	multi-scan	multi-scan
CCDC	1988637	1988644	1988651	1988640

[a] $R_1 = \Sigma||F_0|- |F_c||/ \Sigma|F_0|$; [b] $wR_2 = [\Sigma[w(F_0^2-F_c^2)^2]/\Sigma[w(F_0)^2]]^{1/2}$; $w = [\sigma c^2(F_0^2)+(xP)^2+yP]^{-1}$ and $P = (F_0^2+2F_c^2)/3$; [c] GooF = $\{\Sigma[w(F_o^2-F_c^2)^2]/(n-p)\}^{1/2}$ (n = number of reflections; p = total number of parameters).

Table S4. Crystallographic data of **12b**–**15**.

	12b	**13**	**14**	**15**
Formula	$C_9H_{12}Cl_2CuN_{24}O_8$	$C_{18}H_{20}CuN_{22}O_{18}$	$C_9H_7CuN_{11}O_9$	$C_{18}H_{20}CuN_{22}O_{22}$
FW [g mol^{-1}]	718.87	896.10	476.80	960.10
Crystal system	trigonal	triclinic	orthorhombic	monoclinic
Space Group	*P*−3*c*1	*P*−1	*Fddd*	$P2_1/c$
Color / Habit	blue block	green needle	green rod	green platelet
Size [mm]	0.19 x 0.28 x 0.31	0.10 x 0.18 x 0.50	0.03 x 0.03 x 0.10	0.06 x 0.14 x 0.48
a [Å]	9.5769(4)	5.1257(5)	8.4483(5)	29.4298(18)
b [Å]	9.5769(4)	11.3567(10)	18.9436(10)	5.2957(3)
c [Å]	15.0033(8)	15.7277(14)	40.114(2)	22.6692(16)
α [°]	90	109.709(8)	90	90
β [°]	90	95.177(7)	90	94.205(6)
γ [°]	120	96.948(7)	90	90
V [Å^3]	1191.70(14)	847.11(14)	6419.9(6)	3523.5(4)
Z	2	1	16	4
$\rho_{calc.}$ [g cm^{-3}]	2.003	1.757	1.973	1.810
μ [mm^{-1}]	1.238	0.757	1.445	0.743
F(000)	722	455	3824	1948
$\lambda_{MoK\alpha}$ [Å]	0.71073	0.71073	0.71073	0.71073
T [K]	111	119	103	122
θ Min–Max [°]	2.5, 26.4	2.7, 26.4	3.7, 26.4	1.9, 26.4
Dataset	−11: 11; −11: 11; −17: 18	−6: 6; −14: 13; −16: 19	−10: 10; −23: 23; −50: 50	−36: 28; −6: 6; −28: 27
Reflections collected	6723	5170	21752	18136
Independent refl.	814	3458	1637	7206
R_{int}	0.033	0.025	0.027	0.075
Observed reflections	710	2932	1565	4570
Parameters	68	284	140	616
R_1 (obs)[a]	0.0357	0.0377	0.0267	0.0658
wR_2 (all data)[b]	0.0850	0.0908	0.0780	0.1365
GooF[c]	1.20	1.04	1.11	1.04
Resd. Dens. [e Å^{-3}]	−0.37, 0.30	−0.38, 0.49	−0.38, 0.41	−0.55, 0.72
Absorption correction	multi-scan	multi-scan	multi-scan	multi-scan
CCDC	1988638	1988650	1988641	1988634

[a] $R_1 = \Sigma||F_0|- |F_c||/ \Sigma|F_0|$; [b] $wR_2 = [\Sigma[w(F_0^2-F_c^2)^2]/\Sigma[w(F_0)^2]]^{1/2}$; $w = [\sigma c^2(F_0^2)+(xP)^2+yP]^{-1}$ and $P = (F_0^2+2F_c^2)/3$; [c] GooF = $\{\Sigma[w(F_o^2-F_c^2)^2]/(n-p)\}^{1/2}$ (n = number of reflections; p = total number of parameters).

Table S5. Crystallographic data of **16**–**18**.

	16	**17**	**18**
Formula	$C_{18}H_{16}CuN_{22}O_{16}$	$C_{18}H_{16}CuN_{22}O_{18}$	$C_{18}H_{16}CuN_{22}O_{20}$
FW [g mol^{-1}]	860.07	892.07	924.08
Crystal system	triclinic	monoclinic	monoclinic
Space Group	*P*−1	*C*2/*c*	$P2_1/n$
Color / Habit	yellow-green plate	brown block	light-green platelet
Size [mm]	0.07 x 0.28 x 0.46	0.07 x 0.24 x 0.40	0.06 x 0.20 x 0.42
a [Å]	8.7150(5)	20.1935(8)	9.3445(4)
b [Å]	10.1336(8)	8.7385(3)	8.8131(3)
c [Å]	10.3049(9)	17.9519(8)	18.9573(8)
α [°]	113.289(8)	90	90
β [°]	91.470(6)	91.541(4)	103.347(4)
γ [°]	110.637(7)	90	90
V [Å^3]	767.73(12)	3166.7(2)	1519.04(11)
Z	1	4	2
$\rho_{calc.}$ [g cm^{-3}]	1.860	1.871	2.020
μ [mm^{-1}]	0.827	0.810	0.853
F(000)	435	1804	934
$\lambda_{MoK\alpha}$ [Å]	0.71073	0.71073	0.71073
T [K]	122	120	117
θ Min–Max [°]	2.2, 26.4	3.4, 26.4	3.5, 26.7
Dataset	−9: 10; −12: 10; −12: 12	−25: 25; −10: 7; −22: 22	−11: 11; −11: 9; −23: 23
Reflections collected	4159	12435	12575
Independent refl.	3101	3232	3211
R_{int}	0.027	0.037	0.054
Observed reflections	2537	2585	2498
Parameters	267	280	293
R_1 (obs)[a]	0.0423	0.0444	0.0367
wR_2 (all data)[b]	0.0946	0.1210	0.0822
GooF[c]	1.08	1.04	1.05
Resd. Dens. [e Å^{-3}]	−0.51, 0.46	−0.29, 1.00	−0.41, 0.37
Absorption correction	multi-scan	multi-scan	multi-scan
CCDC	1988635	1988646	1988645

[a] $R_1 = \Sigma||F_0|- |F_c||/ \Sigma|F_0|$; [b] $wR_2 = [\Sigma[w(F_0^2-F_c^2)^2]/\Sigma[w(F_0)^2]]^{1/2}$; $w = [\sigma c^2(F_0^2)+(xP)^2+yP]^{-1}$ and $P = (F_0^2+2F_c^2)/3$; [c] GooF = $\{\Sigma[w(F_o^2-F_c^2)^2]/(n-p)\}^{1/2}$ (n = number of reflections; p = total number of parameters).

Similar to complex **13**, ECC **15** is forming complex monomers with two 1,1-dtm and four aqua ligands around the central metal. The complex unit is completed by two mono-deprotonated and non-coordinating trinitrophloroglucinate anions (Figure S5).

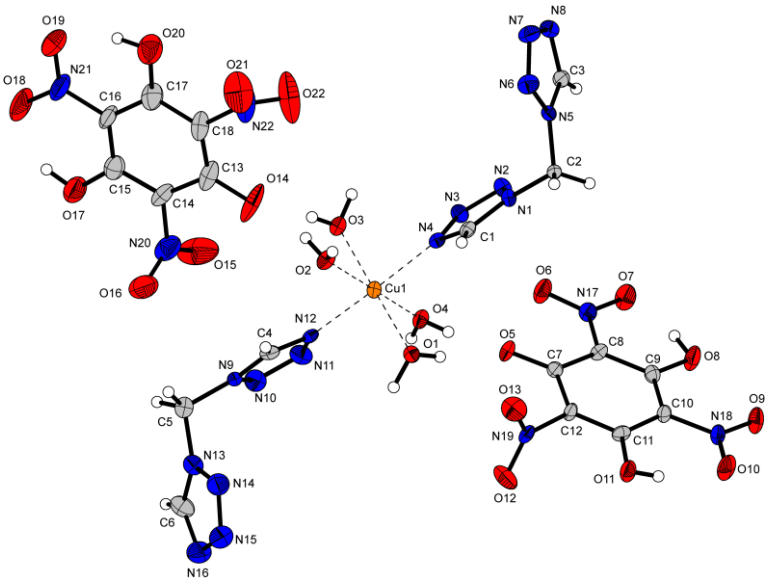

Figure S5. Molecular unit of trinitrophloroglucinate complex **15**. Selected bond lengths (Å): Cu1–O2 1.970(4), Cu1–O3 2.340(4), Cu1–N4 2.007(3). Selected bond angles (°): O1–Cu1–O2 92.69(14), O1–Cu1–O3 178.63(12), O1–Cu1–N4 88.61(13), N4–Cu1–N12 176.53(14).

Nitroaromatic complexes **17** and **18** show the same build up as compound **16**, forming polymeric chains by the bridging of two ditetrazolyl ligands between the same two copper(II) cations. In both cases the anions are mono-deprotonated and non-coordinating (Figures S6 and S7).

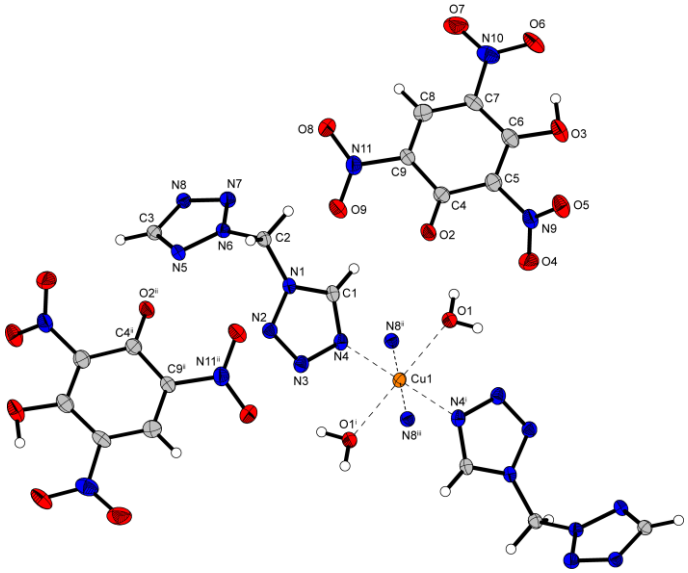

Figure S6. Copper(II) coordination environment of **17**. Selected bond lengths (Å): Cu1–O1 2.264(2), Cu1–N4 2.0225(19), Cu1–N8^{ii} 2.0259(19). Selected bond angles (°): O1–Cu1–N4 87.35(7), O1–Cu1–N8^{ii} 91.47(7), O1^{i}–Cu1–N4 92.65(7). Symmetry codes: (i) 1−x, −y, 1−z; (ii) 1−x, 1−y, 1−z; (iii) x, −1+y, z.

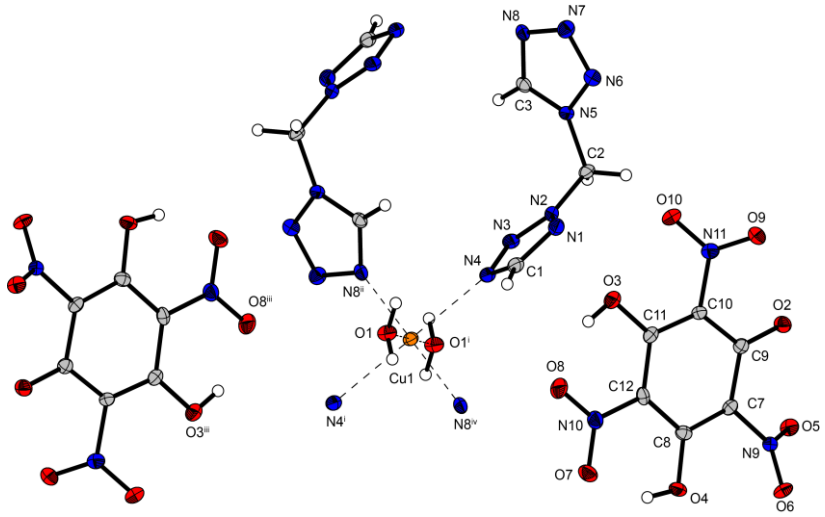

Figure S7. Extended molecular unit of **18**. Selected bond lengths (Å): Cu1–O1 2.0026(19), Cu1–N4 2.405(2), Cu1–N8^{ii} 2.0107(19). Selected bond angles (°): O1–Cu1–N4 89.56(7), O1–Cu1–N8^{ii} 90.94(8), N4–Cu1–N8^{iv} 88.86(7). Symmetry codes: (i) 1−x, 1−y, 1−z; (ii) 1−x, −y, 1−z; (iii) 2−x, 1−y, 1−z; (iv) x, 1+y, z.

6.6.4. DTA Plots

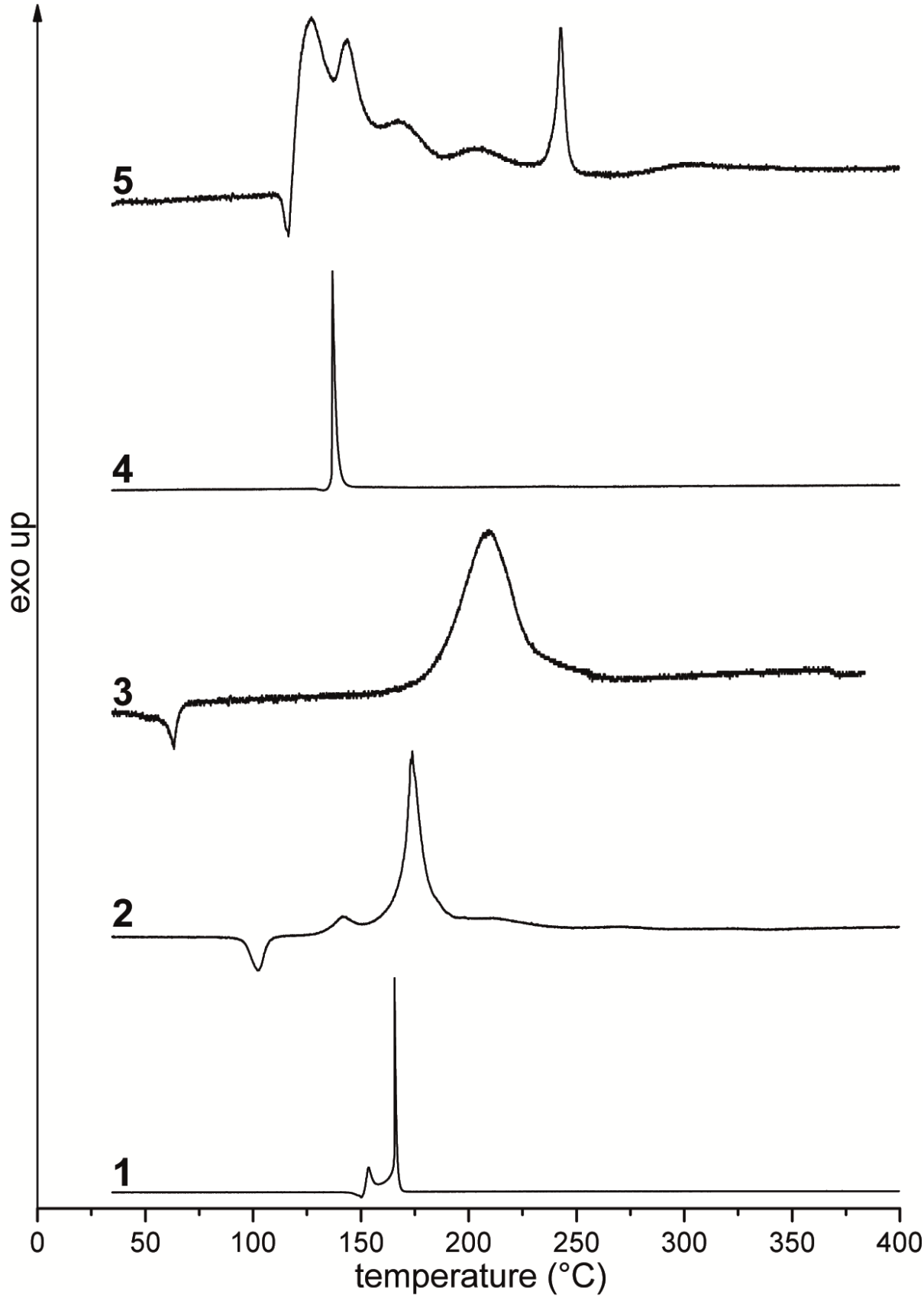

Figure S8. DTA plots of compounds **1**–**5**.

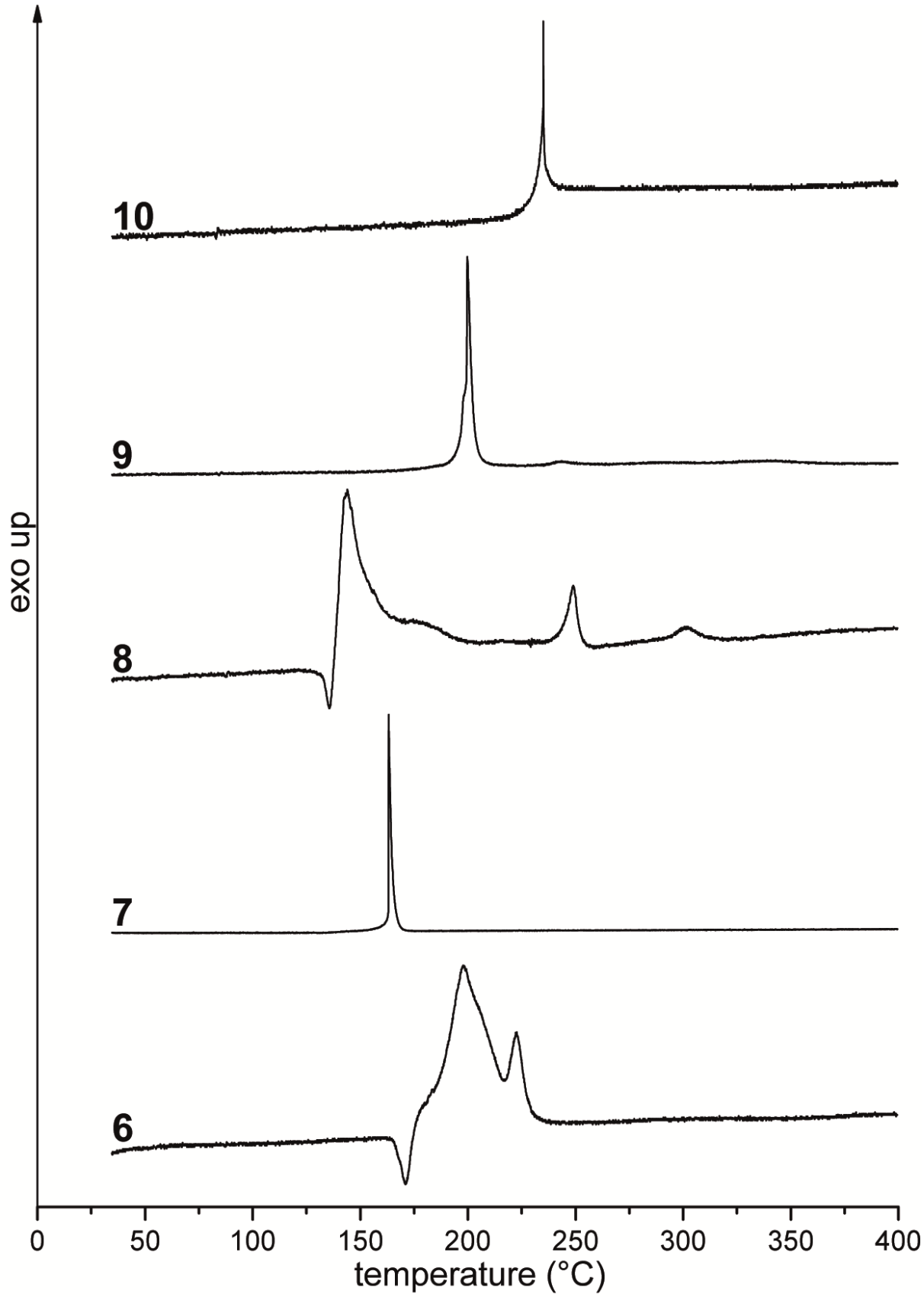

Figure S9. DTA plots of complexes **6**–**10**.

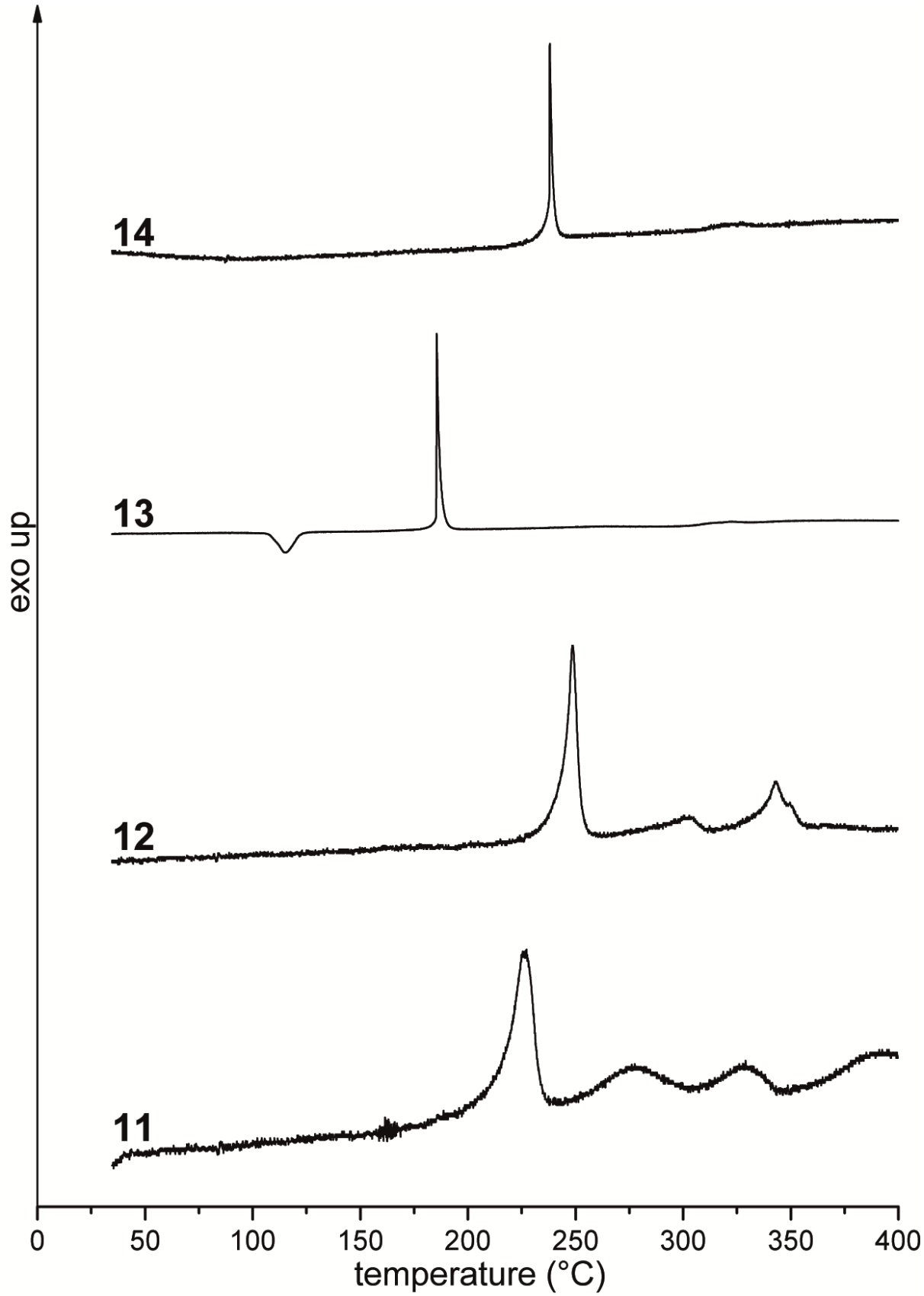

Figure S10. DTA plots of complexes **11**–**14**.

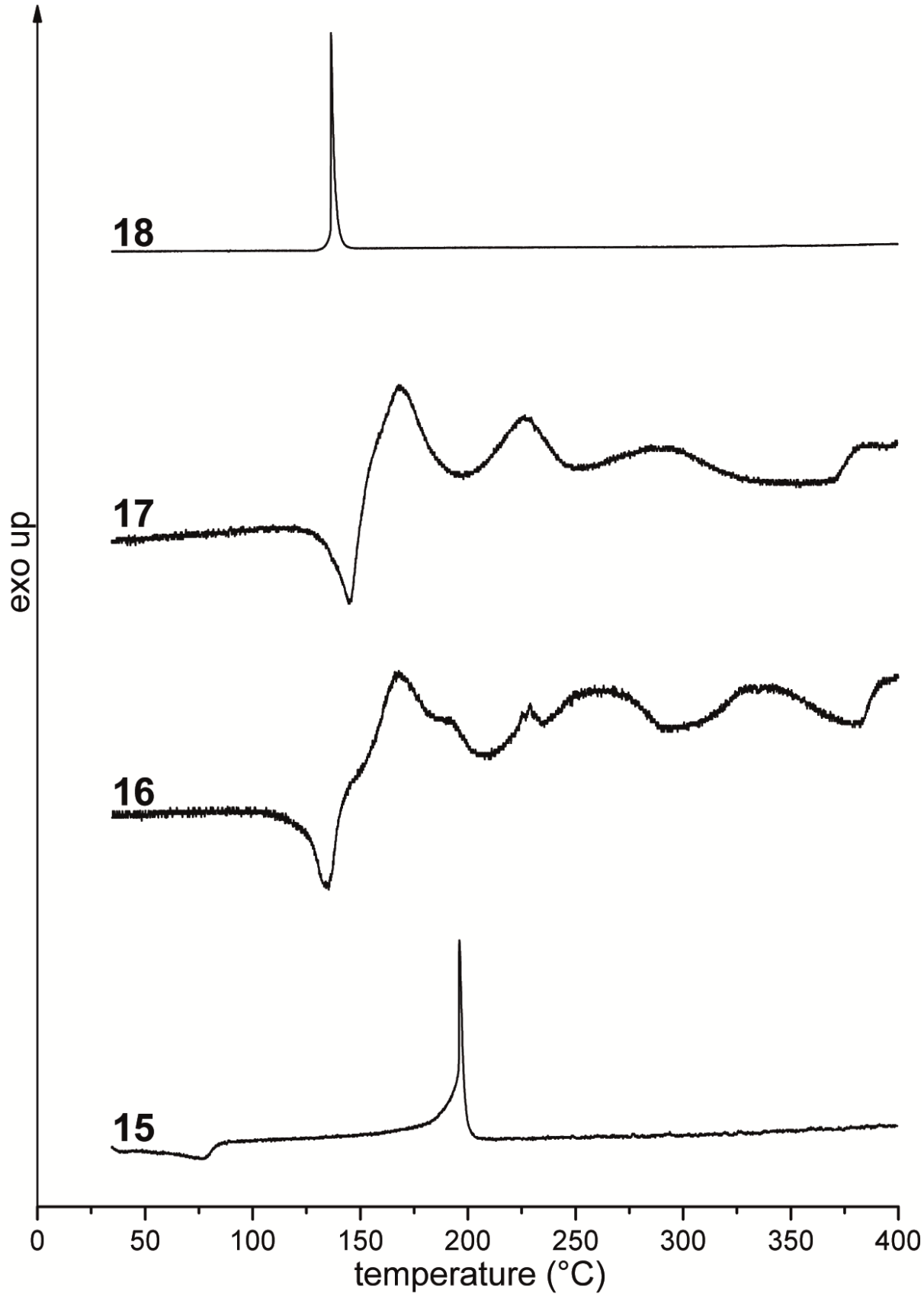

Figure S11. DTA plots of complexes **15**–**18**.

6.6.5. Hot Plate and Hot Needle Tests

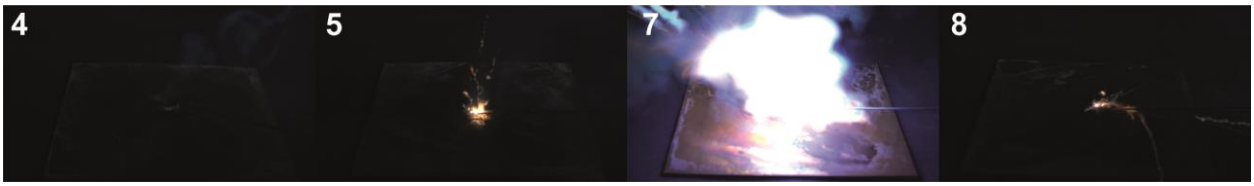

Figure S12. Outcome during HN tests of silver(I) complexes **4**, **5**, **7**, and **8**.

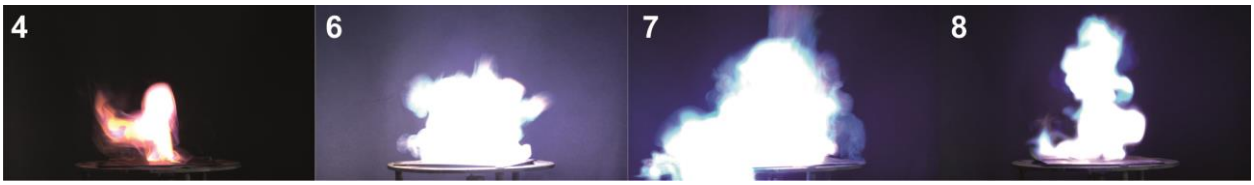

Figure S13. Moments of deflagration of silver(I) complexes **4** and **6**–**8** during HP tests.

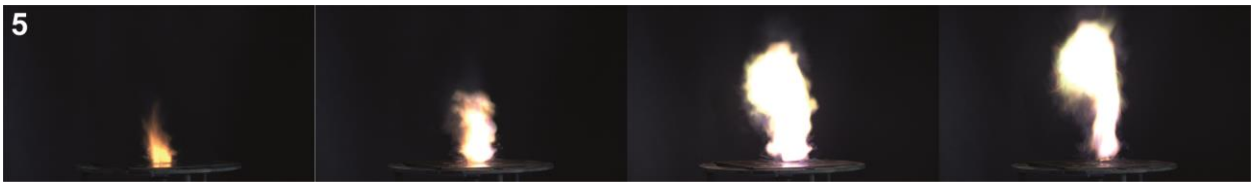

Figure S14. Deflagration of ECC **5** during HP test shown as sequence.

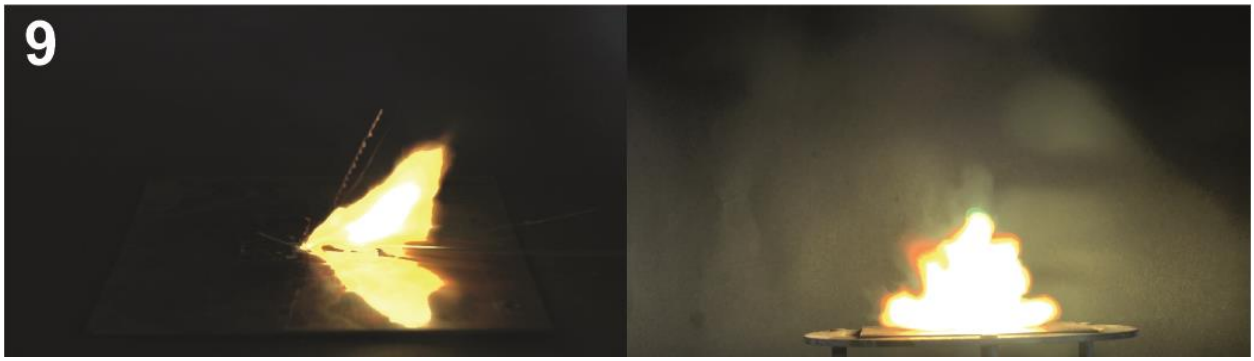

Figure S15. Moment of deflagration of $[Cu_2(NO_3)_4(2,2\text{-dtm})_3]$ (**9**) during HP and HN tests.

Figure S16. Outcome during HN tests of copper(II) perchlorate complexes **10**–**12**.

Figure S17. Moments of deflagration of ECC **14**, **15**, **17**, and **18**.

6.6.6. Initiation Capability Tests

As the initiating capability of compounds indicate their potential use as primary explosives, the most promising ECC (copper(II) perchlorate complexes **10**–**12)** were tested in classical copper shell initiation experiments. The compound to be investigated was loosely filled on top of a pressed (8 kg weight) main charge (200 mg PETN) and ignited using an electrical ignitor (Figure S8).

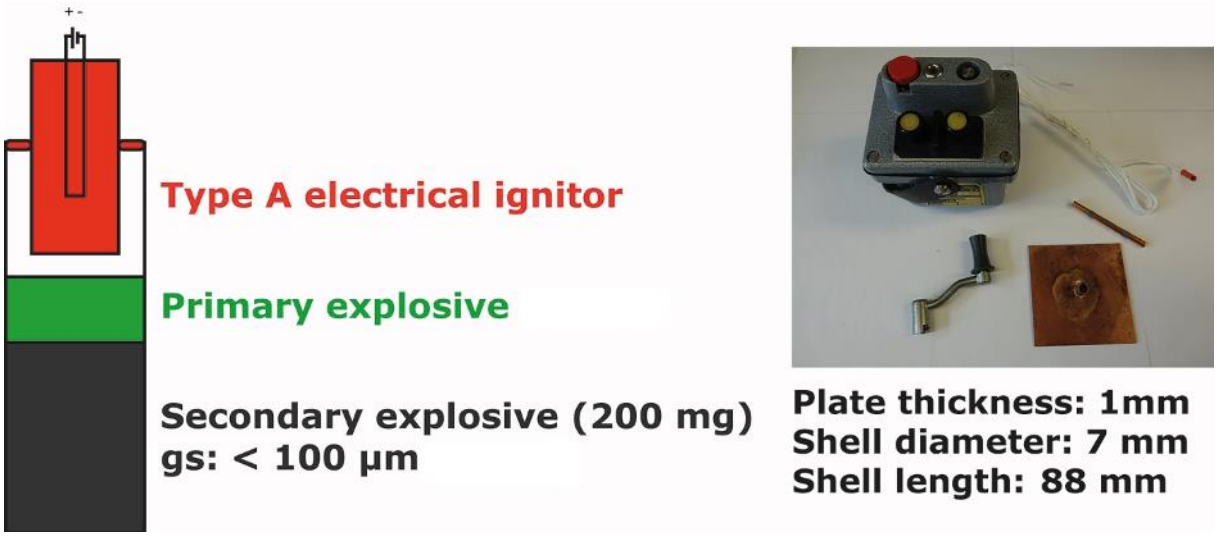

Figure S18. Schematic test setup (left) and used equipment (right) for the initiation capability tests.

6.6.7. Heat of Formation Calculations

All quantum chemical calculations were carried out using the Gaussian G09 program package.[20] The enthalpies (H) and free energies (G) were calculated using the complete basis set (CBS) method of *Petersson* and coworkers in order to obtain very accurate energies. The CBS models are using the known asymptotic convergence of pair natural orbital expressions to extrapolate from calculations using a finite basis set to the estimated CBS limit. CBS-4 starts with an HF/3-21G(d) geometry optimization; the zero-point energy is computed at the same level. It then uses a large basis set SCF calculation as a base energy, and an MP2/6- 31+G calculation with a CBS extrapolation to correct the energy through second order. A MP4(SDQ)/6-31+(d,p) calculation is used to approximate higher order contributions. In this study, we applied the modified CBS-4M method.

Heats of formation of the synthesized neutral compounds **1**–**3** were calculated using the atomization method (equation S1) using room temperature CBS-4M enthalpies, which are summarized in Table S6.[21,22]

$$\Delta_f H^\circ_{(g,\,M,\,298)} = H_{(Molecule,\,298)} - \sum H^\circ_{(Atoms,\,298)} + \sum \Delta_f H^\circ_{(Atoms,\,298)} \quad (S1)$$

Table S6. CBS-4M enthalpies for atoms C, H, N, and O and their literature values for atomic $\Delta H°_f^{298}$ / kJ mol^{-1}.

	$-H^{298}$ / a.u.	NIST
H	0.500991	218.2
C	37.786156	717.2
N	54.522462	473.1
O	74.991202	249.5

The gas-phase enthalpy of formation was converted into the solid state (standard conditions) enthalpy of formation. The calculation results are summarized in Table S7.

Table S7. Heat of formation calculation of **1**–**3**.

M	$-H^{298}$ / a.u.[a]	$\Delta_f H°$(g,M) / kJ mol^{-1}[b]	$\Delta_f H°$(s) / kJ mol^{-1}[c]
1	−553.867082	699.3	620.7
2	−553.878902	668.3	598.9
3	−553.885838	650.1	587.8

[a] CBS-4M electronic enthalpy; [b] gas phase enthalpy of formation; [c] standard solid state enthalpy of formation.

6.6.8. References

[1] NATO standardization agreement (STANAG) on explosives, impact sensitivity tests, no. 4489, 1st ed., Sept. 17, **1999**.

[2] WIWEB-Standardarbeitsanweisung 4-5.1.02, Ermittlung der Explosionsgefährlichkeit, hier der Schlagempfindlichkeit mit dem Fallhammer, Nov. 8, **2002**.

[3] OZM, http://www.ozm.cz, (accessed January 2020).

[4] BAM, http://www.bam.de, (accessed January 2020).

[5] Military Standard 1751A (MIL-STD-1751A): safety and performance tests for qualification of explosives (high explosives, propellants and pyrotechnics), method 1016, Dec. 11, **2001**.

[6] UN Model Regulation: Recommendations on the Transport of Dangerous Goods – Manual of Tests and Criteria, section 13.4.2.3.3, **2015**.

[7] NATO standardization agreement (STANAG) on explosive, friction sensitivity tests, no. 4487, 1st ed., Aug. 22, **2002**.

[8] WIWEB-Standardarbeitsanweisung 4-5.1.03, Ermittlung der Explosionsgefährlichkeit oder der Reibeempfindlichkeit mit dem Reibeapparat, Nov. 8, **2002**.

[9] Impact: insensitive > 40 J, less sensitive ≥ 35 J, sensitive ≥ 4 J, very sensitive ≤ 3 J; Friction: insensitive > 360 N, less sensitive = 360 N, sensitive < 360 N and > 80 N, very sensitive ≤ 80 N, extremely sensitive ≤ 10 N. According to the UN Recommendations on the Transport of Dangerous Goods, 5th ed., **2009**.

[10] a) CrystalExplorer 17.5 Software Package, M. J. Turner, J. J. McKinnon, S. K. Wolff, D. J. Grimwood, P. R. Spackman, D. Jayatilaka, M. A. Spackman; b) D. Jayatilaka, D. J. Grimwood, in Computational Science – ICCS **2003**, Springer, Berlin **2003**, pp. 142–151.

[11] M. A. Spackman, J. J. McKinnon, *CrystEngComm* **2002**, *4*, 378–392.

[12] CrysAlisPRO (Version 171.33.41), Oxford Diffraction Ltd., **2009**.

[13] A. Altomare, G. Cascarano, C. Giacovazzo, A. Guagliardi, *J. Appl. Crystallogr.* **1993**, *26*, 343–350.

[14] a) A. Altomare, G. Cascarano, C. Giacovazzo, A. Guagliardi, A. G. G. Moliterni, M. C. Burla, G. Polidori, M. Camalli, R. Spagna, *SIR97*, **1997**; b) A. Altomare, M. C. Burla, M. Camalli, G. L. Cascarano, C. Giacovazzo, A. Guagliardi, A. G. G. Moliterni, G. Polidori, R. Spagna, *J. Appl. Crystallogr.* **1999**, *32*, 115–119.

[15] a) G. M. Sheldrick, SHELXL-97, University of Göttingen, Germany, **1997**; b) G. M. Sheldrick, *Acta Crystallogr. Sect. A* **2008**, *64*, 112.

[16] A. L. Spek, PLATON, Utrecht University, The Netherlands, **1999**.

[17] L. J. Farrugia, *J. Appl. Cryst.* **2012**, *45*, 849.

[18] Empirical absorption correction using spherical harmonics, implemented in SCALE3 ABSPACK scaling algorithm (CrysAlisPro Oxford Diffraction Ltd., Version 171.33.41, **2009**).

[19] APEX3, Bruker AXS Inc., Madison, Wisconsin, USA.

[20] M. J. Frisch, G. W. Trucks, H. B. Schlegel, G. E. Scuseria, M. A. Robb, J. R. Cheeseman, G. Scalmani, V. Barone, B. Mennucci, G. A. Petersson, H. Nakatsuji, M. Caricato, X. Li, H. P. Hratchian, A. F. Izmaylov, J. Bloino, G. Zheng, J. L. Sonnenberg, M. Hada, M. Ehara, K. Toyota, R. Fukuda, J. Hasegawa, M. Ishida, T. Nakajima, Y. Honda, O. Kitao, H. Nakai, T. Vreven, J. A. Montgomery, Jr., J. E. Peralta, F. Ogliaro, M. Bearpark, J. J. Heyd, E. Brothers, K. N. Kudin, V. N. Staroverov, R. Kobayashi, J. Normand, K. Raghavachari, A. Rendell, J. C. Burant, S. S. Iyengar, J. Tomasi, M. Cossi, N. Rega, J. M. Millam, M. Klene, J. E. Knox, J. B. Cross, V. Bakken, C. Adamo, J. Jaramillo, R. Gomperts, R. E. Stratmann, O. Yazyev, A. J. Austin, R. Cammi, C. Pomelli, J. W. Ochterski, R. L. Martin, K. Morokuma, V. G. Zakrzewski, G. A. Voth, P. Salvador, J. J. Dannenberg, S. Dapprich, A. D. Daniels, O. Farkas, J. B. Foresman, J. V. Ortiz, J. Cioslowski, D. J. Fox, Gaussian 09 A.02, Gaussian, Inc., Wallingford, CT, USA, **2009**.

[21] a) J. W. Ochterski, G. A. Petersson, J. A. Montgomery Jr., *J. Chem. Phys.* **1996**, *104*, 2598–2619; b) J. A. Montgomery Jr., M. J. Frisch, J. W. Ochterski G. A. Petersson, *J. Chem. Phys.* **2000**, *112*, 6532–6542.

[22] a) L. A. Curtiss, K. Raghavachari, P. C. Redfern, J. A. Pople, *J. Chem. Phys.* **1997**, *106*, 1063–1079; b) E. F. C. Byrd, B. M. Rice, *J. Phys. Chem.* A **2006**, *110*, 1005–1013; c) B. M. Rice, S. V. Pai, J. Hare, *Combust. Flame* **1999**, *118*, 445–458.

[23] a) H. D. B. Jenkins, H. K. Roobottom, J. Passmore, L. Glasser, *Inorg. Chem.* **1999**, *38*, 3609–3620; b) H. D. B. Jenkins, D. Tudela, L. Glasser, *Inorg. Chem.* **2002**, *41*, 2364–2367.

7. Salts of Picramic Acid – Nearly Forgotten Temperature-Resistant Energetic Materials

Maximilian H. H. Wurzenberger, Jasmin T. Lechner, Marcus Lommel, Thomas M. Klapötke, and Jörg Stierstorfer

Dedicated to Dr. Klaus Römer on the Occasion of his 80th Birthday

Published in *Propellants, Explosives, Pyrotechnics* **2020**, *45*, 898–907.

DOI: 10.1002/prep.201900402

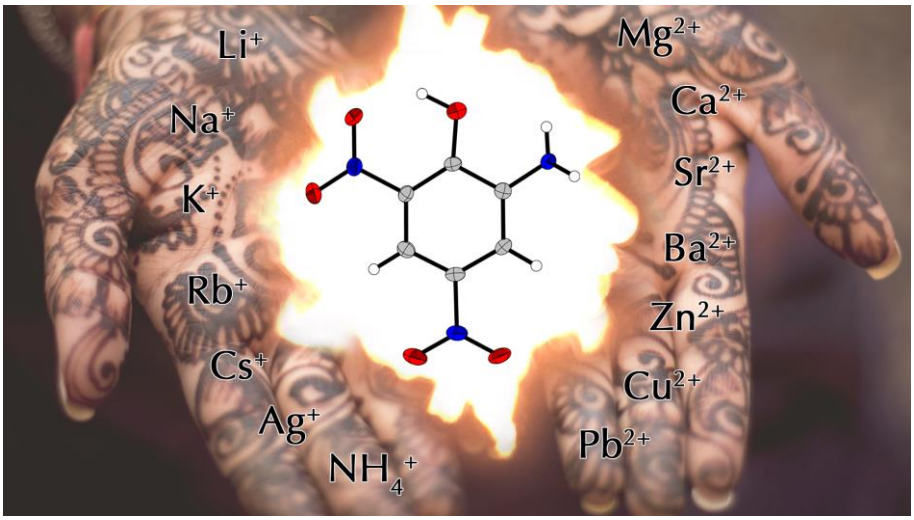

Abstract: Thermally stable explosives are becoming more and more important nowadays due to their important role in the oil and mining industry. The requirements of these explosives are constantly changing. Picramate-based compounds are poorly investigated toward their energetic properties as well as sensitivities. In this work, 13 different salts of picramic acid were synthesized as potential energetic materials with high thermal stability in a simple one-step reaction and compared with commercially used lead picramate. The obtained compounds were extensively characterized by *e.g.*, XRD, IR, EA, DTA, and TGA. In addition, the sensitivities toward impact and friction were determined with the BAM drop hammer and the BAM friction tester. Also, the electrostatic discharge sensitivity was explored. Calculations of the energetic performance of selected compounds were carried out with the current version of EXPLO5 code. Therefore, heats of formation were computed and X-ray densities were converted to room temperature. Some of the synthesized salts show promising characteristics with high exothermic decomposition temperatures. Especially, the water-free rubidium, cesium, and barium salts **5**, **6**, and **10** with decomposition temperatures of almost 300 °C could be promising candidates for future applications.

7.1. Introduction

The field of energetic materials is manifold and can be divided into several subgroups, such as propellants, primary or high explosives, which is leading to numerous and diverse applications.[1–3] Especially, due to the increased environmental awareness, there are many research groups around the world working on the development of ever more efficient molecules. The new compounds should, if possible, be less toxic and harmful to the environment than current molecules and at the same time also cheaper to produce.[4–6] Various strategies exist for designing new energetic materials, like increasing the energy of a molecule by ring or cage strain. Another approach is the synthesis of nitrogen-rich compounds, which release a lot of energy during their decomposition, due to their large endothermic heat of formation. The third strategy is the combination of fuel (carbon-backbone) and oxidizer (nitro groups) in one molecule. Various examples for this concept are displayed in Chart 1, with 2,4,6-trinitrotoluene (TNT) being the most favorite one, since it was the most commonly used explosive in World War I and is still used in explosive charges today.[2,7]

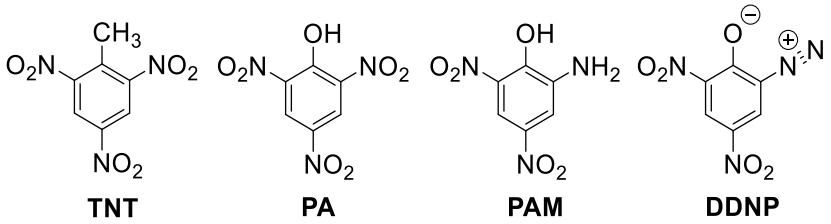

Chart 1. Chemical structures of 2,4,6-trinitrotoluene (TNT), 2,4,6-trinitrophenol (PA), 2-amino-4,6-dinitrophenol (PAM), and diazodinitrophenol (DDNP).

Another famous representative of this group is picric acid (PA), which replaced black powder at the end of the 19th century in military applications.[8] Later it was substituted by TNT itself because it caused undesired formations of very sensitive metal salts in grenades and mines.[2,9] A rather uncommon representative is 2-amino-4,6-dinitrophenol, also known as picramic acid (PAM), which can be obtained by partial reduction of PA with sodium hydrogen sulfide, ammonium sulfide or hydrazine. PAM is known for its explosive character but the neutral compound and the associated sodium salt are more familiar as ingredients for 'henné' color in hair and skin colorants.[10–12] Indeed, picramic acid and some of its soluble salts are more well-known as precursors for the synthesis of diazodinitrophenol (DDNP), an efficient heavy metal-free primary explosive.[10,13] In 1961 Glowiak *et al*. demonstrated, based on lead picrate and lead picramate, that the replacement of a nitro group by an amino group leads to an increase in thermal stability with simultaneously reduced impact sensitivity.[14] This was also confirmed by Agrawal, who developed some approaches to increase the thermal stability of energetic molecules. He particularly emphasized the concepts "salt formation" and "introduction of amino groups".[1] Agrawal *et al*. examined

the energetic characteristics of iron(II), cobalt(II), nickel(II), copper(II), silver(I), zinc(II), cadmium(II), and mercury(I) picramate.[15–17] A few years later, Srivastava and Agrawal investigated titanium(IV), zirconium(IV), and thorium(IV) as well as palladium(IV) and uranium(IV) picramate.[18,19] All metal picramates showed energetic properties but are only partly investigated, except lead picramate, which is the only salt used for industrial applications nowadays, especially in fuse head compositions of electric detonators.[20,21] Accordingly, alkali and alkaline earth picramates, as well as ammonium picramate, could be promising thermally stable energetic compounds. In this work, these compounds were synthesized as well as their energetic properties studied and compared. A few already known salts were reinvestigated in detail, due to the lack of analytical data in the literature.

7.2. Experimental Section

CAUTION! *All investigated compounds are energetic materials and some of them show increased sensitivities toward various stimuli (e.g., elevated temperatures, impact, friction or electronic discharge). Although no hazards occurred, proper security precautions (safety glasses, face shield, earthed equipment and shoes, leather jacket, Kevlar sleeves, and earplugs) have to be worn while synthesizing and handling the described compounds*.

More information on the general methods and syntheses of compounds **2–15** can be found in the Supporting Information.

7.3. Results and Discussion

7.3.1. Synthesis

Sodium picramate monohydrate (**1**) was available in sufficient quantities in the research group and can be synthesized according to a literature procedure (Scheme 1).[22] It was used as starting material to prepare picramic acid (**2**) (Scheme 2) by straightforward protonation with hydrochloric acid.

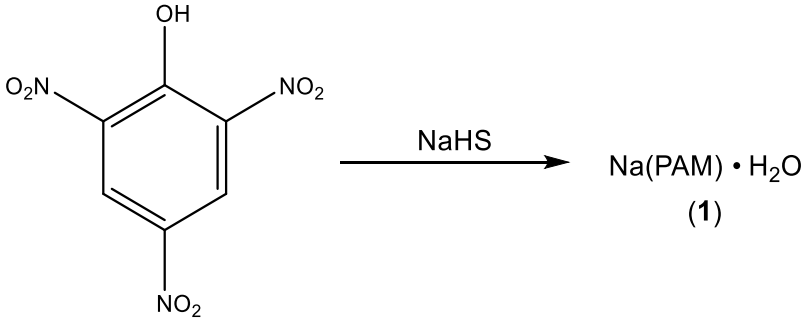

Scheme 1. Synthesis of sodium picramate (**1**, Na(PAM)).

The isolated picramic acid (**2**) was further reacted in simple metathesis reactions to the corresponding salts **3–14**. It was dissolved in ethanol and a metal salt of the desired cation in water was added (Scheme 2), which led in all cases to a darkening of the solution.

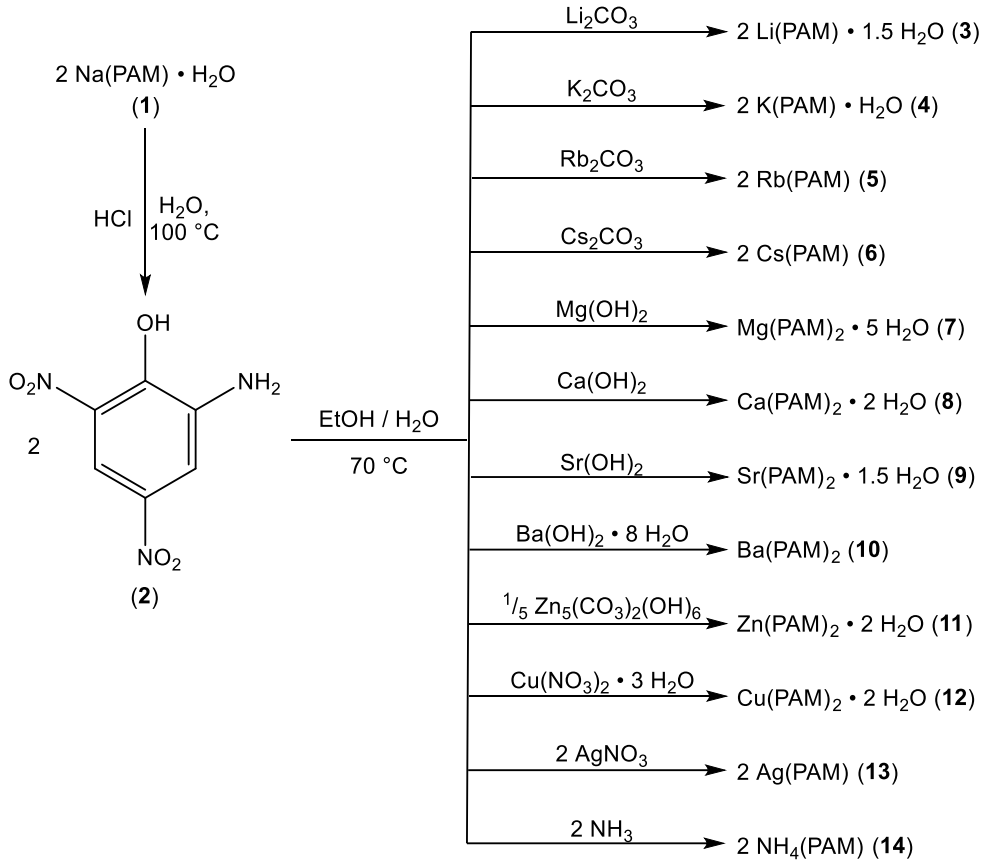

Scheme 2. Reaction scheme for the synthesis of the energetic salts **3**–**14**.

For a successful synthesis, an alkaline milieu had to be ensured during the whole reaction. For obtaining the alkali salts of picramic acid, the corresponding carbonates were used. Compounds **3–6** were filtered off after crystallization of sufficient amounts during evaporation of the solvent in air. For the syntheses of the alkaline earth salts **7–10** the corresponding metal hydroxides were used. Magnesium picramate (**7**) was obtained as pentahydrate in the form of single crystals suitable for X-ray diffraction experiments. The remaining alkaline earth salts could only be isolated as microcrystalline solids, due to their low solubility. For the synthesis of zinc(II) picramate (**11**), basic zinc(II) carbonate was used. The low solubility of $Zn(PAM)_2$ leads to the immediate precipitation of the product after mixing of the solutions. Similar circumstances were observed during the synthesis of silver(I) and copper(II) picramates (**12** and **13**), starting from the corresponding nitrate salts. Single crystals of **11** and **12** were obtained by layering aqueous solution of the nitrate salts with ethanolic solutions of HPAM to ensure slow formation at the phase boundary. The yields can be increased by evaporation of the remaining mother liquor. Ammonium picramate (**14**) was received by the addition of aqueous ammonia to the solution of picramic acid. After

evaporation of the solvent, **14** was obtained as crystalline material. In case of lead picramate (**15**), the reaction of the free acid with a soluble lead salt did not lead to the formation of the desired product. Instead, sodium picramate (**1**) was utilized as starting material (Scheme 3) leading to the direct precipitation of lead picramate.

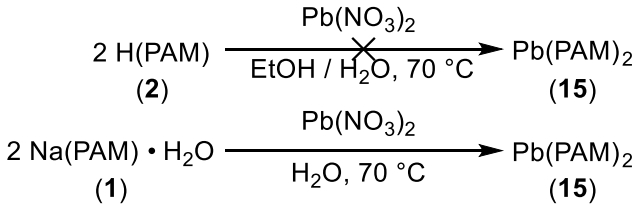

Scheme 3. Reaction scheme for the preparation of lead picramate (**15**).

7.3.2. Crystal Structures

Until today only the crystal structures of the free acid, as well as the potassium salt, were measured at room-temperature and published as private communications.[23,24] Therefore, low-temperature single-crystal X-ray diffraction experiments of compounds **1–7**, **10b**, **11**, **12**, and **14** were performed. The crystal structures have been uploaded to the CSD database and are available under the CCDC numbers 1965957 (**1**), 1965965 (**2**), 1965964 (**3**), 1965963 (**4**), 1965958 (**5**), 1965966 (**6**), 1965967 (**7**), 1965960 (**10b**), 1965962 (**11**), 1965959 (**12**), and 1965961 (**14**). Due to the very low solubility of pure barium picramate (**10**), it was only possible to obtain single crystals from saturated DMSO solutions. This led to the incorporation of both, DMSO and water solvent molecules (**10b**). Details on the measurement and refinement data of all structures are given in the Supporting Information (Tables S1–3). The neutral compound **2** crystallizes in the form of red blocks in the triclinic space group *P*−1 with a density of 1.730 g cm^{-3} (123 K) and four molecules per unit cell. The bond lengths are in the typical range of comparable compounds and all non-hydrogen atoms, except the oxygens of the nitro groups, are within one plane (Figure 1). Latter ones are only slightly twisted out of the benzol layer. Compared to the parent compound **2**, the deprotonation and interaction with the cations in all other compounds are leading to a shortening of the C−O and elongation of the C−N bonds of the amino groups. The only exception is cesium salt **6** with a contraction of both bonds. The nitro groups in all structures show bonds with almost the same lengths and only vary in the level of twisting out of the benzol plane. Except of **3** (*P*−1), all alkali salts are crystallizing in monoclinic space groups (**1**: *Pc* ; **4**/**5**: $P2_1/c$; **6**: $C2/c$) with increasing densities (Li: 1.707 g cm^{-3} (121 K) < Na: 1.791 g cm^{-3} (127 K) < K: 1.837 g cm^{-3} (135 K) < Rb: 2.226 g cm^{-3} (122 K) < Cs: 2.526 g cm^{-3} (135 K)) in terms of atomic number. A similar trend can be observed in terms of the coordination sphere around the cations: Li: CN = 4/5, Na: CN = 6, K: CN = 9, Rb: CN = 9, Cs: CN = 12. This is also influencing the polymeric structures.

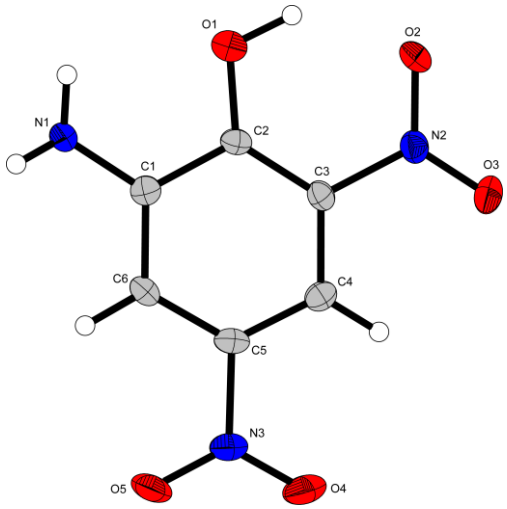

Figure 1. Molecular structure of **2**. Thermal ellipsoids of non-hydrogen atoms in all structures are set to the 50% probability level. Selected bond lengths (Å): C1–N1 1.355(2), C2–O1, 1.331(2), C3–N2 1.453(2), N2–O2 1.244(2), N2–O3 1.220(2), C5–N3 1.464(2), N3–O4 1.225(2), N3–O5 1.224(2), C1–C2 1.419(2), C2–C3 1.399(2), C3–C4 1.395(2), C4–C5 1.376(3), C5–C6 1.395(2), C6–C1 1.394(2).

While lithium compound **3** is building up dimers consisting of two asymmetric units, sodium (**1**), as well as potassium (**4**) picramate, are forming 2D polymeric layers and the rubidium (**5**), as well as cesium (**6**) salt, consist as 3D networks. The dimeric structure of **3** consists of two asymmetric units containing two different lithium ions (Figure 2). While Li1 shows a rather uncommon fivefold coordination by two chelating PAM anions and one additional aqua ligand, Li2 is tetrahedrally coordinated by one amino and one nitro group as well as two water molecules. Furthermore, the two inner anions each are bridging between three cations and the outer two are only coordinating to one lithium ion.

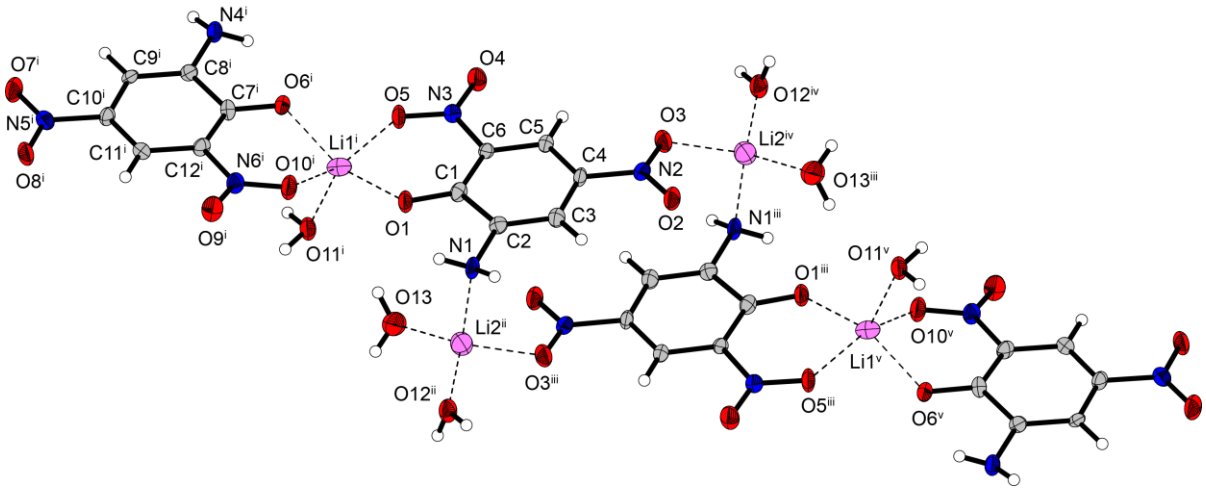

Figure 2. Dimeric structure of **3**. Selected bond lengths (Å): $Li1^{i}$–O1 1.904(8), $Li1^{i}$–O5 2.050(8), $Li1^{i}$–$O6^{i}$ 1.965(8), $Li1^{i}$–$O10^{i}$ 2.062(8), $Li1^{i}$–$O11^{i}$ 2.027(9), $Li2^{ii}$–$O3^{iii}$ 2.018(8), $Li2^{ii}$–$O12^{ii}$ 1.848(9), $Li2^{ii}$–O13 1.903(9). Symmetry codes: (i) 1−x, 1−y, −z; (ii) x, −1+y; (iii) −x, −y, 1−z; (iv) −x, 1−y, 1−z; (v) −1+x, −1+y, 1+z.

Similar to compound **3**, which crystallizes as sesquihydrate, sodium (**1**) and potassium (**4**) picramate are also present as mono- and sesquihydrate, respectively (Figure 3). The only water-free alkaline salts are Rb(PAM) (**5**) and Cs(PAM) (**6**) (Figure 4).

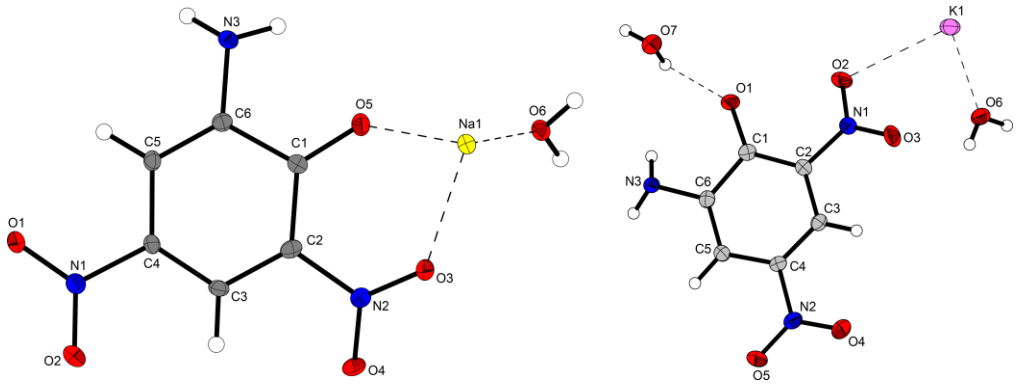

1 **4**

Figure 3. Molecular structure of **1** (left) and extended molecular structure of **4** (right). Selected bond lengths (Å) of **1**: Na1–O3 2.450(6), Na1–O5 2.325(6), Na1–O6 2.359(7). Selected bond lengths (Å) of **4**: K1–O2 2.8133(15), K1–O3 2.9571(16) K1–O6 2.7364(16).

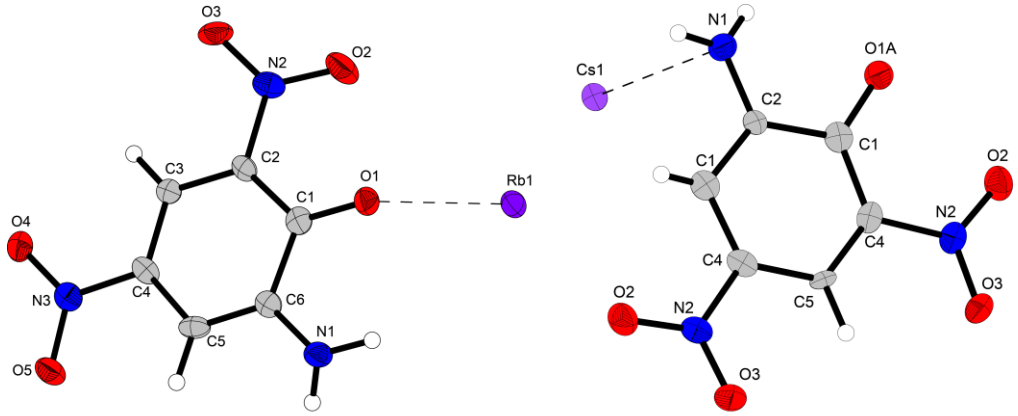

5 **6**

Figure 4. Molecular structure of **5** (left) and **6** (left). Selected bond length (Å) of **5**: Rb1–O1 2.803(3). Selected bond length (Å) of **6**: Cs1–N1 3.4347(9).

Magnesium picramate (**7**) crystallizes as pentahydrate in the form of brown rods in the monoclinic space group $P2_1/c$ with a density of 1.735 g cm^{-3} (109 K) and two molecules per unit cell. There are two different coordinated magnesium cations present, which are both octahedrally coordinated. Mg1 is chelated by two PAM anions and two monodentate aqua ligands, whereas Mg2 is solely bounded by aqua ligands. The unit cell is completed with two non-coordinating water molecules and picramate anions with a significantly twisted nitro group (Figure 5). Recrystallization of water-insoluble Ba(PAM)$_2$ (**10**) from DMSO gave single crystals of **10b** and leads to the incorporation of water as well as solvent molecules. It crystallizes in the form of red rods in the monoclinic space group $P2_1/n$ and a density of 1.949 g cm^{-3}

(127 K). The barium cation is elevenfold coordinated by two anions and one aqua as well as DMSO ligand. The molecular unit is completed by one crystal water molecule (Figure 6).

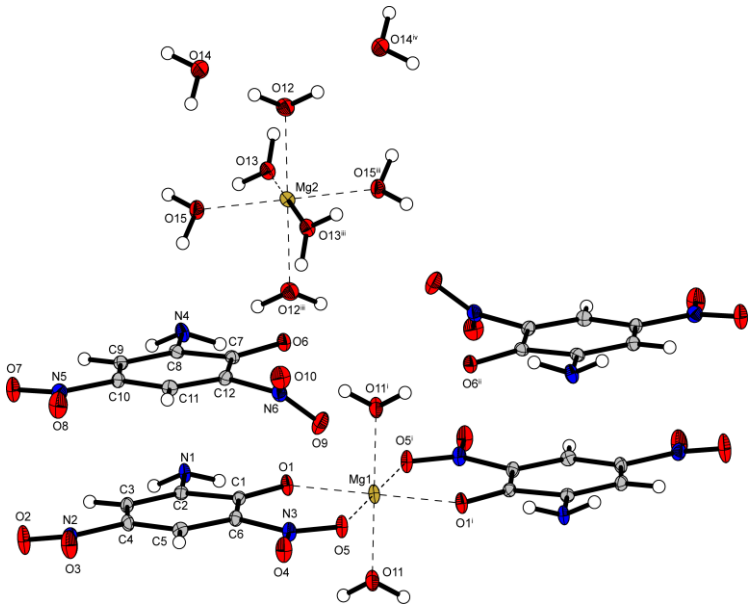

Figure 5. Molecular structure of **7**. Selected bond lengths (Å): Mg1–O1 1.9729(13), Mg1–O5 2.1023(13), Mg1–O11 2.0239(15), Mg2–O12 2.0588(14), Mg2–O13 2.0710(14), Mg2–O15 2.0593(13). Symmetry codes: (i) 2−x, −y, −z; (ii) 1−x, −y, −z; (iii) 1−x, −y, 1−z; (iv) −x, −y, −z.

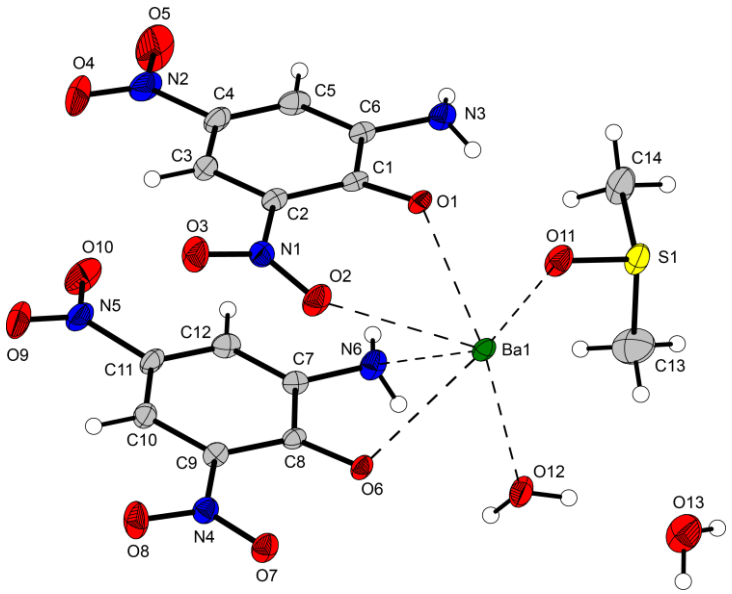

Figure 6. Molecular structure of **10b**. Selected bond lengths (Å): Ba1–O1 2.674(2), Ba1–O2 3.080(2), Ba1–O6 2.833(2), Ba1–O11 2.687(2), Ba1–O12 2.800(3), Ba1–N6 3.051(3).

The zinc(II) (**11**) and copper(II) (**12**) salts of picramic acid crystallize isotypically in the triclinic space group *P*−1 with similar cell axes and volume as well as comparable densities. Both compounds show an octahedral coordination sphere around the central metal, whereas the two aqua ligands occupy the axial positions and two chelating anions are in equatorial positions (Figure 7). Furthermore, a typical Jahn-Teller distortion can be observed along the O6−Cu1−O6^{i} axis.

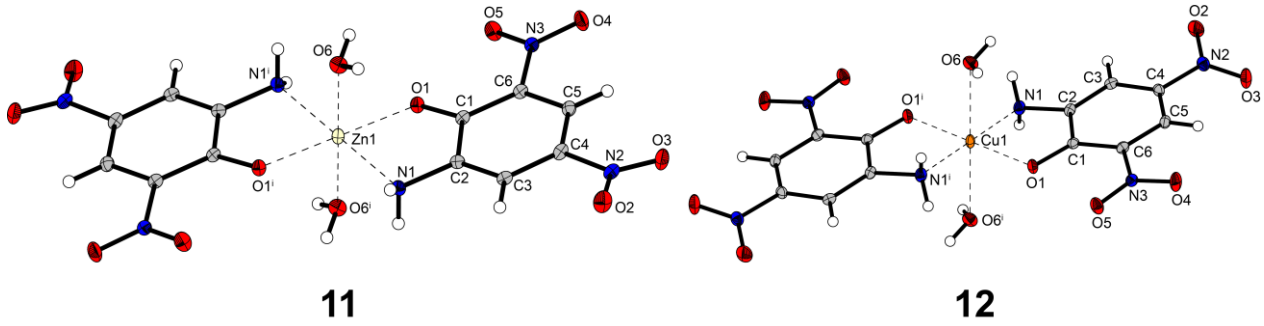

Figure 7. Molecular structures of **11** (left) and **12** (right). Selected bond lengths (Å) of **11**: Zn1–O1 2.0715(16), Zn1–O6 2.1870(18), Zn1–N1 2.117(2). Selected bond lengths (Å) of **12**: Cu1–O1 1.9681(12), Cu1–O6 2.4354(15), Cu1–N1 2.0115(15). Symmetry code of **11**: 1−x, 2−y, 1−z. Symmetry code of **12**: 1−x, 1−y, −z.

Ammonium picramate (**14**) crystallizes as anhydrous salt in the form of orange platelets in the monoclinic space group $P2_1/c$ with four molecules per unit cell (Figure 8). It possesses the lowest density (1.693 g cm^{-3} @ 104 K) of all compounds.

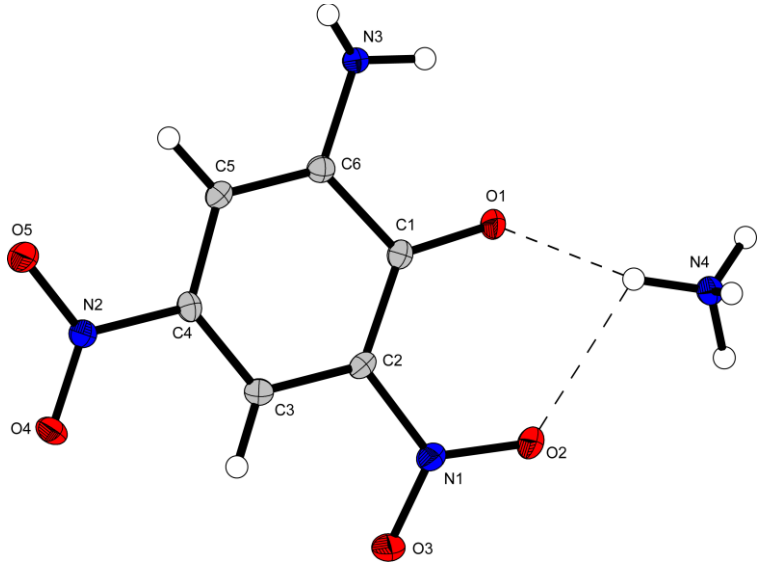

Figure 8. Molecular structure of **14**. Selected bond lengths (Å): C1–O1 1.2697(17), C2–N1 1.4430(18), N1–O2 1.2306(17), N1–O3 1.2336(17), C4–N2 1.4323(18), N2–O4 1.2341(15), N2–O5 1.2485(16), C6–N3 1.3977(18).

7.3.3. Physicochemical Properties

The physicochemical properties of all compounds, except **10b**, were investigated and therefore thermal stability measurements were performed as well as their sensitivities toward external stimuli were determined. Furthermore, calculations of the heat of formations of **2** and **14** were made using the EXPLO5 code. Potassium picramate (**4**), which crystallizes as sesquihydrate, seems to lose half a crystal water molecule when stored at ambient conditions. Elemental analysis as well as thermogravimetric analyses only show the presence of one molecule of water.

7.3.4. Thermal Analysis

The exothermic decomposition temperatures determined via differential thermal analysis (DTA) are listed in Table 1 together with the obtained sensitivity values.

Table 1. Thermal stability measurements by DTA[a] as well as sensitivities toward impact, friction, and ESD of **1**–**15**.[b]

	$T_{exo.}$[c] [°C]	*IS*[d] [J]	*FS*[e] [N]	*ESD*[f] [mJ]
Na(PAM) • H_2O (**1**)	292	20	> 360	> 1500
HPAM (**2**)	217	> 40	> 360	840
Li(PAM) • 1.5 H_2O (**3**)	295	> 40	> 360	1080
K(PAM) • H_2O (**4**)	295	10	> 360	960
Rb(PAM) (**5**)	286	9	> 360	540
Cs(PAM) (**6**)	287	10	360	450
$Mg(PAM)_2$ • 5 H_2O (**7**)	275	> 40	> 360	630
$Ca(PAM)_2$ • 2 H_2O (**8**)	300	10	> 360	740
$Sr(PAM)_2$ • 1.5 H_2O (**9**)	288	40	> 360	227
$Ba(PAM)_2$ (**10**)	291	40	> 360	840
$Zn(PAM)_2$ • 2 H_2O (**11**)	293	> 40	> 360	250
$Cu(PAM)_2$ • 2 H_2O (**12**)	252	30	> 360	270
Ag(PAM) (**13**)	156	> 40	360	480
NH_4(PAM) (**14**)	209	20	> 360	740
$Pb(PAM)_2$ (**15**)	259	< 1	16	0.33

[a] Onset temperatures at a heating rate of 5 °C min^{-1}. [b] Determined at a grain size < 100 µm. [c] Exothermic peak, which indicates decomposition. [d] Impact sensitivity according to the BAM drop hammer (method 1 of 6). [e] Friction sensitivity according to the BAM friction tester (method 1 of 6). [f] Electrostatic discharge sensitivity (OZM ESD tester); impact: insensitive > 40 J, less sensitive ≥ 35 J, sensitive ≥ 4 J, and very sensitive ≤ 3 J; friction: insensitive > 360 N, less sensitive = 360 N, sensitive < 360 N and > 80 N, very sensitive ≤ 80 N, and extremely sensitive ≤ 10 N. According to the UN Recommendations on the Transport of Dangerous Goods.

The DTA measurements were performed with a linear heating rate of β = 5 °C min^{-1} from 30 °C to 400 °C and critical events are given as onset temperatures. The plots of the measurements can be seen in Figures 9 and S5–7. Both, sodium salt **1** and picramic acid (**2**) show an endothermic event at 174 and 175 °C, respectively. Whereas **1** first loses its crystal water and decomposes afterwards at 292 °C, the neutral compound **2** melts shortly before it shows an exothermic decomposition at 217 °C. In general, it can be seen that all exothermic decomposition temperatures, except the one of **13**, are all above 200 °C. Furthermore, the alkali, alkaline earth and zinc(II) picramates are even close to 300 °C, which makes those compounds to interesting energetic compounds for high-temperature applications. The water containing compounds **3**, **7**, **8**, and **11** also show endothermic events between 79 and 223 °C, which can be matched to the loss of water. Interestingly, for the other hydrates (**4**, **9**, and **12**) no loss of water can be detected in the DTA measurements, indicating a too low sensibility of the device for minor endothermic events. Similar to picramic acid (**2**), the ammonium salt shows an endothermic event at 182 °C, that can be assigned to a melting, which was also observed during melting-point measurements. In the case of NH_4(PAM), it is directly followed by an exothermic decomposition at 209 °C (Figure S7). The relatively

low thermal stability of silver picramate (**13**), is in accordance with observations made before, describing the constant decomposition starting above 120 °C.[16]

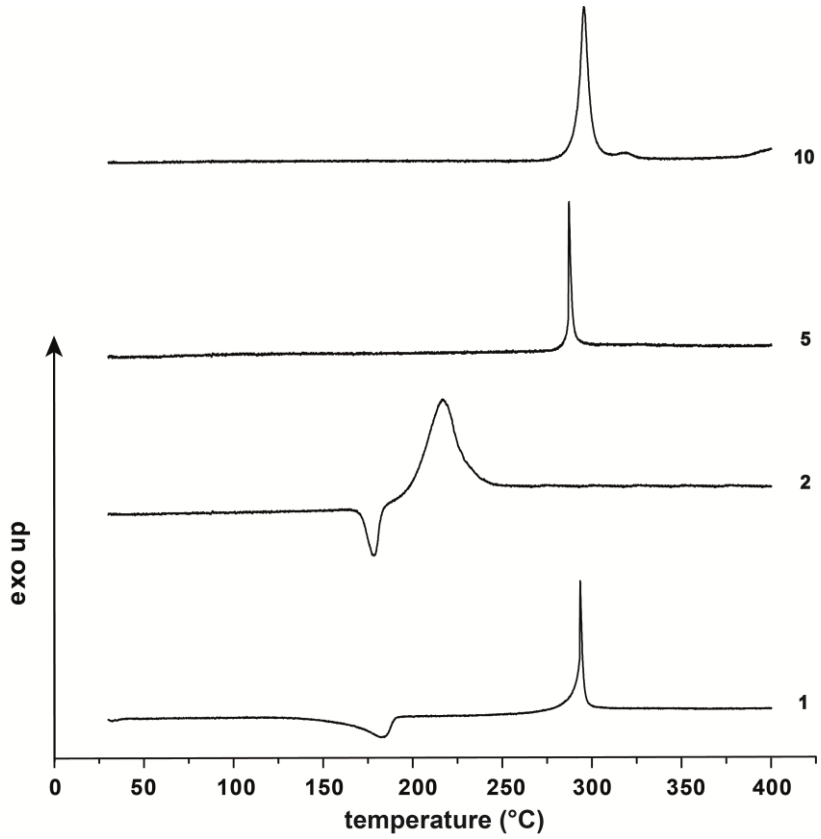

Figure 9. DTA plots of compounds **1**, **2**, **5**, and **10**.

Due to the difficulties in detecting the loss of water in some compounds and to further investigate the occurring endothermic events, thermogravimetric analyses (TGA) were performed. In the TGA measurements, it was heated with a heating rate of $\beta = 5\ °C\ min^{-1}$ from 30 °C to 400 °C. In sodium picramate (**1**) the loss of 7.5 wt% can be clearly seen around 174 °C, which perfectly fits the mass of one crystal water molecule. The temperature is in accordance with the endothermic signal occurring in the DTA measurement. The same can be observed for compound **3** with a mass loss of 11 wt% at 105 °C conforming to the presence of a sesquihydrate. Due to the absence of crystal water molecules in **6** and **15**, loss of mass only can be seen at the corresponding decomposition points of the compounds (Figure 10). Similar trends can be observed for all other picramates (Figures S8–10). Special cases can be observed in substances **4** and **10**, whose compositions were verified by EA, IR, and thermal measurements. Usually, potassium salts are present as anhydrates whereas barium compounds often exist as hydrates. Therefore, both are rare examples in the literature. K(PAM) • H_2O (**4**) which shows no endothermic event during DTA measurements (Figure S5) clearly shows the loss of water till 90 °C in the TGA. When drying **4** for 24 h at 100 °C, an anhydrous substance is obtained, which immediately begins to absorb water under ambient conditions.

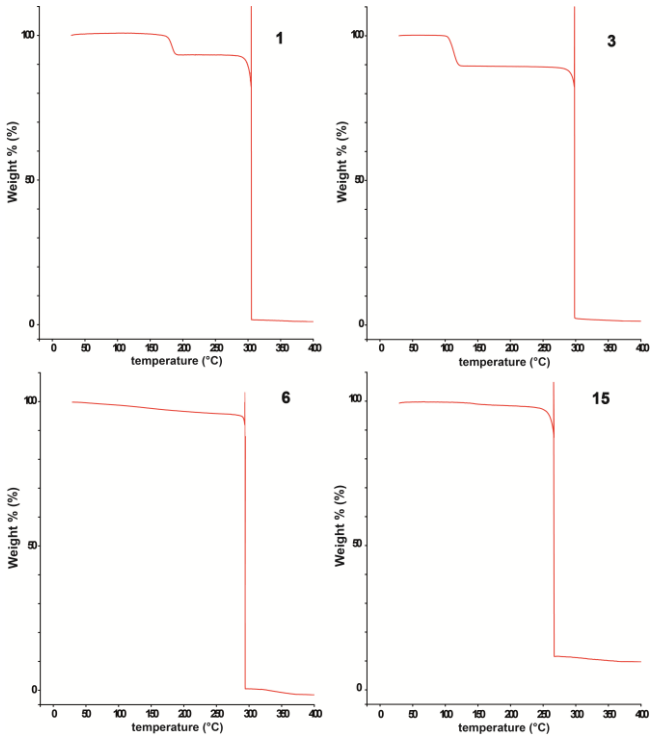

Figure 10. TGA plots of compounds **1**, **3**, **6**, and **15**.

7.3.5. Sensitivities and Energetic Properties

Except for **10b**, all compounds were tested toward their sensitivities against impact, friction as well as electrostatic discharge (Table 1). Lead picramate (**15**) is by far the most sensitive salt of all, with values of a primary explosive (< 1 J, 16 N). Comparing the friction sensitives, the other picramates can be classified as insensitive (> 360 N) according to the UN Recommendations on the Transport of Dangerous Goods. The only exceptions are **6** and **13** with sensitivities of 360 N (less sensitive). In case of impact sensitivity only compounds **2**, **3**, **7**, **11**, and **13** are ranked as insensitive, whereas **9** and **10** are less sensitive. All other compounds are in the range between 9 J (**5**) and 30 J (**12**) and are therefore sensitive. The observed sensitivity of picramic acid (34 J) could not be verified in our tests. The stark contrast of the lead salt compared to all other investigated salts cannot really be explained in detail yet. Hot needle (HN) and hot plate (HP) tests of compounds **10** and **15** prove the energetic character of the water-free picramates salts (Table 2).

Table 2. Hot needle and hot plate tests of **10** and **15**.

	HN[a]	HP[a]
$Ba(PAM)_2$ (**10**)	def.	def.
$Pb(PAM)_2$ (**15**)	det.	def.

[a] def.: deflagration; det.: detonation.

Whereas barium picramate shows deflagrations in both setups (Figure 11), slight confinement of $Pb(PAM)_2$ is already leading to detonations (Figure 12). For a better classification with already used

explosives, important detonation parameters of **2** and **14** were calculated using the EXPLO5 code.[25] It can be seen that **14** is comparable to TNT with values close to it (Table 3).

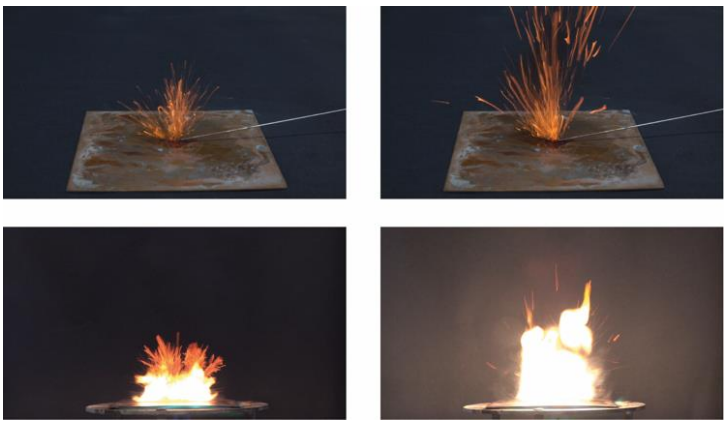

Figure 11. Hot needle (top) and hot plate (bottom) tests of compound **10**.

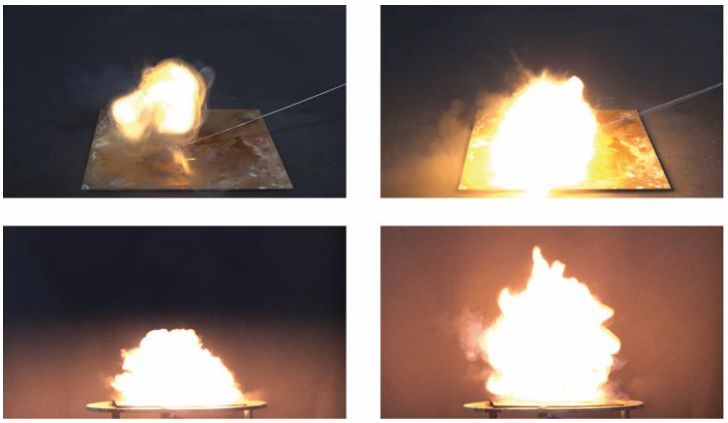

Figure 12. Hot needle (top) and hot plate (bottom) tests of compound **15**.

As seen in Figure S11, only sodium and lithium compounds **1** and **3** could be used as potential flame colorants. Especially lithium picramate is producing an intensive red flame. All other salts show very little to no coloring, which can be explained by their low solubility.

Table 3. EXPLO5 6.05.02 values of **2** and **14** compared to TNT.

	H(PAM) (**2**)	NH_4(PAM) (**14**)	TNT
ρ[a] [g cm^{-3}]	1.69	1.64	1.65
Ω_{CO2}[b] [%]	−76.33	−81.42	−73.96
$\Delta_f H°$[c] [kJ mol^{-1}]	−1299	−1267	−261
$\Delta_f U°$[d] [kJ kg^{-1}]	−1202	−1146	−171
$-\Delta_{ex} H°$[e] [kJ kg^{-1}]	−3362	−3346	−4427
T_{det} [K]	2555	2423	3222
P_{CJ}[f] [GPa]	1.63	1.68	1.94
V_{det}[g] [m s^{-1}]	6546	6780	6824
V_0[h] [L kg^{-1}]	644	729	633

[a] Measured X-ray densities converted to RT. [b] Oxygen balance (Ω=(xO−2yC−1/2zH)M/1600). [c] Calculated enthalpy of formation at 298.15 K. [d] Calculated energy of formation at 298.15 K. [e] Heat of explosion. [f] Detonation pressure. [g] Detonation velocity. [h] Volume of detonation gases (assuming only gaseous products).

7.4. Conclusion

In this work, 14 salts of picramic acid were prepared with simple one-step acid-base reactions whereupon 11 of them were characterized by low-temperature X-ray diffraction. All intensively colored compounds (mostly red) are easily accessible by the reaction of picramic acid with the corresponding bases in hot water/ethanol and were obtained in good yields. Surprisingly, all of the investigated compounds are far less sensitive than lead(II) picramate. The calculation of the ammonium salt showed that its performance is in the range of TNT while possessing a higher decomposition temperature. Most of the metal salts show very high thermal stabilities of up to 300 °C. Especially the water-free barium picramate could be of future interest, due to its low solubility, high stability and energetic performance.

7.5. Acknowledgements

For financial support of this work by Ludwig-Maximilians-University (LMU), the Office of Naval Research (ONR) under grant no. ONR N00014-19-1-2078 and the Strategic Environmental Research and Development Program (SERDP) under contract no. W912HQ19C0033 are gratefully acknowledged. The authors would like to thank Mr. Othmar Janowitz for the inspiration to investigate this topic and Dr. Peter Mayer for helping with X-ray crystal structure analysis. In addition, the authors would like to thank Mr. Moritz Kofen and Mr. Michael Gruhne for their great contribution to this work.

7.6. References

[1] J. P. Agrawal, *High Energy Materials: Propellants, Explosives and Pyrotechnics*, 1st ed., Wiley-VCH, Weinheim, **2010**.

[2] T. M. Klapötke, *Chemistry of High-Energy Materials*, 5th ed., De Gruyter, Berlin, Boston, **2019**.

[3] T. M. Klapötke, *Energetic Materials Encyclopedia*, 1st ed., De Gruyter, Berlin, Boston, **2018**.

[4] E. C. Johnson, E. J. Bukowski, J. J. Sabatini, R. C. Sausa, E. F. C. Byrd, M. A. Garner, D. E. Chavez, *ChemPlusChem* **2019**, *84*, 319–322.

[5] L. L. Fershtat, N. N. Makhova, *ChemPlusChem* **2020**, *85*, 13–42.

[6] J. Zhang, Q. Zhang, T. T. Vo, D. A. Parrish, J. M. Shreeve, *J. Am. Chem. Soc.* **2015**, *137*, 1697–1704.

[7] J. P. Agrawal, R. D. Hodgson, *Organic Chemistry of Explosives*, 1st ed., Wiley-VCH, Weinheim **2006**.

[8] H. Sprengel, *The Discovery of Picric Acid (Melinite, Lyddite) „As a Powerful Explosive“ and of Cumulative Detonation with its Bearing on wet Gun Cotton*, 2nd ed., Eyre & Spottiswoode, London, **1903**.

[9] R. Matyáš, J. Pachman, *Primary Explosives*, 1st ed., Springer, Berlin, **2013**.

[10] J. Köhler, R. Meyer, A. Homburg, *Explosivstoffe*, 10th ed., Wiley-VCH, Weinheim, **2008**.

[11] M. Nicoletti, C. Frezza, L. Tomassini, M. Serafini, A. Bianco, *Nat. Prod. Res.* **2019**, *33*, 2073–2078.

[12] L. C. Becker, W. F. Bergfeld, D. V. Belsito, C. D. Klaassen, J. G. Jr. Marks, R. C. Shank, T. J. Slaga, P. W. Snyder, F. A. Andersen, *Int. J. Toxicol.* **2009**, *28*, 205–216.

[13] Z. Yang, Y. Liu, D. Liu, L. Yan, J. Chen, *J. Hazard. Mat.* **2010**, *177*, 938–943.

[14] B. Glowiak, *Chem. Stosowana* **1961**, *5*, 575–598.

[15] S. P. Agrawal, J. P. Agrawal, *Indian J. Chem.* **1969**, *7*, 1264–1267.

[16] S. P. Agrawal, J. P. Agrawal, *Def. Sci. J.* **1970**, *20*, 237–248.

[17] S. P. Agrawal, B. D. Agrawal, *Indian J. Chem.* **1972**, *10*, 1106–1107.

[18] R. S. Srivastava, S. P. Agrawal, H. N. Bhargava, *Propellants Explos. Pyrotech.* **1976**, *1*, 101–103.

[19] S. Srivastava, S. P. Agrawal, H. N. Bhargava, *Kogyo Kayaku* **1979**, *40*, 38–42.

[20] S. R. Yoganarasimhan, G. O. Reddy, S. Achar, *J. Energ. Mater.* **1992**, *10*, 151–171.

[21] N. Orbovic, A. C. Luco, M. Bozovic, *Propellants Explos. Pyrotech.* **2008**, *33*, 271–278.

[22] L. Molard, J. Vaganay, *Meml. Poudres* **1957**, *39*, 123–136.

[23] H. Adolf, A. L. Rheingold, M. B. Allen, CCDC 1215579 **1996**.

[24] M. A. Menelaou, N. H. Fischer, F. R. Fronczek, CCDC 125117 **1999**.

[25] M. Sućeska, EXPLO5 Version 6.05.02, Zagreb, **2018**.

7.7. Supporting Information

7.7.1. Chemicals and Analytics

All chemicals and solvents were employed as received (Sigma-Aldrich, Fluka, Acros, ABCR). The samples were measured in a range of 25–400 °C at a heating rate of 5 °C min^{-1} through differential thermal analysis (DTA) with an OZM Research DTA 552-Ex instrument. Endothermic and exothermic events of the described compounds, which indicate melting, evaporation, or decomposition, are given as the extrapolated onset temperatures. Partly the compounds were measured also by thermal gravimetric analysis (TGA) with a PerkinElmer TGA4000. Infrared spectra were measured with pure samples on a Perkin-Elmer BXII FT-IR system with a Smith DuraSampler IR II diamond ATR. Determination of the carbon, hydrogen, and nitrogen contents was carried out by combustion analysis using an Elementar Vario El (nitrogen values determined are often lower than those calculated due to their explosive behavior).

Impact sensitivity tests were carried out according to STANAG 4489[1] with a modified instruction[2] using a BAM (Bundesanstalt für Materialforschung und -prüfung) drop hammer.[3,4] Friction sensitivity tests were carried out according to STANAG 4487[5] with a modified instruction[6] using the BAM friction tester. The classification of the tested compounds results from the "UN Recommendations on the Transport of Dangerous Goods".[7] Additionally, all compounds were tested to determine the sensitivity toward electrical discharge using OZM Electric Spark XSpark10 device.[3] Hot plate and hot needle tests were performed in order to further explore the energetic character. The samples were fixed on a copper plate underneath adhesive tape and initiated by a red-hot needle. Strong deflagration or detonation of the compound usually indicates a valuable primary explosive. The safe and straightforward hot plate test only shows the behavior of the unconfined sample toward fast heating on a copper plate.

7.7.2. IR Spectroscopy

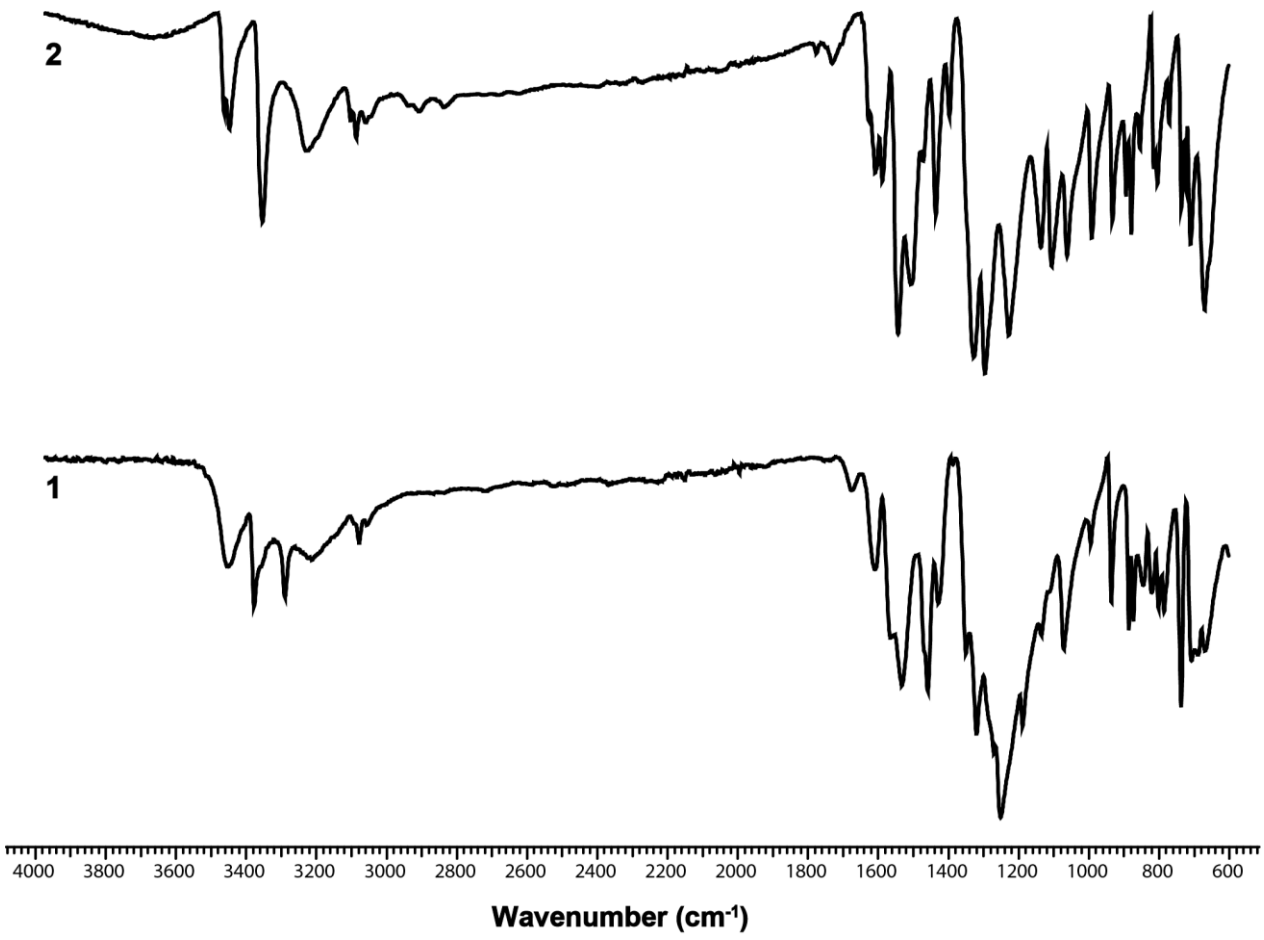

Figure S1. IR spectra of compounds **1** and **2**.

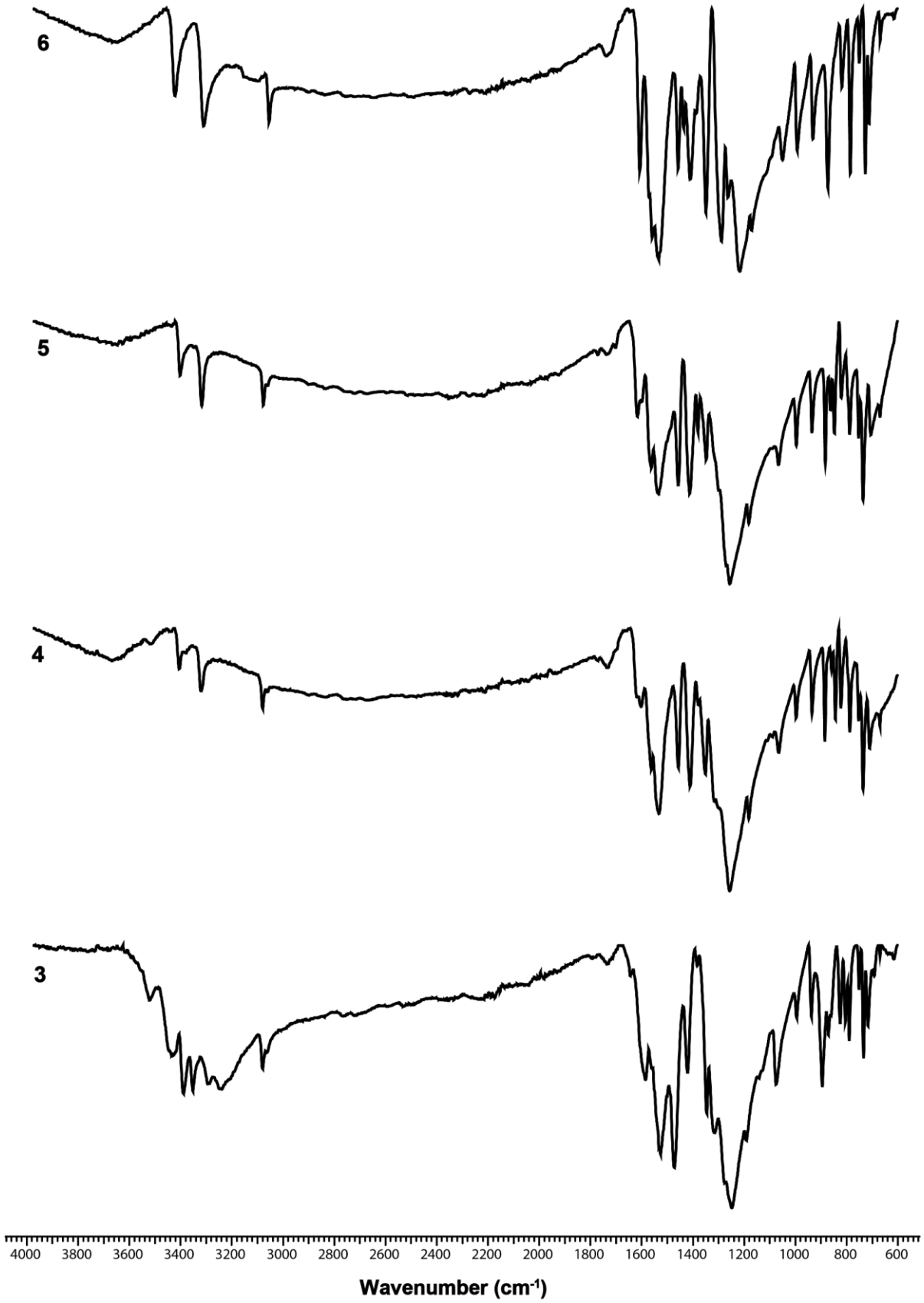

Figure S2. IR spectra of compounds **3**–**6**.

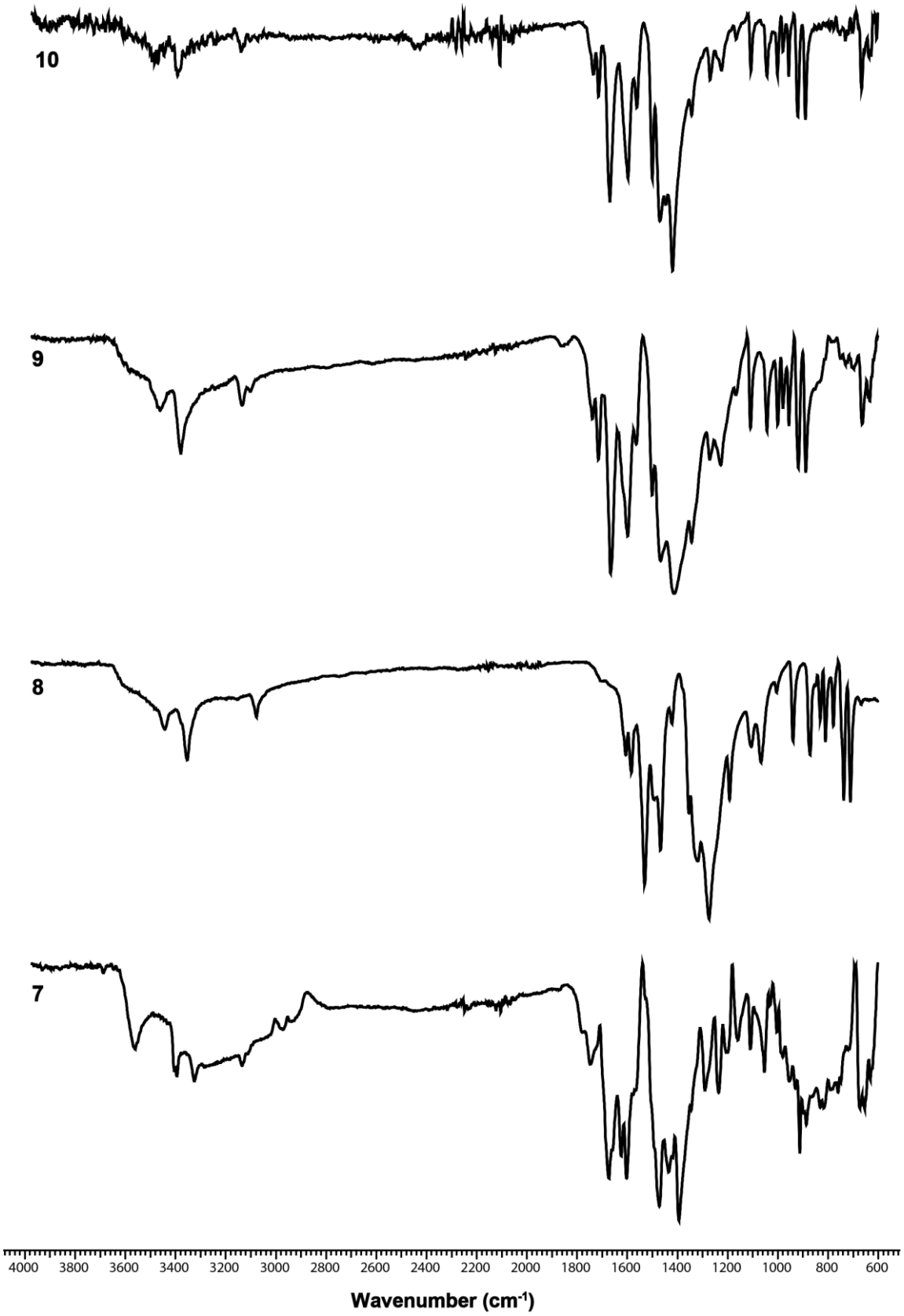

Figure S3. IR spectra of compounds **7**–**10**.

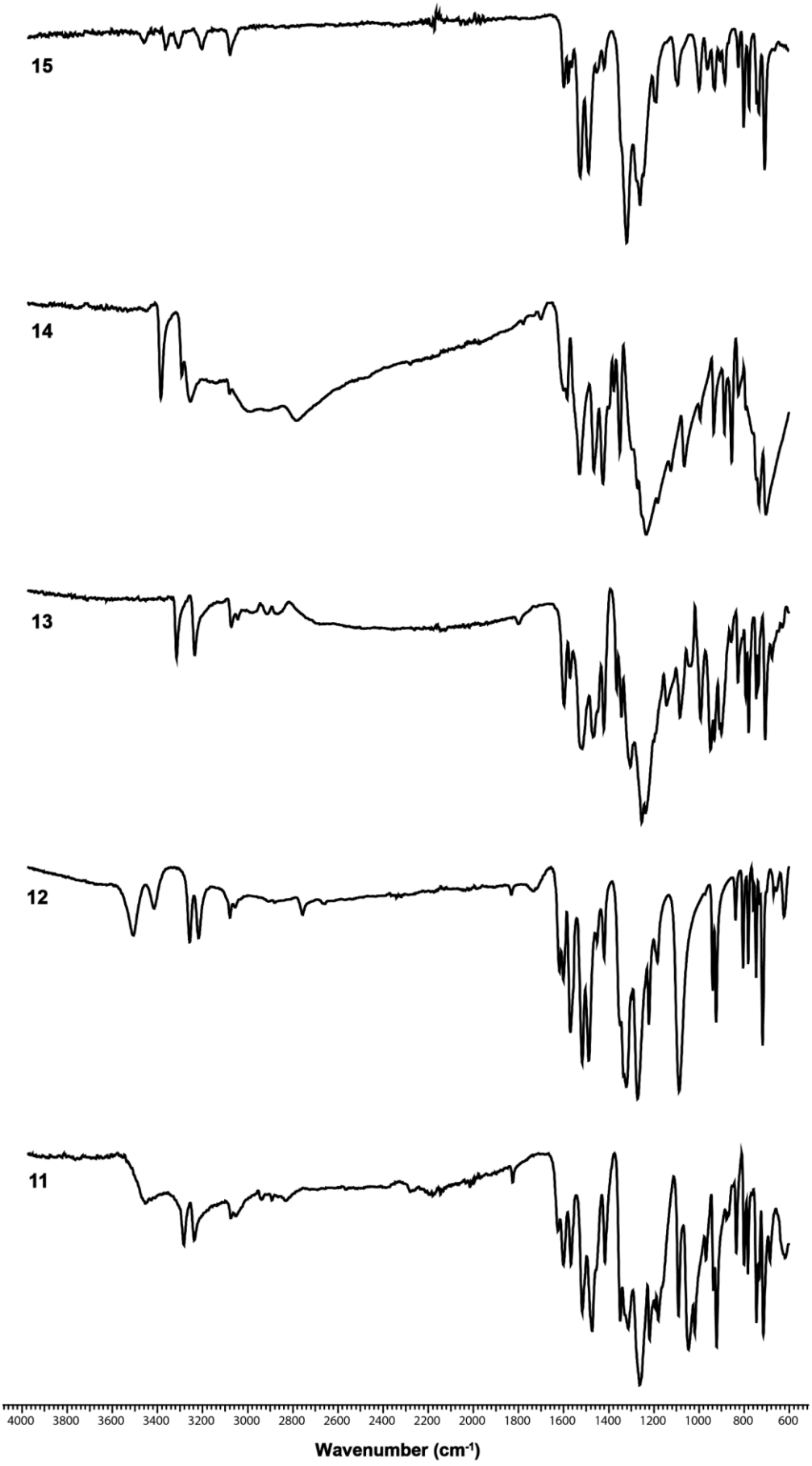

Figure S4. IR spectra of compounds **11**–**15**.

7.7.3. DTA Measurements

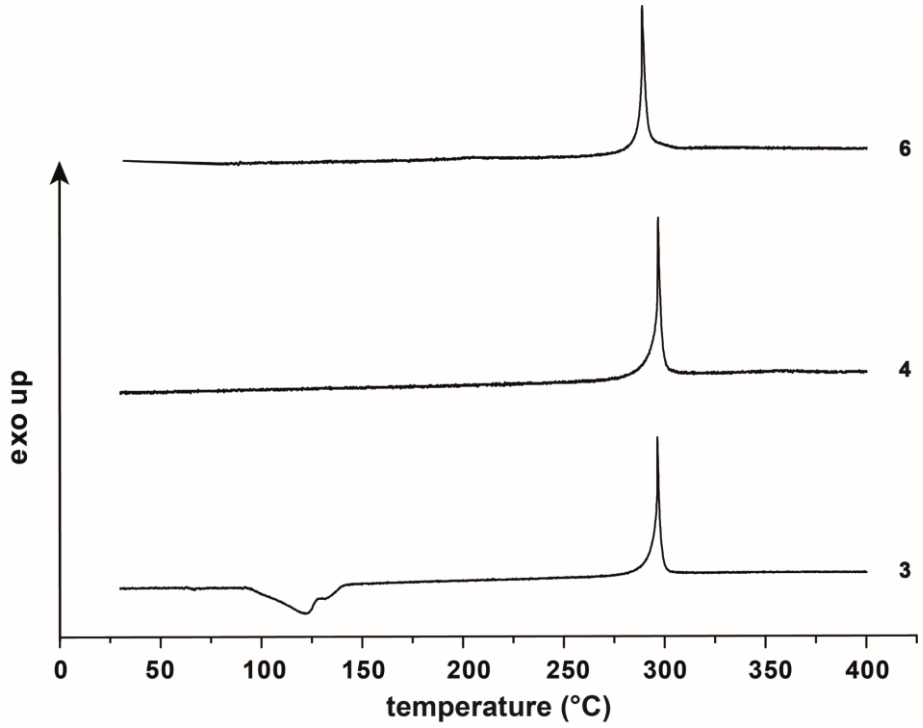

Figure S5. DTA measurements of compounds **3**, **4**, and **6**.

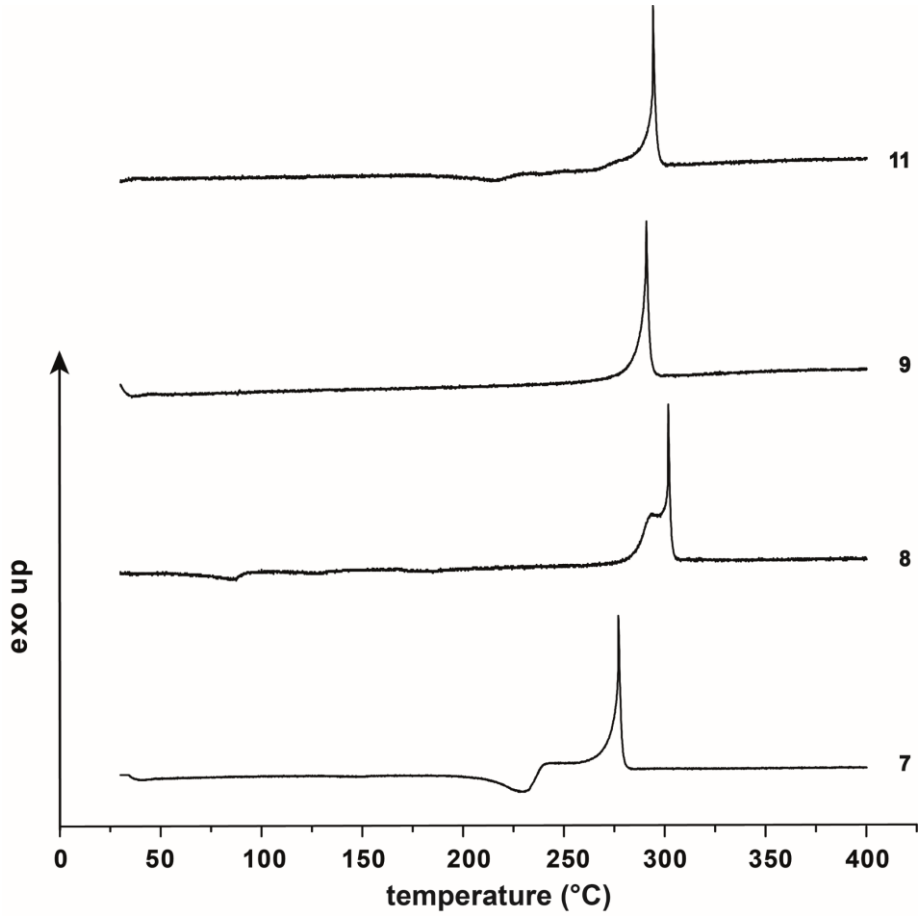

Figure S6. DTA measurements of compounds **7–9**, and **11**.

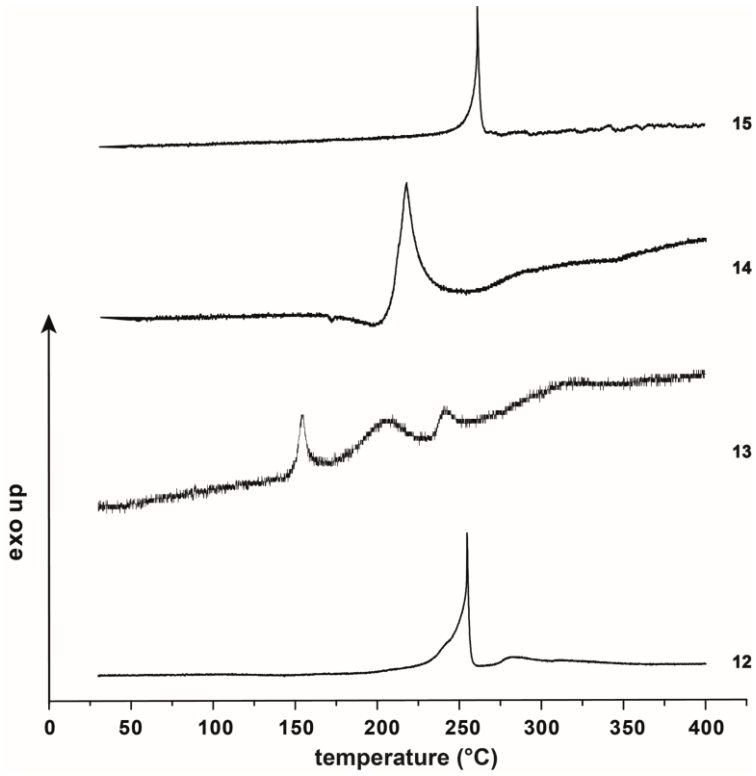

Figure S7. DTA measurements of compounds **12–15**.

7.7.4. TGA Measurements

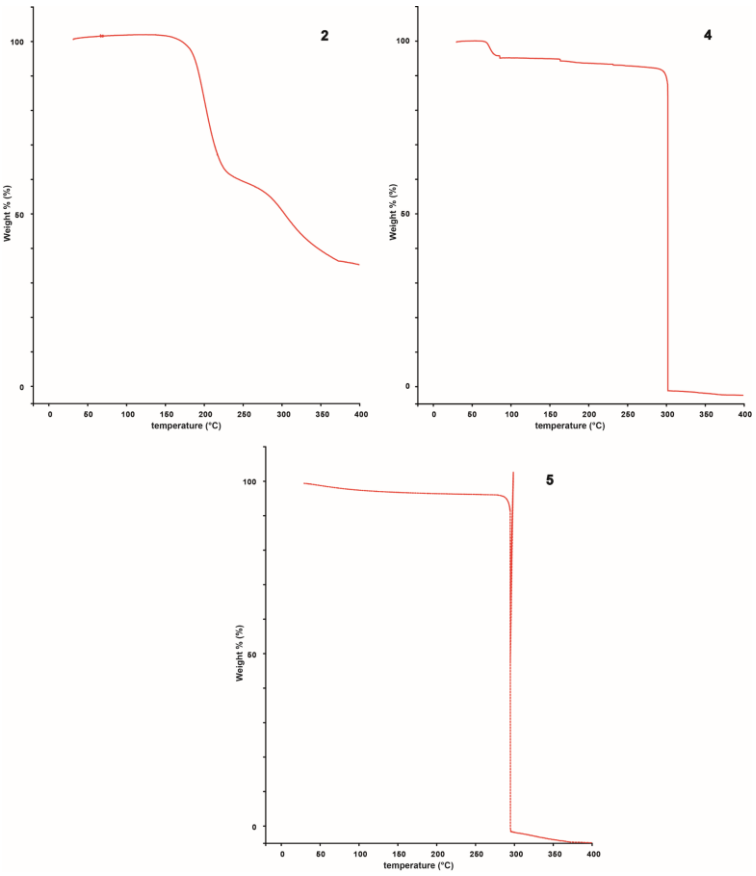

Figure S8. TGA measurements of compounds **2**, **4**, and **5**.

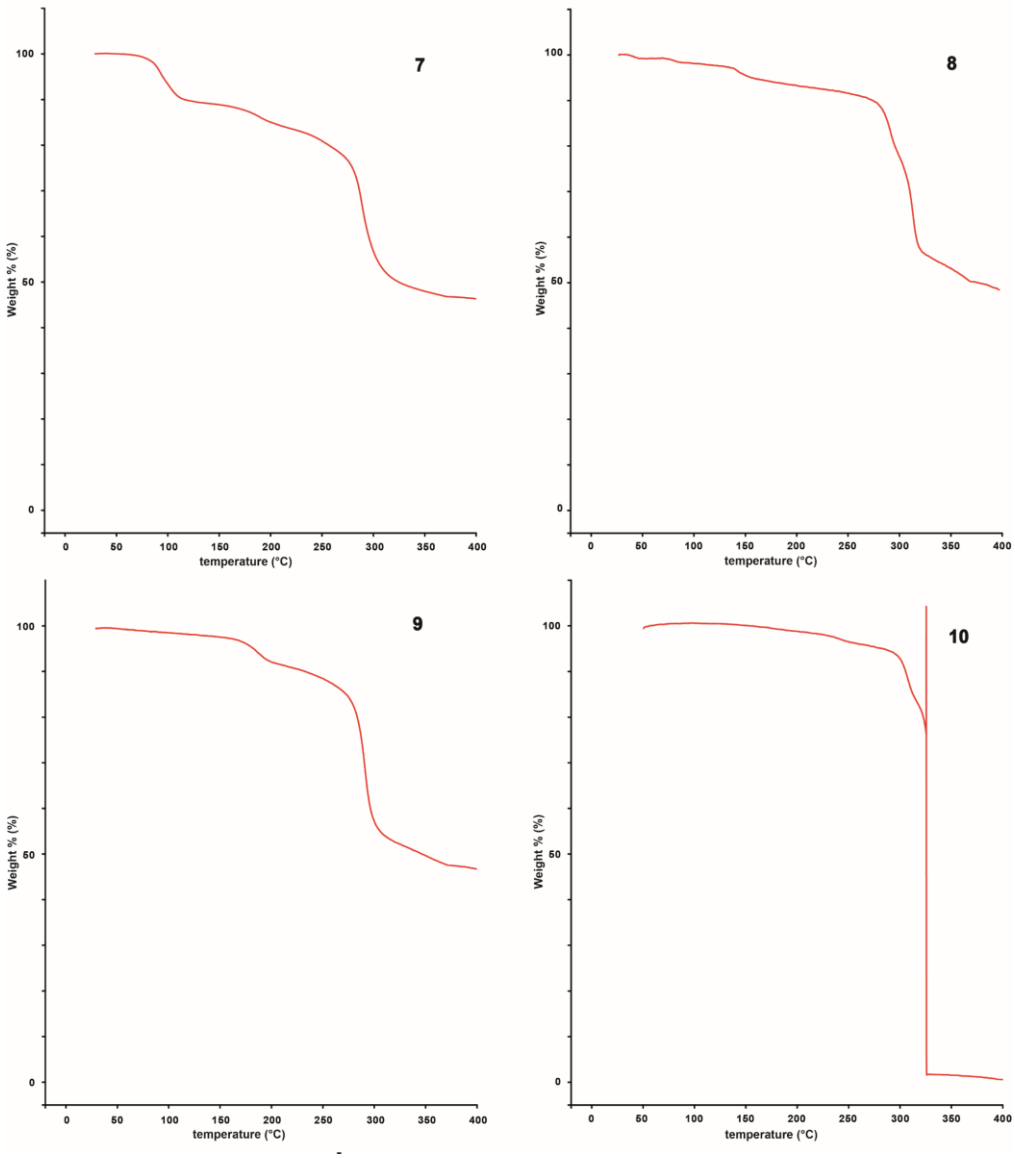

Figure S9. TGA measurements of compounds **7**–**10**.

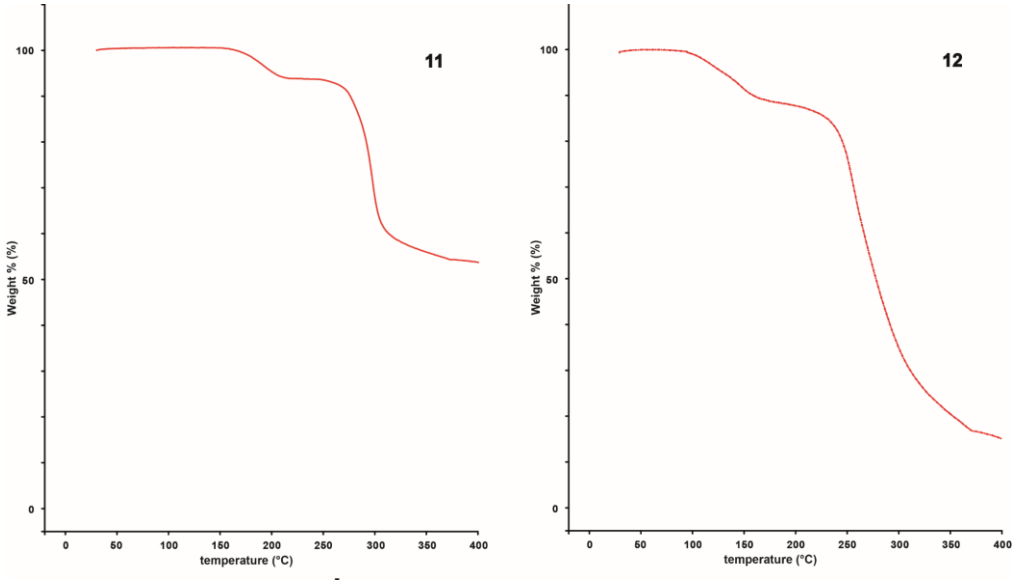

Figure S10. TGA measurements of compounds **11** and **12.**

7.7.5. Spectroscopic Properties

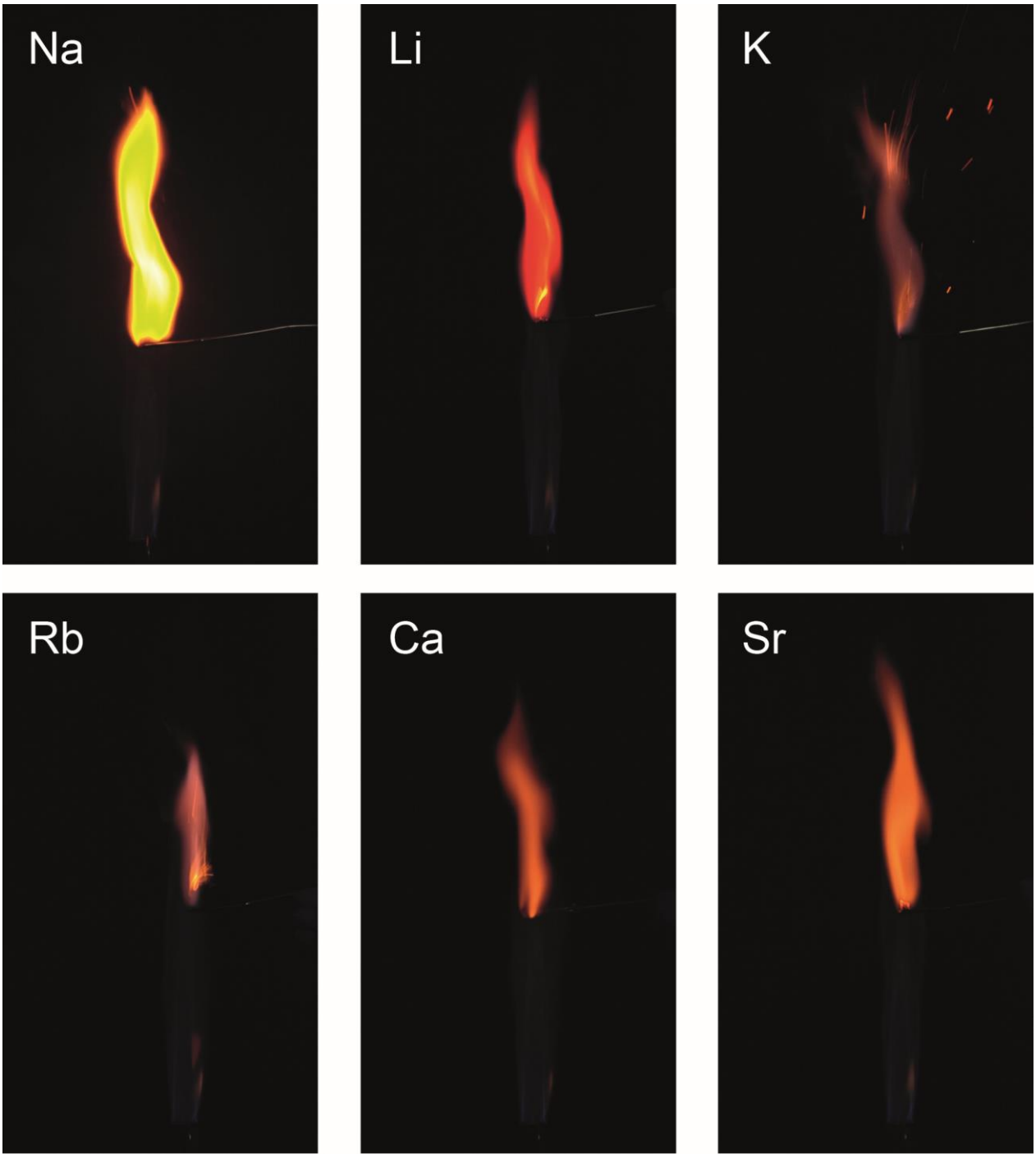

Figure S11. Flame coloration of compounds **1**, **3**–**5**, **8**, and **9**.

7.7.6. X-Ray Diffraction

For all crystalline compounds, an Oxford Xcalibur3 diffractometer with a CCD area detector or Bruker D8 Venture TXS diffractometer equipped with a multilayer monochromator, a Photon 2 detector and a rotating-anode generator were employed for data collection using Mo-*K*α radiation (λ = 0.71073 Å). On

the Oxford device, data collection and reduction were carried out using the CRYSALISPRO software.[8] On the Bruker diffractometer, the data were collected with the Bruker Instrument Service v3.0.21, the data reduction was performed using the SAINT V8.18C software (Bruker AXS Inc., 2011). The structures were solved by direct methods (SIR-92,[9] SIR-97,[10] or SHELXS-97[11]) and refined by full-matrix least-squares on *F*2 (SHELXL[11]) and finally checked using the PLATON software[12] integrated in the WinGX[13] software suite. The non-hydrogen atoms were refined anisotropically and the hydrogen atoms were located and freely refined. The absorptions were corrected by a SCALE3 ABSPACK or SADABS Bruker APEX3 multiscan method.[14,15] All DIAMOND2 plots are shown with thermal ellipsoids at the 50% probability level and hydrogen atoms are shown as small spheres of arbitrary radius.

Table S1. Crystallographic data of **1**–**4**.

	1	**2**	**3**	**4**
Formula	$C_6H_6N_3NaO_6$	$C_6H_5N_3O_5$	$C_{12}H_{14}Li_2N_6O_{13}$	$C_{12}H_{14}K_2N_6O_{13}$
FW [g mol^{-1}]	239.13	199.13	464.17	528.49
Crystal system	monoclinic	triclinic	triclinic	monoclinic
Space Group	*Pc*	*P*−1	*P*−1	$P2_1/c$
Color / Habit	red plate	red block	orange platelet	red block
Size [mm]	0.04 x 0.17 x 0.23	0.25 x 0.50 x 0.50	0.03 x 0.24 x 0.44	0.06 x 0.15 x 0.38
a [Å]	3.5121(3)	7.7506(5)	8.6881(13)	3.6796(1)
b [Å]	11.8013(10)	8.1481(5)	9.7990(15)	25.4195(9)
c [Å]	10.7612(9)	13.7699(8)	11.4482(18)	10.2320(5)
α [°]	90	83.158(5)	81.600(13)	90
β [°]	96.248(8)	74.055(5)	69.628(15)	93.156(3)
γ [°]	90	66.158(6)	85.143(12)	90
V [Å^3]	443.37(7)	764.76(9)	903.3(3)	955.58(6)
Z	2	4	2	2
$\rho_{calc.}$ [g cm^{-3}]	1.791	1.730	1.707	1.837
μ [mm^{-1}]	0.200	0.153	0.153	0.583
F(000)	244	480	176	540
$\lambda_{MoK\alpha}$ [Å]	0.71073	0.71073	0.71073	0.71073
T [K]	127	123	121	135
θ Min–Max [°]	3.5, 26.4	3.7, 26.4	3.5, 26.4	3.8, 26.4
Dataset	−4: 4; −14: 14; −13: 13	−9: 9; −10: 10; −17: 15	−10: 10; −10: 12; −14: 14	−2: 4; −31: 31; −12: 9
Reflections collected	2980	4793	5015	6692
Independent refl.	1609	3107	3623	1962
R_{int}	0.042	0.015	0.043	0.030
Observed reflections	1609	3107	3623	1962
Parameters	162	277	338	178
R_1 (obs)[a]	0.0727	0.0457	0.0672	0.0326
wR_2 (all data)[b]	0.1853	0.12992	0.1405	0.0777
GooF[c]	1.16	1.04	0.98	1.03
Resd. Dens. [e Å^{-3}]	−0.32, 0.98	−0.35, 1.48	−0.32, 0.34	−0.26, 0.34
Absorption correction	multi-scan	multi-scan	multi-scan	multi-scan
CCDC	1965957	1965965	1965964	1965963

[a] $R_1 = \Sigma||F_0|- |F_c||/ \Sigma|F_0|$; [b] $wR_2 = [\Sigma[w(F_0^2-F_c^2)^2]/\Sigma[w(F_0)^2]]^{1/2}$; $w = [\sigma c^2(F_0^2)+(xP)^2+yP]^{-1}$ and $P = (F_0^2+2F_c^2)/3$; [c] GooF = $\{\Sigma[w(F_o^2-F_c^2)^2]/(n-p)\}^{1/2}$ (n = number of reflections; p = total number of parameters).

Table S2. Crystallographic data of **5**–**7**, and **10b**.

	5	**6**	**7**	**10b**
Formula	$C_6H_4N_3O_5Rb$	$C_6H_4CsN_3O_5$	$C_{24}H_{36}Mg_2N_{12}O_{30}$	$C_{14}H_{18}BaN_6O_{13}S$
FW [g mol^{-1}]	283.59	331.03	1021.27	647.74
Crystal system	monoclinic	monoclinic	monoclinic	monoclinic
Space Group	$P2_1/c$	$C2/c$	$P2_1/c$	$P2_1/n$
Color / Habit	red platelet	red block	brown rod	red rod
Size [mm]	0.04 x 0.20 x 0.30	0.04 x 0.14 x 0.19	0.01 x 0.02 x 0.10	0.12 x 0.19 x 0.55
a [Å]	10.2376(8)	9.8508(6)	7.4295(2)	7.7035(3)
b [Å]	3.8764(2)	13.2109(7)	26.2462(8)	11.7210(5)
c [Å]	21.4788(16)	6.8067(4)	10.1243(3)	24.5208(11)
α [°]	90	90	90	90
β [°]	96.821(7)	100.643(5)	97.894(1)	94.363(4)
γ [°]	90	90	90	90
V [Å^3]	846.35(10)	870.57(9)	1955.49(10)	2207.63(16)
Z	4	4	2	4
$\rho_{calc.}$ [g cm^{-3}]	2.226	2.526	1.735	1.949
μ [mm^{-1}]	5.857	4.261	0.188	1.974
F(000)	522	624	1056	1280
$\lambda_{MoK\alpha}$ [Å]	0.71073	0.71073	0.71073	0.71073
T [K]	122	135	109	127
θ Min–Max [°]	3.8, 26.4	3.7, 26.4	2.6, 26.4	3.3, 26.4
Dataset	–12: 8; –4: 4; –24: 26	–12: 11; –14: 16; –8: 7	–9: 9; –32: 32; –12: 12	–9: 9; –14: 10; –29: 30
Reflections collected	4219	2368	34733	12484
Independent refl.	1725	895	3997	4508
R_{int}	0.058	0.047	0.046	0.031
Observed reflections	1725	895	3997	3816
Parameters	144	75	366	350
R_1 (obs)[a]	0.0403	0.03505	0.0377	0.0317
wR_2 (all data)[b]	0.0754	0.0694	0.0875	0.0709
GooF[c]	1.03	1.08	1.08	1.06
Resd. Dens. [e Å^{-3}]	–0.57, 0.69	–0.69, 1.50	–0.24, 0.35	–0.47, 1.36
Absorption correction	multi-scan	multi-scan	multi-scan	multi-scan
CCDC	1965958	1965966	1965967	1965960

[a] $R_1 = \Sigma||F_0|- |F_c||/ \Sigma|F_0|$; [b] $wR_2 = [\Sigma[w(F_0^2-F_c^2)^2]/\Sigma[w(F_0)^2]]^{1/2}$; $w = [\sigma c^2(F_0^2)+(xP)^2+yP]^{-1}$ and $P = (F_0^2+2F_c^2)/3$; [c] GooF = $\{\Sigma[w(F_o^2-F_c^2)^2]/(n-p)\}^{1/2}$ (n = number of reflections; p = total number of parameters).

Table S3. Crystallographic data of **11**, **12**, and **14**.

	11	**12**	**14**
Formula	$C_{12}H_{12}N_6O_{12}Zn$	$C_{12}H_{12}CuN_6O_{12}$	$C_6H_8N_4O_5$
FW [g mol^{-1}]	497.65	495.82	216.16
Crystal system	triclinic	triclinic	monoclinic
Space Group	*P*–1	*P*–1	$P2_1/c$
Color / Habit	colorless rod	green platelet	orange platelet
Size [mm]	0.01 x 0.02 x 0.08	0.02 x 0.07 x 0.08	0.02 x 0.06 x 0.08
a [Å]	4.8201(3)	4.9948(3)	10.0945(3)
b [Å]	8.3510(6)	8.3928(6)	11.0657(3)
c [Å]	10.9634(7)	10.8960(8)	7.7409(2)
α [°]	72.262(2)	70.659(2)	90
β [°]	86.392(2)	84.010(2)	101.224(1)
γ [°]	77.013(2)	74.197(2)	90
V [Å^3]	409.57(5)	414.65(5)	848.14(4)
Z	1	1	4
$\rho_{calc.}$ [g cm^{-3}]	2.018	1.986	1.693
μ [mm^{-1}]	1.590	1.407	0.149
F(000)	252	251	448
$\lambda_{MoK\alpha}$ [Å]	0.71073	0.71073	0.71073
T [K]	105	104	104
θ Min–Max [°]	2.8, 26.4	3.8, 26.4	3.3, 26.4
Dataset	–5: 6; –10: 10; –13: 13	–6: 6; –10: 10; –13: 13	–12: 12; –13: 13; –9: 9
Reflections collected	5461	6009	13210
Independent refl.	1662	1688	1730
R_{int}	0.031	0.029	0.034
Observed reflections	1662	1688	1730
Parameters	158	258	160
R_1 (obs)[a]	0.0284	0.0213	0.0322
wR_2 (all data)[b]	0.0667	0.0573	0.0844
GooF[c]	1.10	1.11	1.08
Resd. Dens. [e Å^{-3}]	–0.67, 0.41	–0.28, 0.41	–0.25, 0.33
Absorption correction	multi-scan	multi-scan	multi-scan
CCDC	1965962	1965959	1965961

[a] $R_1 = \Sigma||F_0|- |F_c||/ \Sigma|F_0|$; [b] $wR_2 = [\Sigma[w(F_0^2-F_c^2)^2]/\Sigma[w(F_0)^2]]^{1/2}$; $w = [\sigma c^2(F_0^2)+(xP)^2+yP]^{-1}$ and $P = (F_0^2+2F_c^2)/3$; [c] GooF = $\{\Sigma[w(F_o^2-F_c^2)^2]/(n-p)\}^{1/2}$ (n = number of reflections; p = total number of parameters).

7.7.7. Heat of Formation Calculation

All quantum chemical calculations were carried out using the Gaussian G09 program package.[16] The enthalpies (H) and free energies (G) were calculated using the complete basis set (CBS) method of *Petersson* and coworkers in order to obtain very accurate energies. The CBS models are using the known asymptotic convergence of pair natural orbital expressions to extrapolate from calculations using a finite basis set to the estimated CBS limit. CBS-4 starts with an HF/3-21G(d) geometry optimization; the zero-point energy is computed at the same level. It then uses a large basis set SCF calculation as a base energy, and an MP2/6- 31+G calculation with a CBS extrapolation to correct the energy through second order. A MP4(SDQ)/6-31+(d,p) calculation is used to approximate higher order contributions. In this study, we applied the modified CBS-4M method.

Heats of formation of the synthesized neutral compound **2** and the ammonium salt **14** were calculated using the atomization method (equation S1) using room temperature CBS-4M enthalpies, which are summarized in Table S4.[17,18]

$$\Delta_f H°_{(g,\,M,\,298)} = H_{(Molecule,\,298)} - \sum H°_{(Atoms,\,298)} + \sum \Delta_f H°_{(Atoms,\,298)} \quad (S1)$$

Table S4. CBS-4M enthalpies for atoms C, H, N, and O and their literature values for atomic $\Delta H°_f^{298}$ / kJ mol^{-1}.

	$-H^{298}$ / a.u.	NIST [S11]
H	0.500991	218.2
C	37.786156	717.2
N	54.522462	473.1
O	74.991202	249.5

For ionic compounds, the lattice energy (*U*L) and lattice enthalpy (Δ*H*L) are calculated from the corresponding X-ray molecular volumes (converted to RT) according to the equations provided by *Jenkins* and *Glasser*.[19] With the calculated lattice enthalpy the gas-phase enthalpy of formation was converted into the solid state (standard conditions) enthalpy of formation. The calculation results are summarized in Table S5.

Table S5. Heat of formation calculation of **2** and **14**.

M	$-H^{298}$ / a.u.[a]	$\Delta_f H°$(g,M) / kJ mol^{-1}[b]	V_M / nm^3[c]	ΔUL, ΔHL / kJ mol^{-1}[d]	$\Delta_f H°$(s) / kJ mol^{-1}[e]	Δn[f]	$\Delta_f U$(s) / kJ kg^{-1}[g]
PAM anion	770.36370	352.77448					
NH_4^+	56.796608	635.8309674					
2					247.95	5.5	2273.36
14			0.14209	556.86005	273.80	8.5	1169.09

[a] CBS-4M electronic enthalpy; [b] gas phase enthalpy of formation; [c] molecular volumes taken from X-ray structures and corrected to room temperature; [d] lattice energy and enthalpy (calculated using Jenkins and Glasser equations); [e] standard solid state enthalpy of formation; [f] Δn being the change of moles of gaseous components when formed; [g] solid state energy of formation.

7.7.8. Experimental Section

Sodium picramate • H_2O (1)
Sodium picramate (**1**) can be synthesized according to Molard *et al.*.[20]

DTA (5 °C min^{-1}): 174 °C (endothermic), 292 °C (exothermic); IR (ATR, cm^{-1}): $\tilde{\nu}$ = 3473 (m), 3399 (m), 3311 (m), 3233 (w), 3097 (w), 1615 (m), 1570 (m), 1562 (m), 1538 (s), 1464 (s), 1433 (m), 1354 (m), 1324 (s), 1273 (s), 1254 (vs), 1191 (s), 1138 (m), 1073 (m), 995 (w), 936 (m), 886 (m), 873 (m), 845 (m), 820 (m), 801 (m), 785 (m), 736 (s), 706 (m), 687 (m), 667 (m); EA ($C_6H_6N_3NaO_6$, 239.11) calcd.: C 30.14, H 2.53, N 17.57%; found: C 30.06, H 2.63, N 17.50%; BAM drop hammer: 20 J; friction tester: > 360 N; ESD: > 1500 mJ (at grain size < 100 μm).

Picramic acid (2)
An aqueous solution (200 mL) of sodium picramate monohydrate (**1**, 1.00 g, 4.18 mmol) was heated to 100 °C and acidified with HCl (2M, 10 mL). After stirring for 10 min, the mixture was extracted three times with toluene (200 mL each) and the combined organic phases were dried over $MgSO_4$. The solvent was removed *in vacuo* to obtain picramic acid (0.68 g, 3.40 mmol, 81%) as a red solid. Single crystals suitable for X-Ray diffraction were obtained by recrystallization from ethanol.

DTA (5 °C min^{-1}): 175 °C (endothermic), 217 °C (exothermic); IR (ATR, cm^{-1}): $\tilde{\nu}$ = 3375 (m), 3121 (w), 3106 (m), 2925 (w), 1783 (w), 1739 (w), 1634 (w), 1615 (m), 1594 (m), 1549 (s), 1512 (s), 1440 (m), 1402 (w), 1331 (vs), 1300 (vs), 1231 (s), 1139 (s), 1108 (s), 1063 (s), 993 (s), 933 (m), 894 (m), 879 (s), 854 (m), 814 (m), 804 (m), 770 (m), 735 (m), 709 (s), 668 (s); EA ($C_6H_5N_3O_5$, 199.12) calcd.: C 36.19, H 2.53, N 21.10%; found: C 35.96, H 2.52, N 20.91%; BAM drop hammer: > 40 J; friction tester: > 360 N; ESD: 840 mJ (at grain size < 100 μm).

General procedure for alkali picramates 3–6:
Under heating, picramic acid (**2**, 99.6 mg, 0.50 mmol, 2 eq) was dissolved in ethanol (10 mL) and stirred for 5 min. The corresponding alkali carbonate (Li: 18.5 mg, K: 34.6 mg, Rb: 57.7 mg, Cs: 81.5 mg, 0.25 mmol, 1 eq) solution in water (10 mL) was slowly added, it was further stirred for 5 min and the reaction mixture left in air for crystallization. All alkali picramates were obtained as red single crystals suitable for X-ray diffraction.

Lithium picramate • 1.5 H_2O (3)
Yield: 83.6 mg (0.18 mmol, 36%).

DTA (5 °C min^{-1}): 105 °C (endothermic), 295 °C (exothermic); IR (ATR, cm^{-1}): $\tilde{\nu}$ = 3544 (w), 3457 (m), 3450 (m), 3411 (m), 3374 (m), 3315 (m), 3270 (m), 3260 (m), 3099 (m), 3082 (m), 1742 (vw), 1651 (w),

1591 (m), 1538 (s), 1532 (s), 1478 (s), 1425 (m), 1350 (s), 1319 (s), 1279 (vs), 1251 (vs), 1194 (s), 1145 (m), 1077 (m), 996 (w), 938 (w), 895 (m), 871 (m), 824 (w), 804 (w); EA ($C_{12}H_{14}Li_2N_6O_{13}$, 464.15) calcd.: C 31.05, H 3.04, N 18.11%; found: C 30.99, H 2.88, N 17.89%; BAM drop hammer: > 40 J; friction tester: > 360 N; ESD: 1080 mJ (at grain size < 100 μm).

Potassium picramate • H_2O (4)
Yield: 243 mg (0.46 mmol, 92%).

DTA (5 °C min^{-1}): 295 °C (exothermic); IR (ATR, cm^{-1}): $\tilde{\nu}$ = 3537 (vw), 3427 (w), 3342 (w), 3099 (m), 3079 (w), 1741 (w), 1568 (m), 1538 (s), 1462 (m), 1415 (s), 1355 (m), 1320 (s), 1260 (vs), 1184 (s), 1112 (m), 1067 (m), 998 (m), 935 (m), 885 (m), 859 (w), 843 (m), 822 (m), 786 (m), 752 (m), 734 (s), 708 (m), 668 (m); EA ($C_6H_{12}KN_3O_6$, 255.23) calcd.: C 28.24, H 2.37, N 16.46%; found: C 28.84, H 2.34, N 16.68%; BAM drop hammer: 10 J; friction tester: > 360 N; ESD: 960 mJ (at grain size < 100 μm).

Rubidium picramate (5)
Yield: 105 mg (0.37 mmol, 74%).

DTA (5 °C min^{-1}): 286 °C (exothermic); IR (ATR, cm^{-1}): $\tilde{\nu}$ = 3424 (w), 3339 (m), 3096 (m), 1779 (w), 1744 (w), 1709 (vw), 1623 (m), 1606 (m), 1568 (m), 1544 (s), 1539 (s), 1463 (s), 1417 (s), 1385 (m), 1352 (m), 1302 (s), 1273 (vs), 1259 (vs), 1184 (s), 1067 (m), 997 (m), 936 (m), 883 (m), 862 (m), 847 (m), 820 (w), 787 (m), 752 (m), 734 (s), 704 (m); EA ($C_6H_4N_3O_5Rb$, 283.58) calcd.: C 25.41, H 1.42, N 14.82%; found: C 25.36, H 1.45, N 14.70%; BAM drop hammer: 9 J; friction tester: > 360 N; ESD: 540 mJ (at grain size < 100 μm).

Cesium picramate (6)
Yield: 89.4 mg (0.27 mmol, 54%).

DTA (5 °C min^{-1}): 287 °C (exothermic); IR (ATR, cm^{-1}): $\tilde{\nu}$ = 3444 (m), 3331 (m), 3073 (m), 1744 (w), 1613 (s), 1576 (s), 1564 (s), 1539 (vs), 1463 (s), 1441 (m), 1415 (s), 1391 (m), 1353 (s), 1292 (s), 1266 (s), 1220 (vs), 1173 (s), 1051 (m), 994 (m), 932 (m), 873 (s), 818 (w), 785 (s), 749 (w), 725 (s), 710 (m), 667 (w), 613 (vw); EA ($C_6H_4CsN_3O_5$, 331.02) calcd.: C 21.77, H 1.22, N 12.69%; found: C 21.88, H 1.26, N 12.91%; BAM drop hammer: 10 J; friction tester: 360 N; ESD: 450 mJ (at grain size < 100 μm).

General procedure for alkaline earth picramates 7–10:
Picramic acid (**2**, 99.6 mg, 0.50 mmol, 2 eq) was dissolved in ethanol (10 mL) while stirring for 5 min under heating. The corresponding aqueous solution (10 mL) of the alkaline earth hydroxide (Mg: 22.0 mg, Ca: 25.0 mg, Sr: 36.9 mg, Ba • 8 H_2O: 78.5 mg, 0.25 mmol, 1 eq) was slowly added, the reaction mixture

stirred for 5 min and left in air. Compound **7** was obtained as red crystals suitable for X-Ray diffraction. In contrast, compounds **8**–**10** were obtained as red microcrystalline solids.

Magnesium picramate • 5 H_2O (7)
Yield: 45.9mg (0.09 mmol, 36%).

DTA (5 °C min^{-1}): 223 °C (endothermic), 275 °C (exothermic); IR (ATR, cm^{-1}): $\tilde{\nu}$ = 3560 (m), 3393 (m), 3383 (m), 3308 (m), 3104 (m), 1658 (w), 1623 (m), 1543 (s), 1529 (s), 1491 (s), 1468 (s), 1440 (m), 1328 (vs), 1289 (s), 1272 (s), 1246 (vs), 1194 (m), 1134 (m), 1076 (m), 994 (w), 941 (m), 882 (m), 857 (w), 809 (m), 776 (m), 750 (m), 731 (s), 715 (m), 703 (s), 644 (m); EA ($C_{12}H_{18}MgN_6O_{15}$, 510.07) calcd.: C 28.23, H 3.55, N 16.46%; found: C 28.40, H 3.56, N 16.25%; BAM drop hammer: > 40 J; friction tester: > 360 N; ESD: 630 mJ (at grain size < 100 μm).

Calcium picramate • 2 H_2O (8)
Yield: 70.9 mg (0.15 mmol, 60%).

DTA (5 °C min^{-1}): 79 °C (endothermic), 300 °C (exothermic); IR (ATR, cm^{-1}): $\tilde{\nu}$ = 3506 (w), 3464 (w), 3375 (m), 3097 (w), 1612 (m), 1589 (m), 1536 (s), 1499 (m), 1473 (s), 1427 (w), 1358 (m), 1323 (s), 1278 (vs), 1195 (m), 1108 (m), 1069 (m), 1006 (w), 940 (m), 871 (m), 830 (w), 810 (m), 778 (w), 736 (m), 709 (m), 666 (w); EA ($C_{12}H_{12}CaN_6O_{12}$, 472.34) calcd.: C 30.51, H 2.56, N 17.79%; found: C 30.08, H 2.62, N 17.36%; BAM drop hammer: 10 J; friction tester: > 360 N; ESD: 740 mJ (at grain size < 100 μm).

Strontium picramate • 1.5 H_2O (9)
Yield: 153 mg (0.15 mmol, 60%).

DTA (5 °C min^{-1}): 288 °C (exothermic); IR (ATR, cm^{-1}): $\tilde{\nu}$ = 3454 (w), 3366 (m), 3104 (w), 1614 (m), 1588 (m), 1537 (vs), 1505 (m), 1464 (s), 1427 (m), 1360 (s), 1324 (s), 1265 (vs), 1192 (s), 1115 (m), 1067 (m), 941 (m), 871 (m), 825 (m), 803 (w), 777 (m), 737 (m), 706 (m), EA ($C_{24}H_{22}N_{12}O_{23}Sr_2$, 1021.74) calcd.: C 28.21, H 2.17, N 16.45%; found: C 28.05, H 2.12, N 16.30%; BAM drop hammer: 40 J; friction tester: > 360 N; ESD: 227 mJ (at grain size < 100 μm).

Barium picramate (10)
Yield: 116 mg (0.21 mmol, 84%).

DTA (5 °C min^{-1}): 291 °C (exothermic); IR (ATR, cm^{-1}): $\tilde{\nu}$ = 3379 (w), 1588 (m), 1539 (s), 1463 (s), 1425 (m), 1359 (s), 1327 (s), 1301 (s), 1273 (vs), 1191 (m), 1113 (w), 1065 (w), 1002 (vw), 871 (w), 826 (w), 803 (w), 778 (w), 739 (m), 707 (m); EA ($C_{12}H_8BaN_6O_{10}$, 533.56) calcd.: C 27.01, H 1.51, N 15.75%;

found: C 26.76, H 1.69, N 15.45%; BAM drop hammer: 40 J; friction tester: > 360 N; ESD: 840 mJ (at grain size < 100 μm).

Zinc picramate • 2 H_2O (11)
Picramic acid (**2**, 99.6 mg, 0.50 mmol, 2 eq) was dissolved in ethanol (10 mL) under heating and stirred for 5 min. A solution of zinc hydroxide carbonate (137 mg, 0.25 mmol, 1 eq) in water (10 mL) was slowly added to the picramic acid mixture, leading to immediate precipitation of the product. Compound **11** was filtered off, washed with a small amount of ethanol and dried in air. Zinc picramate (69.7 mg ,0.14 mmol, 56%) was obtained as a green solid.

Single crystals suitable for X-ray diffraction were obtained by layering an aqueous solution of zinc(II) nitrate hexahydrate with an ethanolic solution of picramic acid.

DTA (5 °C min^{-1}): 206 °C (endothermic), 293 °C (exothermic); IR (ATR, cm^{-1}): $\tilde{\nu}$ = 3476 (w), 3304 (m), 3257 (m), 3157 (w), 3093 (w), 1631 (m), 1607 (m), 1573 (m), 1523 (s), 1479 (s), 1421 (m), 1353 (s), 1318 (s), 1266 (vs), 1222 (s), 1197 (s), 1183 (s), 1092 (s), 1048 (s), 1020 (s), 970 (m), 937 (m), 922 (s), 877 (w), 868 (w), 834 (m), 799 (m), 782 (m), 744 (s), 732 (m); EA ($C_{12}H_{12}N_6O_{12}Zn$, 497.64) calcd.: C 28.96, H 2.43, N 16.89%; found: C 28.70, H 2.35, N 16.80%; BAM drop hammer: > 40 J; friction tester: > 360 N; ESD: 250 mJ (at grain size < 100 μm).

General procedure for copper and silver picramate 12 and 13:
Salts **12** and **13** were synthesized according to a literature procedure.[21] Under heating an ethanolic solution (10 mL) of picramic acid (**2**, 99.6 mg, 0.50 mmol, 2 eq) was stirred for 5 min. The corresponding metal nitrate (Cu(II) • 3 H_2O: 60.4 mg, 0.25 mmol, 1 eq / Ag(I): 42.5 mg, 0.50 mmol, 2 eq) was dissolved in water (10 mL) and slowly added to the solution. The products precipitated immediately as solids (**12**: green; **13**: brown), were filtered off and washed with a small amount of ethanol.

Copper(II) picramate • 2 H_2O (12)
Yield: 84.2 mg (0.17 mmol, 68%).

Single crystals suitable for X-ray diffraction were obtained by layering an aqueous solution of copper(II) nitrate trihydrate with an ethanolic solution of picramic acid.

DTA (5 °C min^{-1}): 252 °C (exothermic); IR (ATR, cm^{-1}): $\tilde{\nu}$ = 3530 (w), 3437 (w), 3278 (m), 3238 (m), 3098 (w), 2773 (w), 2673 (w), 1840 (w), 1741 (w), 1625 (m), 1607 (m), 1576 (s), 1523 (s), 1494 (s), 1456 (m), 1425 (m), 1353 (s), 1338 (vs), 1326 (vs), 1302 (m), 1275 (vs), 1225 (s), 1187 (m), 1089 (vs), 940 (m), 924 (s), 837 (w), 804 (m), 781 (m), 758 (w); EA ($C_{12}H_{12}CuN_6O_{12}$, 494.98) calcd.: C 29.07, H 2.44,

N 16.95%; found: C 28.51, H 2.46, N 16.51%; BAM drop hammer: 30 J; friction tester: > 360 N; ESD: 270 mJ (at grain size < 100 μm).

Silver(I) picramate (13)
Yield: 18.4 mg (0.06 mmol, 12%).

DTA (5 °C min^{-1}): 156 °C (exothermic); IR (ATR, cm^{-1}): $\tilde{\nu}$ = 3337 (w), 3255 (w), 3092 (w), 3062 (w), 2932 (w), 2885 (w), 1809 (w), 1604 (m), 1577 (m), 1523 (s), 1473 (s), 1454 (m), 1426 (s), 1369 (m), 1348 (m), 1307 (s), 1256 (vs), 1239 (vs), 1203 (s), 1146 (m), 1086 (m), 1039 (m), 994 (m), 949 (s), 932 (s), 909 (s), 901 (s), 857 (w), 827 (m), 805 (w); EA ($C_6H_4AgN_3O_5$, 305.98) calcd.: C 23.55, H 1.32, N 13.73%; found: C 23.59, H 1.31, N 13.42%; BAM drop hammer: > 40 J; friction tester: 360 N; ESD: 480 mJ (at grain size < 100 μm).

Ammonium picramate (14)
To a solution of picramic acid (**2**, 99.6 mg, 0.50 mmol, 1 eq) in ethanol (10 mL) conc. ammonia solution (8.52 mg, 0.50 mmol, 1 eq) was added slowly. The mixture was stirred for 5 min and left in air to crystallize. Ammonium picramate (77.8 mg, 0.36 mmol, 72%) was obtained in the form of red crystals suitable for X-Ray diffraction.

DTA (5 °C min^{-1}): 182 °C (endothermic), 209 °C (exothermic); IR (ATR, cm^{-1}): $\tilde{\nu}$ = 3406 (m), 3313 (m), 3274 (m), 3099 (m), 3015 (m), 2800(m), 1707 (vw), 1604 (m), 1590 (m), 1535 (s), 1471 (s), 1430 (s), 1381 (m), 1354 (s), 1276 (s), 1237 (vs), 1185 (s), 1127 (s), 1067 (s), 996 (m), 935 (m), 887 (m), 855 (s), 825 (m), 745 (s), 733 (s), 702 (vs); EA ($C_6H_8N_4O_5$, 216.15) calcd.: C 33.34, H 3.73, N 25.92%; found: C 33.32, H 3.65, N 25.96%; BAM drop hammer: 20 J; friction tester: > 360 N; ESD: 740 mJ (at grain size < 100 μm).

Lead(II) picramate (15)
An aqueous solution (10 mL) of sodium picramate monohydrate (**1**, 120 mg, 0.50 mmol, 2 eq) was stirred for 5 min under heating. Lead(II) nitrate (82.8 mg, 0.25 mmol, 1 eq) was dissolved in water (10 mL) and slowly added. The product precipitated immediately, was filtered off and washed with a small amount of ethanol. Lead picramate (123 mg, 0.20 mmol, 80%) was obtained as orangish brown solid.

DTA (5 °C min^{-1}): 259 °C (exothermic); IR (ATR, cm^{-1}): $\tilde{\nu}$ = 3482 (w), 3386 (w), 3329 (w), 3223 (w), 3097 (w), 1605 (m), 1585 (m), 1570 (w), 1532 (s), 1495 (s), 1458 (w), 1424 (w), 1324 (vs), 1264 (s), 1250 (s), 1200 (m), 1193 (m), 1096 (m), 1000 (m), 963 (w), 931 (m), 908 (w), 885 (m), 825 (w), 801 (m), 777 (m), 743 (m), 733 (m), 707 (s), 663 (w); EA ($C_{12}H_8N_6O_{10}Pb$, 603.43) calcd.: C 23.89, H 1.34,

N 13.93%; found: C 23.72, H 1.41, N 13.89%; BAM drop hammer: < 1 J; friction tester: 16 N; ESD: 0.33 mJ (at grain size < 100 μm).

7.7.9. References

[1] NATO standardization agreement (STANAG) on explosives, impact sensitivity tests, no. 4489, 1st ed., Sept. 17, **1999**.

[2] WIWEB-Standardarbeitsanweisung 4-5.1.02, Ermittlung der Explosionsgefährlichkeit, hier der Schlagempfindlichkeit mit dem Fallhammer, Nov. 8, **2002**.

[3] http://www.ozm.cz, (accessed June 2019).

[4] http://www.bam.de, (accessed June 2019).

[5] NATO standardization agreement (STANAG) on explosive, friction sensitivity tests, no. 4487, 1st ed., Aug. 22, **2002**.

[6] WIWEB-Standardarbeitsanweisung 4-5.1.03, Ermittlung der Explosionsgefährlichkeit oder der Reibeempfindlichkeit mit dem Reibeapparat, Nov. 8, **2002**.

[7] Impact: insensitive > 40 J, less sensitive ≥ 35 J, sensitive ≥ 4 J, very sensitive ≤ 3 J; Friction: insensitive > 360 N, less sensitive = 360 N, sensitive < 360 N and > 80 N, very sensitive ≤ 80 N, extremely sensitive ≤ 10 N. According to the UN Recommendations on the Transport of Dangerous Goods, 5th ed., **2009**.

[8] *CrysAlisPro*, Oxford Diffraction Ltd., version 171.33.41, **2009**.

[9] A. Altomare, G. Cascarano, C. Giacovazzo, A. Guagliardi, *J. Appl. Crystallogr.* **1993**, *26*, 343–350.

[10] a) A. Altomare, G. Cascarano, C. Giacovazzo, A. Guagliardi, A. G. G. Moliterni, M. C. Burla, G. Polidori, M. Camalli, R. Spagna, *SIR97*, **1997**; b) A. Altomare, M. C. Burla, M. Camalli, G. L. Cascarano, C. Giacovazzo, A. Guagliardi, A. G. G. Moliterni, G. Polidori, R. Spagna, *J. Appl. Crystallogr.* **1999**, *32*, 115–119.

[11] a) G. M. Sheldrick, *SHELXL-97*, *Program for the Refinement of Crystal Structures*, University of Göttingen, Germany, **1997**; b) G. M. Sheldrick, *Acta Crystallogr. Sect. A* **2008**, *64*, 112–122.

[12] A. L. Spek, *PLATON*, *A Multipurpose Crystallographic Tool*, Utrecht University, The Netherlands, **1999**.

[13] L. J. Farrugia, *J. Appl. Cryst.* **2012**, *45*, 849–854.

[14] Empirical absorption correction using spherical harmonics, implemented in SCALE3 ABSPACK scaling algorithm (CrysAlisPro Oxford Diffraction Ltd., Version 171.33.41, **2009**).

[15] *APEX3*. Bruker AXS Inc., Madison, Wisconsin, USA.

[16] M. J. Frisch, G. W. Trucks, H. B. Schlegel, G. E. Scuseria, M. A. Robb, J. R. Cheeseman, G. Scalmani, V. Barone, B. Mennucci, G. A. Petersson, H. Nakatsuji, M. Caricato, X. Li, H. P. Hratchian, A. F. Izmaylov, J. Bloino, G. Zheng, J. L. Sonnenberg, M. Hada, M. Ehara, K. Toyota, R. Fukuda, J. Hasegawa, M. Ishida, T. Nakajima, Y. Honda, O. Kitao, H. Nakai, T. Vreven, J. A.

Montgomery, Jr., J. E. Peralta, F. Ogliaro, M. Bearpark, J. J. Heyd, E. Brothers, K. N. Kudin, V. N. Staroverov, R. Kobayashi, J. Normand, K. Raghavachari, A. Rendell, J. C. Burant, S. S. Iyengar, J. Tomasi, M. Cossi, N. Rega, J. M. Millam, M. Klene, J. E. Knox, J. B. Cross, V. Bakken, C. Adamo, J. Jaramillo, R. Gomperts, R. E. Stratmann, O. Yazyev, A. J. Austin, R. Cammi, C. Pomelli, J. W. Ochterski, R. L. Martin, K. Morokuma, V. G. Zakrzewski, G. A. Voth, P. Salvador, J. J. Dannenberg, S. Dapprich, A. D. Daniels, O. Farkas, J. B. Foresman, J. V. Ortiz, J. Cioslowski, D. J. Fox, Gaussian 09 A.02, Gaussian, Inc., Wallingford, CT, USA, **2009**.

[17] a) J. W. Ochterski, G. A. Petersson, J. A. Montgomery Jr., *J. Chem. Phys.* **1996**, *104*, 2598–2619; b) J. A. Montgomery Jr., M. J. Frisch, J. W. Ochterski G. A. Petersson, *J. Chem. Phys.* **2000**, *112*, 6532–6542.

[18] a) L. A. Curtiss, K. Raghavachari, P. C. Redfern, J. A. Pople, *J. Chem. Phys.* **1997**, *106*, 1063–1079; b) E. F. C. Byrd, B. M. Rice, *J. Phys. Chem.* A **2006**, *110*, 1005–1013; c) B. M. Rice, S. V. Pai, J. Hare, *Comb. Flame* **1999**, *118*, 445–458.

[19] a) H. D. B. Jenkins, H. K. Roobottom, J. Passmore, L. Glasser, *Inorg. Chem.* **1999**, *38*, 3609–3620; b) H. D. B. Jenkins, D. Tudela, L. Glasser, *Inorg. Chem.* **2002**, *41*, 2364–2367.

[20] L. Molard, J. Vaganay, *Meml. Poudres* **1957**, *39*, 123–136.

[21] S. P. Agrawal, J. P. Agrawal, *Def. Sor. J.* **1970**, *20*, 237–248.

8. Copper(II) Dicyanamide Complexes with *N*-Substituted Tetrazole Ligands – Energetic Coordination Polymers with Moderate Sensitivities

Maximilian H. H. Wurzenberger, Jasmin T. Lechner, and Jörg Stierstorfer

Published in *ChemPlusChem* **2020**, *85*, 769–775.

DOI: 10.1002/cplu.202000156

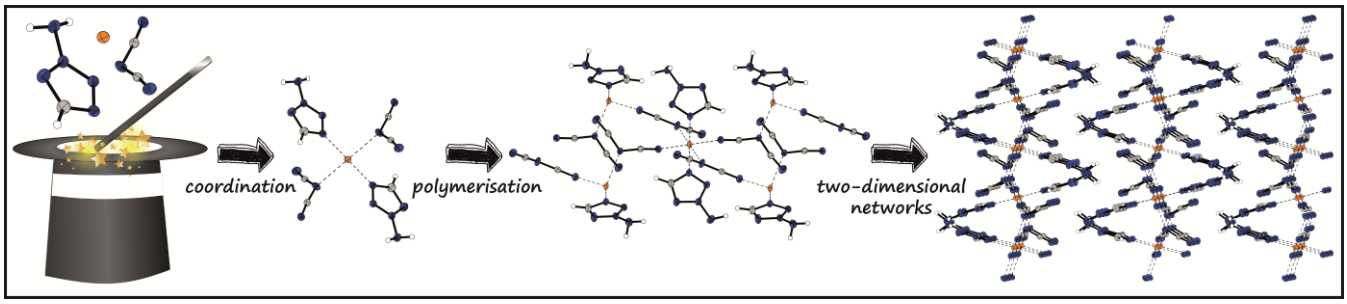

Abstract: Following the useful concept of energetic coordination compounds (ECC), copper(II) dicyanamide was used as a building block for the synthesis of eight new complexes. As ligands, six different *N*-substituted tetrazoles were applied, leading to the formation of high-nitrogen containing complexes. The obtained compounds were characterized in detail by single crystal as well as powder XRD, IR, EA, DTA, and TGA. In addition, the sensitivities toward impact and friction were determined with BAM standard techniques as well as the sensitivity toward electrostatic discharges. All compounds show moderate sensitivities (*IS* > 6 J, *FS* > 80 N) and energetic properties but differ in their polymeric structures forming polymeric chains or layers up to 3D networks.

8.1. Introduction

The dicyanamide moiety belongs to the class of cyanamides, which have manifold applications and are used as precursors or intermediates in industry. Sodium dicyanamide (NaDCA) can be easily obtained by reacting cyanamide with cyanogen chloride and sodium hydroxide.[1] Dicyanamides can be used as starting materials for the synthesis of many different materials such as heterocycles, ionic liquids or transition metal complexes.[2] An interesting heterocycle with regards to its very high nitrogen content on the one hand side and its perfect stability and facile accessibility on the other hand side is 5,5'-bis(1*H*-tetrazol-5-yl)amine (H_2bta). It can easily be prepared by a one-step reaction starting with NaDCA (Chart 1 **A**)).

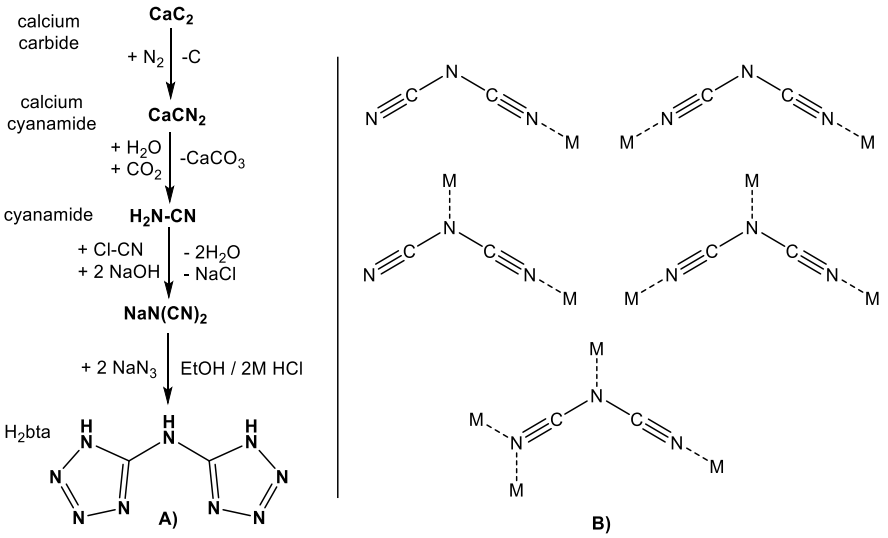

Chart 1. A) Synthesis of the di-heterocyclic compound bis(tetrazolyl)amine H_2bta starting from sodium dicyanamide (NaDCA), which can be produced from calcium carbide; **B)** Different coordination modes of the DCA anion reported in the literature.[3]

The neutral compound and its metal salts were discussed for different applications, especially for the use as energetic materials, *e.g.*, as burn rate modifiers due to their moderate sensitivities.[4] Another important use of the DCA anion is its application in transition metal complexes. Due to its manifold coordination modes and bridging character it can connect between several metal centers forming polymeric compounds with unique features (Chart 1 **B**)).[3] An innumerable amount of complexes mainly based on 3d transition metals are discussed in the literature for different applications such as magnetic switches.[5] Besides the commonly used central metals copper and cobalt there can also be found more exotic ones, like silver or uranium.[6] In the past, strong oxidizing anions such as nitrate or perchlorate were often used for the synthesis of energetic coordination compounds (ECC). The obtained complexes are powerful compounds with great performance but also come along with high sensitivities making their handling considerably more difficult.[7] In recent years, the focus of new energetic compounds shifted strongly toward substances

that are safer to use and therefore possess decreased sensitivities.[8] For the synthesis of novel ECC, we focused on small anions with positive heat of formation (ΔH_f). Most of the anions such as (per)chlorate, nitrate, etc. are formed exothermically in the gas phase (Figure 1). In contrast cyanide, fulminate, azide, and dicyanamide have different positive calculated ΔH_f's and allow therefore the tuning of the desired properties.

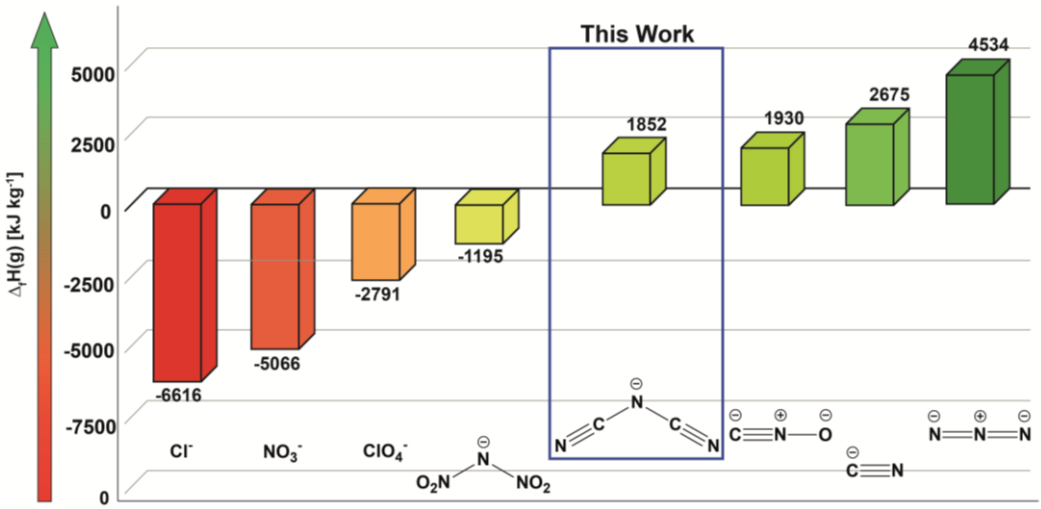

Figure 1. Comparison of the calculated gas-phase enthalpies of formation[9] for several simple negatively charged anions showing positive heat of formation for the DCA anion.

In the case of copper(II) complexes the choices are considerably narrowed. Both, fulminates and cyanides are leading to the reduction to Cu^+, while copper azides are extremely sensitive and dangerous to handle. The optimal compromise for the synthesis of energetic copper complexes with moderate sensitivities is thus the dicyanamide anion showing a moderate positive heat of formation. For the DCA anion, both the pure copper(I) and copper(II) salts are stable at ambient conditions.[10] While many copper(II) dicyanamide complexes were investigated, nitrogen-rich representatives are very rare in the literature. Solely the 1,5-diaminotetrazole compound is mentioned as an energetic combustion catalyst for propellant systems, indicating their potential as possible ECC.[11] Therefore, in this work, new copper(II) coordination polymers based on dicyanamide and tetrazole ligands were synthesized and their energetic properties investigated.

8.2. Results and Discussion

8.2.1. Synthesis

The copper(II) dicyanamide compounds were synthesized using six different tetrazole ligands and started with a metathesis reaction. Therefore, the corresponding copper(II) nitrate complexes were generated *in situ* and further reacted with aqueous sodium dicyanamide solutions (Scheme 1). The used ligands were

available in the research group and prepared according to literature known syntheses.[12] All eight complexes possess polymeric structures due to the bridging nature of the DCA anion and therefore crystallize quickly after the synthesis.

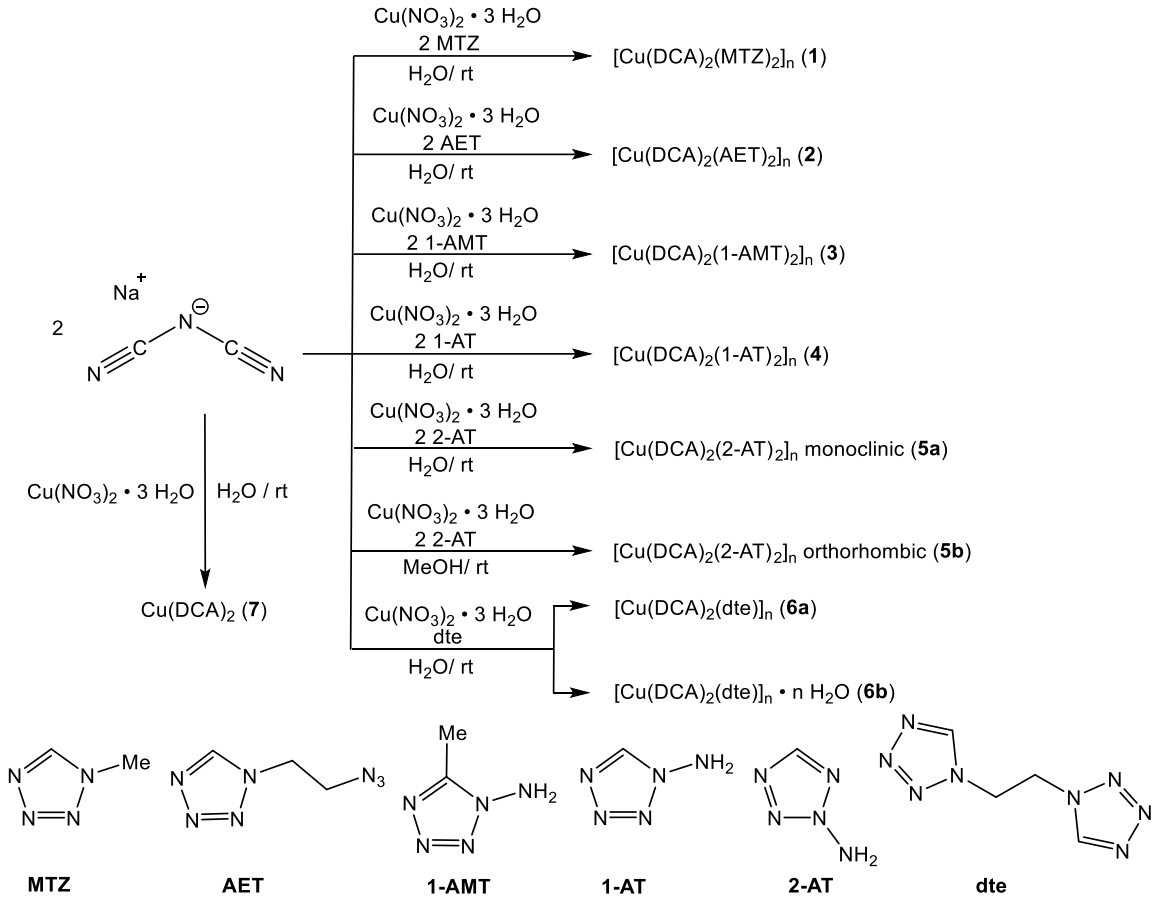

Scheme 1. Syntheses of the coordination compounds **1**–**6** and the pure copper(II) salt **7** (top). Structures of the used ligands (bottom). MTZ: 1-methyl-5*H*-tetrazole; AET: 1-azidoethyl-5*H*-tetrazole; 1-AMT: 1-amino-5-methyltetrazole; 1-AT: 1-amino-5*H*-tetrazole; 2-AT: 2-amino-5*H*-tetrazole; dte: 1,2-di(tetrazol-1-yl)ethane.

During the synthesis of **6a**, sometimes the formation of a second species in very small traces was observed. The side-species **6b** represents a monohydrate of **6a** and is the only water-containing compound. All other complexes were obtained as anhydrous substances. Similar to **6b** only some single-crystals of complex **3** were able to be obtained. Therefore, both compounds could not be further characterized. The pure copper(II) dicyanamide (**7**) was obtained as the main product during the attempted synthesis of **3** and as the only product when 2-amino-5-methyltetrazole was applied as ligand.

8.2.2. Crystal Structures

All compounds were characterized by low-temperature single-crystal X-ray diffraction and details on the measurement and refinement data are given in the Supporting Information (Tables S1−3).[13]

In all eight complexes, the central Cu^{2+} cations are octahedrally coordinated and show typical d^9 Jahn-Teller distortions. Due to the bridging dicyanamide anion, all structures are multidimensional. The spatial structures of compounds **1**, **2**, and **3** with the ligands MTZ (**1**), AET (**2**), and 1-AMT (**3**) are quite similar. The copper atoms are all coordinated by two tetrazole ligands in equatorial positions and four bridging dicyanamido anions. The MTZ complex **1** is crystallizing in the monoclinic space group $P2_1/n$ and compounds **2** and **3** in the triclinic space group $P\bar{1}$ (Figure 2). They show comparable densities between 1.735 and 1.772 g cm^{-3}.

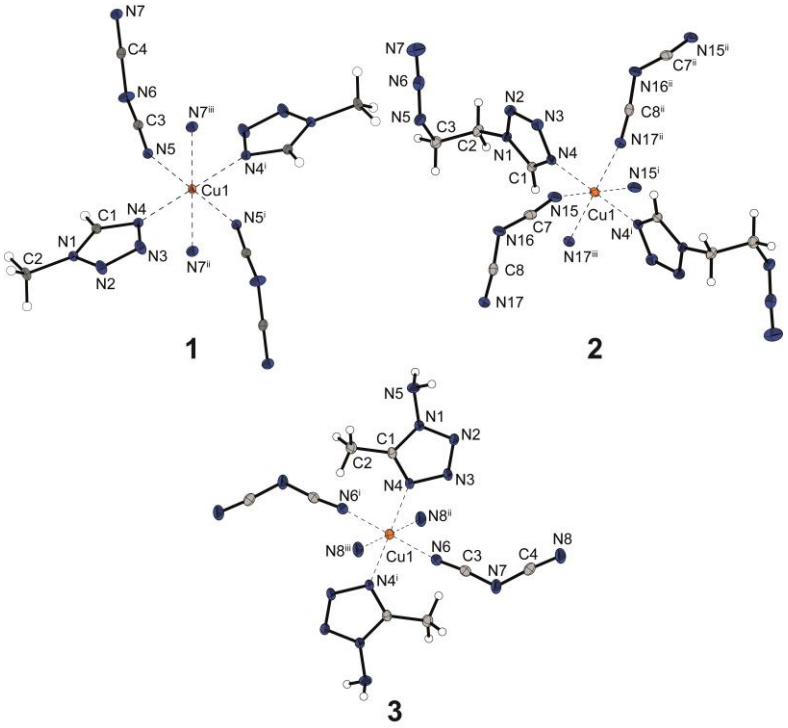

Figure 2. Copper(II) coordination environment of **1** (top left), **2** (top right) and **3** (bottom). Thermal ellipsoids of non-hydrogen atoms in all structures are set to the 50% probability level. Selected bond lengths of **1** (Å): Cu1–N4 2.0179(13), Cu1–N5 1.9892(14), Cu1–$N7^{ii}$ 2.4717(14). Selected bond angles of **1** (°): N4–Cu1–N5 89.07(6), N4–Cu1–$N4^{i}$ 180.00, N4–Cu1–$N7^{ii}$ 85.17(5). Symmetry codes of **1**: (i) 1−x, 1−y, 1−z; (ii) x, −1+y, z; (iii) 1−x, 2−y, 1−z. Selected bond lengths of **2** (Å): Cu1–N4 2.013(2), Cu1–N15 2.459(2), Cu1–$N17^{ii}$ 1.991(2). Selected bond angles of **2** (°): N4–Cu1–N15 90.28(8), N4–Cu1–$N4^{i}$ 180.00, N4–Cu1–$N17^{ii}$ 90.83(9). Symmetry codes of **2**: (i) 2−x, −y, 1−z; (ii) −1+x, y, z; (iii) 3−x, −y, 1−z. Selected bond lengths of **3** (Å): Cu1–N4 2.0459(16), Cu1–N6 1.944(2), Cu1–$N8^{ii}$ 2.544(2). Selected bond angles of **3** (°): N4–Cu1–$N6^{i}$ 90.55(8), N4–Cu1–$N4^{i}$ 180.00, N4–Cu1–$N8^{ii}$ 89.23(6). Symmetry codes of **3**: (i) −x, −y, −z; (ii) −1+x, y, z; (iii) 1−x, −y, −z.

In all three cases, the bridging leads to the formation of one-dimensional chains (Figure 3), which are caused by the binding of the two outer nitrogen atoms of the DCA to the central metals. Two anions each bridging between the same two cations. The heterocycles all bind to the copper via the N4 atom which is located next to the carbon atom. The bond lengths between the Cu1 and the N4 atom are almost the same for all three complexes. The copper complex **4** with 1-AT as ligand has a nearly similar coordination

environment as the previously described complexes **1**–**3**. The central copper atom is coordinated by two 1-AT ligands via N4, and 4 DCA anions again via the outer two nitrogen atoms (Figure 4). It crystallizes in the monoclinic space group $P2_1/c$ with two formula units per unit cell and a calculated density of 1.860 g cm^{-3} at 143 K.

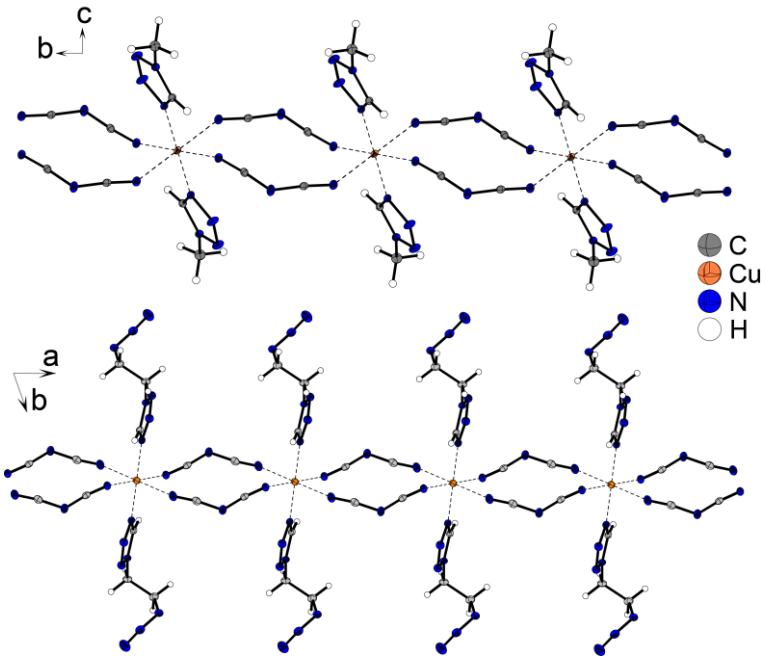

Figure 3. One-dimensional polymeric structure of **1** (top) and **2** (bottom).

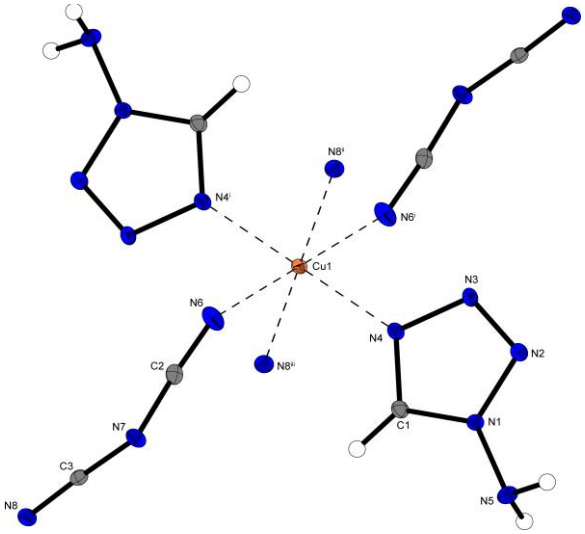

Figure 4. Copper(II) coordination environment of **4**. Selected bond lengths (Å): Cu1–N4 2.0191(12), Cu1–N6 2.3986(14), Cu1–N8^{ii} 1.9884(14). Selected bond angles (°): N4–Cu1–N6^{i} 90.69(5), N4–Cu1–N4^{i} 180.00, N4–Cu1–N8^{iii} 89.55(5). Symmetry codes: (i) x, 2−y, −z; (ii) x, 0.5+y, −0.5−z; (iii) x, 1.5−y, 0.5+z.

However, the compounds differ in their polymeric structure. While in complexes **1**–**3** the dicyanamide anions are bridging always between the same two central metals, the four DCAs in compound **4** link to four different copper cations. This creates a two-dimensional polymeric layer (Figure 5).

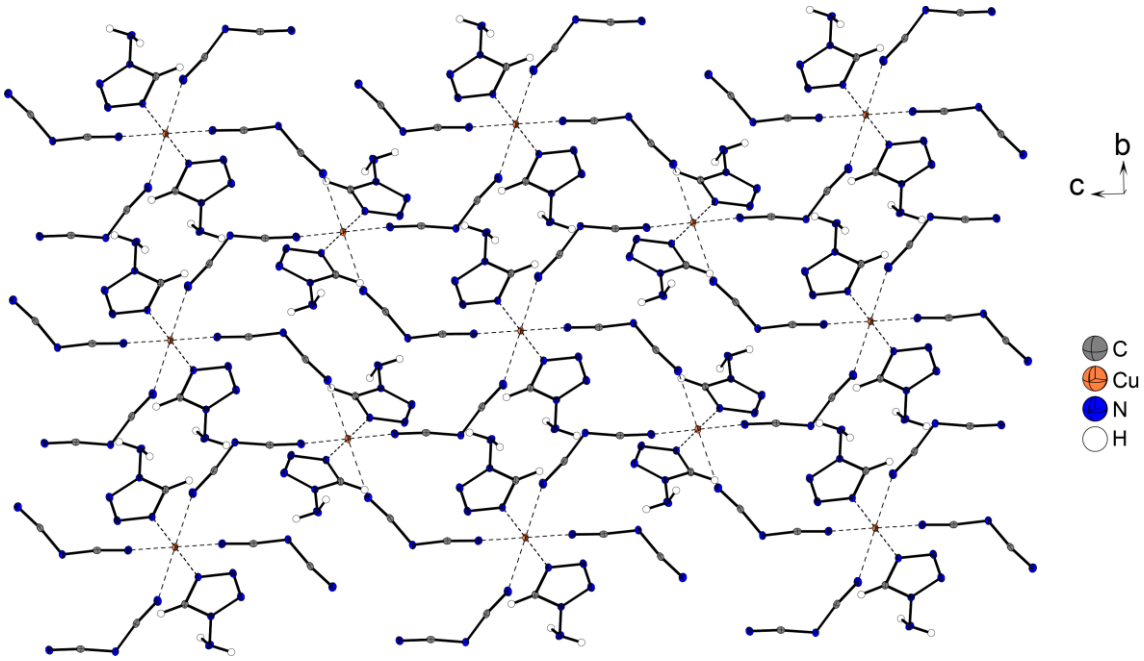

Figure 5. Two-dimensional polymeric structure of **4**, view along the *a* axis.

The coordination polymers of copper(II) dicyanamide with 2-amino-5*H*-tetrazole can be obtained in two different polymorphs **5a** and **5b**. Similar to **4**, both compounds show a coordination structure with the copper central atom bound to two 2-AT ligands via the N4 atom. Furthermore, four dicyanamide anions bind to the Cu(II), but this time each via one outer and the middle nitrogen atom. While **5a** crystallizes in a monoclinic space group ($P2_1/c$), **5b** is present in an orthorhombic one (*Pbca*; Figure 6). Interestingly, they show a difference in density of about 0.1 g cm^{-3}, whereby **5a** has 1.858 g cm^{-3} at 127 K and **5b** 1.757 g cm^{-3} at 143 K.

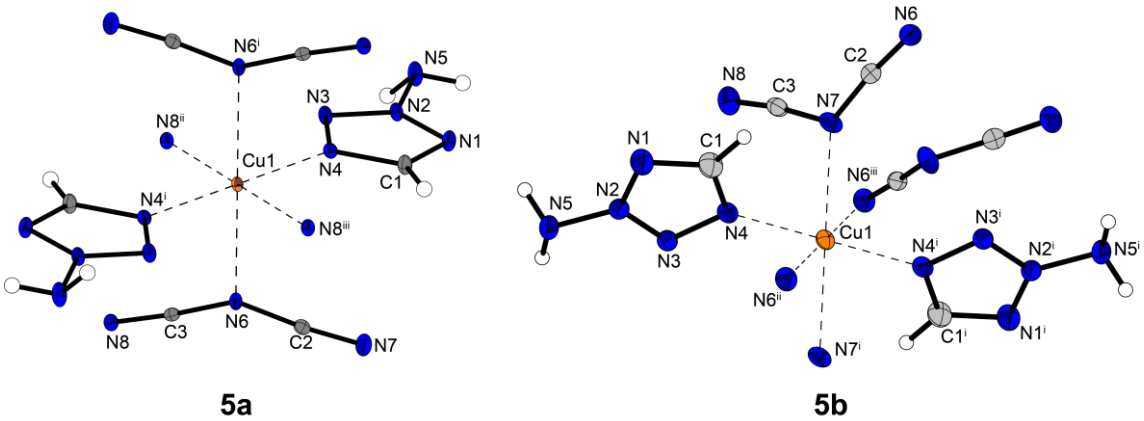

Figure 6. Copper(II) coordination environment of **5a** (left) and of **5b** (right). Selected bond lengths of **5a** (Å): Cu1–N4 2.0321(14), Cu1–N6 2.4280(13), Cu1–N8^{ii} 1.9803(14). Selected bond angles of **5a** (°): N4–Cu1–N6^{i} 92.51(5), N4–Cu1–N4^{i} 180.00, N4–Cu1–N8^{iii} 89.13(5). Symmetry codes of **5a**: (i) −x, 1−y, 1−z; (ii) x, 1.5−y, 0.5+z; (iii) −x, −0.5+y, 0.5−z. Selected bond lengths of **5b** (Å): Cu1–N4 2.0311(18), Cu1–N6^{ii} 1.956(2), Cu1–N7 2.464(2). Selected bond angles of **5b** (°): N4–Cu1–N6^{ii} 89.77(8), N4–Cu1–N4^{i} 180.00, N4–Cu1–N7 86.19(7). Symmetry codes of **5b**: (i) 1−x, 1−y, −z; (ii) −0.5+x, 0.5−y, −z; (iii) 1.5−x, 0.5+y, z.

Both compounds show a comparable coordination behavior with the dicyanamido ligands linking the central metals to four different copper atoms forming two-dimensional polymers. Upon closer examination, it becomes clear that the only difference between the two is the arrangement of the tetrazole ligands. While in **5b** the heterocycles of one side all point to the same side in **5a** they alternate, allowing a denser packing and explaining the higher density (Figure 7).

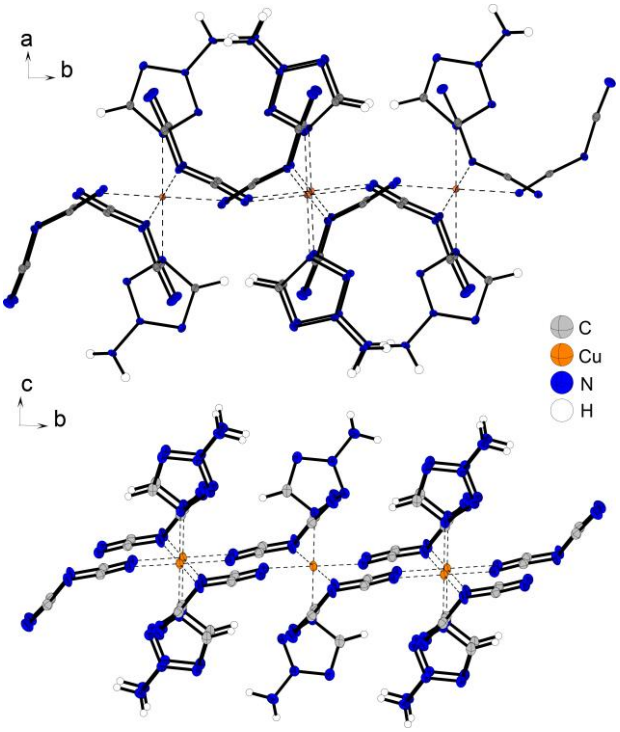

Figure 7. Two-dimensional polymeric structure of **5a** (top) and **5b** (bottom).

Compared to the other complexes, the structures of **6a** and **6b** are outstanding due to the insertion of an additional bridging ligand. The anhydrous compound **6a** crystallizes in the triclinic space group *P*−1 with a density of 1.817 g cm^{-3} (110 K) and the monohydrate in the monoclinic space group *C*2/*c* with a slightly lower density (1.752 g cm^{-3} @ 127 K). In both cases, the central metals are coordinated by two tetrazoles and four DCA nitrogen atoms. Like in **5a** and **5b**, the anions are binding with one outer and the middle nitrogen atom. The molecular unit of **6b** is completed by an additional crystal water molecule (Figure 8). Nevertheless, **6b** is not just simply the monohydrate of **6a**. A closer examination of the crystal structures reveals the difference of **6a** forming a two-dimensional and **6b** a three-dimensional structure. Similar to compounds **1**–**3**, in **6a** two anions each are bridging between the same two central metals leading to the formation of polymeric chains. The additional linking of the ditetrazolyl ligand is causing an enhancement of the dimension to polymeric layers (Figure 9). The dte ligand is also increasing the dimension in complex **6b**, but here the DCA anions are already forming 2D-layers, similar to complex **5a** and **5b**. This results in a three-dimensional polymeric structure of **6b** (Figure 10). The structure favors the storage of water, which is why **6b** crystallizes as monohydrate.

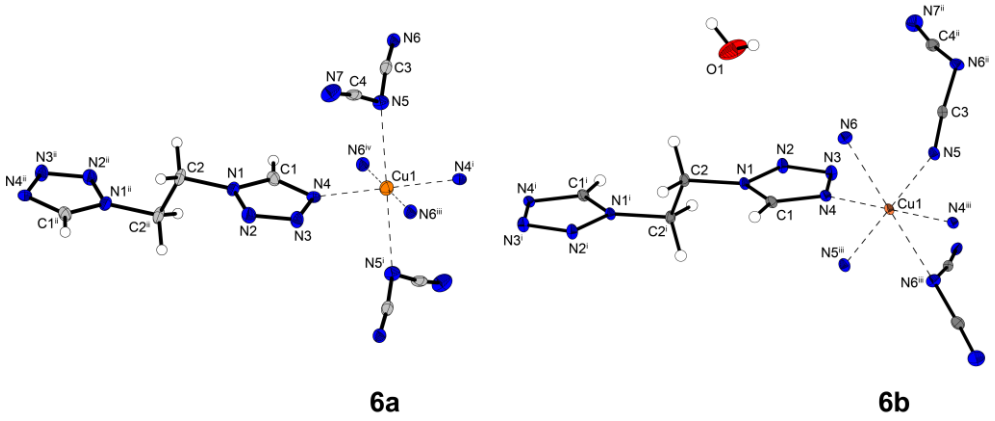

Figure 8. Copper(II) coordination environment of **6a** (left) and of **6b** (right). Selected bond lengths of **6a** (Å): Cu1–N4 2.027(3), Cu1–N5 2.438(3), Cu1–N6^{iii} 1.958(3). Selected bond angles of **6a** (°): N4–Cu1–N5^{i} 93.14(12), N4–Cu1–N4^{i} 180.00, N4–Cu1–N6^{iv} 90.82(13). Symmetry codes of **6a**: (i) 2−x, −y, −z; (ii) 2−x, −1−y, 1−z; (iii) 1−x, −y, −z; (iv) 1+x, y, z. Selected bond lengths of **6b** (Å): Cu1–N4 2.0094(14), Cu1–N5 1.9619(14), Cu1–N6 2.4851(15). Selected bond angles of **6b** (°): N4–Cu1–N6 86.20(5), N4–Cu1–N4^{iii} 180.00, N4–Cu1–N5^{iii} 90.22(6). Symmetry codes of **6b**: (i) −x, −y, 1−z; (ii) x, 1−y, 0.5+z; (iii) 0.5−x, 0.5−y, 1−z.

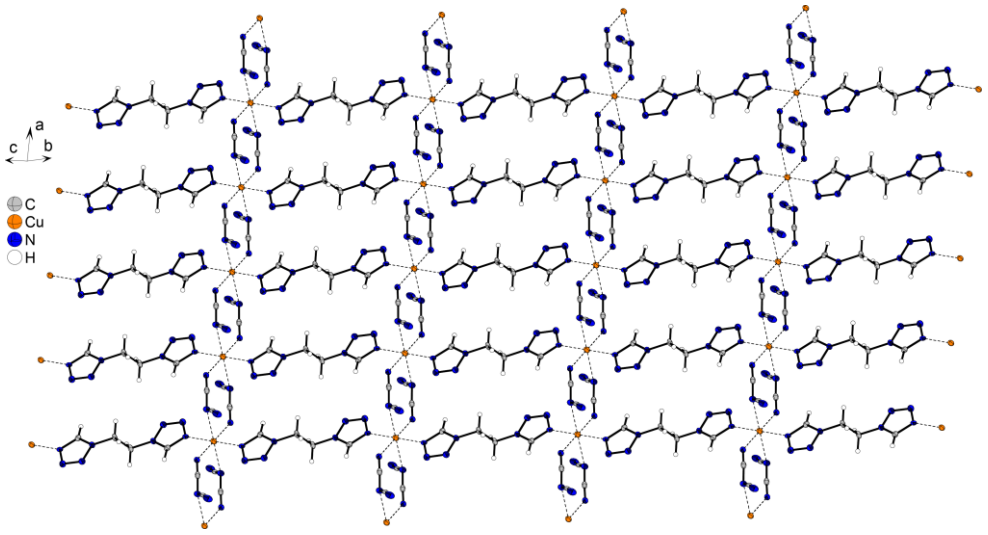

Figure 9. Two-dimensional polymeric structure of **6a**.

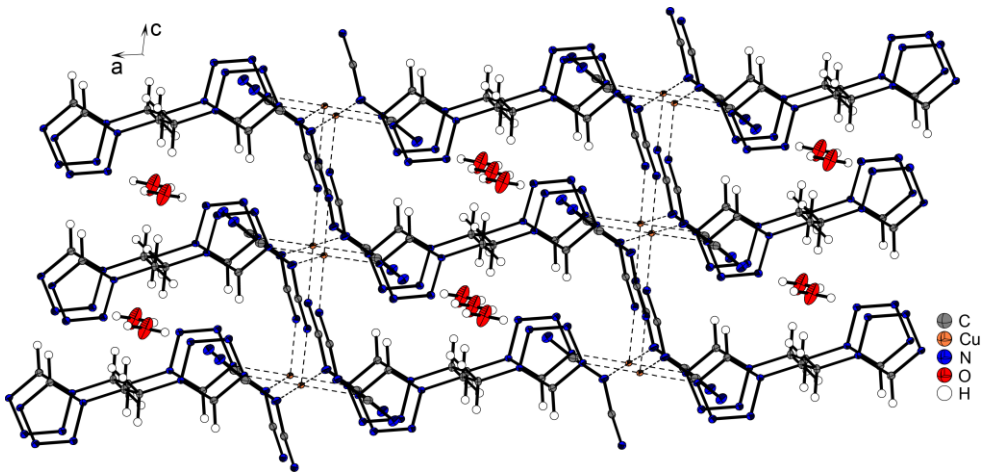

Figure 10. View along the *b* axis of three-dimensional polymeric structure of **6b**.

8.2.3. Physicochemical Properties

All synthesized compounds, except **3** and **6b**, were investigated regarding their thermal properties and sensitivities toward external stimuli. In order to check the isomeric purity of compounds **5a** and **5b**, they were further investigated by powder X-ray diffraction.

8.2.4. Thermal Analysis

Compounds **1**, **2**, **4**, **5a**, **5b**, and **6a** were characterized by differential thermal analysis (DTA) with a linear heating rate of β =5 °C min^{-1} in the range of 30 to 400 °C. The DTA plots are shown in Figures 11 and S3.

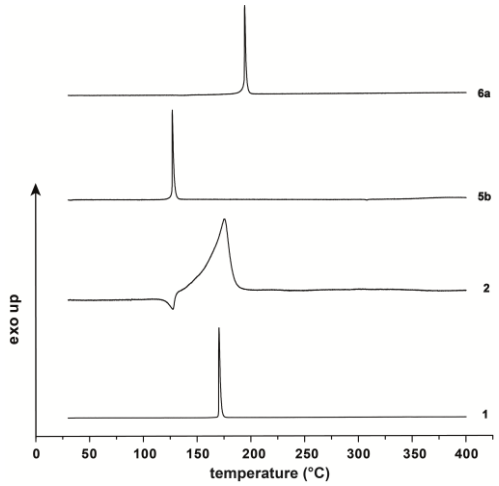

Figure 11. DTA Plots of compounds **1**, **2**, **5b**, and **6a**.

The experiments (Table 1) reveal that all complexes possess lower decomposition points (126–193 °C) compared to pure $Cu(DCA)_2$ (254 °C). Furthermore, compound **2** is the only one showing an endothermic event right before its decomposition. Closer examination using thermogravimetric analysis (TGA) proves the compounds' stability up to their corresponding exothermic decomposition temperatures, revealing a melting point for complex **2** at 126 °C (Figures 12 and S4).

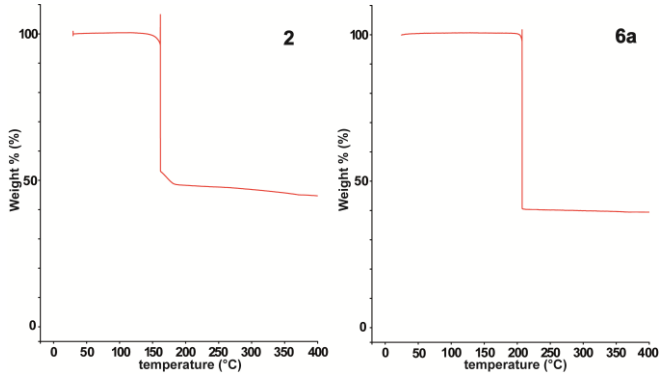

Figure 12. TGA Plots of compounds **2** and **6a**.

8.2.5. Sensitivities

Except for **3** and **6b**, the energetic properties of all compounds were investigated. The sensitivities toward impact, friction, and electrostatic discharge are summarized in Table 1. The impact sensitivities are in the range of 6–10 J and therefore, the complexes have to be classified as sensitive according to the UN Recommendations on the Transport of Dangerous Goods. Only the salt **7** is classified as less sensitive with a value of 40 J.

Table 1. Thermal stability measurements by DTA,[a] as well as sensitivities toward impact, friction and ESD of compounds **1**–**7**.[b]

	$T_{exo.}$[c] [°C]	*IS*[d] [J]	*FS*[e] [N]	*ESD*[f] [mJ]
1	170	8	> 360	> 1500
2	131	6	192	1500
4	141	6	144	1350
5a	129	9	80	540
5b	126	9	80	540
6a	193	10	> 360	1220
7	254	40	> 360	630

[a] Onset temperatures at a heating rate of 5 °C min^{-1}. [b] Determined at a grain size < 100 µm. [c] Exothermic peak, which indicates decomposition. [d] Impact sensitivity according to the BAM drop hammer (method 1 of 6). [e] Friction sensitivity according to the BAM friction tester (method 1 of 6). [f] Electrostatic discharge sensitivity (OZM XSpark10 ESD tester); impact: insensitive > 40 J, less sensitive ≥ 35 J, sensitive ≥ 4 J, and very sensitive ≤ 3 J; friction: insensitive > 360 N, less sensitive = 360 N, sensitive < 360 N and > 80 N, very sensitive ≤ 80 N, and extremely sensitive ≤ 10 N. According to the UN Recommendations on the Transport of Dangerous Goods.

Concerning the friction sensitivities, compounds **1**, **6a**, and **7** can be classified as insensitive (> 360 N). In contrast, complexes **2**, **4**, **5a**, and **5b** have to be classified as sensitive, with values between 80 N (**5a**, **5b**) and 192 N (**2**). It can be seen that the energetic character of pure copper(II) dicyanamide is getting increased through the coordination of nitrogen-rich ligands. Interestingly, the two different polymorphs **5a** and **5b** do not show major aberrations in their energetic properties.

8.2.6. Powder Diffraction

For a more detailed investigation, compounds **5a** and **5b** were applied to X-ray powder diffraction measurements (Figure 13). Small variations in the orthorhombic species **5b** can be attributed to the temperature differences of single-crystal and powder X-ray diffraction. Therefore, it is possible to synthesize **5b** isomerically pure. However, in the case of **5a** contamination with the second polymorph are observable and further research is necessary for selective synthesis of it.

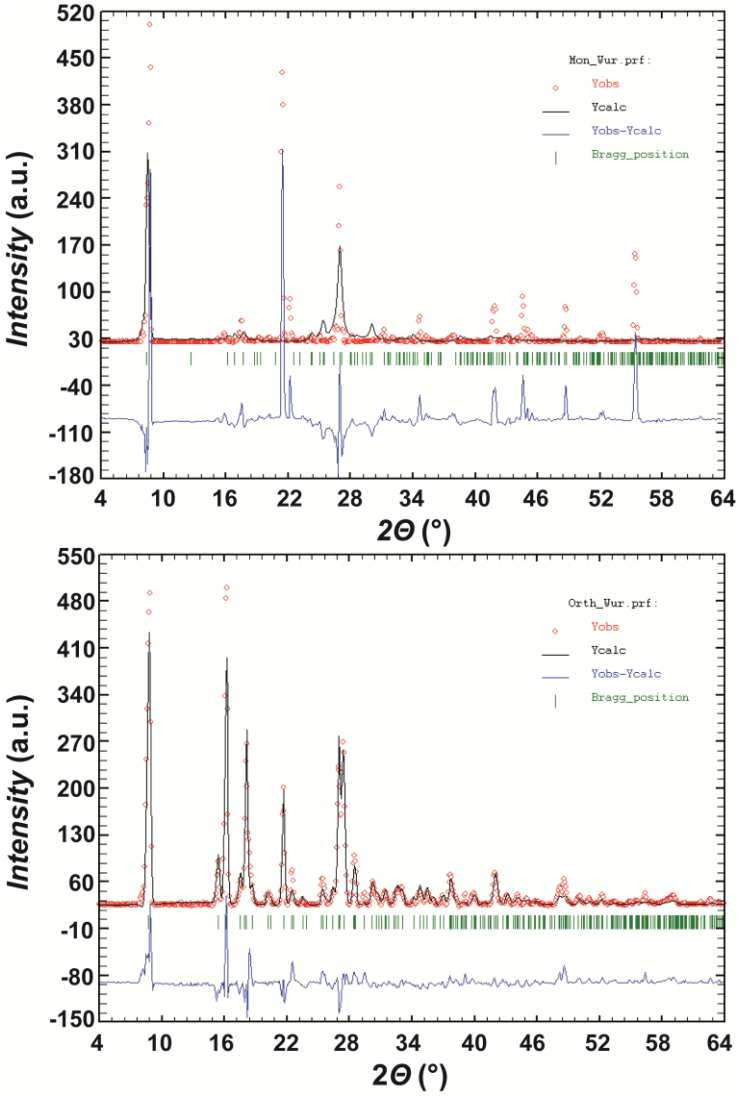

Figure 13. Powder diffraction experiments (comparison (blue) of the measured (red) and calculated (black) data) of compounds **5a** (top) and **5b** (bottom).

8.3. Conclusion

In this work, eight new nitrogen-rich copper(II) dicyanamide complexes based on *N*-substituted tetrazole ligands were synthesized. Due to the good coordination behavior of dicyanamide, they can all be obtained without the inclusion of water. Only the formation of a 3D-polymeric side-species allows the inclusion of guest solvent molecules. All complexes were investigated by low-temperature single-crystal X-ray experiments and their polymeric structure examined in detail. The energetic properties and thermal behavior of the low water-soluble six ECC were determined and showed moderate sensitivities (*IS* > 6 J, *FS* > 80 N). This allows the safe handling of the complexes, which could be used as potential energetic additives *e.g.*, burn rate catalysts. Also, a non-energetic use as magnetic switches could be possible. Especially compounds **4** and **5b** show promising properties for the use as energetic metal-organic frameworks (EMOF).

8.4. Experimental Section

CAUTION! *All investigated compounds are energetic materials, which partly show increased sensitivities toward various stimuli (e.g., elevated temperatures, impact, friction or electronic discharge). Although no incidents occurred, proper security precautions (safety glasses, face shield, earthed equipment and shoes, leather jacket, Kevlar sleeves, and earplugs) have to be worn while synthesizing and handling the described compounds.*

Detailed information on chemicals, syntheses, as well as analytical data and methods of **1**–**6** can be found in the Supplementary Information.

General procedure for the preparation of copper(II) dicyanamide complexes (**1**–**5a** and **6a**): To a solution of copper(II) nitrate trihydrate (60.4 mg, 0.25 mmol, 1 eq) in water (1 mL) the corresponding ligand (**1**: 1-methyl-5*H*-tetrazole (42.0 mg, 0.50 mmol, 2 eq); **2**: 1-azidoethyl-5*H*-tetrazole (69.6 mg, 0.50 mmol, 2 eq); **3**: 1-amino-5-methyltetrazole (49.6 mg, 0.50 mmol, 2 eq); **4**: 1-amino-5*H*-tetrazole (42.5 mg, 0.50 mmol, 2 eq); **5a**: 2-amino-5*H*-tetrazole (42.5 mg, 0.50 mmol, 2 eq); **6a**: 1,2-di(tetrazol-1-yl)ethane (41.6 mg, 0.25 mmol, 1 eq)) was added. After stirring for a minute, an aqueous solution (1 mL) of sodium dicyanamide (44.5 mg, 0.50 mmol, 2 eq) was added, the mixture was stirred for one more minute at room temperature and left for crystallization. After formation of the crystalline products, the compounds were filtered off, washed with cold ethanol and dried in air. All compounds were obtained in the form of single crystals suitable for X-ray diffraction.

8.5. Acknowledgements

For financial support of this work by Ludwig-Maximilians-University (LMU). The authors would like to thank especially Prof. Dr. Thomas M. Klapötke for providing facilities and great scientific support, Prof. Dr. Jürgen Evers for the X-ray powder diffraction experiments, Dr. Peter Mayer for helping with X-ray crystal structure analysis and Mr. Marcus Lommel for his great contribution to this work.

8.6. References

[1] T. Güthner, B. Mertschenk, *Cyanamides. Ullmann's Encyclopedia of Industrial Chemistry*, 1st ed., Wiley-VCH, Weinheim, **2006**.

[2] a) A. M. Kini, U. Geiser, H. H. Wang, K. D. Carlson, J. M. Williams, W. K. Kwok, K. G. Vandervoort, J. E. Thompson, D. L. Stupka, D. Jung, M. Whangbo, *Inorg. Chem.* **1990**, *29*, 2555–2557; b) T. Chivers, D. Gates, X. Li, I. Manners, M. Parvez, *Inorg. Chem.* **1999**, *38*, 70–76; c) N. Delgado-Mellado, J. García, F. Rodríguez, R. D. Rogers, *ChemPlusChem* **2019**, *84*, 872–881; d) S. R. Batten, P. Jensen, B. Moubaraki, K. S. Murray, *Chem. Commun.* **2000**, *23*, 2331–2332; e)

Y.-H. Joo, H. Gao, Y. Zhang, J. M. Shreeve, *Inorg. Chem.* **2010**, *49*, 3282–3288; f) Z. Jalový, Z. Padělková, R. Jirásko, R. Matyáš, M. Holčapek, O. Němec, M. Novotná, L. Mišková, *Polyhedron* **2012**, *44*, 88–100; g) O. Reckeweg, A. Schulz, F. J. DiSalvo, *Z. Naturforsch. B* **2013**, *68*, 296–300; h) J. G. Díaz, A. G. Albor, E. V. Jaime, V. Vrábel, J. Kozísek, *Acta Crystallogr. Sect. E* **2012**, *68*, 89–90.

[3] J. L. Manson, T. Lancaster, S. J. Blundell, Y. Qiu, J. Singleton, P. Sengupta, F. L. Pratt, J. Kang, C. Lee, M.-H. Whangbo, *Polyhedron* **2010**, *29*, 514–520.

[4] a) M. Dahan, E. Komarala, L. Fadeev, A. K. Chinnam, A. Shlomovich, S. Lipstman, S. P. Padi, H. Haustein, M. Gozin, B. A. Rosen, *J. Mater. Chem. A* **2019**, *7*, 141–149; b) J. Lavoie, C.-F. Petre, P.-Y. Paradis, C. Dubois, *Propellants Explos. Pyrotech.* **2017**, *42*, 149–157; c) T. M. Klapötke, P. Mayer, J. Stierstorfer, J. J. Weigand, *J. Mater. Chem.* **2008**, *18*, 5248–5258.

[5] a) M. Havastijova, J. Kohout, H. Köhler, G. Ondrejovic, *Z. Anorg. Allg. Chem.* **1988**, *566*, 111–120; b) J. Carranza, J. Sletten, F. Lloret, M. Julve, *Inorg. Chim. Acta* **2004**, *357*, 3304–3316; c) R. Sen, A. Bhattacharjee, P. Gütlich, Y. Miyashita, K.-I. Okamoto, S. Koner, *Inorg. Chim. Acta* **2009**, *362*, 4663–4670; d) G. A. van Albada, M. G. van der Horst, S. J. Teat, P. Gamez, O. Roubeau, I. Mutikainen, U. Turpeinen, J. Reedijk, *Polyhedron* **2009**, *28*, 1541–1545; e) J. Kozísek, J. G. Díaz, A. G. Albor, *Acta Crystallogr. Sect. E* **2007**, *63*, 125–126; f) M. Biswas, G. M. Rosair, G. Pilet, S. Mitra, *Inorg. Chim. Acta* **2007**, *360*, 695–699; g) J. Ding, H. Ge, Y. Zhang, B. Li, Y. Zhang, *J. Mol. Struct.* **2006**, *782*, 143–149.

[6] a) K. E. Bessler, L. L. Romualdo, V. M. Deflon, *Z. Anorg. Allg. Chem.* **2000**, *626*, 1942–1945; b) M.-J. Crawford, A. Ellern, K. Karaghiosoff, F. Martin, P. Mayer, *Inorg. Chem.* **2010**, *49*, 2674–2683.

[7] a) T. W. Myers, J. A. Bjorgaard, K. E. Brown, D. E. Chavez, S. K. Hanson, R. J. Scharff, S. Tretiak, J. M. Veauthier, *J. Am. Chem. Soc.* **2016**, *138*, 4685–4692; b) Q. Zhang, J. M. Shreeve, *Angew. Chem.* **2014**, *126*, 2574–2576; c) Q. Zhang, J. M. Shreeve, *Angew. Chem. Int. Ed.* **2014**, *53*, 2540–2542; d) N. Szimhardt, M. H. H. Wurzenberger, L. Zeisel, M. S. Gruhne, M. Lommel, J. Stierstorfer, *J. Mater. Chem. A* **2018**, *6*, 16257–16272.

[8] a) E. C. Johnson, J. J. Sabatini, D. E. Chavez, L. A. Wells, J. E. Banning, R. C. Sausa, E. F. C. Byrd, J. A. Orlicki, *ChemPlusChem* **2020**, *85*, 237–239; b) L. M. Foroughi, R. A. Wiscons, D. R. Du Bois, A. J. Matzger, *Chem. Commun.* **2020**, *56*, 2111–2114; c) Ł. Gutowski, W. Trzciński, M. Szala, *ChemPlusChem* **2018**, *83*, 87–91; d) B. Wang, H. Xiong, G. Cheng, H. Yang, *ChemPlusChem* **2018**, *83*, 439–447; e) L. L. Fershtat, N. N. Makhova, *ChemPlusChem* **2020**, *85*, 13–42.

[9] Gas phase enthalpies of formation were calculated using the atomization method ($\Delta_f H^0_{(g,M)} = H_{(M)} - \sum H^0_{(A)} + \sum \Delta_f H^0_{(A)}$) using Gaussian09 computed CBS-4 M electronic enthalpies.

[10] a) O. Reckeweg, R. E. Dinnebier, A. Schulz, B. Blaschkowski, C. Schneck, T. Schleid, *Z. Naturforsch. B: Anorg. Chem. Org. Chem.* **2017**, *72*, 159–165; b) Q. Rayée, P. T. Nguyen, T. Segato, M.-P. Delplancke-Ogletree, T. Doneux, C. Buess-Herman, *J. Electroanal. Chem.* **2018**, *819*, 331–337.

[11] Z. Li, T. Zhang, J. Zhang, L. Wang, Y. Zhong, Beijing Institute Tech, CN Patent 201910821846, China **2019**.

[12] a) P. N. Gaponik, M. M. Degtyarik, A. S. Lyakhov, V. E. Matulis, O. A. Ivashkevih, M. Quesada, J. Reedijk, *Inorg. Chim. Acta* **2005**, *358*, 3949–3957; b) M. H. H. Wurzenberger, M. S. Gruhne,

M. Lommel, N. Szimhardt, T. M. Klapötke, J. Stierstorfer, *Chem. – Asian J.* **2019**, *14*, 2018–2028; c) K. Sakai, J. P. Anselme, *Org. Prep. Proced. Int.* **1975**, *7*, 61–65; d) R. Raap, *Can. J. Chem.* **1969**, *47*, 3677; e) P. J. v. Koningsbruggen, Y. Garcia, G. Bravic, D. Chasseau, O. Kahn, *Inorg. Chim. Acta* **2001**, *326*, 101–105.

[13] CCDC 1986804 (**1**), 1986806 (**2**), 1986801 (**3**), 1986805 (**4**), 1986800 (**5a**), 1986803 (**5b**), 1986802 (**6a**) and 1986807 (**6b**) contains the supplementary crystallographic data for this paper. These data can be obtained free of charge from The Cambridge Crystallographic Data Centre.

8.7. Supporting Information

8.7.1. Chemicals and Analytics

All chemicals and solvents were employed as received (Sigma-Aldrich, Fluka, Acros, ABCR). The samples were measured in a range of 25–400 °C at a heating rate of 5 °C min^{-1} through differential thermal analysis (DTA) with an OZM Research DTA 552-Ex instrument. Endothermic and exothermic events of the described compounds, which indicate melting, evaporation, or decomposition, are given as the extrapolated onset temperatures. Partly, the compounds were measured also by thermal gravimetric analysis (TGA) with a PerkinElmer TGA4000. Infrared spectra were measured with pure samples on a Perkin-Elmer BXII FT-IR system with a Smith DuraSampler IR II diamond ATR. Determination of the carbon, hydrogen, and nitrogen contents was carried out by combustion analysis using an Elementar Vario El (nitrogen values determined are often lower than those calculated due to their energetic behavior). Impact sensitivity tests were carried out according to STANAG 4489[1] with a modified instruction[2] using a BAM (Bundesanstalt für Materialforschung und -prüfung) drop hammer.[3,4] Friction sensitivity tests were carried out according to STANAG 4487[5] with a modified instruction[6] using the BAM friction tester. The classification of the tested compounds results from the "UN Recommendations on the Transport of Dangerous Goods".[7] Additionally, all compounds were tested to determine the sensitivity toward electrical discharge using OZM Electric Spark XSpark10 device.[3]

8.7.2. IR Spectroscopy

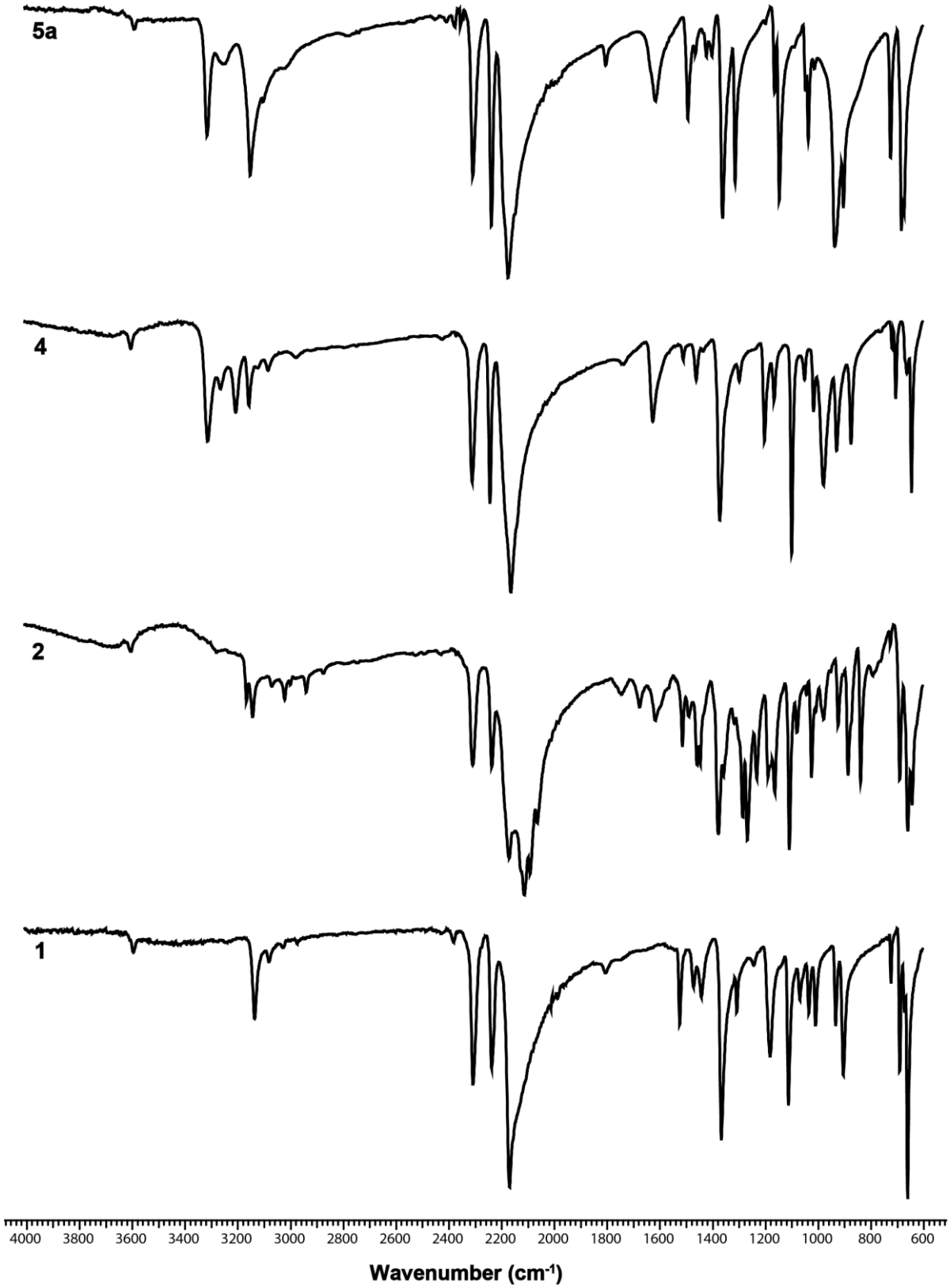

Figure S1. IR spectra of complexes **1**, **2**, **4**, and **5a**.

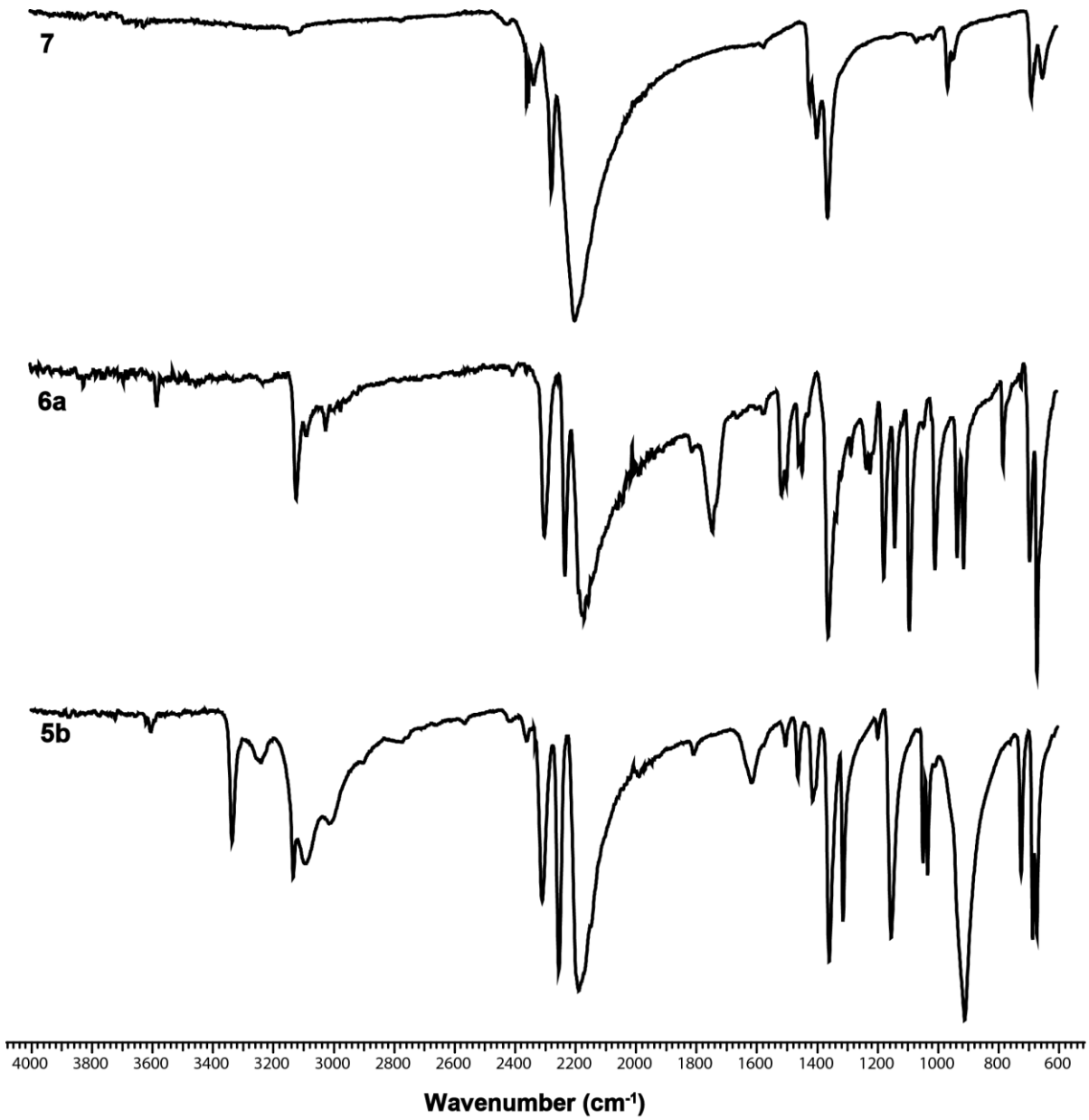

Figure S2. IR spectra of compounds **5b**, **6a**, and **7**.

8.7.3. DTA Measurements

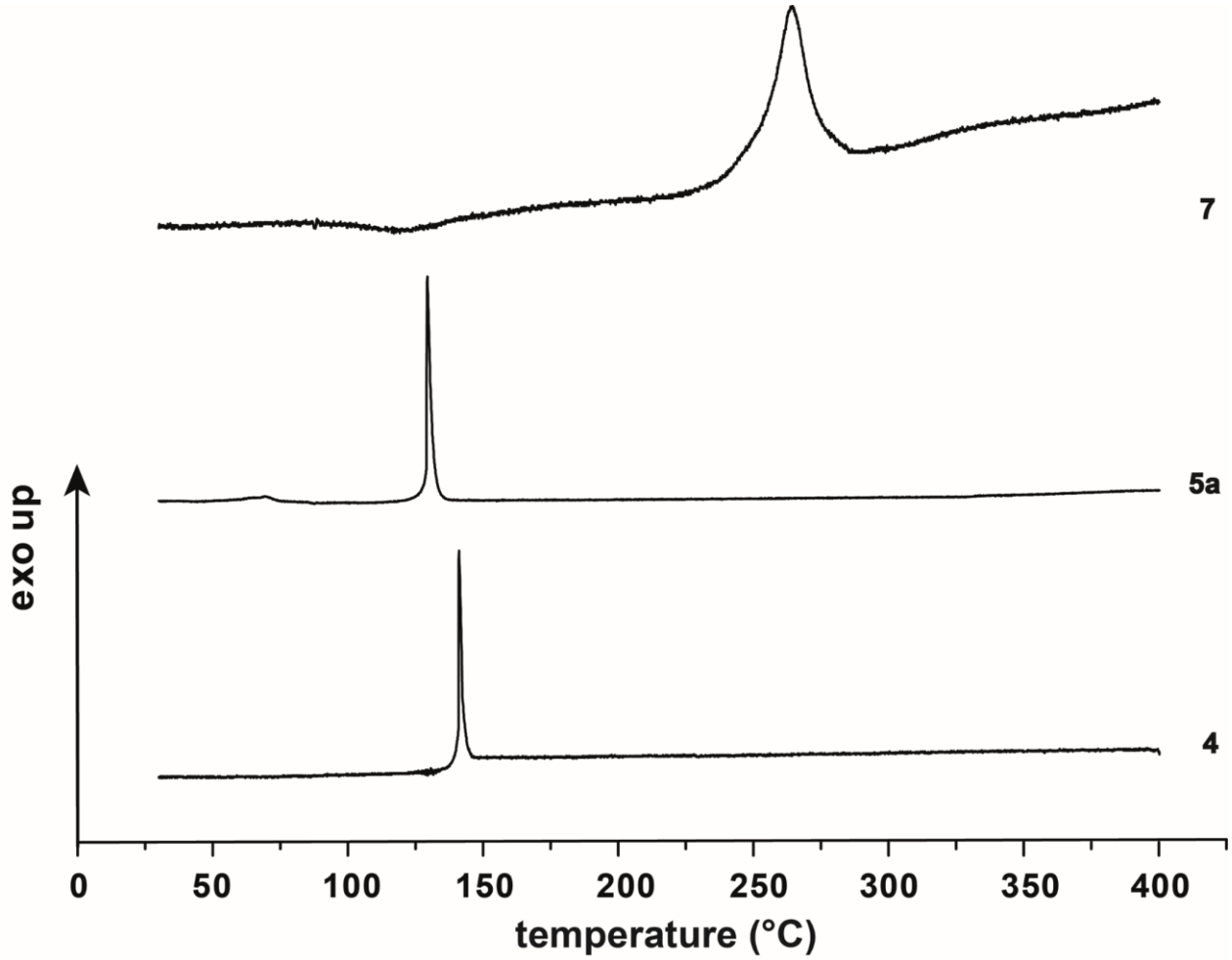

Figure S3. DTA measurements of compound **4**, **5a**, and **7**.

8.7.4. TGA Measurements

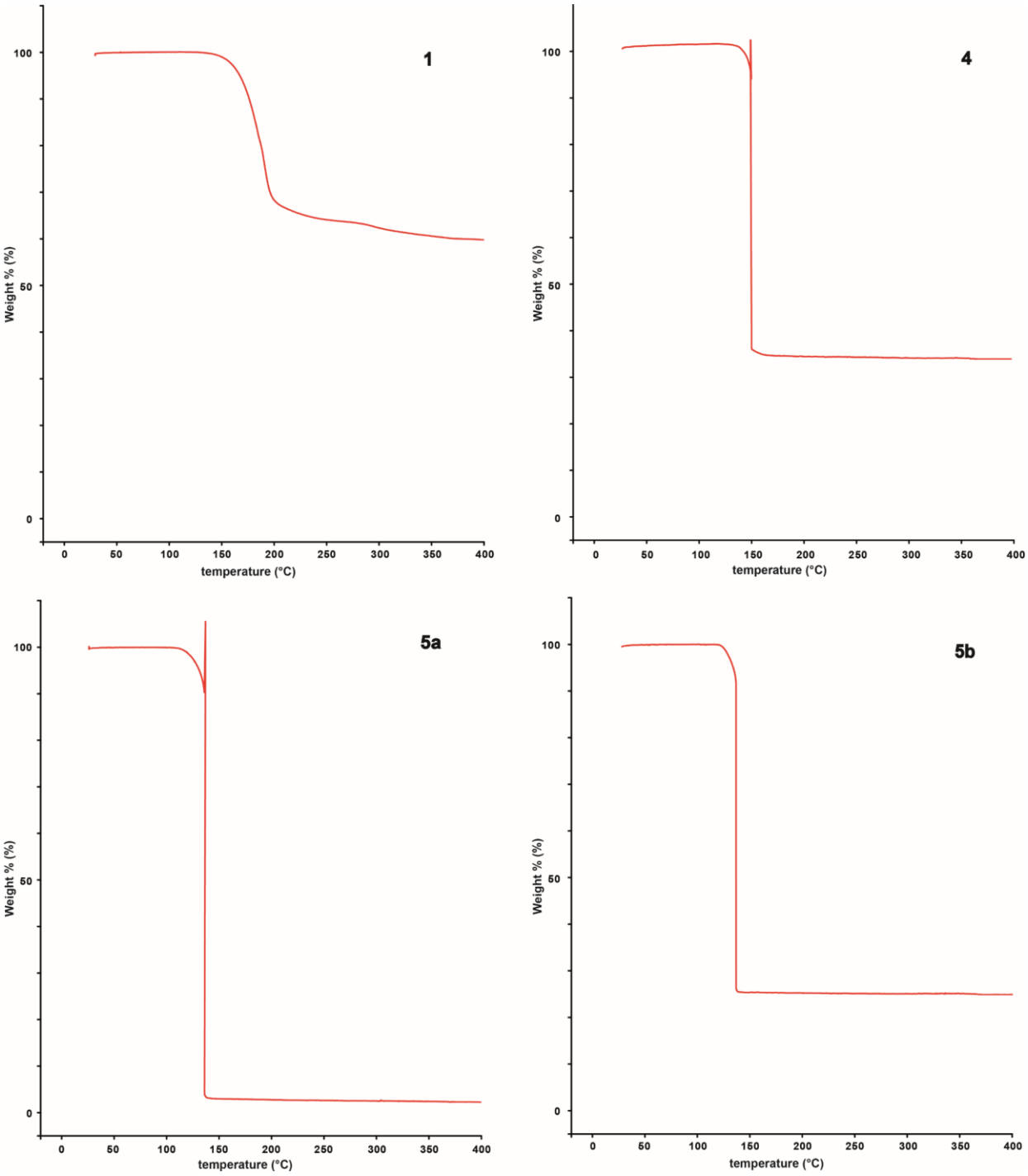

Figure S4. TGA measurements of compounds **1**, **4**, **5a**, and **5b**.

8.7.5. X-Ray Diffraction

For all crystalline compounds, an Oxford Xcalibur3 diffractometer with a CCD area detector or Bruker D8 Venture TXS diffractometer equipped with a multilayer monochromator, a Photon 2 detector and a rotating-anode generator were employed for data collection using Mo-*K*α radiation (λ = 0.71073 Å). On

the Oxford device, data collection and reduction were carried out using the CRYSALISPRO software.[8] On the Bruker diffractometer, the data were collected with the Bruker Instrument Service v3.0.21, the data reduction was performed using the SAINT V8.18C software (Bruker AXS Inc., 2011). The structures were solved by direct methods (SIR-92,[9] SIR-97[10] or SHELXS-97[11]) and refined by full-matrix least-squares on *F*2 (SHELXL[11]) and finally checked using the PLATON software[12] integrated in the WinGX[13] software suite. The non-hydrogen atoms were refined anisotropically and the hydrogen atoms were located and freely refined. The absorptions were corrected by a SCALE3 ABSPACK or SADABS Bruker APEX3 multiscan method.[14,15] All DIAMOND2 plots are shown with thermal ellipsoids at the 50% probability level and hydrogen atoms are shown as small spheres of arbitrary radius.

Table S1. Crystallographic data of **1**–**4**.

	1	**2**	**3**	**4**
Formula	$C_8H_8CuN_{14}$	$C_{10}H_{10}CuN_{20}$	$C_8H_{10}CuN_{16}$	$C_6H_6CuN_{16}$
FW [g mol^{-1}]	363.82	473.92	393.86	365.82
Crystal system	monoclinic	triclinic	triclinic	monoclinic
Space Group	$P2_1/n$	$P\bar{1}$	$P\bar{1}$	$P2_1/c$
Color / Habit	blue block	blue plate	blue block	blue block
Size [mm]	0.08 x 0.35 x 0.45	0.05 x 0.05 x 0.50	0.20 x 0.26 x 0.50	0.15 x 0.17 x 0.22
a [Å]	6.3361(2)	7.5230(6)	7.0512(7)	6.5126(6)
b [Å]	7.3106(3)	10.8125(12)	7.3876(8)	7.7731(6)
c [Å]	15.2047(6)	12.9215(12)	7.9189(7)	12.9955(11)
α [°]	90	65.401(10)	76.323(8)	90
β [°]	98.672(4)	89.071(7)	78.979(8)	96.847(8)
γ [°]	90	70.027(9)	69.756(10)	90
V [Å^3]	696.24(5)	888.38(18)	373.34(7)	653.18(10)
Z	2	2	1	2
$\rho_{calc.}$ [g cm^{-3}]	1.735	1.772	1.752	1.860
μ [mm^{-1}]	1.595	1.282	1.498	1.704
F(000)	366	478	199	366
$\lambda_{MoK\alpha}$ [Å]	0.71073	0.71073	0.71073	0.71073
T [K]	143	125	131	143
θ Min–Max [°]	4.3, 26.4	4.2, 26.4	3.6, 26.4	4.1, 26.4
Dataset	−7: 6; −8: 9; −18: 19	−9: 9; −13: 13; −14: 16	−7: 8; −9: 9; −9: 9	−8: 8; −9: 9; −14: 16
Reflections collected	5191	6690	2844	4879
Independent refl.	1404	3624	1519	1324
R_{int}	0.027	0.030	0.027	0.018
Observed reflections	1269	2850	1413	1261
Parameters	107	283	124	114
R_1 (obs)[a]	0.0228	0.0350	0.0279	0.0198
wR_2 (all data)[b]	0.0602	0.0812	0.0617	0.0526
GooF[c]	1.06	1.06	1.11	1.06
Resd. Dens. [e Å^{-3}]	−0.27, 0.31	−0.43, 0.31	−0.33, 0.31	−0.27, 0.28
Absorption correction	multi-scan	multi-scan	multi-scan	multi-scan
CCDC	1986804	1986806	1986801	1986805

[a] $R_1 = \Sigma||F_0|- |F_c||/ \Sigma|F_0|$; [b] $wR_2 = [\Sigma[w(F_0^2-F_c^2)^2]/\Sigma[w(F_0)^2]]^{1/2}$; $w = [\sigma c^2(F_0^2)+(xP)^2+yP]^{-1}$ and $P = (F_0^2+2F_c^2)/3$; [c] GooF = $\{\Sigma[w(F_o^2-F_c^2)^2]/(n-p)\}^{1/2}$ (n = number of reflections; p = total number of parameters).

Table S1. Crystallographic data of **5a**, **5b**, **6a**, and **6b**.

	5a	**5b**	**6a**	**6b**
Formula	$C_6H_6CuN_{16}$	$C_6H_6CuN_{16}$	$C_8H_6CuN_{14}$	$C_8H_8CuN_{14}O$
FW [g mol^{-1}]	365.81	365.81	361.81	379.82
Crystal system	monoclinic	orthorhombic	triclinic	monoclinic
Space Group	$P2_1/c$	$Pbca$	$P\bar{1}$	$C2/c$
Color / Habit	blue block	blue block	blue platelet	blue plate
Size [mm]	0.19 x 0.38 x 0.48	0.05 x 0.19 x 0.33	0.05 x 0.20 x 0.25	0.06 x 0.29 x 0.40
a [Å]	10.6040(7)	6.9754(3)	5.2672(5)	22.4100(7)
b [Å]	9.0931(6)	9.8736(4)	6.4642(5)	7.1404(2)
c [Å]	6.8092(5)	20.0779(9)	10.3796(11)	9.1402(3)
α [°]	90	90	82.677(7)	90
β [°]	95.261(6)	90	82.001(8)	100.120(3)
γ [°]	90	90	71.515(8)	90
V [Å^3]	653.80(8)	1382.81(10)	330.60(6)	1439.83(8)
Z	2	4	1	4
$\rho_{calc.}$ [g cm^{-3}]	1.858	1.757	1.817	1.752
μ [mm^{-1}]	1.703	1.610	1.679	1.551
F(000)	366	732	181	764
$\lambda_{MoK\alpha}$ [Å]	0.71073	0.71073	0.71073	0.71073
T [K]	127	143	110	127
θ Min–Max [°]	4.3, 26.4	4.1, 26.4	2.0, 26.3	4.3, 26.4
Dataset	−11: 13; −11: 11; −8: 8	−8: 8; −12: 10; −22: 25	−6: 5; −8: 7; −12: 12	−23: 28; −8: 8; −11: 11
Reflections collected	4669	9866	2009	5748
Independent refl.	1332	1406	1341	1465
R_{int}	0.023	0.047	0.051	0.029
Observed reflections	1221	1067	1055	1342
Parameters	114	114	106	115
R_1 (obs)[a]	0.0219	0.0295	0.0502	0.0236
wR_2 (all data)[b]	0.0558	0.0809	0.0999	0.0626
GooF[c]	1.08	1.03	0.99	1.06
Resd. Dens. [e Å^{-3}]	−0.44, 0.30	−0.32, 0.29	−0.51, 0.57	−0.48, 0.36
Absorption correction	multi-scan	multi-scan	multi-scan	multi-scan
CCDC	1986800	1986803	1986802	1986807

[a] $R_1 = \Sigma||F_0|- |F_c||/ \Sigma|F_0|$; [b] $wR_2 = [\Sigma[w(F_0^2-F_c^2)^2]/\Sigma[w(F_0)^2]]^{1/2}$; $w = [\sigma c^2(F_0^2)+(xP)^2+yP]^{-1}$ and $P = (F_0^2+2F_c^2)/3$; [c] GooF = $\{\Sigma[w(F_o^2-F_c^2)^2]/(n-p)\}^{1/2}$ (n = number of reflections; p = total number of parameters).

8.7.6. Experimental Section

General procedure for the preparation of copper(II) dicyanamide complexes (1–5a and 6a):
To a solution of copper(II) nitrate trihydrate (60.4 mg, 0.25 mmol, 1 eq) in water (1 mL) the corresponding ligand (**1**: 1-methyl-5*H*-tetrazole (42.0 mg, 0.50 mmol, 2 eq); **2**: 1-azidoethyl-5*H*-tetrazole (69.6 mg, 0.50 mmol, 2 eq); **3**: 1-amino-5-methyltetrazole (49.6 mg, 0.50 mmol, 2 eq); **4**: 1-amino-5*H*-tetrazole (42.5 mg, 0.50 mmol, 2 eq); **5a**: 2-amino-5*H*-tetrazole (42.5 mg, 0.50 mmol, 2 eq); **6a**: 1,2-di(tetrazol-1-yl)ethane (41.6 mg, 0.25 mmol, 1 eq)) was added. After stirring for a minute, an aqueous solution (1 mL) of sodium dicyanamide (44.5 mg, 0.50 mmol, 2 eq) was added, the mixture was stirred for one more minute at room temperature and left for crystallization. After formation of the crystalline

products, the compounds were filtered off, washed with cold ethanol and dried in air. All compounds were obtained in the form of single crystals suitable for X-ray diffraction.

[Cu(DCA)$_2$(MTZ)$_2$] (1)
Yield: 57.9 mg (0.16 mmol, 64%).

DTA (5 °C min^{-1}): 170 °C (exothermic); IR (ATR, cm^{-1}): $\tilde{\nu}$ = 3587 (vw), 3128 (m), 3074 (w), 3020 (vw), 2375 (vw), 2301 (m), 2231 (m), 2163 (vs), 1800 (w), 1531 (vw), 1519 (m), 1467 (w), 1437 (w), 1361 (s), 1303 (m), 1239 (w), 1177 (m), 1107 (s), 1064 (w), 1030 (m), 1005 (m), 928 (m), 899 (m), 730 (vw), 719 (w), 686 (m), 663 (w), 656 (vs); EA ($C_8H_8CuN_{14}$, 363.80) calcd.: C 26.41, H 2.22, N 53.90%; found: C 26.54, H 2.08, N 53.61%; BAM drop hammer: 8 J; friction tester: > 360 N; ESD: > 1500 mJ (at grain size < 100 μm).

[Cu(DCA)$_2$(AET)$_2$] (2)
Yield: 61.6 mg (0.13 mmol, 52%).

DTA (5 °C min^{-1}): 126 °C (endothermic), 131 °C (exothermic); IR (ATR, cm^{-1}): $\tilde{\nu}$ = 3597 (vw), 3159 (w), 3136 (m), 3063 (w), 3014 (w), 2933 (w), 2868 (w), 2302 (m), 2230 (m), 2164 (s), 2107 (vs), 2085 (vs), 2058 (s), 1738 (w), 1670 (m), 1611 (m), 1508 (m), 1496 (w), 1453 (m), 1441 (m), 1372 (s), 1353 (m), 1280 (s), 1263 (s), 1227 (m), 1184 (m), 1175 (m), 1159 (s), 1104 (s), 1075 (m); EA ($C_{10}H_{10}CuN_{20}$, 478.88) calcd.: C 25.35, H 2.13, N 59.12%; found: C 24.65 , H 2.26, N 60.43%; BAM drop hammer: 6 J; friction tester: 192 N; ESD: 1500 mJ (at grain size < 100 μm).

[Cu(DCA)$_2$(1-AT)$_2$] (4)
Yield: 52.7mg (0.14 mmol, 56%).

DTA (5 °C min^{-1}): 141 °C (exothermic); IR (ATR, cm^{-1}): $\tilde{\nu}$ = 3597 (w), 3306 (m), 3258 (w), 3200 (m), 3150 (m), 3078 (w), 2305 (m), 2237 (s), 2159 (vs), 1731 (w), 1621 (m), 1506 (w), 1456 (w), 1367 (s), 1294 (w), 1198 (m), 1161 (w), 1120 (vw), 1095 (s), 1063 (w), 1012 (m), 975 (s), 925 (m), 870 (m), 715 (vw), 701 (w), 658 (w), 641 (s); EA ($C_6H_6CuN_{16}$, 365.77) calcd.: C 19.70, H 1.65, N 61.27%; found: C 20.06, H 1.59, N 60.46%; BAM drop hammer: 6 J; friction tester: 144 N; ESD: 1350 mJ (at grain size < 100 μm).

[Cu(DCA)$_2$(2-AT)$_2$] monoclinic (5a)
Yield: 71.3 mg (0.19 mmol, 76%).

DTA (5 °C min^{-1}): 129 °C (exothermic); IR (ATR, cm^{-1}): $\tilde{\nu}$ = 3584 (vw), 3308 (m), 3242 (w), 3145 (s), 3096 (m), 2370 (vw), 2349 (vw), 2302 (s), 2232 (s), 2169 (vs), 1799 (w), 1611 (m), 1488 (m), 1459 (w),

1418 (w), 1397 (w), 1356 (s), 1309 (s), 1160 (m), 1142 (s), 1043 (m), 1032 (m), 932 (s), 899 (s), 720 (m), 679 (s), 670 (s); EA ($C_6H_6CuN_{16}$, 365.77) calcd.: C 19.70, H 1.65, N 61.27%; found: C 20.00, H 1.60, N 61.01%; BAM drop hammer: 9 J; friction tester: 80 N; ESD: 540 mJ (at grain size < 100 μm).

[Cu(DCA)$_2$(dte)] (6a)
Yield: 42.2 mg (0.12 mmol, 47%).

DTA (5 °C min^{-1}): 126 °C (exothermic); IR (ATR, cm^{-1}): $\tilde{\nu}$ = 3580 (w), 3118 (m), 3021 (w), 2296 (m), 2228 (s), 2170 (s), 2164 (s), 1739 (m), 1511 (m), 1495 (m), 1454 (m), 1448 (w), 1356 (s), 1229 (m), 1217 (m), 1189 (w), 1172 (s), 1136 (m), 1087 (s), 1002 (s), 929 (s), 907 (s), 777 (m), 689 (s), 664 (vs); EA ($C_8H_6CuN_{14}$, 361.77) calcd.: C 26.56, H 1.67, N 54.20%; found: C 26.58, H 1.78, N 53.65%; BAM drop hammer: 10 J; friction tester: > 360 N; ESD: 1220 mJ (at grain size < 100 μm).

[Cu(DCA)$_2$(2-AT)$_2$] orthorhombic (5b)
To an methanolic solution (1 mL) of copper(II) nitrate trihydrate (60.4 mg, 0.25 mmol, 1 eq) 2-amino-5*H*-tetrazole (42.5 mg, 0.50 mmol, 2 eq) was added. After stirring for a minute an aqueous solution (1 mL) of sodium dicyanamide (44.5 mg, 0.50 mmol, 2 eq) was added. It was stirred for another minute and left in air for crystallization. The precipitate was filtered off, washed with cold ethanol and dried in air. Compound **5b** (67.5 mg, 0.18 mmol, 72%).) could be obtained as blue X-ray suitable crystals.

DTA (5 °C min^{-1}): 126 °C (exothermic); IR (ATR, cm^{-1}): $\tilde{\nu}$ = 3333 (m), 3237 (w), 3131 (m), 3092 (m), 3006 (m), 2357 (w), 2306 (s), 2251 (s), 2185 (vs), 2146 (s), 1806 (w), 1613 (w), 1500 (w), 1460 (w), 1410 (w), 1356 (s), 1310 (s), 1195 (vw), 1151 (s), 1045 (m), 1030 (m), 907 (vs), 720 (m), 682 (s), 668 (s); EA ($C_8H_8CuN_{16}$, 365.77) calcd.: C 19.70, H 1.65, N 61.27%; found: C 19.99, H 1.58, N 60.36%; BAM drop hammer: 9 J; friction tester: 80 N; ESD: 540 mJ (at grain size < 100 μm).

Cu(DCA)$_2$ (7)
The selective synthesis of compound **7** is known from the literature.[16] In this work it was obtained as product of the attempted synthesis of the complex with 2-AMT (2-amino-5-methyltetrazole) as ligand.

DTA (5 °C min^{-1}): 254 °C (exothermic); IR (ATR, cm^{-1}): $\tilde{\nu}$ = 3137 (vw), 2351 (w), 2348 (w), 2332 (w), 2272 (m), 2196 (vs), 1418 (m), 1394 (m), 1358 (s), 960 (w), 942 (w), 684 (w), 647 (w); EA (C_4CuN_6, 195.63) calcd.: C 24.56, N 42.96%; found: C 24.22, N 42.35%; BAM drop hammer: 40 J; friction tester: > 360 N; ESD: 630 mJ (at grain size < 100 μm).

8.7.7. References

[1] NATO standardization agreement (STANAG) on explosives, impact sensitivity tests, no. 4489, 1st ed., Sept. 17, **1999**.

[2] WIWEB-Standardarbeitsanweisung 4-5.1.02, Ermittlung der Explosionsgefährlichkeit, hier der Schlagempfindlichkeit mit dem Fallhammer, Nov. 8, **2002**.

[3] http://www.ozm.cz, (accessed June 2019).

[4] http://www.bam.de, (accessed June 2019).

[5] NATO standardization agreement (STANAG) on explosive, friction sensitivity tests, no. 4487, 1st ed., Aug. 22, **2002**.

[6] WIWEB-Standardarbeitsanweisung 4-5.1.03, Ermittlung der Explosionsgefährlichkeit oder der Reibeempfindlichkeit mit dem Reibeapparat, Nov. 8, **2002**.

[7] Impact: insensitive > 40 J, less sensitive ≥ 35 J, sensitive ≥ 4 J, very sensitive ≤ 3 J; Friction: insensitive > 360 N, less sensitive = 360 N, sensitive < 360 N and > 80 N, very sensitive ≤ 80 N, extremely sensitive ≤ 10 N. According to the UN Recommendations on the Transport of Dangerous Goods, 5th ed., **2009**.

[8] *CrysAlisPro*, Oxford Diffraction Ltd., version 171.33.41, **2009**.

[9] A. Altomare, G. Cascarano, C. Giacovazzo, A. Guagliardi, *J. Appl. Crystallogr.* **1993**, *26*, 343–350.

[10] a) A. Altomare, G. Cascarano, C. Giacovazzo, A. Guagliardi, A. G. G. Moliterni, M. C. Burla, G. Polidori, M. Camalli, R. Spagna, *SIR97*, **1997**; b) A. Altomare, M. C. Burla, M. Camalli, G. L. Cascarano, C. Giacovazzo, A. Guagliardi, A. G. G. Moliterni, G. Polidori, R. Spagna, *J. Appl. Crystallogr.* **1999**, *32*, 115–119.

[11] a) G. M. Sheldrick, *SHELXL-97*, *Program for the Refinement of Crystal Structures*, University of Göttingen, Germany, **1997**; b) G. M. Sheldrick, *Acta Crystallogr. Sect. A* **2008**, *64*, 112–122.

[12] A. L. Spek, *PLATON*, *A Multipurpose Crystallographic Tool*, Utrecht University, The Netherlands, **1999**.

[13] L. J. Farrugia, *J. Appl. Cryst.* **2012**, *45*, 849–854.

[14] Empirical absorption correction using spherical harmonics, implemented in SCALE3 ABSPACK scaling algorithm (CrysAlisPro Oxford Diffraction Ltd., Version 171.33.41, **2009**).

[15] *APEX3*. Bruker AXS Inc., Madison, Wisconsin, USA.

[16] M. Kurmoo, C. J. Kepert, *New J. Chem.* **1998**, *12*, 1515–1524.

9. Nitrogen-Rich Copper(II) Bromate Complexes: an Exotic Class of Primary Explosives

Maximilian H. H. Wurzenberger, Norbert Szimhardt, and Jörg Stierstorfer

Reprinted (adapted) with permission from *Inorganic Chemistry* **2018**, *57*, 7940–7949.

DOI: 10.1021/acs.inorgchem.8b01045

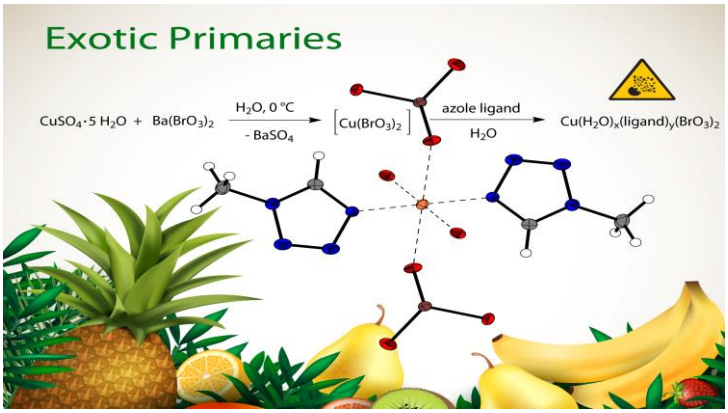

Abstract: Because of the ongoing very challenging search for potential replacements of the currently used toxic lead-based primary explosives, new synthetic strategies have to be developed. In particular, the smart concept of energetic coordination compounds (ECC) has proven to hold great potential to solve this difficult and complex problem. The herein-described approach combines the exotic and neglected class of copper(II) bromate ECC with different environmentally friendly nitrogen-rich heterocycles, which exhibit the energetic properties of powerful primary explosives. The concept is the simple adjustment of the energetic properties of the complexes through alteration of the corresponding azoles. Six new copper(II) bromate complexes with reasonable sensitivities are featured in this study, which were synthesized in a practical and straightforward fashion, assured through easy access to copper(II) bromate obtained by metathesis reaction. Obtained compounds were comprehensively characterized through various analytical methods such as low-temperature X-ray diffraction, IR spectroscopy, and elemental analysis. Their sensitivities toward impact and friction were assessed through BAM standard techniques, together with their sensitivity against electrostatic discharge. Evaluation of the energetic properties of the newly synthesized compounds included examination of the respective thermal stabilities by differential thermal analysis. Furthermore, the complexes were tested regarding their behavior toward laser irradiation. Additionally, to receive insight into a possible correlation between the laser-investigated compounds' optical absorption and their ability to ignite by exposure to laser irradiation, UV-Vis-near-IR spectra were recorded.

9.1. Introduction

Energetic materials include a wide range of chemical compounds and can be classified into four main subgroups: primary explosives, secondary explosives, pyrotechnics, and propellants.[1] In contrast to the high-performing secondary explosives, primaries embody compounds showing a very fast deflagration-to-detonation transition (DDT) after being initiated by a nonexplosive simple initiation impulse.[1,2] The most commonly used primary explosives nowadays are lead styphnate (LS) and lead azide (LA), two compounds that possess highly toxic potential toward human and nature.[3,4] To avoid exposure of toxic chemicals during the utilization and manufacturing of lead-containing primaries, modern research in the field of primary explosives focuses on the synthesis of new green compounds while maintaining the desired properties of LS and LA (Chart 1).[5–10]

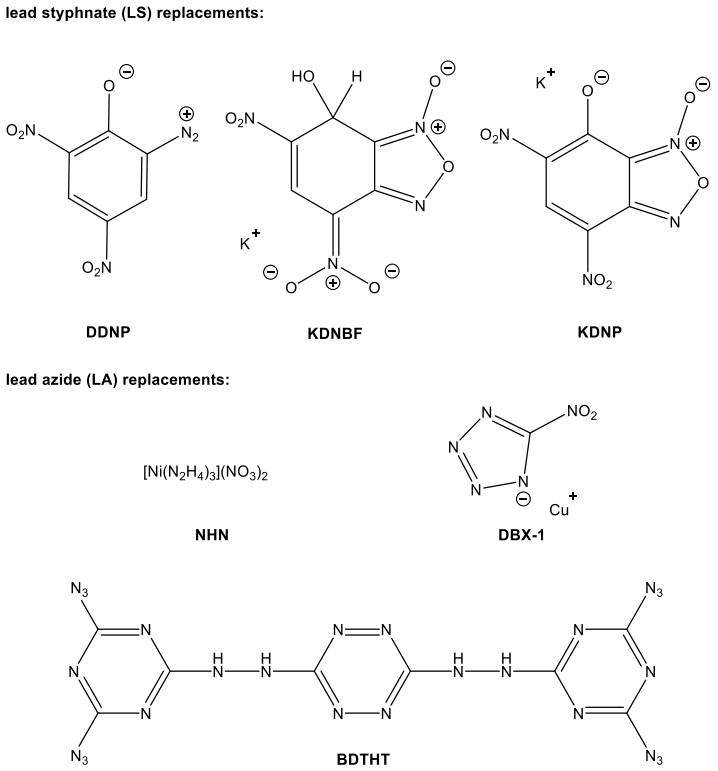

Chart 1. Molecular structures of possible LS and LA replacements: DDNP = diazodinitrophenol,[11] KDNBF = potassium dinitrobenzofuroxan,[12] KDNP = 5,7-dinitro-[2,1,3]-benzoxadiazol-4-olate 3-oxide,[13] NHN = nickel(II) hydrazine nitrate,[14] DBX-1 = copper(I) nitrotetrazolate,[15] and BDTHT = 3,6-bis(2-(4,6-diazido-1,3,5-triazin-2-yl)hydrazinyl)-1,2,4,5-tetrazine.[16]

From all energetic characteristics, the previously discussed sensitivities are of high importance as well as high decomposition temperature and chemical and physical stability during long-term storage.[2] Moreover, to enable the substitution of commonly used compounds, the required synthesis of a new primary explosive should include as few as possible reaction steps and ought to be compatible with conventional materials (detonators, secondaries, and blasting caps).[2] One promising approach to obtain

green primary explosives includes the synthesis of energetic coordination compounds (ECC), a strategy that has gained increased attention in recent years.[7,17–20] Regarding the numerous parameters (metal center, ligand system, and counterion) that can be modified, the specific properties of a desired compound can be tailored incrementally toward the final target. In that manner, copper(II) bears great potential considering previous investigations,[19,21] and, therefore, was examined extensively in combination with bromate as the anion in the course of this work. Besides the tedious search for possible replacements of LS and LA, recently, the research on primary explosives focused on laser-ignitable compounds.[22] In contrast to the conventional methods of initiation through impact, friction, and electrostatic discharge, this new initiation method bears encouraging potential because of the circumstance that examined compounds do not require high sensitivities toward the customary stimuli.[23] Consequently, laser-ignitable energetic materials with high performance, high thermal stability, and an uncritical impact on the environment can be used as insensitive but powerful charges to allow much safer handling and to prevent undesired initiations.[22] On the basis of the idea of primary explosives in the form of coordination compounds, Zhilin *et al.* isolated several very promising complexes in the early 2000s (Chart 2a,b), including the well-known *cis*-bis(5-nitro-2*H*-tetrazolato-*N*2)cobalt(III) perchlorate and 5-hydrazino-1*H*-tetrazolemercury(II) perchlorate.[24–27] On the basis of these promising results, several research groups were starting to examine laser-sensitive ECC for future applications in military and civil areas.[28–30]

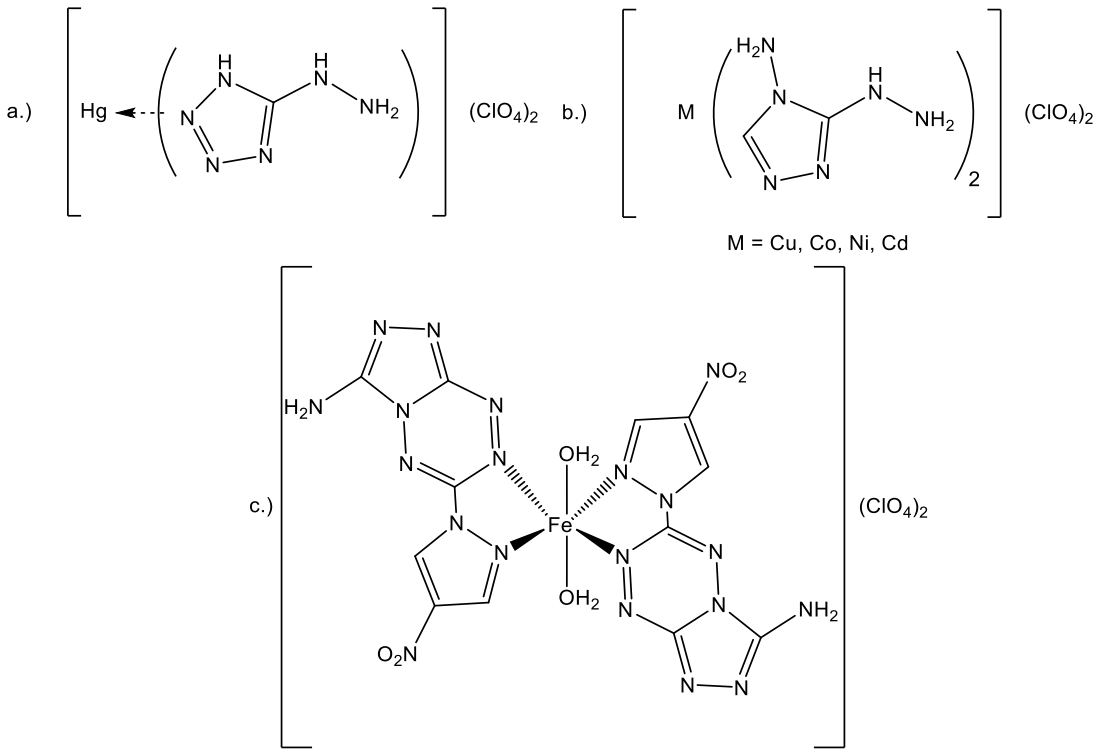

Chart 2. Different laser-ignitable coordination compounds: a) 5-hydrazino-1*H*-tetrazolemercury(II) perchlorate,[26] (b) 3-hydrazino-4-amino-1,2,4-triazole-based metal(II) perchlorates,[27] or (c) $[(H_2NTriTz^{NO2}Pyr)_2Fe(H_2O)_2](ClO_4)_2$.[31]

Bromates, particularly in the form of alkali salts, can be found in many different industrial processes (food production, synthetic reagents, dyeing, cosmetics, etc.) and are therefore an integral part of our daily life. While the use of alkali bromates ($NaBrO_3$ and $KBrO_3$) is rather common, the investigation of transition-metal bromates is relatively poor, especially with copper(II). Their high thermal stabilities,[32] exceptional performances, and relatively low prices make alkali bromates promising candidates in explosive mixtures. The latter fact led to the development of manageable potassium bromate containing concrete cracking agents and airbag-gas-generating compositions, as well as the invention of detectors for bromate-containing explosive mixtures.[33–35] Because of the strong oxidizing power of bromates and their high redox reactivity, mixtures with fuels or reducing agents have to be handled with great care. In particular, compositions with sulfur or organic compounds, such as dinitrotoluene or malonic acid, are highly unstable and tend to self-ignite within hours.[36] Only a very few copper(II) complexes (including complexes with ammonia, primary amines, 4-amino-1,2,4-triazole (4-ATRI)) using bromate as the counter anion are known in the literature so far.[37,38] However, none of them was investigated for its crystal structure or has been described in relation to energetic materials. One of the very few, literature-reported examples uses the compound as a source for *in situ* generated $Cu^{I}Br$ and as an alternative oxidizer (BrO_3^- vs ClO_4^-) in blue-light-emitting pyrotechnics.[39] The current contribution covers, as a further development of our recently published copper(II) chlorate complexes, analogous bromate-containing compounds with sensitivities in the range of primary explosives.[40] Obtained exceptional copper(II) bromate coordination compounds could be initiated by laser irradiation and their energetic character precisely tailored through the application of different nitrogen-donating azole-based ligands.

9.2. Results and Discussion

9.2.1. Synthesis

Copper(II) bromate is poorly accessible, not commercially available, and exists with variable water contents (2–6 H_2O).[41,42] Therefore, the driving force of barium sulfate precipitation was utilized to synthesize copper(II) bromate stoichiometrically *in situ* as an intermediate for further reaction with the ligands (Scheme 1) through metathesis of copper(II) sulfate and barium bromate. All ligands used were commercially available or were synthesized according to the literature. Because of the very good solubility of the used nitrogen-rich azoles and copper(II) bromate, a minimum amount of water was chosen as the reaction medium for the synthesis of ECC **1**–**6**. As a result, the compounds often contain crystal water or aqua ligands. All attempts to change the reaction media to organic solvents led to decomposition of bromate to bromide because of its high redox activity [redox potential of E^0 = 1.45 V

(to BrO^-); pH = 0], which is even slightly higher than that of perchlorate or chlorate [E^0 = 1.43 V (to ClO^-)].[43]

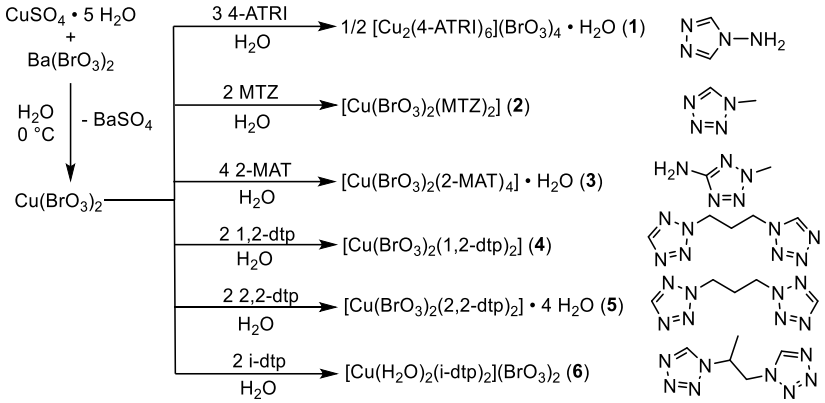

Scheme 1. Synthesis of complexes **1**–**6** starting from copper(II) sulfate and barium bromate. Overview of the nitrogen-rich ligands used: 4-ATRI = 4-amino-1,2,4-triazole; MTZ = 1-methyl-5*H*-tetrazole; 2-MAT = 2-methyl-5-aminotetrazole; 1,2-dtp = 1-(tetrazol-1-yl)-3-(tetrazol-2-yl)propane; 2,2-dtp= 1,3-di(tetrazol-2-yl)propane; i-dtp = 1,1'-(propane-1,2-diyl)bis-(tetrazole).

Most of the compounds were received in decent yields (57–85%) directly from the mother liquor in the form of single crystals suitable for X-ray diffraction. Only the compound $[Cu_2(4\text{-ATRI})_6](BrO_3)_4 \cdot H_2O$ (**1**) was isolated as a light-blue powder, and crystal growth was achieved through layering and very slow formation at the phase boundary. All coordination compounds were filtered off, washed with small amounts of cold water, and dried in air. The complexes can easily be distinguished by IR spectroscopy (Figures S1 and S2) because of the different coordination modes of the anions and the water molecules or through the absence of crystal water.

9.2.2. Crystal Structures

All complexes were characterized by low-temperature single-crystal X-ray diffraction. The crystal structures were uploaded to the CSD database[44] and can be obtained free of charge as CCDC 1836542 (**1**), 1836543 (**2**), 1836539 (**3**), 1836540 (**4**), 1836537 (**5**), 1836541 (**6**), 1836544 (**7**), 1836538 (**8**). The bond lengths and angles of the coordinating ligands in the analyzed complexes are in the typical range of the tetrazole and triazole ligands and nearly the same as in the non-coordinating ligands.[45–47] The ligands are therefore not part of the discussion in any of the following coordination compounds. All copper(II) bromate complexes show octahedral coordination with a Jahn-Teller distortion along the axial coordination sphere. In general, copper(II) bromate complexes tend to crystallize with water as solvent molecules (**1**, $[Cu(BrO_3)_2(2\text{-MAT})_4] \cdot H_2O$ (**3**), and $[Cu(BrO_3)_2(2,2\text{-dtp})_2] \cdot 4\ H_2O$ (**5**)) or in the form of aqua ligands ($[Cu(H_2O)_2(i\text{-dtp})_2](BrO_3)_2$ (**6**) and $[Cu(H_2O)_2(en)_2](BrO_3)_2$ (**7**)). Only the bridging bromato anions in compounds $[Cu(BrO_3)_2(MTZ)_2]$ (**2**) and $[Cu(BrO_3)_2(1,2\text{-dtp})_2]$ (**4**) prevented the inclusion of

aqua molecules. The monohydrated complex **1** is the only one presented with copper(II) ions exclusively coordinated by nitrogen atoms. It crystallizes in the form of blue blocks in the monoclinic space group *C*2/*c* with four formula units per unit cell and a calculated density of 2.299 g cm^{-3} at 143 K. The molecular unit contains two different copper(II) cations (Figure 1), and each is octahedrally coordinated by six triazole ligands. Both central atoms show a Jahn-Teller distortion, whereas the axial Cu–N bonds of Cu1 are shorter compared with those of Cu2. Three ligands are bridging between the same two copper(II) atoms and form polymeric chains. **2** shows the highest density (2.491 g cm^{-3} at 143 K) of all bromate complexes and crystallizes in the form of blue plates in the monoclinic space group $P2_1/c$ with two formula units per unit cell. The bromate anions in **2** are now coordinating to the transition-metal(II) center in comparison to compound **1** (Figure 2). Each of the bromato ligands is bridging between two different metal(II) atoms, building up polymeric 2D layers. The monodentate ligand 2-MAT leads to the formation of a closed octahedral coordination sphere in complex **3**. It crystallizes in the form of green blocks in the monoclinic space group $P2_1/c$ with four formula units per unit cell and exhibits the lowest density (1.983 g cm^{-3} at 143 K) of all compounds.

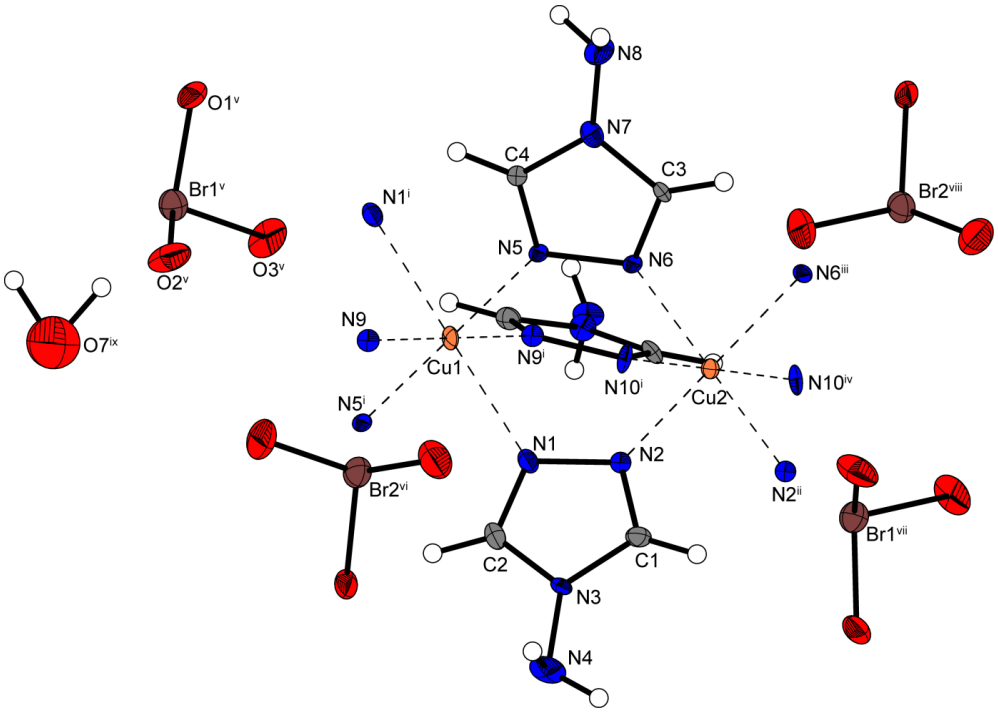

Figure 1. Copper(II) coordination environment of **1**. Thermal ellipsoids of non-hydrogen atoms in all structures are set to the 50% probability level. Selected bond lengths (Å): Cu1–N1 2.298(6), Cu1–N5 2.052(6), Cu1–N9 2.022(7), Cu2–N2 2.019(6), Cu2–N6 2.036(6), Cu2–N10^{i} 2.408(7). Selected bond angles (°): N1–Cu1–N5 88.6(2), N1–Cu1–N9 88.8(2), N5–Cu1–N9 89.7(2), N2–Cu2–N6 91.4(2), N2–Cu2–N10^{i} 89.7(2), N6–Cu2–N10^{i} 88.0(2). Symmetry codes: (i) −x, −y, 1−z; (ii) −x, y, 1.5−z; (iii) −x, y, 1.5−z; (iv) x, −y, 0.5+z; (v) −1.5+x, 0.5+y, z; (vi) 0.5−x, −0.5−y, 1−z; (vii) 0.5+x, −0.5−y, 0.5+z; (viii) 0.5−x, 0.5+y, 1.5−z; (ix) −1+x, y, z.

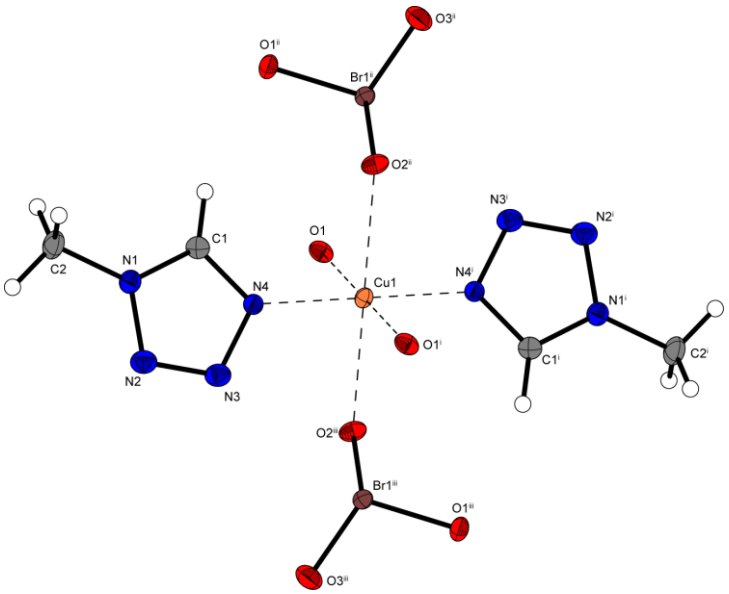

Figure 2. Copper(II) coordination environment of **2**. Selected bond lengths (Å): Cu1–O1 2.009(2), Cu1–$O2^{ii}$ 2.346(2), Cu1–N4 1.987(3). Selected bond angles (°): O1–Cu1–N4 90.71(10), O1–Cu1–$O2^{ii}$ 87.89(8), $O2^{ii}$–Cu1–N4 89.80(9). Symmetry codes: (i) −x, 2−y, −z; (ii) −x, 0.5+y, 0.5−z; (iii) x, 1.5−y, −1.5+z.

The molecular unit consists of one copper(II) cation (Figure 3), coordinated by two bromato and four tetrazole ligands together with an additional crystal water molecule. In contrast to compound **2**, the bromatos are only coordinating to one copper(II) central atom; therefore, the formation of polymeric structures does not occur.

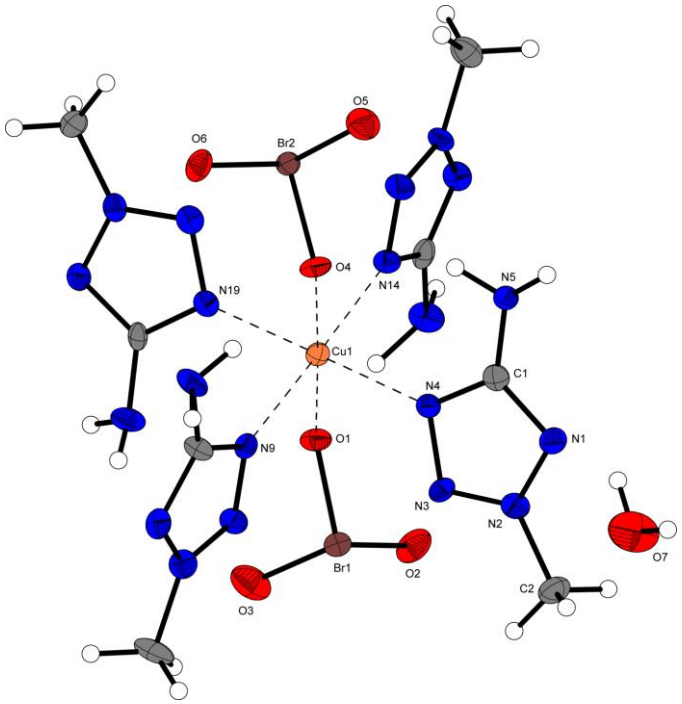

Figure 3. Molecular unit of **3**. Selected bond lengths (Å): Cu1–O1 2.367(4), Cu1–O4 2.381(4), Cu1–N4 2.018(5), Cu1–N9 2.057(5), Cu1–N14 2.043(5), Cu1–N19 2.033(5). Selected bond angles (°): O1–Cu1–N9 88.57(17), O4–Cu1–N9 90.95(17), N4–Cu1–N9 91.08(19), N4–Cu1–N14 89.84(19).

The water-free compound **4** crystallizes in the form of blue blocks in the monoclinic space group $P2_1/c$ with two formula units per unit cell and a calculated density of 2.142 g cm^{-3} at 130 K. The molecular unit is built up by one copper(II) cation (Figure 4), two coordinating ligands in equatorial positions, and two bridging bromato anions. The ditetrazole ligands are only connected with the 1-substituted tetrazole ring, while the 2-substituted ring is not coordinating at all. Similar to complex **2**, every bromato is bridging between two different copper(II) atoms, building up polymeric 2D layers.

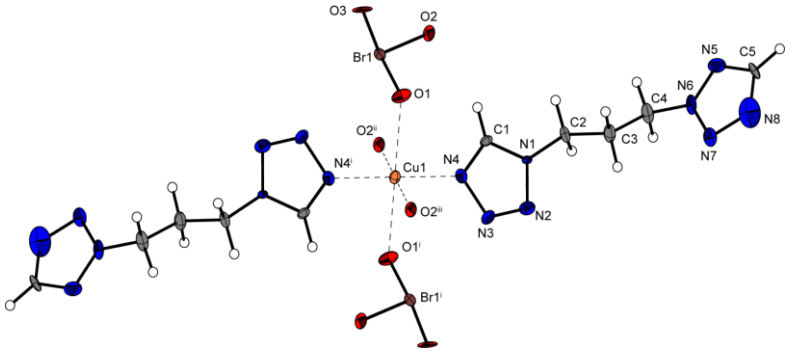

Figure 4. Copper(II) coordination environment of **4**. Selected bond lengths (Å): Cu1–O1 2.352(11), Cu1–O2^{ii} 2.033(12), Cu1–N4 1.976(12). Selected bond angles (°): O1–Cu1–N4 90.9(5), O1–Cu1–O2^{ii} 96.2(4), O2^{ii}–Cu1–N4 90.4(5). Symmetry codes: (i) 2−x, −y, −z; (ii) x, −0.5−y, −0.5+z; (iii) 2−x, 0.5+y, 0.5−z.

5 crystallizes in the form of blue blocks in the triclinic space group $P\bar{1}$ with one formula unit per unit cell and a calculated density of 2.002 g cm^{-3} at 143 K. The molecular unit is composed of a copper(II) cation (Figure 5) with two coordinating bromato ligands in the axial positions, two 2,2-dtp ligands in the plane, and four non-coordinating crystal water molecules. In contrast to compounds **2** and **3**, the bromates are not bridging, but two neutral ligands are linking between two central metals, building up polymeric chains.

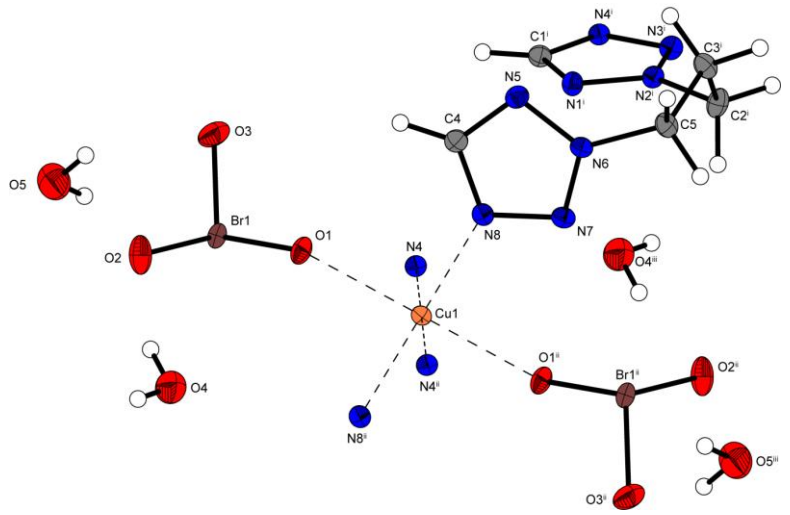

Figure 5. Copper(II) coordination environment of **5**. Selected bond lengths (Å): Cu1–O1 2.3200(13), Cu1–N4 2.0042(15), Cu1–N8 2.0335(15). Selected bond angles (°):O1–Cu1–N4 93.85(5), O1–Cu1–N8 86.72(5), N4–Cu1–N8 91.38(6). Symmetry codes: (i) 3−x, −y, 2−z; (ii) 2−x, −y, 2−z; (iii) 1−x, 1−y, 2−z.

The diaqua coordination compound **6** crystallizes in the form of blue blocks in the monoclinic space group *C*2/*c* with four formula units per unit cell and a calculated density of 1.989 g cm^{-3} at 143 K. In contrast to the other aqua complexes, the water molecules act as ligands whereas the bromate counterions are not coordinating. The molecular unit contains one central metal(II) (Figure 6) with two aqua ligands in axial positions, two equatorial ditetrazole molecules, and two non-coordinating counterions. Analogously to complex **5**, the ligands are bridging between the copper(II) ions, building up polymeric chains.

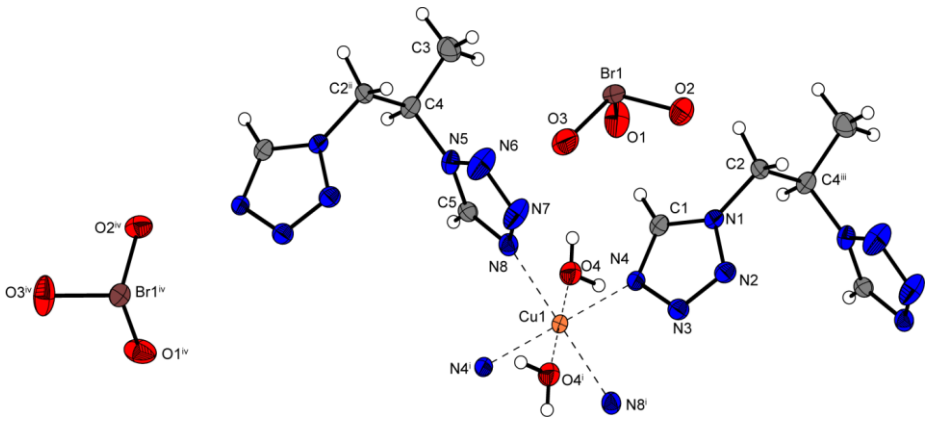

Figure 6. Copper(II) coordination environment of **6**. Selected bond lengths (Å): Cu1–O4 2.258(2), Cu1–N4 2.030(2), Cu1–N8 2.078(2). Selected bond angles (°):O4–Cu1–N4 91.46(9), O4–Cu1–N8 85.56(9), N4–Cu1–N8 89.45(9). Symmetry codes: (i) 2−x, 2−y, 1−z; (ii) 0.5+x, −0.5+y, z; (iii) −0.5+x, 0.5+y, z; (iv) 0.5+x, 0.5−y, −0.5+z.

Amiel described the synthesis of one of the first ever copper(II) bromate complexes with ethylenediamine (en) as the ligand in 1935 (Scheme 2). He suggested a monoclinic space group for the obtained violet compound with a formula of $(BrO_3)_2Cu(en)_2(H_2O)$.[37] This compound was reinvestigated by single-crystal X-ray diffraction. The reinvestigation of this compound (Figure 7) verifies indeed a monoclinic space group ($P2_1/c$) for compound **7**.

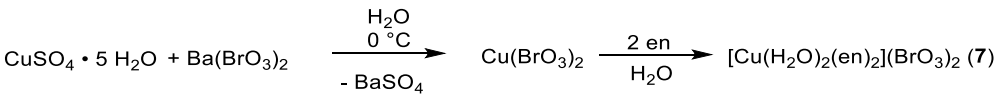

Scheme 2. Synthesis of the reinvestigated complex **7**.

Two chelating en molecules in the equatorial position and two aqua ligands in the axial position are building up closed octahedral coordination spheres around the copper(II) center with non-coordinating bromate counter anions in the molecular unit. The diaqua coordination compound crystallizes in the form of purple blocks with six formula units per unit cell and a calculated density of 2.201 g cm^{-3} at 143 K. The ligands highly influence the coordination mode of the bromate counterions. This affinity can also be observed in the various hydrates of copper(II) bromate. In $[Cu(BrO_3)_2(H_2O)_2]$, the coordination sphere around the metal(II) center is built up of four bridging bromato and two aqua ligands.[41] Blackburn *et al.*

published the crystal structure of $[Cu(H_2O)_6](BrO_3)_2$ with non-coordinating anions, and the up-to-now unknown structure of $[Cu(BrO_3)_2(H_2O)_4]$ (**8**), measured in the course of this work, shows coordination but no linking of the bromato ligands.[42] The tetraaqua form of copper(II) bromate (**8**) crystallizes in the form of blue blocks in the orthorhombic space group *Pbca* with four formula units per unit cell and a calculated density of 2.975 g cm^{-3} at 143 K. Similar to complexes **3** and **5**, the coordination sphere around the copper(II) atom contains nonbridging bromato ligands in the axial positions and four extra equatorial aqua ligands (Figure 8).

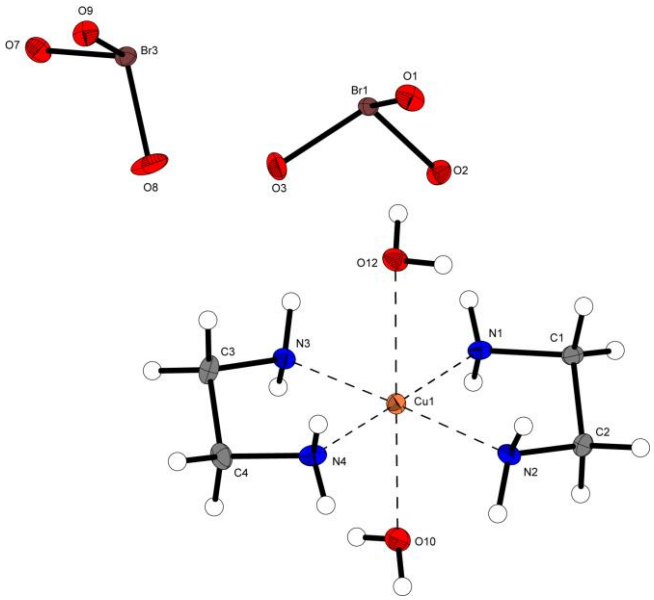

Figure 7. Molecular unit of **7**. Selected bond lengths (Å): Cu1–N1 2.000(4), Cu1–N2 2.027(3), Cu1–N3 2.014(4), Cu1–N4 1.995(4), Cu1–O10 2.555(4), Cu1–O12 2.551(3). Selected bond angles (°): N1–Cu1–N2 84.82(16), N1–Cu1–N3 94.90(16), N1–Cu1–N4 179.17(17), N1–Cu2–O10 83.98(15), N1–Cu2–O12 92.00(15).

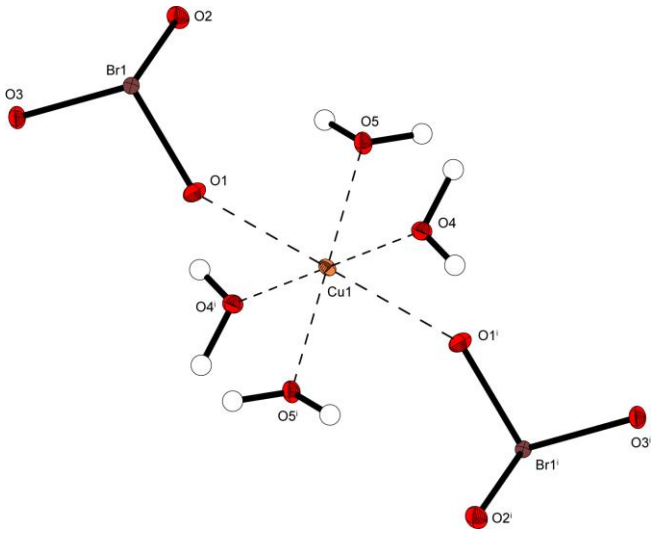

Figure 8. Molecular unit of **8**. Selected bond lengths (Å): Cu1–O1 2.399(2), Cu1–O4 1.9572(19), Cu1–O5 1.9520(19). Selected bond angles (°): O1–Cu1–O4 88.94(7), O1–Cu1–O5 95.11(7), O4–Cu1–O5 89.07(8). Symmetry code: (i) 1−x, −y, 1−z.

9.2.3. Sensitivities and Thermal Stability

For the investigation of endothermic events, like dehydration or melting, and for determination of the thermal stabilities, differential thermal analysis (DTA) measurements with a heating rate of $\beta = 5$ °C min^{-1} were performed. The sensitivities of the complexes toward electric discharge as well as against impact and friction have been determined according to BAM standards, and all compounds were classified in accordance with the UN recommendations on the transport of dangerous goods.[48] An overview of the physicochemical properties of all compounds is given in Table 1. The sensitivities toward mechanical stress are comparable to those for LS and LA, whereas the susceptibility against electrostatic discharge sensitivity (ESD) is lower, making them more secure.[49]

Table 1. Physicochemical properties of compounds **1**–**6** as well as LS and LA.[50]

	IS[a] [J]	*FS*[b] [N]	*ESD*[c] [mJ]	$T_{endo.}$[d] [°C]	$T_{exo.}$[e] [°C]	grain size [µm]
1	2	< 5	25	-	137	< 100
2	1	< 5	60	-	169	100–500
3	2	< 5	90	-	92	100–500
4	< 1	10	150	-	146	100–500
5	8	108	260	103	150	100–500
6	1	40	150	129	146	100–500
LS	2.5–5	1.5	0.02–1.0	115	275–280	-
LA	2.5–4	0.1–1	6–12	-	320–360	-

[a] Impact sensitivity according to the BAM drop hammer (method 1 of 6). [b] Friction sensitivity according to the BAM friction tester (method 1 of 6). [c] Electrostatic discharge sensitivity (OZM ESD tester). [d] Endothermic peak indicating dehydration or loss of aqua ligands according to DTA (onset temperatures at a heating rate of 5 °C min^{-1}). [e] Exothermic peak indicating decomposition according to DTA (onset temperatures at a heating rate of 5 °C min^{-1}).

The only endothermic occasions occurred during heating of coordination compounds **5** and **6** (Figure 9C) were the loss of their crystal water (**5**) or aqua (**6**) ligands at 103 and 129 °C, respectively. The loss of crystal water molecules after heating in compounds **1** and **3** leads to instability of the whole molecule and results therefore in exothermic decomposition. One possible explanation of the higher thermal stability of compounds **5** and **6** could be the formation of water-free species that decompose at a later stage. Nevertheless, stable water-free products of **5** and **6** could not be obtained through dehydration. All ECC have an exothermic decomposition temperature above 130 °C, except complex **3**, which possesses a very low thermal stability of 92 °C due to the loss of crystal water. The highest temperature stability (169 °C) shows the water-free 2D polymer **2**. The general trend becoming apparent is that bridging bromatos lead to crystallization of anhydrous complexes with higher thermal stabilities. Determination of the compounds' DDT capability by hot-plate and hot-needle testing (Figure 9A,B) was performed. Hot-needle tests were conducted by fixation of the sample underneath adhesive tape on a copper plate, followed by penetration with a red-heated needle. A compound's detonation typically indicates a valuable primary explosive, whereas the safe and practicable hot-plate test shows the performance of the

unconfined sample toward fast heating on a copper plate. It does not necessarily allow any conclusions on a compound's capability as a primary explosive. All compounds, except complex **1**, showed deflagration in both tests. While the water-free compound **2** shows relatively high-temperature stability and only weak DDT, it is the other way around with compound **1**, possessing a great DDT but a low decomposition temperature.

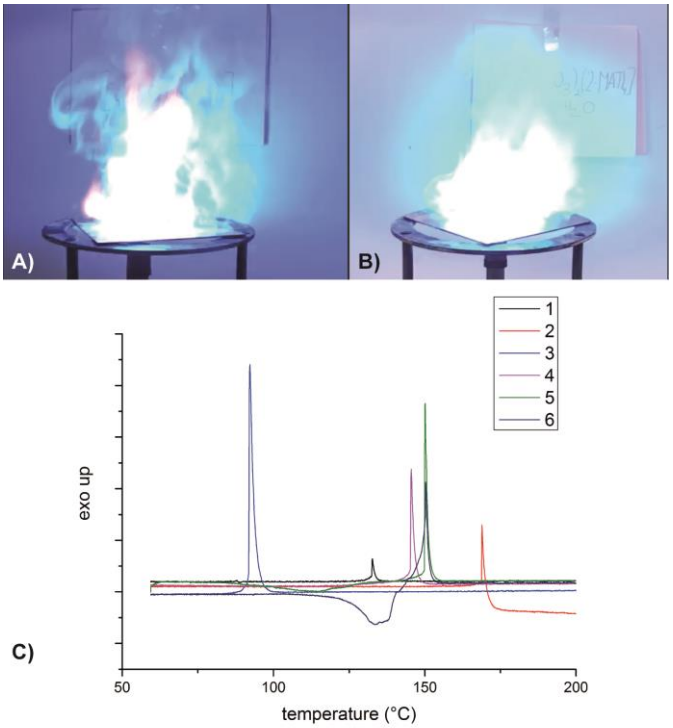

Figure 9. Hot-plate test of compound **2** (A) and **3** (B). (C) DTA plots (5 °C min^{-1}) of complexes **1**–**6** shown in the range of 50–200 °C.

9.2.4. Laser Initiation Tests and UV-Vis Measurements

The laser ignition tests were performed with a 45 W InGaAs laser diode in the single-pulsed mode. The diode was coupled directly to an optical fiber with a core diameter of 400 µm and a cladding diameter of 480 µm. The optical fiber was linked via a SMA-type connecter directly to the laser and to a collimator. The collimator, in turn, was connected to an optical lens, which was stationed in its focal distance (f = 29.9 mm) to the sample. The lens was shielded from the explosive with sapphire glass. Transparent polycarbonate percussion caps were filled with approximately 25 mg of the compound, pressed with a pressure force of 1 kN, and sealed by a UV-curing adhesive. The confined samples were irradiated at a wavelength of 915 nm, a varying current of 7–8 A, a voltage of 4 V, and a varying pulse length of 0.10–15 ms, which combined the results in an approximate energy output of 0.17–30 mJ. The results of the laser experiments, which are classified in decomposition, deflagration, or detonation according to the generated sound, are summarized in Table 2.

Table 2. Results of the laser ignition tests of compounds **1**–**6**.

	1	**2**	**3**	**4**	**5**	**6**
E_{max} [mJ]	0.17	30.0	0.20	0.17	5.10	2.55
outcome[a]	det.	det.	det.	det.	dec.	det.

[a] det. = detonation; dec = decomposition. Operating parameters: current I = 7–8 A; voltage U = 4 V; theoretical maximal output power P_{max} = 45 W; wavelength λ = 915 nm; pulse length τ = 0.10–15 ms.

All complexes, except tetraaqua compound **5**, showed a detonation (Figure 10A,B) differing in the required energy input between 0.17 and 2.55 mJ. Compared to LA[51] (3–30 mJ cm^{-2}) and LS[52] (1.3 J cm^{-2}), the ignition of most of the ECC is possible with lower energy input, although the results are difficult to compare because of their different setups. These results correlate with the observed sensitivities and make copper(II) bromate complexes promising compounds for laser ignition with low initiation energies. In order to gain insight toward the laser-initiation mechanism, solid-state UV-Vis measurements were performed in the range of 350–1000 nm for all complexes (Figure 10C). The step in the absorption intensity at 800 nm in the spectra is caused by a detector change. The UV-Vis spectra exhibit only qualitative character.

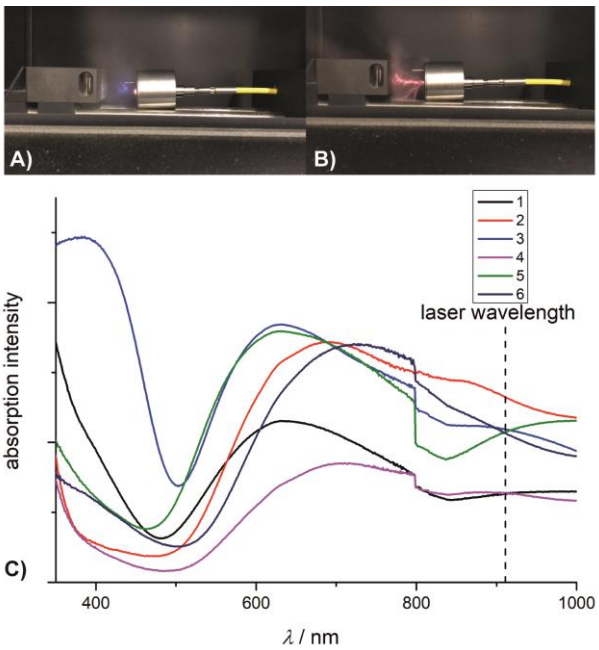

Figure 10. Positive laser initiation tests of compound **2** (A) and **6** (B). (C) Solid-state UV-Vis measurements that were correlated with the laser-initiation experiments.

Because of the characteristic d-d transitions, the spectra show absorptions in the UV, visible, and near-IR regions typical for copper(II) compounds. The mechanism for laser initiation is still not fully understood, and many pathways, such as electronic or thermal, are imaginable.[53] Because of the different coordination spheres, no conclusions can be drawn about the influence of the metal-ligand bond energy toward the color of the compounds. Compound **3**, the only green copper(II) bromate complex, shows absorption maxima close to 400 and 600 nm. All other copper(II) bromate complexes show absorption

maxima close to 350 and 600 nm with only minor deviations among each other. All complexes show only minor absorptions at the laser wavelength of 915 nm. The excitation at 915 nm could be a conceivable explanation for the initiation. The process of laser ignition probably depends on multiple parameters, and more investigations are necessary for a better understanding of the laser-initiation mechanism in the future.

9.2.5. Toxicity Determination and Mass Spectrometry (MS) of Decomposition Gases

The commercially available bioassay system LUMIStox test (luminescent marine bacterium *Vibrio fischeri* NRRL-B-11177), which measures the toxicity in aqueous media, is a valuable indicating device when it comes to groundwater contamination. The half-maximal effective concentration EC_{50} of these compounds was determined after an incubation time of 30 min (the toxicity level after 30 min of incubation: very toxic, < 0.10 g L^{-1}; toxic, 0.10–1.00 g L^{-1}; nontoxic, > 1.00 g L^{-1}).[54] With an EC_{50} (30 min) value of 0.21 g L^{-1} for compound **2**, it has to be considered as toxic, which is not surprising, because of the known toxicity of copper(II) compounds toward microorganisms.[55] Compared to the corresponding copper(II) chlorate and perchlorate complex, recently published by our group,[56,40] with EC_{50} values of 0.19 and 0.13 g L^{-1}, respectively, the lower toxicity toward aquatic life of bromate compounds is proven. For analysis of the gaseous decomposition products, a sample of approximately 40 mg of compound **2** was heated to 200 °C in a nitrogen gas flow and the formed gases were detected with a Cirrus3-XD quadrupole mass spectrometer (Figure 11). The spectra show the formation of oxygen (32), CO_2 (44), and small amounts of water (18). No formation of toxic Br_2 or HBr was observed.

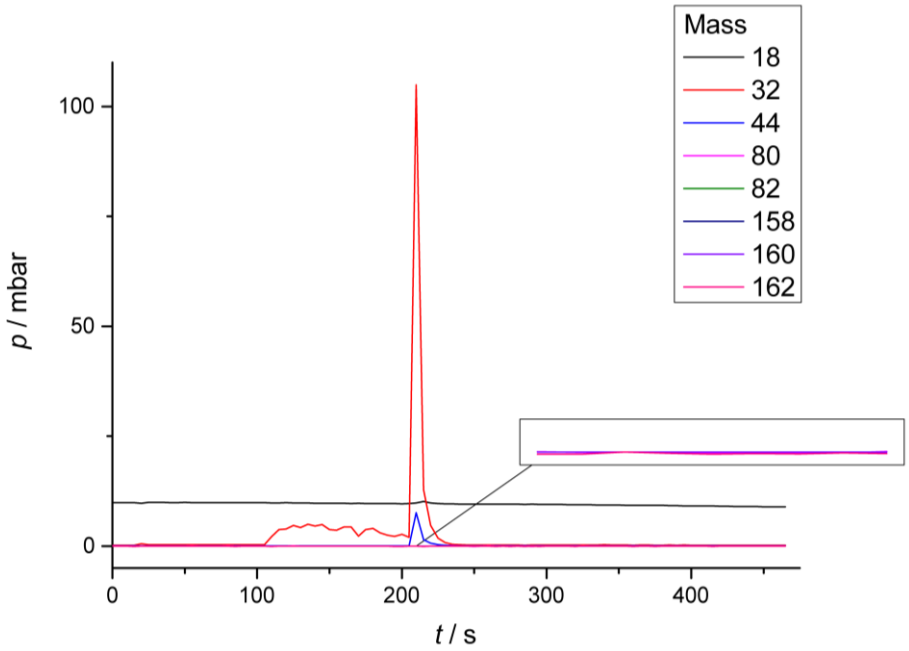

Figure 11. Results of the MS gas analysis of the decomposition products of compound **2**.

9.3. Conclusion

We demonstrated the next step in the development toward environmentally benign perchlorate-free ECC with our exclusive concept of using bromate anions as “exotic” oxidizing species. The six newly synthesized and investigated copper(II) bromate compounds with azole ligands represent a considerable contribution to the coordination chemistry in general and in particular to ECC because of the enormous lack of literature regarding this topic. The displayed synthesis of the complexes is a straightforward and low-cost synthetic route toward modern lead-free primary explosives with promising performance characteristics. The simple complexation of $Cu(BrO_3)_2$ with different nitrogen-rich ligands based on tri- and tetrazole derivatives assures the formation of energetic compounds with high densities. The trend of inclusion of water into many of the structures can hardly be explained by the average oxophilicity of copper(II); however, it can be prevented by the formation of 2D polymeric layers caused by bridging bromato ligands. X-ray studies of all compounds gave insight into the fascinating coordination variety of copper(II) bromate complexes highly depending on the ligands used. The compositions of complexes **1**–**6** were confirmed by elemental analysis and are in accordance with the crystal structures observed. In addition, the X-ray structure of the up-to-now unknown tetrahydrate of copper(II) bromate **8** could successfully be determined and the previously predicted structures of **1**[38] and **7**[37] proven wrong. Most of the compounds showed exothermic decomposition temperatures above 135 °C in thermal stability measurements by DTA. In comparison to the analogous perchlorate and chlorate complexes, ECC **2** showed a lower environmental hazardousness toward aquatic life in toxicity assessments using *V. fischeri*, which proves the higher environmental friendliness of bromate compounds. Within preliminary analysis of decomposition gases, no HBr and Br_2 formation was observed in the MS spectra. Detonations during laser-ignition experiments of nearly every single compound revealed the great capability of copper(II) bromate complexes in future laser-initiation systems.

9.4. Experimental Section

All chemicals and solvents were employed as received (Sigma-Aldrich, Fluka, Acros, and ABCR). ^{1}H and ^{13}C NMR spectra were recorded with neat solids as samples at ambient temperature using a JEOL Eclipse 270, JEOL EX 400, or JEOL Eclipse 400 instrument. The chemical shifts quoted in parts per million in the text refer to typical standards such as tetramethylsilane (^{1}H and ^{13}C). Dehydration, melting, and decomposition temperatures of the described compounds were measured through DTA with an OZM Research DTA 552-Ex instrument. The samples were measured in a range of 25–400 °C at a heating rate of 5 °C min^{-1}. IR spectra were measured with pure samples on a PerkinElmer BXII FT-IR system with a

Smith DuraSampler IR II diamond attenuated total reflectance instrument. Determination of the carbon, hydrogen, nitrogen, and sulfur contents was carried out by combustion analysis using an Elementar Vario El analyzer (the nitrogen values determined are often lower than the calculated ones because of their explosive behavior). UV-Vis spectra were recorded in the solid state using a Varian Cary 500 spectrometer in the wavelength range of 350–1000 nm. Impact sensitivity tests were carried out according to STANAG 4489[57] modified instruction[58] using a BAM (Bundesanstalt für Materialforschung und -prüfung) drop hammer.[59] Friction sensitivity tests were carried out according to STANAG 4487[60] modified instruction[60,61] using the BAM friction tester. The classification of the tested compounds results from the "UN Recommendations on the Transport of Dangerous Goods".[62] Additionally, all compounds were tested for their sensitivity toward electrical discharge using the Electric Spark Tester ESD 2010 EN.S7.[63] Liquid-dried luminescent bacteria of the strain *V. fischeri* NRRL-B-11177 provided by the HACH LANGE GmbH were used for the luminescent bacteria inhibition test to determine their toxicity toward aquatic organisms according to a modified procedure.[64] All of the obtained coordination compounds were washed with cold water, dried overnight in air, and used for analytics without further purification.

CAUTION! *All investigated compounds are potentially explosive energetic materials, which show partly increased sensitivities toward various stimuli (e.g., elevated temperatures, impact, friction, or electrostatic discharge). Therefore, proper security precautions (safety glass, face shield, earthed equipment and shoes, leather coat, Kevlar gloves, Kevlar sleeves, and ear plugs) have to be applied while synthesizing and handling the described compounds. Especially compound **1** must be handled with great care!*

General Procedure for the Preparation of Complexes 1–7

Copper(II) sulfate pentahydrate (62.4 mg, 0.25 mmol) and barium bromate (98.3 mg, 0.25 mmol), each dissolved in 5 mL of water, were combined and stirred mechanically for 10 min, and the precipitated barium sulfate was filtered off. The aqueous filtrate was dried under reduced pressure and the obtained copper(II) bromate dissolved in 2 mL of water. Stoichiometric amounts of the ligand dissolved in 1 mL of water were added under stirring. The reaction mixtures were left to crystallize, and the solids were filtered off, washed with cold water (2 mL), and dried in air. Only one single crystal of compound **7** was picked for X-ray determination experiments, and the complex was not further analyzed. The up-to-now unknown structure of **8** was picked out of a complex solution, which was left for crystallization as a single crystal, and a pure product for further investigation was not obtained.

$[Cu_2(4\text{-ATRI})_6](BrO_3)_4 \cdot H_2O$ (1)

Compound **1** was isolated as a light-blue precipitate. Yield: 116 mg (0.20 mmol, 80%). Single-crystal growth was achieved by overlaying an aqueous solution (8 mL) of copper(II) bromate with an ethanolic solution (8 mL) of 4-ATRI, separated by a mixture (4 mL) of water/ethanol (50/50). After 7 days, blue rods suitable for X-ray determination were obtained.

DTA (5 °C min^{-1}) onset: 137 °C (exothermic). IR (ATR, cm^{-1}): $\tilde{\nu}$ = 3545 (vw), 3250 (m), 3208 (w), 3153 (m), 3126 (m), 3089 (m), 3063 (m), 3018 (w), 2965 (w), 1644 (w), 1631 (w), 1553 (w), 1539 (w), 1491 (vw), 1424 (vw), 1396 (w), 1373 (w), 1321 (vw), 1222 (m), 1207 (w), 1095 (m), 1085 (m), 1050 (m), 1007 (w), 992 (w), 979 (w), 913 (w), 890 (w), 818 (s), 808 (s), 783 (vs), 761 (vs), 693 (w), 679 (w), 622 (vs). EA ($C_{12}H_{26}Br_4Cu_2N_{24}O_{13}$, 1161.29) calcd.: C 12.41, H 2.26, N 28.95%; found: C 12.78, H 2.28, N 28.64%. BAM drop hammer: 2 J; friction tester: < 5 N; ESD: 25 mJ (at grain size < 100 μm).

$[Cu(BrO_3)_2(MTZ)_2]$ (2)

Blue platelike crystals of complex **2** were obtained within 5 days and were suitable for X-ray determination. Yield: 89.4 mg (0.18 mmol, 73%).

DTA (5 °C min^{-1}) onset: 169 °C (exothermic). IR (ATR, cm^{-1}): $\tilde{\nu}$ = 3143 (m), 3034 (w), 1762 (vw), 1522 (m), 1472 (w), 1304 (w), 1202 (m), 1178 (vw), 1109 (m), 1066 (w), 1036 (w), 1003 (w), 883 (m), 862 (vs), 788 (s), 726 (s), 708 (s), 686 (vs), 652 (s). EA ($C_4H_8Br_2CuN_8O_6$, 487.51) calcd.: C 9.85, H 1.65, N 22.99%; found: C 10.11, H 1.81, N 23.13%. BAM drop hammer: 1 J; friction tester: < 5 N; ESD: 60 mJ (at grain size 100–500 μm).

$[Cu(BrO_3)_2(2\text{-}MAT)_4] \cdot H_2O$ (3)

Green blocks suitable for X-ray determination of the monohydrated complex **3** crystallized within 3 days. Yield: 106 mg (0.14 mmol, 58%).

DTA (5 °C min^{-1}) onset: 92 °C (exothermic). IR (ATR, cm^{-1}): $\tilde{\nu}$ = 3359 (m), 3317 (m), 3306 (m), 3223 (m), 3174 (w), 3020 (w), 2962 (w), 1629 (m), 1606 (m), 1557 (s), 1439 (m), 1422 (m), 1383 (w), 1345 (w), 1333 (w), 1195 (m), 1132 (w), 1103 (w), 1075 (w), 1023 (w), 803 (vs), 760 (vs), 749 (vs), 680 (m), 670 (w), 631 (m), 571 (w). EA ($C_8H_{22}Br_2CuN_{20}O_7$, 733.75) calcd.: C 13.10, H 3.02, N 38.18%; found: C 13.13, H 2.95, N 38.37%. BAM drop hammer: 2 J; friction tester: < 5 N; ESD: 90.0 mJ (at grain size 100–500 μm).

$[Cu(BrO_3)_2(1,2\text{-}dtp)_2]$ (4)

Blue blocklike crystals of the water-free compound **4** were isolated within 7 days and were suitable for X-ray determination. Yield: 96.9 mg (0.14 mmol, 57%).

DTA (5 °C min^{-1}) onset: 146 °C (exothermic). IR (ATR, cm^{-1}): $\tilde{\nu}$ = 3144 (m), 1764 (w), 1741 (m), 1571 (w), 1516 (m), 1466 (m), 1457 (m), 1446 (m), 1396 (w), 1381 (m), 1366 (m), 1301 (w), 1287 (m), 1198 (m), 1180 (m), 1141 (m), 1134 (m), 1108 (w), 1059 (w), 1031 (m), 1015 (m), 1008 (m), 886 (m), 860 (s), 786 (s), 751 (m), 727 (s), 713 (s), 700 (vs), 677 (m), 654 (s). EA ($C_{10}H_{16}Br_2CuN_{16}O_6$, 679.70) calcd.: C 17.67, H 2.37, N 32.97%; found: C 17.20, H 2.47, N 32.51%. BAM drop hammer: <1 J; friction tester: 10 N; ESD: 150 mJ (at grain size 100–500 μm).

$[Cu(BrO_3)_2(2,2\text{-dtp})_2] \cdot 4H_2O$ (5)
The four-crystal water-containing complex **5** crystallized within 7 days in the form of blue blocks suitable for X-ray determination. Yield: 113 mg (0.15 mmol, 60%).

DTA (5 °C min^{-1}) onset: 103 °C (loss of water), 150 °C (exothermic). IR (ATR, cm^{-1}): $\tilde{\nu}$ = 3524 (w), 3441 (w), 3367 (w), 3151 (w), 3125 (w), 3014 (w), 2985 (vw), 2970 (vw), 2945 (vw), 1741 (vw), 1737 (vw), 1652 (vw), 1623 (w), 1608 (w), 1573 (vw), 1512 (w), 1488 (w), 1474 (w), 1464 (w), 1447 (w), 1438 (w), 1382 (w), 1373 (w), 1359 (w), 1322 (w), 1306 (w), 1285 (w), 1254 (vw), 1209 (w), 1199 (w), 1187 (w), 1172 (m), 1153 (m), 1137 (m), 1101 (m), 1086 (m), 1076 (w), 1059 (w), 1031 (m), 1021 (m), 1012 (w), 982 (w), 936 (w), 890 (vw), 861 (w). EA ($C_{10}H_{24}Br_2CuN_{16}O_{10}$, 751.76) calcd.: C 15.98, H 3.22, N 29.81%; found: C 16.46, H 3.36, N 31.06%. BAM drop hammer: 8 J; friction tester: 108 N; ESD: 260 mJ (at grain size 100–500 μm).

$[Cu(H_2O)_2(i\text{-dtp})_2](BrO_3)_2$ (6)
Product **6** was received within 8 days in the form of blue blocks suitable for X-ray determination. Yield: 152 mg (0.21 mmol, 85%).

DTA (5 °C min^{-1}) onset: 129 °C (loss of water followed by decomposition). IR (ATR, cm^{-1}): $\tilde{\nu}$ = 3357 (w), 3267 (w), 3151 (w), 3116 (w), 3016 (w), 2986 (w), 2945 (vw), 2776 (vw), 2661 (vw), 1741 (vw), 1652 (w), 1571 (vw), 1512 (w), 1489 (w), 1437 (m), 1391 (w), 1376 (w), 1360 (w), 1321 (vw), 1304 (w), 1287 (w), 1211 (w), 1187 (m), 1173 (m), 1160 (w), 1127 (w), 1100 (m), 1086 (m), 1039 (m), 1031 (w), 1011 (m), 990 (w), 916 (w), 891 (w), 840 (s), 782 (vs), 753 (s), 719 (w), 675 (m), 665 (m), 632 (m), 532 (vw). EA ($C_{10}H_{20}Br_2CuN_{16}O_8$, 715.73) calcd.: C 16.78, H 2.82, N 31.31%; found: C 16.91, H 2.92, N 31.81%. BAM drop hammer: 1 J; friction tester: 40 N; ESD: 150 mJ (at grain size 100–500 μm).

9.5. Acknowledgements

Financial support of this work by the Ludwig-Maximilians-University of Munich and the Office of Naval Research under Grant ONR.N00014-16-1-2062 is gratefully acknowledged. Prof. Dr. Thomas M.

Klapötke is thanked for great financial support and indispensable scientific assistance. The authors additionally thank Mrs. Cornelia Unger for her great contribution in the form of toxicity assessments.

9.6. References

[1] T. M. Klapötke, *Chemistry of High-Energy Materials*, 3rd ed., De Gruyter, Berlin, Boston, **2015**.

[2] T. Brinck, *Green Energetic Materials*, 1st ed., John Wiley & Sons, Ltd., Chichester, **2014**.

[3] L. T. Fairhall, W. V. Jenrette, S. W. Jones, E. A. Pritchard, *Public Health Rep.* **1943**, *58*, 607–617.

[4] D. A. Gidlow, *Occup. Med.* **2015**, *65*, 348–356.

[5] R. Haiges, K. O. Christe, *Inorg. Chem.* **2013**, *52*, 7249–7260.

[6] M. H. V. Huynh, M. D. Coburn, T. J. Meyer, M. Wetzler, *Proc. Natl. Acad. Sci. U. S. A.* **2006**, *103*, 10322–10327.

[7] J.-G. Xu, C. Sun, M.-J. Zhang, B.-W. Liu, X.-Z. Li, J. Lu, S.-H. Wang, F.-K. Zheng, G.-C. Guo, *Chem. Mater.* **2017**, *29*, 9725–9733.

[8] T. Liu, X. Qi, K. Wang, J. Zhang, W. Zhang, Q. Zhang, *New J. Chem.* **2017**, *41*, 9070–9076.

[9] Y. Tang, C. He, L. A. Mitchell, D. A. Parrish, J. M. Shreeve, *Angew. Chem. Int. Ed.* **2016**, *55*, 5565–5567.

[10] P. He, L. Wu, J. Wu, Q. Wang, Z. Li, M. Gozin, J. Zhang, *Chem. – Eur. J.* **2017**, *23*, 11159–11168.

[11] L. V. Clark, *Ind. Eng. Chem.* **1933**, *25*, 663–669.

[12] R. J. Spear, W. P. Norris, *Propellants Explos. Pyrotech.* **1983**, *8*, 85–88.

[13] J. W. Fronabarger, M. D. Williams, W. B. Sanborn, D. A. Parrish, M. Bichay, *Propellants Explos. Pyrotech.* **2011**, *36*, 459–470.

[14] Z. Shunguan, W. Youchen, Z. Wenyi, M. Jingyan, *Propellants Explos. Pyrotech.* **1997**, *22*, 317–320.

[15] J. W. Fronabarger, M. D. Williams, W. B. Sanborn, J. G. Bragg, D. A. Parrish, M. Bichay, *Propellants Explos. Pyrotech.* **2011**, *36*, 541–550.

[16] D. Chen, H. Yang, Z. Yi, H. Xiong, L. Zhang, S. Zhu, G. Cheng, *Angew. Chem. Int. Ed.* **2018**, *57*, 2081–2084.

[17] M. A. Ilyushin, M. A. Aleksandrova, I. V. Bachurina, A. V. Smirnov, I. V. Tselinskii, *Russ. J. Appl. Chem.* **2010**, *83*, 92–96.

[18] S. Chen, W. Guo, Y. Bi, T. Zhang, *Z. Anorg. Allg. Chem.* **2016**, *642*, 761–765.

[19] M. B. Talawar, A. P. Agrawal, S. N. Asthana, *J. Hazard. Mater.* **2005**, *120*, 25–35.

[20] N. Szimhardt, M. H. H. Wurzenberger, T. M. Klapötke, J. T. Lechner, H. Reichherzer, C. C. Unger, J. Stierstorfer, *J. Mater. Chem. A* **2018**, *6*, 6565–6577.

[21] J. Evers, I. Gospodinov, M. Joas, T. M. Klapötke, J. Stierstorfer, *Inorg. Chem.* **2014**, *53*, 11749–11756.

[22] S. R. Ahmad, M. Cartwright, *Laser Ignition of Energetic Materials*, 1st ed., John Wiley & Sons, Ltd., Chichester **2014**, pp 247–268.

[23] R. Schirra, H. Zöllner, *Proceedings of the 42nd International Pyrotechnics Seminar*, Grand Junction, CO, July 10–15, **2016**; IPSUSA, pp 422–428.

[24] A. Y. Zhilin, M. A. Ilyushin, I. V. Tselinskii, A. S. Brykov, *Russ. J. Appl. Chem.* **2001**, *74*, 99–102.

[25] A. Y. Zhilin, M. A. Ilyushin, I. V. Tselinskii, A. S. Kozlov, I. S. Lisker, *Russ. J. Appl. Chem.* **2003**, *76*, 572.

[26] M. A. Ilyushin, I. V. Tselinsky, I. A. Ugryumov, A. Y. Zhilin, A. S. Kozlov, *Proceedings of the 6th Seminar on New Trends in Research of Energetic Materials*, Pardubice, Czech Republic, Apr 22–24, **2003**; University of Pardubice, pp 146–152.

[27] I. A. Ugryumov, M. A. Ilyushin, I. V. Tselinskii, A. S. Kozlov, *Russ. J. Appl. Chem.* **2003**, *76*, 439–441.

[28] T. W. Myers, K. E. Brown, D. E. Chavez, R. J. Scharff, J. M. Veauthier, *Eur. J. Inorg. Chem.* **2016**, *2016*, 3178–3183.

[29] T. W. Myers, J. A. Bjorgaard, K. E. Brown, D. E. Chavez, S. K. Hanson, R. J. Scharff, S. Tretiak, J. M. Veauthier, *J. Am. Chem. Soc.* **2016**, *138*, 4685–4692.

[30] M. Joas, dissertation, Ludwig-Maximilians-University Munich, **2014**.

[31] T. W. Myers, K. E. Brown, D. E. Chavez, R. J. Scharff, J. M. Veauthier, *Inorg. Chem.* **2017**, *56*, 2297–2303.

[32] D. Yoffe, R. Frim, S. D. Ukeles, M. J. Dagani, H. J. Barda, T. J. Benya, D. C. Sanders, *Bromine Compounds. In Ullmann's Encyclopedia of Industrial Chemistry*, 7th ed., Wiley-VCH Verlag, Weinheim, **2013**; pp 27–28.

[33] S. Yoshinaga, M. Matsumoto, T. Nagaishi, *Kogyo Kayaku* **1979**, *40*, 101–108.

[34] T. Yoshida, Otsuka Chemical Co Ltd, Daicel Corp, Nippon Koki Co Ltd, US Patent 5898126A, USA **1999**.

[35] R. E. Menzel, US Patent 7910376B2, USA **2011**.

[36] P. G. Urben, *Bretherick's Handbook of Reactive Chemical Hazards*, 8th ed., Elsevier, Amsterdam, **2017**, pp 69–70.

[37] J. Amiel, *Compt. rend.* **1935**, *200*, 672–674.

[38] V. P. Sinditskii, T. Y. Vernidub, A. E. Fogel'zang, N. A. Zueva, *Izv. Vyssh. Uchebn. Zaved. Khim. Khim. Tekhnol.* **1991**, *34*, 15–19.

[39] D. Juknelevicius, E. Karvinen, T. M. Klapötke, R. Kubilius, A. Ramanavicius, M. Rusan, *Chem. – Eur. J.* **2015**, *21*, 15354–15359.

[40] M. H. H. Wurzenberger, N. Szimhardt, J. Stierstorfer, *J. Am. Chem. Soc.* **2018**, *140*, 3206–3209.

[41] V. N. Markin, I. V. Rozhdestvenskaya, O. I. Fedosova, *Vestn. Leningr. Univ. Ser. 4: Fiz. Khim.* **1985**, *1*, 104–107.

[42] A. C. Blackburn, J. C. Gallucci, R. E. Gerkin, *Acta Crystallogr. Sect. C* **1991**, *47*, 2019–2023.

[43] A. F. Holleman, E. Wiberg, N. Wiberg, *Lehrbuch der Anorganischen Chemie*; De Gruyter, Berlin, **2007**, pp 464–474.

[44] Crystallographic data for the structures have been deposited with the Cambridge Crystallographic Data Centre. Copies of the data can be obtained free of charge upon application to The Director, CCDC, 12 Union Road, Cambridge CB2 1EZ, UK (fax int.code_(1223)336-033; e-mail for inquiry fileserv@ccdc.cam.ac.uk; e-mail for deposition deposit@ccdc.cam.ac.uk).

[45] L. Wiehl, *Acta Crystallogr. Sect. B* **1993**, *49*, 289–303.

[46] P. J. van Koningsbruggen, Y. Garcia, O. Kahn, L. Fournès, H. Kooijman, A. L. Spek, J. G. Haasnoot, J. Moscovici, K. Provost, A. Michalowicz, F. Renz, P. Gütlich, *Inorg. Chem.* **2000**, *39*, 1891–1900.

[47] G. V. Romanenko, Z. A. Savelieva, N. V. Podberezskaya, S. V. Larionov, *J. Struct. Chem.* **1997**, *38*, 171– 176.

[48] Impact: insensitive, > 40 J; less sensitive, ≥ 35 J; sensitive, ≥ 4 J; very sensitive, ≤ 3 J. Friction: insensitive, > 360 N; less sensitive, 360 N; sensitive, < 360 and > 80 N, very sensitive, ≤ 80 N, extremely sensitive, ≤ 10 N. According to the UN Recommendations on the Transport of Dangerous Goods, 5th ed., **2009**.

[49] R. Meyer, J. Köhler, A. Homburg, *Explosives*, 5th ed., Wiley-VCH Verlag, Weinheim, **2002**, pp 196–197.

[50] R. Meyer, J. Köhler, A. Homburg, *Explosives*, 5th ed., Wiley-VCH, Weinheim, **2002**, pp 196–197.

[51] J. T. Hagan, M. M. Chaudhri, *J. Mater. Sci.* **1981**, *16*, 2457–2466.

[52] L. de Yon, T. Nguyen, J. Waschl, *Laser ignition of explosives, pyrotechnics and propellants*, Defence Science and Technology Organization, **1995**.

[53] E. D. Aluker, A. G. Krechetov, A. Y. Mitrofanov, D. R. Nurmukhametov, M. M. Kuklja, *J. Phys. Chem. C* **2011**, *115*, 6893–6901.

[54] C. J. Cao, M. S. Johnson, M. M. Hurley, T. M. Klapötke, *JANNAF J. Propuls. Energet.* **2012**, *5*, 41–51.

[55] V. Ochoa-Herrera, G. Léon, Q. Banihani, J. A. Field, R. Sierra-Alvarez, *Sci. Total Environ.* **2011**, *412-413*, 380–385.

[56] N. Szimhardt, M. H. H. Wurzenberger, A. Beringer, L. Daumann, J. Stierstorfer, *J. Mater. Chem. A* **2017**, *5*, 23753–23765.

[57] NATO standardization agreement (STANAG) on explosives, impact sensitivity tests, no. 4489, 1st ed., Sept 17, **1999**.

[58] WIWEB-Standardarbeitsanweisung 4-5.1.02, Ermittlung der Explosionsgefährlichkeit, hier der Schlagempfindlichkeit mit dem Fallhammer, Nov 8, **2002**.

[59] http://www.bam.de, (accessed Apr 2018).

[60] NATO standardization agreement (STANAG) on explosive, friction sensitivity tests, no. 4487, 1st ed., Aug 22, **2002**.

[61] WIWEB-Standardarbeitsanweisung 4-5.1.03, Ermittlung der Explosionsgefährlichkeit oder der Reibeempfindlichkeit mit dem Reibeapparat, Nov 8, **2002**.

[62] Impact: insensitive, > 40 J; less sensitive, ≥ 35 J; sensitive, ≥ 4 J; very sensitive, ≤ 3 J. Friction: insensitive, > 360 N; less sensitive, 360 N; sensitive, < 360 and > 80 N; very sensitive, ≤ 80 N, extremely sensitive, ≤ 10 N. According to the UN Recommendations on the Transport of Dangerous Goods, 5th ed., **2009**.

[63] http://www.ozm.cz, (accessed April 2018).

[64] R. Scharf, dissertation, Ludwig-Maximilians-University Munich, **2016**.

9.7. Supporting Information

9.7.1. X-Ray Diffraction

For all crystalline compounds, an Oxford Xcalibur3 diffractometer with a CCD area detector or Bruker D8 Venture TXS diffractometer equipped with a multilayer monochromator, a Photon 2 detector and a rotating-anode generator were employed for data collection using Mo-*K*α radiation (λ = 0.7107 Å). The data collection and reduction were carried out using the CRYSALISPRO software.[1] The structures were solved by direct methods (SIR-92,[2] SIR-97,[3,4] or SHELXS-97[5,6]) and refined by full-matrix least-squares on *F*2 (SHELXL4[5]) and finally checked using the PLATON software[7] integrated in the WinGX software suite. The non-hydrogen atoms were refined anisotropically and the hydrogen atoms were located and freely refined. The absorptions were corrected by a SCALE3 ABSPACK multiscan method.[8] All DIAMOND2 plots are shown with thermal ellipsoids at the 50% probability level and hydrogen atoms are shown as small spheres of arbitrary radius.

Table S1. Crystallographic data of **1**–**4**.

	1	**2**	**3**	**4**
Formula	$C_{12}H_{26}Br_4Cu_2N_{24}O_{13}$	$C_4H_8Br_2CuN_8O_6$	$C_8H_{22}Br_2CuN_{20}O_7$	$C_{10}H_{16}Br_2CuN_{16}O_6$
FW [g mol^{-1}]	1161.21	487.51	733.75	679.70
Crystal system	monoclinic	monoclinic	monoclinic	monoclinic
Space Group	*C*2/*c*	*P*2$_1$/*c*	*P*2$_1$/*c*	*P*2$_1$/*c*
Color / Habit	blue rod	blue plate	green block	blue block
Size [mm]	0.03 x 0.06 x 0.46	0.07 x 0.39 x 0.45	0.04 x 0.10 x 0.25	0.10 x 0.10 x 0.20
a [Å]	13.7831(16)	10.5446(5)	7.7919(6)	16.5302(7)
b [Å]	15.7896(17)	6.8317(3)	16.8822(11)	6.5743(3)
c [Å]	15.4202(13)	9.2634(5)	18.8716(14)	9.7369(5)
α [°]	90	90	90	90
β [°]	91.373(10)	103.055(5)	98.031(7)	95.125(4)
γ [°]	90	90	90	90
V [Å^3]	3354.9(6)	650.07(6)	2458.1(3)	1053.92(9)
Z	4	2	4	2
$\rho_{calc.}$ [g cm^{-3}]	2.299	2.491	1.983	2.142
μ [mm^{-1}]	6.129	7.871	4.215	4.899
F(000)	2272	470	1460	670
$\lambda_{MoK\alpha}$ [Å]	0.71073	0.71073	0.71073	0.71073
T [K]	143	143	143	143
θ Min–Max [°]	4.1, 26.2	4.5, 26.0	4.2, 26.0	4.2, 26.0
Dataset	−16: 16; −18: 19; −11: 18	−11: 12; −8: 7; −11: 11	−9: 8; −20: 18; −22: 23	−20: 20; −8: 8; −12: 11
Reflections collected	10717	4552	20093	7371
Independent refl.	2913	1272	4813	2040
R_{int}	0.091	0.034	0.101	0.043
Observed reflections	1891	1204	3188	1906
Parameters	238	98	341	160
R_1 (obs)[a]	0.0578	0.0269	0.0492	0.1017
wR_2 (all data)[b]	0.1179	0.0733	0.1142	0.2582
GooF[c]	1.03	1.11	1.03	1.23
Resd. Dens. [e Å^{-3}]	−0.78, 0.77	−0.67, 0.75	−0.78, 1.06	−2.78, 3.75
Absorption correction	multi-scan	multi-scan	multi-scan	multi-scan
CCDC	1836542	1836543	1836539	1836540

[a] $R_1 = \Sigma||F_0|- |F_c||/ \Sigma|F_0|$; [b] $wR_2 = [\Sigma[w(F_0^2-F_c^2)^2]/\Sigma[w(F_0)^2]]^{1/2}$; $w = [\sigma c^2(F_0^2)+(xP)^2+yP]^{-1}$ and $P = (F_0^2+2F_c^2)/3$; [c] GooF = $\{\Sigma[w(F_o^2-F_c^2)^2]/(n-p)\}^{1/2}$ (n = number of reflections; p = total number of parameters).

Table S2. Crystallographic data of **5**–**8**.

	5	**6**	**7**	**8**
Formula	$C_{10}H_{24}Br_2CuN_{16}O_{10}$	$C_{10}H_{20}Br_2CuN_{16}O_8$	$C_4H_{20}Br_2CuN_4O_8$	$H_8Br_2CuO_{10}$
FW [g mol^{-1}]	751.76	715.73	475.60	874.04
Crystal system	triclinic	monoclinic	monoclinic	orthorhombic
Space Group	*P*−1	*C*2/*c*	$P2_1/c$	*Pbca*
Color / Habit	blue block	blue block	purple block	blue block
Size [mm]	0.16 x 0.34 x 0.36	0.09 x 0.15 x 0.25	0.08 x 0.15 x 0.40	0.10 x 0.23 x 0.36
a [Å]	7.8692(3)	15.1113(5)	7.2970(3)	9.6361(5)
b [Å]	8.0515(2)	8.9694(3)	15.3327(5)	7.2172(4)
c [Å]	10.2521(3)	17.7869(7)	19.2554(7)	12.5678(6)
α [°]	76.605(2)	90	90	90
β [°]	80.773(3)	97.542(3)	92.154(3)	90
γ [°]	87.471(2)	90	90	90
V [Å^3]	526.60(12)	2155.44(19)	2152.82(14)	874.04(8)
Z	1	4	6	4
$\rho_{calc.}$ [g cm^{-3}]	2.002	1.989	2.201	2.974
μ [mm^{-1}]	4.160	4.332	7.128	11.675
F(000)	375	1420	2410	748
$\lambda_{MoK\alpha}$ [Å]	0.71073	0.71073	0.71073	0.71073
T [K]	143	143	143	143
θ Min–Max [°]	4.1, 26.0	4.2, 26.0	4.1, 26.0	4.2, 26.0
Dataset	−8: 9; −9: 9; −12: 12	−18: 18; −10: 11; −21: 21	−9: 8; −18: 18; −23: 22	−10: 11; −8: 8; −13: 15
Reflections collected	4757	9165	16689	5975
Independent refl.	2432	2336	4198	856
R_{int}	0.014	0.033	0.054	0.039
Observed reflections	2288	2046	3401	731
Parameters	194	178	323	62
R_1 (obs)[a]	0.0188	0.0279	0.0315	0.0218
wR_2 (all data)[b]	0.0485	0.0648	0.0688	0.0584
GooF[c]	1.07	1.09	1.06	1.13
Resd. Dens. [e Å^{-3}]	−0.41, 0.57	−0.38, 0.70	−0.64, 0.76	−0.59, 0.60
Absorption correction	multi-scan	multi-scan	multi-scan	multi-scan
CCDC	1836537	1836541	1836544	1836538

[a] $R_1 = \Sigma||F_0|- |F_c||/ \Sigma|F_0|$; [b] $wR_2 = [\Sigma[w(F_0^2-F_c^2)^2]/\Sigma[w(F_0)^2]]^{1/2}$; $w = [\sigma c^2(F_0^2)+(xP)^2+yP]^{-1}$ and $P = (F_0^2+2F_c^2)/3$; [c] GooF = $\{\Sigma[w(F_o^2-F_c^2)^2]/(n-p)\}^{1/2}$ (n = number of reflections; p = total number of parameters).

9.7.2. IR Spectroscopy of 1–6

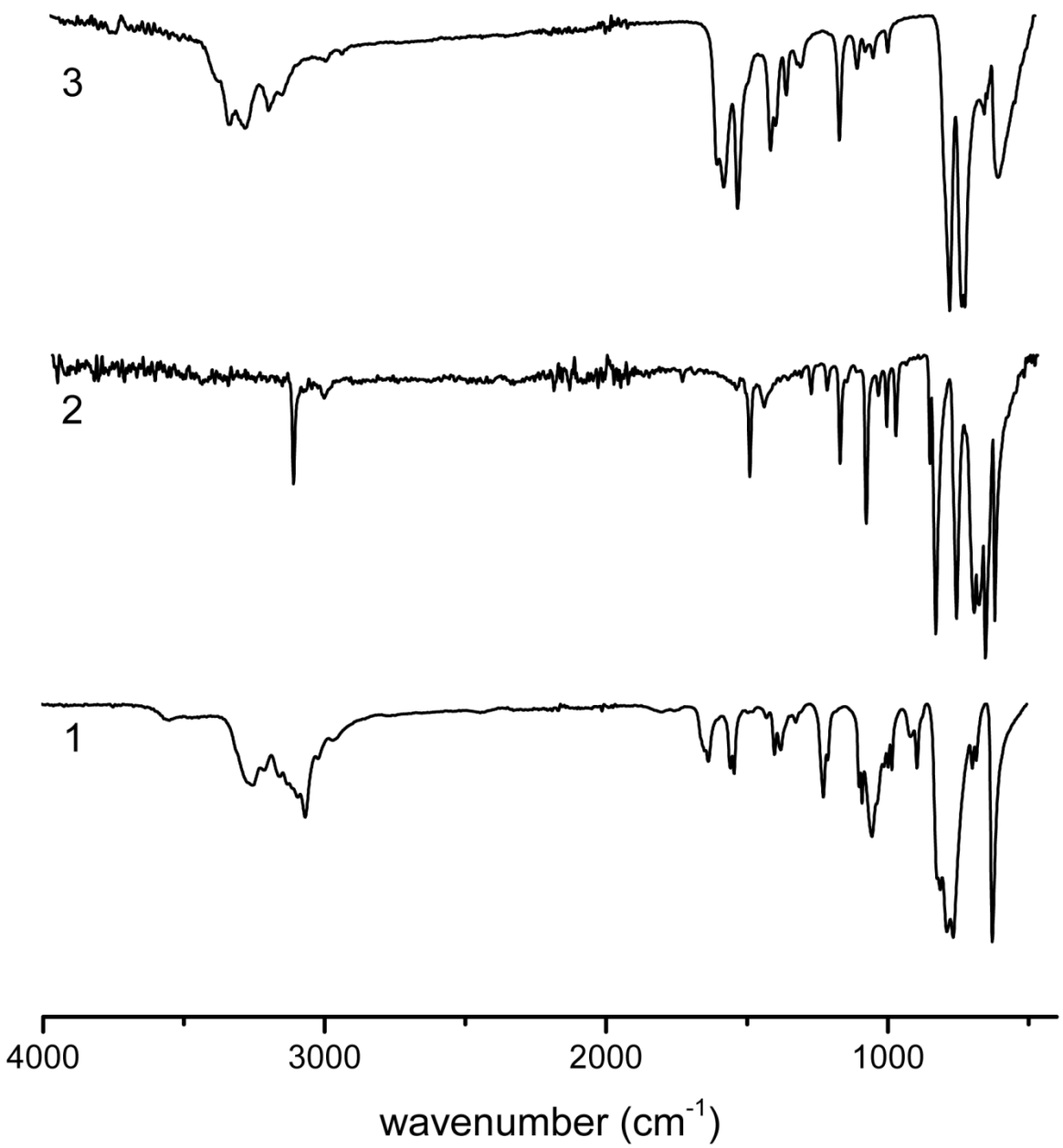

Figure S1. Infrared spectra of compounds **1**–**3**.

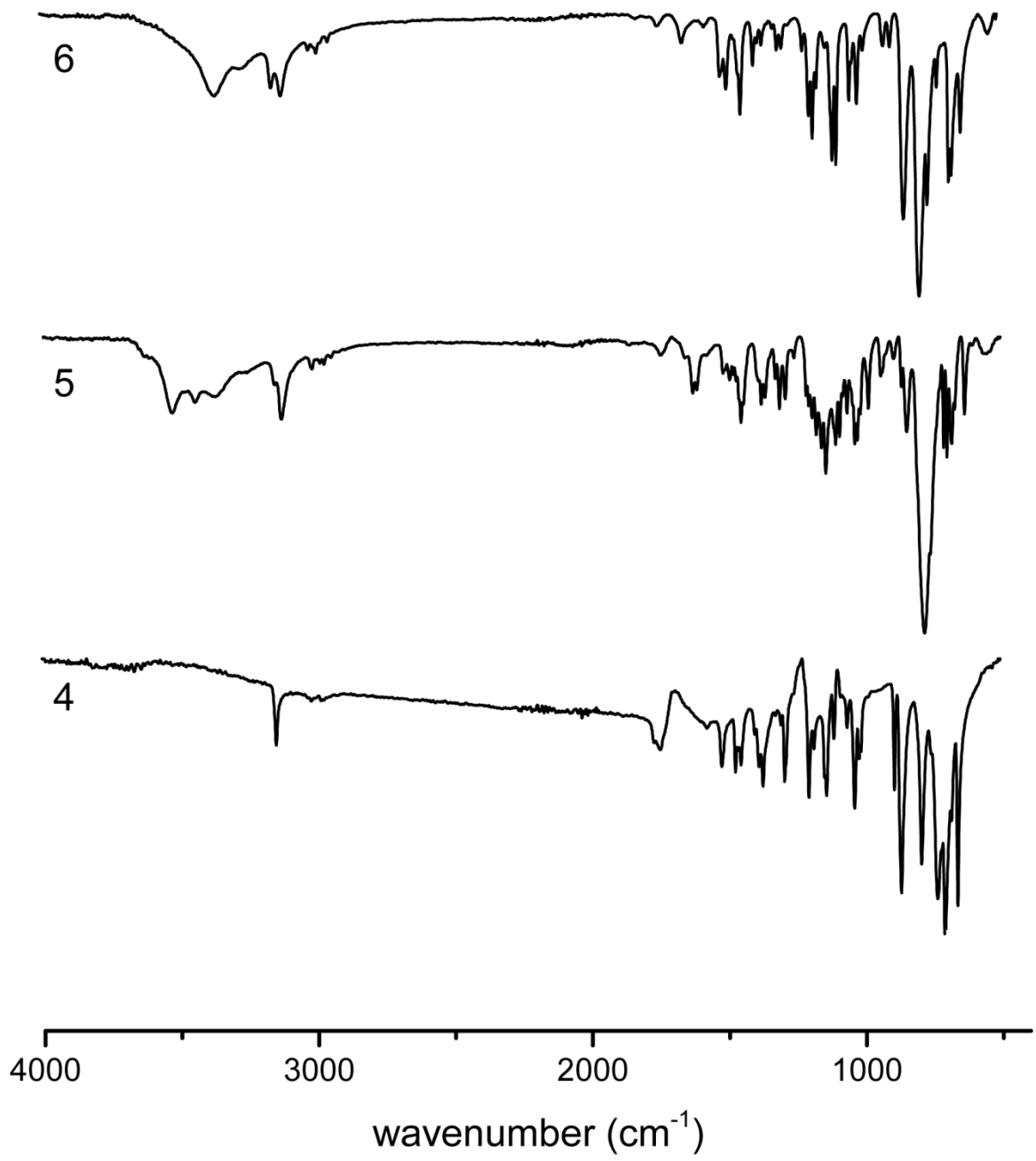

Figure S2. Infrared spectra of compounds **4**–**6**.

9.7.3. References

[1] *CrysAlisPro*, Oxford Diffraction Ltd., version 171.33.41, **2009**.

[2] A. Altomare, G. Cascarano, C. Giacovazzo, A. Guagliardi, *J. Appl. Crystallogr.* **1993**, *26*, 343–350.

[3] A. Altomare, G. Cascarano, C. Giacovazzo, A. Guagliardi, A. G. G. Moliterni, M. C. Burla, G. Polidori, M. Camalli, R. Spagna, *SIR97*, **1997**.

[4] A. Altomare, M. C. Burla, M. Camalli, G. L. Cascarano, C. Giacovazzo, A. Guagliardi, A. G. G. Moliterni, G. Polidori, R. Spagna, *J. Appl. Crystallogr.* **1999**, *32*, 115–119.

[5] G. M. Sheldrick, *SHELXL-97, Program for the Refinement of Crystal Structures*, University of Göttingen, Germany, **1997**.

[6] G. M. Sheldrick, *Acta Crystallogr. Sect. A* **2008**, *64*, 112–122.

[7] A. L. Spek, *PLATON, A Multipurpose Crystallographic Tool*, Utrecht University, The Netherlands, **1999**.

[8] Empirical absorption correction using spherical harmonics, implemented in SCALE3 ABSPACK scaling algorithm (CrysAlisPro Oxford Diffraction Ltd., Version 171.33.41, **2009**).

10. Copper(II) Chlorate Complexes: The Renaissance of a Forgotten and Misjudged Energetic Anion

Maximilian H. H. Wurzenberger, Norbert Szimhardt, and Jörg Stierstorfer

Reprinted (adapted) with permission from *Journal of the American Chemical Society* **2018**, *140*, 3206–3209.

DOI: 10.1002/asia.201900269

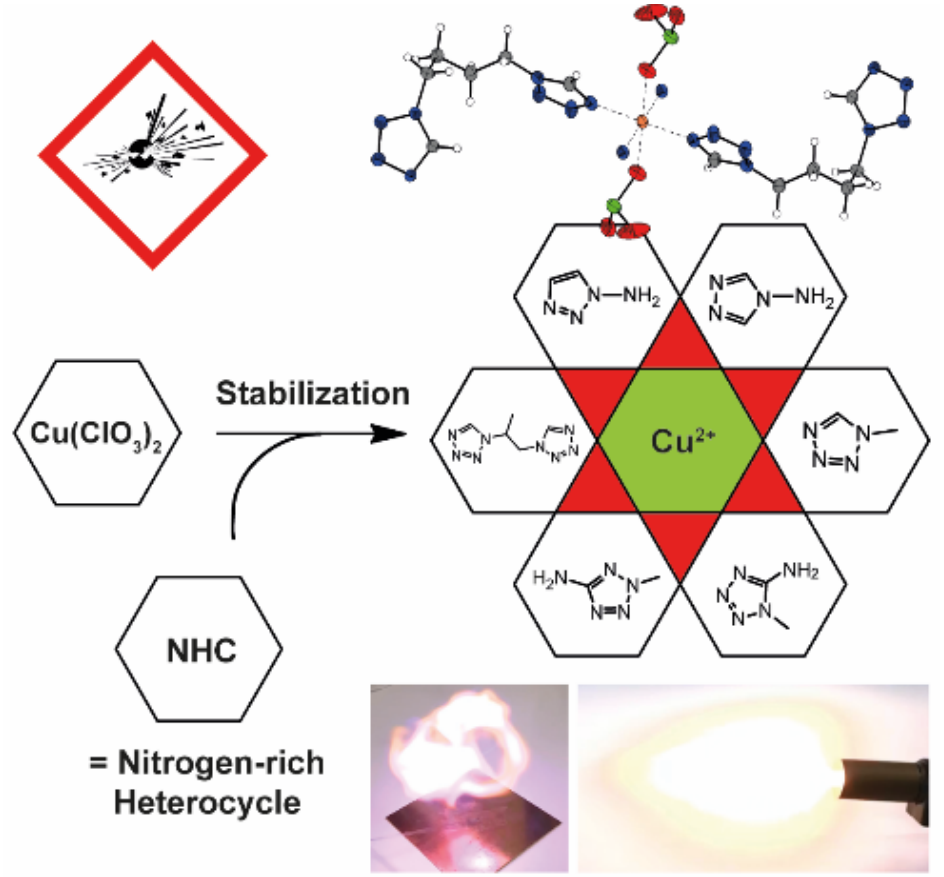

Abstract: A convenient synthetic route toward new copper(II) chlorate complexes with potential use in modern advanced ignition or initiation systems is described. Obtained compounds were not only accurately characterized (XRD, IR, UV-Vis EA and DTA) but also investigated for their energetic character (sensitivities, initiation capability, and laser ignition). The copper(II) 4-aminotriazolyl chlorate complex showed excellent initiation of PETN, while also being thermally stable and safe to handle. Solid-state UV-Vis measurements were performed to get a possible insight toward the laser initiation mechanism. In contrast to expectations, the presented copper(II) chlorate energetic coordination compounds show manageable sensitivities that can be tamed or boosted by the appropriate choice of nitrogen-rich ligands.

10.1. Introduction

The use of chlorates is still ever-present in everyday life with applications in bleach (both $NaClO_3$ and $KClO_3$ are responsible for the production of ClO_2 in elemental chlorine-free bleaching processes), oxygen candles (for aircrafts or submarines), herbicides and even medicine (*e.g.*, $Al(ClO_3)_3$ in mouth washes against mild inflammation in the pharynx due to its astringent effect).[1] The mixture of approximately 65–80 w% potassium chlorate together with 20–35 w% red phosphorus in one of the most spectacular and sensitive formulations, called the Armstrong's mixture (Figure 1A), can cause disastrous accidents. The composition tends to spontaneous ignite when mixed or grinded. It is used in matches, fireworks, toy cap guns and earlier in primers and guns. It has nearly been completely replaced due to corrosion issues. Also, the risk of misuse is high and may lead to accidents through incorrect handling.[2] Mixtures containing chlorates with different reducing agents such as sugar, metal powders, saw dust, carbon black or graphite are extremely dangerous.[3]

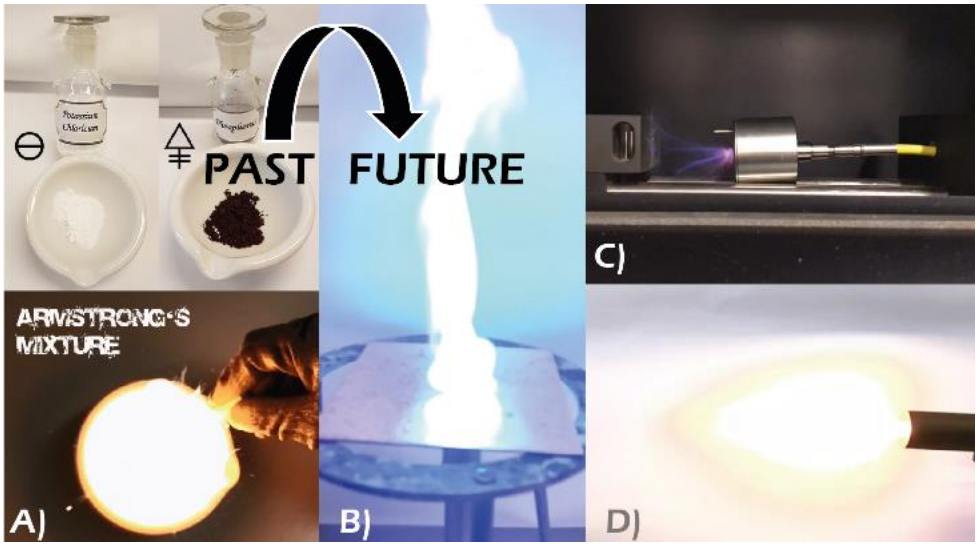

Figure 1. Old versus new: (A) Armstrong's mixture containing potassium chlorate and red phosphorus; (B) hot plate test showing blue light emission during the decomposition from copper(II) chlorates; (C) laser ignition of copper(II) chlorate complex **8**; (D) smokeless muzzle flash of a new ignition mixture.

Chlorates possess a high oxidation potential (performance), are thermally stable (T_{dec} $NaClO_3$: 255 °C, $KClO_3$: 368 °C) and show low toxicities (LD_{50} ($NaClO_3$) 1200 mg kg^{-1}).[4] Investigations by the European Food Safety Authority showed that the potency of chlorate to the human body is 10 times lower compared with perchlorate and only chronic exposure over a long time period could cause inhibition of the thyroid iodine uptake.[5] The ongoing use of lead containing priming mixtures and the accompanied environmental accumulation holds a high ecological risk. Finally, lead styphnate and lead azide, the most commonly used substances in primer mixtures, were put on the candidate list of authorization (substances of very high concern, Annex XIV) during the REACH (Registration, Evaluation, Authorization and

Restriction of Chemicals)[6] regulations in 2011 due to their high toxicity. This could lead to prohibition or restriction of the compounds, which makes research into possible alternatives very important.[7]

10.2. Results and Discussion

The described approach herein for the replacement of lead containing primary explosives is the use of energetic copper(II) chlorate complexes, which were stabilized and tuned with different endothermic nitrogen-rich ligands. Interestingly, very few copper(II) complexes using chlorate as the counter anion or ligand have been described in literature. These include ammonia, a few primary amines, ethylenediamine, and 4-amino-1,2,4-triazole (4-ATRI).[8] However, crystal structures and sensitivities have not been reported and energetic investigations are limited to their decomposition temperatures. This may be a consequence of the poor accessibility toward copper(II) chlorate, which is not commercially available, exists with variable water contents (4–6 H_2O) and is highly hygroscopic.[9] Although perchlorates are stronger oxidizers, the reduction of chlorates is favored, leading to an easier initiation.[10] The higher reactivity can also be explained by the missing shielding of the chlorine(+V) atom. The difficult main goal in the synthesis of metal chlorate complexes is the stabilization of the desired products. For that reason, neutral tri- and tetrazole derivatives were utilized, which are either commercially available or easy to synthesize.[11] The next challenge we faced was the difficult access to copper(II) chlorate, which was solved by a simple metathesis reaction exploiting the precipitation of barium sulfate as the driving force (Scheme 1). Due to the high hygroscopicity of copper(II) chlorate, freshly prepared alcoholic solutions (except **6**) of copper(II) chlorate were combined with respective stoichiometric amounts of the ligands dissolved in organic solvents (MeOH, EtOH, MeCN). All compounds were analyzed by low temperature single crystal X-ray diffraction. Figure 2 shows six different coordination modes in the complexes with no (**2**, **6**, and **9**), one (**4**) and two (**5** and **8**) coordinating chlorato ions. The most favored mode in this study is the octahedral coordination sphere with two coordinating chlorato ligands surrounding the copper(II) metal center. Also, an extraordinary square pyramidal coordination in compound **4** with both a coordinating chlorato ligand and a nonbinding chlorate counter anion was observed. Monodentate ligands such as 1-ATRI, MTZ, and 2-MAT lead to the formation of closed octahedral coordination spheres in the complexes **1** and **3**–**5**. Whereas 4-ATRI and the propyl-linked ditetrazole isomers are bidentate and form 1D polymeric chains by coordinating between the same copper(II) cation in compounds **2** and **6**–**9**. A different situation can be found in complex **10**, where each butyl ligand bridges two different center metals forming 2D polymeric networks. Though complexes **2** and **6** are the only presented compounds with copper(II) ions exclusively coordinated by six nitrogen donors, the coordination sphere of **5** shows the greatest variety with two aqua, chlorate, and tetrazole ligands each.

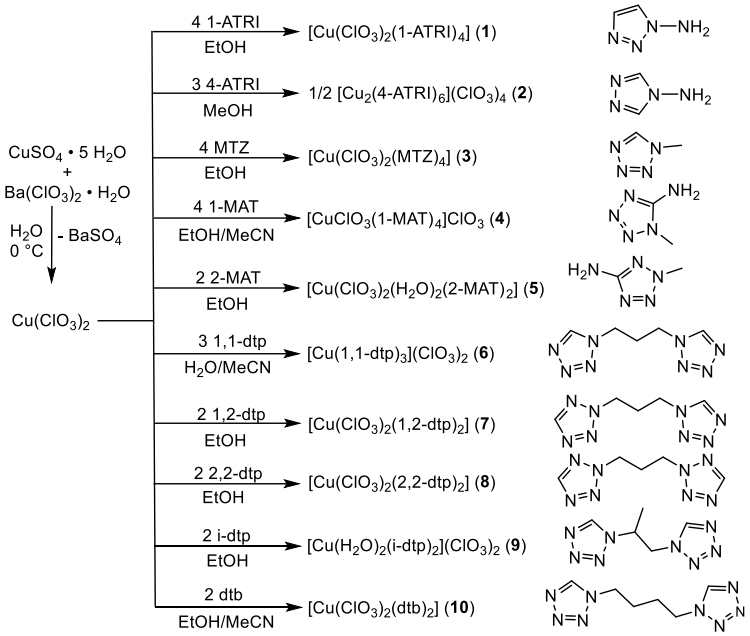

Scheme 1. Synthesis of the complexes **1**–**10** starting from copper(II) sulfate and barium chlorate. Overview of used nitrogen-rich ligands: 1-ATRI: 1-amino-1,2,3-triazole; 4-ATRI: 4-amino-1,2,4-triazole; MTZ: 1-methyl-5*H*-tetrazole; 1-MAT: 1-methyl-5-aminotetrazole; 2-MAT: 2-methyl-5-aminotetrazole; 1,1-dtp: 1,3-di(tetrazol-1-yl)propane; 1,2-dtp: 1-(tetrazol-1-yl)-3-(tetrazol-2-yl)propane; 2,2-dtp: 1,3-di(tetrazol-2-yl)propane; i-dtp: 1,1'-(propane-1,2-diyl)bis(tetrazole); dtb: 1,4-di(tetrazol-1-yl)butane.

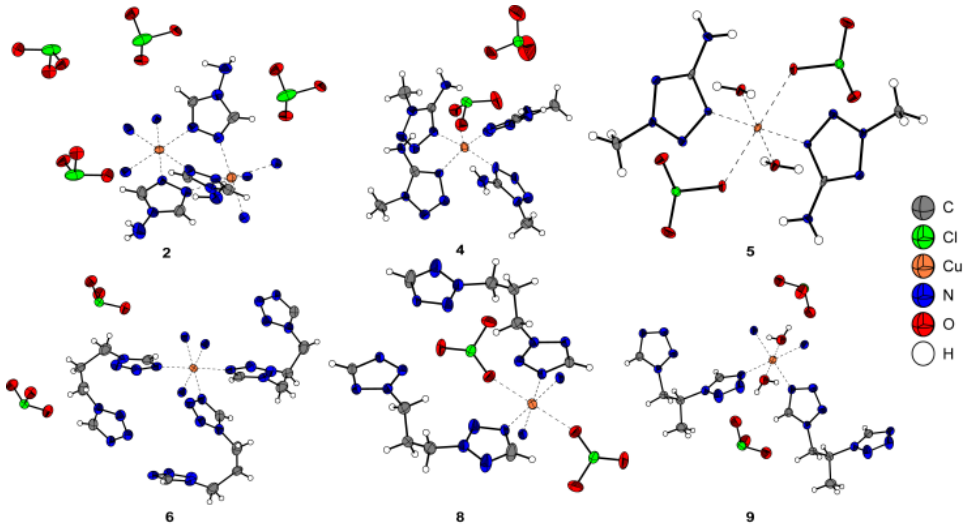

Figure 2. Different coordination modes of copper(II) chlorate complexes $[Cu_2(4\text{-ATRI})_6](ClO_3)_4$ (**2**), $[CuClO_3(1\text{-MAT})_4]ClO_3$ (**4**), $[Cu(ClO_3)_2(H_2O)_2(2\text{-MAT})_2]$ (**5**), $[Cu(1,1\text{-dtp})_3](ClO_3)_2$ (**6**), $[Cu(ClO_3)_2(2,2\text{-dtp})_2]$ (**8**), and $[Cu(H_2O)_2(i\text{-dtp})_2](ClO_3)_2$ (**9**) determined by low temperature X-ray diffraction. Ellipsoids are drawn at the 50% probability level.[12]

The molecular unit of **2** consists of two different crystallographic center atoms, both showing a Jahn-Teller distortion. Whereas Cu1 exhibits a rare compressed coordination sphere with shorter axial Cu–N-bonds compared to the equatorial ones, the stretched coordination environment of Cu2 is composed of longer axial and shorter equatorial Cu–N-bonds. In contrast, the copper(II) centers in complex **6** show no

distortion at all, possessing six Cu–N-bond lengths of almost the same distance. For the determination of the compounds' deflagration to detonation transition (DDT) capability the hot plate test, hot needle test, and plate dent test (Figure 3) were performed.

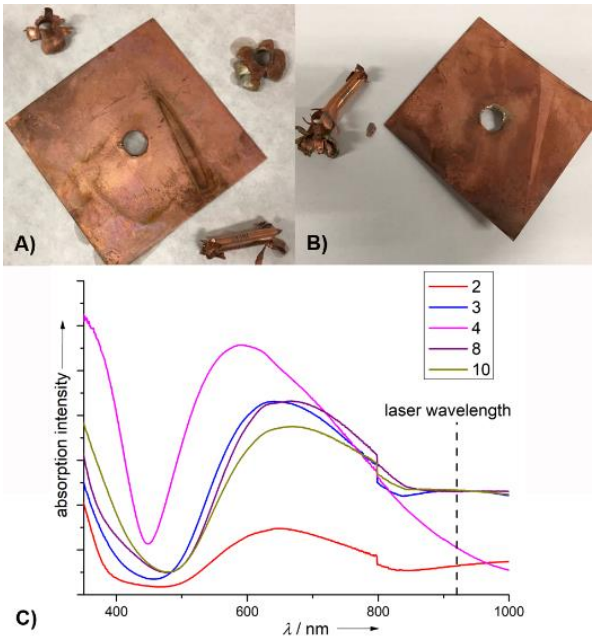

Figure 3. Positive PETN initiation test of compound **2** (A) and **8** (B); (C): solid-state UV-Vis measurements which were correlated to the laser initiation experiments.

The most promising compounds in terms of performance and thermal stability are complexes **2** and **8**. Their physicochemical properties are summarized in Table 1 and compared with that of lead azide.

Table 1. Physicochemical properties of compounds **2** and **8** compared to lead azide.[15]

	2	**8**	**$Pb(N_3)_2$**
Formula	$C_{12}H_{24}Cl_4Cu_2N_{24}O_{12}$	$C_{10}H_{16}Cl_2CuN_{16}O_6$	PbN_6
FW [g mol^{-1}]	965.37	590.79	291.24
$\rho_{calc.}$ [g cm^{-3}] (*T* [K])	1.964 (143)	1.821 (173)	4.8
IS [J][a]	1	1	2.5–4
FS [N][b]	< 5	< 5	0.1–1
ESD [mJ][c]	15	50	6–12
$T_{exo.}$ [°C][d]	186	176	320–360

[a] Impact sensitivity according to the BAM drop hammer (method 1 of 6). [b] Friction sensitivity according to the BAM friction tester (method 1 of 6). [c] Electrostatic discharge sensitivity (OZM ESD tester). [d] Temperature of decomposition indicated by exothermic event according to DTA (onset temperatures at a heating rate of 5 °C min^{-1}).

The sensitivities toward mechanical stimuli are comparable to those observed for $Pb(N_3)_2$, whereas the susceptibility against electrostatic discharge is lower, making them safer to handle. The compounds possess both good densities and thermal stabilities. Copper(II) chlorate complexes **2** and **8** were tested in copper shell initiation tests and showed positive DDTs toward the secondary explosive PETN (Figure 3A,B). In the laser ignition tests (Figure 1C), all complexes, except diaqua compound **9**, showed a detonation differing in the required energy input between 0.17–25.5 mJ. However, UV-Vis measurements

showed that the complexes only exhibit moderate absorption in the laser wavelength area (Figure 3C). Complex **8** cannot be compared with its perchlorate analogue since no energetic properties were explored.[13] Comparing **2** to the corresponding perchlorate complex (4-ATRI as ligand), a higher decomposition temperature (250 °C), and a significantly lower density can be observed. It shows a higher friction sensitivity (8.8 N) and was positive in PETN initiation tests.[14] The toxicity measurements, using luminescent marine bacterium *Vibrio fischeri* NRRL-B-11177, for compound **3** and comparison with the corresponding copper(II) perchlorate complex, recently published by our group,[16] prove the lower toxicity toward aquatic life of chlorate compounds.

10.3. Conclusion

In conclusion, we demonstrated a straightforward and low-cost synthetic route toward energetic copper(II) chlorate complexes. Complexation of $Cu(ClO_3)_2$ assures stabilization and tuning of the energetic character by the simple selection of different nitrogen-rich ligands based on tri- and tetrazole derivatives. In the course of this work, ten new coordination compounds were successfully synthesized and comprehensively compared with each other. All ten ligands lead to a disappearance of the high hygroscopy of pure copper(II) chlorate. For the first time, X-ray crystal structures of all compounds were determined and the previously predicted structure of **2**[8c] successfully proven. Thermal stability measurements by DTA showed exothermic decomposition temperatures above 150 °C for most of the compounds. Easy ignition by heat was proven by the hot needle and hot plate tests. In addition, the most promising primary explosives **2** and **8** showed excellent initiation capabilities toward the secondary PETN indicated by positive deflagration to detonation transitions. The use of alkyl-bridged ditetrazoles with longer chain lengths leads to an improvement of the mechanical sensitivities while maintaining a highly energetic character. This could be a promising concept for desensitization of energetic (copper(II) chlorate) complexes in the future. Toxicity measurements using *Vibrio fischeri* of compound **3** showed a lower toxicity in comparison to the analogous perchlorate complex and confirmed the higher environmental friendliness of chlorate compounds. During the laser ignition experiments, detonation of almost every compound was observed and demonstrated the great suitability of chlorate complexes in future laser initiation systems.

10.4. Acknowledgements

Financial support of this work by the Ludwig-Maximilians-University of Munich (LMU). The authors thank Prof. Dr. Thomas M. Klapötke for providing the research facilities but also for invaluable scientific input.

10.5. References

[1] (a) A. F. Holleman, E. Wiberg, N. Wiberg, *Lehrbuch der Anorganischen Chemie*, De Gruyter, Berlin, **2007**, pp 469–470; (b) F. v. Bruchhausen, *Hagers Handbuch der pharmazeutischen Praxis*; Springer, Berlin, **1995**, pp 171; (c) A. Glasner, L. Weidenfeld, *J. Am. Chem. Soc.* **1952**, *74*, 2464–2467.

[2] K. L. Kosanke, B. J. Kosanke, *Selected Pyrotechnic Publications of K. L. and B. J. Kosanke, Part 4 (1995 Through 1997)*; Journal of Pyrotechnis, Whitewater, **1999**, 42–43.

[3] K. A. Hofmann, *Anorganische Chemie*, 21st ed., Springer, Berlin, **2013**, 447.

[4] www.sigmaaldrich.com, (accessed November 2017).

[5] European Food Safety Authority (EFSA) *EFSA J.* **2015**, *13*, 4135–4238.

[6] https://echa.europa.eu/de/candidate-list-table, (accessed November 2017).

[7] (a) J. Zhang, S. Dharavath, J. M. Shreeve, L. A. Mitchell, D. A. Parrish, *J. Am. Chem. Soc.* **2016**, *138*, 7500–7503; (b) T. W. Myers, J. A. Bjorgaard, K. E. Brown, D. E. Chavez, S. K. Hanson, R. J. Scharff, S. Tretiak, J. M. Veauthier, *J. Am. Chem. Soc.* **2016**, *138*, 4685–4692; (c) K. B. Landenberger, O. Bolton, A. J. Matzger, *J. Am. Chem. Soc.* **2015**, *137*, 5074–5079; (d) M. A. Ilyushin, I. V. Tselinsky, I. V. Shugalei, *Cent. Eur. J. Energy Mater.* **2012**, *9*, 293–327; (e) M. A. Petrie, J. A. Sheehy, J. A. Boatz, G. Rasul, G. K. S. Prakash, G. A. Olah, K. O. Christe, *J. Am. Chem. Soc.* **1997**, *119*, 8802–8808; (f) Z. Mi, S. Chen, Z. Jing, L. Yang, T. Zhang, *Eur. J. Inorg. Chem.* **2016**, *2016*, 3978–3983; (g) T. M. Klapötke, C. Petermayer, D. G. Piercey, J. Stierstorfer, *J. Am. Chem. Soc.* **2012**, *134*, 20827–20836.

[8] (a) J. Amiel, *Compt. rend.* **1934**, *199*, 51–53; (b) J. Amiel, *Compt. rend.* **1934**, *199*, 201–203; (c) V. P. Sinditskii, T. Y. Vernidub, A. E. Fogel'zang, N. A. Zueva, *Izv. Vyssh. Uchebn. Zaved. Khim. Khim. Tekhnol.* **1991**, *34*, 15–19.

[9] (a) A. C. Blackburn, J. C. Gallucci, R. E. Gerkin, *Acta Crystallogr. Sect. B* **1991**, *47*, 474–479; (b) D. L. Perry, S. L. Phillips, *Handbook of Inorganic Compounds*, 1st ed., CRC Press, Boca Raton, **1995**, 139.

[10] G. M. Brown, B. Gu, *Perchlorate Environmental Occurrence, Interactions and Treatment*, 1st ed., Springer, New York, **2006**, 17–47.

[11] (a) https://www.abcr.de/startseite/, (accessed October 2017); (b) P. J. van Koningsbruggen, Y. Garcia, O. Kahn, L. Fournès, H. Kooijman, A. L. Spek, J. G. Haasnoot, J. Moscovici, K. Provost, A. Michalowicz, F. Renz, P. Gütlich, *Inorg. Chem.* **2000**, *39*, 1891–1900; (c) P. J. van Koningsbruggen, Y. Garcia, H. Kooijman, A. L. Spek, J. G. Haasnoot, O. Kahn, J. Linares, E. Codjovi, F. Varret, *J. Chem. Soc. Dalton Trans.* **2001**, *4*, 466–471.

[12] Selected X-ray data: **2**: *C*2/*m*, *a* 13.5622(16) Å, *b* 15.5713(18) Å, *c* 7.7338(15) Å, β 91.559(12)°, *V* 1632.6(4) Å^3, *Z* 4, ρ 1.964 g cm^{-3}; **4**: $P2_1/n$, *a* 13.1028(10) Å, *b* 10.7288(8) Å, *c* 16.2265(14) Å, β 95.036(7)°, *V* 2272.3(3) Å^3, *Z* 4, ρ 1.832 g cm^{-3}; **5**: $P\bar{1}$, *a* 6.5617(3) Å, *b* 7.5260(4) Å, *c* 9.0097(4) Å, α 111.762(2)°, β 98.711(2)°, γ 104.197(2)°, *V* 385.81(3) Å^3, *Z* 1, ρ 2.000 g cm^{-3}; **6**: $P\bar{3}c1$, *a* 10.9642(2) Å, *c* 14.3772(4) Å, *V* 1496.78(8) Å^3, *Z* 2, ρ 1.711 g cm^{-3}; **8**: *C*2/*c*, *a* 14.6638(7) Å, *b* 8.9883(5) Å, *c* 16.3538(8) Å, β 90.324(5)°, *V* 2155.44(19) Å^3, *Z* 4, ρ

1.821 g cm^{-3}; **9**: *C*2/*c*, *a* 15.0672(5) Å, *b* 9.0113(3) Å, *c* 17.5426(6) Å, β 97.696(3)°, *V* 2360.39(14) Å^3, *Z* 4, ρ 1.764 g cm^{-3}.

[13] R. Bronisz, *Eur. J. Inorg. Chem.* **2004**, *18*, 3688–3695.

[14] S. Cudziło, M. Nita, *J. Hazard. Mater.* **2010**, *177*, 146–149.

[15] R. Meyer, J. Köhler, A. Homburg, *Explosives*, 5th ed., Wiley-VCH, Weinheim, **2002**, pp 196–197.

[16] N. Szimhardt, M. H. H. Wurzenberger, A. Beringer, L. Daumann, J. Stierstorfer, *J. Mater. Chem. A* **2017**, *5*, 23753–23765.

10.6. Supporting Information

10.6.1. Experimental Procedure and General Methods

All chemicals and solvents were employed as received (Sigma-Aldrich, Fluka, Acros, ABCR). ^{1}H and ^{13}C NMR spectra were recorded with neat solids as samples at ambient temperature using a JEOL Eclipse 270, JEOL EX 400 or a JEOL Eclipse 400 instrument. The chemical shifts quoted in ppm in the text refer to typical standards such as tetramethylsilane (^{1}H, ^{13}C). Critical temperatures such as dehydration, melting and decomposition points of the described compounds were measured through differential thermal analysis (DTA) with an OZM Research DTA 552-Ex instrument. In addition, thermogravimetric measurements on a Perkin Elmer TG4000 were carried out for selected compounds. The samples were measured in a range of 25–400 °C at a heating rate of 5 °C min^{-1}. Infrared spectra were measured with pure samples on a Perkin-Elmer BXII FT-IR system with a Smith DuraSampler IR II diamond ATR. Determination of the carbon, hydrogen and nitrogen contents was carried out by combustion analysis using an Elementar Vario El (nitrogen values determined are often lower than the calculated ones due to their explosive behavior). UV-Vis spectra were recorded in the solid state using a Varian Cary 500 spectrometer in the wavelength range of 350–1000 nm. Impact sensitivity tests were carried out according to STANAG 4489[1] modified instruction[2] using a BAM (Bundesanstalt für Materialforschung und -prüfung) drop hammer.[3] Friction sensitivity tests were carried out according to STANAG 4487[4] modified instruction[5] using the BAM friction tester. The classification of the tested compounds results from the "UN Recommendations on the Transport of Dangerous Goods".[6] Additionally all compounds were tested upon the sensitivity toward electrical discharge using the Electric Spark Tester ESD 2010 EN.[7] Liquid-dried luminescent bacteria of the strain *Vibrio fischeri* NRRL-B-11177 provided by the HACH LANGE GmbH were used for the luminescent bacteria inhibition test to determine their toxicity toward aquatic organisms according to a modified procedure. All the obtained coordination compounds were washed with cold ethanol,[8] dried over night in air and used for analytics without further purification.

CAUTION! *All investigated compounds and mixtures of copper(II) chlorate and organic solvents are potentially explosive, which show partly increased sensitivities toward various stimuli (e.g., elevated temperatures, impact, friction or electrostatic discharge). Therefore, proper security precautions (safety glass, face shield, earthed equipment and shoes, leather coat, Kevlar gloves, Kevlar sleeves and ear plugs) have to be applied while synthesizing and handling the described compounds. Especially compounds **2** and **8** must be handled with great care!*

General procedure for the preparation of complexes 1–10:
Copper(II) sulfate pentahydrate (62.4 mg, 0.25 mmol) and barium chlorate monohydrate (80.6 mg, 0.25 mmol), each dissolved in 3 mL water, were combined and stirred mechanically for 10 min. The precipitated barium sulfate was filtered off and the aqueous filtrate concentrated under reduced pressure. Obtained copper(II) chlorate was dissolved in 2 mL ethanol (**1**, **3**–**5**, **7**–**10**), methanol (**2**) or water (**6**) and stoichiometric amounts of the ligand dissolved in 1 mL ethanol (**1**, **3**, **5**, **7**–**9**) or acetonitrile (**4**, **6**, **10**) were added under stirring. The solids were filtered off, washed with cold ethanol (2 mL) and dried in air.

$[Cu(ClO_3)_2(1\text{-ATRI})_4]$ (1)
The copper(II) chlorate complex **1** was obtained as blue powder. Yield: 128 mg (0.23 mmol, 90%). Evaporation of the ethanolic residue overnight gave single crystals in the form of blue blocks suitable for X-ray determination.

DTA (5 °C min^{-1}) onset: 119 °C (exothermic); IR (ATR, cm^{-1}): $\tilde{\nu}$ = 3346 (w), 3320 (m), 3257 (w), 3190 (w), 3172 (w), 3144 (w), 3121 (w), 1608 (w), 1505 (w), 1476 (w), 1339 (vw), 1239 (vw), 1220 (w), 1202 (w), 1138 (m), 1094 (m), 1047 (vw), 978 (s), 947 (vs), 925 (vs), 879 (m), 805 (s), 782 (s), 706 (w), 700 (w), 687 (w), 659 (vw), 637 (w), 608 (m); EA ($C_8H_{16}Cl_2CuN_{16}O_6$, 566.77) calcd.: C 16.95, H 2.85, N 39.54%; found: C 17.17, H 2.84, N 39.33%; BAM drop hammer: 1 J; friction tester: < 5 N; ESD: 20 mJ (at grain size < 100 µm).

$[Cu_2(4\text{-ATRI})_6](ClO_3)_4$ (2)
The water-free chlorate complex **2** was isolated as blue precipitate. Yield: 112 mg (23 mmol, 93%). Single crystal growth was achieved by overlaying an aqueous solution (8 mL) of copper(II) chlorate with an ethanolic solution (8 mL) of 4-ATRI, separated by a mixture (4 mL) of water/ethanol (50:50). After 5 days blue rods suitable for X-ray determination were obtained.

DTA (5 °C min^{-1}) onset: 186 °C (exothermic); IR (ATR, cm^{-1}): $\tilde{\nu}$ = 3279 (w), 3217 (w), 3175 (w), 3103 (w), 3078 (w), 1638 (w), 1554 (w), 1536 (w), 1401 (w), 1379 (w), 1327 (vw), 1225 (w), 1217 (w), 1096 (m), 1085 (m), 1051 (m), 974 (vs), 941 (vs), 918 (s), 903 (s), 883 (vs), 694 (w), 680 (w), 624 (s), 606 (m);

EA ($C_6H_{12}Cl_2CuN_{12}O_6$, 965.37) calcd.: C 14.93, H 2.51, N 34.82%; found: C 15.26, H 2.51, N 34.47%; BAM drop hammer: 1 J; friction tester: < 5 N; ESD: 15 mJ (at grain size < 100 µm).

$[Cu(ClO_3)_2(MTZ)_4]$ (3)
Complex **3** was isolated within 15 min in the form of blue blocks suitable for X-ray determination. Yield: 94.5 mg (0.17 mmol, 67%).

DTA (5 °C min^{-1}) onset: 159 °C (exothermic); IR (ATR, cm^{-1}): $\tilde{\nu}$ = 3175 (w), 3152 (w), 3036 (vw), 2963 (vw), 1518 (m), 1498 (w), 1471 (w), 1437 (w), 1431 (w), 1302 (w), 1188 (m), 1113 (m), 1101 (s), 1028 (w), 988 (s), 952 (vs), 899 (vs), 883 (s), 871 (s), 719 (w), 682 (m), 652 (vs), 609 (m); EA ($C_8H_{16}Cl_2CuN_{16}O_6$, 566.77) calcd.: C 16.95, H 2.85, N 39.54%; found: C 17.13, H 2.84, N 39.30%; BAM drop hammer: 3 J; friction tester: 7 N; ESD: 100 mJ (at grain size 100–500 µm).

$[Cu(ClO_3)(1\text{-}MAT)_4]ClO_3$ (4)
The square pyramidal complex **4** crystallized within 5 days in the form of blue blocks suitable for X-ray determination. Yield: 94.1 mg (0.15 mmol, 60%).

DTA (5 °C min^{-1}) onset: 157 °C (exothermic); IR (ATR, cm^{-1}): $\tilde{\nu}$ = 3420 (w), 3321 (w), 3207 (w), 1644 (s), 1593 (m), 1505 (m), 1454 (w), 1427 (vw), 1378 (w), 1355 (w), 1233 (vw), 1138 (vw), 1074 (w), 1056 (w), 1042 (w), 984 (m), 952 (vs), 921 (vs), 780 (m), 736 (w), 689 (m), 680 (w), 608 (w); EA ($C_8H_{20}Cl_2CuN_{20}O_6$, 626.83) calcd.: C 15.33, H 3.22, N 44.69%; found: C 15.58, H 3.23, N 43.73%; BAM drop hammer: 2 J; friction tester: 16 N; ESD: 110 mJ (at grain size < 100 µm).

$[Cu(ClO_3)_2(H_2O)_2(2\text{-}MAT)_2]$ (5)
Single crystals of compound **5** in the form of colorless blocks were obtained by slow evaporation overnight. Yield: 113 mg (0.24 mmol, 98%).

DTA (5 °C min^{-1}) onset: 125 °C (exothermic); IR (ATR, cm^{-1}): $\tilde{\nu}$ = 3417 (m), 3321 (m), 3245 (m), 3173 (m), 3052 (w), 1641 (s), 1565 (w), 1445 (m), 1422 (w), 1388 (w), 1349 (vw), 1334 (w), 1195 (w), 1138 (vw), 1108 (vw), 1013 (s), 909 (vs), 813 (m), 748 (m), 678 (vw), 649 (m), 609 (m), 533 (w), 525 (w); EA ($C_4H_{14}Cl_2CuN_{10}O_8$, 464.67) calcd.: C 10.34, H 3.04, N 30.14%; found: C 10.52, H 2.91, N 29.93%; BAM drop hammer: 2 J; friction tester: < 5 N; ESD: 50 mJ (at grain size 100–500 µm).

$[Cu(1,1\text{-}dtp)_3](ClO_3)_2$ (6)
Compound **7** crystallized within one day in the form of blue blocks. Yield: 143 mg (0.19 mmol, 74%).

DTA (5 °C min^{-1}) onset: 168 °C (exothermic); IR (ATR, cm^{-1}): $\tilde{\nu}$ = 3107 (m), 2999 (vw), 2977 (vw), 1573 (vw), 1505 (m), 1451 (w), 1431 (m), 1376 (w), 1341 (vw), 1289 (vw), 1250 (vw), 1174 (s), 1146

(w), 1097 (s), 1068 (w), 969 (vs), 937 (s), 910 (m), 877 (m), 721 (vw), 697 (w), 667 (w), 648 (m), 619 (m), 604 (m); EA ($C_{15}H_{24}Cl_2CuN_{24}O_6$, 770.97) calcd.: C 23.37, H 3.14, N 43.60%; found: C 23.10, H 3.03, N 42.52%; BAM drop hammer: 2 J; friction tester: 18 N; ESD: 100 mJ (at grain size < 100 µm).

$[Cu(ClO_3)_2(1,2\text{-dtp})_2]$ (7)

The water-free coordination compound **7** precipitated as a blue powder. Yield: 90.2 mg (0.15 mmol, 61%). Blue crystals suitable for X-ray determination were obtained from methanol as solvent.

DTA (5 °C min^{-1}) onset: 162 °C (exothermic); IR (ATR, cm^{-1}): $\tilde{\nu}$ = 3159 (w), 3126 (w), 1517 (w), 1460 (m), 1446 (w), 1366 (w), 1356 (w), 1304 (w), 1247 (w), 1198 (w), 1188 (m), 1163 (w), 1147 (m), 1108 (m), 1088 (w), 1059 (vw), 1044 (vw), 1030 (w), 992 (s), 962 (vs), 920 (s), 904 (m), 888 (s), 828 (m), 724 (w), 701 (m), 683 (m), 659 (m), 639 (w), 601 (m), 506 (vw); EA ($C_{10}H_{16}Cl_2CuN_{16}O_6$, 590.79) calcd.: C 20.33, H 2.73, N 37.93%; found: C 20.42, H 2.69, N 37.63%; BAM drop hammer: 1 J; friction tester: 9 N; ESD: 100 mJ (at grain size 100–500 µm).

$[Cu(ClO_3)_2(2,2\text{-dtp})_2]$ (8)

Compound **8** precipitated as blue powder. Yield: 82.9 mg (0.14 mmol, 56%). Single crystals were obtained within 9 days by slow evaporation of an aqueous solution in the form of blue plates.

DTA (5 °C min^{-1}) onset: 176 °C (exothermic); IR (ATR, cm^{-1}): $\tilde{\nu}$ = 3130 (w), 3044 (vw), 2997 (vw), 1469 (w), 1450 (w), 1427 (vw), 1373 (w), 1346 (w), 1309 (w), 1301 (w), 1195 (w), 1157 (w), 1144 (m), 1137 (m), 1065 (vw), 1049 (w), 994 (s), 962 (vs), 930 (m), 889 (vs), 839 (m), 799 (w), 763 (w), 728 (vw), 702 (m), 691 (m), 659 (vw), 632 (m), 606 (m); EA ($C_{10}H_{16}Cl_2CuN_{16}O_6$, 590.79) calcd.: C 20.33, H 2.73, N 37.93%; found: C 20.61, H 2.74, N 37.68%; BAM drop hammer: 1 J; friction tester: < 5 N; ESD: 50 mJ (at grain size 100–500 µm).

$[Cu(H_2O)_2(i\text{-dtp})_2](ClO_3)_2$ (9)

The diaqua complex **9** was isolated as light blue solid. Yield: 84.7 mg (0.14 mmol, 54%). Slow evaporation of an aqueous solution resulted in single crystals in the form of blue blocks suitable for X-ray determination.

DTA (5 °C min^{-1}) onset: 140 °C (endothermic), 156 °C (exothermic); IR (ATR, cm^{-1}): $\tilde{\nu}$ = 3399 (w), 3148 (w), 3121 (w), 1644 (w), 1514 (w), 1491 (w), 1437 (m), 1393 (w), 1378 (vw), 1361 (vw), 1306 (w), 1286 (w), 1212 (vw), 1186 (m), 1175 (m), 1161 (w), 1130 (w), 1110 (w), 1097 (m), 1087 (m), 1040 (w), 1004 (s), 921 (vs), 894 (s), 754 (m), 719 (w), 675 (m), 667 (m), 633 (m), 603 (s); EA ($C_{10}H_{20}Cl_2CuN_{16}O_8$, 626.82) calcd.: C 19.16, H 3.22, N 35.75%; found: C 19.25, H 3.17, N 35.62%; BAM drop hammer: 1 J; friction tester: 32 N; ESD: 65 mJ (at grain size 100–500 µm).

[Cu(ClO$_3$)$_2$(dtb)$_2$] (10)

Product **10** was obtained as blue solid. Yield: 115 mg (0.19 mmol, 74%). Evaporation of aqueous solutions gave small amounts of single crystals suitable for X-ray determination.

DTA (5 °C min^{-1}) onset: 157 °C (exothermic); IR (ATR, cm^{-1}): $\tilde{\nu}$ = 3156 (vw), 3107 (w), 1511 (w), 1503 (w), 1468 (w), 1452 (w), 1442 (w), 1434 (w), 1392 (w), 1355 (vw), 1187 (m), 1169 (w), 1149 (w), 1106 (m), 1095 (m), 1055 (vw), 1013 (s), 950 (s), 898 (s), 877 (vs), 841 (m), 733 (m), 715 (w), 679 (m), 659 (m), 645 (m), 604 (s); EA ($C_{12}H_{20}Cl_2CuN_{16}O_6$, 618.85) calcd.: C 23.29, H 3.26, N 36.21%; found: C 23.31, H 3.21, N 35.01%; BAM drop hammer: 3 J; friction tester: 32 N; ESD: 100 mJ (at grain size < 100 µm).

10.6.2. Synthesis

The copper(II) complexes **3**–**6** (Scheme S1) were obtained as single crystals suitable for X-ray diffraction within minutes or days directly from the mother liquor in reasonable to very good yields (60–98%). Compound **1**, **2**, and **7**–**10** precipitated within 5 minutes as light to dark blue solids in satisfying to very good yields (54–93%). It was possible to isolate small amounts of single crystals suitable for X-ray experiments out of the ethanolic (**1**), methanolic (**7**), or aqueous (**8**–**10**) reaction mixtures. Crystal growth of **2** was achieved by layering to ensure slow formation at the phase boundary. All products were filtered off, washed with cold ethanol to remove unreacted starting materials and dried in air.

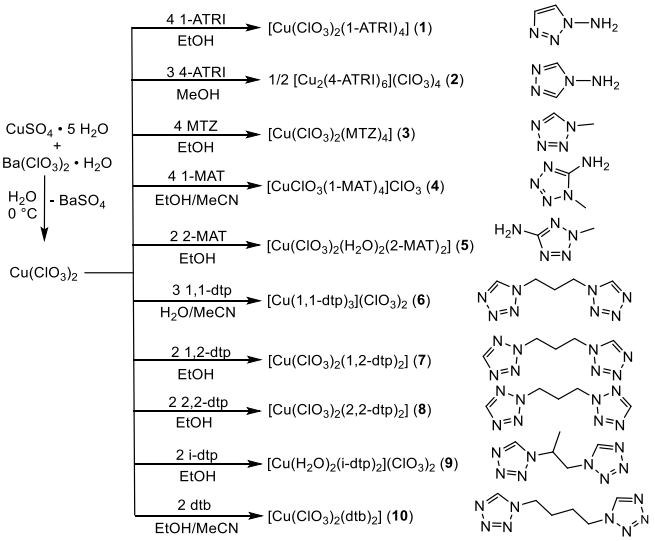

Scheme S1. Synthesis of the complexes **1**–**10** starting from copper(II) sulfate and barium chlorate; Overview of used nitrogen-rich ligands: 1-ATRI: 1-amino-1,2,3-triazole; 4-ATRI: 4-amino-1,2,4-triazole; MTZ: 1-methyl-5*H*-tetrazole; 1-MAT: 1-methyl-5-aminotetrazole; 2-MAT: 2-methyl-5-aminotetrazole; 1,1-dtp: 1,3-di(tetrazol-1-yl)propane; 1,2-dtp: 1-(tetrazol-1-yl)-3-(tetrazol-2-yl)propane; 2,2-dtp: 1,3-di(tetrazol-2-yl)propane; i-dtp: 1,1'-(propane-1,2-diyl)bis(tetrazole); dtb: 1,4-di(tetrazol-1-yl)butane.

10.6.3. Crystal Structures

All complexes were characterized by low temperature single crystal X-ray diffraction. The crystal structures were uploaded to the CSD database[9] and can be obtained free of charge with the CCDC nos. 1574490 (**1**), 1574486 (**2**), 1574482 (**3**), 1574487 (**4**), 1574489 (**5**), 1574485 (**6**), 1574481 (**7**), 1574484 (**8**), 1574483 (**9**), 1574488 (**10**). The bond lengths and angles of the coordinating ligands in the analyzed complexes are in the typical range of tetrazole and triazole ligands and nearly the same as in the non-coordinating ligands.[10] The ligands are therefore not part of the discussion in any of the following coordination compounds. All copper(II) chlorate complexes, except compound **4**, show an octahedral coordination with a Jahn-Teller distortion along the axial coordination sphere. $[Cu(ClO_3)_2(1\text{-ATRI})_4]$ (**1**) crystallizes in the form of blue blocks in the triclinic space group *P*−1 with one formula unit per unit cell and a calculated density of 1.916 g cm^{-3} at 100 K. The octahedral coordination sphere around the copper(II) cation (Figure S1) is built up of two chlorato ligands in axial positions and four aminotriazole molecules in a plane.

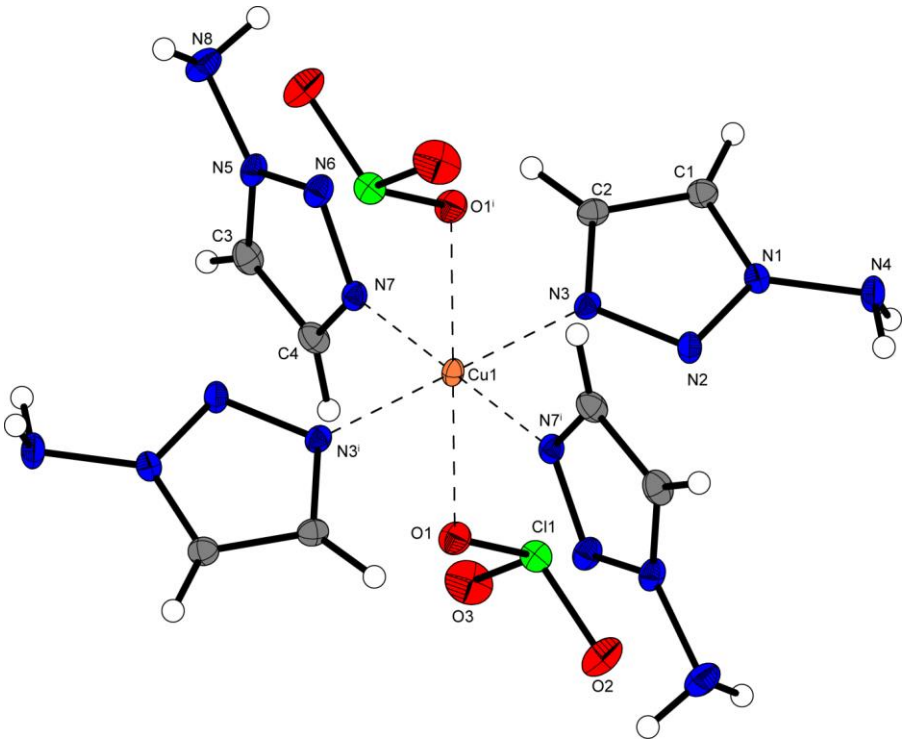

Figure S1. Molecular unit of $[Cu(ClO_3)_2(1\text{-ATRI})_4]$ (**1**). Selected bond lengths (Å): Cu1–O1 2.3698(17), Cu1–N3 2.027(2), Cu1–N7 2.026(2); selected bond angles (°): O1–Cu1–N3 93.77(7), O1–Cu1–N7 90.47(7), N3–Cu1–N7 88.76(8). Symmetry code: (i) 1−x, −y, 2−z.

The water-free compound **2** crystallizes in the form of blue rods in the monoclinic space group *C*2/*m* with four formula units per unit cell and a calculated density of 1.964 g cm^{-3} at 143 K. The molecular unit

contains two different copper(II) ions (Figure S2), each is octahedrally coordinated by six donor atoms. Complex **2** and **6** are the only presented compounds with copper(II) ions exclusively coordinated by nitrogen atoms. Both center atoms show a Jahn-Teller distortion, whereas Cu1 shows a rare compressed coordination sphere with shorter axial Cu–N bonds compared to the equatorial ones. The stretched coordination environment of Cu2 is composed of longer axial and shorter equatorial Cu–N-bonds. Two copper(II) atoms are bridged by three bidental ligands building up polymeric chains. In comparison to compound **1**, the chlorates are not participating in coordination and act only as counter anions. $[Cu(ClO_3)_2(MTZ)_4]$ (**3**), the structural isomer of **1**, crystallizes in the form of blue blocks in the monoclinic space group $P2_1/n$ with two formula units per unit cell and a calculated density of 1.807 g cm^{-3} at 173 K. Similar to compound **1**, the molecular unit is composed of one central metal (Figure S3) with two coordinating chlorato ligands in axial positions and four ligand molecules in a plane with comparable bond lengths to complex **1**. In comparison to complex **1**, coordination compound **4** with a calculated density of 1.832 g cm^{-3} at 173 K, crystallizes in the same monoclinic space group $P2_1/n$ but with an extraordinary square pyramidal coordination sphere and four formula units per unit cell. The molecular unit is made up of one metal cation (Figure S4), one axial coordinated chlorato ligand, four coordinating ligands in a plane and one non-coordinating counter anion. Compared to all other presented coordination compounds, the lower number of ligands around the copper(II) ion leads to shorter Cu–N-bonds.

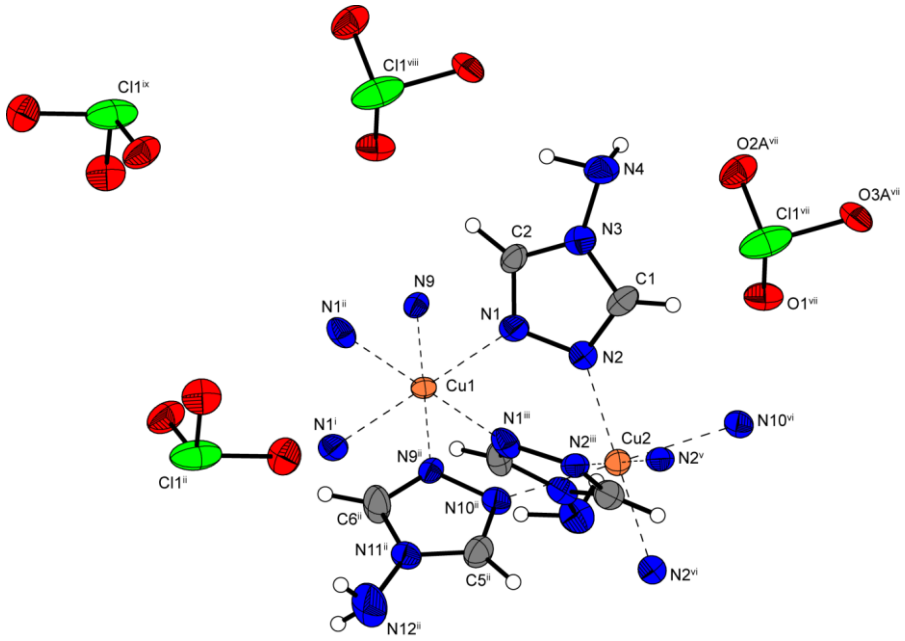

Figure S2. Copper(II) coordination environment of $[Cu_2(4\text{-ATRI})_6](ClO_3)_4$ (**2**). Selected bond lengths (Å): Cu1–N1 2.172(6), Cu1–N9 2.035(7), Cu2–N2 2.039(5), Cu2–N10^{ii} 2.411(7); selected bond angles (°): N1–Cu1–N9 89.34(17), N1–Cu1–N1^{ii} 91.5(2), N1^{ii}–Cu1–N9 90.66(17), N2–Cu2–N2^{iii} 91.01(19), N2–Cu2–N10^{ii} 87.66(17). Symmetry codes: (i) 1−x, 1−y, −z; (ii) 1−x, y, −z; (iii) x, 1−y, z; (iv) 1−x, 1−y, 1−z; (v) 1−x, y, 1−z; (vi) x, y, 1+z; (vii) 0.5−x, 0.5−y, 1−z; (viii) 0.5−x, 0.5−y; −z; (ix) 0.5+x, 0.5−y, −1+z.

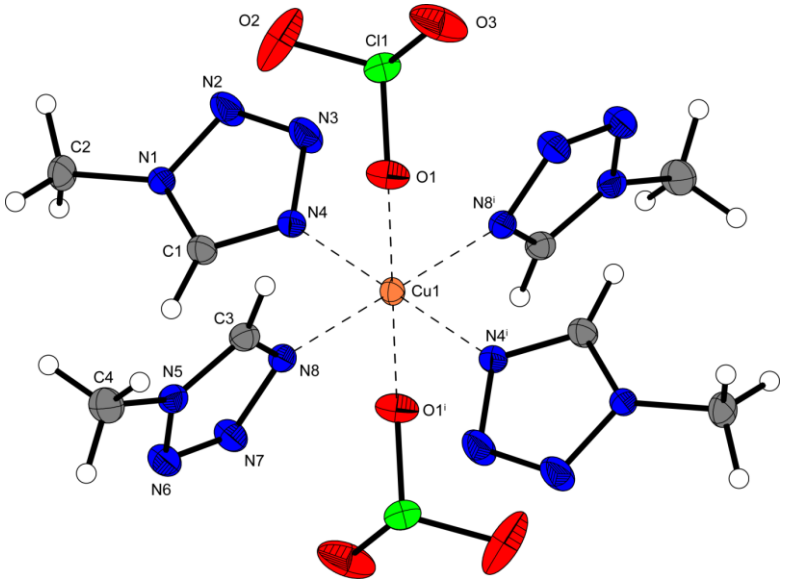

Figure S3. Molecular unit of $[Cu(ClO_3)_2(MTZ)_4]$ (**3**). Selected bond lengths (Å): Cu1–O1 2.3458(14), Cu1–N4 2.0206(15), Cu1–N8 2.0254(15); selected bond angles (°): O1–Cu1–N4 94.78(6), O1–Cu1–N8 85.91(5), N4–Cu1–N8 89.02(6). Symmetry code: (i) 1−x, 1−y, −z.

The diaqua complex **5** crystallizes in the form of colorless blocks in the triclinic space group *P*−1 with one formula unit per unit cell and possesses the highest density (2.000 g cm^{-3} at 100 K) of all compounds. The use of 2-MAT, a constitutional isomer of 1-MAT, is favoring an octahedral coordination sphere around the copper(II) cation (Figure S5) with two chlorato, two aqua and two tetrazole ligands.

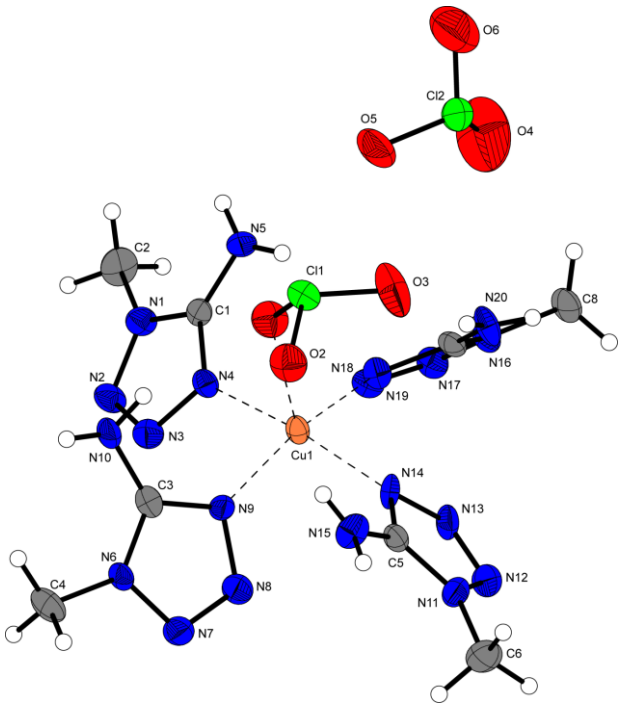

Figure S4. Molecular unit of $[CuClO_3(1\text{-}MAT)_4]ClO_3$ (**4**). Selected bond lengths (Å): Cu1–O1 2.369(7), Cu1–N4 2.020(7), Cu1–N9 1.963(6), Cu1–N14 2.003(7), Cu1–N19 1.982(7); selected bond angles (°): O1–Cu1–N9 96.9(2), O1–Cu1–N14 106.3(2), O1–Cu1–N19 97.2(2), N4–Cu1–N9 90.2(3), N9–Cu1–N19 165.9(3).

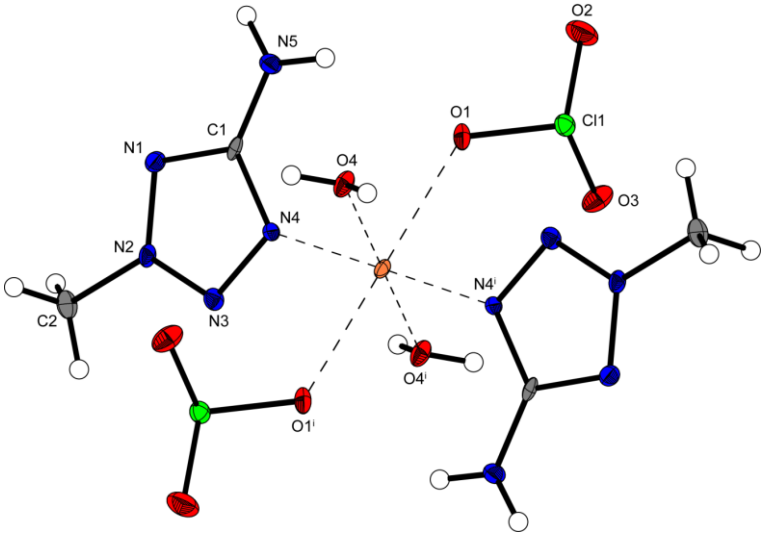

Figure S5. Molecular unit of $[Cu(ClO_3)_2(H_2O)_2(2\text{-MAT})_2]$ (**5**). Selected bond lengths (Å): Cu1–O1 2.422(3), Cu1–O4 1.983(3), Cu1–N4 1.995(3); selected bond angles (°): O1–Cu1–O4 88.56(10), O1–Cu1–N4 86.89(9), O4–Cu1–N4 91.09(12). Symmetry code: (i) −x, −y, 2−z.

The copper(II) chlorate complex **6** shows the lowest density (1.711 g cm^{-3} at 123 K) of all compounds and is the only trigonal crystal structure. It crystallizes in the form of blue blocks in the space group *P*−3*c*1 with two formula units per unit cell. The molecular unit contains one copper(II) cation (Figure S6) with three coordinating ditetrazole ligands and two non-coordinating chlorate anions. Two copper(II) cations are linked by three bidental ligands, building up linear polymeric chains.

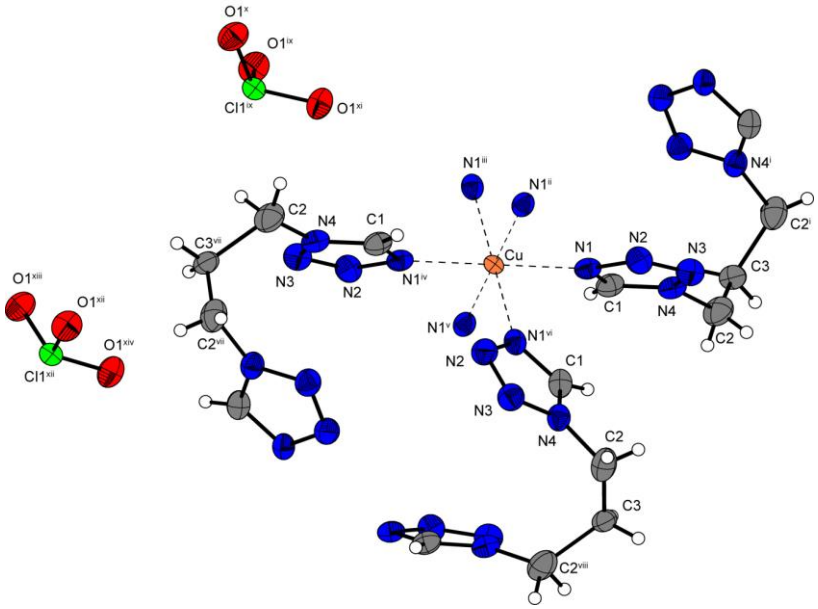

Figure S6. Copper(II) coordination environment of $[Cu(1,1\text{-dtp})_3](ClO_3)_2$ (**6**). Selected bond length (Å): Cu–N1 2.1280(17); selected bond angles (°): N1–Cu1–N1^{ii} 91.17(7), N1–Cu1–N1^{iii} 91.18(8), N1–Cu1–N1^{v} 88.82(8). Symmetry codes: (i) −x, −x+y, 0.5−z; (ii) −x+y, −x, z; (iii) −y, x−y, z; (iv) −x, −y, −z; (v) x−y, x, −z; (vi) y, −x+y, −z; (vii) x, x−y, −0.5+z; (viii) −x+y, y, 0.5+z; (ix) −1+x, −1+y, −1+z; (x) −y, −1+x−y, −1+z; (xi) −x+y, −x, −1+z; (xii) −x+y, −1+y, −1.5+z; (xiii) −1+x, −1+x−y, −1.5+z; (xiv) −y, −x, −1.5+z.

$[Cu(ClO_3)_2(1,2\text{-dtp})_2]$ (**7**) crystallizes in the form of blue blocks in the triclinic space group *P*−1 with one formula unit per unit cell and a calculated density of 1.863 g cm^{-3} at 173 K. Compared to complex **6**, the central metal (Figure S7) is linked to one ditetrazole ligand less due to the two coordinating chlorato ligands in axial positions. Two equatorial ligands each are bridging between two cations, building up linear chains.

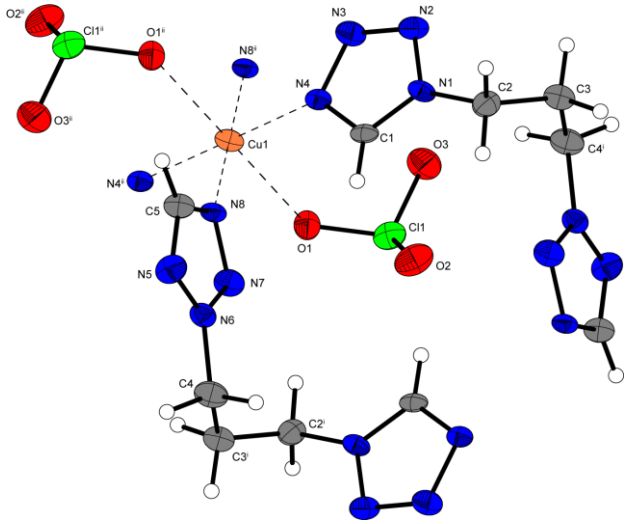

Figure S7. Copper(II) coordination environment of $[Cu(ClO_3)_2(1,2\text{-dtp})_2]$ (**7**). Selected bond lengths (Å): Cu1–O1 2.410(3), Cu1–N4 2.004(4), Cu1–N8 2.020(4); selected bond angles (°): O1–Cu1–N4 91.31(14), O1–Cu1–N8 92.09(14), N4–Cu1–N8 89.88(16). Symmetry codes: (i) 1−x, 1−y, 1−z; (ii) 1−x, −y, 1−z.

Complex compound **8** crystallizes in the form of blue plates in the monoclinic space group *C2/c* with four formula units per unit cell and a calculated density of 1.821 g cm^{-3} at 173 K. The coordination sphere around the copper(II) central metal (Figure S8) is identical to compound **7** with two coordinating chlorato ions in axial positions and two neutral ditetrazole molecules in a plane, bridging between copper(II) atoms and building up polymeric chains.

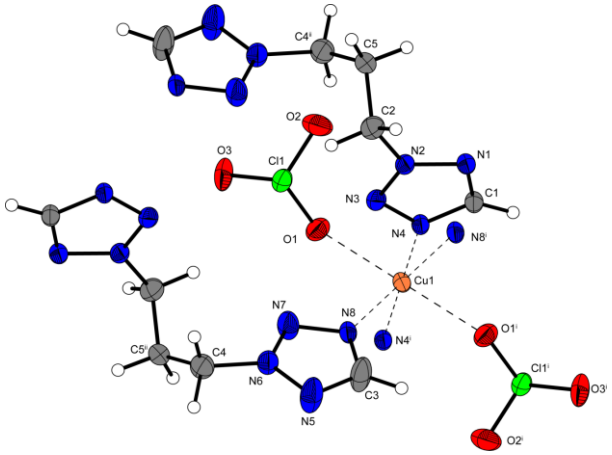

Figure S8. Copper(II) coordination environment of $[Cu(ClO_3)_2(2,2\text{-dtp})_2]$ (**8**). Selected bond lengths (Å): Cu1–O1 2.312(3), Cu1–N4 2.011(3), Cu1–N8 2.046(3); selected bond angles (°): O1–Cu1–N4 95.27(10), O1–Cu1–N8 92.25(10), N4–Cu1–N8 90.12(11). Symmetry codes: (i) 1−x, −y, 1−z; (ii) 0.5−x, 0.5−y, 1−z.

Like complex **8**, coordination compound **9**, with a calculated density of 1.764 g cm^{-3} at 173 K, crystallizes in the monoclinic space group *C*2/*c* with four formula units per unit cell. However, the chlorate counterions are not involved in the formation of the octahedron. The central metal (Figure S9) is again coordinated by two equatorial ditetrazole molecules and by two axial complexing aqua ligands instead of the chlorates. Like complex **6** and **7**, the nitrogen-rich ligands are bridging between the copper(II) ions, building up polymeric chains.

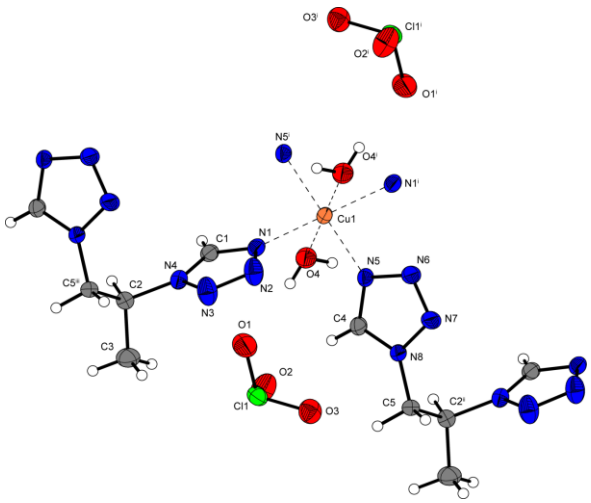

Figure S9. Copper(II) coordination environment of $[Cu(H_2O)_2(i\text{-}dtp)_2](ClO_3)_2$ (**9**). Selected bond lengths (Å): Cu1–O4 2.2951(18), Cu1–N1 2.0498(18), Cu1–N5 2.0307(17); selected bond angles (°): O4–Cu1–N1 86.35(7), O4–Cu1–N5 90.43(7), N1–Cu1–N5 89.54(7). Symmetry codes: (i) 1−x, −y, −z; (ii) −0.5+x, −0.5+y, z; (iii) 0.5+x, 0.5+y, z.

The copper(II) chlorate complex **10** crystallizes in the form of blue blocks in the monoclinic space group $P2_1/n$ with two formula units per unit cell and a calculated density of 1.840 g cm^{-3} at 143 K. The molecular unit consists of one copper(II) cation (Figure S10), two coordinating chloratos and two bridging ditetrazole ligands. In contrast to compounds **7**–**9**, each ligand is linking two different copper(II) atoms, which leads to the formation of a 2D-network.

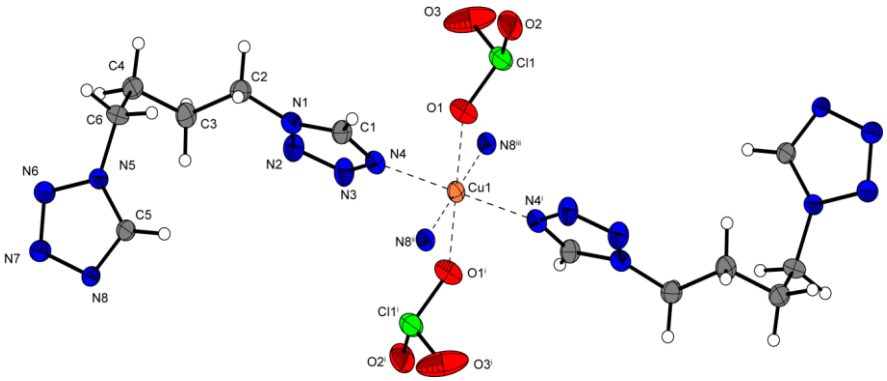

Figure S10. Copper(II) coordination environment of $[Cu(ClO_3)_2(dtb)_2]$ (**10**). Selected bond lengths (Å): Cu1–O1 2.360(3), Cu1–N4 2.017(3), Cu1–N8 2.050(2); selected bond angles (°): O1–Cu1–N4 86.63(10), O1–Cu1–N8 96.25(9), N4–Cu1–N8 91.93(10). Symmetry code: (i) 1−x, −1−y, 1−z.

10.6.4. Sensitivities and Thermal Stability

For the investigation of endothermic events, like dehydration or melting and for the determination of the thermal stabilities, DTA measurements with a heating rate of $\beta = 5\ °C\ min^{-1}$ were performed. The sensitivities of the complexes toward impact, friction and electric discharge have been determined according to BAM standards and all compounds were classified in accordance to the UN recommendations on the transport of dangerous goods. An overview of the physicochemical properties of all compounds is given in Tables S1 and S2. Only one endothermic occasion has been observed for coordination compound **9** (Figure S12) which loses its aqua ligands at 140 °C. The other diaqua complex **5** (Figure S11) exhibits only an exothermic event at 125 °C. One possible explanation for the thermal stability of compound **9** could be the formation of a stable water-free species which decomposes at a later stage, whereas compound **5** directly decomposes after the loss of the water molecules.

Table S1. Physicochemical properties of compounds **1**–**5**.

	1	**2**	**3**	**4**	**5**
Formula	$C_8H_{16}Cl_2CuN_{16}O_6$	$C_{12}H_{24}Cl_4Cu_2N_{24}O_{12}$	$C_8H_{16}Cl_2CuN_{16}O_6$	$C_8H_{20}Cl_2CuN_{20}O_6$	$C_4H_{14}Cl_2CuN_{10}O_8$
FW [g mol^{-1}]	566.77	965.37	566.77	626.83	464.67
$\rho_{calc.}$ [g cm^{-3}] (*T* [K])	1.916 (100)	1.964 (143)	1.807 (173)	1.832 (173)	2.000 (100)
IS [J][a]	1	1	3	2	2
FS [N][b]	< 5	< 5	7	16	< 5
ESD [mJ][c]	20	15	100	110	50
$T_{exo.}$ [°C][d]	119	186	159	157	125
Grain size [µm]	< 100	< 100	100–500	< 100	100–500

[a] Impact sensitivity according to the BAM drop hammer (method 1 of 6). [b] Friction sensitivity according to the BAM friction tester (method 1 of 6). [c] Electrostatic discharge sensitivity (OZM ESD tester). [d] Temperature of decomposition indicated by exothermic event according to DTA (onset temperatures at a heating rate of 5 °C min^{-1}).

Table S2. Physicochemical properties of compounds **6**–**10**.

	6	**7**	**8**	**9**	**10**
Formula	$C_{15}H_{24}Cl_2CuN_{24}O_6$	$C_{10}H_{16}Cl_2CuN_{16}O_6$	$C_{10}H_{16}Cl_2CuN_{16}O_6$	$C_{10}H_{20}Cl_2CuN_{16}O_8$	$C_{12}H_{20}Cl_2CuN_{16}O_6$
FW [g mol^{-1}]	770.97	590.79	590.79	626.82	618.85
$\rho_{calc.}$ [g cm^{-3}] (*T* [K])	1.711 (123)	1.863 (173)	1.821 (173)	1.764 (173)	1.840 (143)
IS [J][a]	2	1	1	1	3
FS [N][b]	18	9	< 5	32	32
ESD [mJ][c]	100	100	50	65	100
T_{dec} [°C][d]	168	162	176	156	157
Grain size [µm]	< 100	100–500	100–500	100–500	< 100

[a] Impact sensitivity according to the BAM drop hammer (method 1 of 6). [b] Friction sensitivity according to the BAM friction tester (method 1 of 6). [c] Electrostatic discharge sensitivity (OZM ESD tester). [d] Temperature of decomposition indicated by exothermic event according to DTA (onset temperatures at a heating rate of 5 °C min^{-1}).

All other energetic coordination compounds show a higher exothermic decomposition temperature between 157 °C (**4**, **10**) and 186 °C (**2**), except complex **1**, which possesses a very low thermal stability of 119 °C. Even though no general trend for the thermal stability, regarding the coordination mode of the

chlorates, the bridging or non-bridging ligands and the chain length of the ditetrazole ligands, can be observed, it stands out that $[Cu_2(4\text{-ATRI})_6](ClO_3)_4$ (**2**) with alternating stretched and compressed Jahn-Teller distortions shows the highest decomposition temperature. This makes it, together with complex **8** (T_{dec} = 176 °C), the most promising candidates of all the presented compounds.

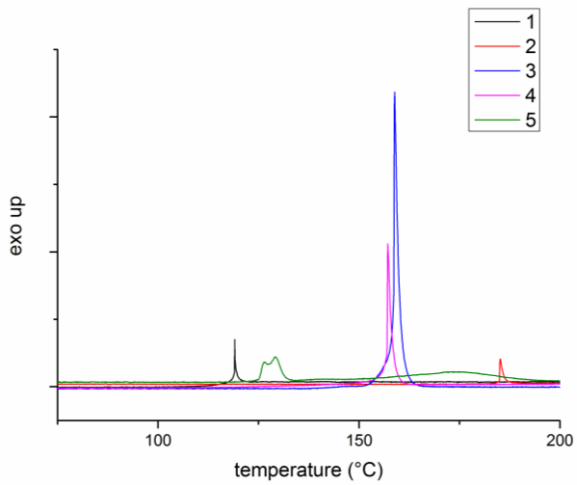

Figure S11. DTA plots (5 °C min^{-1}) of chlorate complexes **1**–**5** shown in the range of 75–200 °C.

The parameters given in Tables S1 and S2 show that all complexes are, in accordance to the UN recommendations on the transport of dangerous goods, very sensitive toward impact and friction.[21] Even though the chlorate complexes show relatively high impact sensitivities from 1–3 J, the compounds can be still handled in a safe way. In the row of ditetrazole ligands it can be seen that dtb complex **10** shows decreased sensitivities (3 J, 32 N) compared to the propyl linked compounds. Additionally, coordination compounds with non-coordinating chlorates (**6**, **9**) show a slightly higher stability (2 J, 16 N/ 1 J, 32 N) than complexes with coordinating chlorato ligands (**7**, **8**) (1 J, 9 N/ 1 J, < 5 N). Surprisingly the two aqua ligands in compound **5** do not lead to a higher stability (1 J, < 5 N) of the explosive compound compared with the anhydrous complexes.

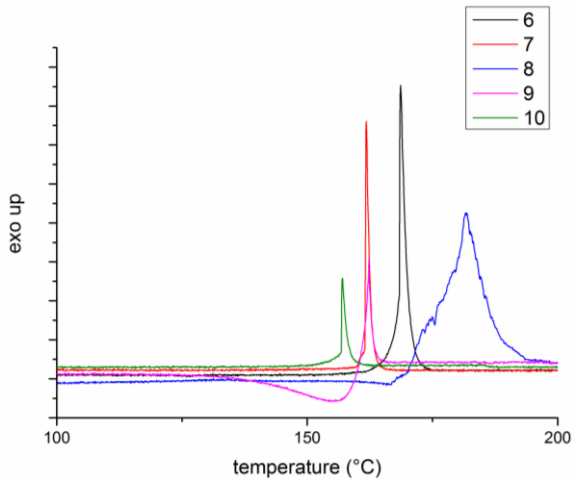

Figure S12. DTA plots (5 °C min^{-1}) of ditetrazole complexes **6**–**10** shown in the range of 100–200 °C.

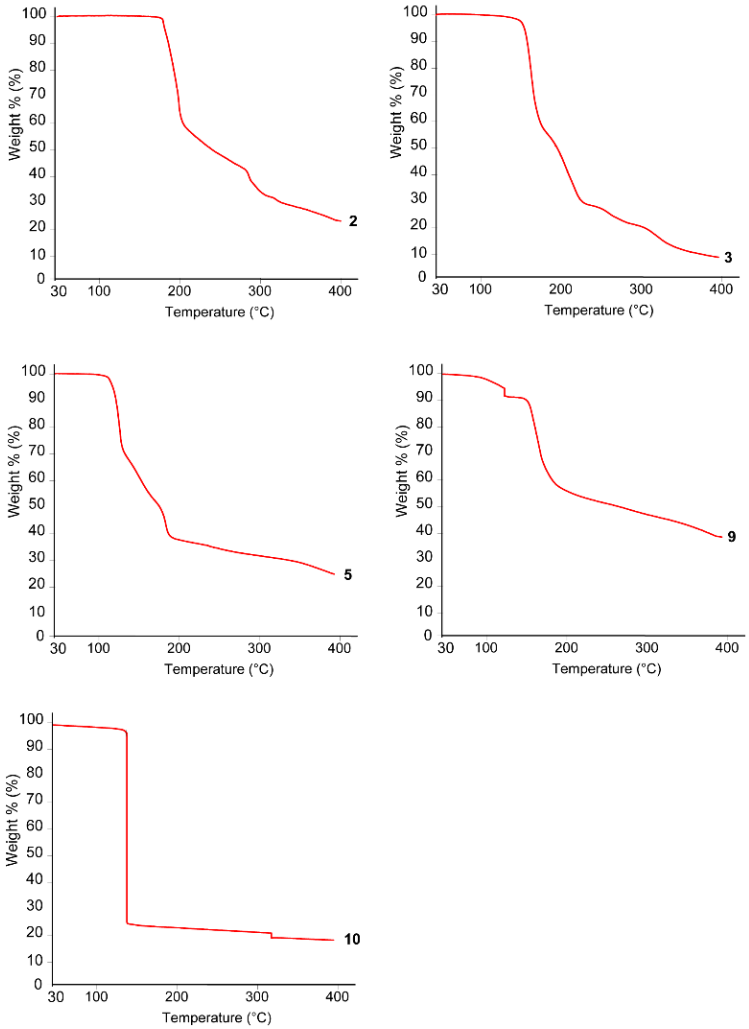

Figure S13. TG plots of selected compounds.

10.6.5. Laser Ignition Tests

The laser ignition tests were performed with a 45 W InGaAs laser diode in the single-pulsed mode. The diode was coupled directly to an optical fiber with a core diameter of 400 µm and a cladding diameter of 480 µm. The optical fiber was linked via a SMA type connecter directly to the laser and to a collimator. The collimator, in turn, was connected to an optical lens, which was stationed in its focal distance (f = 29.9 mm) to the sample. The lens was shielded from the explosive with sapphire glass. Transparent polycarbonate firing caps were filled with approx. 25 mg of the compound, pressed with a pressure force of 1 kN, and sealed by a UV-curing adhesive. The confined samples were irradiated at a wavelength of 915 nm, a varying current of 7–8 A, a voltage of 4 V, and a varying pulse length of 0.10–15 ms, which combined results in an approximately energy output of 0.17–25.5 mJ. The results of the laser experiments are summarized in Table S3. All complexes, except diaqua compound **9**, showed a detonation (Figure S14) differing in the required energy input. These results make copper(II) chlorate complexes promising compounds for laser ignition with low initiation energies.

Table S2. Results of the laser ignition tests.

	1	**2**	**3**	**4**	**5**	**6**	**7**	**8**	**9**	**10**
E_{max} [mJ]	0.20	1.70	25.5	0.43	0.20	0.20	0.43	0.85	1.70	0.85
outcome[a]	det.	det.	det.	det.	det.	det.	det.	det.	def.	det.

[a] (det. = detonation; def. = deflagration). Operating parameters: current I = 7 A; voltage U = 4 V; theoretical maximal output power P_{max} = 45 W; wavelength λ = 915 nm; pulse length τ = 0.10–15 ms.

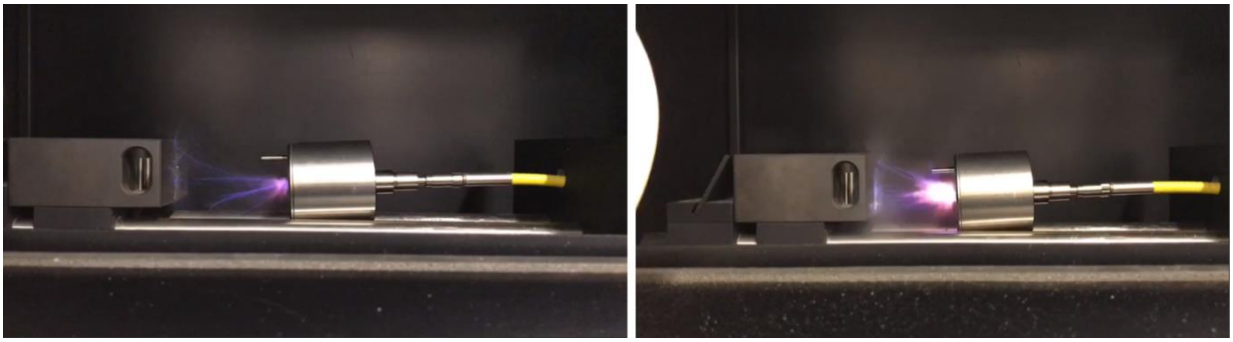

Figure S14. Moment of detonation of compounds **6** (left) and **10** (right).

10.6.6. UV-Vis Spectroscopy

In order to get insight toward a possible laser initiation mechanism, solid-state UV-Vis spectra were measured in the range of 350–1000 nm for all complexes. Compounds are shown in Figure S15. The step in the absorption intensity at 800 nm in the spectra is caused by a detector change. The UV-Vis spectra exhibit only qualitative character.

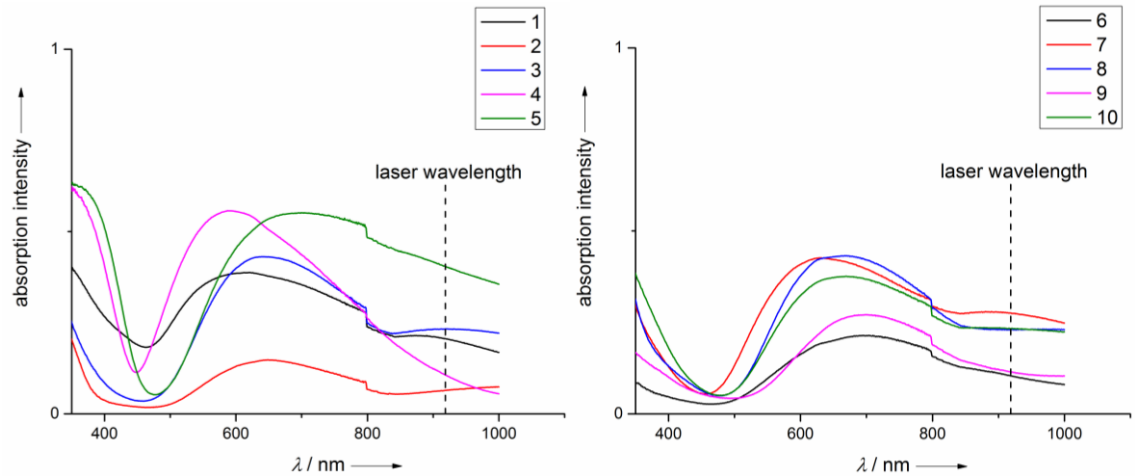

Figure S15. UV-Vis spectra in the solid-state of compounds **1**–**10**.

Due to the characteristic d-d-transitions, the spectra show absorptions in the UV, visible, and near-infrared region typical for blue copper(II) compounds with only minor deviations among each other. The mechanism for laser initiation is still not understood and many pathways such as electronically or thermally are imaginable.[11] All copper(II) chlorate complexes show absorption maxima close to 350 and 600 nm, whereas only minor absorptions occur at the laser wavelength of 915 nm. The excitation at

915 nm could be a conceivable explanation for the initiation. It is quite sure that the process of laser ignition depends on multiple parameters and more investigations are necessary for a better understanding of the laser initiation mechanism in the future.

10.6.7. Initiation Capability Tests

For the determination of the compounds' deflagration to detonation transition (DDT) capability hot plate and hot needle test were performed (Figure S16). The most promising complexes were tested in copper shell initiation tests with PETN as secondary explosive. Hot needle tests were performed by fixation of the sample underneath adhesive tape on a copper plate followed by penetration with a red heated needle.

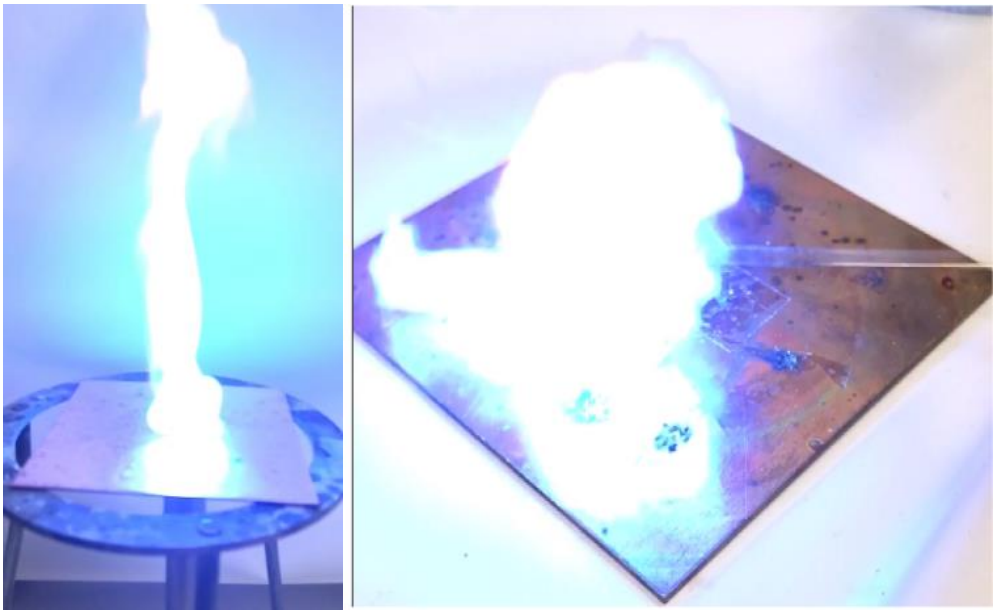

Figure S16. Left: moment of deflagration of compound **3** during the hot plate test; right: moment of detonation of compound **2** during the hot needle test.

A compound's detonation typically indicates a valuable primary explosive, whereas the safe and practicable hot plate test shows only the performance of the unconfined sample toward fast heating on a copper plate. It does not necessarily allow any conclusions on a compound's capability as a primary explosive. For the copper shell initiation tests, 200 mg of sieved PETN (grain size 100–500 µm) were filled into a shell (diameter of 7 mm, length of 88 mm) and pressed with a weight of 8 kg. On top 50 mg of the primary explosive were pressed with the same pressure force. The shell was placed in a retaining ring on a copper plate with a thickness of 1 mm and ignited with a type A electrical igniter (Figure S17). A positive DDT from the primary explosive toward the secondary PETN is indicated by a hole in the copper plate. Figure S18 illustrates the remnants of the copper plate and shell from the positive initiation tests with the most promising compounds **2** and **8**. The only other tested compound **3** showed no positive DDT from the primary explosive toward PETN.

Figure S17. left: schematic diagram of the initiation test; right: copper shell and plate test setup.

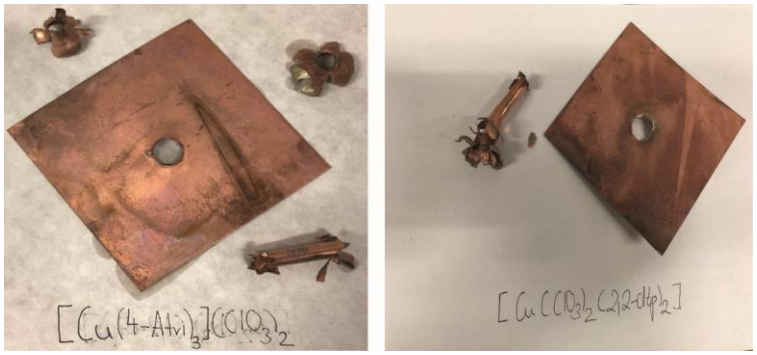

Figure S18. Positive initiation test of compound **2** (left) and **8** (right).

10.6.8. Toxicity

The toxicity measurements using the commercially available bioassay system LUMIStox test (luminescent marine bacterium *Vibrio fischeri* NRRL-B-11177) in aqueous media is a valuable indicating device when it comes to groundwater contamination. The half maximal effective concentration EC_{50} of these compounds was determined after an incubation time of 30 min (toxicity level after 30 min incubation: very toxic < 0.10 g/L; toxic 0.10–1.00 g/L; non-toxic > 1.00 g/L).[12] With a EC_{50} (30 min) value of 0.19 g/L for compound **3** it has to be considered as toxic, which is not surprising, due to the known toxicity of copper(II) compounds toward microorganisms.[13] Compared to the corresponding copper(II) perchlorate complex with a EC_{50} value of 0.13 g/L – recently published by our group[14] – the lower toxicity toward aquatic life of chlorate compounds is proven.

10.6.9. X-Ray Diffraction

For all crystalline compounds, an Oxford Xcalibur3 diffractometer with a CCD area detector or Bruker D8 Venture TXS diffractometer equipped with a multilayer monochromator, a Photon 2 detector and a rotating-anode generator were employed for data collection using Mo-*K*α radiation (λ = 0.7107 Å). The

data collection and reduction were carried out using the CRYSALISPRO software.[15] The structures were solved by direct methods (SIR-92,[16] SIR-97,[17] or SHELXS-97[18]) and refined by full-matrix least-squares on *F*2 (SHELXL[4]) and finally checked using the PLATON software[19] integrated in the WinGX software suite. The non-hydrogen atoms were refined anisotropically and the hydrogen atoms were located and freely refined. The absorptions were corrected by a SCALE3 ABSPACK multiscan method.[20] All DIAMOND2 plots are shown with thermal ellipsoids at the 50% probability level and hydrogen atoms are shown as small spheres of arbitrary radius.

Table S4. Crystallographic data of **1**–**4**.

	1	**2**	**3**	**4**
Formula	$C_8H_{16}Cl_2CuN_{16}O_6$	$C_{12}H_{24}Cl_4Cu_2N_{24}O_{12}$	$C_8H_{16}Cl_2CuN_{16}O_6$	$C_8H_{20}Cl_2CuN_{20}O_6$
FW [g mol^{-1}]	566.77	965.37	566.77	626.83
Crystal system	triclinic	monoclinic	monoclinic	monoclinic
Space Group	*P*−1	*C*2/*m*	$P2_1/n$	$P2_1/n$
Color / Habit	blue block	blue rod	blue block	blue block
Size [mm]	0.03 x 0.05 x 0.07	0.10 x 0.10 x 0.15	0.16 x 0.18 x 0.21	0.09 x 0.10 x 0.19
a [Å]	7.2932(2)	13.5622(16)	7.6403(3)	13.1028(10)
b [Å]	10.9456(3)	15.5713(18)	10.0072(4)	10.7288(8)
c [Å]	12.4170(3)	7.7338(15)	13.6230(5)	16.2265(14)
α [°]	93.041(1)	90	90	90
β [°]	96.845(1)	91.559(12)	90.400(5)	95.036(7)
γ [°]	91.156(1)	90	90	90
V [Å^3]	982.43(4)	1632.6(4)	1041.56(7)	2272.3(3)
Z	2	4	2	4
$\rho_{calc.}$ [g cm^{-3}]	1.916	1.964	1.807	1.832
μ [mm^{-1}]	1.455	1.725	1.372	1.272
F(000)	574	972	574	1276
$\lambda_{MoK\alpha}$ [Å]	0.71073	0.71073	0.71073	0.71073
T [K]	100	143	173	173
θ Min–Max [°]	2.4, 26.0	4.2, 27.0	4.3, 26.0	4.2, 26.0
Dataset	−8: 8; −13: 13; −15: 15	−17: 17; −19: 19; −9: 9	−9: 8; −12: 12; −16: 16	−16: 16; −7: 13; −18: 20
Reflections collected	17068	6915	7926	17379
Independent refl.	3838	1844	2038	4436
R_{int}	0.033	0.109	0.021	0.071
Observed reflections	3421	1166	1852	3224
Parameters	333	158	153	370
R_1 (obs)[a]	0.0243	0.0716	0.0244	0.0853
wR_2 (all data)[b]	0.0940	0.1861	0.0628	0.2549
GooF[c]	1.26	1.03	1.10	1.13
Resd. Dens. [e Å^{-3}]	−0.59, 0.45	−0.57, 2.21	−0.34, 0.26	−0.81, 2.22
Absorption correction	multi-scan	multi-scan	multi-scan	multi-scan
CCDC	1574490	1574486	1574482	1574487

[a] $R_1 = \Sigma||F_0|- |F_c||/ \Sigma|F_0|$; [b] $wR_2 = [\Sigma[w(F_0^2-F_c^2)^2]/\Sigma[w(F_0)^2]]^{1/2}$; $w = [\sigma c^2(F_0^2)+(xP)^2+yP]^{-1}$ and $P = (F_0^2+2F_c^2)/3$; [c] GooF = $\{\Sigma[w(F_o^2-F_c^2)^2]/(n-p)\}^{1/2}$ (n = number of reflections; p = total number of parameters).

Table S5. Crystallographic data of **5**–**8**.

	5	**6**	**7**	**8**
Formula	$C_4H_{14}Cl_2CuN_{10}O_8$	$C_{15}H_{24}Cl_2CuN_{24}O_6$	$C_{10}H_{16}Cl_2CuN_{16}O_6$	$C_{10}H_{16}Cl_2CuN_{16}O_6$
FW [g mol^{-1}]	464.67	770.97	590.79	590.79
Crystal system	triclinic	trigonal	triclinic	monoclinic
Space Group	*P*−1	*P*−3*c*1	*P*−1	*C*2/*c*
Color / Habit	colorless block	blue block	blue block	blue plate
Size [mm]	0.03 x 0.03 x 0.04	0.10 x 0.22 x 0.29	0.04 x 0.09 x 0.13	0.08 x 0.16 x 0.34
a [Å]	6.5617(3)	10.9642(2)	6.7837(8)	14.6638(7)
b [Å]	7.5260(4)	10.9642(2)	8.182(1)	8.9883(5)
c [Å]	9.0097(4)	14.3772(4)	10.1959(12)	16.3538(8)
α [°]	111.762(2)	90	108.068(11)	90
β [°]	98.711(2)	90	101.188(10)	90.324(5)
γ [°]	104.197(2)	120	90.137(10)	90
V [Å^3]	385.81(3)	1496.78(8)	526.60(12)	2155.44(19)
Z	1	2	1	4
$\rho_{calc.}$ [g cm^{-3}]	2.000	1.711	1.863	1.821
μ [mm^{-1}]	1.826	0.987	1.361	1.331
F(000)	235	786	299	1196
$\lambda_{MoK\alpha}$ [Å]	0.71073	0.71073	0.71073	0.71073
T [K]	100	123	173	173
θ Min–Max [°]	3.0, 26.0	4.3, 26.0	4.2, 25.2	4.5, 26.0
Dataset	−8: 7; −9: 8; 0: 11	−13: 13; −13: 9; −17: 17	−7: 7; −9: 6; −10: 10	−18: 18; −11: 11; −20: 20
Reflections collected	1500	10648	2222	8158
Independent refl.	1500	989	1471	2109
R_{int}	0.040	0.032	0.039	0.058
Observed reflections	1392	825	987	1607
Parameters	144	98	160	160
R_1 (obs)[a]	0.0295	0.0289	0.0439	0.0437
wR_2 (all data)[b]	0.0635	0.0818	0.0658	0.1043
GooF[c]	1.12	1.06	0.89	1.06
Resd. Dens. [e Å^{-3}]	−0.33, 0.41	−0.24, 0.34	−0.49, 0.38	−0.34, 0.75
Absorption correction	multi-scan	multi-scan	multi-scan	multi-scan
CCDC	1574489	1574485	1574481	1574484

[a] $R_1 = \Sigma||F_0|- |F_c||/ \Sigma|F_0|$; [b] $wR_2 = [\Sigma[w(F_0^2-F_c^2)^2]/\Sigma[w(F_0)^2]]^{1/2}$; $w = [\sigma c^2(F_0^2)+(xP)^2+yP]^{-1}$ and $P = (F_0^2+2F_c^2)/3$; [c] GooF = $\{\Sigma[w(F_o^2-F_c^2)^2]/(n-p)\}^{1/2}$ (n = number of reflections; p = total number of parameters).

Table S6. Crystallographic data of **9** and **10**.

	9	**10**
Formula	$C_{10}H_{20}Cl_2CuN_{16}O_8$	$C_{12}H_{20}Cl_2CuN_{12}O_6$
FW [g mol^{-1}]	626.82	618.85
Crystal system	monoclinic	monoclinic
Space Group	*C*2/*c*	$P2_1/n$
Color / Habit	blue block	blue block
Size [mm]	0.17 x 0.23 x 0.36	0.08 x 0.17 x 0.31
a [Å]	15.0672(5)	10.7286(6)
b [Å]	9.0113(3)	6.8178(4)
c [Å]	17.5426(6)	15.5263(12)
α [°]	90	90
β [°]	97.696(3)	100.469(6)
γ [°]	90	90
V [Å^3]	2360.39(14)	1116.77(13)
Z	4	2
$\rho_{calc.}$ [g cm^{-3}]	1.764	1.840
μ [mm^{-1}]	1.226	1.289
F(000)	1276	630
$\lambda_{MoK\alpha}$ [Å]	0.71073	0.71073
T [K]	173	143
θ Min–Max [°]	4.3, 26.0	4.1, 26.0
Dataset	−18: 18; −11: 11; −21: 21	−13: 13; −8: 8; −19: 19
Reflections collected	9395	8061
Independent refl.	2306	2186
R_{int}	0.034	0.046
Observed reflections	2094	1756
Parameters	198	169
R_1 (obs)[a]	0.0310	0.0433
wR_2 (all data)[b]	0.0834	0.1155
GooF[c]	1.08	1.09
Resd. Dens. [e Å^{-3}]	−0.45, 0.61	−0.44, 0.90
Absorption correction	multi-scan	multi-scan
CCDC	1574483	1574488

[a] $R_1 = \Sigma||F_0|- |F_c||/ \Sigma|F_0|$; [b] $wR_2 = [\Sigma[w(F_0^2-F_c^2)^2]/\Sigma[w(F_0)^2]]^{1/2}$; $w = [\sigma c^2(F_0^2)+(xP)^2+yP]^{-1}$ and $P = (F_0^2+2F_c^2)/3$; [c] GooF = $\{\Sigma[w(F_o^2-F_c^2)^2]/(n-p)\}^{1/2}$ (n = number of reflections; p = total number of parameters).

10.6.10. IR Spectroscopy

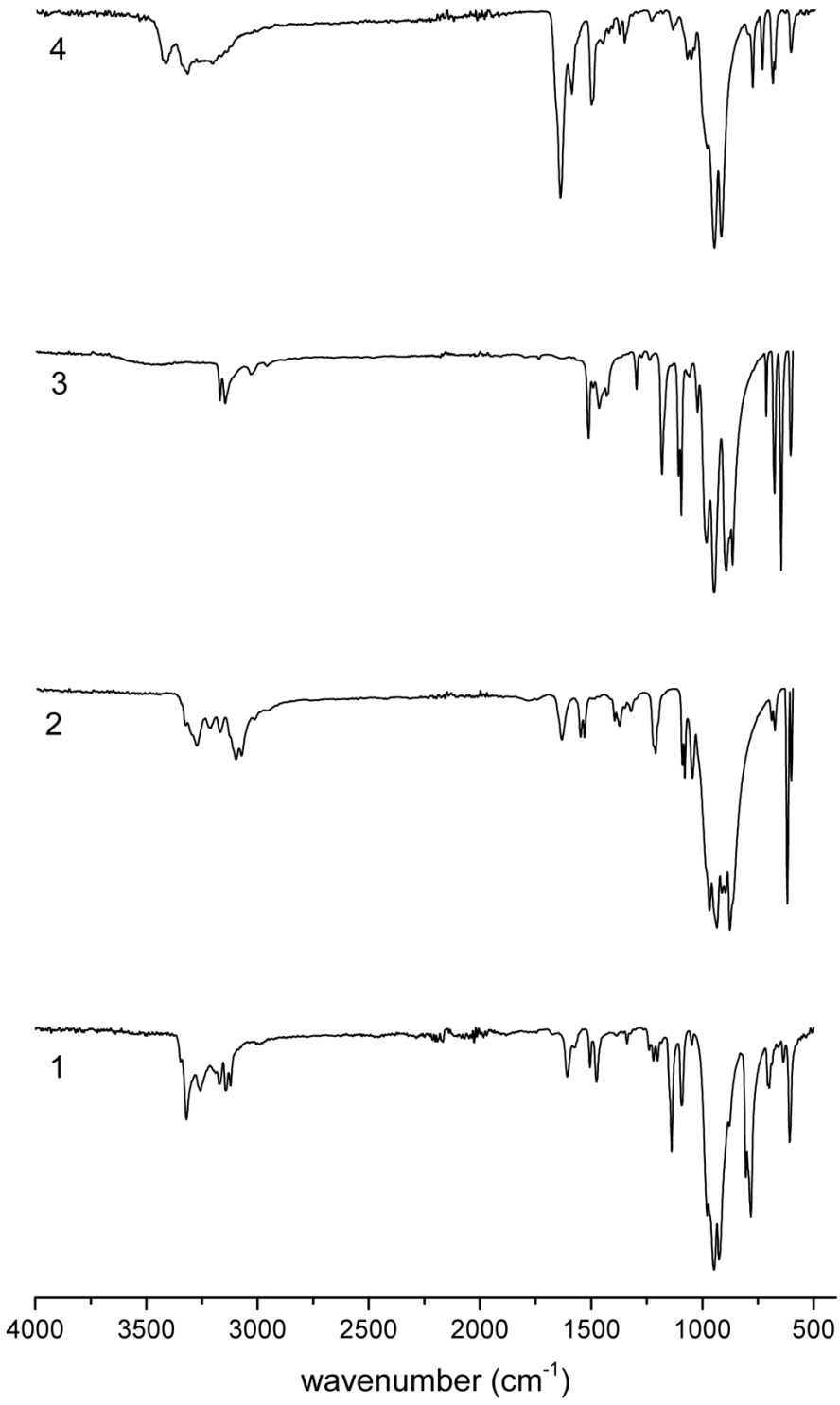

Figure S19. Infrared spectra of compounds **1**–**4**.

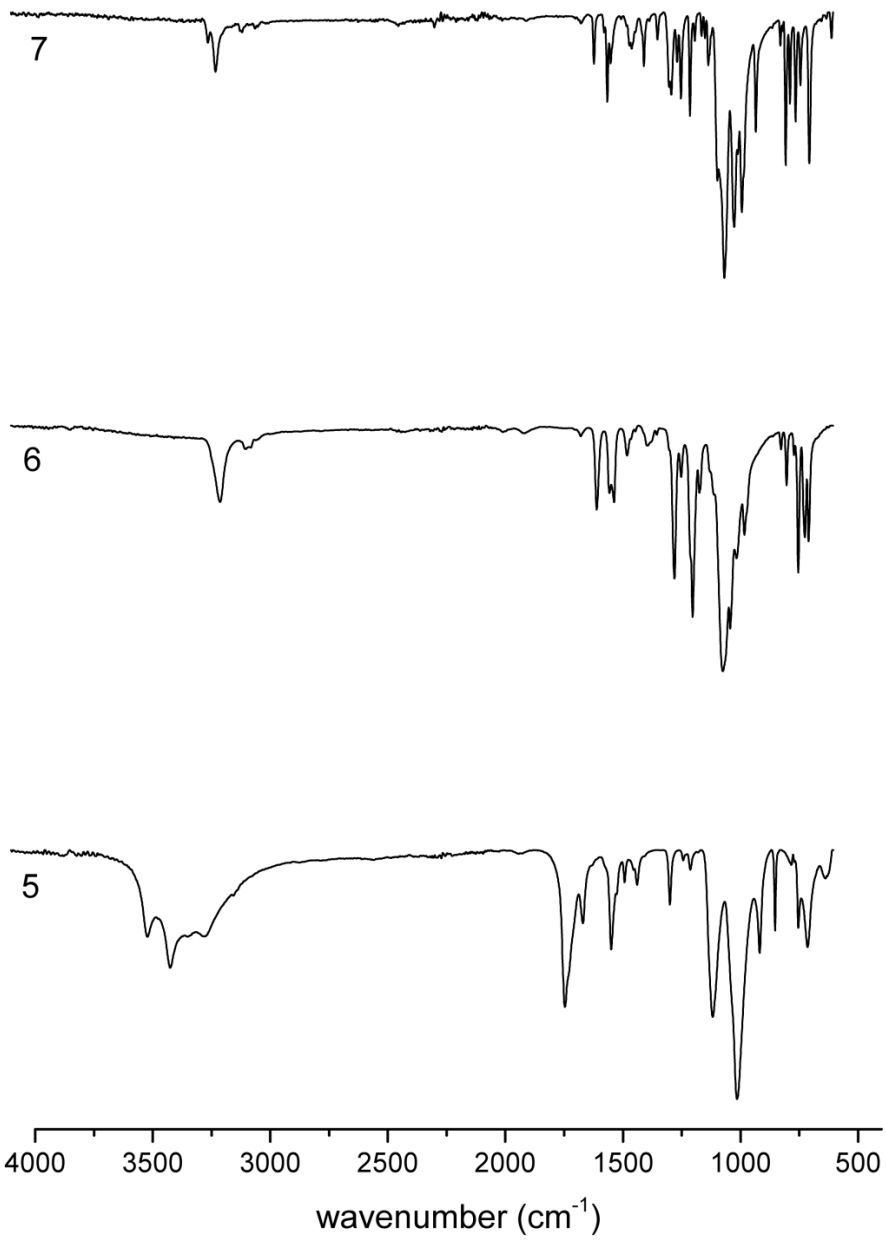

Figure S20. Infrared spectra of compounds **5**–**7**.

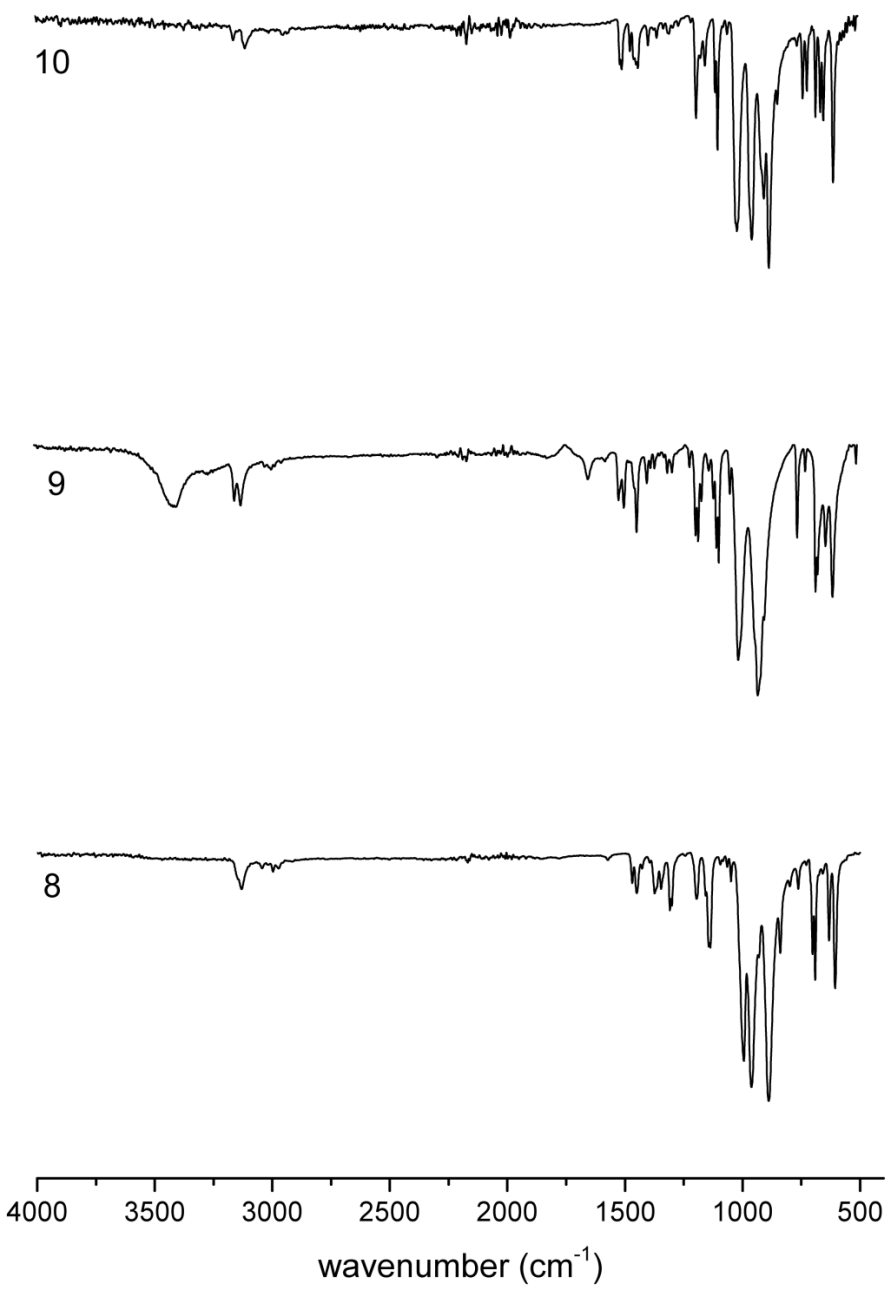

Figure S21. Infrared spectra of compounds **8**–**10**.

10.6.11. References

[1] NATO standardization agreement (STANAG) on explosives, impact sensitivity tests, no. 4489, 1st ed., Sept. 17, **1999**.

[2] WIWEB-Standardarbeitsanweisung 4-5.1.02, Ermittlung der Explosionsgefährlichkeit, hier der Schlagempfindlichkeit mit dem Fallhammer, Nov. 8, **2002**.

[3] http://www.bam.de, (accessed December 2017).

[4] NATO standardization agreement (STANAG) on explosive, friction sensitivity tests, no. 4487, 1st ed., Aug. 22, **2002**.

[5] WIWEB-Standardarbeitsanweisung 4-5.1.03, Ermittlung der Explosionsgefährlichkeit oder der Reibeempfindlichkeit mit dem Reibeapparat, Nov. 8, **2002**.

[6] Impact: insensitive > 40 J, less sensitive ≥ 35 J, sensitive ≥ 4 J, very sensitive ≤ 3 J; Friction: insensitive > 360 N, less sensitive = 360 N, sensitive < 360 N and > 80 N, very sensitive ≤ 80 N, extremely sensitive ≤ 10 N. According to the UN Recommendations on the Transport of Dangerous Goods, 5th ed., **2009**.

[7] http://www.ozm.cz, (accessed December 2017).

[8] R. Scharf, dissertation, Ludwig-Maximilians-University Munich, **2016**.

[9] Crystallographic data for the structures have been deposited with the Cambridge Crystallographic Data Centre. Copies of the data can be obtained free of charge on application to The Director, CCDC, 12 Union Road, Cambridge CB2 1EZ, UK (Fax: int.code_(1223)336-033; e-mail for inquiry: fileserv@ccdc.cam.ac.uk; e-mail for deposition: (deposit@ccdc.cam.ac.uk).

[10] (a) L. Wiehl, *Acta Cryst. B.* **1993**, *49*, 289–303. (b) D. Mueller, C. Knoll, B. Stoeger, W. Artner, M. Reissner, P. Weinberger, *Eur. J. Inorg. Chem.* **2013**, *2013*, 984–991. (c) P. J. van Koningsbruggen, Y. Garcia, O. Kahn, L. Fournès, H. Kooijman, A. L. Spek, J. G. Haasnoot, J. Moscovici, K. Provost, A. Michalowicz, F. Renz, P. Gütlich, *Inorg. Chem.* **2000**, *39*, 1891–1900.

[11] E. D. Aluker, A. G. Krechetov, A. Y. Mitrofanov, D. R. Nurmukhametov, M. M. Kuklja, *J. Phys. Chem. C* **2011**, *115*, 6893–6901.

[12] C. J. Cao, M. S. Johnson, M. M. Hurley, T. M. Klapötke, *JANNAF J. Propuls. Energet.* **2012**, *5*, 41–51.

[13] V. Ochoa-Herrera, G. Léon, Q. Banihani, J. A. Field, R. Sierra-Alvarez, *Sci. Total Environ.* **2011**, *380*, 412–413.

[14] N. Szimhardt, M. H. H. Wurzenberger, A. Behringer, L. Daumann, J. Stierstorfer *J. Mater. Chem. A* **2017**, *5*, 23753–23765.

[15] *CrysAlisPro*, Oxford Diffraction Ltd., version 171.33.41, **2009**.

[16] A. Altomare, G. Cascarano, C. Giacovazzo, A. Guagliardi, *J. Appl. Crystallogr.* **1993**, *26*, 343–350.

[17] (a) A. Altomare, G. Cascarano, C. Giacovazzo, A. Guagliardi, A. G. G. Moliterni, M. C. Burla, G. Polidori, M. Camalli, R. Spagna, *SIR97*, **1997**; (b) A. Altomare, M. C. Burla, M. Camalli, G. L. Cascarano, C. Giacovazzo, A. Guagliardi, A. G. G. Moliterni, G. Polidori, R. Spagna, *J. Appl. Crystallogr.* **1999**, *32*, 115–119.

[18] (a) G. M. Sheldrick, *SHELXL-97, Program for the Refinement of Crystal Structures*, University of Göttingen, Germany, **1997**; (b) G. M. Sheldrick, *Acta Crystallogr. Sect. A* **2008**, *64*, 112–122.

[19] A. L. Spek, *PLATON, A Multipurpose Crystallographic Tool*, Utrecht University, The Netherlands, **1999**.

[20] Empirical absorption correction using spherical harmonics, implemented in SCALE3 ABSPACK scaling algorithm (CrysAlisPro Oxford Diffraction Ltd., Version 171.33.41, **2009**).

11. Refinement of Copper(II) Azide with 1-Alkyl-5*H*-tetrazoles: Adaptable Energetic Complexes

Maximilian H. H. Wurzenberger, Marcus Lommel, Michael S. Gruhne, Norbert Szimhardt, and Jörg Stierstorfer

Published in *Angewandte Chemie International Edition* **2020**, *59*, 12367–12370 and *Angewandte Chemie* **2020**, *132*, 12466–12469.

In Memory of Rolf Huisgen

DOI: 10.1002/anie.202002823 and 10.1002/ange.202002823

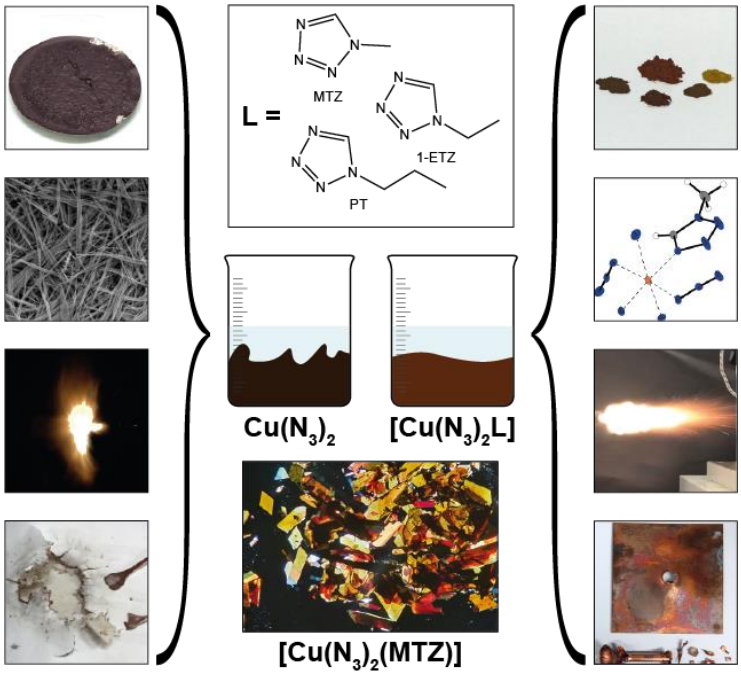

Abstract: A concept for stabilizing highly sensitive and explosive copper(II) azide with 1-*N*-substituted tetrazoles is described. It was possible to stabilize the system by the use of highly endothermic, nitrogen-rich ligands. The sensitivities of the resulting energetic copper(II) coordination compounds can be tuned further by variation of the alkyl chain of the ligands and by phlegmatization of the complexes with classical additives during the synthesis. It is demonstrated, using the compound based on 1-methyl-5*H*-tetrazole ([$Cu(N_3)_2(MTZ)$], **1**) that this class of complexes can be applied as a potential replacement for both lead azide (LA) and lead styphnate (LS). The complex was extensively investigated according to its chemical (elemental analysis, single-crystal, and powder X-ray diffraction, IR spectroscopy, scanning electron microscopy) and physicochemical properties (differential thermal analysis, sensitivities toward impact, friction, and electrostatic discharge) compared to pure copper(II) azide.

11.1. Introduction

The azide anion (N_3^-) has attracted the attention of chemists worldwide for centuries. While some are scared because of its high nitrogen content and consequent explosive character, others are attracted for the same reason. Due to their highly versatile nature, azides are not only commonly used in organic synthesis and pharmaceutics but also in energetic materials such as in airbags, propellants, and explosives.[1] In recent years, numerous new pentazolate (N_5^-) derivatives synthesized by selective C–N bond cleavage of pentazoles using mCPBA and iron glycinate generated excitement in the field.[2] The first compound of these five-membered heterocycles was described by Huisgen and Ugi. It was detected after a 1,3-dipolar cycloaddition (Huisgen reaction) of a benzene diazonium chloride and lithium azide.[3] A further current global interest is the replacement of lead-containing explosives, particularly lead azide and lead styphnate, with safer and less toxic energetic materials.[4] Various metal salts have been described as substitutes, mainly silver azide and rarely copper azides, although only cupric $Cu(N_3)_2$ (and not cuprous CuN_3) might be of practical interest. However, both azides are extremely sensitive toward impact and friction. Furthermore, $Cu(N_3)_2$ is decomposed by mineral acids as well as bases and slowly forms basic cupric azides (*e.g.*, $Cu(N_3)_2 \cdot x\ Cu(OH)_2$ (x = 1–3) and $Cu(N_3)_2 \cdot 8\ CuO$) when exposed to humidity (Figure S18 in the Supporting Information).[5] In this work, a procedure is described for the syntheses of nitrogen-rich copper(II) azide complexes involving 5*H*-tetrazoles. This concept is explained using three ligands exemplarily (1-methyl-5*H*-tetrazole (MTZ), 1-ethyl-5*H*-tetrazole (1-ETZ), and 1-propyl-5*H*-tetrazole (PT)). Moreover, many different tetrazoles, as well as triazoles, are potential candidates. The application of these compounds yielded two independent patents,[6] which can be discussed and described scientifically. In general, it is known that metal azides (*e.g.*, Mn, Nb, Ti, Zr, Hf, V, W, and Mo) can be stabilized with nitrogen donor ligands, although only some complexes of $Cu(N_3)_2$ have been reported in the literature and are rarely discussed as energetic materials.[7]

11.2. Results and Discussion

For the preparation of energetic coordination compounds (ECC) based on copper(II) azide, the implementation of nitrogen-rich ligands leads to the blockage of one coordination site, resulting in stabilization in comparison to the pure metal azide (Figure 1). The azide anion is extremely toxic to the environment and all life forms, but its effect on the ecological system depends strongly on the compounds' solubility. High water solubility implies a potent absorption through the skin and mucous membranes, leading to serious consequences for even relatively small amounts (≈ 10 mg).[8] Copper(II) azide was

chosen as the main building block due to the expected low solubility of the obtained compounds, resulting in a low risk to the environment.

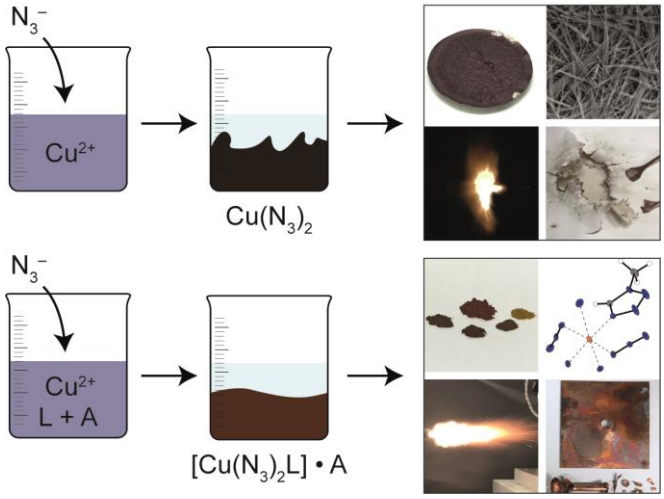

Figure 1. Top: Addition of azide to an aqueous solution of copper(II) leads to instant precipitation of copper(II) azide. Safe handling is almost impossible as the material shows characteristics of a contact explosive. Bottom: Addition of azide to an aqueous solution of copper(II), ligand (L), and additive (A) leads to precipitation of a copper(II) azide complex. The resulting compound can be safely applied as primary explosive.

The driving force for the synthesis of the copper(II) azide complexes is the instantaneous precipitation of the compounds after the addition of sodium azide. To prevent the formation of pure copper(II) azide, an aqueous solution of sodium azide was slowly added to *in situ* generated complexes of soluble copper(II) salts with ligands (Scheme 1).

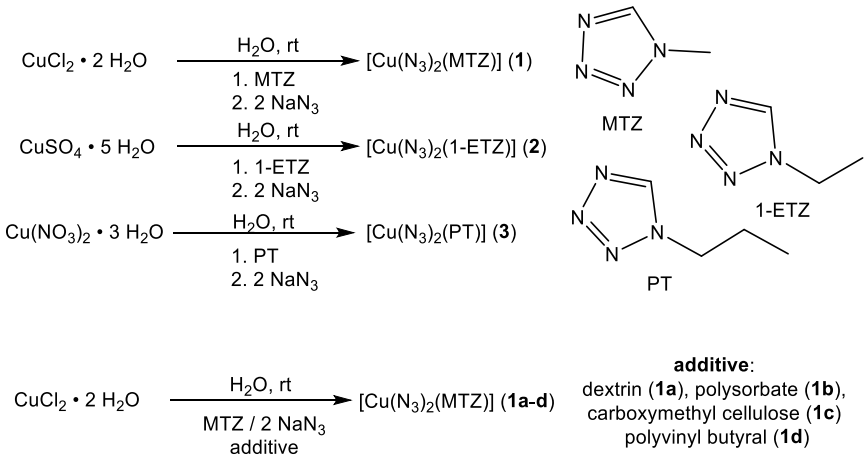

Scheme 1. Syntheses of selected tetrazole complexes **1**–**3** as pure and as phlegmatized compounds **1a**–**1d**.

The tetrazoles were synthesized starting from the corresponding alkyl amines or bromides.[9] The addition of sodium azide led to the products' formation as brown precipitates in very good yields (90–93%). The suspensions were mechanically stirred for 10 min, filtered off, washed with water as well as ethanol, and

dried in air. Single crystals suitable for X-ray diffraction were obtained by layering concentrated aqueous and ethanolic solutions to ensure slow formation at the phase boundary. It is also possible to phlegmatize the energetic coordination compounds by using common additives such as carboxymethyl cellulose during the synthesis according to modified literature procedures.[10] All compounds show a similar coordination behavior and therefore $[Cu(N_3)_2(MTZ)]$ (**1**) is discussed exemplarily for all three presented complexes. The other structures can be found in the Supporting Information (Figures S3 and S4). Compound **1** crystallizes in the form of red-brown plates in the monoclinic space group $P2_1/c$ with four formula units per unit cell and a calculated density of 2.036 g cm^{-3} at 123 K.[11] The molecular unit consists of one copper(II) central cation coordinated by one MTZ ligand in equatorial position and five azido anions (Figure 2A). The two different bridging modes of the azides (Figure 2C) favor the formation of 2D layers (Figure 2B). Two of three equatorial counterions bridge between the same two central metals (N4) and the other three azides link three different copper(II) atoms (N1 and N3).

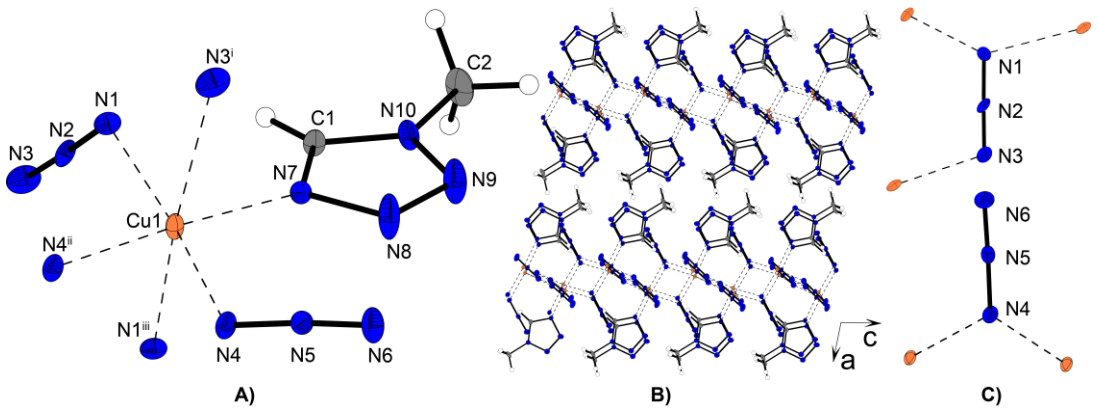

Figure 2. A) Copper(II) coordination environment of $[Cu(N_3)_2(MTZ)]$ (**1**). Selected bond lengths (Å): Cu1−N1 2.013(3), Cu1−N3^{i} 2.563(5), Cu1−N4 2.003(3), Cu1−N7 1.996(3); selected bond angles (°): N1−Cu1−N4 171.74(12), N1−Cu1−N7 90.96(12), N1−Cu1−N3^{i} 84.99(15), N4−Cu1−N7 96.59(13). Symmetry codes: (i) $-x$, $0.5+y$, $0.5-z$; (ii) $-x$, $1-y$, $1-z$; (iii) $-x$, $-0.5+y$, $0.5-z$. B) Polymeric structure of **1** caused by bridging anions along the *b* and *c* axes, leading to the formation of 2D layers stacked above each other along the *a* axis. C) Two different coordination modes of the azide anions in **1**.

Even though no difficulties were encountered during the synthesis or handling of the ECC, pure $[Cu(N_3)_2(MTZ)]$ (**1**) must be classified as very sensitive and does not possess a no-fire-level against impact and friction stimuli according to standard BAM methods. Compared to pure $Cu(N_3)_2$, which shows capricious properties when handled and can even explode when slightly touched (Figure S20), compound **1** can be easily controlled. For even safer handling and regulation of the particle size in powder form, the compound can be phlegmatized during crystallization. For the stabilization of complex **1**, the commonly used additives dextrin (**1a**), polysorbate 80 (**1b**), carboxymethyl cellulose (**1c**), and polyvinyl butyral (**1d**) were used. The phlegmatization has no significant effect on the exothermic decomposition points but in every case a more or less successful desensitization is evident. The most effective additive is

carboxymethyl cellulose (**1c**), leading to sensitivities of 2 J and 0.75 N, which are in the range of those of LA and LS (Table 1). Another approach for reducing the sensitivities of copper(II) azide complexes is the usage of tetrazole ligands with longer alkyl chains at the N1 position. The elongation of the alkyl chain to an ethyl substituent decreases the friction sensitivity to 4.5 N (**2**) and the further extension with a propyl rest to 10 N (**3**). A similar proportionality can be observed for the electrostatic discharge (ESD) values.

Table 1. Thermal stability and sensitivities against external stimuli of pure complexes **1**–**3** and phlegmatized **1** compared to pure cupric azide as well as commercially used lead azide (LA) and lead styphnate (LS).[12]

	$T_{exo.}$ [°C][a]	*IS* [J][b]	*FS* [N][c]	*ESD* [mJ][d]
$Cu(N_3)_2$	205	<< 1[5]	<< 0.1	< 0.28
1	148	< 1	< 0.1	0.79
2	134	3	4.5	33
3	148	2.5	10	112
1a	148	< 1	0.40	8.3
1b	149	1.5	0.60	3.9
1c	150	2	0.75	0.54
1d	151	4	0.45	0.33
LA	320–360	2.5–4.0	0.1–1.0	6.0–12
LS	275–280	2.5–5.0	0.5–1.5	0.02–1.0

[a] Temperature of decomposition indicated by exothermic event according to DTA (onset temperatures at a heating rate of 5 °C min^{-1}). [b] Impact sensitivity according to the BAM drop hammer (method 1 of 6). [c] Friction sensitivity according to the BAM friction tester (method 1 of 6). [d] Electrostatic discharge sensitivity (OZM XSpark10 ESD tester).

Due to the possible formation of different species, elemental analysis may represent only an average value. Confirmation of the purity of the bulk material was therefore exemplarily achieved through powder diffraction measurements of compounds **1** and **2** (Figure S5). Scanning electron microscopy (SEM) was performed to investigate the compounds' morphology and to further examine the influence of the phlegmatization on the crystal habitus and size. It can be seen that the pure copper(II) azide forms agglomerates made of very fine, intergrown crystalline fibers, which are the reason for its high mechanical sensitivity. Pure complex **1** shows a distribution of crystallites. The different additives used for phlegmatization make it possible to tune the crystal morphology (plate- or needle-like) and corresponding size distribution (Figure 3 and S6–S11). For use as a potential LA replacement, ECC **1** was tested in classical initiation capability tests. Therefore, 200 mg of the common secondary explosives pentaerythritol tetranitrate (PETN) and 1,3,5-trinitro-1,3,5-triazinane (RDX) was pressed into copper shells and initiated with either pure complex **1** or the most promising phlegmatized complex (**1c**). Further information on the test setup can be found in the Supporting Information (Figure S14). As little as 5 mg of compound **1** is able to initiate RDX reliably, making the compound an extremely efficient initiating substance (Figure 4).

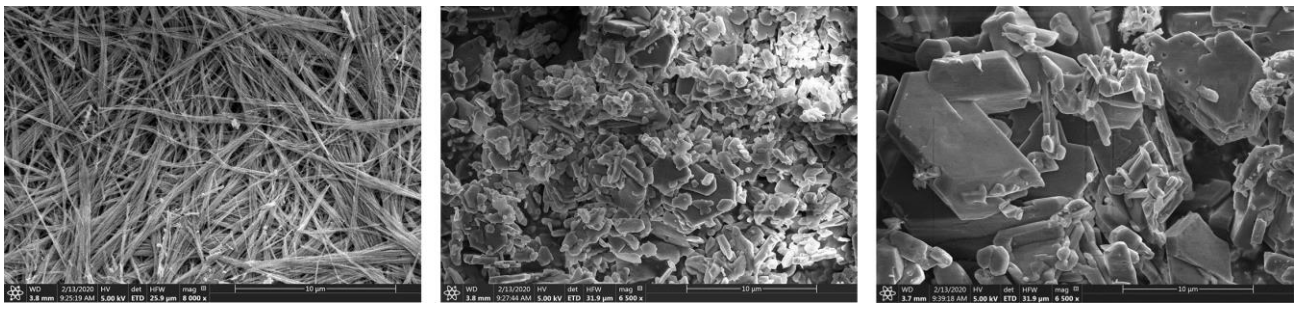

Figure 3. SEM images of $Cu(N_3)_2$ (8000× enlargement), pure complex **1** (6500× enlargement) and dextrinated **1a** (6500× enlargement).

Figure 4. Positive PETN (left) and RDX (right) initiation tests with 5 mg of the coordination compound **1**.

The initiating properties of **1** far outstrip those of recently published green primary explosives with claimed outstanding initiation efficiency.[13] The phlegmatized complex **1c** (50 mg) also showed positive results in initiating both PETN and RDX (Figure S15). Apart from its intended use as a potential replacement for lead azide, **1** can also serve as a replacement for lead styphnate for the use in priming mixtures (PM). Since the beginning of the 20th century, LS has been one of the most commonly used primary explosives in PM, which are applied to produce a flame instead of a detonation and are mostly utilized in percussion caps.[5] Complex **1** was used for the preparation of a lead-free PM, which was compared to a commercially available one based on lead styphnate. The PM consisted of 15% $[Cu(N_3)_2(MTZ)]$ as well as 85% of a mixture made up of barium nitrate, aluminum, antimony trisulfide, and PETN. The created flame is sufficient for the inflammation of propellant powder (Figure 5). The resulting time-pressure curve generated with a 7.62 NATO cartridge filled with nitrocellulose powder shows an ideal gradient (Figure S17 and Table S3). The sensitivities of the new PM are similar to values of a commercial mixture (Table S2).

Figure 5. Components for the preparation of lead-free percussion caps based on $[Cu(N_3)_2(MTZ)]$ (**1**) (left and middle) and moment of ignition thereof (right).

11.3. Conclusion

Finally, it was successfully shown that copper(II) azide can be stabilized with *N*-substituted tetrazole ligands and the sensitivities can be adjusted by the choice of ligand or phlegmatization during the synthesis. The resulting complexes are manageable energetic materials, which can be used as potential lead-free primary explosives.

11.4. Acknowledgements

This work was supported financially by Ludwig-Maximilians-University (LMU). We thank especially Prof. Dr. Thomas M. Klapötke for providing his research facilities, Prof. Dr. Jürgen Evers for the recording of the X-ray powder diffraction, Dr. Steffen Schmidt for investigating compounds by SEM, and Mr. Simon Endraß for his great contribution to this work. We also thank Dr. Manuel Joas for helpful discussions as well as Mrs. Cornelia Unger and Mrs. Esra Soner for proofreading of the manuscript.

11.5. References

[1] S. Bräse, C. Gil, K. Knepper, V. Zimmermann, *Angew. Chem. Int. Ed.* **2005**, *44*, 5188–5240.

[2] a) Y. Xu, Q. Wang, C. Shen, Q. Lin, P. Wang, M. Lu, *Nature* **2017**, *549*, 78–81; b) C. Zhang, C. Sun, B. Hu, C. Yu, M. Lu, *Science* **2017**, *355*, 374–376.

[3] R. Huisgen, I. Ugi, *Angew. Chem.* **1956**, *68*, 705–706.

[4] a) J. C. Bennion, N. Chowdhury, J. W. Kampf, A. J. Matzger, *Angew. Chem. Int. Ed.* **2016**, *55*, 13118–13121; b) A. A. Larin, N. V. Muravyev, A. N. Pivkina, K. Yu. Suponitsky, I. V. Ananyev, D. V. Khakimov, L. L. Fershtat, N. N. Makhova, *Chem. – Eur. J.* **2019**, *25*, 4225–4233; c) G. Bélanger-Chabot, M. Rahm, R. Haiges, K. O. Christe, *Angew. Chem. Int. Ed.* **2015**, *54*, 11730–11734.

[5] R. Matyáš, J. Pachman, *Primary Explosives*, 1st ed., Springer, Berlin, **2013**, pp. 96–100.

[6] a) H. Zöllner, M. Joas, R. Schirra, K. Kaplan, DynITEC GmbH, WO Patent 2018011134A1, Germany, **2018**; b) T. Klapötke, J. Stierstorfer, M. H. H. Wurzenberger, N. Szimhardt, EMTO GmbH, WO Patent 2019134867A1, Germany, **2019**.

[7] a) A. Hinz, M. Köckerling, *ChemistrySelect* **2017**, *2*, 9654–9657; b) J.-C. Liu, D.-G. Fu, J.-Z. Zhuang, C.-Y. Duana, X.-Z. You, *J. Chem. Soc. Dalton Trans.* **1999**, *14*, 2337–2342; c) P.-P. Liu, A.-L. Cheng, N. Liu, W.-W. Sun, E.-Q. Gao, *Chem. Mater.* **2007**, *19*, 2724–2726; d) R. Haiges, R. J. Buszek, J. A. Boatz, K. O. Christe, *Angew. Chem. Int. Ed.* **2014**, *53*, 8200–8205; e) T. Saal, P. Deokar, K. O. Christe, R. Haiges, *Eur. J. Inorg. Chem.* **2019**, *2019*, 2388–2391; f) T. Saal, P. Deokar, K. O. Christe, R. Haiges, *Dalton Trans.* **2019**, *48*, 806–813.

[8] J. J. Jobelius, H.-D. Scharff, *Ullmann's Encyclopedia of Industrial Chemistry*, 7th ed., Wiley-VCH, Weinheim, **2012**, pp. 97–101.

[9] a) P. N. Gaponik, V. P. Karavai, Yu. V. Grigor′ev, *Chem. Heretocycl. Compd.* **1985**, *21*, 1255–1258; b) P. N. Gaponik, M. M. Degtyarik, A. S. Lyakhov, V. E. Matulis, O. A. Ivashkevich, M. Quesada, J. Reedijk, *Inorg. Chim. Acta* **2005**, *358*, 3949–3957.

[10] T. Costain, F. B. Wells, *Technology of the inorganic azides*, 1st ed., Plenum Press, New York, **1977**, pp. 11–54.

[11] Selected X-ray data: red-brown plate, monoclinic, $P2_1/c$, a 11.4746(7), b 6.1867(3), c 10.8165(5) Å, β 100.078(5)°, V 756.01(7) Å^3, Z 4, ρ 2.036 g cm^{-3}, *wR2* 10.69%, *S* 1.06, CCDC 1985252 contains the supplementary crystallographic data for this paper. These data can be obtained free of charge from The Cambridge Crystallographic Data Centre.

[12] a) J. Köhler, R. Meyer, A. Homburg, *Explosivstoffe*, 10th ed., Wiley-VCH, Weinheim, **2008**; b) T. M. Klapötke, *Energetic Materials Encyclopedia*, De Gruyter, Berlin, Boston, **2018**; c) M. S. Gruhne, M. Lommel, M. H. H. Wurzenberger, N. Szimhardt, T. M. Klapötke, J. Stierstorfer, *Propellants Explos. Pyrotech.* **2020**, *45*, 147–153.

[13] a) W. Huang, Y. Tang, G. H. Imler, D. A. Parrish, J. M. Shreeve, *J. Am. Chem. Soc.* **2020**, *142*, 3652–3657; b) M. Deng, Y. Feng, W. Zhang, X. Qi, Q. Zhang, *Nat. Commun.* **2019**, *10*, 1339.

11.6. Supporting Information

11.6.1. Experimental Part and General Methods

All chemicals and solvents were employed as received (Sigma-Aldrich, Fluka, Acros, ABCR). Exothermic events of the described compounds, which indicate decomposition, are given as the extrapolated onset temperatures. The samples were measured in a range of 25–300 °C at a heating rate of 5 °C min^{-1} through differential thermal analysis (DTA) with an OZM Research DTA 552-Ex instrument. Infrared spectra were measured with pure samples on a Perkin-Elmer BXII FT-IR system with a Smith DuraSampler IR II diamond ATR. Determination of the carbon, hydrogen and nitrogen contents was carried out by combustion analysis using an Elementar Vario El (nitrogen values determined are often lower than the calculated ones due to their explosive behavior). Impact sensitivity tests were carried out according to STANAG 4489[1] with a modified instruction[2] using a BAM (Bundesanstalt für

Materialforschung und -prüfung) drop hammer.[3,4] Friction sensitivity tests were carried out according to STANAG 4487[5] with a modified instruction[6] using the BAM friction tester. The classification of the tested compounds results from the "UN Recommendations on the Transport of Dangerous Goods".[7] Additionally all compounds were tested upon the sensitivity toward electrical discharge using the OZM Electric Spark XSpark10 device.[3] The morphology of selected samples was determined by a scanning electron microscope (SEM) NanoLab G3 (Helios). The samples were carbon-coated (BAL-TEC MED 020, Bal Tec AG) to hinder electrostatic charging and to increase the conductivity.

The obtained coordination compounds were washed with cold water and ethanol when stated, dried overnight in air and used for analytics without further purification.

CAUTION! *All investigated compounds are highly energetic materials, which show increased sensitivities toward various stimuli (e.g., elevated temperatures, impact, friction or electrostatic discharge). Therefore, proper security precautions (safety glasses, face shield, earthed equipment and shoes, leather jacket, Kevlar gloves, Kevlar sleeves and ear plugs) have to be worn while synthesizing and handling the described compounds. It is recommended not to handle more than 250 mg at once.*

Procedure for the preparation of pure copper(II) azide

The pure cupric azide was prepared according to a modified procedure outlined by STRAUMANIS and CIRULIS in 1943.[8] Diluted aqueous hydrazoic acid was prepared by ion exchange techniques, according to literature.[9]

Copper(II) nitrate trihydrate (4.14 mmol, 1.00 g) was dissolved in water (50 mL) and stirred magnetically. An aqueous solution of sodium azide (7.70 mmol, 500 mg, 10 mL) was added dropwise. The gluey, dark brown precipitate was filtered off and washed with water. For purification, the wet azide was brought into an enclosed container of 2–3% hydrazoic acid (50 mL) and stored for 24 h under HN_3. During filtration, the product was washed several times with ethanol and finally with diethyl ether. After drying in air, pure copper(II) azide was obtained as a brown product with a slight reddish shine. Yield: 371 mg (2.51 mmol, 61%).

DTA (5 °C min^{-1}) onset: 205 °C (exothermic); IR (ATR, cm^{-1}): $\tilde{\nu}$ = 2123 (vs), 2089 (vs), 1302 (m), 1260 (s), 687 (m), 582 (w), 572 (m); EA (CuN_6, 147.59) calcd.: Cu 10.37, N 60.46%; found: too sensitive for measurement; BAM drop hammer: n.d.; friction tester: < 0.10 N; ESD: < 0.29 mJ (at grain size < 100 µm).

General procedure for the preparation of copper(II) azide complexes 1–3

Stoichiometric amounts of copper(II) chloride dihydrate (**1**, 3 mmol, 511 mg), copper(II) sulfate pentahydrate (**2**, 3 mmol, 749 mg) or copper(II) nitrate trihydrate (**3**, 3 mmol, 725 mg) and the ligand (**1**,

1-methyl-5*H*-tetrazole, 3 mmol, 252 mg; **2**, 1-ethyl-5*H*-tetrazole, 3 mmol, 294 mg; **3**, 1-propyl-5*H*-tetrazole, 3 mmol, 336 mg) were stirred mechanically in 12 mL of water. Two equivalents of sodium azide, dissolved in 5 mL water, were added dropwise within 1 min and the suspension was stirred for 15 min. The precipitated complex compounds were filtered off, washed with water and ethanol and dried in air.

Single crystals growth was achieved by overlaying an aqueous solution (8 mL) of sodium azide and the ligand with an ethanolic solution (8 mL) of copper(II) chloride dihydrate, separated by a mixture (4 mL) of water/ethanol (50/50). After 7 to 14 days crystals suitable for X-ray determination were obtained.

[Cu(N$_3$)$_2$(MTZ)] (1)
ECC **1** was obtained as fine brown powder. Yield: 647 mg (2.79 mmol, 93%).

DTA (5 °C min^{-1}) onset: 157 °C (exothermic); IR (ATR, cm^{-1}): $\tilde{\nu}$ = 3366 (vw), 3326 (vw), 3121 (m), 3026 (vw), 2955 (vw), 2638 (vw), 2570 (vw), 2074 (s), 2044 (vs), 1818 (vw), 1646 (vw), 1522 (m), 1477 (vw), 1425 (w), 1346 (w), 1297 (m), 1284 (m), 1177 (m), 1107 (m), 1067 (w), 1022 (m), 1000 (m), 912 (w), 715 (w), 682 (m), 656 (m), 603 (w), 589 (w), 411 (w); EA ($C_2H_4CuN_{10}$, 231.67) calcd.: C 10.37, H 1.74, N 60.46%; found: C 10.29, H 1.75, N 59.84%; BAM drop hammer: < 1 J; friction tester: < 0.10 N; ESD: 0.79 mJ (at grain size < 100 µm).

[Cu(N$_3$)$_2$(ETZ)] (2)
The complex compound **2** was received in the form of a brown precipitate. Yield: 680 mg (2.77 mmol, 92%).

DTA (5 °C min^{-1}) onset: 134 °C (exothermic); IR (ATR, cm^{-1}): $\tilde{\nu}$ = 3367 (vw), 3322 (vw), 3115 (w), 2992 (vw), 2949 (vw), 2691 (vw), 2631 (vw), 2559 (vw), 2074 (s), 2040 (vs), 1573 (vw), 1511 (m), 1438 (w), 1382 (w), 1350 (w), 1294 (m), 1279 (m), 1204 (w), 1180 (s), 1115 (m), 1099 (m), 1082 (m), 1032 (w), 1010 (m), 967 (w), 907 (w), 891 (w), 803 (w), 718 (vw), 690 (w), 678 (m), 661 (w), 647 (m), 602 (m), 593 (w), 587 (w); EA ($C_3H_6CuN_{10}$, 245.70) calcd.: C 14.67, H 2.46, N 57.01%; found: C 14.38, H 2.38, N 55.90%; BAM drop hammer: 3 J; friction tester: 4.5 N; ESD: 33 mJ (at grain size < 100 µm).

[Cu(N$_3$)$_2$(PT)] (3)
Complex **3** was obtained as brown precipitate. Yield: 699 mg (2.69 mmol, 90%).

DTA (5 °C min^{-1}) onset: 148 °C (exothermic); IR (ATR, cm^{-1}): $\tilde{\nu}$ = 3124 (w), 2975 (w), 2945 (w), 2883 (w), 2092 (s), 2041 (vs), 1511 (w), 1469 (w), 1446 (w), 1375 (w), 1342 (w), 1294 (m), 1279 (m), 1180 (m), 1118 (w), 1091 (w), 1057 (vw), 1034 (vw), 1013 (w), 903 (w), 885 (w), 758 (w), 744 (w), 716 (w), 691 (w), 662 (m), 602 (w), 592 (w), 587 (w), 410 (w); EA ($C_4H_8CuN_{10}$, 259.73) calcd.: C 18.50 H 3.10

N 53.93%; found: C 18.34 H 3.14 N 52.95%; BAM drop hammer: 2.5 J; friction tester: 10 N; ESD: 112 mJ (at grain size < 100 µm).

Phlegmatized $[Cu(N_3)_2(MTZ)]$ + 6% Dextrin (1a)

The phlegmatized compound was prepared analogous to the synthesis of dextrinated lead azide.[10] While heating to 60 °C, dextrin from potato starch (120 mg) was added to water (36 mL) under stirring. As soon as the solution became clear, sodium azide was added (17.3 mmol, 1.12 g). An aqueous solution of copper(II) chloride dihydrate (8.63 mmol, 1.47 g) and MTZ (8.63 mmol, 0.73 g) in water (20 mL) was prepared. To this solution of metal salt and ligand, the dextrinated sodium azide solution was added dropwise over the course of 30 min while stirring and heating at 60 °C continued. After addition, the solution was allowed to cool down and the brown complex filtered, washed with ethanol and air-dried overnight. Yield: 1.72 g (6.91 mmol, 80%).

DTA (5 °C min^{-1}) onset: 148 °C (exothermic); IR (ATR, cm^{-1}): $\tilde{\nu}$ = 3565 (vw), 3365 (vw), 3326 (w), 3120 (m), 3025 (w), 2954 (vw), 2638 (vw), 2567 (vw), 2075 (s), 2044 (vs), 1941 (m), 1816 (w), 1521 (m), 1424 (w), 1346 (w), 1297 (m), 1282 (m), 1176 (m), 1106 (m), 1066 (w), 1021 (m), 999 (m), 912 (w), 715 (w), 681 (m), 656 (m), 603 (w), 589 (m), 471 (vw), 412 (w); BAM drop hammer: < 1 J; friction tester: 0.40 N; ESD: 8.3 mJ (at grain size < 100 µm).

Phlegmatized $[Cu(N_3)_2(MTZ)]$ + 5% Span 80 (1b)

An emulsion of Span 80 (50 mg) in water (9.8 mL) was prepared and heated to 60 °C while stirring vigorously. Copper(II) chloride dihydrate (4.32 mmol, 736 mg) and MTZ (4.32 mmol, 363 mg) were added. A solution of sodium azide (8.63 mmol, 561 mg) in water (18 mL) was added dropwise to the emulsion containing metal salt and ligand over the course of 10 min. The precipitated brown complex was filtered, washed with ethanol and air-dried overnight. Yield: 763 mg (3.08 mmol, 71%).

DTA (5 °C min^{-1}) onset: 149 °C (exothermic); IR (ATR, cm^{-1}): $\tilde{\nu}$ = 3583 (w), 3444 (vw), 3367 (w), 3326 (w), 3118 (m), 3025 (w), 2925 (w), 2855 (w), 2637 (vw), 2571 (w), 2149 (w), 2075 (s), 2044 (vs), 1809 (w), 1739 (m), 1626 (w), 1521 (m), 1468 (w), 1424 (w), 1377 (w), 1347 (w), 1283 (m), 1272 (m), 1175 (m), 1105 (s), 1066 (w), 1021 (m), 998 (m), 909 (m), 715 (w), 681 (s), 655 (s), 603 (m), 588 (m), 572(w), 474(vw), 411(w); BAM drop hammer: 1.5 J; friction tester: 0.60 N; ESD: 63 mJ (at grain size < 100 µm).

Phlegmatized $[Cu(N_3)_2(MTZ)]$ + 5% CMC (1c)

The phlegmatized compound was prepared analogous to a modified procedure, describing the production of RD1333 lead azide.[10] Sodium carboxymethylcellulose (25 mg) with medium viscosity (400–800 cP, 2% in H_2O at 25 °C) was dissolved in water while stirring at room temperature. Copper(II) chloride dihydrate (2.16 mmol, 368 mg) and MTZ (2.16 mmol, 182 mg) were dissolved in water (10 mL). A

solution of sodium azide (4.32 mmol, 281 mg) in water (10 mL) was prepared. The solution containing copper(II) salt and ligand, as well as the solution containing the sodium azide were simultaneously added dropwise to the CMC solution. After complete addition and precipitation of the complex, it was allowed to stir for another 5 min. The brown powder was filtrated, washed with ethanol and air-dried overnight. Yield: 452 mg (1.84 mmol, 85%).

DTA (5 °C min^{-1}) onset: 150 °C (exothermic); IR (ATR, cm^{-1}): $\tilde{\nu}$ = 3366 (vw), 3326 (vw), 3120 (w), 3025 (vw), 2953 (vw), 2637 (vw), 2565 (vw), 2544 (vw), 2074 (s), 2045 (vs), 1818 (w), 1672 (w), 1612 (w), 1522 (m), 1477 (w), 1425 (w), 1346 (w), 1283 (m), 1177 (m), 1106 (m), 1067 (w), 1022 (m), 999 (m), 912 (w), 715 (w), 682 (m), 656 (m), 603 (w), 589 (w), 413 (w); BAM drop hammer: 2 J; friction tester: 0.75 N; ESD: 3.9 mJ (at grain size < 100 µm).

Phlegmatized $[Cu(N_3)_2(MTZ)]$ + 5% PVB (1d)

A solution of polyvinyl butyral (25 mg) in methanol was prepared while stirring at room temperature. After the additive was completely dissolved, copper(II) nitrate trihydrate (2.16 mmol, 522 mg) and MTZ (2.16 mmol, 182 mg) were added and dissolved in the PVA solution. An aqueous solution of sodium azide (4.32 mmol, 281 mg) was dripped to the *in situ* formed nitrate complex. The precipitated complex was allowed to stir for five more minutes and, after filtration, washing with ethanol and air-drying overnight, obtained as brown powder. Yield: 508 mg (2.06 mmol, 95%).

DTA (5 °C min^{-1}) onset: 151 °C (exothermic); IR (ATR, cm^{-1}): $\tilde{\nu}$ = 3368 (vw), 3120 (w), 3009 (vw), 2968 (vw), 2638 (vw), 2580 (vw), 2084 (vs), 2048 (vs), 1783 (vw), 1515 (m), 1483 (w), 1343 (w), 1290 (s), 1184 (m), 1105 (m), 1063 (w), 1032 (w), 1000 (m), 893 (m), 835 (vw), 812 (vw), 719 (vw), 686 (m), 655 (s), 598 (w), 587 (w), 499 (vw), 408 (w); BAM drop hammer: 4 J; friction tester: 0.45 N; ESD: 0.54 mJ (at grain size < 100 µm).

11.6.2. IR Spectroscopy

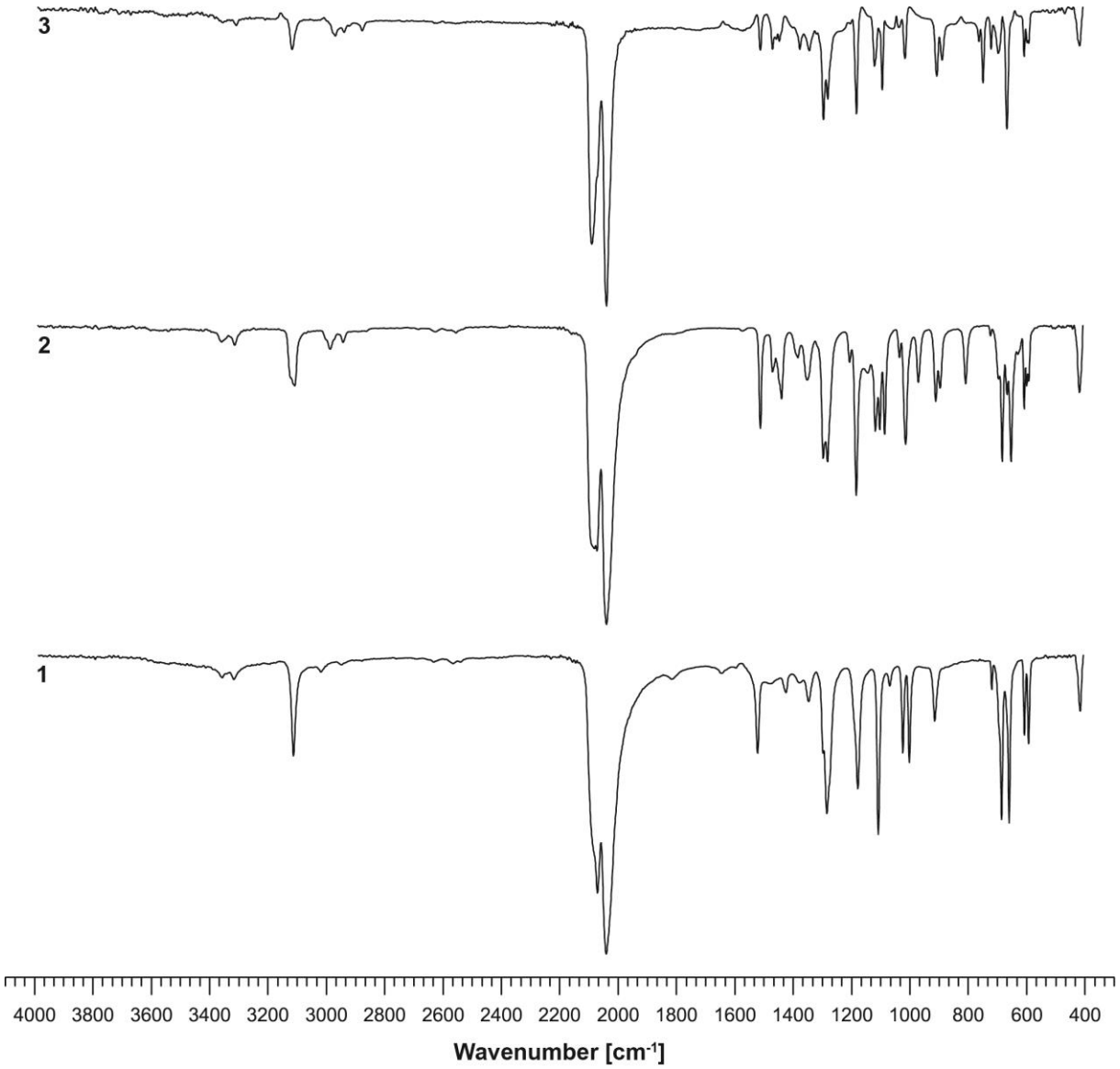

Figure S1. Infrared spectra of ECC **1**–**3**.

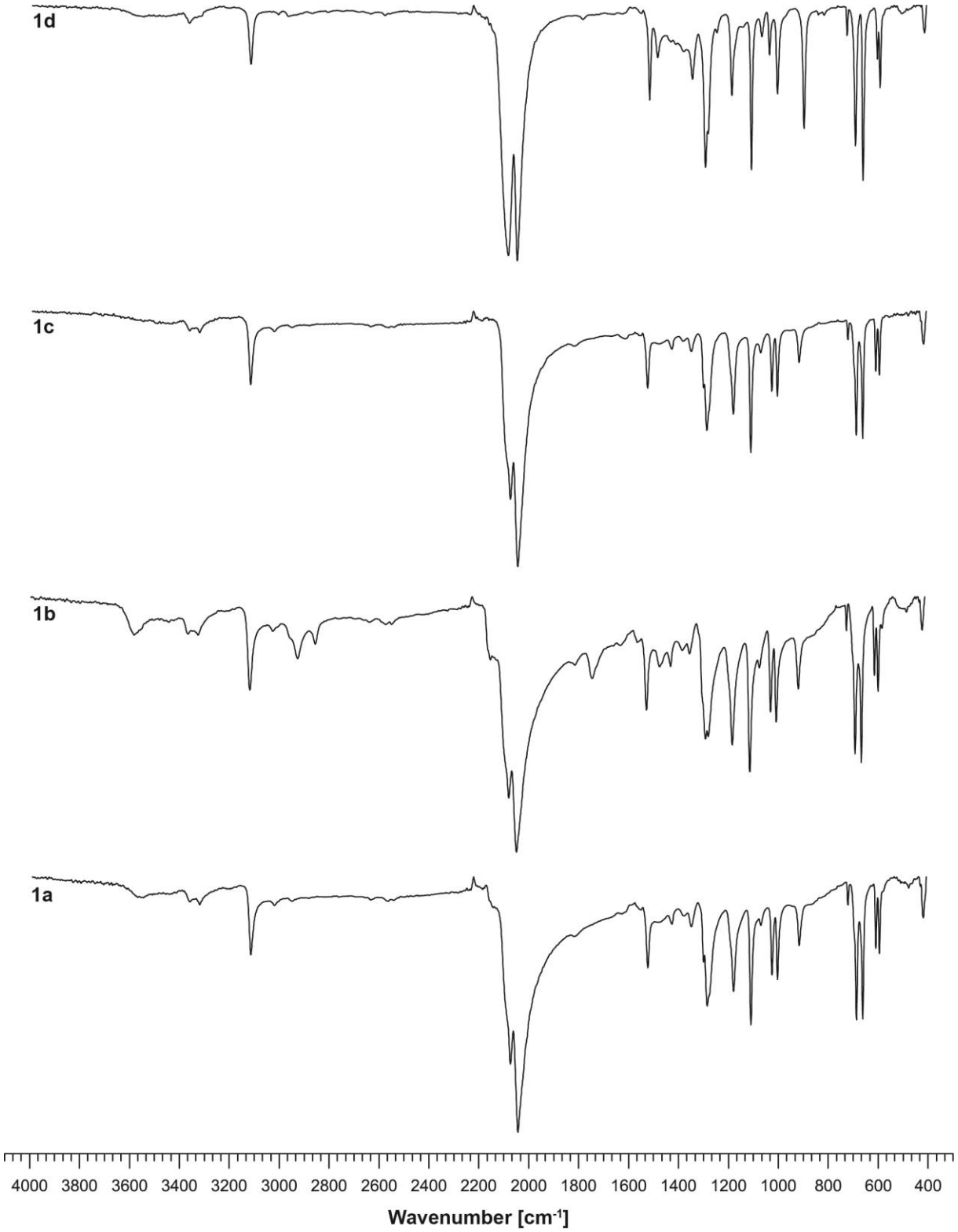

Figure S2. Infrared spectra of phlegmatized complexes **1a**–**d**.

11.6.3. X-Ray Diffraction

For all crystalline compounds, an Oxford Xcalibur3 diffractometer with a CCD area detector or Bruker D8 Venture TXS diffractometer equipped with a multilayer monochromator, a Photon 2 detector and a

rotating-anode generator were employed for data collection using Mo-*K*α radiation (λ = 0.7107 Å). On the Oxford device, data collection and reduction were carried out using the CRYSALISPRO software.[11] On the Bruker diffractometer, the data were collected with the Bruker Instrument Service v3.0.21, the data reduction was performed using the SAINT V8.18C software (Bruker AXS Inc., 2011). The structures were solved by direct methods (SIR-92,[12] SIR-97,[13] or SHELXS-97[14]) and refined by full-matrix least-squares on *F*2 (SHELXL[14]) and finally checked using the PLATON software[15] integrated in the WinGX[16] software suite. The non-hydrogen atoms were refined anisotropically and the hydrogen atoms were located and freely refined. The absorptions were corrected by a SCALE3 ABSPACK or SADABS Bruker APEX3 multiscan method.[17,18] All DIAMOND2 plots are shown with thermal ellipsoids at the 50% probability level and hydrogen atoms are shown as small spheres of arbitrary radius.

Table S1. Crystallographic data of **1**–**3**.

	1	**2**	**3**
Formula	$C_2H_4CuN_{10}$	$C_6H_{12}Cu_2N_{20}$	$C_8H_{16}Cu_2N_{20}$
FW [g mol^{-1}]	231.69	491.44	519.49
Crystal system	monoclinic	triclinic	triclinic
Space Group	$P2_1/c$	$P\bar{1}$	$P\bar{1}$
Color / Habit	red-brown plate	yellow platelet	brown block
Size [mm]	0.05 x 0.16 x 0.21	0.01 x 0.03 x 0.04	0.03 x 0.05 x 0.10
a [Å]	11.4746(7)	6.2573(3)	6.3931(5)
b [Å]	6.1867(3)	10.7256(4)	10.6917(8)
c [Å]	10.8165(5)	12.8661(5)	14.0603(11)
α [°]	90	98.438(2)	107.276(2)
β [°]	100.078(5)	98.221(2)	90.120(2)
γ [°]	90	90.230(1)	90.221(2)
V [Å^3]	756.01(7)	845.09(6)	917.70(12)
Z	4	2	2
$\rho_{calc.}$ [g cm^{-3}]	2.036	1.931	1.880
μ [mm^{-1}]	2.858	2.563	2.365
F(000)	460	492	524
$\lambda_{MoK\alpha}$ [Å]	0.71073	0.71073	0.71073
T [K]	123	103	102
θ Min–Max [°]	4.4, 26.0	2.3, 26.0	2.8, 26.4
Dataset	−14: 13; −3: 7; −9: 13	−7: 7; −13: 13; −15: 15	−7: 7; −13: 13; −17: 17
Reflections collected	2684	8592	12240
Independent refl.	1547	3320	3702
R_{int}	0.032	0.029	0.031
Observed reflections	1326	2702	3439
Parameters	119	255	273
R_1 (obs)[a]	0.0406	0.0366	0.0722
wR_2 (all data)[b]	0.1069	0.0926	0.1837
GooF[c]	1.07	1.07	1.18
Resd. Dens. [e Å^{-3}]	−0.90, 1.02	−0.51, 1.89	−0.99, 2.16
Absorption correction	multi-scan	multi-scan	multi-scan
CCDC	1984071	1984070	1984069

[a] $R_1 = \Sigma||F_0|- |F_c||/ \Sigma|F_0|$; [b] $wR_2 = [\Sigma[w(F_0^2-F_c^2)^2]/\Sigma[w(F_0)^2]]^{1/2}$; $w = [\sigma c^2(F_0^2)+(xP)^2+yP]^{-1}$ and $P = (F_0^2+2F_c^2)/3$; [c] GooF = $\{\Sigma[w(F_o^2-F_c^2)^2]/(n-p)\}^{1/2}$ (n = number of reflections; p = total number of parameters).

Copper(II) azide complex **2** crystallizes as yellow platelets in the triclinic space group *P*−1 with two formula units per unit cell and a calculated density of 1.931 g cm^{-3} at 103 K. The molecular unit is built of two different copper(II) cations, each coordinated octahedrally by one ligand in equatorial position and five bridging azide anions (Figure S3). The coordination spheres show strong Jahn-Teller distortions along the N14–Cu1–N12^{i} and N9–Cu2–N11^{iv} axes and the azido ligands possess the same bridging behavior like in compound **1** again forming 2D-polymeric layers. ECC **3** crystallizes as brown blocks in the triclinic space group *P*−1. It possesses two formula units per unit cell and the lowest calculated density (1.880 g cm^{-3} at 102 K) of all three compounds. Again, the molecular unit consists of two different metal(II) cations, each coordinated octahedrally by one ligand in equatorial position and five bridging azide anions (Figure S4). The coordination spheres show strong Jahn-Teller distortions along the N15^{iii}–Cu1–N17 and N8–Cu2–N10^{ii} axes and the azido ligands possess the same bridging behavior like in compound **1** and **2** leading to the formation of layers.

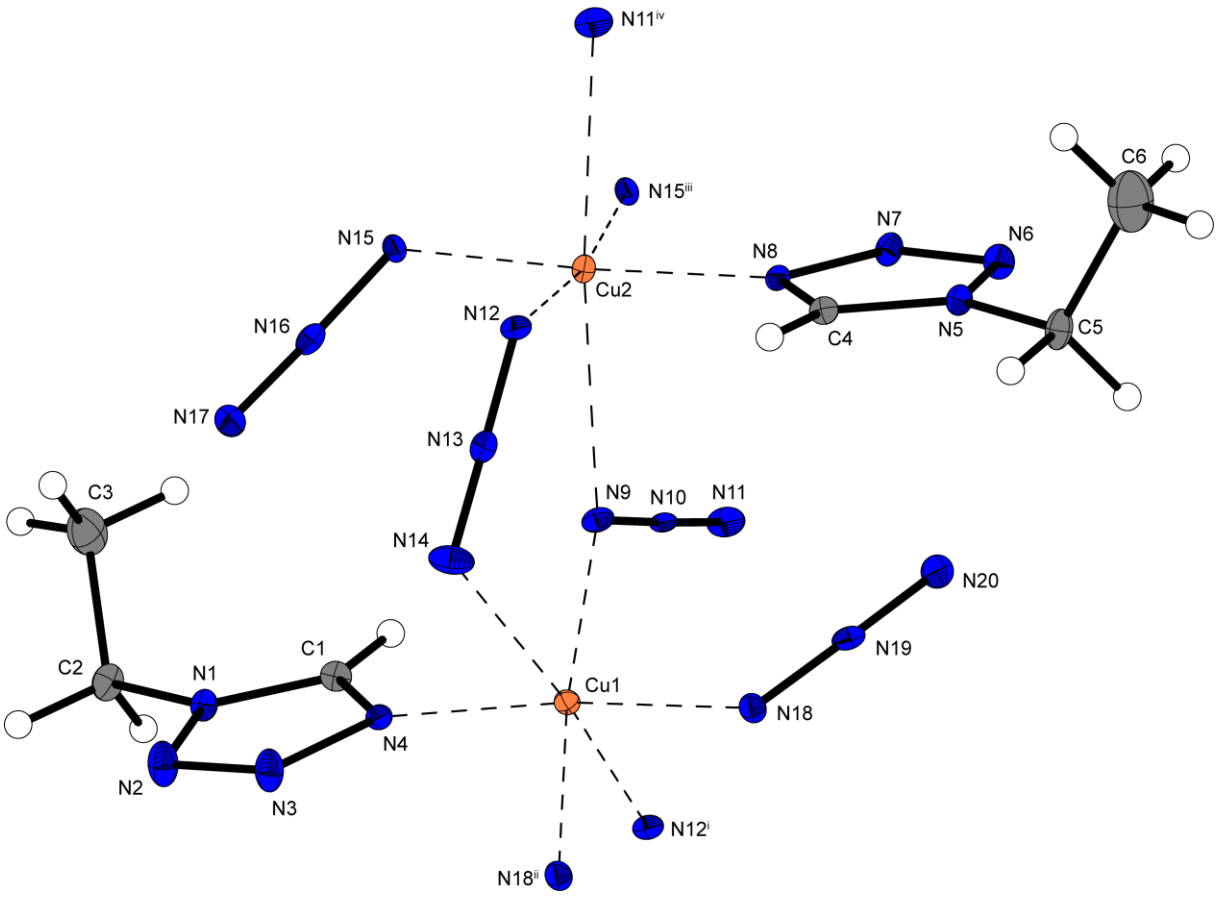

Figure S3. Coordination environment of [Cu(N$_3$)$_2$(ETZ)] (**2**). Selected bond lengths (Å): Cu1–N4 1.996(3), Cu1–N9 2.001(3), Cu1–N14 2.594(3), Cu1–N18^{ii} 2.010(3), Cu2–N8 1.993(3), Cu2–N9 2.545(3), Cu2–N11^{iv} 2.600(3), Cu2–N12 2.008(3); selected bond angles (°): N4–Cu1–N9 91.87(14), N4–Cu1–N14 85.33(12), N9–Cu1–N14 85.11(12), N8–Cu2–N9 89.54(12), N8–Cu2–N12 91.51(12), N9–Cu2–N12 89.83(12). Symmetry codes: (i) −1+x, y, z; (ii) 2−x, 1−y, −z; (iii) 1−x, 2−y, −z; (iv) −1+x, y, z.

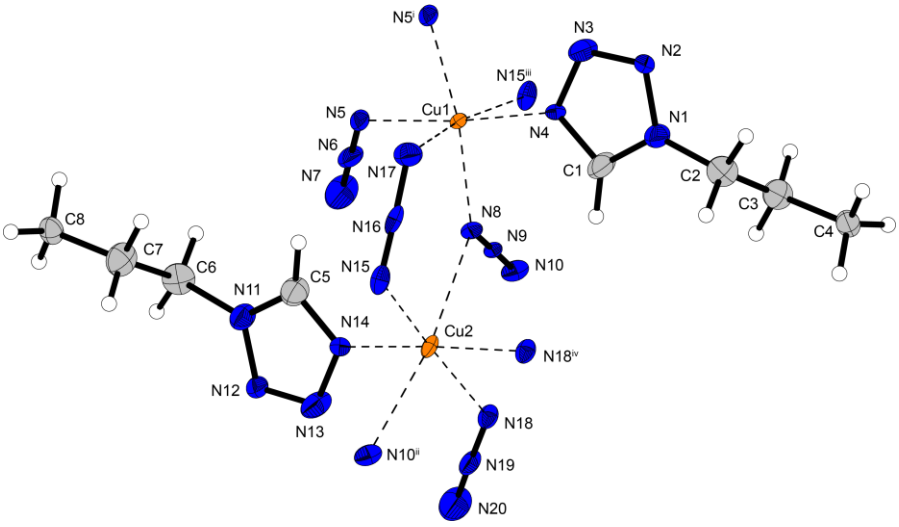

Figure S4. Coordination environment of [Cu(N$_3$)$_2$(PT)] (**3**). Selected bond lengths (Å): Cu1–N4 2.000(6), Cu1–N5 2.006(7), Cu1–N8 2.005(7), Cu1–N5^{i} 2.000(7), Cu1–N15^{iii} 2.592(7), Cu1–N17 2.639(7), Cu2–N8 2.637(7), Cu2–N14 1.989(6), Cu2–N15 2.016(7), Cu2–N18 1.994(7), Cu2–N10^{ii} 2.593(7); selected bond angles (°): N5–Cu1–N4 95.9(2), N5–Cu1–N5 79.0(3), N4–Cu1–N5 174.8(2), N8–Cu1–N5 93.6(3), N14–Cu2–N8 96.0(3), N14–Cu2–N18 174.1(2), N8–Cu2–N18 78.3(3), N14–Cu2–N15 91.5(3), N18–Cu2–N15 171.9(3), N8–Cu2–N15 94.2(2), N8–Cu2–N10 171.3(2). Symmetry codes: (i) 1−x, 1−y, 1−z; (ii) 1+x, y, z; (iii) −1+x, y, z; (iv) 2−x, −y, 1−z.

11.6.4. Powder Diffraction

X-ray powder experiments were performed on a Gunier diffractometer (Huber G644) with Mo-Kα1 radiation (λ = 0.7093 Å, quartz monochromator) in Lindemann capillaries (0.7 mm diameter). The angle calibration was performed with electronic grade germanium. In the 2θ range between 4 and 34° with an increment of 0.04°, 750 data points were collected with a counting rate of 10 s for each increment. The Rietveld parameters were analyzed with the program FullProf.[19]

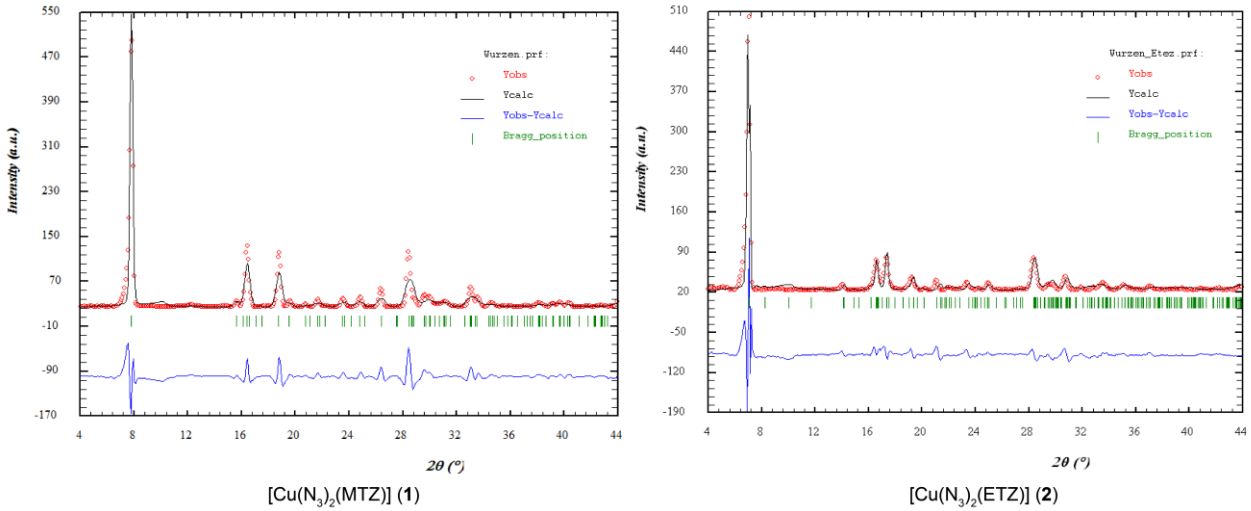

Figure S5. Powder diffraction of compounds **1** and **2**. Small aberrations of observed and calculated data are caused by the temperature difference of single crystal and powder diffraction experiments.

11.6.5. Scanning Electron Microscopy

Since all of the prepared compounds differ in their physicochemical properties and appearance, scanning electron microscopy (SEM) was performed to investigate the morphology of pure copper azide as well as the prepared coordination compound with (**1a**–**1d**) and without (**1**) additives.

The pure azide consists of thin fibers with a diameter of less than 1 µm, forming intergrown agglomerates (Figure S6). This is also represented in the macroscopic scale, as the dry compound does not form a fine powder but keeps the shape of the filter paper and crumbles into large chunks.

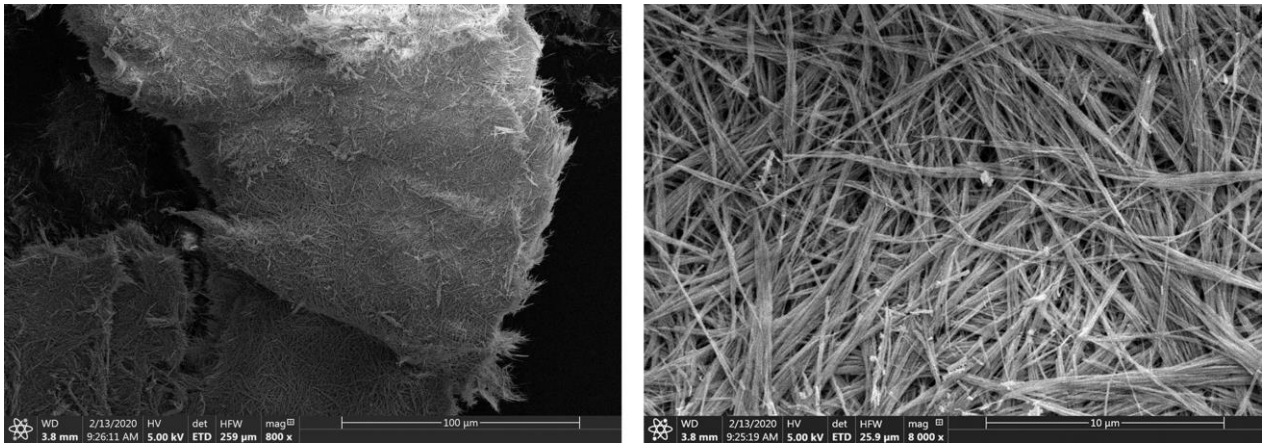

Figure S6. SEM images with 800x magnitude (left) and 8000x magnitude (right) of pure $Cu(N_3)_2$.

The coordination compound (**1**) shows a completely different crystal habit, as small crystallites are homogenously distributed (Figure S7). Most of them have a plate-like morphology, rounded edges and a size in the range of 0.5–5 µm. This can also be confirmed by the compound's macroscopic appearance, as it precipitates as a fine powder and retains this morphology after drying.

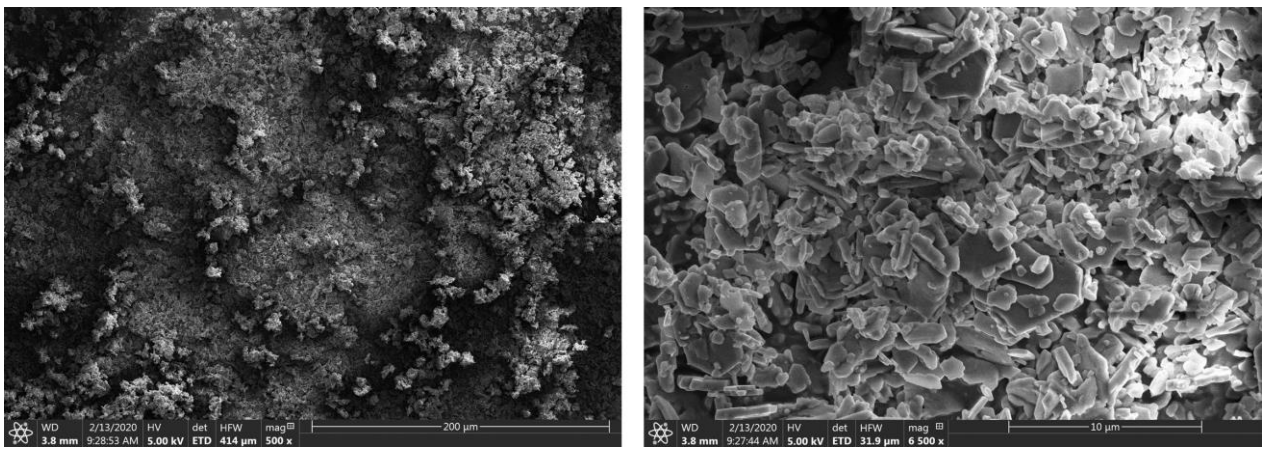

Figure S7. SEM images with 500x magnitude (left) and 6500x magnitude (right) of compound **1**.

The dextrinated complex (**1a**) shows a similar overall morphology but with bigger crystallites (up to 30 µm) tending to take on more geometric shapes (Figure S8).

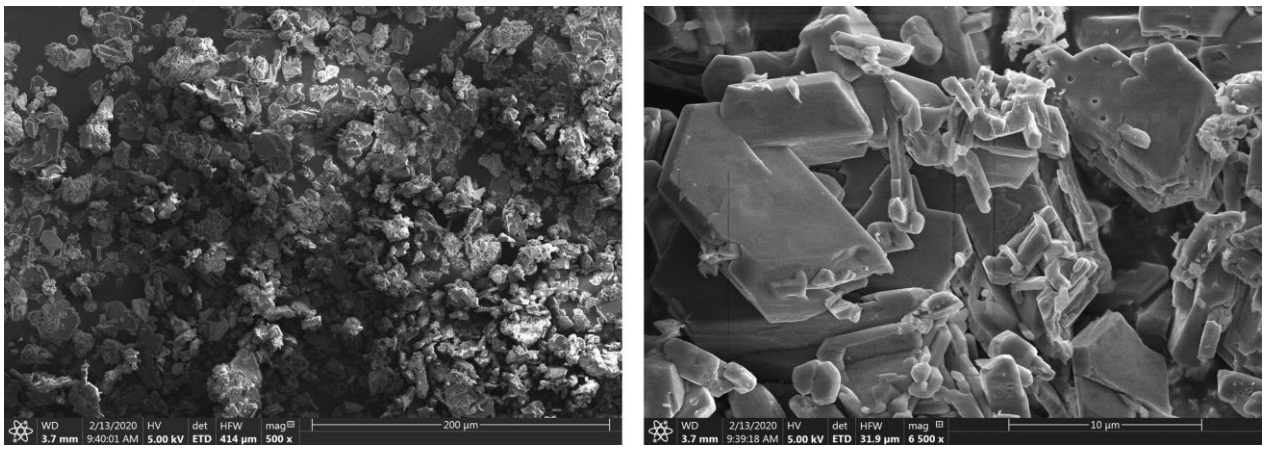

Figure S8. SEM images with 500x magnitude (left) and 6500x magnitude (right) of compound **1a**.

The complex **1b** precipitated from an aqueous solution of polysorbate (Span 80) shows a larger particle size distribution and forms even bigger chunks (up to 80 µm) which are partially intergrown and possess soft edges (Figure S9).

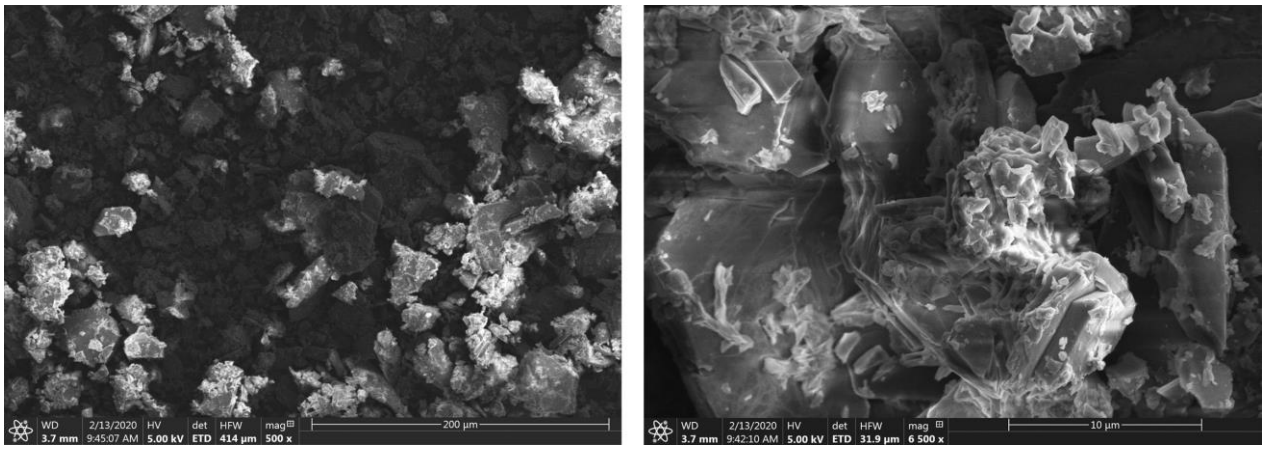

Figure S9. SEM images with 500x magnitude (left) and 6500x magnitude (right) of compound **1b**.

Interestingly, compound **1c**, which is prepared using carboxymethyl cellulose as an additive, forms agglomerates consisting of two different crystal morphologies (Figure S10). Firstly, a plate-like structure (as present in pure complex **1**) can be found, as well as a needle-like species. With no structures being much bigger than 10 µm, the overall morphology seems to be very compact due to space-filling needles between layers of platelets.

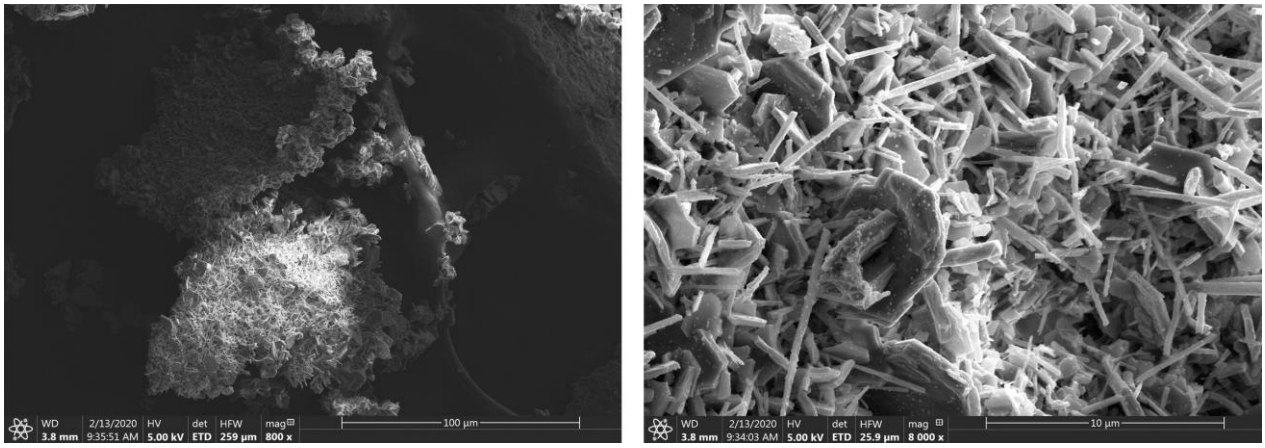

Figure S10. SEM images with 800x magnitude (left) and 8000x magnitude (right) of compound **1c**.

The complex **1d**, precipitated out of an aqueous solution of polyvinyl butyral, shows a morphology with the smallest structures (Figure S11) in this row. With very short needle-like crystals in the range of 0.2–2 µm, the formation of agglomerates is facilitated as well as a homogeneous general morphology.

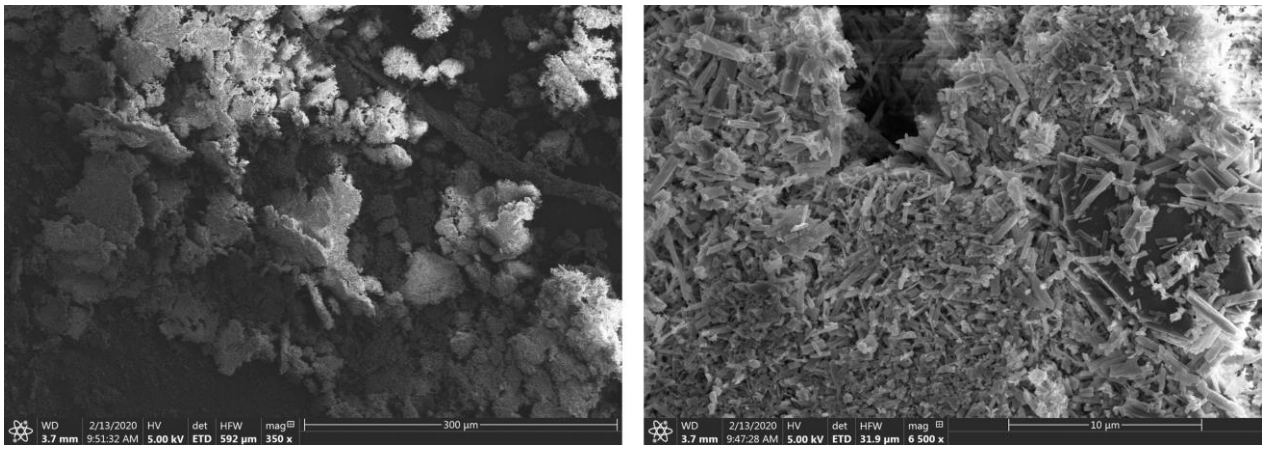

Figure S11. SEM images with 350x magnitude (left) and 6500x magnitude (right) of compound **1c**.

11.6.6. DTA Plots

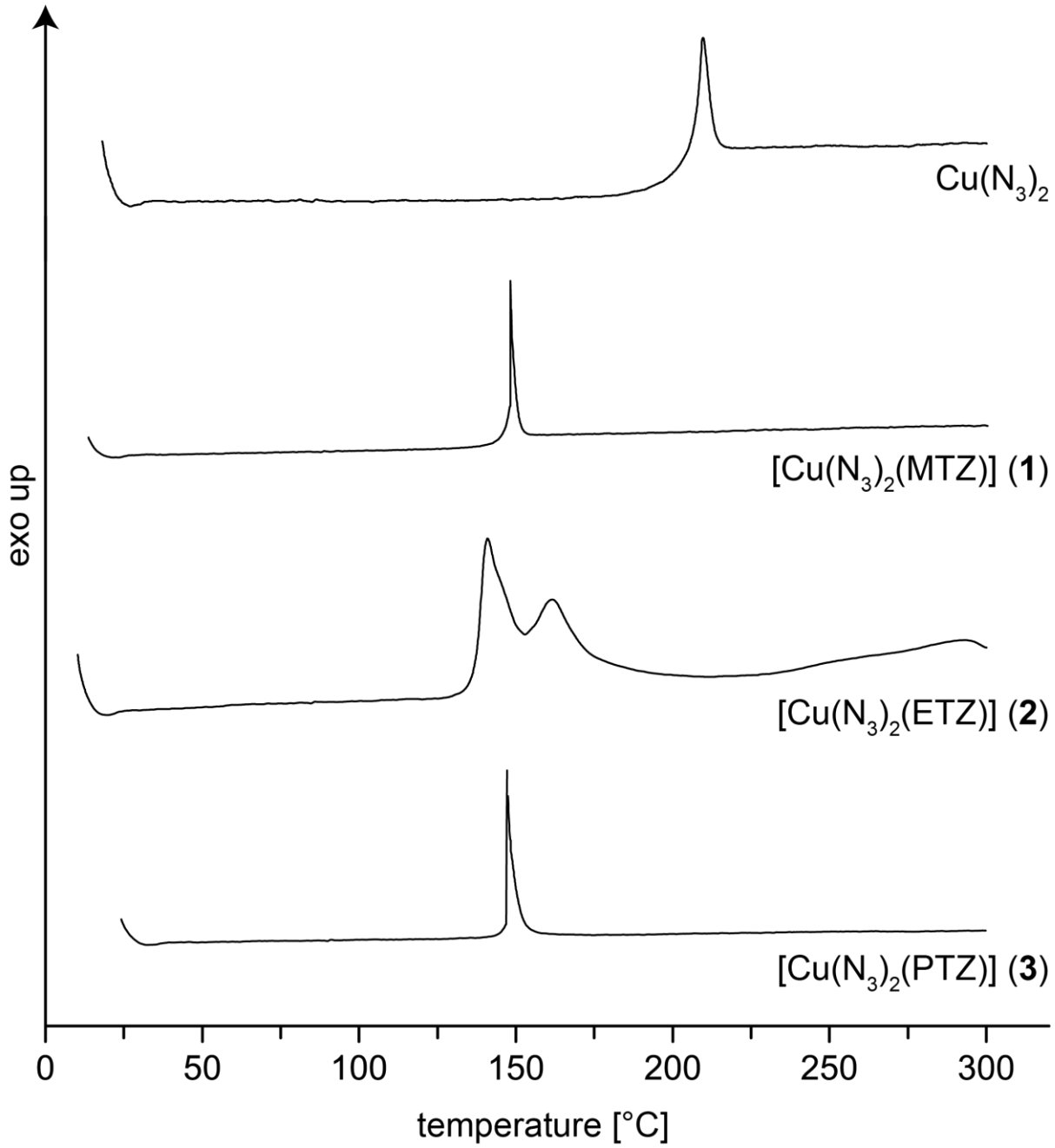

Figure S12. DTA plots of copper(II) azide and ECC **1**–**3**.

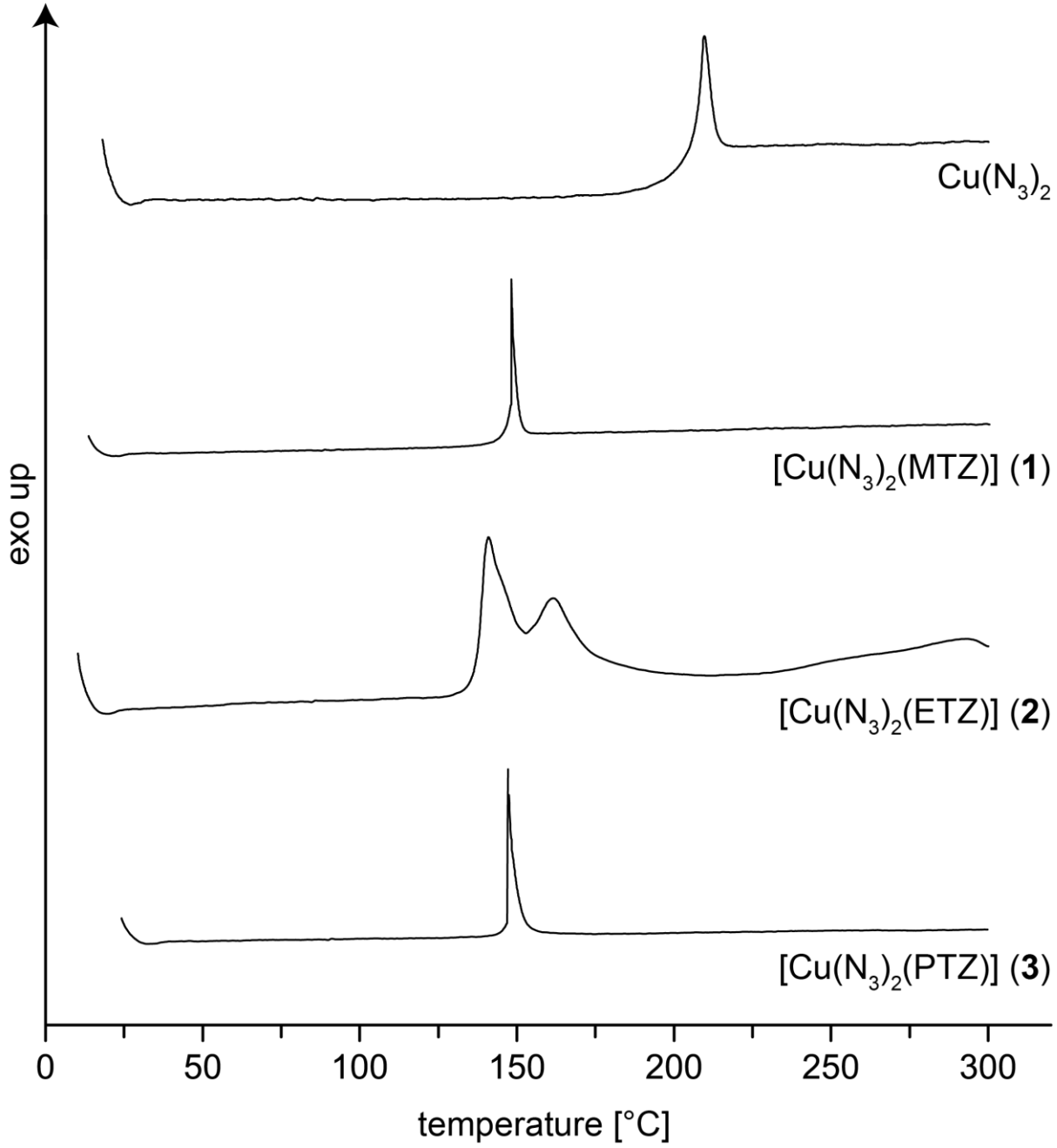

Figure S13. DTA plots of phlegmatized complexes **1a**–**c**.

11.6.7. Initiation Capability Tests

As the initiating capability of a compound indicates its suitability as a primary explosive, selected ECC were tested in initiation experiments. The compound to be evaluated was loosely filled on top of a pressed (8 kg weight) main charge (200 mg of PETN or RDX) in a copper shell (Figure S14). The primary explosive was ignited using an electrical ignitor.

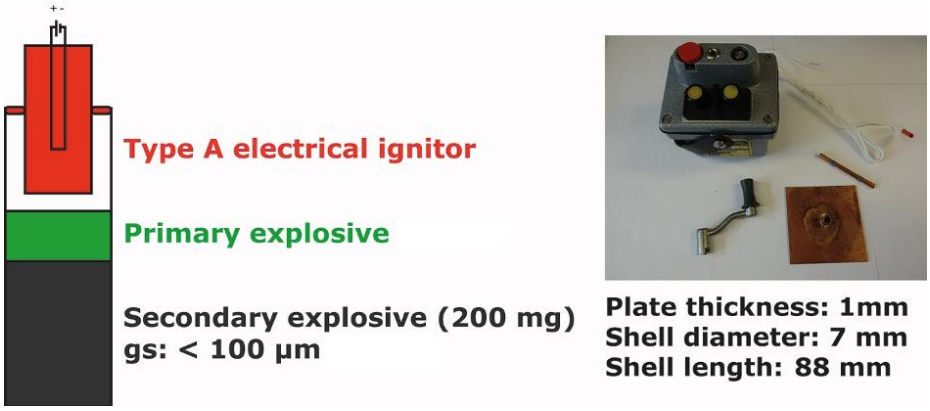

Figure S14. Schematic test setup (left) and used equipment (right) for the initiation capability tests.

Figure S15. Positive PETN (left) and RDX (right) initiation tests with 50 mg of the phlegmatized coordination compound **1c**.

11.6.8. Priming Mixtures

In order to test the suitability in priming mixtures (PM), $[Cu(N_3)_2(MTZ)]$ (**1**) was applied as a lead styphnate (LS) replacement in a priming composition similar to the so called FA-956.[20] Instead of using 41% of primary explosive by mass (37% LS, 4% tetrazene), the mixture was tested with 15% of $[Cu(N_3)_2(MTZ)]$ as a primary explosive. For obtaining homogenous priming mixtures in lab scale, weighted quantities of all compounds were brought into a sample container and placed into a Heidolph Reax 2 overhead shaker. After several hours at 60 rpm, a homogenous mixture was attained, which was further characterized regarding sensitivities, thermal behavior, and the produced flame. Therefore, the PM was filled in commonly used large-rifle percussion primer consisting of a brass primer cup (B) covered with a paper disc (C), which is pressed onto the mixture. Lastly an anvil (D) is pressed on top of the paper (Figure S16). As soon as the firing pin hits the primer cup (A), mechanical stimulus ignites the priming mixture (B), which is confined by the anvil (D) and subjected to impact and friction.

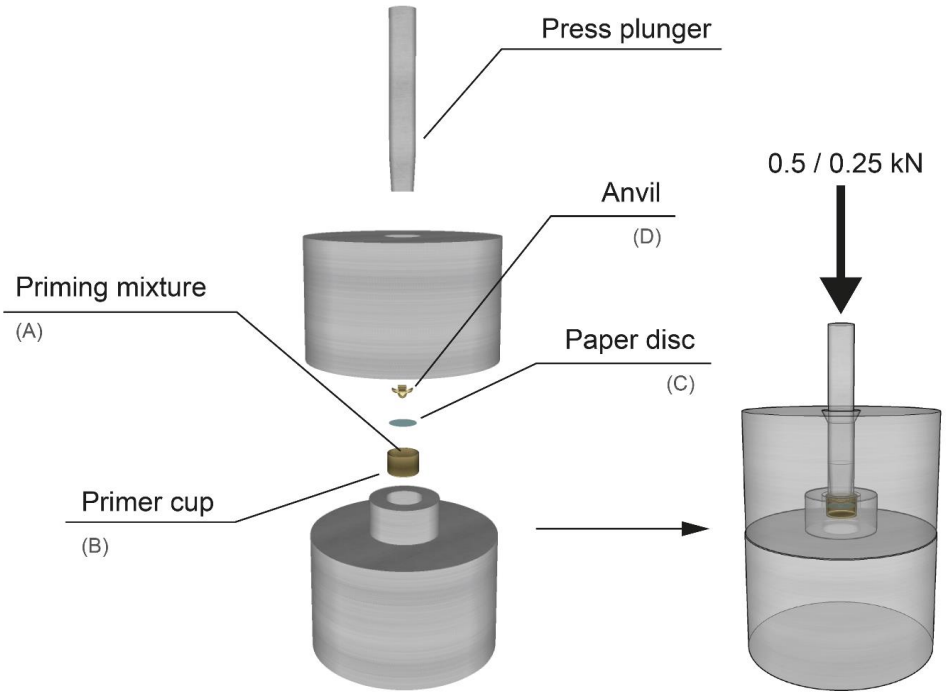

Figure S16. Primer processing.

Table S2. Sensitivities of the new PM compared to a commercially available one.

Compound	*IS* [J][a]	*FS* [N][b]	*ESD* [mJ][c]
Lead-free mixture	1	10	3.3
Commercial mixture	1	30	0.79

[a] Impact sensitivity according to the BAM drop hammer (method 1 of 6). [b] Friction sensitivity according to the BAM friction tester (method 1 of 6). [c] Electrostatic discharge sensitivity (OZM XSpark10 ESD tester).

A primer filled with the new mixture was pressed into a 7.62 mm cartridge and the priming mixture ignited with the impact of a firing pin. Nitrocellulose was used as propellant. The building up gas pressure was measured and compared to a cartridge with a commercial large rifle primer. The results can be found in Table S3 and Figure S17. The generated gas pressure [bar] is plotted against time [ms].

Table S3. Results of the gas pressure measurements.

Compound	Pressure [bar]	Velocity [m/s]	Energy [J]
Lead-free mixture	2998.0	822.1	3228
Commercial mixture	3232.4	839.8	3366

[a] Impact sensitivity according to the BAM drop hammer (method 1 of 6). [b] Friction sensitivity according to the BAM friction tester (method 1 of 6). [c] Electrostatic discharge sensitivity (OZM XSpark10 ESD tester).

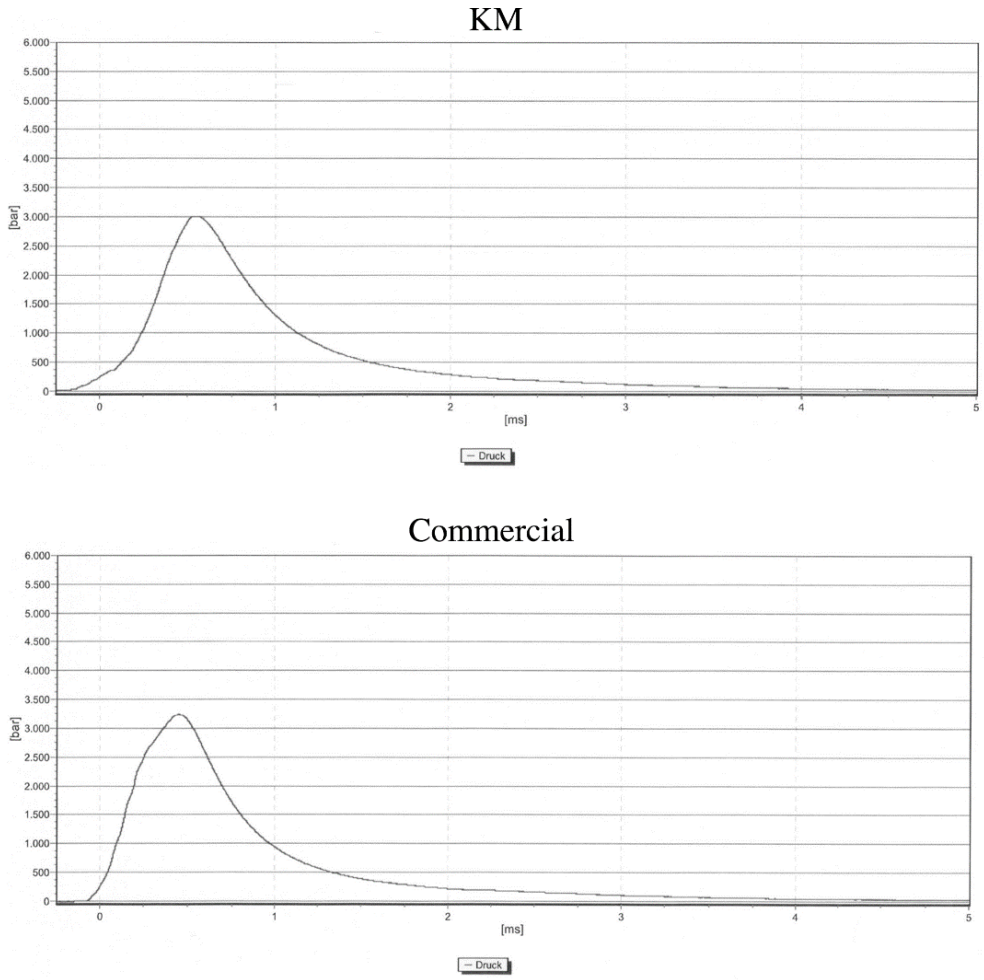

Figure S17. Generated gas pressure of two mixtures, plotted against time.

11.6.9. Notes on the Preparation of Copper(II) Azide

Cupric azide was prepared as outlined in the Experimental Section, according to STRAUMANIS and CIRULIS.[8] After the addition of azide to a solution of copper nitrate, crude copper azide precipitates immediately. The formation of a 3D-polymeric network, which is built up according to the crystal structure,[21] leads to the appearance of very fine fibers (observable during electron microscopy, Figure S6) and ultimately to an intergrown polymeric mass of product which is hard to filter and process. This crude product is impure, as it contains basic copper azides. It has to be stored under diluted hydrazoic acid for a certain period of time, leading to the destruction of basic byproducts (Figure S19). That process was monitored by IR spectroscopy, showing a significant reduction of the broad hydroxy band (O–H bond stretching vibration at 3600–3400 cm^{-1}) and sharper remaining bands, *e.g.*, azide band at 2130–2070 cm^{-1} (Figure S18).

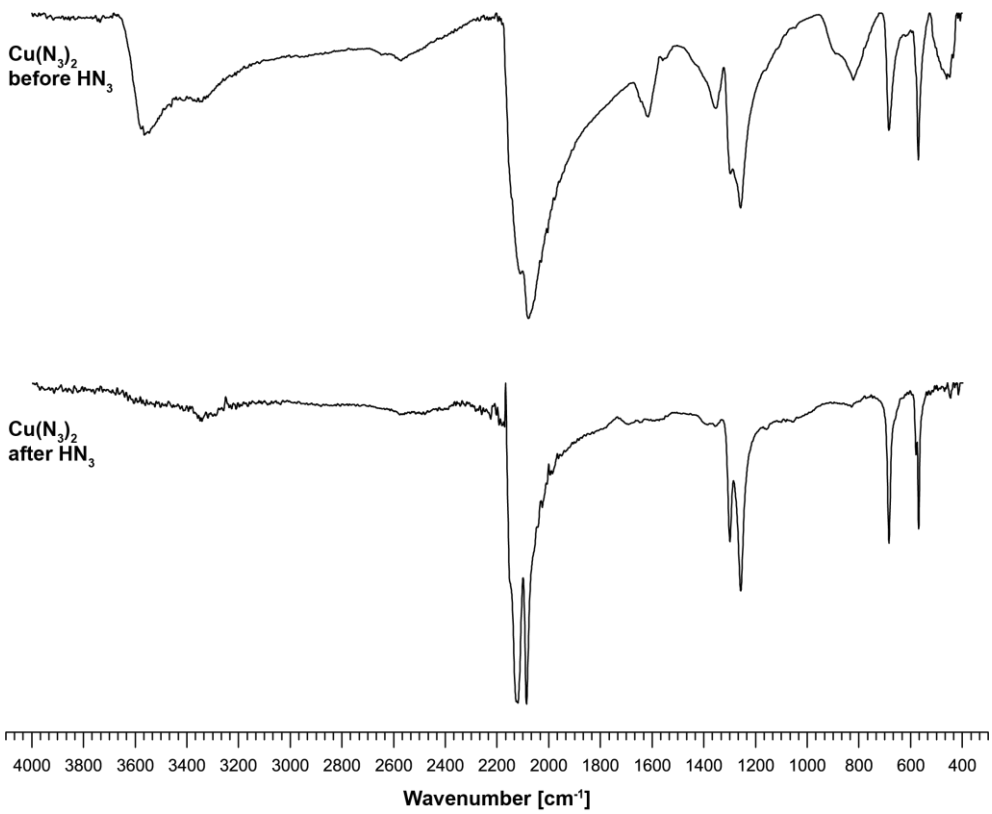

Figure S18. IR spectra of copper(II) azide before and after treatment with diluted HN_3.

$Cu(N_3)_2$ appears to be significantly less sensitive when wet (H_2O, EtOH). It is however very sensitive in the dry state (also when wetted with Et_2O), exploding occasionally during manipulation, *e.g.*, due to slight scratches when being removed from the filter paper (Figure S20).

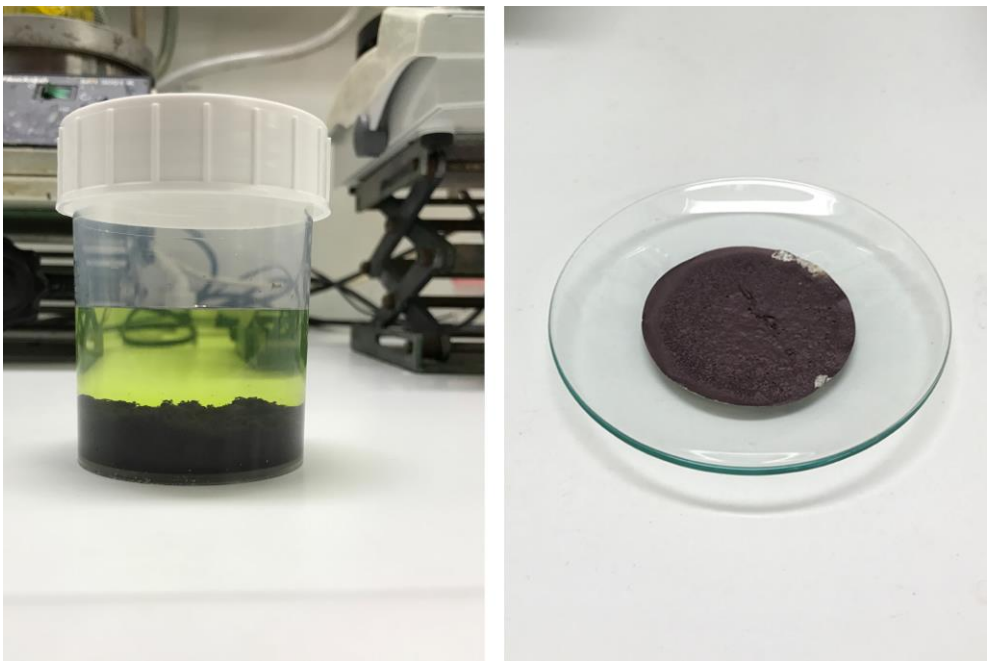

Figure S19. Copper azide under HN_3 (left) and on a filter paper, after washing with ether.

Figure S20. Failed attempt to remove $Cu(N_3)_2$ from a filter paper (left), successful attempt (right).

11.6.10. References

[1] NATO standardization agreement (STANAG) on explosives, impact sensitivity tests, no. 4489, 1st ed., Sept. 17, **1999**.

[2] WIWEB-Standardarbeitsanweisung 4-5.1.02, Ermittlung der Explosionsgefährlichkeit, hier der Schlagempfindlichkeit mit dem Fallhammer, Nov. 8, **2002**.

[3] OZM, http://www.ozm.cz, (accessed January 2020).

[4] BAM, http://www.bam.de, (accessed January 2020).

[5] NATO standardization agreement (STANAG) on explosive, friction sensitivity tests, no. 4487, 1st ed., Aug. 22, **2002**.

[6] WIWEB-Standardarbeitsanweisung 4-5.1.03, Ermittlung der Explosionsgefährlichkeit oder der Reibeempfindlichkeit mit dem Reibeapparat, Nov. 8, **2002**.

[7] Impact: insensitive > 40 J, less sensitive ≥ 35 J, sensitive ≥ 4 J, very sensitive ≤ 3 J; Friction: insensitive > 360 N, less sensitive = 360 N, sensitive < 360 N and > 80 N, very sensitive ≤ 80 N, extremely sensitive ≤ 10 N. According to the UN Recommendations on the Transport of Dangerous Goods, 5th ed., **2009**.

[8] M. Straumanis, A. Cīrulis, *Z. Anorg. Allg. Chem.* **1943**, *251*, 315–331.

[9] J. I. Bryant, H. Rosenwasser, *J. Chem. Educ.* **1962**, *39*, 296.

[10] T. Costain, F. B. Wells, *Technology of the inorganic azides*, Plenum Press, New York **1977**, pp. 11–54.

[11] CrysAlisPRO (Version 171.33.41), Oxford Diffraction Ltd., **2009**.

[12] A. Altomare, G. Cascarano, C. Giacovazzo, A. Guagliardi, *J. Appl. Crystallogr.* **1993**, *26*, 343–350.

[13] a) A. Altomare, G. Cascarano, C. Giacovazzo, A. Guagliardi, A. G. G. Moliterni, M. C. Burla, G. Polidori, M. Camalli and R. Spagna, SIR97, **2003**; b) A. Altomare, M. C. Burla, M. Camalli, G. L. Cascarano, C. Giacovazzo, A. Guagliardi, A. G. G. Moliterni, G. Polidori and R. Spagna, *J. Appl. Crystallogr.* **1999**, *32*, 115.

[14] a) G. M. Sheldrick, SHELXL-97, University of Göttingen, Germany, **1997**; b) G. M. Sheldrick, *Acta Crystallogr. Sect. A* **2008**, *64*, 112.

[15] A. L. Spek, PLATON, Utrecht University, The Netherlands, **1999**.

[16] L. J. Farrugia, *J. Appl. Cryst.* **2012**, *45*, 849.

[17] Empirical absorption correction using spherical harmonics, implemented in SCALE3 ABSPACK scaling algorithm (CrysAlisPro Oxford Diffraction Ltd., Version 171.33.41, **2009**).

[18] APEX3, Bruker AXS Inc., Madison, Wisconsin, USA.

[19] J. R. Rodriguez-Carvajal, Abstracts of the Satellite Meeting on Powder Diffraction of XV Congress of the IUCr, Toulouse, France, **1990**, 127.

[20] C. M. Csernica, *40th Int. Pyro. Symp.*, Colorado **2014**, pp. 114–133.

[21] I. Agrell, *Acta Chem. Scand.* **1967**, *21*, 2647–2658.

12. Taming the Dragon: Complexation of Silver Fulminate with Nitrogen-rich Azole Ligands

Maximilian H. H. Wurzenberger, Michael S. Gruhne, Marcus Lommel, Vanessa Braun, Norbert Szimhardt, and Jörg Stierstorfer

Reprinted (adapted) with permission from *Inorganic Chemistry* **2020**, *59*, 17875–17879.

DOI: 0.1021/acs.inorgchem.0c03027

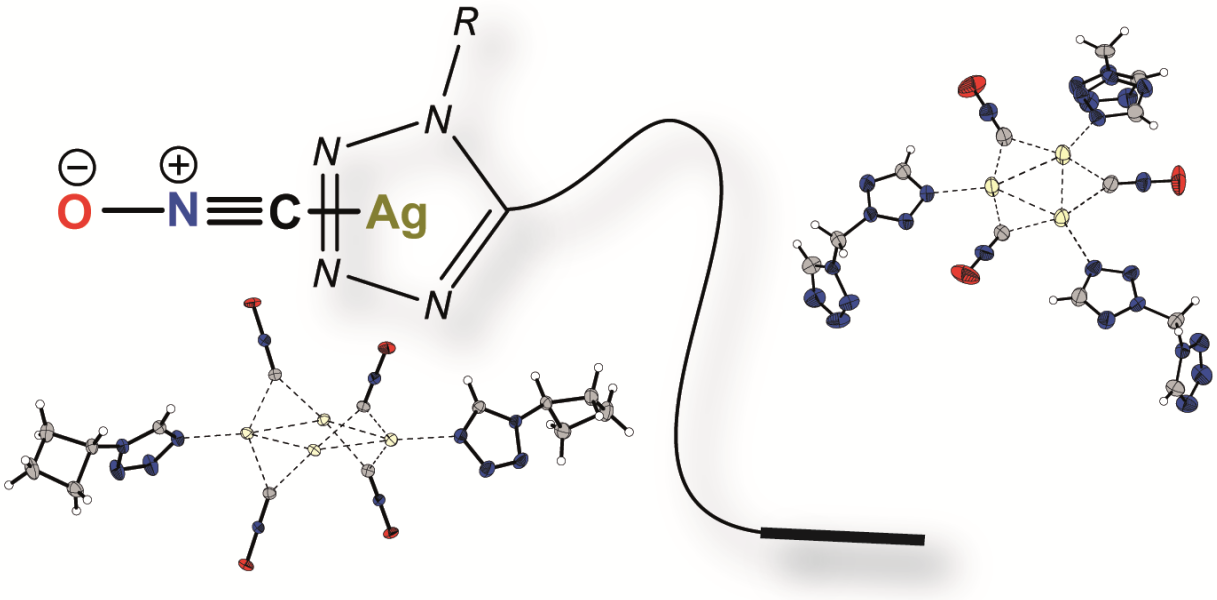

Abstract: The almost ancient and very sensitive silver fulminate (SF), which was involved in the establishment of fundamental chemical concepts, was desensitized for the first time with different nitrogen-rich triazoles and tetrazoles, yielding SF complexes $[Ag_x(CNO)_x(N\text{-Ligand})_y]$ (x = 1–4; y = 1–3). These were accurately characterized (X-ray diffraction, scanning electron microscopy, IR, elemental analysis, differential thermal analysis, and thermogravimetric analysis) and investigated concerning their energetic character. The highly energetic coordination compounds suddenly show, in contrast to SF, sensitivities in a manageable range and are therefore safer to handle. In particular, compounds $[Ag_4(CNO)_4(BTRI)]$ [**3**; BTRI = 4,4'-bis(1,2,4-triazole)] and $[Ag_4(CNO)_4(2,2\text{-dtp})]$ [**8**; 2,2-dtp = 1,3-di(tetrazol-2-yl)propane] show values in the range of desired lead styphnate alternatives with similar energetic performances. The crystal structure experiments reveal silver cluster formation in all complexes with distinct argentophilic interactions close to 2.77 Å. Furthermore, it was possible to synthesize **8** in a one-pot reaction, avoiding the isolation of highly sensitive SF.

12.1. Introduction

During a time when alchemy turned into chemistry and attempts were made to transmute elements into gold and silver, the first fulminates were born. The history of fulminates dates back at least to the 17th century, when the unintentional synthesis of mercury fulminate (MF) by Kunckel led to a severe explosion.[1] This incident demonstrates the highly sensitive nature that all fulminates have in common and that is affected by the type of bonding (ionic vs covalent) within the compounds.[2] The explosive characteristics are also responsible for the compounds' designation, which is derived from the Latin word "fulminare", which means "to strike with lightning".[3] Since the first isolation of MF, the most common compound of this class, by Howard in 1799, several famous chemists have investigated fulminates (*e.g.*, Liebig, Gay-Lussac, Kekulé, Pauling, Huisgen, Beck, and many more), which has led to breakthrough discoveries such as the concept of isomerism.[4] Besides the acquisition of fundamental comprehensions and its use for military applications, MF has played a crucial role for peaceful purposes. It enabled, for the first time, the detonation of safely manageable dynamite at the end of the 19th century, thus facilitating civil engineering in general as well as allowing megaprojects such as construction of the Panama Canal (Figure 1A).[1,5]

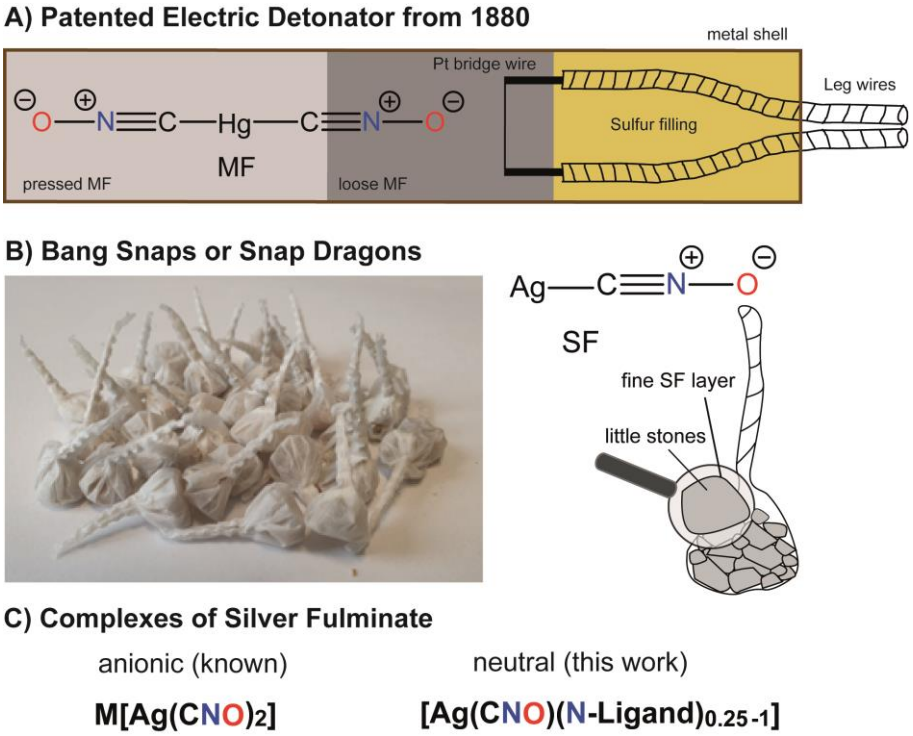

Figure 1. A) MF in detonators for dynamite initiation. B) SF for bang snaps. C) Complexation of SF.

Except for MF, the only other readily accessible metal fulminate, starting from the corresponding metal, nitric acid, and ethanol, is represented by its silver salt. Silver fulminate (SF) is an extremely dangerous primary explosive (especially toward electrostatic discharge) that can even explode during filtration or

underwater and that is therefore too sensitive for almost any application (this corresponds with our experiences!).[6] To the best of our knowledge, the only application of SF is in “bang snaps”, also called “snap dragons” (Figure 1B). Small amounts of SF, which coats tiny stones that are wrapped in thin paper, instantly detonate when dropped. Nevertheless, it was intensively examined by Liebig, who was able to handle up to 100 g of this compound. This not only led to the perfection of his well-known carbon, hydrogen, and nitrogen analysis but also proved his exceptional abilities and great skills.[7] He was also the first one who investigated simple fulminato complexes such as $K[Ag(CNO)_2]$ (Figure 1C). Soon, several more compounds followed, which were discovered by Nef,[8] Wöhler and Martin,[9] and Wieland.[10] Despite their explosive and sensitive character, all of these complexes had in common that they did not receive much attention regarding their coordination behavior at that time. More detailed examinations on the complexing nature of the CNO^- anion were carried out by Beck, whose work with metal fulminates was extensive.[11] For the first time, it was also possible to obtain nonexplosive and thermally stable fulminato complexes by using large-volume cations.[12] Completely unknown in the literature are fulminate complexes with nitrogen-donor ligands, and especially rare are single-crystal X-ray diffraction (XRD) investigations of fulminate compounds. In recent years, the concept of energetic coordination compounds (ECC) gained increasing interest among scientists worldwide, and various reports set the stage for their future applications.[13–18] Herein, we report the first-ever SF complexes based on nitrogen-rich azole ligands.

12.2. Results and Discussion

Following the concept of ECC, highly sensitive SF was combined with (highly) endothermic nonacidic triazole and tetrazole ligands. The incorporation reveals practicable ECC with very diverse and interesting coordination spheres compared to pure SF. Therefore, AgCNO was synthesized according to our preferred literature procedure, which starts with elementary silver, nitric acid, and absolute ethanol.[19] SF was further reacted with readily obtained azole ligands.[20–22] The reaction conditions are highly dependent on the ligand systems used, and all compounds were obtained as colorless solids with satisfactory to very good yields (56–89%). All ECC can be stored at ambient conditions and do not show any evidence for decomposition. However, safety precautions (such as Kevlar gloves, face shields, ear protection, etc.) must be applied when handling pure SF and its complexes. Complexes **2**, **4**, and **6**–**8** can easily be crystallized by dissolving AgCNO in a solution of the appropriate amount of ligand in acetonitrile/water (50:50). Whereas the ECC **5** can be synthesized in the same solvent system using an excess of ligand to prevent the formation of pure SF, the coordination compound **2** can be crystallized by adding some drops of aqueous ammonia to the reaction mixture (Scheme 1). When SF is added to the

dissolved ligands in a relatively small amount of solvent, complexes **2**, **6**, and **8** can also be precipitated from the reaction solution, which has to be stirred for 15 (**6** and **8**) to 45 min (**2**). Interestingly, the ECC **8** can be synthesized in a one-pot reaction, avoiding isolation of the highly sensitive SF. Therefore, elemental silver is reacted with nitric acid, and 1,3-di(tetrazol-2-yl)propane (2,2-dtp) dissolved in ethanol is added, which results in the formation of a colorless precipitate (most probably the corresponding silver nitrate complex). When heated with stirring, the solid dissolves around 70 °C, and the typical formation (gas generation accompanied by the precipitation of an off-white solid) of SF occurs. However, instead of pure AgCNO, the corresponding ECC **8** is formed in a very high yield of 89%.

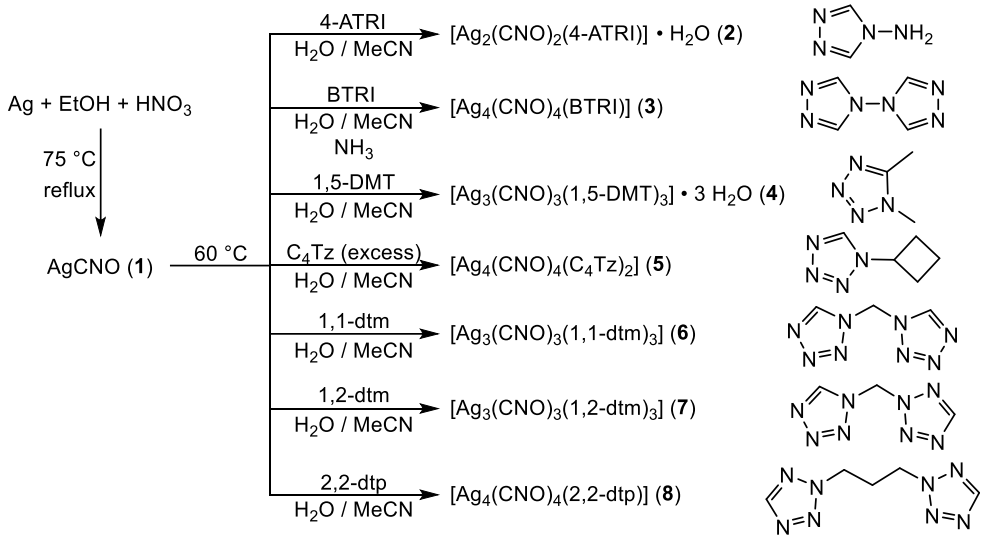

Scheme 1. Synthesis of SF and its conversion to practical ECC. Overview of the azole ligands used: 4-ATRI: 4-amino-1,2,4-triazole; BTRI: 4,4'-bi(1,2,4-triazole); 1,5-DMT: 1,5-dimethyltetrazole; C_4Tz: 1-cyclobutyl-5*H*-tetrazole; 1,1-dtm: di(tetrazol-1-yl)methane; 1,2-dtm: (tetrazol-1-yl)(tetrazol-2-yl)methane; 2,2-dtp: 1,3-di(tetrazol-2-yl)propane.

All ECC were investigated by single-crystal XRD experiments. Pure SF occurs in two different polymorphic forms, an orthorhombic one as well as a trigonal one.[23] In both cases, coordination of the fulminate anions can be described as a bridging of the terminal carbon and oxygen atoms (Figure 2, **A**) with shorter Ag–C bond lengths (~2.2 Å) compared to the Ag–O ones, leading to 3D polymeric structures. Because some of the Ag–O distances are longer than 2.7 Å, the linking of the anion is better represented as being in mode **B** or between that of **A** and **B**. The addition of nitrogen-donor ligands to SF reveals very diverse and worthwhile coordination chemistry. The same two main coordination modes can be observed in the ECC **2**–**8** (Figures 2 and S3–S9 and Tables S1 and S2). While all structures have the bridging behavior of the fulminate carbon atom between two silver cations in common (Ag–C–Ag = 77–91°), in compounds **2**–**4**, **6**, and **7**, no Ag–O interactions are observed at all. The Ag–O distances in the ECC **5** and **8** are in the range of 2.49–3.01 Å, with most of them above 2.6 Å, which indicates rather weak bonding between them. In all structures, the clear presence of Ag–Ag interactions is observable. These

argentophilic interactions are defined as sub van der Waals contacts (<3.44 Å) and have gained increasing attention within the last years.[24–27] The closest Ag–Ag distance with 2.7705(5) Å can be found in the ECC **8**, which is very close to the shortest reported argentophilic interaction [2.7599(3) Å].[28]

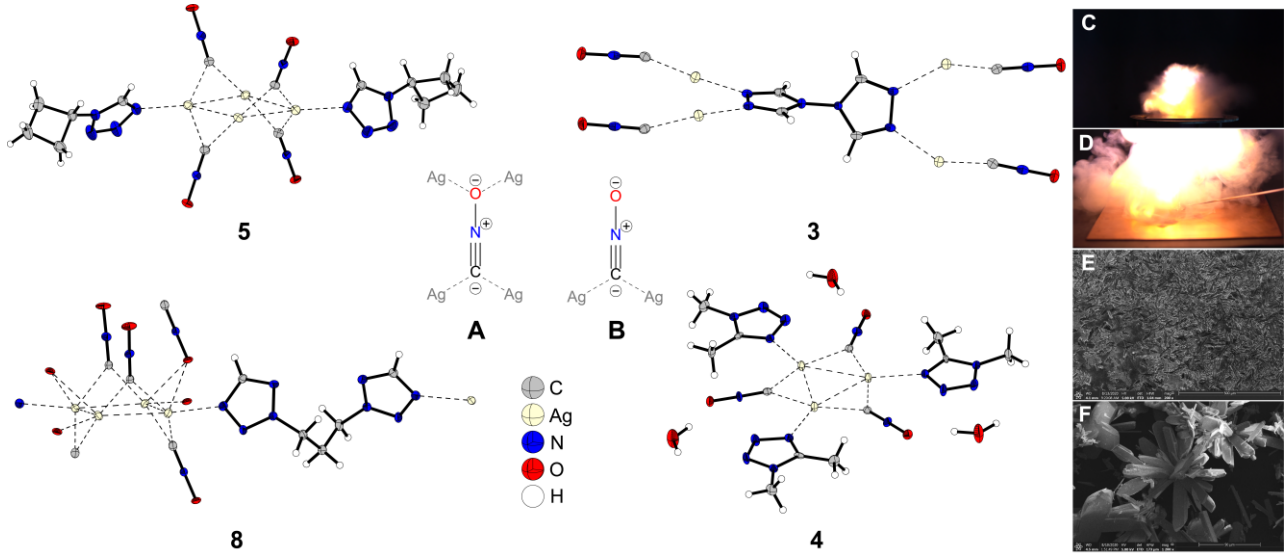

Figure 2. Different bridging modes **A** and **B** of the fulminate anion and molecular units of **3**–**5** as well as the extended molecular unit of **8**. Ellipsoids are set to the 50% probability level.[29] Physicochemical properties: (C) detonation of the ECC **3** during the hot plate test; (D) deflagration of **3** during the hot needle test; (E) SEM image of decomposed AgCNO (200× enlargement); (F) SEM image of complex **8** (1200× enlargement).

The ECC **4**, **6**, and **7** are the only compounds that form complex monomers that consist of silver trimers. Coordination of the ditetrazolylmethane ligands with only one of their rings in **6** and **7** is a literature-known issue.[22] In complexes **4** and **8**, tetrameric clusters of silver are present, which build up 2D polymeric layers via Ag–Ag and Ag–O bonding. The additional linking of the ligand in **8** is connecting the layers and leads to the formation of a 3D polymeric network. Contrary to **8**, formation of the 3D structure in **3** is caused by 4-fold coordination of the ligand to different silver atoms, preventing the formation of Ag–O bonds. All ECC were analyzed regarding their physicochemical properties, and their sensitivities toward various external stimuli were determined and are summarized in Table 1. Whereas pure SF does not possess no-fire limits for friction and electrostatic discharge sensitivities, in every case, the incorporation of nitrogen-rich ligands leads to stabilization. Considering the friction sensitivity, it becomes clear that it corresponds with the SF to ligand ratio. Therefore, complexes **3** and **8** are the most sensitive ones, with values close to those of lead styphnate (LS). The incorporation of water molecules creates compounds that are completely insensitive and therefore safe to handle. All ECC show lower thermal stabilities compared to pure SF, except compound **3**, which exceeds 200 °C. Interestingly, the incorporation of bridging ligands (**2**, **3**, and **8**) causes higher exothermic decomposition temperatures, whereas monodentate acting ligands (**4**–**7**) lead to lower thermal stabilities.

Table 1. Summary of the compounds' thermal stability,[a] sensitivities toward various external stimuli, and results of hot plate (HP) and hot needle (HN) tests compared to SF and LS.

	$T_{endo.}$ [°C][b]	$T_{exo.}$ [°C][c]	*IS* [J][d]	*FS* [N][e]	*ESD* [mJ][f]	*BDIS* [mJ][g]	HP[h]	HN[h]
AgCNO (**1**)	-	196	5[19]	≤ 0.1[19]	≤ 0.28	≤ 4[19]	det.	det.
$[Ag_2(CNO)_2(4\text{-ATRI})] \cdot H_2O$ (**2**)	64, 89	187	> 40	> 360	> 1000	> 200	def.	dec.
$[Ag_4(CNO)_4(BTRI)]$ (**3**)	-	215	5	10	2.5	55	det.	def.
$[Ag_3(CNO)_3(1,5\text{-DMT})_3] \cdot 3\ H_2O$ (**4**)	82	138	> 40	> 360	740	> 200	def.	dec.
$[Ag_4(CNO)_4(C_4Tz)_2]$ (**5**)	-	133	20	84	7.3	> 200	det.	def.
$[Ag_3(CNO)_3(1,1\text{-dtm})_3]$ (**6**)	-	152	6	72	25	28	def.	def.
$[Ag_3(CNO)_3(1,2\text{-dtm})_3]$ (**7**)	-	144	7	64	203	41	def.	def.
$[Ag_4(CNO)_4(2,2\text{-dtp})]$ (**8**)	-	177	8	1	0.7	8	det.	det.
LS[19,30]	-	275–280	2.5–5	0.5–5	0.02–1	15	det.	det.

[a] Onset temperature at a heating rate of 5 °C min^{-1} measured by DTA; [b] Endothermic peak, which indicates melting or dehydration; [c] Exothermic peak, which indicates decomposition. [d] Impact sensitivity according to the BAM drop hammer (method 1 of 6). [e] Friction sensitivity according to the BAM friction tester (method 1 of 6). [f] Electrostatic discharge sensitivity (OZM Electric Spark XSpark10). [g] Ball drop impact sensitivity determined with the 1 of 6 method in accordance with the MIL-STD 1751A (method 1016). [h] dec.: decomposition; def.: deflagration; det.: detonation.

Hot plate and hot needle tests reveal the energetic character of the complexes, which all show deflagrations or even detonations (Figures 2 and S13–S20). Whereas none of the ECC can detonate nitropenta in classical initiation tests, the energetic performances of complexes **3** and **8** are similar to that of LS, making them potential lead-free replacements. Scanning electron microscopy (SEM) was performed to examine the morphology of some of the compounds and compare it with that of pure SF (Figures 2 and S21–S24). Interestingly, SF is the first primary explosive in our research group that is too sensitive to be investigated using SEM. During the sample preparation, the substances have to be sputtered using a high-voltage pulse. Most likely, it is the high electrostatic discharge sensitivity of **1** that causes decomposition during the process. In contrast, the ECC show different crystal morphologies with differing crystal sizes, demonstrating their improved stability.

12.3. Conclusion

In conclusion, we successfully synthesized seven new SF complexes based on different neutral nitrogen-rich azole ligands. All ECC show fascinating coordination behavior with cluster formation and argentophilic interactions close to the shortest reported Ag–Ag distances. The resulting compounds possess manageable sensitivities, and ligands with bridging character increased the thermal stability up to 215 °C. The possible synthesis of complex **8** in a one-pot reaction from elemental silver, ethanol, nitric acid, and ligand in high yields avoids the isolation of pure SF and opens the field to a safe synthesis of SF complexes, which could be used as a potential replacement for LS.

12.4. Acknowledgements

The authors are grateful for financial support of this work by Ludwig-Maximilians-University (LMU). The authors want to thank Prof. Dr. Thomas M. Klapötke for scientific input and for providing research infrastructure and Prof. Dr. Wolfgang Beck for inspiring discussions. Furthermore, we are very grateful to Mr. Moritz Kofen and Mrs. Jasmin Lechner for providing 1,5-DMT and graphical support and to Mrs. Lisa Eichacker for proofreading.

12.5. References

[1] F. Kurzer, *J. Chem. Educ.* **2000**, *77*, 851–857.

[2] Z. Iqbal, A. D. Yoffe, *Proc. Roy. Soc. A.* **1967**, *302*, 35–49.

[3] W. R. Martin, D. W. Ball, *J. Energ. Mater.* **2019**, *37*, 70–79.

[4] W. Beck, J. Evers, M. Göbel, G. Oehlinger, T. M. Klapötke, *Z. Anorg. Allg. Chem.* **2007**, *633*, 1417–1422.

[5] A. J. Moss, *Ann. Noninvasive Electrocardiol.* **2007**, *12*, 79–80.

[6] R. Matyáš, J. Pachman, *Primary Explosives*, 1st ed., Springer, Berlin, Heidelberg, **2013**.

[7] W. Beck, *Eur. J. Inorg. Chem.* **2003**, *24*, 4275–4288.

[8] J. U. Nef, *Ann. Chem.* **1894**, *280*, 263–342.

[9] L. Wöhler, F. Martin, *Ber. Dtsch. Chem. Ges.* **1917**, *50*, 586–596.

[10] H. Wieland, *Justus Liebigs Ann. Chem.* **1925**, *444*, 7–40.

[11] W. Beck, *Organometal. Chem. Rev. A* **1971**, *7*, 159–190.

[12] W. Beck, P. Swoboda, K. Feldl, E. Schuierer, *Chem. Ber.* **1970**, *103*, 3591–3604.

[13] T. W. Myers, J. A. Bjorgaard, K. E. Brown, D. E. Chavez, S. K. Hanson, R. J. Scharff, S. Tretiak, J. M. Veauthier, *J. Am. Chem. Soc.* **2016**, *138*, 4685–4692.

[14] Q. Zhang, J. M. Shreeve, *Angew. Chem. Int. Ed.* **2014**, *53*, 2540–2542.

[15] M. H. H. Wurzenberger, N. Szimhardt, J. Stierstorfer, *J. Am. Chem. Soc.* **2018**, *140*, 3206–3209.

[16] M. A. Ilyushin, A. A. Kotomin, S. A. Dushenok, *Russ. J. Phys. Chem. B* **2019**, *13*, 119–138.

[17] Q. Sun, X. Li, Q. Lin, M. Lu, *J. Mater. Chem. A* **2019**, *7*, 4611–4618.

[18] T.-A. D. Nguyen, J. M. Veauthier, G. F. Angles-Tamayo, D. E. Chavez, E. Lapsheva, T. W. Myers, T. R. Nelson, E. J. Schelter, *J. Am. Chem. Soc.* **2020**, *142*, 4842–4851.

[19] M. S. Gruhne, M. Lommel, M. H. H. Wurzenberger, N. Szimhardt, T. M. Klapötke, J. Stierstorfer, *Propellants Explos. Pyrotech.* **2020**, *45*, 147–153.

[20] A. F. Brigas, *Sci. Synth.* **2004**, *13*, 861–915.

[21] A. A. Kirilchuk, A. A. Yurchenko, Yu. G. Vlasenko, A. N. Kostyuk, A. B. Rozhenko *Chem. Heterocycl. Compd.* **2015**, *50*, 1559–1566.

[22] M. H. H. Wurzenberger, V. Braun, M. Lommel, T. M. Klapötke, J. Stierstorfer, *Inorg. Chem.* **2020**, *59*, 10938–10952.

[23] D. Britton, J. D. Dunitz, *Acta Cryst.* **1965**, *19*, 662–668.

[24] G.-G. Gao, P.-S. Cheng, T. C. W. Mak, *J. Am. Chem. Soc.* **2009**, *131*, 18257–18259.

[25] H. Schmidbaur, A. Schier, *Angew. Chem. Int. Ed.* **2015**, *54*, 746–784.

[26] L. Mistry, O. El-Zubir, G. Dura, W. Clegg, P. G Waddell, T. Pope, W. A. Hofer, N. G. Wright, B. R. Horrocks, A. Houlton, *Chem. Sci.* **2019**, *10*, 3186–3195.

[27] Q.-Y. Wang, J. Wang, S. Wang, Z.-Y. Wang, M. Cao, C.-L. He, J.-Q. Yang, S.-Q. Zang, T. C. W. Mak *J. Am. Chem. Soc.* **2020**, *142*, 12010–12014.

[28] P. Ai, A. A. Danopoulos, P. Braunstein, K. Yu. Monakhov, *Chem. Commun.* **2014**, *50*, 103–105.

[29] Selected X-ray data: **3**: *Ccca*, *a* 11.8399(9) Å, *b* 20.8348(16) Å, *c* 5.8163(3) Å, *V* 1434.78(17) Å^3, *Z* 8, *ρ* 3.406 g cm^{-3}; **4**: *P*6$_3$/*m*, *a* 15.0648(5) Å, *c* 6.1186(4) Å, *V* 1202.57(13) Å^3, *Z* 2, *ρ* 2.204 g cm^{-3}; **5**: *C*2/*c*, *a* 32.653(3) Å, *b* 5.4602(5) Å, *c* 12.9896(11) Å, *β* 97.805(3)°, *V* 2294.5(4) Å^3, *Z* 8, *ρ* 2.454 g cm^{-3}; **8**: *P*2/*c*, *a* 12.5173(11) Å, *b* 5.6400(4) Å, *c* 12.8877(10) Å, *β* 100.146(8)°, *V* 895.61(12) Å^3, *Z* 2, *ρ* 2.891 g cm^{-3}.

[30] T. M. Klapötke, *Energetic Materials Encyclopedia*, 1st ed., De Gruyter, Berlin, Boston, **2018**.

12.6. Supporting Information

12.6.1. Experimental Part and General Methods

All chemicals and solvents were employed as received (Sigma-Aldrich, Fluka, Acros, ABCR). Exothermic events of the described compounds, which indicate decomposition, are given as the extrapolated onset temperatures. The samples were measured in a range of 25–400 °C at a heating rate of 5 °C min^{-1} through differential thermal analysis (DTA) with an OZM Research DTA 552-Ex instrument and in some cases additional by thermal gravimetric analysis (TGA) with a PerkinElmer TGA4000. Infrared spectra were measured with pure samples on a Perkin-Elmer BXII FT-IR system with a Smith DuraSampler IR II diamond ATR. Determination of the carbon, hydrogen and nitrogen contents was carried out by combustion analysis using an Elementar Vario El (nitrogen values determined are often lower than the calculated ones due to their explosive behavior). Impact sensitivity tests were carried out according to STANAG 4489[1] with a modified instruction[2] using a BAM (Bundesanstalt für Materialforschung und -prüfung) drop hammer.[3,4] Ball drop impact sensitivity tests were determined for selected compounds on an OZM ball drop machine (BIT-132), following MIL-STD-1751A (method

1016) by dropping a free falling steel ball onto the explosive compound.[5] A sample of approximately 30 mg was placed on a steel block and spread into a 0.33 mm layer of substance. The steel ball guide was set to the desired height and the loaded impact block positioned underneath. By releasing the ball shield, a 0.500-inch steel ball, weighing 8.35 g, was allowed to fall onto the sample. Any visual observation of decomposition was regarded as a positive result. If no reaction occurred, the remaining substance was disposed, and the impact block loaded with a freshly prepared sample. The limiting impact energy was determined in conformity with the recommended UN method for testing impact and friction sensitivities (1-in-6 approach), according to ST/SG/AC.10/11Rev.6 (s. 13.4.2.3.3).[6] The impact energy was calculated as the product of the weight of the steel ball and its fall height. An initial drop height was chosen, at which an explosion of the sample could be ensured. The impact energy level (ball guide height) was now stepwise decreased until no reaction was observed. At this point, testing was continued up to a total of six trials at that certain energy level. If an explosion occurred, the procedure was repeated by decreasing the drop height. As soon as six trials at a fixed energy level emerged as negative, the next higher energy level, where at least one out of at least six trials resulted in an explosion, is determined as the limiting impact energy. Friction sensitivity tests were carried out according to STANAG 4487[7] with a modified instruction[8] using the BAM friction tester. The classification of the tested compounds results from the "UN Recommendations on the Transport of Dangerous Goods".[9] Additionally, all compounds were tested upon the sensitivity toward electrical discharge using the OZM Electric Spark XSpark10 device.[3] Hot plate and hot needle tests were performed in order to classify the initiation capability of selected complexes. The samples were fixed on a copper plate underneath adhesive tape and initiated by a red-hot needle. Strong deflagration or detonation of the compound usually indicates a valuable primary explosive. The safe and straightforward hot plate test only shows the behavior of the unconfined sample toward fast heating on a copper plate. It does not necessarily allow any conclusions on a compound´s capability as a suitable primary explosive. Initiation capability tests of the newly investigated complexes toward pentaerythritol tetranitrate (PETN) were carried out in a copper shell with a diameter of 7 mm and a length of 88 mm filled with 200 mg of sieved PETN (grain size < 100 µm). First, nitropenta was pressed with a weight of 8 kg, then the primary explosive to be investigated was subsequently filled loosely on top of the main charge. The shell was sealed by an insulator, placed in a retaining ring, which was soldered to a copper witness plate with a thickness of 1 mm and finally initiated by a type A electric igniter. A positive test is indicated by a hole in the copper plate and fragmentation of the shell caused by a deflagration-to-detonation transition (DDT) of PETN. None of the compounds was able to successfully transfer a detonation toward PETN. The morphology of selected samples was determined by a scanning

electron microscope (SEM) NanoLab G3 (Helios). The samples were carbon-coated (BAL-TEC MED 020, Bal Tec AG) to hinder electrostatic charging and to increase the conductivity.

The obtained coordination compounds were washed with cold ethanol and water when stated, dried overnight in air and used for analytics without further purification.

CAUTION! *All investigated compounds are highly energetic materials, which show increased sensitivities toward various stimuli (e.g., elevated temperatures, impact, friction or electrostatic discharge). Especially pure silver fulminate is highly unpredictable and sometimes is blowing up during filtration. Therefore, proper security precautions (safety glasses, face shield, earthed equipment and shoes, leather jacket, Kevlar gloves, Kevlar sleeves and ear plugs) have to be worn while synthesizing and handling the described compounds and it is recommended to handle a maximum amount of 500 mg of pure SF.*

Procedure for the preparation of silver fulminate

Silver fulminate was synthesized according to a literature procedure by dissolving silver (432 mg, 4.00 mmol) in 65% nitric acid (5.60 mL, 124 mmol) and water (2.40 mL).[10] The mixture was added to 96% EtOH (9.60 mL, 164 mmol) and under stirring heated to reflux. After the vigorous formation of gas, a solid precipitated and the solution was allowed to cool to room temperature while stirring. The reaction mixture was decanted with water several times until a neutral pH value was obtained. The colorless solid was very carefully filtrated off and dried at ambient conditions over night yielding 474 mg pure silver fulminate (3.16 mmol, 79%).

DTA (5 °C min^{-1}) onset: 196 °C; IR (ATR, cm^{-1}): $\tilde{\nu}$ = 3184 (w), 2244 (m), 2096 (s), 1738 (m), 1569 (m), 1370 (m), 1230 (w), 1130 (vs), 493 (m), 462 (m); EA (CAgNO, 149.89) calcd.: C 8.01, N 9.54%; found: C 8.46, N 9.54%; BAM drop hammer: 5 J; friction tester: ≤ 0.1 N; ESD: ≤ 0.28 mJ (at grain size < 100 µm).

General procedure for the preparation of complexes 2, 4, and 6–8

The ligand (**2**: 0.50 mmol, 42.0 mg, (4-ATRI); **4**: 1.00 mmol, 98.1 mg, (1,5-DMT); **6**: 1.00 mmol, 152 mg, (1,1-dtm); **7**: 1.00 mmol, 152 mg, (1,2-dtm); **8**: 0.25 mmol, 45.0 mg, (2,2-dtp)) was dissolved in 10 mL of water and acetonitrile (50:50) at 60 °C and silver fulminate (1.00 mmol, 150 mg) was added. The resulting reaction mixture was stirred at elevated temperatures and solvent was added until a complete dissolution was obtained. Afterwards the solutions were left in air for crystallization, filtered off and washed with cold ethanol.

$[Ag_2(CNO)_2(4\text{-ATRI})] \cdot H_2O$ (2)

Monohydrate complex **2** crystallized within one day as colorless needles. Yield: 152 mg (0.38 mmol, 76%)

DTA (5 °C min^{-1}) onset: 64 °C (endothermic), 89 °C (endothermic), 187 °C (exothermic); IR (ATR, cm^{-1}): $\tilde{\nu}$ = 3563 (w), 3443 (m), 3314 (s), 3253 (m), 3207 (m), 3005 (m), 2575 (m), 2321 (m), 2075 (s), 2039 (s), 2009 (s), 1710 (m), 1621 (s), 1546 (s), 1528 (m), 1475 (m), 1399 (m), 1370 (m), 1318 (m), 1225 (w), 1212 (w), 1165 (s), 1078 (s), 1021 (s), 993 (vs), 979 (vs), 866 (s), 692 (w), 670 (w), 616 (s), 571 (m), 483 (m); EA ($C_4H_6Ag_2N_6O_3$, 401.87) calcd.: C 11.96, H 1.50, N 20.91%; found: C 12.05, H 1.42, N 20.81%; BAM drop hammer: > 40 J; friction tester: > 360 N; ESD: > 1000 mJ; ball drop impact tester: > 200 mJ (at grain size 100–500 µm).

$[Ag_3(CNO)_3(1,5\text{-}DMT)_3] \cdot 3\ H_2O$ (4)
Coordination compound **3** was obtained within one hour. Yield: 225 mg (0.28 mmol, 85%)

DTA (5 °C min^{-1}) onset: 82 °C (endothermic), 138 °C (exothermic); IR (ATR, cm^{-1}): $\tilde{\nu}$ = 3587 (w), 3500 (w), 3267 (w), 2374 (vw), 2100 (s), 2013 (w), 1603 (w), 1546 (m), 1483 (w), 1466 (w), 1451 (w), 1414 (w), 1398 (w), 1389 (w), 1383 (w), 1301 (w), 1258 (w), 1221 (vw), 1190 (vs), 1107 (m), 1044 (w), 1020 (w), 731 (m), 670 (s), 513 (m), 505 (m), 497 (m); EA ($C_{12}H_{24}Ag_3N_{15}O_6$, 798.03) calcd.: C 18.06, H 3.03, N 26.33%; found: C 18.22, H 2.93, N 26.34%; BAM drop hammer: > 40 J; friction tester: > 360 N; ESD: 740 mJ; ball drop impact tester: > 200 mJ (at grain size < 100 µm).

$[Ag_3(CNO)_3(1,1\text{-}dtm)_3]$ (6)
ECC **6** crystallized within one day. Yield: 205 mg (0.23 mmol, 68%)

DTA (5 °C min^{-1}) onset: 152 °C (exothermic); IR (ATR, cm^{-1}): $\tilde{\nu}$ = 3268 (w), 3144 (m), 3121 (w), 3058 (w), 3007 (w), 2095 (s), 1572 (w), 1497 (w), 1467 (m), 1427 (m), 1391 (w), 1383 (w), 1306 (w), 1227 (w), 1198 (s), 1172 (s), 1095 (vs), 1021 (m), 985 (m), 943 (w), 891 (w), 879 (w), 790 (s), 740 (vs), 714 (m), 649 (m), 501 (w); EA ($C_{12}H_{12}Ag_3N_{27}O_3$, 906.03) calcd.: C 15.91, H 1.34, N 41.74%; found: C 15.80, H 1.48, N 41.87%; BAM drop hammer: 6 J; friction tester: 72 N; ESD: 25 mJ; ball drop impact tester: 28 mJ (at grain size 100–500 µm).

$[Ag_3(CNO)_3(1,2\text{-}dtm)_3]$ (7)
Complex **7** crystallized as colorless rods within one day. Yield: 169 mg (0.19 mmol, 56%)

DTA (5 °C min^{-1}) onset: 144 °C (exothermic); IR (ATR, cm^{-1}): $\tilde{\nu}$ = 3269 (w), 3143 (w), 3057 (w), 3002 (w), 2391 (w), 2092 (s), 1775 (w), 1572 (w), 1476 (m), 1465 (w), 1436 (w), 1421 (m), 1358 (m), 1348 (m), 1300 (w), 1293 (w), 1199 (s), 1168 (s), 1140 (m), 1125 (s), 1095 (vs), 1040 (s), 1018 (s), 966 (w), 944 (m), 889 (m), 836 (w), 797 (s), 775 (w), 747 (vs), 717 (m), 701 (w), 675 (s), 649 (m), 624 (w), 503

(w); EA ($C_{12}H_{12}Ag_3N_{27}O_3$, 906.03) calcd.: C 15.91, H 1.34, N 41.74%; found: C 15.87, H 1.33, N 41.49%; BAM drop hammer: 7 J; friction tester: 64 N; ESD: 203 mJ; ball drop impact tester: 41 mJ (at grain size 100–500 µm).

[$Ag_4(CNO)_4$(2,2-dtp)] (8)

Complex **8** was obtained after one day in the form of single-crystals. Yield: 138 mg (0.18 mmol, 71%)

To avoid the isolation and handling of silver fulminate as well as increasing the yield of compound **8**, it can also be synthesized in a one-pot reaction. Therefore, silver (432 mg, 4.00 mmol) was dissolved in 65% nitric acid (5.60 mL, 124 mmol) and water (2.40 mL) and the ligand dissolved in 96% EtOH (9.60 mL, 164 mmol) was added. The resulting dispersion was stirred under reflux until the formation of silver fulminate occurred. It was stirred for further 15 min and afterwards the reaction mixture was allowed to cool to room temperature. The formed precipitate was filtered off and washed three times with water. Pure coordination compound **8** was obtained in a yield of 694 mg (0.89 mmol, 89%)

DTA (5 °C min^{-1}) onset: 177 °C (exothermic); IR (ATR, cm^{-1}): $\tilde{\nu}$ = 3196 (w), 3145 (w), 3012 (w), 2279 (w), 2241 (w), 2187 (vw), 2103 (s), 2083 (s), 2016 (w), 1971 (w), 1961 (w), 1786 (w), 1457 (w), 1440 (w), 1420 (w), 1383 (w), 1351 (w), 1294 (m), 1188 (w), 1147 (s), 1123 (vs), 1043 (m), 1021 (m), 1014 (m), 976 (m), 895 (m), 832 (m), 731 (w), 693 (m), 673 (w), 638 (w), 480 (w) 463 (m), 411 (w); EA ($C_9H_8Ag_4N_{12}O_4$, 779.72) calcd.: C 13.86, H 1.03, N 21.56%; found: C 14.09, H 1.24, N 21.49%; BAM drop hammer: 8 J; friction tester: 1 N; ESD: 0.7 mJ; ball drop impact tester: 15 mJ (at grain size < 100 µm).

[$Ag_4(CNO)_4(BTRI)_3$] (3)

For synthesizing complex **3**, BTRI (0.25 mmol, 34.0 mg) was dissolved in 20 mL of a mixture of water and acetonitrile (50:50) at 60 °C. AgCNO (1.00 mmol, 150 mg) was added under stirring and 10 drops of aqueous ammonia (25%) were added to dissolve all solids. The complex was obtained within two days. Yield: 157 mg (0.21 mmol, 85%)

DTA (5 °C min^{-1}) onset: 215 °C (exothermic); IR (ATR, cm^{-1}): $\tilde{\nu}$ = 3231 (w), 3109 (m), 2081 (m), 2005 (w), 1992 (w), 1527 (w), 1493 (w), 1351 (w), 1328 (w), 1312 (w), 1222 (vw), 1185 (s), 1103 (s), 1027 (m), 973 (w), 936 (w), 852 (m), 607 (vs), 510 (w), 491 (w), 444 (vw), 419 (w); EA ($C_8H_4Ag_4N_{10}O_4$, 735.66) calcd.: C 13.06, H 0.55, N 19.04%; found: C 12.86, H 0.54, N 18.80%; BAM drop hammer: 5 J; friction tester: 10 N; ESD: 2.5 mJ; ball drop impact tester: 55 mJ (at grain size < 100 µm).

[$Ag_4(CNO)_4(C_4Tz)_2$] (5)

ECC **5** was synthesized using an excess of ligand to prevent the crystallization of pure silver fulminate. C_4Tz (4.00 mmol, 497 mg) was dissolved in 10 mL of a mixture of water and acetonitrile (50:50) at 60 °C and AgCNO (1.00 mmol, 150 mg) was added under stirring. The resulting reaction mixture was left in air for crystallization and the complex was obtained after three days. Yield: 160 mg (0.19 mmol, 75%)

DTA (5 °C min^{-1}) onset: 133 °C (exothermic); IR (ATR, cm^{-1}): $\tilde{\nu}$ = 3122 (w), 2989 (w), 2952 (w), 2297 (w), 2253 (w), 2105 (m), 2087 (s), 1478 (m), 1445 (w), 1430 (m), 1352 (w), 1290 (w), 1249 (w), 1227 (w), 1189 (w), 1154 (vs), 1129 (vs), 1112 (vs), 1079 (s), 1007 (s), 980 (s), 940 (m), 900 (s), 839 (m), 720 (m), 671 (s), 559 (w), 480 (m), 462 (m), 410 (w); EA ($C_{14}H_{16}Ag_4N_{12}O_4$, 847.84) calcd.: C 19.83, H 1.90, N 19.83%; found: C 19.77, H 1.85, N 19.66%; BAM drop hammer: 20 J; friction tester: 84 N; ESD: 7.3 mJ; ball drop impact tester: > 200 mJ (at grain size 100–500 µm).

12.6.2. IR Spectroscopy

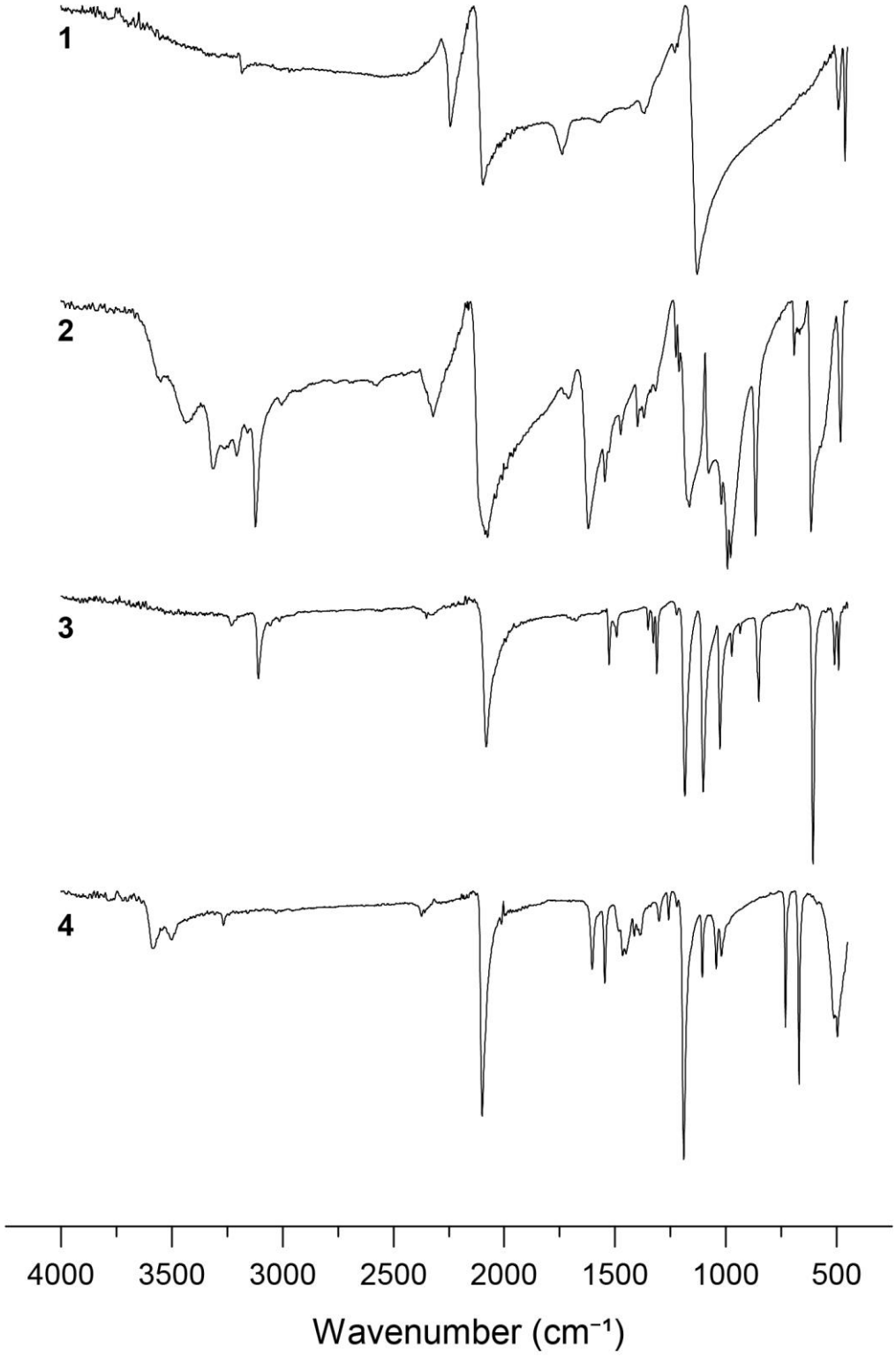

Figure S1. Infrared spectra of compounds **1**–**4**.

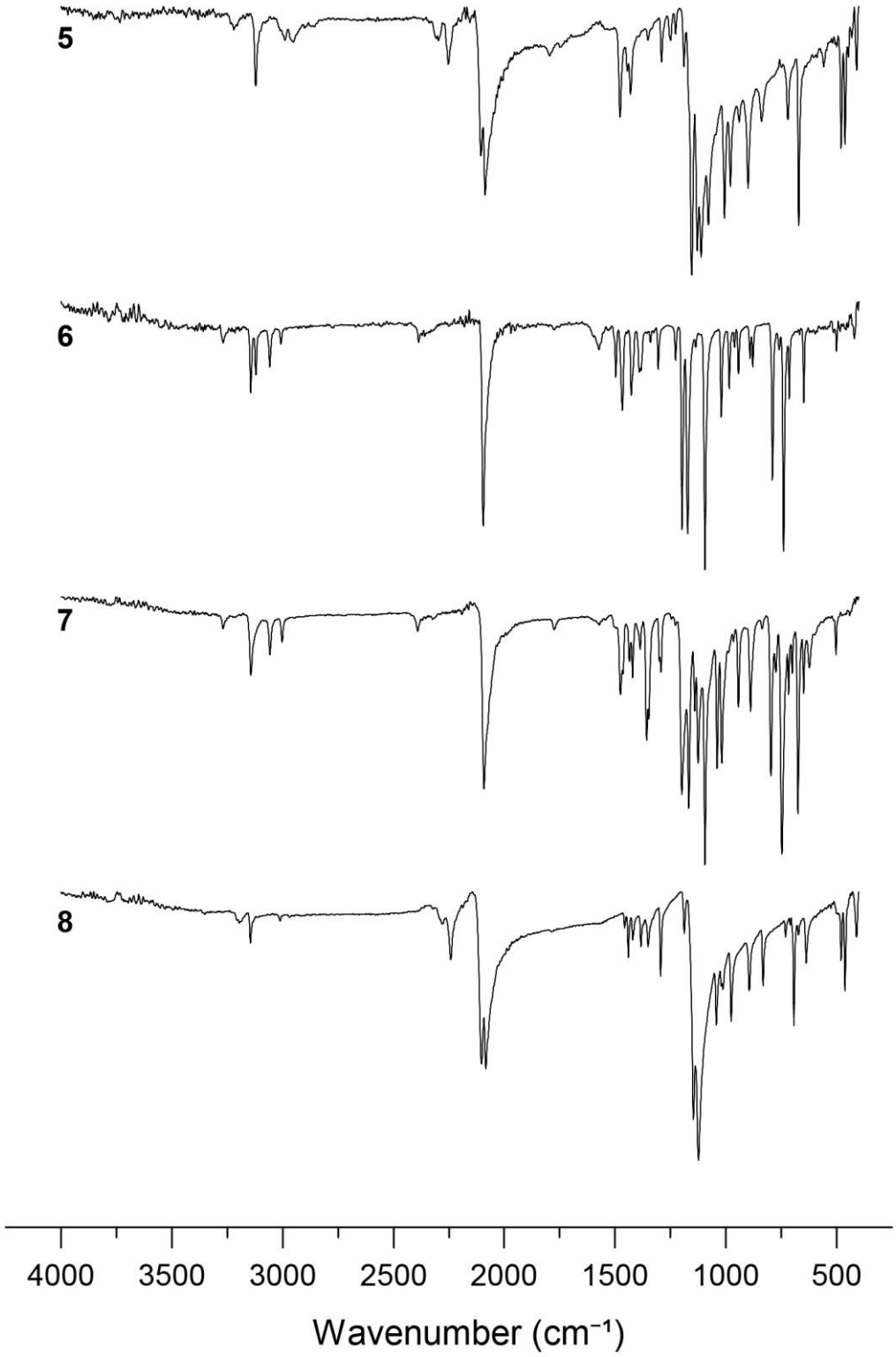

Figure S2. Infrared spectra of complexes **5**–**8**.

12.6.3. X-Ray Diffraction

For all crystalline compounds, an Oxford Xcalibur3 diffractometer with a CCD area detector or Bruker D8 Venture TXS diffractometer equipped with a multilayer monochromator, a Photon 2 detector and a rotating-anode generator were employed for data collection using Mo-*K*α radiation (λ = 0.7107 Å). On

the Oxford device, data collection and reduction were carried out using the CRYSALISPRO software.[11] On the Bruker diffractometer, the data were collected with the Bruker Instrument Service v3.0.21, the data reduction was performed using the SAINT V8.18C software (Bruker AXS Inc., 2011). The structures were solved by direct methods (SIR-92,[12] SIR-97,[13] or SHELXS-97[14]) and refined by full-matrix least-squares on *F*2 (SHELXL[14]) and finally checked using the PLATON software[15] integrated in the WinGX[16] software suite. The non-hydrogen atoms were refined anisotropically and the hydrogen atoms were located and freely refined. The absorptions were corrected by a SCALE3 ABSPACK or SADABS Bruker APEX3 multiscan method.[17,18] All DIAMOND2 plots are shown with thermal ellipsoids at the 50% probability level and hydrogen atoms are shown as small spheres of arbitrary radius.

Table S1. Crystallographic data of **2**–**5**.

	2	**3**	**4**	**5**
Formula	$C_4H_6Ag_2N_6O_3$	$C_4H_2Ag_2N_5O_2$	$C_{12}H_{24}Ag_3N_{15}O_6$	$C_7H_8Ag_2N_6O_2$
FW [g mol^{-1}]	401.89	367.85	798.07	423.93
Crystal system	monoclinic	orthorhombic	hexagonal	monoclinic
Space Group	*Ia*	*Ccca*	$P6_3/m$	$C2/c$
Color / Habit	colorless needle	colorless platelet	colorless rod	colorless rod
Size [mm]	0.03 x 0.04 x 0.45	0.07 x 0.24 x 0.29	0.01 x 0.01 x 0.05	0.02 x 0.03 x 0.07
a [Å]	6.0684(7)	11.8399(9)	15.0648(5)	32.653(3)
b [Å]	24.774(2)	20.8348(16)	15.0648(5)	5.4602(5)
c [Å]	6.3761(8)	5.8163(3)	6.1186(4)	12.9896(11)
α [°]	90	90	90	90
β [°]	111.436(14)	90	90	97.805(3)
γ [°]	90	90	120	90
V [Å^3]	892.27(19)	1434.78(17)	1202.57(13)	2294.5(4)
Z	4	8	2	8
$\rho_{calc.}$ [g cm^{-3}]	2.992	3.406	2.204	2.454
μ [mm^{-1}]	4.387	5.425	2.482	3.413
F(000)	760	1368	780	1616
$\lambda_{MoK\alpha}$ [Å]	0.71073	0.71073	0.71073	0.71073
T [K]	108	112	293	103
θ Min–Max [°]	3.3, 26.4	3.4, 26.3	2.7, 26.4	3.2, 26.4
Dataset	−7: 7; −30: 30; −7: 7	−14: 13; −26: 17; −5: 7	−18: 18; −18: 18; −7: 7	−40: 40; −6: 6; −16: 16
Reflections collected	5132	3953	20386	19544
Independent refl.	1812	739	904	2347
R_{int}	0.058	0.048	0.096	0.049
Observed reflections	1608	563	759	2082
Parameters	144	60	73	154
R_1 (obs)[a]	0.0456	0.0317	0.0340	0.0213
wR_2 (all data)[b]	0.1063	0.0773	0.0857	0.0522
GooF[c]	1.06	1.06	1.26	1.08
Resd. Dens. [e Å^{-3}]	−0.88, 1.12	−0.66, 1.31	−1.13, 0.66	−0.49, 0.65
Absorption correction	multi-scan	multi-scan	multi-scan	multi-scan
CCDC	2021064	2021070	2021069	2021067

[a] $R_1 = \Sigma||F_0|- |F_c||/ \Sigma|F_0|$; [b] $wR_2 = [\Sigma[w(F_0^2-F_c^2)^2]/\Sigma[w(F_0)^2]]^{1/2}$; $w = [\sigma c^2(F_0^2)+(xP)^2+yP]^{-1}$ and $P = (F_0^2+2F_c^2)/3$; [c] GooF = $\{\Sigma[w(F_o^2-F_c^2)^2]/(n-p)\}^{1/2}$ (n = number of reflections; p = total number of parameters).

Table S2. Crystallographic data of **6**–**8**.

	6	**7**	**8**
Formula	$C_{12}H_{12}Ag_3N_{27}O_3$	$C_{12}H_{12}Ag_3N_{27}O_3$	$C_9H_8Ag_4N_{12}O_4$
FW [g mol^{-1}]	906.10	906.10	779.75
Crystal system	trigonal	trigonal	monoclinic
Space Group	*R*−3	*R*−3	*P*2/*c*
Color / Habit	colorless needle	colorless rod	colorless platelet
Size [mm]	0.02 x 0.02 x 0.50	0.01 x 0.02 x 0.10	0.09 x 0.35 x 0.44
a [Å]	26.5151(9)	26.8557(5)	12.5173(11)
b [Å]	26.5151(9)	26.8557(5)	5.6400(4)
c [Å]	6.3674(4)	6.3972(3)	12.8877(10)
α [°]	90	90	90
β [°]	90	90	100.146(8)
γ [°]	120	120	90
V [Å^3]	3876.9(4)	3995.7(3)	895.61(12)
Z	6	6	2
$\rho_{calc.}$ [g cm^{-3}]	2.329	2.259	2.891
μ [mm^{-1}]	2.330	2.260	4.358
F(000)	2628	2628	732
$\lambda_{MoK\alpha}$ [Å]	0.71073	0.71073	0.71073
T [K]	108	298	110
θ Min–Max [°]	2.7, 26.3	3.6, 26.3	3.2, 26.4
Dataset	−32: 32; −31: 33; −7: 7	−33: 33; −33: 33; −7: 7	−15: 15; −7: 7; −13: 16
Reflections collected	7571	25811	5054
Independent refl.	1752	1802	1825
R_{int}	0.059	0.029	0.027
Observed reflections	1426	1667	1543
Parameters	136	136	132
R_1 (obs)[a]	0.0334	0.0214	0.0258
wR_2 (all data)[b]	0.0680	0.0455	0.0652
GooF[c]	1.05	1.07	1.07
Resd. Dens. [e Å^{-3}]	−0.55, 0.78	−0.62, 0.66	−0.88, 0.90
Absorption correction	multi-scan	multi-scan	multi-scan
CCDC	2021066	2021065	2021068

[a] $R_1 = \Sigma||F_0|- |F_c||/ \Sigma|F_0|$; [b] $wR_2 = [\Sigma[w(F_0^2-F_c^2)^2]/\Sigma[w(F_0)^2]]^{1/2}$; $w = [\sigma c^2(F_0^2)+(xP)^2+yP]^{-1}$ and $P = (F_0^2+2F_c^2)/3$; [c] GooF = $\{\Sigma[w(F_o^2-F_c^2)^2]/(n-p)\}^{1/2}$ (n = number of reflections; p = total number of parameters).

Monohydrate compound **2** is crystallizing as colorless needles in the monoclinic space group *Ia* with a calculated density of 2.992 g cm^{-3} at 108 K. Both the neutral triazole and the fulminato ligand are each bridging between two different silver cations leading to the formation of a 2D layer. Whereas 4-ATRI is coordinating with two of the ring nitrogen atoms, the anion is solely binding with its carbon atom. The molecular unit is completed by the incorporation of one crystal water molecule (Figure S3). Complex **3** based on 4,4'-bi(1,2,4-triazole) as ligand is present in the orthorhombic space group *Ccca* with a very high density of 3.406 g cm^{-3} at 112 K. The use of a bitriazole instead of 4-ATRI is on the one hand side further increasing the dimensionality to a 3D polymeric network, due to the linking of the ligand to four different central metals (Figure S4). On the other side the absence of an amino group is avoiding the

incorporation of a water molecule. Like in **2** the fulminato ligands are solely binding with their carbon atom to two cations.

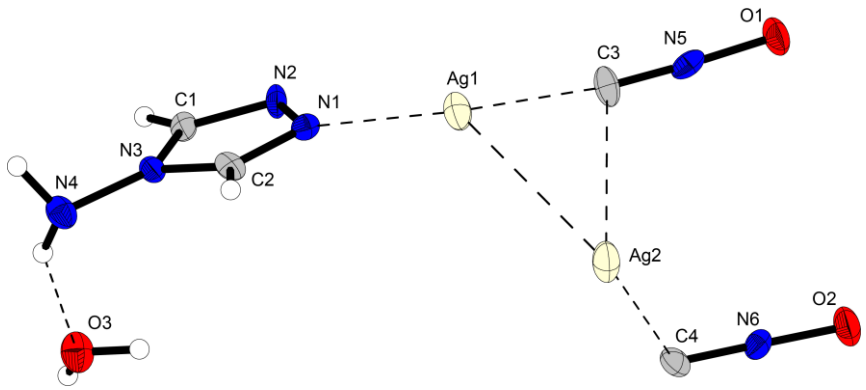

Figure S3. Molecular unit of $[Ag_2(CNO)_2(4\text{-ATRI})] \bullet H_2O$ (**2**) Ellipsoids of all structures are set to the 50% probability level. Selected bond lengths (Å): Ag1–Ag2 3.1536(14), Ag1–N1 2.144(12), Ag1–C3 2.063(15), Ag2–C4 2.479(19). Selected bond angles (°): Ag2–Ag1–N1 131.0(3), Ag2–Ag1–C3 59.7(5), N1–Ag1–C3 162.7(6), Ag1–Ag2–C4 106.1(4).

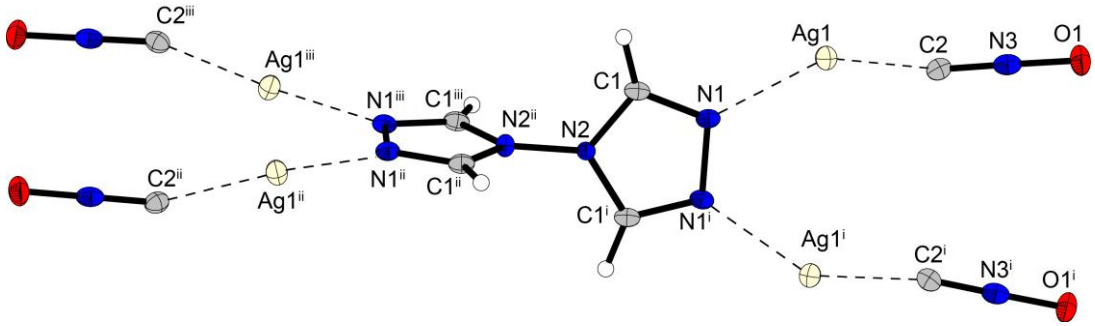

Figure S4. Molecular unit of $[Ag_4(CNO)_4(BTRI)]$ (**3**). Selected bond lengths (Å): Ag1–N1 2.250(4), Ag1–C2 2.121(6). Selected bond angle (°): N1–Ag1–C2 140.23(18). Symmetry codes: (i) −x, y, 1.5−z; (ii) −x, 0.5−y, z; (iii) x, 0.5−y, 1.5−z.

In contrast to compounds **2** and **3**, **4** is forming complex monomers consisting of silver trimers (Figure S5). It is crystallizing in the hexagonal space group $P6_3/m$ with a density of 2.204 g cm^{-3} at 293 K. Again, the fulminato ligands are solely coordinating and bridging through their carbon atoms and the presence of methyl groups is leading to the incorporation of crystal water molecules. The molecular unit of **5** consists of a silver tetramer, four bridging anions and two tetrazole ligands (Figure S6). It is crystallizing in the monoclinic space group $C2/c$ with a density of 2.454 g cm^{-3} at 103 K. Two of the cations are coordinated by one tetrazole ligand, whereas the other two are only coordinated by fulminate anions. The tetrameric units are formed by the bridging of two silver central metals of the fulminate carbon atoms. The tetramers are further linked by the coordination of silver with the fulminate oxygens (Ag–O 2.69–2.73 Å) leading to the formation of 2D polymeric layers. Like **4**, ECC **6** and **7** are present as complex monomers consisting of silver trimers with the only difference of no crystal water presence (Figures S7 and S8). They both crystallize isotypically in the trigonal space group $R\bar{3}$ with similar cell axes and

densities. The coordination in both structures is similar to compound **4** and interestingly, the ditetrazolyl ligands are solely binding with one of their two tetrazole substituents.

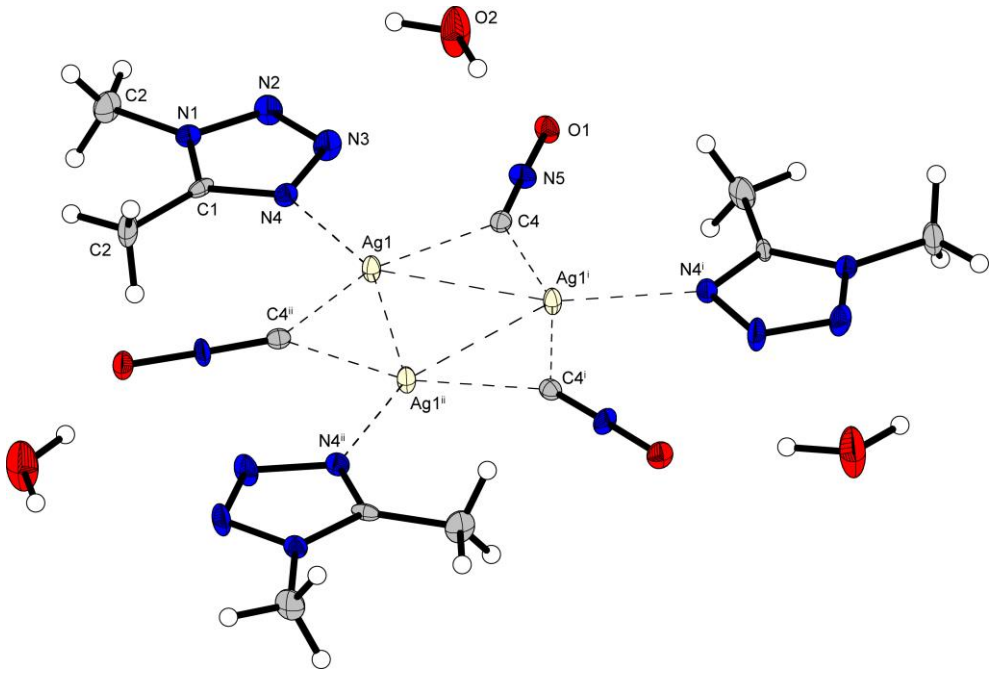

Figure S5. Trimeric unit of $[Ag_3(CNO)_3(1,5\text{-DMT})] \bullet 3\ H_2O$ (**4**). Selected bond lengths (Å): Ag1–N4 2.316(8), Ag1–C4 2.228(11), Ag1–Ag1^{i} 2.8801(11). Selected bond angles (°): N4–Ag1–C4 94.4(3), N4–Ag1–C4^{ii} 107.0(4), C4–Ag1–C4^{ii} 158.7(4), Ag1–C4–Ag1^{i} 81.4(3). Symmetry codes: (i) −x+y, −x, z; (ii) −y, x−y, z.

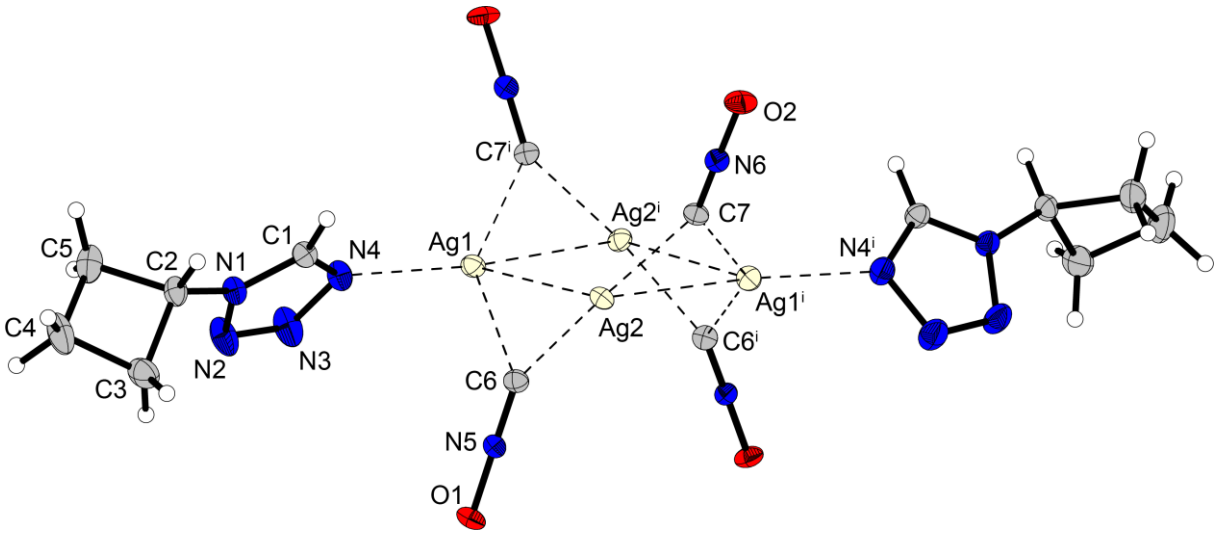

Figure S6. Tetrameric cluster of $[Ag_4(CNO)_4(C_4Tz)_2]$ (**5**). Selected bond lengths (Å): Ag1–Ag2 2.9133(9), Ag1–N4 2.286(3), Ag1–C6 2.303(3), Ag2–C7 2.163(3). Selected bond angles (°): N4–Ag1–C6 98.53(10), Ag1–C6–Ag2 81.31(11). Symmetry code: (i) −x, y, 0.5−z.

Complex **8** is present in the monoclinic space group *P*2/*c* with a calculated density of 2.891 g cm^{-3} at 110 K In contrast to ECC **6** and **7** the ditetrazolyl ligand shows a bridging behavior. Similar to compound **5** the linking of fulminato anions via the oxygen as well as carbon atoms is forming 2D polymeric layers

consisting of silver tetramer (Figure S9). These layers are further connected by the 2,2-dtp ligand to 3D networks.

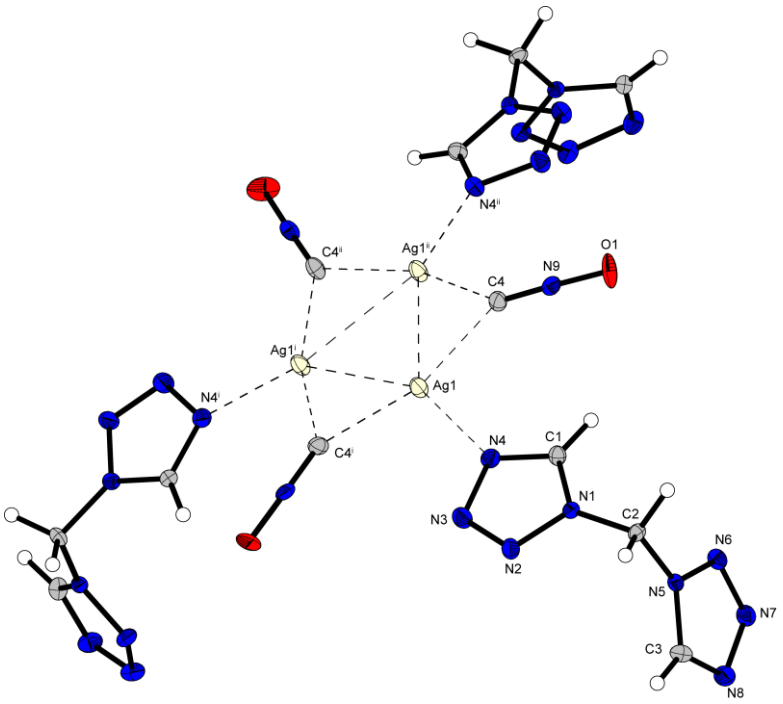

Figure S7. Trimeric cluster of $[Ag_3(CNO)_3(1,1\text{-dtm})_3]$ (**6**). Selected bond lengths (Å): Ag1–N4 2.287(4), Ag1–C4 2.211(5), Ag1–$Ag1^{ii}$ 2.8238(9). Selected bond angles (°): N4–Ag1–C4 96.33(16), N4–Ag1–$C4^{i}$ 104.2(2), C4–Ag1–$C4^{i}$ 159.4(2), Ag1–C4–$Ag1^{ii}$ 79.99(15). Symmetry codes: (i) −x+y, −x, z; (ii) −y, x−y, z.

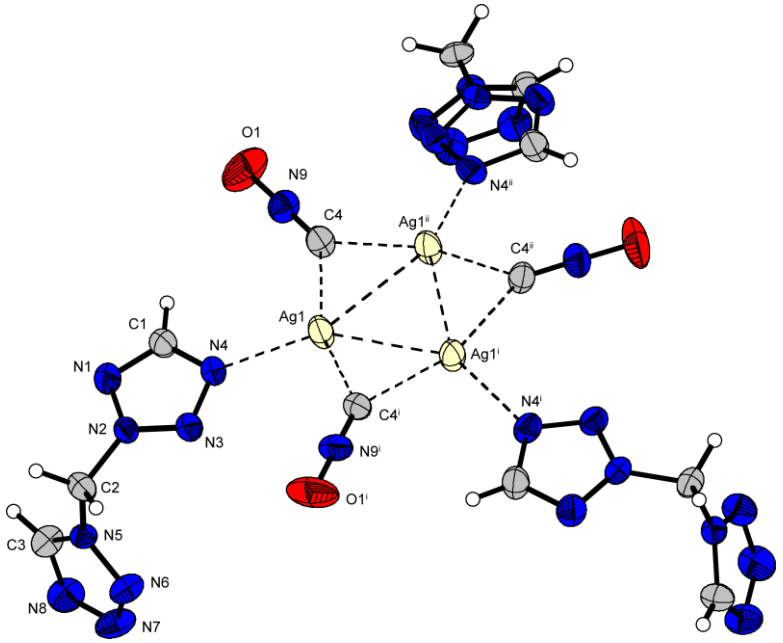

Figure S8. Trimeric unit of $[Ag_3(CNO)_3(1,2\text{-dtm})_3]$ (**7**). Selected bond lengths (Å): Ag1–N4 2.302(3), Ag1–C4 2.197(3), Ag1–$Ag1^{i}$ 2.8271(9). Selected bond angles (°): N4–Ag1–C4 100.70(10), C4–Ag1–$C4^{i}$ 159.14(14), N4–Ag1–$C4^{i}$ 100.08(13), Ag1–C4–$Ag1^{ii}$ 80.09(9). Symmetry codes: (i) −x+y, −x, z; (ii) −y, x−y, z; (iii) x, −1+y, z.

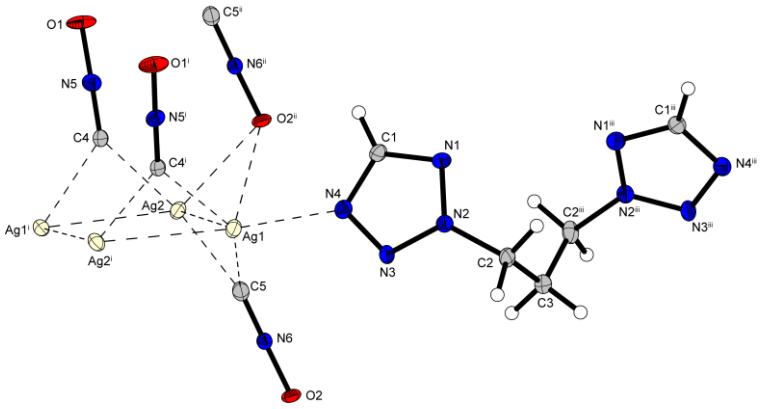

Figure S9. Tetrameric unit of $[Ag_4(CNO)_4(2,2\text{-dtp})]$ (**8**). Selected bond lengths (Å): Ag1–Ag2 2.8884(6), Ag1–N4 2.303(4), Ag1–C5 2.247(4), Ag1–$O2^{ii}$ 2.739(2), Ag1–$Ag2^{i}$ 2.7705(5), Ag2–C4 2.182(4). Selected bond angles (°): N4–Ag1–C5 102.78(13), $O2^{ii}$–Ag1–N4 78.49(11), N4–Ag1–$C4^{i}$ 116.58(13), Ag1–C5–Ag2 81.00(13). Symmetry codes: (i) −x, y, 0.5−z; (ii) x, −1+y, z; (iii) 1−x, y, 1.5−z.

12.6.4. DTA Plots

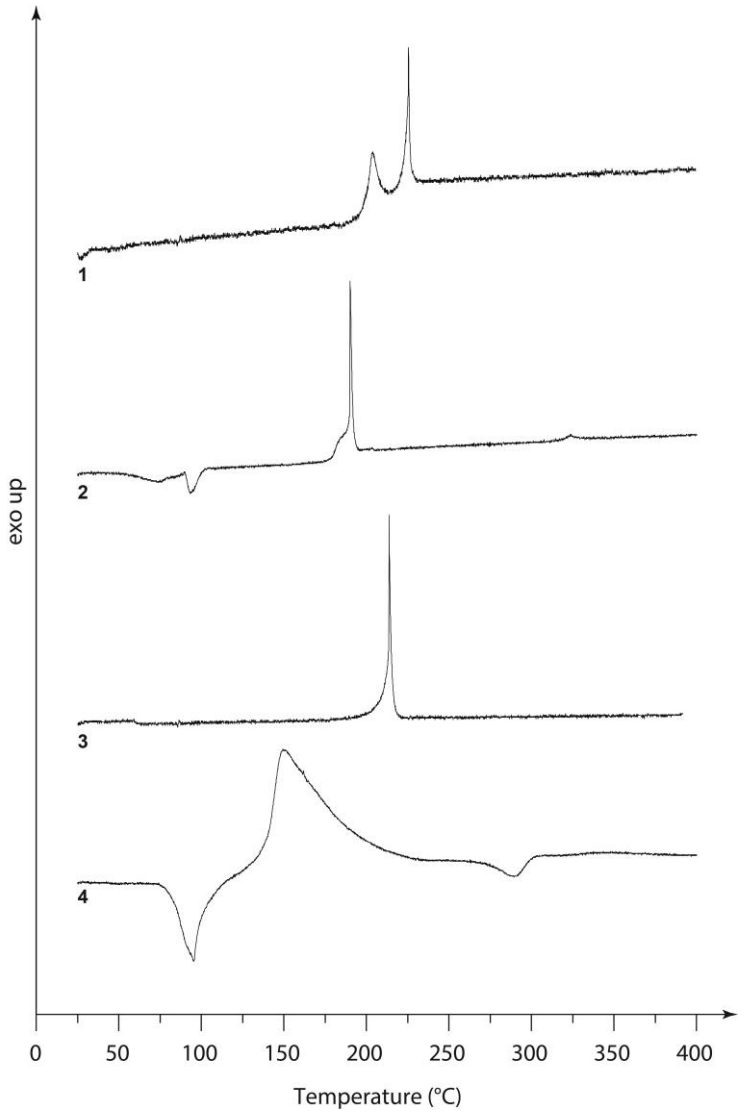

Figure S10. DTA plots of compounds **1**–**4**.

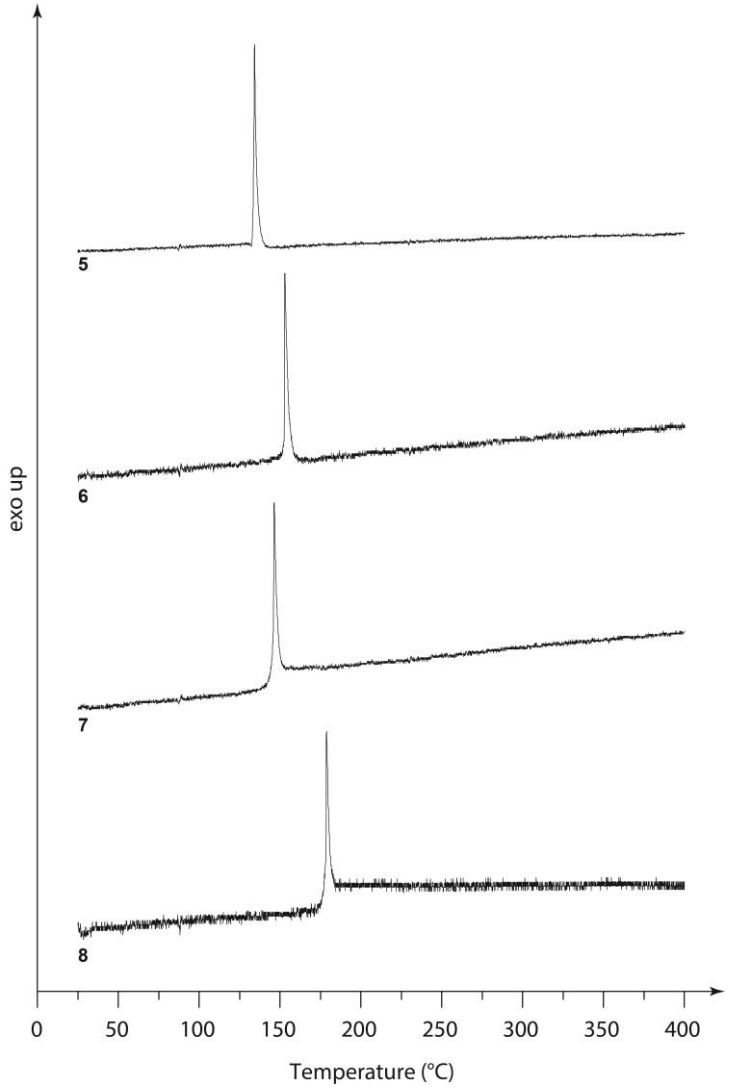

Figure S11. DTA plots of complexes **5**–**8**.

12.6.5. TGA Plots

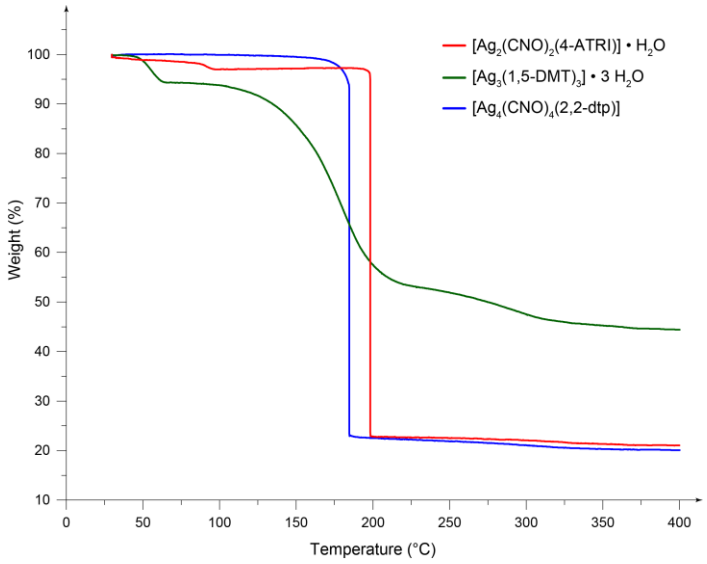

Figure S12. TG measurements of ECC **2**, **5**, and **8**.

12.6.6. Hot Plate and Hot Needle Tests

Figure S13. Deflagration during HN tests of complex **2** shown as a sequence.

Figure S14. Outcome of ECC **3** during HN test shown as a sequence.

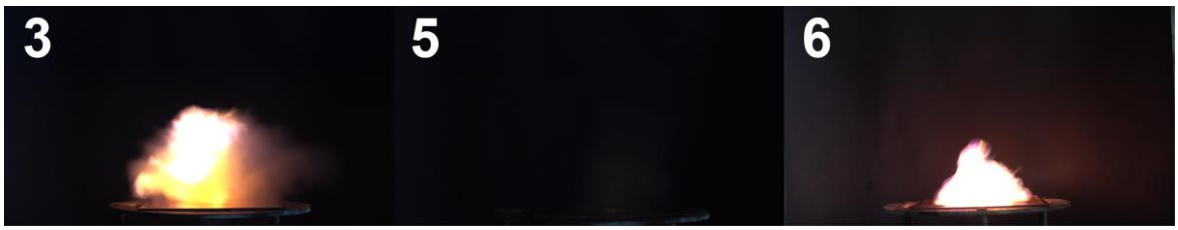

Figure S15. Moments of detonation or deflagration of during HP of complexes **3**, **5**, and **6**.

Figure S16. Deflagration of $[Ag_3(CNO)_3(1,5\text{-}DMT)_3] \bullet 3\ H_2O$ (**4**) during HP test.

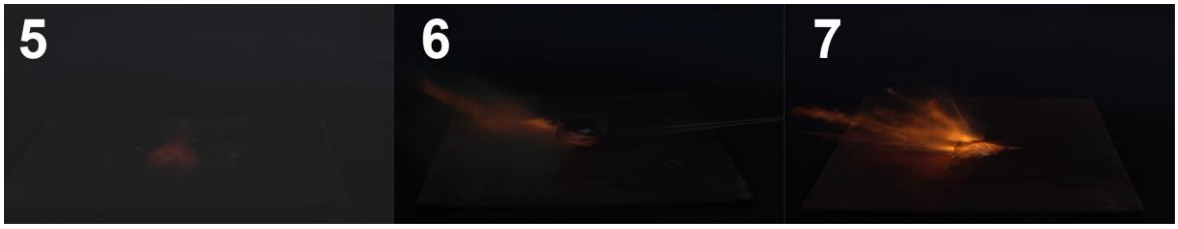

Figure S17. Moments of deflagration during HN tests of complexes **5**–**7**.

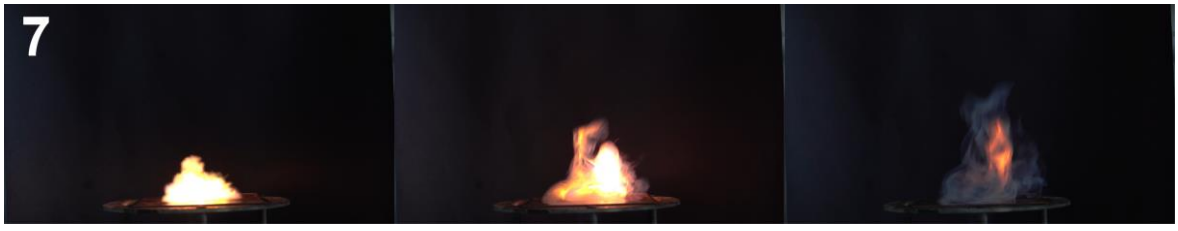

Figure S18. Deflagration of ECC **7** during HP test shown as a sequence.

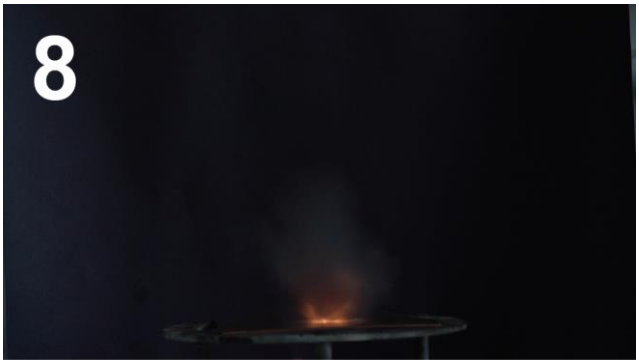

Figure S19. Moment of detonation of complex **8** during HP test.

Figure S20. Detonation of complex **8** during HN test shown as a sequence.

12.6.7. Scanning Electron Microscopy

Scanning electron microscopy (SEM) was performed for imaging the microstructure and morphology of the prepared materials. Pure silver fulminate (**1**) as well as coordination compounds **3**, **6**, and **9** were investigated in detail using this particular technique.

As described in the paper, sample preparation for SEM requires coating of the sample with a thin layer of graphite for increased conductivity. This process is called sputtering (graphite vapor deposition). The process is enabled by vaporization of a graphite wire in high vacuum using a high voltage pulse. Due to the extremely high sensitivity toward electrostatic discharge, the sample is assumed not to withstand these conditions and decomposed during sample preparation. The SEM images show therefore only decomposition products of **1** (Figure S21).

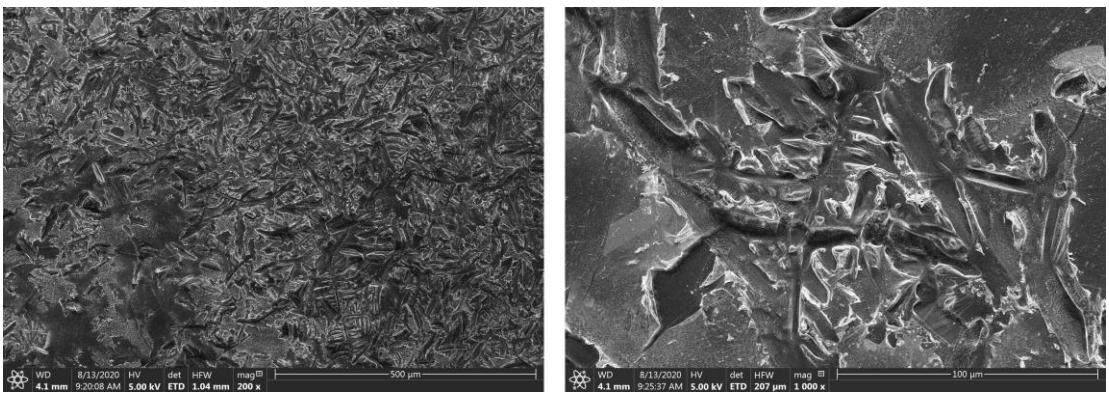

Figure S21. SEM images with 200x magnitude (left) and 3000x magnitude (right) of decomposed compound **1**.

The dominant morphology of compound **3** is represented by intergrown plates with sizes up to 500 µm. A closer look at the plates' surfaces reveals a partly porous structure with attached spongelike agglomerates (Figure S22).

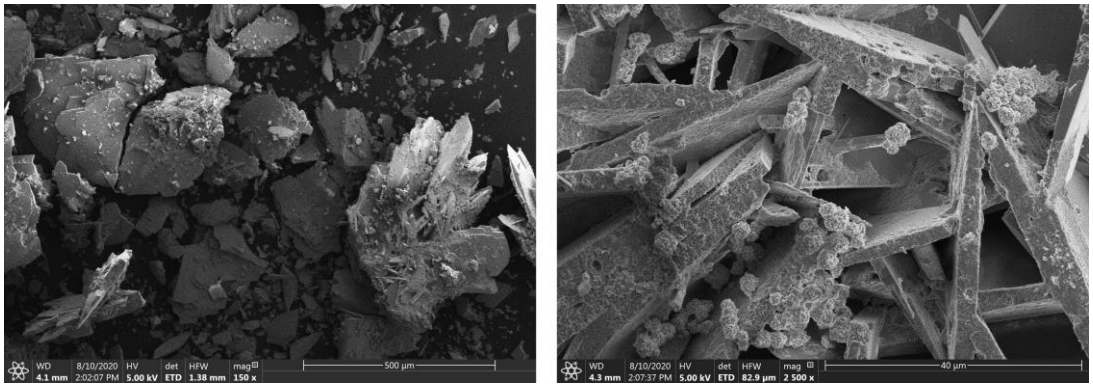

Figure S22. SEM images with 150x magnitude (left) and 2500x magnitude (right) of compound **3**.

Coordination compound **6** shows needle like morphology (Figure S23). Due to the absence of any additives, the crystal size varies widely from 5 to over 500 µm. The majority of the needles is very thin and therefore easily broken into multiple fragments.

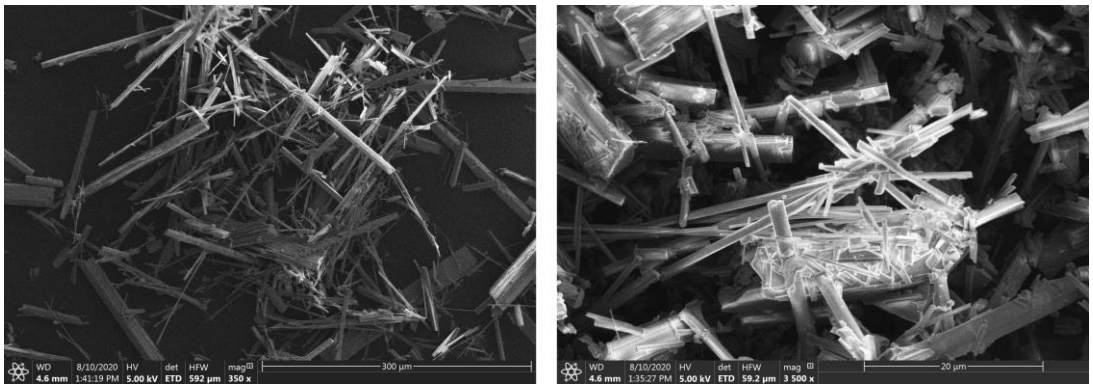

Figure S23. SEM images with 350x magnitude (left) and 3500x magnitude (right) of compound **6**.

Compound **8** forms radiating stellate aggregates consisting of bladed crystals in the range of 10–100 µm (Figure S24).

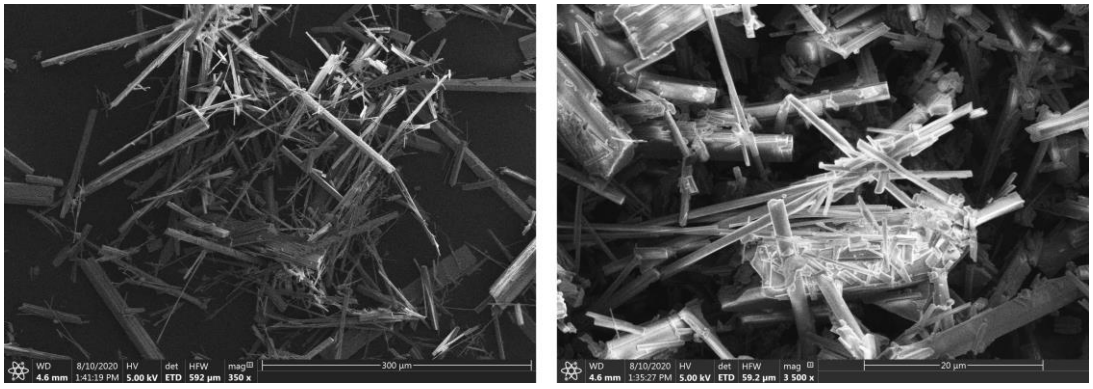

Figure S24. SEM images with 500x magnitude (left) and 1500x magnitude (right) of compound **8**.

12.6.8. References

[1] NATO standardization agreement (STANAG) on explosives, impact sensitivity tests, no. 4489, 1st ed., Sept. 17, **1999**.

[2] WIWEB-Standardarbeitsanweisung 4-5.1.02, Ermittlung der Explosionsgefährlichkeit, hier der Schlagempfindlichkeit mit dem Fallhammer, Nov. 8, **2002**.

[3] OZM, http://www.ozm.cz, (accessed July 2020).

[4] BAM, http://www.bam.de, (accessed July 2020).

[5] Military Standard 1751A (MIL-STD-1751A): safety and performance tests for qualification of explosives (high explosives, propellants and pyrotechnics), method 1016, Dec. 11, **2001**.

[6] UN Model Regulation: Recommendations on the Transport of Dangerous Goods – Manual of Tests and Criteria, section 13.4.2.3.3, **2015**.

[7] NATO standardization agreement (STANAG) on explosive, friction sensitivity tests, no. 4487, 1st ed., Aug. 22, **2002**.

[8] WIWEB-Standardarbeitsanweisung 4-5.1.03, Ermittlung der Explosionsgefährlichkeit oder der Reibeempfindlichkeit mit dem Reibeapparat, Nov. 8, **2002**.

[9] Impact: insensitive > 40 J, less sensitive ≥ 35 J, sensitive ≥ 4 J, very sensitive ≤ 3 J; Friction: insensitive > 360 N, less sensitive = 360 N, sensitive < 360 N and > 80 N, very sensitive ≤ 80 N, extremely sensitive ≤ 10 N. According to the UN Recommendations on the Transport of Dangerous Goods, 5th ed., **2009**.

[10] M. S. Gruhne, M. Lommel, M. H. H. Wurzenberger, N. Szimhardt, T. M. Klapötke, J. Stierstorfer, *Propellants Explos. Pyrotech.* **2020**, *45*, 147–153.

[11] CrysAlisPRO (Version 171.33.41), Oxford Diffraction Ltd., **2009**.

[12] A. Altomare, G. Cascarano, C. Giacovazzo, A. Guagliardi, *J. Appl. Crystallogr.* **1993**, *26*, 343.

[13] a) A. Altomare, G. Cascarano, C. Giacovazzo, A. Guagliardi, A. G. G. Moliterni, M. C. Burla, G. Polidori, M. Camalli, R. Spagna, SIR97, **2003**; b) A. Altomare, M. C. Burla, M. Camalli, G. L. Cascarano, C. Giacovazzo, A. Guagliardi, A. G. G. Moliterni, G. Polidori, R. Spagna, *J. Appl. Crystallogr.* **1999**, *32*, 115.

[14] a) G. M. Sheldrick, SHELXL-97, University of Göttingen, Germany, **1997**; b) G. M. Sheldrick, *Acta Crystallogr. Sect. A* **2008**, *64*, 112.

[15] A. L. Spek, PLATON, Utrecht University, The Netherlands, **1999**.

[16] L. J. Farrugia, *J. Appl. Cryst.* **2012**, *45*, 849.

[17] Empirical absorption correction using spherical harmonics, implemented in SCALE3 ABSPACK scaling algorithm (CrysAlisPro Oxford Diffraction Ltd., Version 171.33.41, **2009**).

[18] APEX3, Bruker AXS Inc., Madison, Wisconsin, USA.

13. Summary and Conclusion

In the scope of this work, extensive investigations based on energetic materials were conducted, and a vast number of new compounds were synthesized. The results are summarized in Chapters 2–12, all of which represent independent publications in peer-reviewed scientific journals (Figure1). While Chapter 2 deals with the comprehensive sensitivity examination of 16 literature-known and partly commercially utilized primary explosives, the remaining thesis almost exclusively covers the preparation of novel energetic substances.

Section	Topic	Reference
Chapter 2	Sensitivity examination of 16 literature-known and partly commercially utilized primary explosives using different sensitivity devices.	M. S. Gruhne, M. Lommel, M. H. H. Wurzenberger, N. Szimhardt, T. M. Klapötke, J. Stierstorfer, *Propellants Explos. Pyrotech* **2020**, *45*, 147–153.
Chapter 3	Synthesis of copper(II) trinitrophenolate complexes with four different *N*-aminotetrazole ligands.	M. H. H. Wurzenberger, B. R. G. Bissinger, M. Lommel, M. S. Gruhne, N. Szimhardt, J. Stierstorfer, *New J. Chem.* **2019**, *44*, 18193–18202.
Chapter 4	Comparison of energetic complexes based on 1-ethyl- and 1-azido-5*H*-ethyltetrazole.	M. H. H. Wurzenberger, M. S. Gruhne, M. Lommel, N. Szimhardt, T. M. Klapötke, J. Stierstorfer, *Chem. – Asian J.* **2019**, *14*, 2018–2028.
Chapter 5	Comparing of ECC consisting of 1-propyl- and 1-azidopropyl-5*H*-tetrazole.	M. H. H. Wurzenberger, S. M. J. Endraß, M. Lommel, T. M. Klapötke, J. Stierstorfer, *ACS Appl. Energy Mater.* **2020**, *3*, 3798–3806.
Chapter 6	Synthesis of three *N*,*N*-ditetrazolylmethane isomers and their energetic copper(II) and silver(I) coordination compounds.	M. H. H. Wurzenberger, V. Braun, M. Lommel, T. M. Klapötke, J. Stierstorfer, *Inorg. Chem.* **2020**, *59*, 10938–10952.
Chapter 7	Investigation of the energetic properties of picramic acid based compounds.	M. H. H. Wurzenberger, J. T. Lechner, M. Lommel, T. M. Klapötke, J. Stierstorfer, *Propellants Explos. Pyrotech* **2020**, *45*, 898–907.
Chapter 8	Preparation of copper(II) dicyanamide coordination polymers with various tetrazole ligands.	M. H. H. Wurzenberger, J. T. Lechner, J. Stierstorfer, *ChemPlusChem* **2020**, *85*, 769–775.
Chapter 9	Investigation of ECC based on copper(II) bromate and tetrazole or triazole ligands.	M. H. H. Wurzenberger, N. Szimhardt, J. Stierstorfer, *Inorg. Chem.* **2018**, *57*, 7940–7949.
Chapter 10	Synthesis of energetic copper(II) chlorate complexes using different nitrogen-rich azole ligands.	M. H. H. Wurzenberger, N. Szimhardt, J. Stierstorfer, *J. Am. Chem. Soc.* **2018**, *140*, 3206–3209.
Chapter 11	Tuning of the energetic properties of copper(II) azide ECC by varying the alkyl chain length of the tetrazole molecules.	M. H. H. Wurzenberger, M. Lommel, M. S. Gruhne, N. Szimhardt, J. Stierstorfer, *Angew. Chem. Int. Ed.* **2020**, *132*, 12466–12469.
Chapter 12	Stabilization of very sensitive silver fulminate by complexation with nitrogen-rich azole ligands.	M. H. H. Wurzenberger, M. S. Gruhne, M. Lommel, V. Braun, N. Szimhardt, J. Stierstorfer, *Inorg. Chem.* **2020**, *59*, 17875–17879.

Figure 1. Overview of the eleven different chapters and their topics.

The characterization comprises standard techniques such as elemental analysis, infrared spectroscopy, differential thermal analysis, thermogravimetric analysis, single-crystal X-ray diffraction experiments, and sensitivity determinations toward impact (IS), ball drop impact (BDIS), friction (FS), and electrostatic discharge (ESD). In addition to ^{1}H and ^{13}C NMR spectroscopy, proton-coupled ^{15}N NMR or the superior two-dimensional ^{1}H-^{15}N-NMR HMBC spectroscopy was applied to investigate the ligands. The trends of different tetrazole isomers were explained by using Hirshfeld surface and fingerprint analysis. Furthermore, the detonation properties of several materials were calculated using the EXPLO5 code. The corresponding ECC were further examined in hot plate (HP) and hot needle (HN) tests to attain an insight into their energetic performance. The most promising compounds were subjected to classical initiation experiments using nitropenta and laser experiments. UV-Vis spectroscopy of laser ignitable materials was

used to gain a deeper understanding of the initiation mechanism. Some compounds were investigated using X-ray powder diffraction or scanning electron microscopy (SEM) to ensure their purity. In order to obtain conclusions on sensitivities and performance parameters regarding grain size and habitus, the crystal morphology of several compounds was determined by light microscopy. The toxicity to aquatic organisms of ligands and corresponding complexes was investigated using luminescent marine bacterium of the strain *Vibrio fischeri*.

Chapter 2: The sensitivity determination of primary explosives with three different devices (BAM drop hammer, BAM friction tester, BIT-132 ball drop impact tester) and several evaluation methods represents fundamental research. It reveals a higher dependency of ball drop impact with BAM friction sensitivity than with BAM impact sensitivity, which can be explained by the slight spinning of the ball when hitting the sample. Nevertheless, the test setup of the BIT-132 illustrates more realistic circumstances and avoids distorting effects such as adiabatic compression compared to the BAM drop hammer device. Through the application of the advantageously Probit evaluation, literature findings were successfully proved, and it was possible to obtain the whole sensitivity curve of the materials.[1] This allows not only the determination of a compound's no-fire level, but also its all-fire level, which is an essential parameter for the reliability. However, compared to the 1 out of 6 (or 1 out of 10) method, the Probit procedure is enormously time-consuming and, in some rare cases, not conclusive, which can void its validity. In conclusion, it can be stated that the BIT-132 is a useful enrichment, especially for sensitivity testing of primary explosives when using the 1 out of 6 method. The results of this work allowed the implementation of the BIT-132 as a standard measuring device for a more detailed examination of explosives, and it was successfully applied in the following publications. Furthermore, it facilitates the comparison with values that were not determined according to standard BAM techniques.

Chapters 3–6: The main focus is the investigation of different ligand systems and their influence toward the energetic properties. Therefore, several isomers or different substituted molecules were compared within the single publications. In this context, eleven ligands were implemented: 1-amino-5*H*-tetrazole (1-AT), 2-amino-5*H*-tetrazole (2-AT), 1-amino-5-methyltetrazole (1-AMT), 2-amino-5-methyltetrazole (2-AMT), 1-azidoethyl-5*H*-tetrazole (AET), 1-ethyl-5*H*-tetrazole (1-ETZ), 1-propyl-5*H*-tetrazole (PT), 1-azidopropyl-5*H*-tetrazole (APT), di(tetrazol-1-yl)methane (1,1-dtm), (tetrazol-1-yl)(tetrazol-2-yl)methane (1,2-dtm), and di(tetrazol-2-yl)methane (2,2-dtm), the latter four of which were literature-unknown and isolated for the first time (Figure 2). The complexes were based on the 3d transition metals manganese, iron, copper, and zinc, all in the oxidation state +II, as well as on silver in the form of Ag^{+}. The utilized metals are all less toxic than lead, making them potential and promising

candidates for its replacement. As counterions, a broad range of different components was examined for a detailed investigation of their trends toward the energetic properties as well as toward thermal stability. The anions were either applied as high-oxidizing (nitrate, chlorate, perchlorate) or less oxidizing building blocks based on trinitrophenol derivatives (picric acid, styphnic acid, trinitrophloroglucinol).

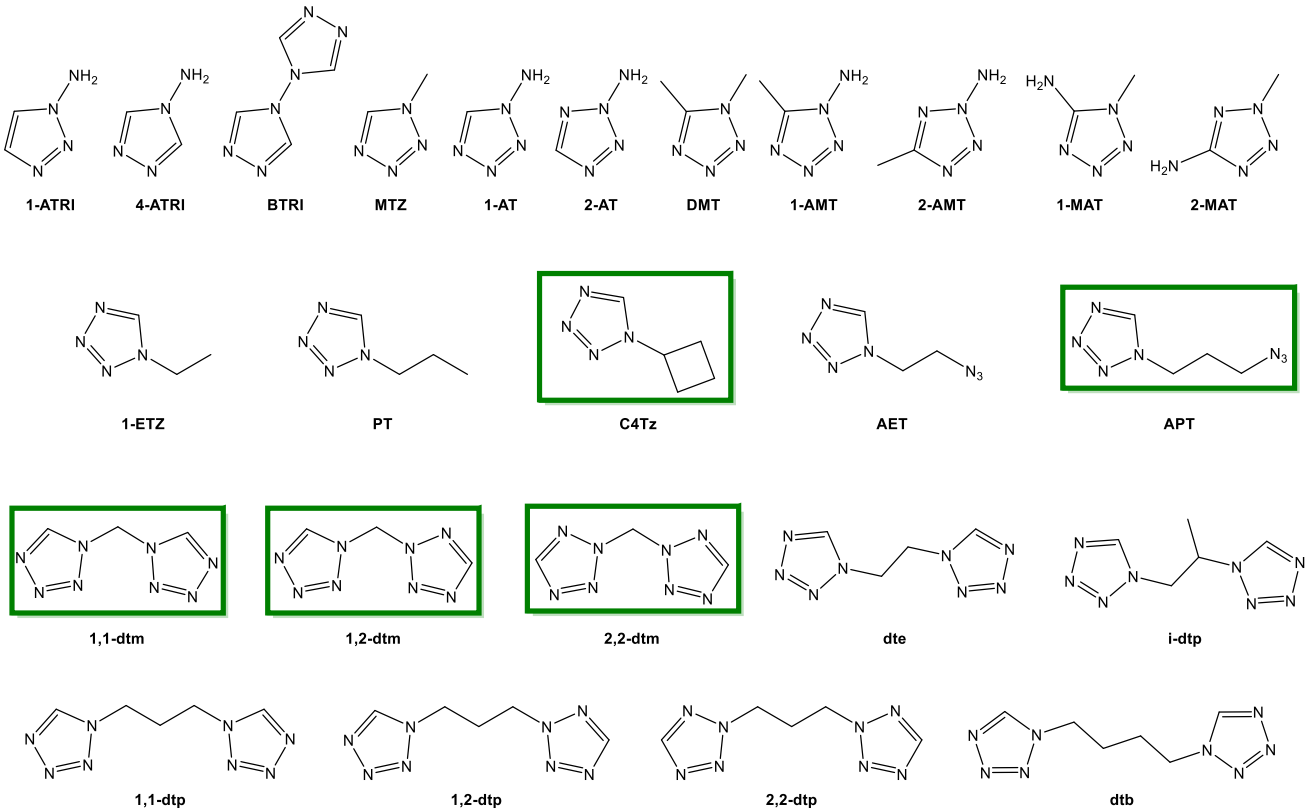

Figure 2. Overview of successfully applied nitrogen-rich azole ligands for the design of energetic coordination compounds. Green marked molecules represent literature-unknown substances. 1-ATRI: 1-amino-1,2,3-triazole; 4-ATRI: 4-amino-1,2,4-triazole; BTRI: 4,4'-bi(1,2,4-triazole); MTZ: 1-methyl-5*H*-tetrazole; 1-AT: 1-amino-5*H*-tetrazole; 2-AT: 2-amino-5*H*-tetrazole; DMT: 1,5-dimethyltetrazole; 1-AMT: 1-amino-5-methyltetrazole; 2-AMT: 2-amino-5-methyltetrazole; 1-MAT: 1-methyl-5-aminotetrazole; 2-MAT: 2-methyl-5-aminotetrazole; 1-ETZ: 1-ethyl-5*H*-tetrazole; PT: 1-propyl-5*H*-tetrazole; C4Tz: 1-cyclobutyl-5*H*-tetrazole; AET: 1-azidoethyl-5*H*-tetrazole; APT: 1-azidopropyl-5*H*-tetrazole; 1,1-dtm: di(tetrazol-1-yl)methane; 1,2-dtm: (tetrazol-1-yl)(tetrazol-2-yl)methane; 2,2-dtm: di(tetrazol-2-yl)methane; dte: 1,2-di(tetrazol-1-yl)ethane; i-dtp: 1,1'-(propane-1,2-diyl)bis(tetrazole); 1,1-dtp: 1,3-di(tetrazol-1-yl)propane; 1,2-dtp: 1-(tetrazol-1-yl)-3-(tetrazol-2-yl)propane; 2,2-dtp: 1,3-di(tetrazol-2-yl)propane; dtb: 1,4-di(tetrazol-1-yl)butane.

In this part of the thesis, not only the newly synthesized complexes but also the nitrogen-rich ligands were thoroughly characterized and investigated toward their energetic and thermal properties. Therefore, a detailed comparison of the pure substances and the effect of their incorporation in coordination compounds was possible. The synthesis of complexes based on highly oxidizing anions and the nitrogen-rich ligands 1-amino-5*H*-tetrazole (1-AT) and 2-amino-5*H*-tetrazole (2-AT) is already described in the

literature.[2] The resulting ECC all show very high sensitivities and performances in the range of primary explosives. Unfortunately, the compounds do not allow safe handling for any industrial application and sometimes even explode during crystallization. Therefore, in Chapter 3, two different strategies were demonstrated for obtaining compounds with practicable properties. Initially, instead of highly oxidizing ones, counterions based on the trinitrophenol compounds picric and styphnic acid as well as on trinitrophloroglucinol were utilized. Secondly, by introducing an additional methyl group at the five position of the tetrazole ring (1-AMT and 2-AMT), the enthalpies of formation of the ligands and, therefore, the resulting energy input in the complexes was drastically lowered in comparison to 1-AT and 2-AT. All obtained ECC show decreased sensitivities compared to complexes based on *N*-aminotetrazole with strong oxidizing anions, and furthermore, they possess very high thermal stabilities up to 212 °C. Interestingly, the additional methyl group in 1-AMT and 2-AMT often favors the formation of compounds with double-deprotonated anions leading to the creation of polymeric structures. The coordination polymers show higher thermal stabilities as well as higher sensitivities compared to the complex monomers based on aminotetrazole. Two of the 1-amino-5-methyltetrazole coordination compounds ($[Cu(TNR)(1\text{-}AMT)_2]$ and $[Cu(HTNPG)(1\text{-}AMT)_2]$) possess a fast DDT and are able to initiate PETN, which marks them as potential lead azide replacements. In contrast, the complexes based on 1-AT and 2-AT show decreased sensitivities and positive outcomes during laser initiation experiments.

The substitution of one hydrogen in 1-ethyl- (1-ETZ) and 1-propyl-5*H*-tetrazole (PT) with an azide group highly increases the performance of the resulting ECC (Figure 3). Whereas complexes based on AET are promising lead azide replacements ($[Fe(AET)_6](ClO_4)_2$ and $[Ag(AET)]ClO_4$), APT compounds show decreased sensitivities and promising properties for laser ignitable explosives ($[Fe(APT)_6](ClO_4)_2$ and $[Cu(APT)_6](ClO_4)_2$). The only drawback is the relatively low thermal stability of ECC based on azido-substituted tetrazoles. Most likely, the degradation of the ligands is catalyzed by the present central metals. Similar to the perchlorate complexes of 1-ETZ and PT, the pure nitrogen-rich ligands 1-ETZ, PT, AET, and APT all show decomposition temperatures close to 200 °C. When coordinating AET or APT to copper(II) or iron(II), the stability drops by approximately 50 °C. In contrast, the non-catalytically central metals zinc(II) and manganese(II) have no or only a slightly destabilizing effect.

As already shown, the formation of coordination polymers is a useful tool for increasing the thermal stability of ECC. Besides the application of bridging anions, it is also possible to deploy the linking of bidentate ligands for the buildup of higher dimensional coordination structures. *N*,*N*-substituted ditetrazolylalkanes are a suitable class of nitrogen-rich ligands to be efficiently utilized to design energetic coordination polymers with high thermal stabilities.[3,4] One of the last missing representatives of this

class of ligands are ditetrazolylmethane isomers (dtm). Therefore, 1,1-dtm, 1,2-dtm, and 2,2-dtm were synthesized and applied for the preparation of ECC. The calculation of the energetic performance of the three molecules using the EXPLO5 code reveals comparable properties to the secondary explosive TNT, and their sensitivities were successfully explained by deploying the useful Hirshfeld surface and fingerprint analysis.

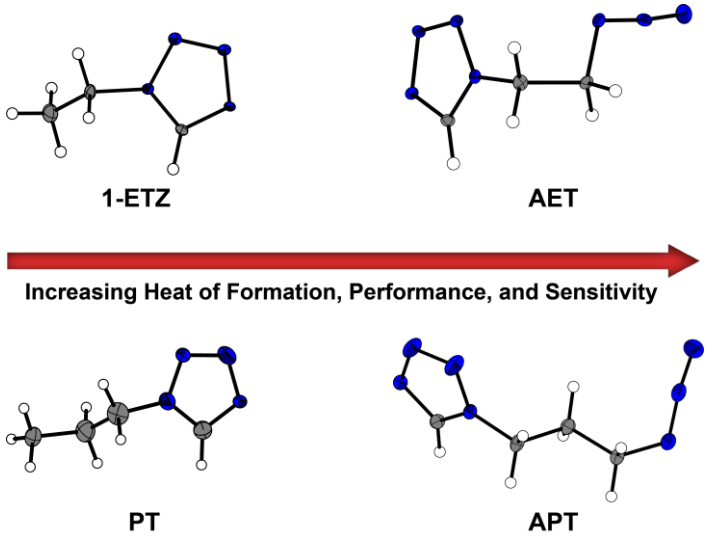

Figure 3. Comparison of *N*-alkyl- and *N*-azidoalkyl-substituted tetrazole ligands.

Interestingly, it was only possible to obtain complexes based on copper(II) and silver(I) as central metals, whereas no complexing behavior was observed with Mn^{2+}, Fe^{2+}, and Zn^{2+}. Furthermore, the ligands often exhibit terminal coordination, which leaves one binding site vacant. The monodentate behavior leads to the reduction or complete prevention of the dimensional structure, which is uncommon for ditetrazolyl substances. Nevertheless, in all copper(II) nitrate and perchlorate complexes, the dtm isomers show bridging behavior, which leads to ECC with very high thermal stabilities up to 242 °C ($[Cu(2,2\text{-}dtm)_3](ClO_4)_2$). Moreover, the exothermic decomposition temperature of 198 °C of $[Cu_2(NO_3)_4(2,2\text{-}dtm)_3]$ is significantly higher compared to other literature-known nitrogen-rich copper(II) nitrate complexes. The most promising compounds are represented by $[Cu(1,2\text{-}dtm)_3](ClO_4)_2$ and $[Cu(2,2\text{-}dtm)_3](ClO_4)_2$, which were both able to successfully transfer a detonation toward PETN.

Chapters 7–12: The main emphasis is the investigation of the anions' influence toward the sensitivities and performance of energetic materials. Therefore, a wide range of different compounds based on the counterions picramate, dicyanamide, bromate, chlorate, azide, and fulminate (Figure 4) were synthesized and thoroughly characterized. The suitable application of trinitrophenolates for the design of ECC as laser ignitable and primary explosives led to the investigation of the closely related 2-amino-4,6-dinitrophenol, which is also called picramic acid. Whereas the neutral compound's explosive properties

are a well-known fact, its simple salts are almost entirely unfamiliar to the energetic community. Therefore, several alkali and alkaline earth salts, together with the ammonium, copper(II), zinc(II), and silver(I) compounds were examined and compared with the commercially used lead(II) picramate. In spite of the lead salt's performance and sensitivities in the range of a primary explosive, all other substances show very high stability and low DDT. Unfortunately, it was not possible until now to incorporate the picramate anion for the synthesis of energetic coordination compounds.

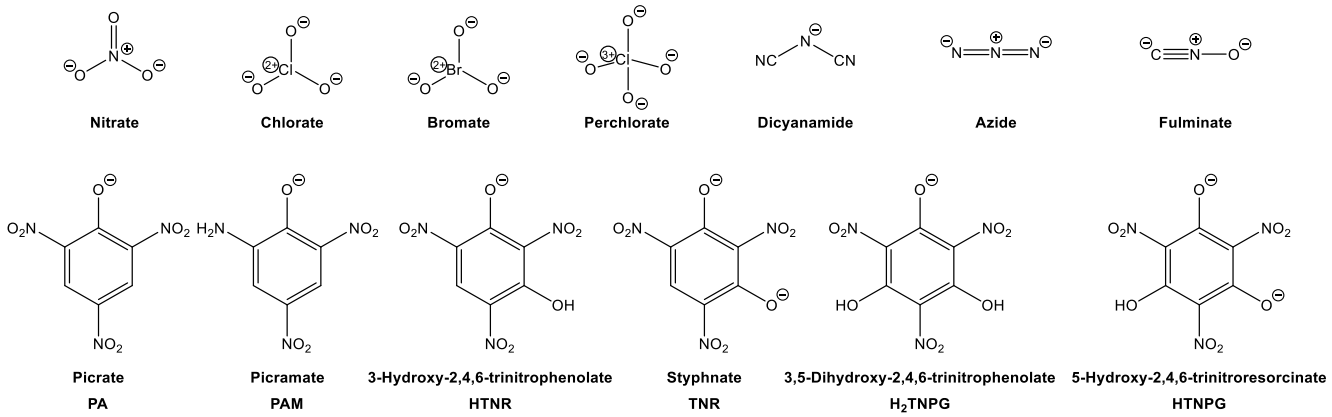

Figure 4. Illustration of different investigated anions.

Nesxt to the use of commercially available starting materials, such as perchlorate or nitrate salts, other, more exotic anions can be utilized for the preparation of ECC. Unpurchasable copper(II) compounds based on oxidizing anions, like copper(II) chlorate and bromate, or endothermic ones, such as copper(II) dicyanamide, are well-known and stable substances. To attain a deeper understanding of the concept of ECC, these three starting materials were synthesized and reacted with different nitrogen-rich azole ligands. Whereas most ECC based on copper(II) chlorate and bromate show increased sensitivities close to the values of primary explosives, dicyanamide complexes are more stable and require the incorporation of more powerful ligands, such as 1-AT and 2-AT. The comparison of similar complexes based on the same ligand systems 1-methyl-5*H*-tetrazole (MTZ) allows several conclusions to be drawn. $[Cu(DCA)_2(MTZ)_2]$ and $[Cu(BrO_3)_2(MTZ)_2]$, both with bridging anions, show higher thermal stability (170 and 169 °C, respectively) than $[Cu(ClO_3)_2(MTZ)_4]$ (159 °C), which is present as a complex monomer. All three compounds possess a lower thermal stability compared to the analogous copper(II) perchlorate complex $[Cu(MTZ)_6](ClO_4)_2$.[5] The sensitivities of the chlorate and bromate ECC are increased in comparison to the perchlorate one, while the dicyanamide complex is less sensitive. Furthermore, the bromate and chlorate compounds can be detonated in laser ignition experiments, whereas the dicyanamide complex only shows decomposition. Besides the laser ignitability of copper(II) chlorate and bromate materials, the most promising compound is represented by 4-amino-1,2,4-triazole complex $[Cu_2(4\text{-ATRI})_6](ClO_3)_4$. The bidentate triazole ligands lead to the formation of polymeric chains,

accompanied by an exothermic decomposition temperature of 186 °C. The successful initiation of PETN makes it a promising lead azide replacement.

Chapters 11 and 12: The inclusion of highly endothermic ligands in the coordination sphere of metal salts allows the formation of exceedingly energetic materials. They can also be applied to stabilize extremely sensitive primary explosives, which are arduous to handle in their pure form. Two of the most prominent substances of this class are represented by copper(II) azide and silver fulminate (SF). Based on them, the synthesis of ECC was successfully demonstrated. In both cases, the nitrogen-rich heterocycles block one of the central metals' coordination sites, which leads to the formation of complexes with practicable properties. Depending on the choice of ligand, the materials' characteristics can be highly modified. For example, the incorporation of crystal water molecules in SF forms insensitive materials, and by variation of the alkyl substituent, the sensitivities of azide complexes can be easily adjusted toward the desired range. In the case of the fulminate compounds, the sensitivities highly correlate with the azole to metal ratio. The most promising ECC examined in Chapter 12 is $[Ag_4(CNO)_4(2,2\text{-dtp})]$, in which one ligand per four silver fulminate units is present, which is the lowest ligand concentration observed. The silver complex shows a temperature stability of 177 °C, comparable performances to lead styphnate, and most beneficially, it can be prepared in a one-pot synthesis which avoids the isolation of pure silver fulminate. By means of $[Cu(N_3)_2(MTZ)]$, the further stabilization of copper(II) azide compounds with different phlegmatization agents was accomplished. Both the pure substance and the phlegmatized compounds are able to detonate PETN, and they can also be used as a lead styphnate replacement in priming mixtures, which was successfully demonstrated. The primer caps, which contain 15% $[Cu(N_3)_2(MTZ)]$ and 85% of a mixture of barium nitrate, aluminum, antimony trisulfide, and PETN, created a flame sufficient for the ignition of gun propellants.

Over the course of this thesis, a total number of 150 different chemical compounds were synthesized, including 25 nitrogen-rich azole ligands, one precursor, and 91 materials based on energetic coordination compounds (Figure 5). The crystal structures of 93 substances were determined for the first time by single-crystal X-ray experiments and uploaded to the CSD database. Of the 150 materials, 129 were studied in more detail, while the remaining compounds are ligands already described in the literature, are side species, or were synthesized exclusively for academic interest. The comparison of the different ECC, makes it clear that their properties are not only dependent on the different combination of the building blocks, but they are also highly influenced by various factors, such as the coordination sphere, ligand to central metal ratio, coordinating or non-coordinating anions, and formation of coordination polymers. Still, it is possible to summarize some blanket trends for their energetic properties. In general, the thermal

stability increases in the following order: $Fe^{2+} < Cu^{2+} < Zn^{2+} < Mn^{2+}$. A similar tendency can be observed for the impact ($Fe^{2+} \approx Cu^{2+} < Mn^{2+} < Zn^{2+}$) and friction sensitivity ($Fe^{2+} \leq Cu^{2+} < Mn^{2+} < Zn^{2+}$), wherein iron and copper complexes are always less stable toward outer stimuli. Concerning the anions, perchlorate silver(I) and copper(II) complexes show the highest thermal stabilities, and nitrate compounds are less stable. Trinitrophenolate based ECC are in between them, whereas the presence of double deprotonated anions always leads to an increase of the exothermic decomposition temperature compared to similar complex monomers. In the case of copper compounds, the anions bromate, chlorate, dicyanamide, and azide show similar temperature stabilities, and in each instance, the chlorate-based materials possess lower stability than analogous perchlorate ones. The sensitivities increase in the following order: DCA < NO_3^- < ClO_4^- < BrO_3^- ≤ ClO_3^- < N_3^-, and the sensitivities of trinitrophenolate compounds when existing as mono-deprotonated anions are in between those of nitrate and perchlorate. However, double deprotonated nitroaromatic ECC show increased sensitivities. In addition to the observed trends, many exceptions can be perceived. Especially the incorporation of aqua ligands and crystal water molecules alters the thermal stability as well as the sensitivities highly.

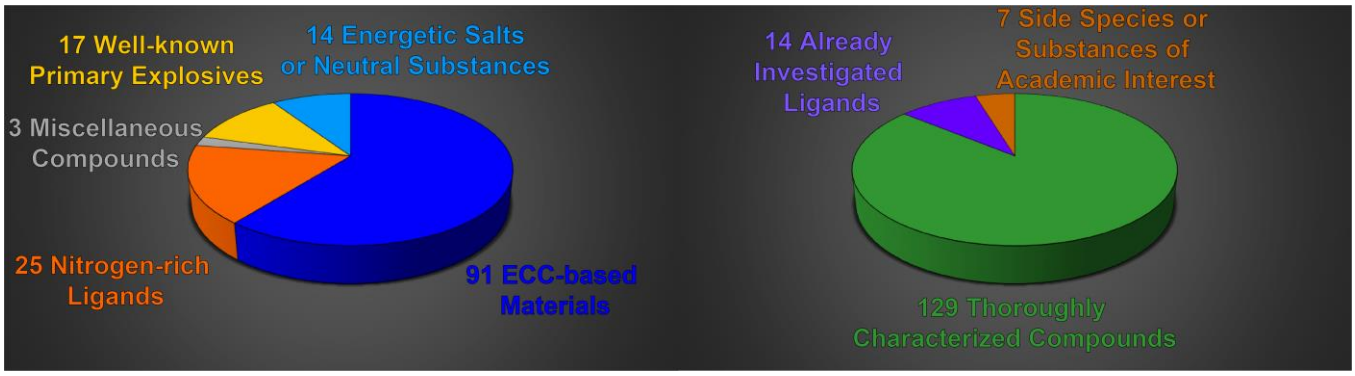

Figure 5. Segmentation of synthesized compounds and level of characterization.

Out of the 91 investigated ECC-based materials, ten complexes were successfully applied to detonate PETN or RDX, which makes them potential LA replacements (Table 1). The compounds consist of the three different central metals iron, silver, and copper, combined with chlorate, azide, or perchlorate as the anion. All of the building blocks possess decreased environmental effects compared to lead. Furthermore, toxicity measurements of chlorate complexes using the luminescent marine bacterium *Vibrio fischeri* prove the reduced toxicity of the anion compared to perchlorate-based materials.[6] Laser initiation experiments revealed 30 feasible candidates for the use as laser-ignitable explosives. In all these cases, a single pulse with energies of just a few mJ was required to trigger either a deflagration or detonation. UV-Vis studies of the ECC allow the inference of a photothermal ignition, but further details of the mechanism could not be discovered, and more detailed investigations are necessary in the future. Besides a few exceptions, the clear trend of the laser experiments' outcome highly depends on the overall sensitivity

and performance of the compounds, which leads to stronger reactions with increasing sensitivities. The deployment of water-free compounds based on strong oxidizing anions, such as (per)chlorate, bromate, or nitrate is especially suitable for the design of new laser-ignitable explosives.

Table 1. Overview of the properties of the ten potential LA replacements.

	$T_{exo.}$ [°C][a,b]	*IS* [J][c]	*FS* [N][d]	*ESD* [mJ][e]	*BDIS* [mJ][f]	Positive initiation
$[Cu(TNR)(1\text{-}AMT)_2$	212	2	16	6.3	10	PETN
$[Cu(HTNPG)(1\text{-}AMT)_2$	202	1	7	4.9	8	PETN
$[Fe(AET)_6](ClO_4)_2$	151	3	3.75	65.0	< 4	PETN
$[Ag(AET)]ClO_4$	165	< 1	0.6	65.0	< 4	PETN
$[Cu(1,2\text{-}dtm)_3](ClO_4)_2$	215	1.5	1	47	< 4	PETN
$[Cu(2,2\text{-}dtm)_3](ClO_4)_2$	242	< 1	0.75	37	< 4	PETN
$[Cu_2(4\text{-}ATRI)_6](ClO_3)_4$	186	1	< 5	15	n.d.	PETN
$[Cu(ClO_3)_2(2,2\text{-}dtp)_2]$	176	1	< 5	50	n.d.	PETN
$[Cu(N_3)_2(MTZ)]$	148	< 1	< 0.1	0.79	n.d.	PETN and RDX
$[Cu(N_3)_2(MTZ)]$ 5% CMC	150	2	0.75	0.54	n.d.	PETN and RDX

[a] Onset temperature at a heating rate of 5 °C min^{-1} measured by DTA; [b] Exothermic peak, which indicates decomposition. [c] Impact sensitivity according to the BAM drop hammer (method 1 of 6). [d] Friction sensitivity according to the BAM friction tester (method 1 of 6). [e] Electrostatic discharge sensitivity (method 1 of 6). [f] Ball drop impact sensitivity determined with the 1 of 6 method in accordance with the MIL-STD 1751A (method 1016).

The most outstanding compound which was investigated in this thesis is copper(II) azide complex $[Cu(N_3)_2(MTZ)]$ (Figure 6). Even though, its thermal stability is close to 150 °C, it shows superior energetic properties and can be used as a substituent for lead azide as well as lead styphnate. The sensitivities can be easily adjusted by applying common phlegmatization agents, such as dextrin, polysorbate, carboxymethyl cellulose, and polyvinyl butyral to ensure safe handling of the primary explosive. Just 5 mg of both the pure compound or of the desensitized material is sufficient for the reliable initiation of PETN as well as of RDX in classical detonators, which makes it to a potential lead azide replacement. Furthermore, the ECC was utilized as a LS alternative in priming mixtures for the ignition of gun propellants and successfully tested in cartridges at the shooting range. The extraordinary insolubility of the azide complex prevents the toxicity toward aquatic organisms, which is a known issue of water-soluble copper compounds.[7] To overcome the relatively low thermal stability of $[Cu(N_3)_2(MTZ)]$, future studies with copper(II) azide have to focus on the assignment of bridging ligands, such as ditetrazolylalkanes or bitriazoles. Another auspicious candidate for future applications can be found in $[Ag_4(CNO)_4(2,2\text{-}dtp)]$, which has performance and sensitivities comparable to that of LS and a thermal stability of 177 °C. The silver fulminate ECC can be readily synthesized in a one-pot reaction, which starts with harmless silver, ethanol, nitric acid, and 1,3-di(tetrazol-2-yl)propane, and which thus avoids the isolation of pure and very dangerous silver fulminate. The only drawback is the strongly restricted selective access toward 2*N*-substituted tetrazoles, the preparation of which requires elaborate and highly time-consuming workup procedures with simultaneously distinctly limited yields. Recent

advancements in organic synthesis seem to overcome this longstanding problem,[8,9] and therefore, future investigations should deal with the selective synthesis of 2,2-dtp and the application of $[Ag_4(CNO)_4(2,2\text{-dtp})]$ in green priming mixtures.

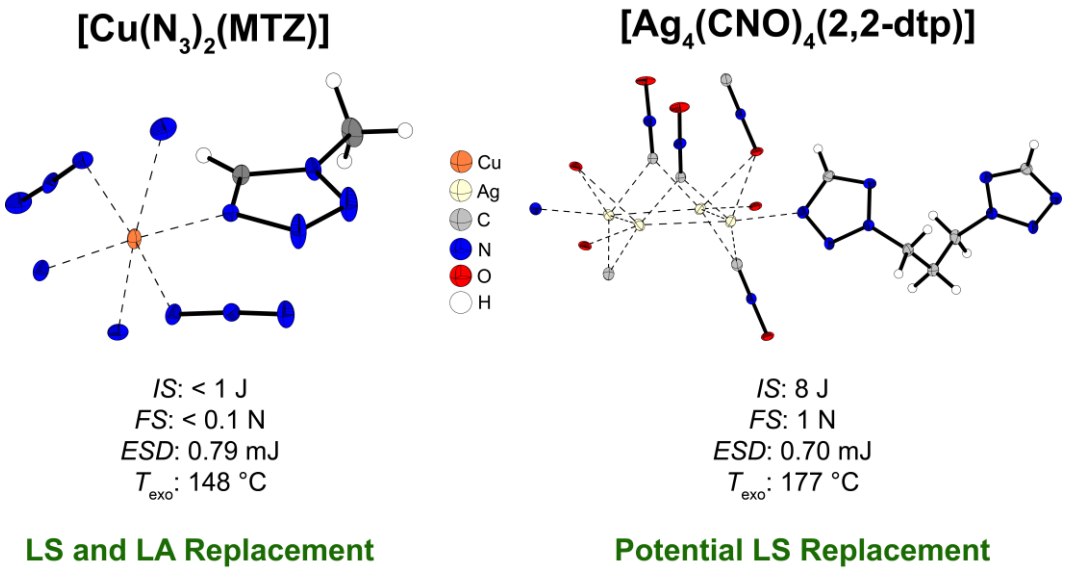

Figure 6. Illustration of the most promising compounds based on copper(II) azide and silver(I) fulminate.

The most conspicuous primary explosives with high thermal stabilities above 180 °C are $[Cu(2,2\text{-dtm})_3](ClO_4)_2$ (242 °C), $[Cu(TNR)(1\text{-AMT})_2]$ (212°C), and $[Cu_2(4\text{-ATRI})_6](ClO_3)_4$ (186 °C). All three materials form coordination polymers (Figure 7) and are able to detonate PETN in classical initiation experiments.

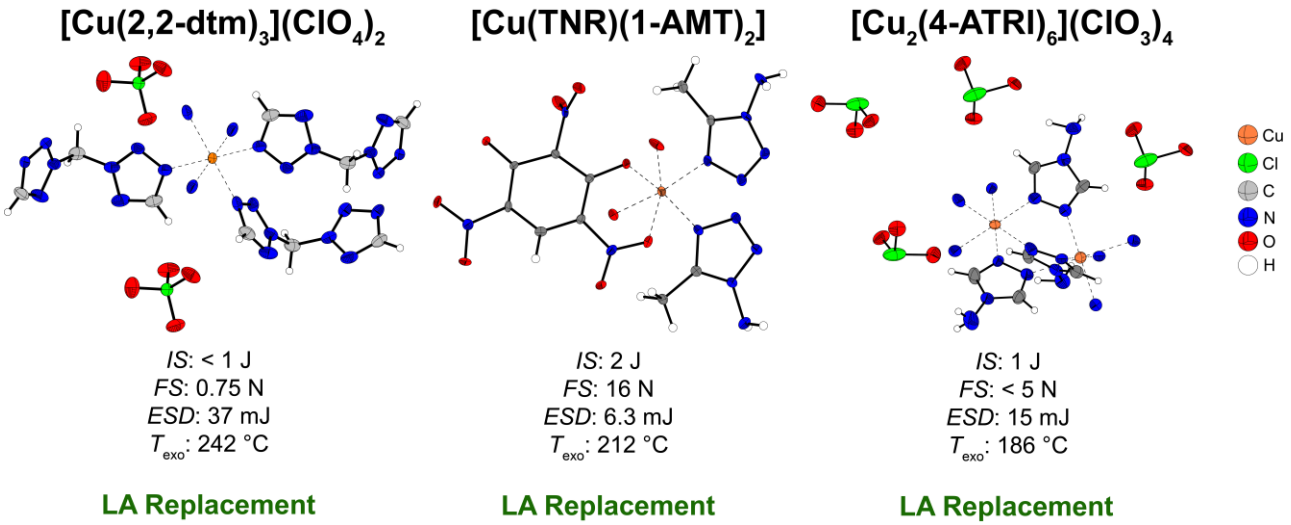

Figure 7. Depiction of lead azide replacements with high thermal stability.

The ditetrazolylmethane compound shows the highest decomposition temperature of all investigated ECC in this thesis and possesses a reliable initiation capacity. The copper(II) styphnate and chlorate complexes are promising candidates to further overcome the minor toxicity of the perchlorate anion, but accompanied

by either slightly decreased performance (styphnate) or lower temperature stability (chlorate). Concerning laser ignitable explosives, the two most considerable materials are $[Cu(APT)_6](ClO_4)_2$ and $[Cu(ClO_3)_2(dtb)_2]$, which show detonations at 51 and 0.81 mJ, respectively (Figure 8). Both possess decreased sensitivities (IS: 2.5–3 J; FS: 32 N) compared to classical primary explosives and temperature stabilities above 150 °C, which makes them potential candidates for future laser application, and which allows safer handling.

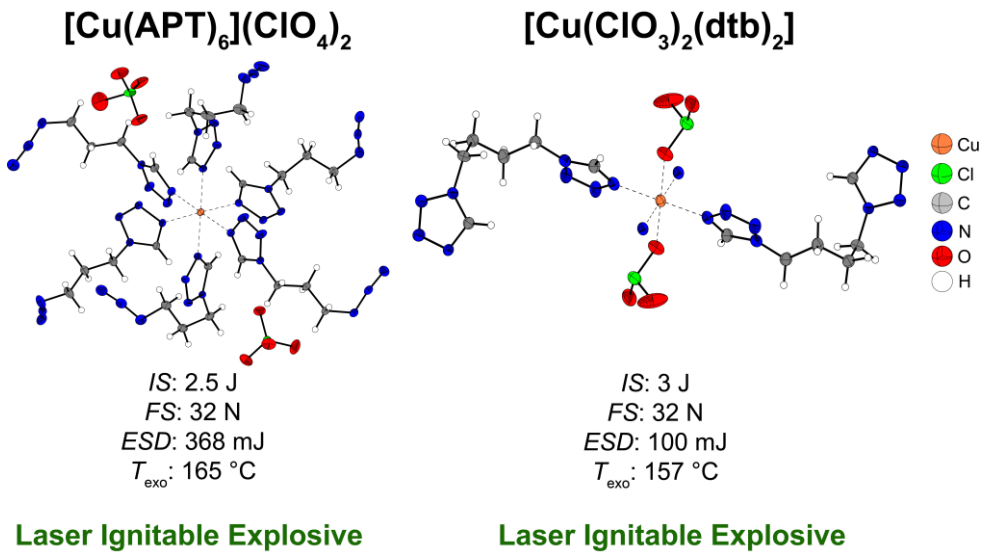

Figure 8. Illustration of detonation laser ignitable explosives with decreased sensitivities.

In conclusion, the understanding of the concept of energetic coordination compounds was further deepened, and it was possible to synthesize complexes with variable sensitivities ranging from primary explosives to completely insensitive materials by the variation of the building blocks. Furthermore, it was successfully demonstrated that highly sensitive materials like copper(II) azide and silver(I) fulminate can be stabilized by incorporating endothermic nitrogen-rich azole ligands, and their properties can be tuned toward suitable primary explosives with practicable properties. Once again, the enormous potential of the concept of ECC was proven, and it was demonstrated that it possesses the capability to replace toxic lead compounds in future applications.

13.1. References

[1] J. Šelešovský, J. Pachman, *Cent. Eur. J. Energ. Mater.* **2010**, *7*, 269–277.

[2] N. Szimhardt, M. H. H. Wurzenberger, L. Zeisel, M. S. Gruhne, M. Lommel, J. Stierstorfer, *J. Mater. Chem. A* **2018**, *6*, 16257–16272.

[3] M. Joas, T. M. Klapötke, *Z. Anorg. Allg. Chem.* **2014**, 1886–1891.

[4] N. Szimhardt, M. H. H. Wurzenberger, T. M. Klapötke, J. Lechner, H. Reichherzer, C. C. Unger, J. Stierstorfer, *J. Mater. Chem. A* **2018**, *6*, 6565–6577.

[5] N. Szimhardt, M. H. H. Wurzenberger, A. Beringer, L. Daumann, J. Stierstorfer, *J. Mater. Chem. A* **2017**, *5*, 23753–23765.

[6] European Food Safety Authority (EFSA). *EFSA J.* **2015**, *13*, 4135−4238.

[7] V. Ochoa-Herrera, G. Leon, Q. Banihani, J. A. Field, R. Sierra-Alvarez, *Sci. Total Environ.* **2011**, *412–413*, 380–385.

[8] S. A. Egorov, M. A. Ishchenko, A. S. Alikberov, *Russ. J. Org. Chem.* **2020**, *56*, 1204–1210.

[9] S. A. Egorov, M. A. Ishchenko, Ya. V. Prokopovich, V. I. Ivanov, *Russ. J. Org. Chem.* **2020**, *56*, 1196–1203.

14. Appendix

14.1. List of Publications

Publications (Peer-Reviewed)

1. N. Szimhardt, M. H. H. Wurzenberger, A. Beringer, L. J. Daumann, J. Stierstorfer, Coordination chemistry with 1-methyl-5*H*-tetrazole: cocrystallization, laser-ignition, lead-free primary explosives - one ligand, three goals, *J. Mater. Chem. A* **2017**, *5*, 23753–23765.

2. M. H. H. Wurzenberger, N. Szimhardt, J. Stierstorfer, Copper(II) Chlorate Complexes: The Renaissance of a Forgotten and Misjudged Energetic Anion, *J. Am. Chem. Soc.* **2018**, *140*, 3206–3209.

3. N. Szimhardt, M. H. H. Wurzenberger, T. M. Klapötke, J. Lechner, H. Reichherzer, C. C. Unger, J. Stierstorfer, Highly functional energetic complexes: stability tuning through coordination diversity of isomeric propyl-linked ditetrazoles, *J. Mater. Chem. A* **2018**, *6*, 6565–6577.

4. M. H. H. Wurzenberger, N. Szimhardt, J. Stierstorfer, Nitrogen-Rich Copper(II) Bromate Complexes: an Exotic Class of Primary Explosives, *Inorg. Chem.* **2018**, *57*, 7940–7949.

5. N. Szimhardt, M. H. H. Wurzenberger, L. Zeisel, M. S. Gruhne, M. Lommel, J. Stierstorfer, Maximization of the energy capability level in transition metal complexes through Application of 1-amino- and 2-amino-5*H*-tetrazole ligands, *J. Mater. Chem. A* **2018**, *6*, 16257–16272.

6. N. Szimhardt, M. H. H. Wurzenberger, P. Spieß, T. M. Klapötke, J. Stierstorfer, Potassium *N*-Nitramino-5*H*-Tetrazolates – Powerful Green Primary Explosives with High Initiation Capabilities, *Propellants Explos. Pyrotech.* **2018**, *43*, 1203–1209.

7. N. Szimhardt, M. S. Gruhne, M. Lommel, A. Hess, M. H. H. Wurzenberger, T. M. Klapötke, J. Stierstorfer, 2,2-Bis(5-tetrazolyl)propane as Ligand in Energetic 3d Transition Metal Complexes, *Z. Anorg. Allg. Chem.* **2019**, 6*45*, 354–361.

8. N. Szimhardt, M. H. H. Wurzenberger, L. Zeisel, M. S. Gruhne, M. Lommel, T. M. Klapötke, J. Stierstorfer, 1-Amino-triazole Transition Metal Complexes as Laser Ignitable and Lead-free Primary Explosives, *Chem. Eur. J.* **2019**, *25*, 1963–1974.

9. L. Zeisel, N. Szimhardt, M. H. H. Wurzenberger, T. M. Klapötke, J. Stierstorfer, 2-Methyl-substituted monotetrazoles in copper(II) perchlorate complexes: manipulating coordination chemistry and derived energetic properties, *New J. Chem.* **2019**, *43*, 609–616.

10. M. H. H. Wurzenberger, M. S. Gruhne, M. Lommel, N. Szimhardt, T. M. Klapötke, J. Stierstorfer, Comparison of 1-Ethyl-5*H*-tetrazole and 1-Azidoethyl-5-tetrazole as Ligands in Energetic Transition Metal Complexes, *Chem. – Asian J.* **2019**, *14*, 2018–2028.

11. M. H. H. Wurzenberger, B. R. G. Bissinger, M. Lommel, M. S. Gruhne, N. Szimhardt, J. Stierstorfer, Synthesis and comparison of copper(II) complexes with various *N*-aminotetrazole ligands involving trinitrophenol anions, *New J. Chem.* **2019**, *43*, 18193–18202.

12. M. S. Gruhne, M. Lommel, M. H. H. Wurzenberger, N. Szimhardt, T. M. Klapötke, J. Stierstorfer, OZM Ball Drop Impact Tester (BIT-132) vs. BAM Standard Method - a Comparative Investigation, *Propellants Explos. Pyrotech.* **2020**, *45*, 147–153.

13. M. H. H. Wurzenberger, J. T. Lechner, M. Lommel, T. M. Klapötke, J. Stierstorfer, Salts of Picramic Acid – Nearly forgotten temperature-resistant energetic materials, *Propellants Explos. Pyrotech.* **2020**, *45*, 898–907.

14. S. D. Schnell, L. V. Hoff, A. Panchagnula, M. H. H. Wurzenberger, T. M. Klapötke, S. Sieber, A. Linden, K. Gademann, 3-Bromotetrazine: Labelling of Macromolecules via Monosubstituted Bifunctional s-Tetrazines, *Chem. Sci.* **2020**, *11*, 3042–3047.

15. M. H. H. Wurzenberger, S. M. J. Endraß, M. Lommel, T. M. Klapötke, J. Stierstorfer, Comparison of 1-Propyl-5*H*-tetrazole and 1-Azidopropyl-5*H*-tetrazole as Ligands for Laser Ignitable Complexes, *ACS Appl. Energy Mater.* **2020**, *3*, 3798–3806.

16. a) M. H. H. Wurzenberger, M. Lommel, M. S. Gruhne, N. Szimhardt, J. Stierstorfer, Refinement of Copper(II) Azide with 1-Alkyl-5*H*-Tetrazoles into Fully Adaptable Energetic Complexes, *Angew. Chem. Int. Ed.* **2020**, *59*, 12367–12370; b) M. H. H. Wurzenberger, M. Lommel, M. S. Gruhne, N. Szimhardt, J. Stierstorfer, Veredelung von Kupfer(II)-azid mittels 1-Alkyl-5*H*-tetrazolen: Leistungsfähige energetische Komplexverbindungen, *Angew. Chem.* **2020**, *132*, 12466–12469.

17. M. H. H. Wurzenberger, J. T. Lechner, J. Stierstorfer, Copper(II) Dicyanamide Complexes with *N*-Substituted Tetrazole Ligands – Energetic Polymers with Moderate Sensitivities, *ChemPlusChem* **2020**, *85*, 769–775.

18. M. H. H. Wurzenberger, V. Braun, M. Lommel, T. M. Klapötke, J. Stierstorfer, Closing the Gap: Synthesis of Three Isomeric *N*,*N*-Ditetrazolymethane Ligands and Their Coordination Proficiency in Adaptable Laser Responsive Copper(II) and Sensitive Silver(I) Complexes, *Inorg. Chem.* **2020**, *59*, 10938–10952.

19. T. M. Klapötke, B. Krumm, C. Riedelsheimer, J. Stierstorfer, C. C. Unger, M. H. H. Wurzenberger, Urazine – a Long Established Heterocycle and Energetic Chameleon, *Eur. J. Org. Chem.* **2020**, *31*, 4916–4924.

20. M. H. H. Wurzenberger, M. S. Gruhne, M. Lommel, V. Braun, N. Szimhardt, J. Stierstorfer, Taming the Dragon: Complexation of Silver Fulminate with Nitrogen-rich Azole Ligands, *Inorg. Chem.* **2020**, *59*, 17875–17879.

21. M. Reichel, M. H. H. Wurzenberger, M. Lommel, M. Kofen, B. Krumm, J. Stierstorfer, K. Karaghiosoff, *N*-Fluoromethylated (Amino)Tetrazoles: Manipulating Thermal and Energetic Properties, *Z. Anorg. Allg. Chem.*, ahead of print.

Patents

1. T. M. Klapötke, J. Stierstorfer, N. Szimhardt, M. H. H. Wurzenberger, EP 18150491.1-1132 and 18151497.7-1116, application date: 12.01.2018.

Poster Presentations

1. M. H. H. Wurzenberger, N. Szimhardt, T. M. Klapötke, J. Stierstorfer, *Energetic Copper(II) Bromate Complexes as Replacement of Lead and Perchlorate Containing Primary Explosives*, New Trends in Research of Energetic Materials, Proceedings of the Seminar, 21th, Pardubice, Czech Republic, **2018**.

Oral Presentations

1. M. H. H. Wurzenberger, T. M. Klapötke, N. Szimhardt, M. S. Gruhne, M. Lommel, J. Stierstorfer, *Energetische Koordinationsverbindungen für den Einsatz als Primär- und laserzündbare Sprengstoffe*, 15th Coordination Chemistry Conference, Munich, Germany, **2019**.

2. M. H. H. Wurzenberger, T. M. Klapötke, N. Szimhardt, M. S. Gruhne, M. Lommel, J. Stierstorfer, *New ligands and energetic coordination compounds for use as primary and laser ignitable explosives*, New Trends in Research of Energetic Materials, Proceedings of the Seminar, 22th, Pardubice, Czech Republic, **2019**.